Late Holocene surface water changes in the eastern Nordic Seas : the message from carbonate and organic-walled phytoplankton microfossils

Christian Dylmer

THÈSE

PRÉSENTÉE A

L'UNIVERSITÉ BORDEAUX 1

ÉCOLE DOCTORALE DES SCIENCES ET ENVIRONNEMENTS

Par **Christian V. DYLMER**

POUR OBTENIR LE GRADE DE

DOCTEUR

SPÉCIALITÉ : SEDIMENTOLOGIE MARINE ET PALEOCLIMATS

Paléohydrologie de surface des Mers Nordiques à l'Holocène Terminal (derniers 3000 ans) : le message du phytoplancton à squelette calcaire et organique.

Directeur de recherche : Jacques GIRAUDEAU

Soutenue le : 17 Décembre 2013

Devant la commission d'examen formée de :

Mme. SEIDENKRANTZ, Marit-S.	Professeur, Dpt Geoscience, Univ. d'Aarhus, Danemark	Rapporteur
M. KNIES, Jochen	Chercheur, Geological Survey of Norway, Norvège	Rapporteur
Mme. HUSUM, Katrine	Chercheur, Dpt Geology, Univ. Tromsø, Norvège	Examinateur
M. CROSTA, Xavier	DR CNRS, EPOC, Univ. Bordeaux 1	Examinateur
Mme. EYNAUD, Frédérique	MCF, EPOC, Univ. Bordeaux 1	Examinateur
M. GIRAUDEAU, Jacques	DR CNRS, EPOC, Univ. Bordeaux 1	Dir. de thèse

Abstract

Five marine sediment cores distributed along the Norwegian, western Barents Sea, and Svalbard continental margins have been investigated in order to reconstruct late Holocene changes in the poleward flow of the Norwegian Atlantic Current (NwAC) and West Spitsbergen Current (WSC) and the nature of the upper surface water masses within the eastern Nordic Seas. This research project is based on the use of dinocyst and coccolith assemblages for qualitative and quantitative reconstructions of surface water conditions from high resolution sediment cores, and involve upstream investigations on proxy reliabilities.
The investigated area (66 to 77°N) was affected by an overall increase in the strength of the AW flow from 3000 cal. yrs BP to the Present. The long-term modulation of westerlies strength and location which are essentially driven by the dominant mode of the North Atlantic Oscillation (NAO), is thought to explain the observed dynamics of the AW flow. The same mechanism also reconciles the recorded opposite zonal shifts in the location of the Arctic Front between the area off western Norway and the western Barents Sea-eastern Fram Strait region. Submillenial changes in AW flow are organised according to known pre-Anthropocene warm (RWP, MCA and the Modern period: strong poleward flow) and cold (LIA, DA: weak poleward flow) climatic spells. A sudden short pulse of resumed high WSC flow interrupted the LIA in the eastern Nordic Seas from 330 to 410 cal. yrs BP. Our results are indicative of a major impact of AW flow dynamics on the Arctic sea ice distribution during the last millenium, when changes in reconstructed sea-ice extent are negatively correlated with the strength of the WSC flow off western Barents Sea and western Svalbard. The extensive decrease in sea ice extent during the last century is synchronous with an exceptional increase in AW flow. The previously reconstructed high amplitude warming of surface waters in eastern Fram Strait at the turn of the 19th century was therefore primarily induced by an excess flow of AW which stands as unprecedented over the last 3000 years.

Keywords: Eastern Nordic Seas, late Holocene, Atlantic water flow, surface waters, coccoliths, dinocysts.

Résumé

La variabilité de l'intensité du flux d'eaux atlantiques et de la nature des masses d'eau de surface le long des marges occidentales de la Norvège, de la mer de Barents et du Svalbard a été reconstituée sur la base des assemblages de coccolithes et dinokystes présents dans cinq carottes sédimentaires marines représentatives de l'Holocène terminal. Les résultats sont présentés sous la forme de reconstructions qualitatives et quantitatives (fonctions de transfert MAT) à haute résolution temporelle (échelle décennale à sub-séculaire). Un travail visant à valider les traceurs micropaléontologiques utilisés a été réalisé en parallèle à l'objectif principal, et s'est en particulier nourri de la collecte et de l'examen de populations vivantes distribuées le long de plusieurs transects zonaux en mer de Norvège, mer d'Islande et à travers le détroit de Fram.
Nos résultats indiquent que la partie orientale des mers Nordiques (66 à 77°N) a été sujette à une tendance globale à l'augmentation du flux d'eaux atlantiques (AW) au cours des derniers 3000 ans. La dynamique récente de ce flux méridien est supposée répondre à la modulation long-terme de la force et de la localisation de la ceinture des vents d'ouest qui est essentiellement pilotée par l'Oscillation Nord Atlantique. Ce même mécanisme atmosphérique réconcilie le déplacement zonal et contradictoire du front arctique entre le domaine ouest-norvégien, et les façades occidentales de la mer de Barents et du détroit de Fram. La variabilité rapide du flux d'AW reproduit la succession des phases climatiques historiques classiques chaudes (Période Chaude Romaine, Période Chaude Médiévale, Période Moderne : flux accentué d'AW) et froides (Période Sombre, Petit Age Glaciaire : flux réduit d'AW) des derniers 2500 ans. Un événènement rapide de renforcement du flux d'AW en mers Nordiques a été identifié pendant le Petit Age Glaciaire entre 330 et 410 ans BP (cal.). Nos résultats indiquent que les variations d'intensité du flux d'AW vers l'Océan Arctique ont eu un impact majeur sur la distribution de la glace de mer arctique au cours du dernier millier d'années, les variations reconstruites de l'extension du couvert de glace à l'echelle de l'océan arctique étant parfaitement corrélées (échelle sub-séculaire) avec nos reconstructions qualitatives de la dynamique de l'AW au large du Svalbard et de la mer de Barents. La diminution importante de l'extension de la banquise durant le 20ème siècle est synchrone d'un flux record d'AW à travers le détroit de Fram, flux qui, d'après nos données, est sans précédent pour les derniers 3000 ans.
Mots clés : Mers Nordiques, Holocène terminal, flux d'eaux atlantiques, eaux de surface, coccolithes, dinokystes.

Résumé étendu

Les Mers Nordiques (mers d'Islande, de Norvège et du Groenland) et domaines marins adjacents (Mer de Barents et Détroit de Fram), constituent, avec l'Océan Arctique, un des domaines océaniques les plus sensibles aux changements climatiques actuelles et passés. Cette région est caractérisée par de forts contrastes de flux méridionaux entrants et sortants de masses d'eaux de surface et intermédiaires sous la forme de transfert de chaleur vers le pole sur sa façade orientale, et d'export vers les basses latitudes d'eaux polaires et de glace de mer sur sa façade occidentale. Site majeur de formation d'eaux profondes (Mers du Groenland et de Norvège), et de formation de glace de mer (plateforme Est-Groenlandaise, Détroit de Fram, Mer de Barents), ce domaine est considéré comme un acteur clé de la variabilité de la circulation thermohaline et du climat global globale aux échelles orbitales et sub-orbitales. La formation (phénomènes de brines, albédo) et la fonte de glace de mer (dessalure) constituent d'importants mécanismes de rétroaction aux changements climatiques globaux. Les changements dans le mode de circulation atmosphérique (Oscillation Nord Atlantique – NAO-) ainsi que la variabilité du flux méridien d'eaux atlantiques vers l'Océan Arctique par le Courant de Norvège (NwAC) sont fortement impliqués dans l'extension présente et passée de la banquise aux très hautes latitudes de l'Atlantique Nord.

L'amplification polaire du changement climatique actuel motive aujourd'hui une série d'initiatives visant à étudier, sur la base d'analogues passés, le déroulement de ce processus et les mécanismes associés, et ce afin de nourrir le plus correctement possible les modèles prédictifs d'évolution du climat futur. L'Holocène terminal, soit les derniers 3000 ans, gouverné par un refroidissement général (Néoglaciation), a été ponctué par une série d'épisodes de réchauffement (Période Chaude Romaine –RWP-, Période Chaude Médiévale – MCA-) et de refroidissement (Petit Age Glaciaire –LIA-) du climat à l'échelle du bassin Atlantique voire de l'hémisphère Nord. Les archives terrestres et marines indiquent que la fin du LIA a été marqué par un renversement des températures selon une amplitude sans précédant pour le dernier millier d'années.

L'objectif général de la présente étude est de contraindre, pour le tardi-Holocène, la variabilité des conditions hydrologiques et de la structure des masses d'eaux de surface des Mers Nordiques dans les régions proches ou actuellement affectées par la formation saisonnière de glace de mer. Cet objectif repose sur des reconstructions qualitatives et quantitatives à très haute résolution temporelle (décennale à séculaire) des conditions des eaux de surface à partir des assemblages de coccolithes (squelettes de phytoplancton calcaire) et dinokystes (restes

fossilisés de phytoplancton organique) contenus dans des carottes marines. Un point particulier de ce travail concerne la reconstruction de la variabilité tardi-holocène du flux d'eaux atlantiques à l'Océan Arctique à travers les seuils de Fram et de la Mer de Barents.
Cette étude repose sur l'analyse de 5 carottes sédimentaires réparti le long des marges de la Norvège, de la Mer de Barents et du Svalbard, et sous l'influence du flot principal d'eaux atlantiques vers l'Océan Arctique. Les traceurs micropaléontologiques retenus (coccolithes et dinokystes) ainsi que des traceurs annexes dont les constituants élémentaires du sédiment (basés sur analyses XRF), les assemblages de foraminifères planctoniques et l'abondance des grains lithiques, ont été analysés afin d'identifier les changements tardi-holocènes des circulation de surface et de sub-surface de la NwAC et de son extension, le West Spitsbergen Current (WSC). Un travail de validation des traceurs micropaléontologiques a été mené en parallèle au travail de reconstructions paléocéanographiques.
Ce travail a permis de dégager plusieurs messages importants :

- <u>Distribution des populations de coccolithophores à travers les Mers de Norvège et d'Islande et le détroit de Fram</u> :
La distribution géographique des populations de coccolithophores collectées le long de 2 transects zonaux (Norvège-Groenland ; Spitsberg-Groenland), et ce à deux périodes distinctes (été et automne), a été discutée en fonction de la distribution des masses d'eaux et fronts hydrologiques déduits de cartes satellites synoptiques et de profils CTD et Argo. Les changements saisonniers observés en terme de distribution et de stratification des masses d'eaux de surface, se traduisent par un déplacement vers l'Ouest de la zone de production maximale du phytoplancton calcaire dominé par l'espèce *Emiliania huxleyi*, de juillet à octobre. Les eaux de surface proches de l'île de Jan Mayen, fortement influencées par une augmentation de la stratification de la zone photique en automne, en relation avec la fonte de la glace de mer, sont sujettes à un changement drastique dans la composition des assemblages de coccolithophores entre l'été (*Coccolithus pelagicus*) et l'automne (*E. huxleyi*). La température seuil (maximale) de 6°C semble limiter la production de l'espèce *C. pelagicus* en Mers de Norvège et d'Islande, ce seuil chutant à 4°C pour les eaux de surface du Détroit de Fram. Contrairement aux eaux de surface des Mers de Norvège et d'Islande, les eaux du Détroit de Fram portent une population de coccolithophores essentiellement contrôlée (stocks et composition) par la présence de glace de mer et l'irradiance solaire.

- Les traceurs de la localisation du Front Arctique, et de l'intensité du flux d'eaux atlantiques :
La distribution spatiale des espèces de coccolithes *E. huxleyi* et *C. pelagicus*, d'une part, et des dinokystes *O. centrocarpum* et *N. labyrinthus* d'autre part suggère que leur rapport d'abondance dans les sédiments de surface des Mers Nordiques définit relativement bien la localisation du front Arctique (AF). L'application de ces rapports aux sédiments de nos 5 carottes marines a fourni des résultats contradictoires. Trois facteurs, pris séparément ou ensemble, permettent d'expliquer ces apparentes contradictions : (1) le choix de la valeur seuil du rapport définissant la position de l'AF ; (2) l'homogénéité de la distribution des échantillons de surface ayant été utilisés pour définir ces traceurs ; (3) une connaissance encore limitée de l'écologie des espèces concernées. Il est ainsi possible d'affirmer que le rapport *E. huxleyi/C. pelagicus* est fiable en tant que traceur de la localisation de l'AF à l'exception des domaines affectés par le Courant Côtier de Norvège, et que conformément à sa distribution dans les carottes étudiées, il traduit au cours des derniers 3000 ans une augmentation progressive dans le temps de l'influence de la NwAC et du WSC vers les très hautes latitudes. Nos données suggèrent également que le rapport *O. centrocarpum/N. labyrinthus* est peu fiable dans les régions affectées par la glace de mer saisonnière, ainsi que sur les domaines de plateforme et bordure de talus.

L'abondance de l'espèce de coccolithe allochtone *Gephyrocapsa muellerae* a été discutée en terme de variation relative de l'intensité du flux méridien d'eaux atlantiques en relation avec l'intensité et la localisation de la ceinture des vents d'ouest (modulé par l'Oscillation Nord Atlantique –NAO-). Les tendances générales pour un mode NAO globalement positif durant le MCA et la période moderne, et un mode globalement négatif durant le LIA, sont exceptionnellement bien exprimées par le renforcement ou de réduction de l'intensité de la NwAC (tels que défini par les variations d'abondance de *G. muellerae*). Ceci répond aux processus actuels influant sur la circulation de surface et de subsurface en Mers Nordiques.
La variabilité du flux d'eaux atlantiques sur la bordure orientale des Mers Nordiques, telle que reconstruite par notre traceur *G. muellerae*, est remarquablement synchrone des changements ayant affecté la distribution de la banquise arctique au cours des derniers 1500 ans. En particulier, la diminution exceptionnelle de la banquise au cours du dernier siècle correspond à un flux reconstruit record du WSC à travers le détroit de Fram, sans précédant pour les derniers 1500 ans.

- Évolution de la circulation de surface au cours des derniers 3000 ans :

L'examen des enregistrements obtenus sur les 5 carottes sédimentaires de notre transect latitudinal nous a permis de reconstruire l'évolution de la distribution des masses d'eaux de surface et du flux de la NwAC et du WSC au cours des derniers 3000 ans. Tous les enregistrements sont représentatifs d'un renforcement de la circulation méridienne des eaux atlantiques tout au long des derniers 3000 ans. Cette modulation long-terme du transfert de chaleur vers les hautes latitudes Nord répond à la dynamique long-terme de la NAO. Ce mécanisme atmosphérique explique également les déplacements reconstruits de la localisation du Front Arctique, déplacements zonaux qui présentent une histoire opposée entre la mer de Barents-Détroit de Fram, et la mer de Norvège. La variabilité sub-millénaire de l'intensité de la NwAC et du WSC est synchrone des évènements climatiques pré-Anthropocène (RWP, DA, MCA and LIA). L'initiation du LIA vers 650 ans cal. BP s'est manifestée par la détérioration du flux méridien d'eaux atlantiques, et une plus forte contribution des eaux arctiques et polaires dans la région du Svalbard et de l'ouest de la mer de Barents. La réduction maximale de l'intensité du WSC n'intervient qu'à partir de 300 ans cal. BP et est couplée avec une extension maximale d la glace de mer à l'ouest de la Mer de Barents. Une courte période d'amélioration hydrologique et climatique caractérise l'intervalle 410-330 ans cal. BP.

Au terme de ce travail, il apparait essentiel de concentrer nos futurs investigations sur les quelques points suivants :

- contribuer à l'amélioration des connaissances sur l'écologie des populations vivantes de coccolithophores et dinoflagellés dans des environnements aussi extrêmes que ceux des hautes latitudes Nord, ainsi que sur la distribution géographique de leurs restes squelettiques.

Outre les paramètres températures et salinités, le rôle de la stratification saisonnière de la zone photique sous l'influence de la fonte de la banquise, doit faire l'objet d'un examen spécifique.

- améliorer la qualité des enregistrements obtenus sur nos 5 sites de travail.

Outre une amélioration du contexte stratigraphique, en partie via la prise en compte de téphras caractéristiques d'éruptions islandaises du dernier millénaire (coll. E. Ducassou, EPOC), le cadre collaboratif du projet CASE permettra très rapidement de coupler nos données avec celles en cours de valorisation sur les mêmes séries sédimentaires (assemblages de foraminifères planctoniques et benthiques, biomarqueurs IP25, parmi les plus importantes).

Acknowledgement

This thesis would not have been possible without the help and support of a large variety of people during the past 3 years.
First of all I want to sincerely thank my supervisor Jacques Giraudeau, who gave me this great opportunity and in spite of other duties always managed to find the time for constructive critique, discussions and scientific advice. Who strongly aided me in keeping the focus on the main objective of my thesis when my focus went too broad and of course thanks for being patient beyond a limit which even I could have mastered. I have learnt a lot from our discussions.
In addition I want to send both Jacques and Isabelle Deme a huge thanks for taking the time to assist in getting settled in France and for going even further than the call of duty, when needed.

A huge thanks to F. Eynaud (EPOC) for her strong help in the micropaleontological investigations, interpretation and for her massive aid in running the Modern Analogue Technique.
Thanks to Katrine Husum (University of Tromsø) and Jochen Knies (NGU, Trondheim) for their contribution to my work and for sharing samples.
Obviously massive thanks also go to my colleagues within the CASE ITN for good discussions, many great experiences and enlighting opportunities!
Following this, I would like to thank my paper co-authors for their help and insightful comments on this work. They are Katrine Husum, Jochen Knies, Vincent Hanquiez (EPOC) and Anne de Vernal (GEOTOP UQAM).
For additional academic and laboratory support I thank the academic and technical staff and PhD students in our research group at EPOC L. Rossignol, M. Georget, I. Billy, J.-M. Escalier, S. Schmidt, M. Sanchez-Goni, L. Londeix, X. Crosta, Aurelie, Marie-Louise, Melanie, Loïc, Dunia, Phillipine and many others.
Thank you to Marit-Solveig for encouraging me to stay in science, for her continuous help and support, and for having accepted to participate to the thesis committee!
On the more personal level, I would like to thank everybody who accompanied and supported me throughout the last three years in Bordeaux. Thanks for being there when needed and for helping me to make these three last years such a great experience! My deepest thanks goes to Weiwei, Bin & Peipei, Wiljam, Hanna and Xin for your friendship, support, great game & dinner evenings and all the nice moments we have spend together here in Bordeaux. Thanks to Gesa for being a nice co-PhD and all the many experiences and fun times during the last 3 years. A thanks also go to Florent, Benjamin, Ana, Floriant & Jinwin for their fantastic friendship during good and bad times.

Et stort tak gaar ogsaa til mine venner i Danmark: Lasse, Anja, Anne-Sophie, Daniel, Anders & Camilla, Aargaard og Martin for altid at vaere dér! Tusind Tak!!!

Til sidst har jeg ingen ord for min tak til min Familie. Tak fordi i altid er der og altid har vaeret der for mig, paa trods af at jeg de sidste tre aar har boet 1000 km. fra jer, saa er i der altid for mig i medgang og i modgang!

I dedicate this work to my entire family!

Thanks!!!

Table of Content

Figure and Table List

Figure and Table List (Articles)

Article: "The coccolithophores *Emiliania huxleyi* and *Coccolithus pelagicus*: extant populations from the Norwegian-Iceland Sea and Fram Strait".

Article: "Northward Advection of Atlantic water in the eastern Nordic Seas over the last 3000 years".

Abbreviation List

AF	Arctic Front
AO	Arctic Oscillation
ArW	Arctic Water
AW	Atlantic Water
BIC	Bear Island Current
BIT	Bear Island Trench
DA	(the) Dark Ages
EB	Eastern Branch (NwAC)
EGC	East Greenland Current
EIC	East Icelandic Current
ESC	East Spitsbergen Current
Gba	(the) Great Bank
HTM	Holocene Thermal Maximum
IRD	Ice Rafted Detritus
JMC	Jan Mayern Current
LF	Lithofacies
LIA	(the) Little Ice Age
MAT	Modern Analogue Technique
MCA	Medieval Climate Anomaly
MIZ	Marginal Ice Zone
M	Modern period
NAC	North Atlantic Current
NAO	North Atlanic Oscillation
NwAC	Norwegian Atlantic Current
NCC	Norwegian Coastal Current
NCaC	North Cape Current
NH	Northern Hemisphere
PC	Percey Current
PW	Polar Water
PF	Polar Front
RAC	Return Atlantic Current
RWP	Roman Warm Period
Sba	Spitsbergen Bank
THC	Thermohaline circulation
WB	Western Branch (NwAC)
WSC	West Spitsbergen Current

Chapter 1 : General Introduction

1.1 Introduction and Thesis Overview

Getting a better knowledge on the dynamics of natural climate changes during the present Interglacial (the Holocene) is of outmost importance to distinguish the anthropogenic vs. natural impacts and feedbacks at play in present times of global warming, and to assess the evolution of the global climate in the coming decades and centuries. The northern North Atlantic (Iceland, Greenland, Norwegian, Barents Seas and Fram Strait) is, together with the Arctic Ocean, one of the most sensitive climatic regions of the modern oceans. As the main connection to the Arctic Ocean, this region is characterized by strong contrasting meridional inflow and outflow of surface and intermediate waters in the form of heat import to the northernmost latitudes on the eastern side of the Nordic Seas, and polar water and sea ice export through Denmark Strait in the western part, respectively. As a major site of deep water convection in the Greenland and Norwegian Sea, and sea-ice formation off western Greenland, Fram Strait and Barents Sea, this area has long been considered as a key player in the variability of the Atlantic Meridional Overturning Circulation, hence in global climate changes at orbital (glacial/interglacial) to shorter time-scales.

A dramatic decline over the last 30 years has been observed in the summer distribution and thickness of Arctic sea ice through satellite imagery, a phenomenom which is now also observed during winter months (Serreze et al., 2003; Comiso et al., 2008). Sea ice formation and melting constitute some of the most important feedback mechanisms to the global climate system (Aargaard and Carmack, 1994). Sea ice effectively insulates the atmosphere from the ocean, restricting the exchanges of heat, mass, momentum and chemical components (Divine and Dick, 2006). Also, together with snow-covered continental areas, sea-ice from its high albedo (higher than that of open ocean surface waters) contributes to a high extent to the radiative balance of the Earth. Changing modes of atmospheric circulation (North Atlantic Oscillation, NAO) as well as variability in poleward flow of the Norwegian Atlantic Current (NwAC) waters are strongly involved into present and past sea ice extent in the northern North Atlantic (Blindheim et al., 2000; Vinje, 2001; Visbeck et al., 2003). Hence, as changes in the global climate necessarily involve changes in sea-ice cover (Divine and Dick, 2006), which again is strongly linked to the northward meridional flow of warm saline waters to the Arctic Oceans, a strong need has arisen to improve our understanding of the effects of the past decades' strengthened heat advection to the Arctic on the decreased sea ice extent (Vinje, 2001; Dick and Divine, 2006) .

An often asked question concerning the last decades' climatic and oceanographic changes is whether or not our present interglacial contains analogues for the present and future climate development. Although the amount of literature on Holocene (last ~11.600 years) climate changes is large and steadily increasing (Wanner et al., 2008), there is still limited information on the geographic patterns and the mechanisms behind this variability. Past naturally-driven Holocene climate shifts had strong social impacts: civilizations' developments and collapses occurring synchronously with abrupt shifts to drier and/or colder climate regimes (Wanner et al., 2008, and references therein). Naturally-driven rapid climate changes will therefore contribute extensively, together with the anthropogenic forcing, to the future climate changes (Sejrup et al., 2011). Despite the role oceans play in the climate system, they are often excluded from general data compilations of Holocene climate archives due to lower time resolutions of marine sediment cores compared to ice cores and tree rings (Overpeck et al., 1997; Kaufman et al., 2009). In addition, the chronology of most ocean sediment cores is primarily based on radiocarbon dates on marine carbonate fossils, which are often hampered by uncertainties in the estimation of reservoir effects, and which, therefore, often limit their reliability to the investigation of low resolution centennial to millennial scale variability (Sejrup et al., 2011).

Reconstructions of sea surface temperature in the North Atlantic generally show a decreasing trend throughout the Holocene which has been attributed to insolation changes (e.g. Marshall et al., 2001). Nevertheless, previous studies (e.g. Dahl-Jensen et al., 1998; Calvo et al., 2002; Sarnthein et al., 2003; Solignac, 2008) showed that hydrographical changes in the mid- and high latitudes of the northern North Atlantic were not uniform in terms of amplitude and spatial extent. As an example, the Late Holocene was governed by a cooling trend known as the Neoglaciation (Porter and Denton, 1967), which was punctuated by several warm and cold spells such as the Roman Warm Period (RWP) and Medieval Climate Anomaly (MCA) and the Little Ice Age (LIA). Over the last century, the LIA was reversed by an overall increase in temperature, as depicted from terrestrial high resolution proxy records of the Arctic region (Overpeck et al., 1997; Kaufman et al., 2009) and proxy records from marine sediment cores of the northern North Atlantic (Spielhagen et al., 2011; Hald et al., 2011; Wilson et al., 2011). Marine proxy-based reconstructions suggest that this recent temperature increase in the subsurface layer west of Spitsbergen (Spielhagen et al., 2011) and in shallow settings of Northwest Norway (Hald et al., 2011) was unprecedented over the past two millenniums.

Both studies implied that this warming was probably caused by enhanced advection of Atlantic Water (AW) to the Arctic Ocean during modern times, although neither (of them) were able to strictly infer the dynamical history of AW, i.e. the history of the strength of the North Atlantic Current (NAC). The hypothesis of an increased AW inflow during the modern period was further supported by Wanamaker et al. (2012) based on living and fossil molluscan remains found north of Iceland. These authors additionally related known pre-Anthropocene warm (MCA) and cold (LIA) climatic spells of the last ~1500 years to modulations of the surface Atlantic-derived water dynamics within the North Atlantic. This modulation was further evidenced off Florida, at the inception of the Gulf Stream, by Lund et al. (2006) who estimated a 10 percent decrease in the flow of this current at the transition from the MCA to the LIA. Similarly, in the close Chesapeake Bay, such modulations were also evidenced by Cronin et al. (2005) who linked them to North Atlantic Oscillation (NAO) forcing of sea-surface temperatures in the western North Atlantic.

The overarching objective of the present research project is to obtain a more complete knowledge on Late Holocene (last ~3000 years) natural variability of physical parameters affecting ecosystem processes and structure in the northern North Atlantic within, or close to areas presently affected by seasonal sea-ice, and based on the investigations of skeleton remains of two marine phytoplankton groups: dinocysts and coccoliths. This goal involves qualitative and quantitative reconstructions of surface water conditions (temperature, salinity, stratification and sea ice distribution) from high resolution (decadal to centennial scales) Holocene sediment cores, and comparisons with other terrestrial and marine datasets. Reconstructing the Late Holocene changes within surface water masses in the eastern Nordic Seas as well as the variability in the Atlantic water inflow to the Arctic Ocean through the Fram Strait and Barents Sea gateways is of particular interest to this research project.

To achieve these objectives, a selection of five records (3 short cores and 2 long cores) were selected along the continental margin of the Northeast Atlantic within the main pathway of Atlantic Water to the Arctic Ocean (i.e. NwAC and the West Spitsbergen Current, WSC) (Fig. 1.1). The main micropaleontological tracers (coccoliths and dinoflagellate cysts) as well as a few additional proxies (XRF-derived elemental contents, planktonic foraminiferal assemblages and lithic grains) were analyzed to identify Holocene changes in the surface (and subsurface) circulation of the NwAC and its extensions into the Arctic Ocean with a focus on the WSC.

The distributions of dinoflagellate and coccolithophore species in surface waters are strongly driven by the physical-chemical state of the upper photic layer, in particular sea-surface temperatures, sea-surface salinities as well as stratification within the water column. A prerequisite for the application of fossilizable phytoplankton to paleoceanographical reconstructions therefore implies a fair understanding of the regional and local oceanography, the governing atmospheric wind systems (**CHAPTER 1**) and the ecological preferences of the investigated species groups, as well as evidence that the distributions of dinocyst and coccolith assemblages in surface sediments are related to the spatial distribution of the surface water masses (**CHAPTER 2**) (Baumann et al., 2000; de Vernal and Marret, 2007). Coccoliths and dinocysts may suffer from specific drawbacks, such as calcite dissolution in coccoliths (Samtleben and Schröder, 1992) or species-specific sensitivity to oxidation of dinocysts (Zonneveld et al., 2001). Applying both proxies and additional minor proxies therefore allows us to discriminate somewhat between true ecological signals and biased information linked to variable preservation and transport processes, and thus to obtain a more accurate picture of the recent paleoceanographic and paleoclimatic variability in the northeastern Atlantic. The rational for the selection of the sediment cores, their chronology and the applied methods are dealt with in **CHAPTER 3.** The location of the five core sites, within the main pathway of the meridional northward flow of AW (Fig. 1.1) provides the perfect conditions for a compilation of datasets covering the Late Holocene with the aim of investigating paleoceanographic changes in the physical parameters and their effect on the ecosystem as well as the inflow variability of the WSC. This will be the focus of **CHAPTER 4**. Finally **CHAPTER 5** provides the conclusions and perspectives of this study.

1.2 State of the Art: The Holocene

The present interglacial climate is considered to be fairly stable on centennial and longer time scales compared to glacial climates which underwent extreme temperature changes within decades along with the 1500-year Dansgaard Oeschger cycles (Dansgaard et al., 1993; Grootes and Stuiver, 1997). During recent decades, a debate has been going on concerning the continuation of earlier glacial cyclicities into the Holocene. Increasing evidence indicates a persistency of these millennial scale cycles during our interglacial, although with generally weaker amplitudes than during glacial times. These dominant periods are under continuous discussion (Bond et al., 1997, 2001). Earlier studies by Bond et al. (1997, 2001) suggested that cycles of ice-rafting and SST changes averaged 1000–2000 years over the entire Holocene, but only 600–1000 years in the early Holocene, and proposed this cycle to

represent the Holocene expression of Dansgaard-Oeschger cycles. Other recorded pacings of Holocene hydrological/climatological changes include 1500 year Dansgaard-Oeschger cycles in Atlantic deep water circulation changes (Bianchi and McCave, 1999) as well as a 890-year periodicity from the Holocene GISP2 ^{18}O (temperature) signal, a period which Schulz and Paul (2002) ascribe to an internal oscillation of the North Atlantic thermohaline circulation (THC). Similar frequencies have been deduced for 10Be variations as measured in GISP2 (Bond et al., 2001). According to O'Brien et al. (1995), the Summit ice core displays several periods of colder conditions between 0-600, 2400-3100, 5000-6100, 7800-8800 years BP and more than 11300 years BP ago, which were not strictly referred to cyclical patterns. Shuman et al. (2005) argued against Holocene cyclicity in climate variability based on results showing that there is not much evidence in Holocene vegetation and lake-level changes of this cyclic behavior.

Whether or not glacial cyclicity has persisted during the Holocene, this period experienced significant climatic variations (Sarnthein et al., 2003). In the northern North Atlantic realm, these climate shifts have been recorded by glacier advances and tree-line changes in Scandinavia (e.g. Dahl and Nesje, 1996; Svendsen and Mangerud, 1997; Nesje et al., 2001; Davis et al., 2003), isotopic, physical and chemical anomalies in the Greenland ice core (O'brien et al., 1995; Dahl-Jensen et al., 1998), fluctuations in sea ice and iceberg-derived lithic grains in the northern North Atlantic (Bond et al., 1997, 2001; Jennings et al., 2002; Moros et al., 2004), subsurface and surface temperatures (Koç et al., 1993; Voronina et al., 2001; Calvo et al., 2002; Sarnthein et al., 2003; Risebrobakken et al., 2003; Hald et al., 2007; Solignac et al., 2008; Risebrobakken et al., 2010; Spielhagen et al., 2011), North Atlantic atmospheric circulation changes (Trouet et al., 2009; Olsen et al., 2012), variability in Atlantic Water heat advection to the Arctic Oceans (Duplessy et al., 2001; Giraudeau et al., 2010) and compilations of Arctic terrestrial datasets (Kaufmann et al., 2009). Hence, although an in-depth assessment of Holocene millennial scale cyclical patterns in climate changes is not part of the main goal of the research presented here, the topic is an inherent feature of paleoclimate proxy record studies.

In general, the climate of the NH was governed by a long-term cooling during the Holocene due to orbital variations that produced declining summer insolation in the higher northern latitudes (Wright et al., 1993). The Holocene followed the Younger Dryas, a period characterized by a significant and extended cooling across higher latitude regions of the northern hemisphere (Cabedo-Sanz et al., 2012). This interglacial can roughly be divided into

three phases. The first phase, from 11.600 to roughly ~9000 cal. years BP (Wanner et al., 2008), was governed by a maximum in NH summer insolation, peaking at 11000 cal. years BP, and downstream cooling effects of the remnant ice sheets (Laurentide, Fennoscandia) on the climate of the North Atlantic and Eurasia (Kaufmann et al., 2004). The second phase covers the period from ~9000 to ~6000-5000 cal. years BP, also known as the Holocene Thermal Maximum (HTM). This phase corresponds to a period of sustained high summer insolation on the NH, and the disapperance of the North American ice sheet. Wanner et al. (2008) suggested that the third phase extended from ~5000 cal. years BP to the pre-industrial period and referred to it as a period of glacier advances, the "Neoglaciation", governed by declining summer insolation on the NH. The phase which I particularly investigated during this PhD project includes several warm and cold spells known as the Roman Warm Period (RWP, until 300 BC - ~600 AD or ~2250-1350 cal. years BP; Wang et al., 2012), the Dark Ages (DA, ~600-900 AD or ~1350-1050 cal. years BP), the Medieval Climate Anomaly (MCA, ~900-1500 AD or ~1050-450 years BP), the Little Ice Age (LIA, ~1500-1900 AD or ~450-50 cal. years BP) and the Modern (Industrial) period (M, ~1900 AD -present) (Spielhagen et al., 2011, and references therein).

1.3 Physical Oceanography

The following includes a short introduction to the physical oceanography of the northern North Atlantic (Iceland, Greenland, Norwegian, Barents Seas and Fram Strait) in the form of a summary of the bathymetry, oceanography and sea ice distribution within this ocean realm.

1.3.1 Bathymetry

The Nordic Seas are comprised by the Norwegian Sea, the Greenland Sea and the Iceland Sea, separated from the rest of the North Atlantic in the south by the Greenland-Scotland Ridge and connected to the Arctic Ocean by two major gateways: the Fram Strait and the Barents Sea. The bathymetry of the Nordic Seas is characterized by a complex ridge system dividing the ocean into four major basins (Schäfer et al., 2001). The Norwegian and Lofoten Basins are located in the eastern part of the Nordic Seas below the Norwegian Sea which is separated from the Greenland Sea (Greenland Basin) by the Mohn Ridge in the north and from the shallower Iceland Sea (Icelandic Plateau) by the Jan Mayen Ridge in the south (Loeng and Drinkwater, 2007; Koszalka et al., 2011) (Fig. 1.1).

The shallow shelf area of the Barents Sea is limited by the shelf break on its western boundary towards the Norwegian Sea, by Novaya Zemlya on its eastern boundary, in the

south by Norway and Russia and finally by the continental shelf break in the north towards the deep Arctic Ocean (Loeng and Drinkwater, 2007). The Barents Sea has a complex bathymetry and is the deepest of the Arctic Oceans shelf areas with a mean depth of 230 meters (Carmack et al., 2006) and a maximum depth situated in the western part of the Bear Island Trench (BIT, ~500 m) (Loeng and Drinkwater, 2007). Extensive shallow areas as well as large isolated banks, e.g. the Central Bank (Cba), the Great Bank (Gba) and the Svalbard Bank (Sba), separated by deeper troughs and depressions can be found west and southwest of Novaya Zemly and around Svalbard. (Wassmann et al., 2006) (Fig. 1.1).

1.3.2 Oceanographic Setting

The overall surface circulation in the northern North Atlantic is in general steered (Johannessen, 1986) and governed by two meridional boundary currents. The eastern boundary current is represented by the northward flowing warm and saline Norwegian Atlantic Current (NwAC) (<500-600 m) (Furevik et al., 2007), a topographically steered two branch extension of the North Atlantic Current (NAC) (7-13 °C, ~≥35) entering the Nordic Seas through the Iceland-Scotland ridge (ca. 7 Sv, Hansen and Østerhus, 2000; Orvik and Niller, 2002; Andersson et al., 2011) (Fig. 1.1).

The Eastern Branch (EB, 4 Sv) of the NwAC dominates the upper water masses on its northward path along the Norwegian margin, except on the shelf where its traveling companion the Norwegian Coastal Current (NCC) rules the conditions with low salinity coastal waters (~34.4), driven by freshwater discharge from the Baltic and the Norwegian fjords (Hansen and Østerhus, 2000; Orvik et al., 2001). The NwAC and the NCC are separated by a salinity front (Loeng and Drinkwater, 2007). North of the Lofoten Islands, the EB splits into two additional branches: a meridional branch, the West Spitsbergen Current (WSC) (T>3 °C, >35), and a zonal component, the North Cape Current (NCaC) (Loeng, 1991; Wassmann et al., 2006; Koszalka et al., 2011) (Fig. 1.1).

Figure 1.1 : Bathymetric map of the Nordic Seas showing the most important topographic features (top), as well as the core locations (red stars). Bottom map shows major surface currents, according to Jakobsen et al. (2003), Olsson et al. (2005) and Andersson et al. (2011). Red arrows show the flow direction of warm saline Atlantic Water; NwAC: Norwegian Atlantic Current, WB: Western Branch, EB: Eastern Branch, NCaC: North Cape Current, WSC: West Spitsbergen Current. Blue arrows show the flow direction of cold low saline Arctic/Polar surface waters; EGC: East Greenland Current, JMC: Jan Mayen Current, EIC: East Icelandic Current, BIC: Bear Island Current, ESC: East Spitsbergen Current, PC : Percey Current. Green arrow shows the flow direction of coastal waters; NCC: Norwegian Coastal Current. Orange dashed line shows the relative location of the Arctic Front. Other abbreviations: NB: Norwegian Basin, LB: Lofoten Basin, GB: Greenland Basin, IP: Icelandic Plateau, Sba: Svalbard Bank, Gba: Great Bank, Cba: Central Bank, BIT: Bear Island Trench.

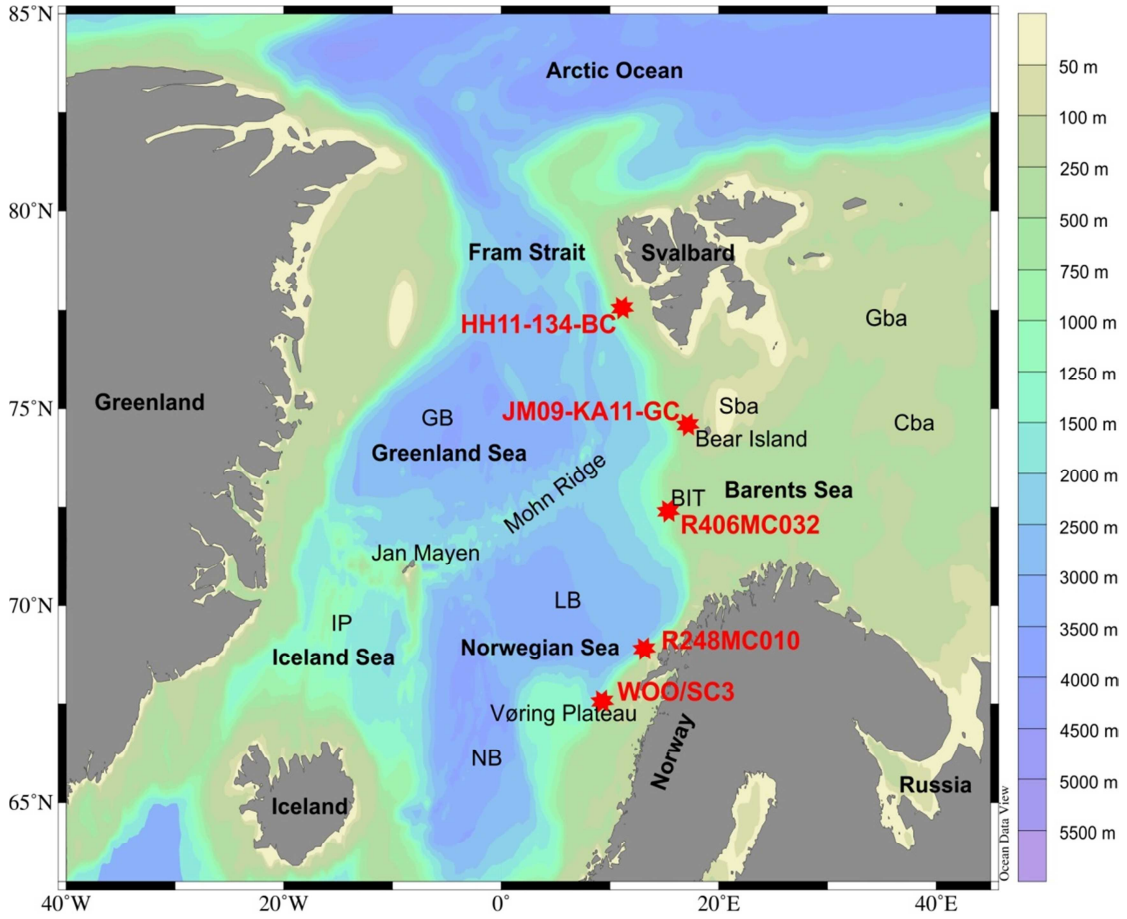
Arctic Ocean
Fram Strait
Svalbard
HH11-134-BC
Gba
Greenland
GB
JM09-KA11-GC
Sba
Bear Island
Cba
Greenland Sea
Mohn Ridge
BIT
Barents Sea
R406MC032
Jan Mayen
LB
IP
Iceland Sea
Norwegian Sea
R248MC010
WOO/SC3
Vøring Plateau
NB
Norway
Russia
Iceland
85°N
80°N
75°N
70°N
65°N
40°W
20°W
0°
20°E
40°E
50 m
100 m
250 m
500 m
750 m
1000 m
1250 m
1500 m
2000 m
2500 m
3000 m
3500 m
4000 m
4500 m
5000 m
5500 m
Ocean Data View

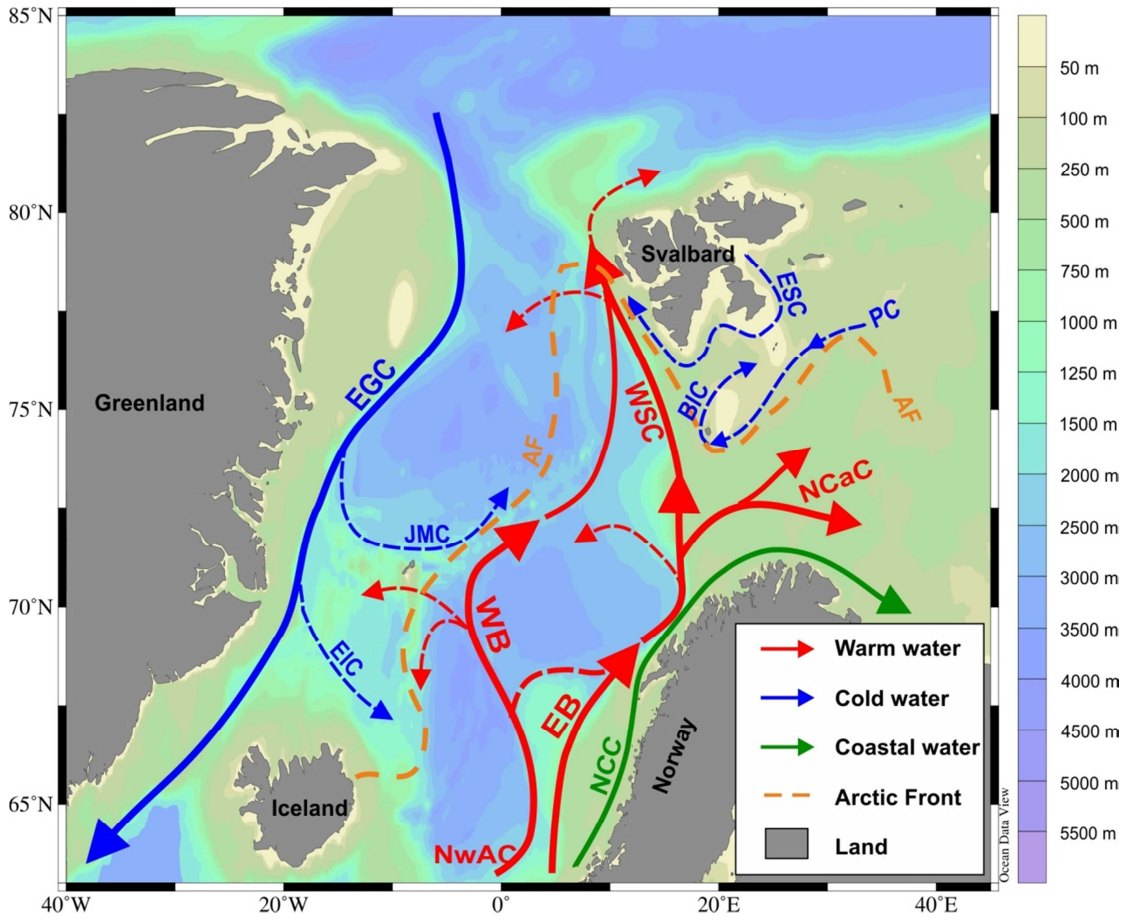
Svalbard
Greenland
EGC
ESC
PC
AF
WSC
BIC
AF
NCaC
JMC
WB
EIC
EB
NCC
Norway
Iceland
NwAC
Warm water
Cold water
Coastal water
Arctic Front
Land
85°N
80°N
75°N
70°N
65°N
40°W
20°W
0°
20°E
40°E
50 m
100 m
250 m
500 m
750 m
1000 m
1250 m
1500 m
2000 m
2500 m
3000 m
3500 m
4000 m
4500 m
5000 m
5500 m
Ocean Data View

The WSC flows along the continental margin of the western Barents Sea and western Spitsbergen and enters the Arctic Ocean as a subsurface current insulated from the atmosphere by fresh PW in the upper mixed layer (3-5 Sv; Blindheim and Østerhus, 2005). The current carries along two Polar Water (PW) companions on the shelf i.e. the Bear Island Current (BIC) (1-3 °C, <34.4) and the Sørkapp Current (extension of the East Spitsbergen Current, <0 °C, 34.3-34.8) towards the north (Loeng, 1991; Saloranta and Svendsen, 2001; Wassmann et al., 2006). The BIC origins from the Percey Current, a current which crosses the Barents Sea along the southern "border" of the Spitsbergen as well as the Cba and Sba, turns around Bear Island and travels north as the BIC (Loeng, 1991; Wassmann et al., 2006) (Fig. 1.1). The Western Branch of the NwAC (WB, 3 Sv, >34.9) rounds the southern rim of the Lofoten Basin and flows north as a baroclinic jet along the Mohn Ridge, contributing with Atlantic Water (AW) to the development of the Nordic Sea Frontal Zone (Hansen and Østerhus, 2000; Orvik et al., 2001; Orvik and Niller, 2002; Jakobsen et al., 2003; Koszalka et al., 2011). The western boundary current is represented by the southward flowing East Greenland Current (EGC; <0°C, <34.5), which is considered as the largest and most concentrated meridional ice flow in the World Oceans (Blindheim and Østerhus, 2005). Its two zonal components, the Jan Mayen Current (JMC) at the Jan Mayen Fracture Zone and the East Icelandic Current (EIC) flowing over the Icelandic Plateau, supply fresh PW to the gyre systems and hence contribute to the Frontal Zone (Johannessen, 1986; Olsson et al., 2005) (Fig. 1.1). The mixing of PW and AW creates Arctic Water (ArW) (0-4°C, 34.6-34.9) (Johannessen, 1986). The northeast-southwest trending boundary between PW and ArW is termed the Polar Front (PF) and characterizes the maximum summer sea-ice extent, whereas the boundary between ArW and AW is referred to as the Arctic Front (AF) and characterizes the maximum winter sea ice extent (Swift, 1986; van Aken et al., 1995; Saloranta and Svendsen, 2001). Generally, the positions of the fronts in the Nordic Seas are well correlated with the bathymetry due to topographic steering of the currents (Johannessen, 1986). This is seen north of Jan Mayen along the mid-ocean ridge, where the AF only exhibits small fluctuations in contrast to the zone between Iceland and Jan Mayen, where large shifts within the position of the AF occur due to variations in the inflow of PW/ArW from the EIC (Blindheim et al., 2000). Hence the supply of PW/ArW carried by the EGC (especially the EIC) and its mixing with North Atlantic water may be an important, but not the only, mechanism to create fluctuations in the atlantic inflow to the Nordic Seas (Blindheim et al., 2000). The Frontal Zone term is used for the area where horizontal gradients in temperature,

salinity and density are high in comparison with the mean parent water types (i.e. AW and PW) (van Aken et al., 1995). A series of cyclonic gyres are present over the Greenland, Lofoten and Norwegian Basins as well as the Icelandic Plateau. These four gyres are strongly linked to the local bottom topography and are areas of strong mixing and transformation of water masses (Poulain et al., 1996; Jakobson et al., 2003; Koszalka et al., 2011) (Fig. 1.1).

The Barents Sea is not just a shelf area but also a major passageway of AW entering the Arctic Ocean, i.e. a flow through shelf (Carmack et al., 2006). The wide but relatively shallow Barents Sea allows for a much stronger transformation of the entering waters than its deeper sister gateway to the west through the Fram Strait. In contrast to Fram Strait, which is characterized by extensive recirculation of the Return Atlantic Current (RAC), the Barents Sea is, generally speaking, a one-way passage only permitting waters to enter the Arctic Ocean (Wassmann et al., 2006). The inflow does not, however, flood the entire shelf as the current is not strong enough, hence the AW of the NCaC is mainly confined to the southern part (Wassmann et al., 2006). The relatively warm Atlantic Waters (T>3 °C, >35) enter between Bear Island and northern Norway together with the coastal waters of the NCC (T>2 °C, <34.7) (Loeng, 1991) (Fig. 1.1). The inflow of AW increases during winter conditions, where the current system is deep and narrow, while it decreases and becomes wide and shallow during summer conditions (Loeng and Drinkwater, 2007); a feature which has been observed along the entire coast of Norway as a result of monsoon-like seasonal shifts of surface winds in the region (Olsen et al., 2003). Southwesterly winds prevail in winter, pushing the NCC onshore, whereas northerly winds dominate the summer conditions and a low salinity wedge is deflected away from the coast (over 100-150 km) (Sætre et al., 1988; Helland, 1963).

The northern North Atlantic is also of special importance as it contains, together with the Wedell and Ross Seas, some of the few key areas of deep water formation; hence it contributes to the functioning of the global THC. This gigantic system slowly turns over the water masses of the entire ocean as a result of density contrasts (Schmittner et al., 2007) (Fig. 1.2). The flow of the Gulf current is primarily wind-driven, where the Atlantic THC contributes with as much as 20% (Rahmstorf, 2006).

Figure 1.2 : Schematic of the Thermohaline Circulation (THC) within the northern North Atlantic (i.e. Nordic Seas and the Labrador Sea). Red arrows: direction of surface flow, blue arrows: direction of deep flow.

1.3.3 Sea Ice Distribution in the Northern North Atlantic

Sea ice and fresh water from the Arctic Ocean are essentially transmitted to the Nordic Seas via Fram Strait and the southward flowing cold and fresh EGC (Buch, 1990) with a yearly export of roughly 10% of the total Arctic sea ice mass (Kwok et al., 2004) (Fig. 1.1, 1.3). Hence the general distribution of sea ice in Fram Strait and the Greenland Sea is strongly influenced by the prevailing conditions within the Arctic Ocean (Ramseier et al., 2001; Kwok et al., 2004) and the AW in Fram Strait. Sea ice along the eastern coast of Greenland drifts southward between the coast and the continental shelf slope and includes both new ice and Multi Year Ice, with highest flow speeds occurring in Fram Strait and decreasing toward the south (Ramseier et al., 2001).

The drift is weakest in summer time and increases again when surface wind fields increase, resulting in a winter ice-drift speed nearly twice as high as summer values (Ramseier et al., 2001, and references therein) (Fig. 1.3). The onset of enhanced seasonal melt in the Greenland Sea varies with latitude, initiating as early as March/April south of 70 °N and as late as July at 86 °N (Ramseier et al., 2001), with an annual minimum sea-ice extent in the northern North Atlantic occurring in September (Dickson et al., 2007). As the ice flows through the Greenland Sea, it encounters warm water mainly from the Return Atlantic Current (RAC), which leads to a strong temperature gradient and, hence, a continuous melting along the ice edge (Ramseier et al., 2001). In contrast, low air temperatures and high wind velocities cause a strong upward heat flux, which again leads to new ice production. Therefore the spatial and

temporal distribution of sea ice within the Greenland Sea is a result of the advection of ice through Fram Strait but also of local new production (Ramseier et al., 2001).

As in the Greenland Sea, most of the sea ice that reaches the Iceland Sea originates from the Arctic Ocean and is transported there by the EGC (Wadhams, 1986). In most years, however, sea ice is only a temporary wind-dependent feature on the Icelandic plateau (Astthorsson et al., 2007, and references therein). It is initially observed in the northwest and then transported along the north coast as part of the general clockwise circulation around Iceland. During so-called "normal" inflow of AW over the northern shelf, the ice usually melts quickly, but if the flow of AW is blocked and PW persists over the shelf, sea ice can drift to the eastern coast of Iceland and in extreme cases even as far as the south coast (Astthorsson et al., 2007).

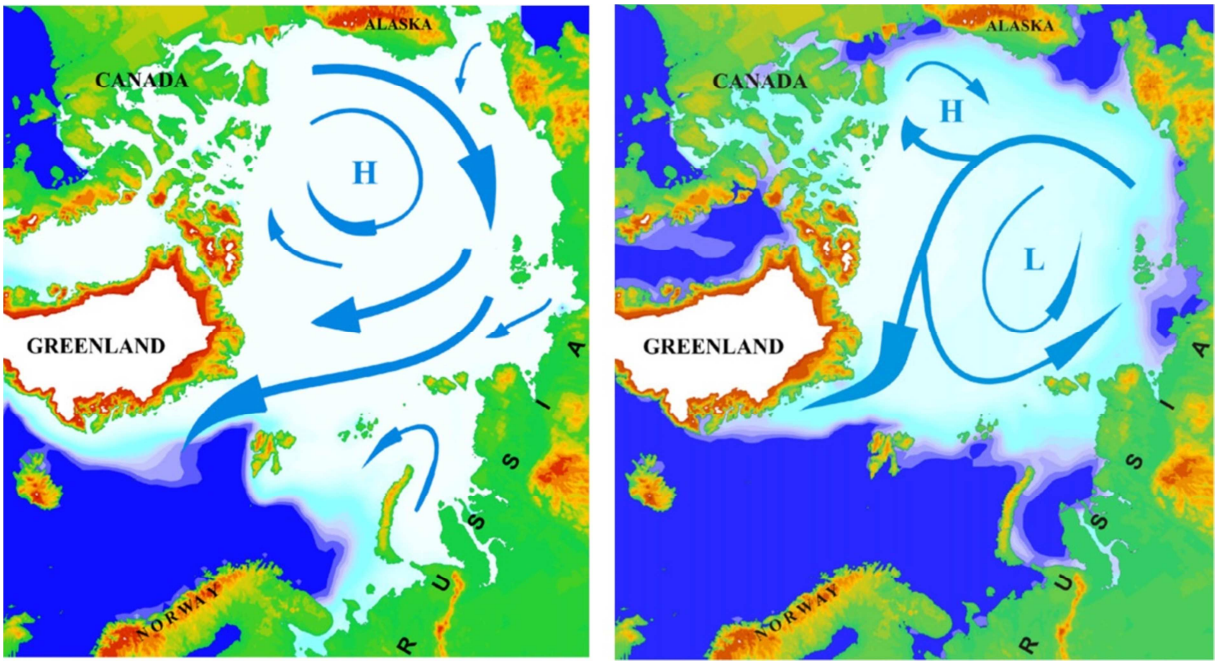

Figure 1.3 : Average Arctic ice cover and ice drift patterns in winter (left) and summer (right), as influenced by the distribution of high and low pressure systems over the Arctic region. Note the considerable difference in the southward extent of sea ice East of Greenland, as well as the winter-summer distribution of sea ice in the Barents Sea. Adapted from Wassmann et al. (2006).

The sea ice extent within this area has a large variability, but appears to have an average seasonal cycle represented by a maximum ice extent towards the end of February and a minimum in mid-September (1978-1996) (Ramseier et al., 2001) (Fig. 1.3). Unusual outflows of sea ice contribute significantly to the freshening of the surface waters of the Greenland and Labrador Seas (Kwok et al., 2004), which, in turn, influences the primary productivity as well as the strength of the global ocean thermohaline circulation through the impact on convective overturning of water masses (Dickson et al., 1988).

Strong seasonal variations in sea ice extent can be observed in the Barents Sea (incl. the ice stream on the western coast of Spitsbergen) especially toward the East (Vinje, 2001; Wassmann et al., 2006) (Fig. 1.3). As the formation of sea-ice in the north closes of the possibility of drift ice entering the Barents Sea, sea-ice within the Barents Sea area is generally locally formed, and therefore the ice export from the Arctic Ocean over the Barents Sea is only a small fraction of that passing through Fram Strait (Wassmann et al., 2006). An annual average of 40% of the region is being ice covered, although with strong seasonal variability (0-60%) (Loeng, 1979; Loeng and Drinkwater, 2007). Minimum ice extent occurs in August/September with a peak usually occurring in March or April, although it might be occasionally postponed until early June (Loeng and Drinkwater, 2007).

The area along the eastern coast of Greenland and the Fram Strait has experienced a 46% reduction in sea ice distribution in the period 1864-1998, compared with a 24% reduction around Svalbard and in the Barents Sea (Vinje, 2001).

1.4 The North Atlantic Oscillation (NAO)

The atmospheric variability over the middle and high latitudes of the Northern Hemisphere is strongly governed by the North Atlantic Oscillation (NAO), a part of the Northern Hemisphere annular mode (Marshall et al., 2001), especially during the cold season months (November-April) (Hurrell et al., 2003). The NAO is often defined as the difference in atmospheric pressure at sea level between the Icelandic low and the Azores high (Jones et al., 2003; Olsen et al., 2012). The NAO pattern essentially refers to a redistribution of atmospheric mass between the Arctic and the subtropical Atlantic, as the NAO swings between its positive and negative phases (Fig. 1.4). Changes in NAO modes influence the mean wind speed and direction over the Atlantic, the heat and moisture transport between the Atlantic and nearby continents, the intensity and number of storms, the oceanic meridional overturning circulation (Hurrell et al., 2003) and the strength and width of the NwAC, NCC and equatorward ice export through the EGC (Blindheim et al., 2000; Kwok et al., 2004; Skagseth et al., 2004). A low NAO index results in a more zonal path of low pressure systems across the Atlantic (a southward storm track), a generally reduced and wider flow of the NwAC and less precipitation in Northern Europe (Hurrell et al., 2003). In contrast, a high index results in a passage of low pressure systems toward Northern Europe from the North Atlantic, favoring stronger precipitation, a strengthened NwAC flow and an eastward shift of the Arctic Front toward the slope of Norway (Blindheim et al., 2000; Pinto and Raible, 2012).

In addition, modern observations have indicated a significant correlation between the NAO indexes and the Greenland and Barents Sea ice extent, with less sea ice and warmer SST during the positive NAO phases and conversely more ice during negative NAO (cold) phases (Vinje, 2001; Visbeck et al., 2003; Ingvaldsen, 2005; Sorteberg and Kvingedal, 2006). A result which is most likely related to variations in southwestern wind patterns and intensity of the AW flow (Blindheim et al., 2000).

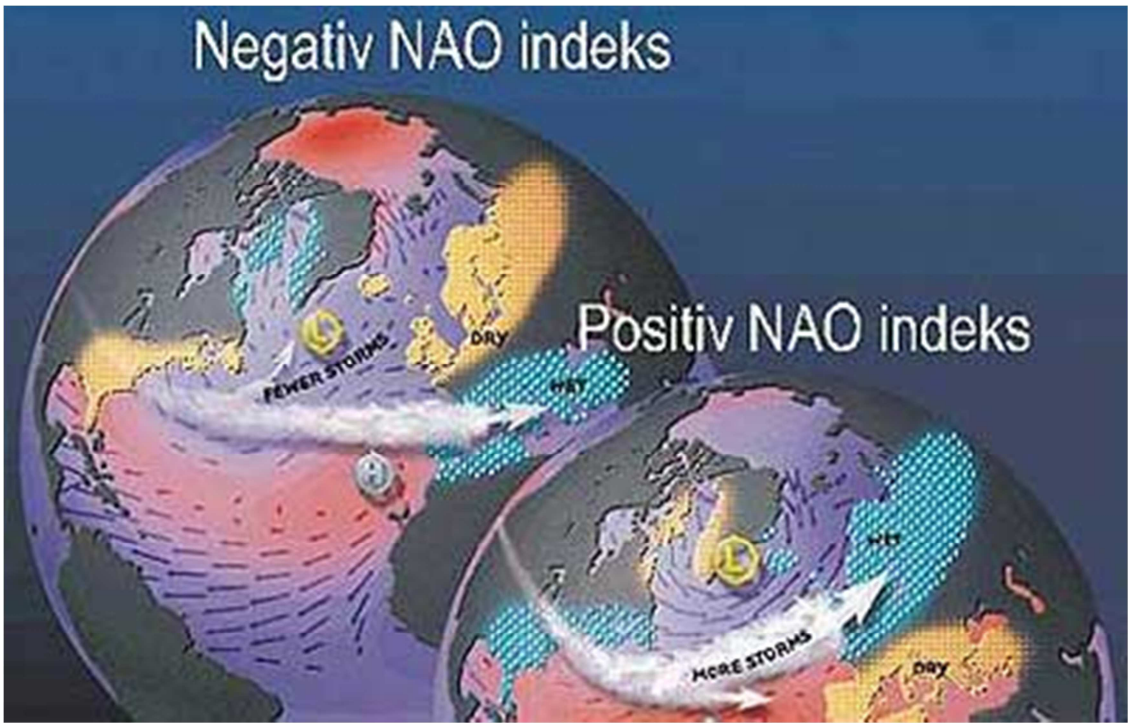

Figure 1.4: A schematic view of NAO modes and the overall effects on precipitation and AW flow.

Considering the impact of NAO on the heat advection to the Arctic Ocean, on the amount of sea ice export, on precipitations on land, and on ocean circulation, with implications on human, plant (incl. phytoplankton) and animal life (Drinkwater et al., 2003; Mysterud et al., 2003), a great deal of effort has been spent on observing and modeling its present and past dynamics, in order to develop a predictive model of its behavior.

NAO records spanning the past 130 years show a decadal scale variability (Ribergaard, 2005; Pinto and Raible, 2012), indicated by a predominantly negative mode before 1900 AD followed by an overall positive phase during the last century only pertubated by a clear negative shift during the 1950's and 1960's (Fig. 1.5).

The origin of the NAO variability over time is currently under debate and various anthropogenic and natural forcing agents have been proposed (i.e. volcanic eruptions, solar activity, tropospheric aerosols, greenhouse gases and links to tropical oceans), although none

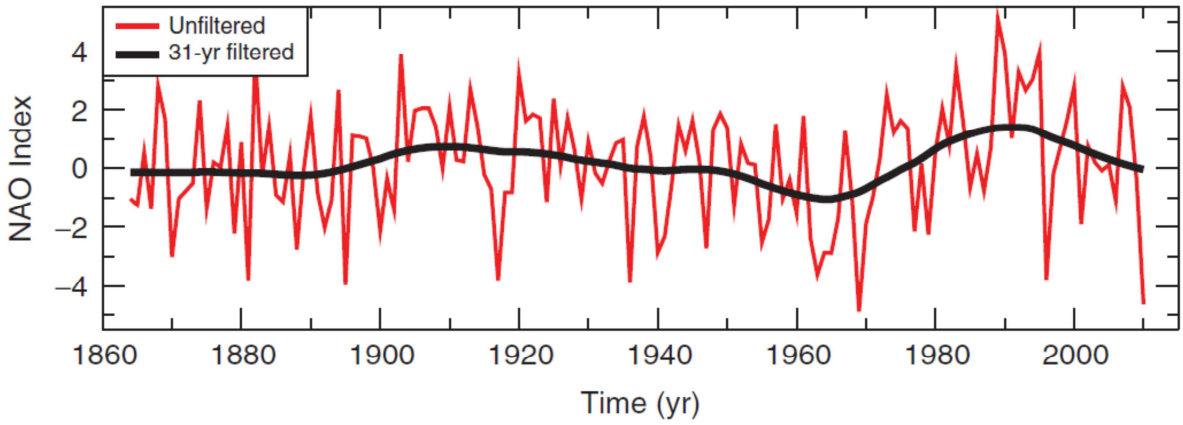

Figure 1.5 : Time series of the station-based NAO index from 1864 to 2009 (instrumental period) for the season DJFM (December, January, February, March). In red unfiltered data from year to year. In black a 31-year filter illustrating the low-frequency behavior. Adapted from Pinto and Raible (2012).

seem to be able to explain the annual to decadal variability on its own. Hence distinguishing between natural and human induced changes still seems difficult (Gillet et al., 2003; Pinto and Raible, 2012). There is, therefore, a “pressing” need to develop longer records of the NAO to place recent variability in a long-term, naturally-driven context in order to fully understand the impact of the anthropogenic rise in greenhouse gases upon NAO (Jones et al., 2003). Assessing the importance of the NAO on the modern hydrography and climate of the Nordic Seas and its significance for paleoceanographic changes in the northern North Atlantic has long been hampered by the lack of instrumental records prior to the 19th century. In addition, prior to 2012, proxy- and model-based NAO reconstructions based on single proxy archives (e.g. ice cores), historical data or multiproxies from different archives (e.g. tree rings, speleotherms) only reached back up to one millennia (i.e. Luterbacher et al., 2002; Jones et al., 2003; Cook et al., 2003; Trouet et al., 2009). These reconstructions usually relied on different statistical methods, assuming a stationary relationship between the proxy and the climate data through time and estimating a statistical relationship between the proxy and climate data in the overlapping calibration period (instrumental period) (Cook et al., 2003; Pinto and Raible, 2012). A recent high resolution reconstruction of NAO variability from a lake record in southwestern Greenland (Olsen et al., 2012) extended these previous NAO records back to 5200 cal. years (BP), and thereby offered a new way to investigate links between atmospheric processes and ocean circulation changes in the northern North Atlantic over the mid to late Holocene.

Although these paleo-studies might under- or over-estimate the strength of the NAO variability during the past (Pinto and Raible, 2012), they still provide us with a strong

guideline-tool to understand the general paleo-climatic changes in the region at the time of interest.

Chapter 2 : The Micropaleontological Proxies: Distribution, Export and Alteration of Fossilizable Phytoplankton within the Northern North Atlantic and Adjacent Seas

2.1 Chapter Overview

This chapter provides a general introduction to the two major micropaleontologic proxies applied within this study. It begins with a brief overview of the net primary phytoplankton production within the northern North Atlantic and the physiochemical processes affecting it, with a particular attention given to the timing and order of spring blooms within the fossilizable phytoplankton community. A review of the export and alteration processes, which affect the sediment assemblages in the Nordic Seas related to dissolution and transport processes, is given. This is followed by a full description of the two major micropaleontological proxies (coccolithophores and dinocysts) in terms of morphology, biology, ecology and sediment distribution. In addition, a submitted paper on the hydrological and ecological factors controlling the species distribution of the extant coccolithophores across Fram Strait and the Norwegian-Iceland Sea is included at the end of the coccolithophore description.

2.2 A General Introduction to Phytoplankton within the Northern North Atlantic

The influence of light and nutrient availability on primary productivity within the world oceans is enormous. As light only penetrates the upper water masses of the oceans, it strongly limits the depth of the photosynthetic zone, and is even further limited by the availability of nutrients. In the world oceans the primary productivity is generally increased within higher latitudes, nutrient rich coastal areas, and the warm nutrient-rich NAC waters (Fig. 2.1).

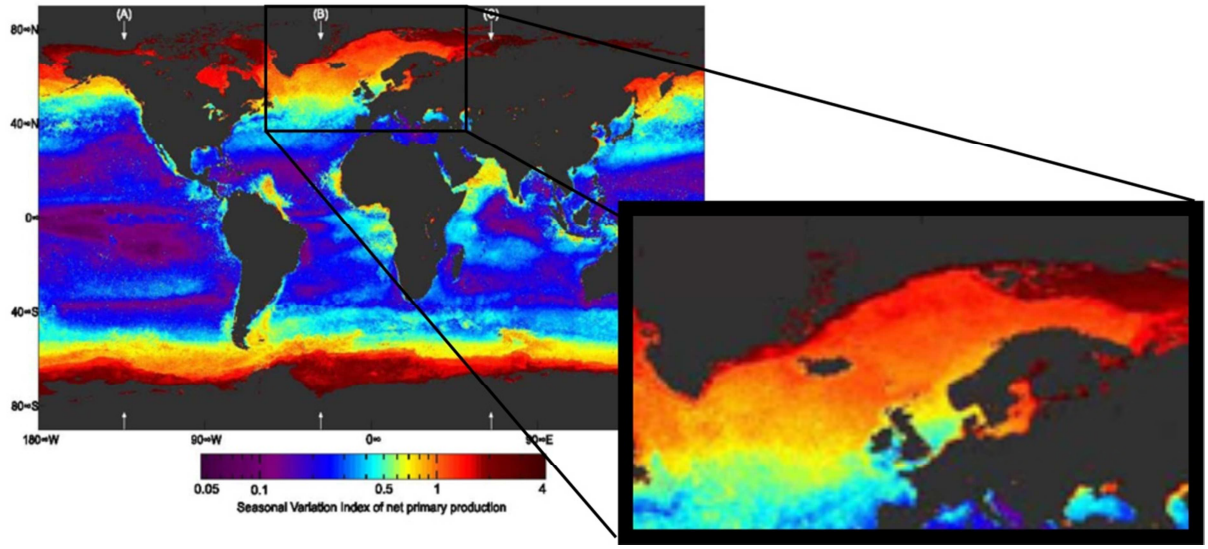

Figure 2.1: Seasonal variation index of net primary production the world's net primary productivity (grams per m^2 per year), zooming in on the northern North Atlantic (highest variation is shown in the high latitudes). Modified after Lutz et al. (2007).

Together with these two forcing factors, physical and biological conditions, which are directly affected by climatic changes , also condition the composition and distribution of modern phytoplankton communities in the world oceans (Fig. 2.2). This is especially of major importance in the North Atlantic region due to the complex relation between cryospheric (ice sheets and sea-ice), atmospheric (winds related to strong gradients in sea-level pressures) and oceanic (opposition of northward flowing AW and southward flowing PW) processes, which together determine the nature and rate of new production transferred to the higher trophic level through the marine food web (Hunt et al., 2002).

The phytoplankton community within the northern North Atlantic is especially influenced by major differences in hydrography and seasonal irradiance, resulting in large variability in the onset of the biological spring as well as the seasonal development and composition of the fossilizable microplankton community within the upper water masses (e.g. diatoms, coccolithophores, dinoflagellates, radiolarians and foraminifera) (Samtleben et al., 1995a;

Schröder-Ritzrau et al., 2001; Wassmann et al., 1990, 1991, 2006), which lie as the base of the Arctic food web (Fig. 2.2). The annual onset of the enhanced biological activity may be as early as March in the southeastern Norwegian Sea and as late as August/September in the Greenland Sea, with a progressive NNW transition in between (Samtleben et al., 1995a; Schröder-Ritzrau et al., 2001; Loeng and Drinkwater, 2007, and references therein) and an overall low production during winter (Baumann et al., 2000; Schröder-Ritzrau et al., 2001; Loeng and Drinkwater, 2007, and references therein). In general, the spring (phytoplankton) bloom develops as soon as the shallow surface layer is stratified. However, previous observations have shown that high primary production might also occur in poorly stratified well mixed waters within high latitudes (Fig. 2.2, 2.3) (Eilertsen, 1993; Dylmer et al., 2013, this study).

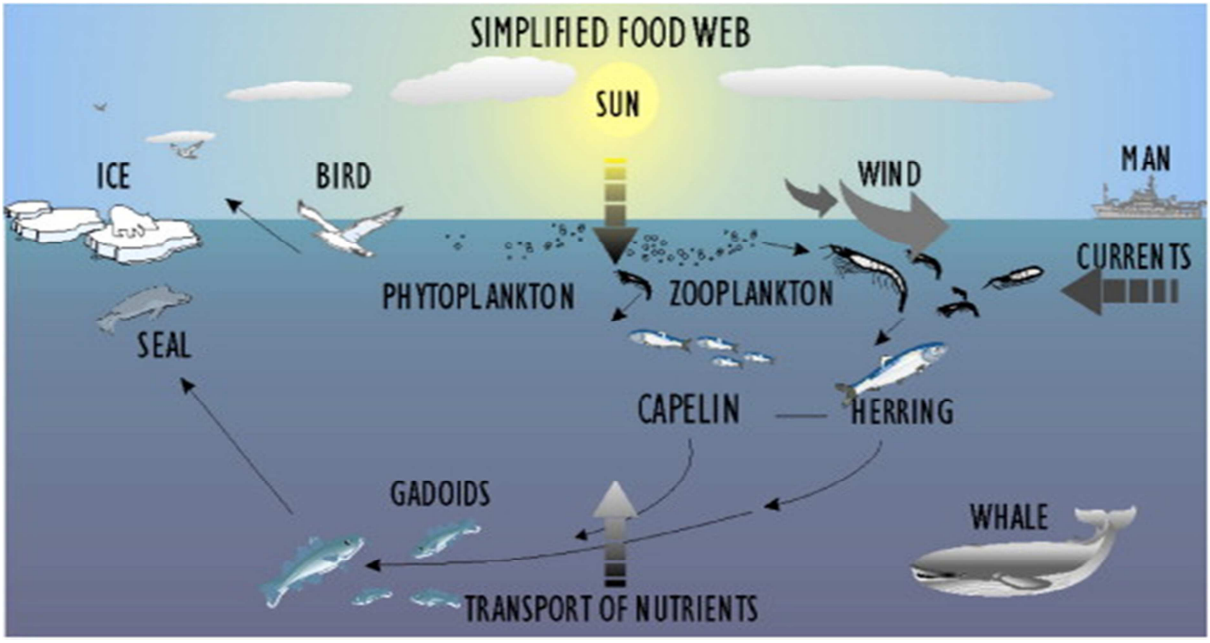

Figure 2.2: Schematic of a typical Arctic food web. Adapted from Svendsen et al. (2007).

2.2.1 The Norwegian Sea

In the Norwegian Sea, winter convection extends to a water depth of ~300 m with spring-summer stratification being almost entirely dependent on solar radiation (thermal stratification) (Wassmann et al., 1991). The spring bloom initiates as early as March in this region with the production of diatoms followed by coccolithophores and dinoflagellates (Wassmann et al., 1990; Loeng and Drinkwater, 2007). Previous investigations on the annual phytoplankton abundances at weather station Mike within the NwAC has generally shown that the spring period from April to June is followed by high phytoplankton concentrations

from July to September which is followed by decreasing populations from September to December. Finally, diatom, coccolithophore and dinoflagellate populations were found to be scarce during winter months from December to March. In addition, the investigations showed that peak cell concentrations of diatoms and coccolithophores reached the same order of magnitude (10^5 to 10^6 ind./l) while dinoflagellates never exceeded 10^4 ind./l (Schröder-Ritzrau et al., 2001, and references therein).

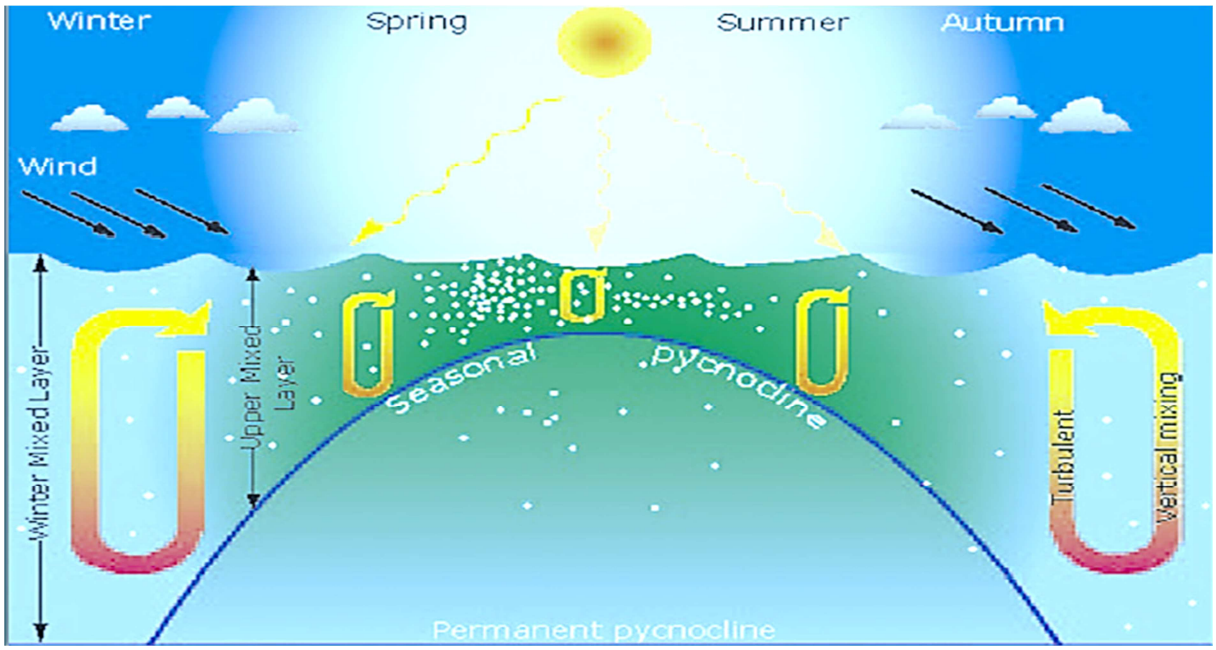

Figure 2.3 : Schematic representation of the seasonal development of phytoplankton and the main physical factors affecting it. White dots represent phytoplankton biomass. Adapted from Loeng and Drinkwater (2007), and references therein.

2.2.2 The Greenland Sea

In this area, the initial surface spring stratification is mainly induced by melt water from sea-ice (Bauerfeind et al., 1994), although in years when the sea ice is poorly developed, thermal warming may initiate spring stratification within most of the region (Schröder-Ritzrau et al., 2001). The most important contributors to the phytoplankton production within the Greenland Sea are diatoms and flagellates, which show maximum abundances in the vicinity of the sea-ice edge (Smith et al., 1991).

2.2.3 The Iceland Sea

The stratification in the Icelandic Sea varies between the socalled “cold” (stronger) and “warm” (weaker) years with the influence of AW (Gudmundsson, 1998). Given favorable conditions, the spring bloom may start to develop in early April and usually peaks in the

beginning of May (Gudmundsson, 1998). Diatoms typically dominate the phytoplankton spring bloom over the Icelandic shelf, followed by an increase in the abundance of dinoflagellates after the spring bloom, while diatoms continue to be relatively abundant (Thordardottir and Gudmundsson, 1998). Coccolithophores seem to peak in August (Samtleben and Bickert, 1990).

2.2.4 Fram Strait

In Fram Strait the primary productivity is strongly influenced by the large hydrological gradients between the dominating water masses (AW, ArW, PW) and sea-ice cover. The maximum primary production was found along the ice-edge and, therefore, naturally varies with the movement of the Marginal Ice Zone (MIZ) (Smith et al., 1987; Birgel and Ruediger, 2004). Phytoplankton production, although generally numerically dominated by small flagellates, initiates with a spring bloom of diatoms (Hirche et al., 1991), followed by summer-early autumn production of coccolithophores (Dylmer et al., 2013, this study). Below the ice, flagellates may be very abundant and comprise up to 98% of the phytoplankton biomass (Wassmann et al., 2006).

2.2.5 The Barents Sea

The Barents Sea primary production rapidly increases in spring, when the mixed layer depth decreases above a critical depth (from 300 to <50m) (Olsen et al., 2003). However, this might occur earlier in the northern Barents Sea along the MIZ, where ice-melt induces an early stratification which supports an earlier initiation of phytoplankton blooms (especially during years where the sea-ice cover exhibits a large southern extent, and sea-ice can drift across the frontal systems and into AW) (Olsen et al., 2003; Wassmann et al., 2006; Loeng and Drinkwater, 2007). At the southwestern entrance to the Barents Sea, the bloom starts when the low-salinity waters from the NCC spread northward, while it is triggered by thermal stratification in the central region (Loeng and Drinkwater, 2007). The abundance of diatoms is low in March, but increases steadily throughout the season along with the dominating flagellates and later the summer-blooming coccolithophores (Wassmann et al., 2006).

The shallow area of the Barents Sea is known for its high primary productivity and is one of the places in the world where the influence of the present global warming on the distribution and composition of phytoplankton communities is most clearly reflected. Recent compilations of satellite observations (AVHRR, SeaWiFS and MODIS-Aqua) are indicative of an

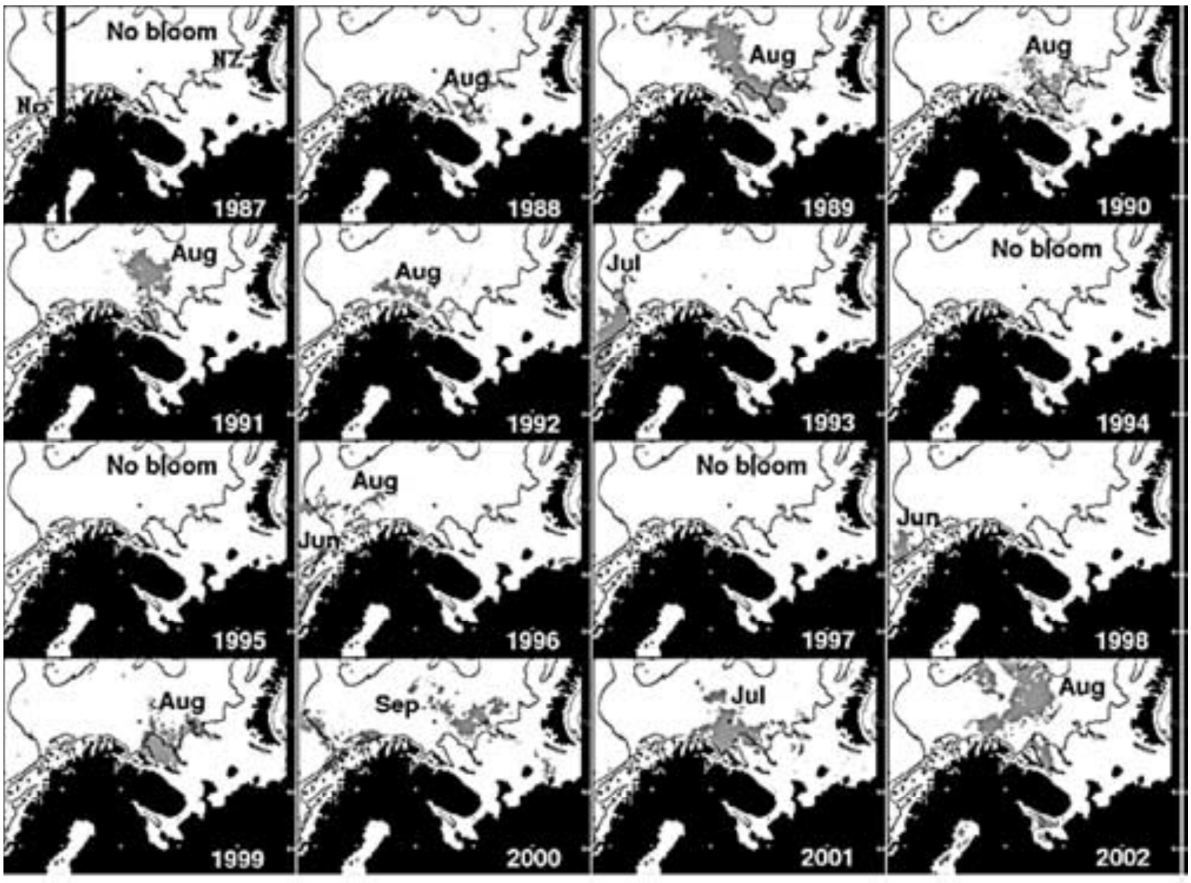

Figure 2.4: Location and timing of coccolithophore blooms in the southern Barents Sea, determined using composite reflectance imagery between 1987 and 2002. Maximum bloom extents are shaded in grey. Adapted from Smyth et al. (2004).

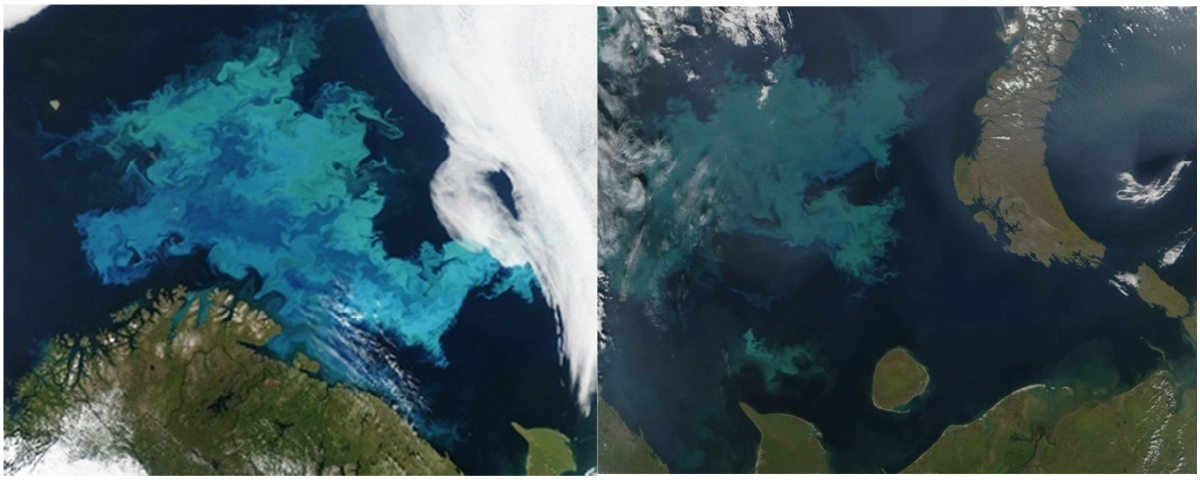

Figure 2.5: MODIS satellite images of coccolithophore blooms in the Barents Sea. Left image: August 2011, north of Norway; right image: September 2005, west of Novaya Zemlya http://modis.gsfc.nasa.gov/gallery/individual.php?db_date=2011-08-17.

increased occurrence of summer blooms of coccolithophores in the Barents and Nordic Seas since the late 80s (Fig. 2.4, 2.5) (Smyth et al., 2004; Burenkov et al., 2011), a phenomenom which has been linked with extensive sea-ice melting (Parkinson et al., 1999; Guan and Gao,

2010) and increased inflow of AW to the northern North Atlantic (Hatun et al., 2005; Hegseth and Sundfjord, 2008; Dimitrenko et al., 2010).

2.3 The Export of Phytoplankton Remains from Surface Waters to Surface Sediments of the Nordic Seas: Dissolution Processes and Lateral Transport

In the Nordic Seas, all microfossil assemblages, irrespective of the faunal or floral plankton group they belong to, display similar regional differences in species richness with a corresponding decrease from the Norwegian Sea to the Greenland Sea (Fig. 2.6), a decrease also observed in the living extant populations (Schröder-Ritzrau et al., 2001).

Therefore, changes in species richness of the different microplankton groups are naturally suitable for defining biogeographic provinces in the Nordic Seas. However, since the tests of the main fossilizable microplankton groups - diatoms, coccolithophores, dinoflagellate cysts, radiolarians and foraminifera – are made of variable skeletal material (calcareous, siliceous and organic tests), they are subject to differences in their resistance to dissolution and, hence, fossilization potential (Schröder-Ritzrau et al., 2001). The geological record of biogenic production might, therefore, be strongly biased by dissolution processes both within the water column during sinking of the skeletal remains (as a function of the residence time in the water column) and within the top centimeters of the sediment layer (Schlüter et al., 2001). These processes not only alter the total fluxes of biogenic particles but also the composition of assemblages, according to the species-specific resistance to degradation of microfossils within each biotic group (Matthiessen et al., 2001).

The mode by which phytoplankton remains leave the permanent thermocline and are transported to the sediment controls their residence time in the water column and thus their rate of degradation, which in turn determines the ultimate fate of the sinking biogenic material (Peinert et al., 2001). Thus the composition of the phytoplankton communities and their bloom phases, grazing and dissolution processes, and their mode of transport throughout the water column (autotrophic or heterotrophic export, i.e. aggregates or fecal pellets, marine snow; Samtleben and Schröder, 1992; Mudie, 1996; Andruleit, 1997; Zonneveld and Brummer, 2000), can be expected to influence the transfer of surface signals to deeper water layers and ultimately the surface sediment. From which valuable information about the origin, composition and modification of exported particles can be derived from microscopic examination of their skeletal remains (Peinert et al., 2001).

Coccoliths

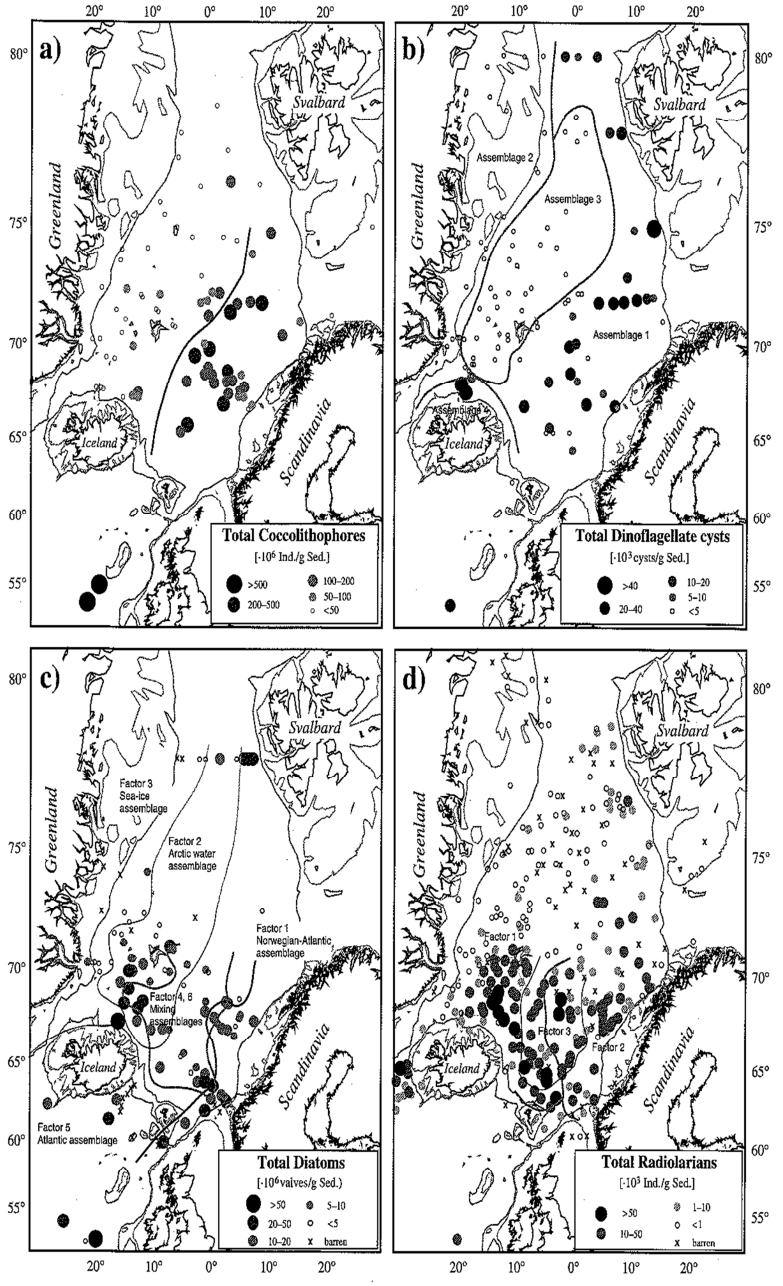

Dinocysts

Diatoms

Radiolarian

Figure 2.6 : Absolute abundances (ind./g dry sediment) of a) coccolithophores, b) dinoflagellate cysts, c) diatoms and d) radiolarians in surface sediments of the Nordic Seas. The distribution of species assemblages in plots b, c and d are based on factor analyses of species weight %. Modified after Matthiessen et al. (2001).

2.3.1 Dissolution Processes within the Nordic Seas

The dissolution of biogenic opal in the water column and in the sediment is a major alteration process worldwide and is particularly important in the Nordic Seas, resulting in generally less than 1% of the original opal production preserved in the sediment (Schröder-Ritzrau et al., 2001, and references therein). This opal dissolution is especially pronounced within diatom assemblages (Samtleben et al., 1995a), where the most abundant species have already been dissolved within the top 500 meters of the water column and are even further destroyed

through grazing, which enhances dissolution by destroying the fecal pellets. Grazing is a strong process especially in the Norwegian Sea, leading to stronger diatom alterations in the upper surface waters compared to the Greenland Sea (Schröder-Ritzrau et al., 2001). Consequently, surface sediments are the relict assemblages of the most resistant diatom species. Similar low preservation seems to influence the radiolarians in the Nordic Seas, except for the Icelandic Plateau (Fig. 2.6, 2.7) (Samtleben et al., 1995a; Schröder-Ritzrau et al., 2001).

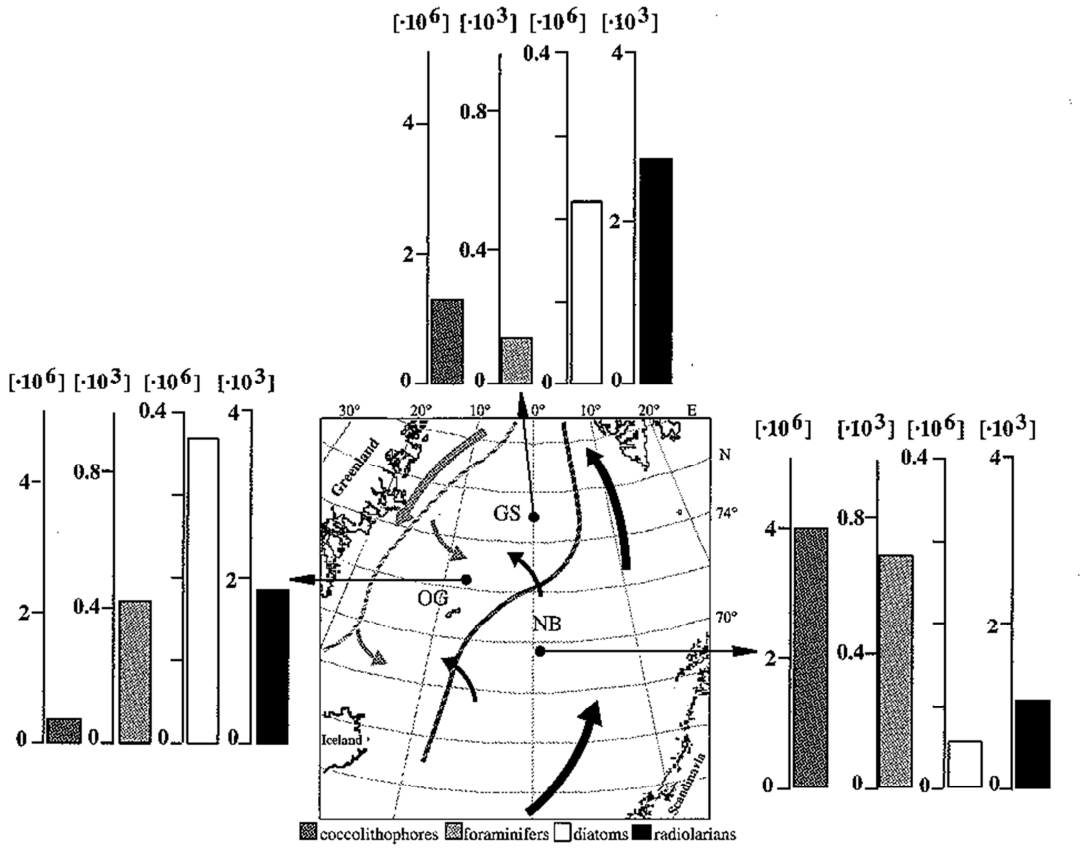

Figure 2.7: Mean daily fluxes (expressed as ind. $m^{-2}d^{-1}$) of coccolithophores, foraminifers, diatoms and radiolarians at 300/500 meters from sediment traps deployed in three different areas of the Nordic Seas. Adapted from Schröder-Ritzrau et al. (2001).

The dominant microplankton producers of biogenic carbonate within the Nordic Seas are coccolithophores and foraminifers (Fig. 2.7) (Matthiessen et al., 2001; Hass et al., 2001). The relatively shallow bathymetry of the Nordic Seas, above the carbonate compensation depth, limits the dissolution of carbonate tests in the deep waters and sediments (Matthiessen et al. 2001). Sediment trap investigations, however, showed that the pattern of carbonate dissolution displays some regional discrepancies with reduced impact in the Norwegian Sea

and the JMC areas, where, in contrast to the Greenland Sea (Andruleit, 2000), grazing is suggested to be the major alteration mechanism (Andruleit, 1997).

The Holocene sediments within the Greenland Sea, in fact, confirm the above mentioned dissolution patterns, showing strongly reduced amounts of diatoms and radiolarians where samples still contain calcareous and organic-walled microfossils (Hass et al., 2001). The test of the organic-walled dinocysts are made of a very complex organic compound (dinosporin), making this species group highly resistant to degradation processes in the water column and the sediment, compared with carbonate and siliceous microfossils. Still, they might degrade under certain environmental conditions (i.e oxidation, Zonneveld et al., 1997). In sediments, the degradation pathway of organic matter is related to aerobic respiration, which depends on the amount of oxygen and the organic carbon content. When the rate of carbon deposition exceeds that of oxygen supply, suboxic or anoxic conditions prevail and, thus, yield well-preserved organic matter (dinocyst) records (e.g. Marret and Zonneveld, 2003). Dinocysts have a sedimentary behavior comparable to fine silt and can, therefore, be subject to transport on their way to the sea floor. Previous experiments, however, showed that dinocysts sink relatively rapidly in the water column (e.g. Zonneveld and Brummer, 2000). As a result, the environmental conditions of the overlying surface water are reasonably well reflected by the assemblages in the bottom sediments (Marret and Zonneveld, 2003), although only ~10-15 % of the world's dinoflagellates are able to produce a fossilizable cyst record (e.g. Dale, 1976; Head, 1996). Nevertheless, the strong preservation potential of dinocysts and their high diversity in a wide range of environments explain their potential for paleoceanographic investigations.

2.3.2 The Importance of Transport Processes on the Spatial Distribution of Microfossils

Although fossil assemblages of phytoplankton are distributed in sediment surface according to major oceanographic domains, the pelagic realm is a highly dynamic environment in which plankton drifting along with major surface (and deep currents) is a common mechanism (Matthiessen et al., 2001). The transport of extant and fossil plankton organisms, which occur in all oceanic regions, can be divided in to three main types (Schröder-Ritzrau et al., 2001).

The *first type* is transport by major geostrophic currents (e.g. the NwAC and the EGC), a mechanism which can cause large biogeographic displacements, resulting in the occurrence of subtropical species in Arctic environments and vice versa (e.g. Samtleben and Schröder, 1992; Samtleben et al., 1995b; Matthiessen, 1995).

The *second type* describes the lateral transport of material in the upper water column from shelf areas to deep ocean basins (Dale and Dale, 1992; Matthiessen, 1995; Schröder-Ritzrau et al., 2001; Fohrmann et al., 2001; Rumohr et al., 2001).

The *third type* is lateral transport of resuspended material within bottom nepheloid layers. A process responsible for the recorded higher accumulation rates of material in deep (more than 300 meters above the sea floor) than in shallow sediment traps, of the Nordic Seas (Schröder-Ritzrau et al., 2001).

Sediment trap investigations within the Nordic Seas revealed that transport mechanisms, including all types described above, affect the sinking plankton microfossils in both the eastern and western parts of the northern North Atlantic to a high extent (Samtleben and Schröder, 1992; Matthiessen, 1995; Samtleben et al., 1995a; Schröder-Ritzrau et al., 2001). Particle fluxes in the central Greenland Sea revealed similar seasonal patterns at shallow and deep water column layers. Sediment traps in the JMC indicated a slightly increased flux in the deeper traps, especially during the low export period between late autumn and spring, although a seasonal flux pattern was still recorded in all planktonic groups of the deep traps. There, lateral advection of resuspended material into deeper traps has been suggested to origin from the Jan Mayen Fracture Zone, while surface to deep particle fluxes partly originated from transport by surface to intermediate ocean currents (e.g. the RAC and JMC) (Schröder-Ritzrau et al., 2001).
In the Norwegian Sea, the total fluxes of all groups are up to 10 fold higher in deep than in shallow sediment traps (Schröder-Ritzrau et al., 2001); the lateral advection of resuspended material within bottom nepheloid layers being strong enough to erase seasonal differences in export between calcareous and siliceous planktonic groups (Andruleit, 1997; Schröder-Ritzrau et al., 2001, and references therein). Investigations of sediment material from deeper basins of the Norwegian Sea must therefore take potential biaises in paleoceanographical reconstructions induced by the presence of a high amount of reworked and exotic material in the sediment, in to account. The majority of the allochtonous material collected in deep sediment traps of the Norwegian Sea has been suggested to originate from the shelf of the Barents Sea (related to brine formation during winter), the shelf and slope of the Norwegian continental margin, and the Jan Mayen Fracture Zone (Dale and Dale, 1992; Matthiessen,

1995; Schröder-Ritzrau et al., 2001; Fohrmann et al., 2001; Rumohr et al., 2001). The present material only rely on upper slope and depression area along the Norwegian-western Barents Sea-Svalbard margin.

2.4 Generalities on Coccolithophore Morphology, Biology, Ecology, and Sediment Distribution within the North Atlantic Region.

Coccoliths are the skeletal remains of the calcareous primary producers, coccolithophores, which are strictly marine and autotrophic, and are considered as one of the three main marine eukaryotic phytoplankton groups in terms of abundance along with diatoms and dinoflagellates.

Coccolithophores are unicellular eukaryotes (division of haptophytes) and thrive in all oceans of the world, although they show the highest biodiversity in temperate and subtropical zones (Okada and McIntyre, 1979). They are considered the largest producers of calcareous skeletal remains on Earth and play a major role on the marine carbon cycle, as the formation of calcite skeletons in the surface layer and their following sinking to the ocean floor modify the upper-ocean alkalinity (Rost and Riebesell, 2004). Furthermore, massive blooms of coccolithophores, commonly depicted from satellite remote sensing images, are likely to affect the oceanic surface albedo (Smyth et al., 2004). This combined influence on the biological and carbonate pumps and the following potential climate feedback mechanisms seem immense (albedo – masses of detached coccoliths reflect incoming light; dimethylsulfide – acting as a source molecule for cloud nucleation) (Westbroek et al., 1993), which makes the understanding of this group of marine algae of crucial importance to further comprehend the mechanisms of past, present and future climate changes.

2.4.1 The Morphology of Coccolithophores

Earlier studies on the morphology of coccolithophores indicated that these unicellular phytoplankton organisms are characterized by a motile phase (free swimming) and a non-motile phase (floating) during their life cycle. In the motile phase, a coccolithophore cell carries two smooth, whip-like flagella, rising from one end of an oval to elongate body, between which a third, so called, haptonema is attached (generally coiled, although it can also be straight) (Fig. 2.8) (Billard and Inouye, 2004, and references therein). During the non-motile stage, the flagella disappear but the haptonema may remain (Bown, 1998; Billard and Inouye, 2004). Living coccolithophores are covered by a layer of organic scales on which

small calcite platelets are resting: the coccoliths (~1 to 50 µm, with a common size range between 2 and 25 µm) (Siesser, 1993; Young et al., 1997).

Coccolithophores have earlier been divided into two general groups: heterococcolithophores and holococcolithophores. This division is based on the size and shape of the calcite cristals, which compose the coccoliths (hetero-coccoliths, made of a limited amount of cristals of different shape and size; holo-coccoliths, made of hundreds to thousands of cristals of similar size and shape) (Young et al., 1997, and references therein). Heterococcoliths are formed of rhombohedral crystals (although a few species are built of hexagonal prisms), whose simplest arrangement is shaped as a single disk with a raised wall of rhombohedral crystals at the circumference. A more complex arrangement of heterococcoliths consist of two circular or elliptical shields (a proximal shield on the inner "concave" side of the coccolith and a distal shield on the outer "convex" side of the coccolith), joined by a central cylindrical column but without a raised wall (Fig. 2.8) (Siesser, 1993). In this setup, the central column is either a solid pillar or hollow tube with its wall composed of rhombohedral crystals, either joined like staves in a barrel or spiraling down the wall of the tube. A distinctive closed or open central area from which crystal elements of the radiate shield radiate outward has been found on most heterococcoliths, where shield elements taper near the central area in order to fit better around a circular center. Contrary to heterococcoliths, holococcoliths are hardly preserved in marine sediments, their structure being prone to rapid disaggregation in the water column at the sediment-water interface (Siesser, 1993).

The calcite crystals in the coccolith plates have different arranged optical axes, resulting in a strong variability of optic extinction patterns as observed through crossed nicols of polarizing microscopes. These varying structural arrangements produce the species-specific recognizable optic extinction patterns used for routine identification (Siesser, 1993).

2.4.2 A short Introduction to Coccolithophore Biology

Internally, the coccolithophore cells contain a nucleus, two chloroplasts, mitochondria, vacuoles and the golgi body (Fig. 2.8). The mitochondrial bodies produce the energy needed for the cellular systems to function and are enclosed in membranes, which have tubular extensions into the cell interior (Bown, 1998). The vacuoles store waste product before it gets "thrown out", and the golgi body consists of closely packed, swollen, sac-like structures called "cisterne", which are used for secreting organic scales to cover the cell and later the coccoliths (Bown, 1998; Billard and Inouye, 2004). The cell's protoplasm is enclosed within a

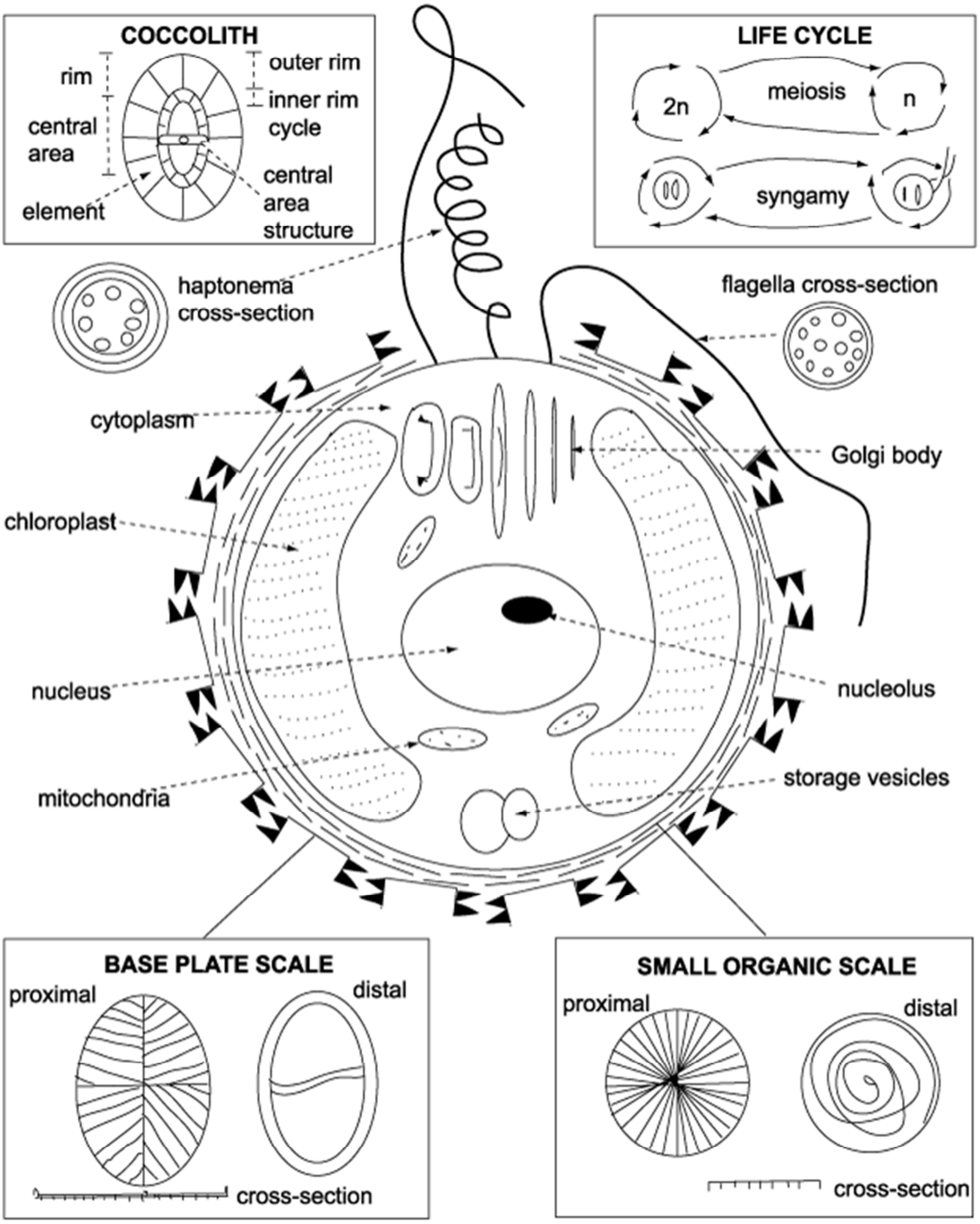

Figure 2.8: Diagrammatic cross-section of a coccolithophore cell and cell wall coverings. The defining feature of the haptophytes is the flagella-like haptonema, which is generally coiled. It differs from the other flagella in its internal structure and its basal attachment. The algal cell contains a nucleus and two chloroplasts, which may move around to optimize collection of available light. Mitochondria contains enzymes to produce energy for the different cell functions, vacuoles deal with waste products and the Golgi body is the site of coccolith secretion. In many species, overlapping oval organic scales coat the outer cell membrane. These have concentric ridges on their distal faces and radiating ridges on their proximal faces. The organic scales might act as bases for calcite coccolith precipitation. The function of coccoliths is not known but they may be used as: a protection from bacteria, protection from physical damage and predators, easiness of flotation and buoyancy, light reflection. Adapted from Bown, (1998).

double membrane that in turn is covered by an organic skin, the pellicle. These organic scales cover the outer cell membrane and act as organic bases for the calcite precipitation that forms the coccoliths. They are oval and have concentric ridges on their distal surfaces as well as radiating ridges on their proximal surfaces (Fig. 2.8) (Siesser, 1993). A variety of coccolith secretion strategies has been observed in different species, yet the most common cause of the production of coccoliths is probably light (Bown, 1998). The function of coccoliths is not known, but may be a protection from bacteria or a barrier against physical damages and predators.

The reproduction of coccolithophores occurs by single or double fission sometimes accompanied by a swarm-spore stage. The information on coccolithophore reproduction is however only based on a few species making it dangerous to generalize. Nevertheless the general consensus is that the coccolith-bearing phase is diploid (produces daughter cells which are exact replicas of the former cell, 2N) and capable of asexual reproduction (Fig. 2.8) (Bown, 1998; Billard and Inouye, 2004). This allows rapid population growth during periods of optimum conditions and is the base of coccolithophore "blooms".

Although coccolithophores have been classified according to coccolith plate morphology (hetero- and holo-coccolithophores), recent studies have shown that these differences are more likely related to stages in the life cycle of coccolithophores rather than different species (Billard and Inouye, 2004). This results in a continuous reevaluation of the taxonomy of this phytoplankton group and calls for additional studies on its ecology and life cycle.

improvement of buoyancy and/or light reflection (Bown, 1998).

2.4.3 Ecology of the Major and Subordinate Fossilizable Coccolithophores of the Nordic Seas.

As other phytoplankton organisms, the biomass and diversity of coccolithophores are constrained by environmental conditions of which salinity, temperature, stratification and light have earlier been found to be of particular importance. The depth range occupied by coccolithophores in the mixed layer is strictly constrained by the thickness of the photic layer, maximum bulk concentrations of these organisms occuring within the top 20 to 10 meters in mesotrophic to eutrophic areas of the high latitudes (Siesser, 1993).

Coccolithophores rival dinoflagellates and diatoms as the most abundant phytoplankton group within the world oceans and are without doubt dominant in the low to mid-latitudes. While outnumbered by organic and opal-walled phytoplankton in sub-polar to polar areas and characterized by a low diversity, coccolithophores, however, display higher concentrations

(cells/liters) in higher than in lower latitudes (Siesser, 1993), a phenomenon which tends to amplify toward the northernmost part of the Atlantic as a result of global warming (Smyth et al., 2004). Numerous investigations over the last two decades have strongly contributed to our knowledge on the distribution and ecology of extant coccolithophore populations and their fossil remains (coccoliths) within the North Atlantic region by using surface water samples, remote sensing, sediment traps and surface sediment sampling, (e.g. Samtleben and Bickert, 1990; Samtleben and Schröder, 1990, 1992; Samtleben et al., 1995a, 1995b; Andruleit, 1997, 2000; Andruleit and Baumann, 1998; Baumann et al., 2000; Cachão and Moita, 2000; Matthiessen et al., 2001; Schröder-Ritzrau et al., 2001; Beaufort and Heussner, 2001; Balestra et al., 2004; Smyth et al., 2004; Hegseth and Sundfjord, 2008; Solignac et al., 2008; Giraudeau et al., 2000, 2004, 2010; Dylmer et al., 2013, this study). These studies identified a total of ~20-25 extant coccolithophore species within the Nordic Seas using Scanning Electron Microscopy, of which the majority thrive along the path of the NwAC resulting in a generally north/northwest decrease in species numbers (Samtleben and Schröder, 1992; Baumann et al., 2000) (Fig. 2.6).

In the higher latitudes the coccolithophore production is generally dependent on seasonal factors, such as temperature, light regime, stratification and nutrients, as reflected in previous observations of extant coccolithophore numbers within the northern North Atlantic, which are consistently higher during high-production period (summer) conditions compared to low production period (late summer-spring) conditions (Baumann et al., 2000; Dylmer et al., 2013, this study).

Due to the naturally varying stability of different coccoliths a strong shift is seen between the extant coccolithophore diversity and the coccolith sediment assemblages (Samtleben and Bickert, 1990), with generally only the two dominating species (*Emiliania huxleyi* and *Coccolithus pelagicus*) and three minor species (*Gephyrocapsa muellerae*, *Calcidiscus leptoporus* and *Syracosphaer* sp.) left for paleoceanographic and paleoclimatic investigations (Samtleben and Schröder, 1992; Baumann et al., 2000).

Emiliania huxleyi

This cosmopolitan opportunistic euryhaline species blossoms during the summer and is frequently involved into massive blooms observed through remote sensing (satellite imagery) (Baumann et al., 2000, and references therein; Tyrrell and Merico, 2004). The Arctic Ocean is one of the only areas where this species is either absent from surface waters or occurs in very

low cell densities in stratified conditions after sea-ice melting (Tyrrell and Merico, 2004, and references therein; Balestra et al., 2004; Hegseth and Sundfjord, 2008; Dylmer et al., 2013, this study).

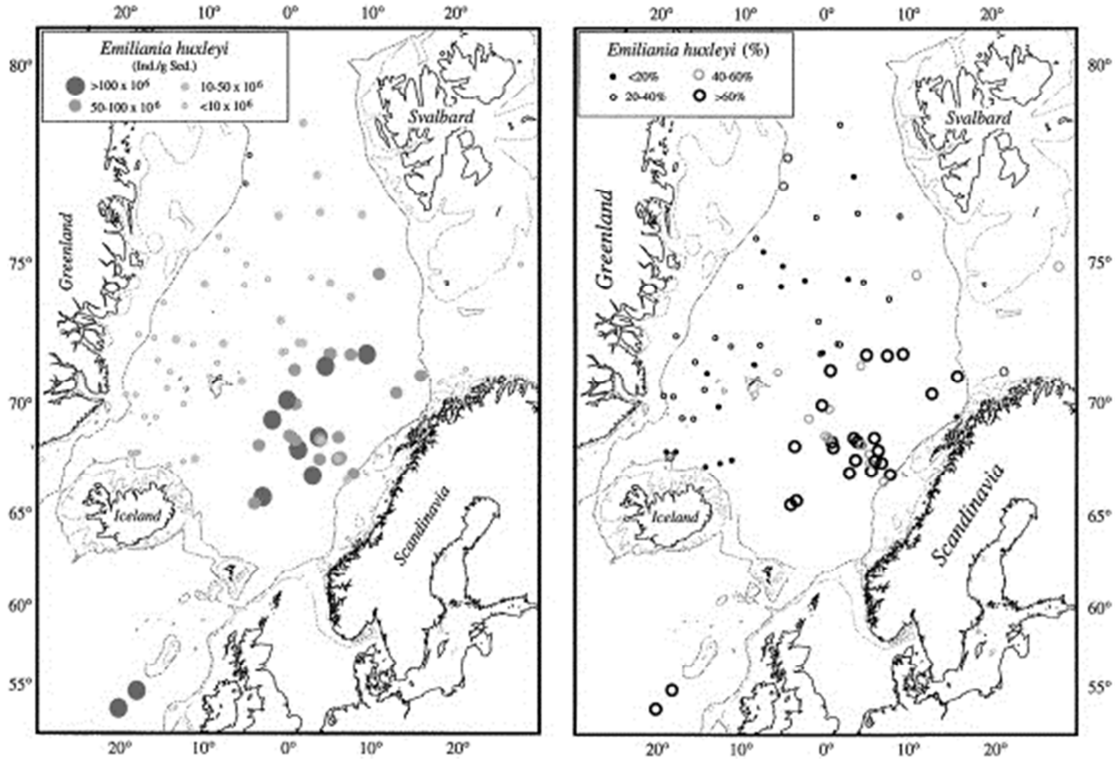

Figure 2.9: Absolute (left) and relative (right) abundances of *E. huxleyi* in surface sediments of the Nordic Seas. Adapted from Baumann et al. (2000).

In the northern North Atlantic, it has a strong affinity for warm, saline, Atlantic-derived surface waters and dominates both the extant population and fossil assemblages in sediment surface samples of the eastern Nordic Seas (Fig. 2.9) (Baumann et al., 2000; Dylmer et al., 2013, this study). In addition to a shallow mixed layer, increased irradiance, high carbonate saturation state and a limited silicate level (restricting the competitive growth of diatoms) in the photic layer within a wide range of sea-surface temperature (0-22°C) have all been suggested as essential parameters, favoring the success of *E. huxleyi*, which, in combination with a high growth rate, explains its frequent occurrence in massive blooms (Samtleben and Schröder, 1990, 1992; Samtleben et al., 1995a; Baumann et al., 2000; Beaufort and Heussner, 2001; Schröder-Ritzrau et al., 2001, and references therein; Tyrrell and Merico, 2004).

Coccolithus pelagicus

C. pelagicus has been subdivided into two sub-species on the grounds of morphological, genetical and ecological preference aspects (Baumann et al., 2000; Geisen et al., 2004; Zivery

et al., 2004): a sub-Arctic sub-species *C. pelagicus pelagius* (<10µm) and a larger temperate sub-species *C. pelagicus braarudii* (>10µm) (Zivery et al., 2004). While no differentiation is made between the two sub-species in the present thesis, we believe that most of the specimens we identified within our surface water or sediment samples belong to the sub-arctic form. Earlier work has shown that *C. pelagicus* preferentially grows during summer in surface waters of temperatures ranging between 1 and 14 °C, with an optimum at 8 °C (Samtleben and Schröder, 1992: Samtleben et al., 1995a; Beaufort and Heussner, 2001). Our own observations (Dylmer et al., 2013, this study) indicate an apparent maximum boundary temperature of 6 °C within the northern North Atlantic for this species, which explains its overwhelming dominance, albeit with low standing stocks, in the extant sub-polar to polar coccolithophore community along the East Greenland Current and below the thermocline in the eastern Norwegian Sea (Fig. 2.10) (Samtleben and Schröder, 1992; Samtleben et al,

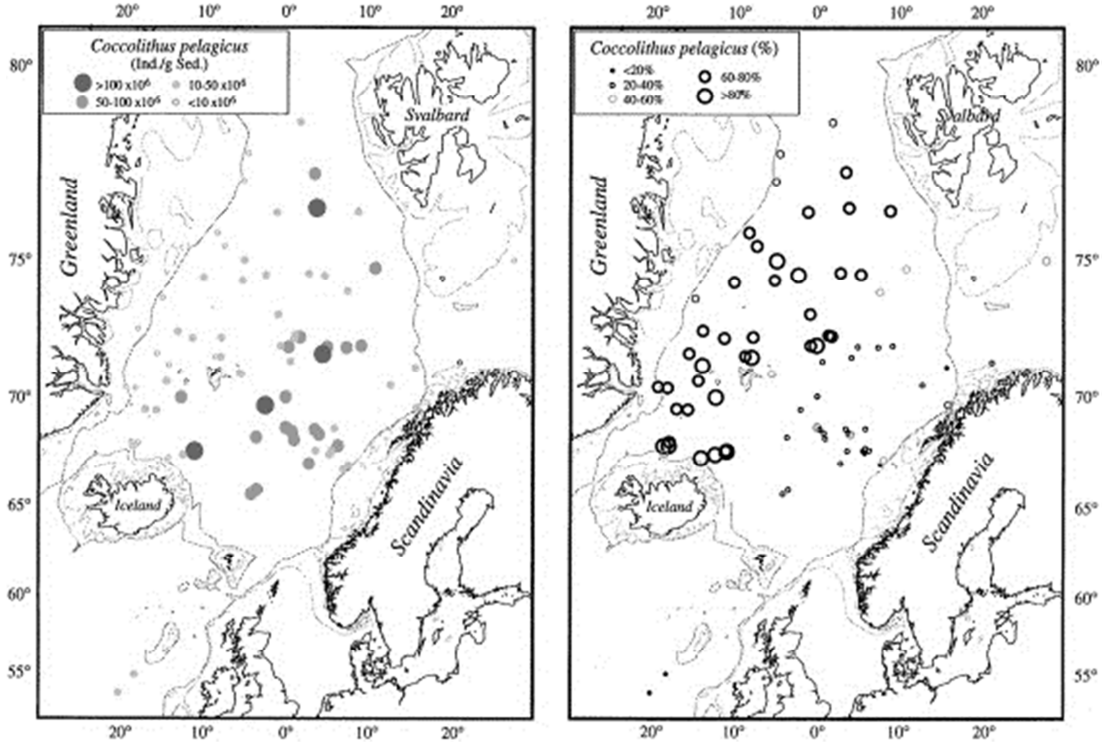

Figure 2.10: Absolute (left) and relative (right) abundances of *Coccolithus pelagicus* in surface sediments of the Nordic Seas. Adapted from Baumann et al. (2000).

1995a). This species constitutes the main component of the coccolith assemblages in surface sediments of the Greenland, Iceland, Irminger and Labrador Seas (Solignac et al., 2008).

C. pelagicus has no known salinity preferences suggesting an ecology controlled by other factors e.g. turbulence, temperature, nutrients and irradiance (Baumann et al., 2000; Schröder-Ritzrau et al., 2001; Balestra et al., 2004; Giraudeau et al., 2004). Indeed, this species has been suggested to occupy a particular ecological niche associated with moderate frontal

boundaries of different origins (thermal, upwelling and haline) (Cachao and Moita, 2000). Therefore, *C. pelagicus* appears to be associated with moderately turbulent conditions and might be a reliable proxy for meso- to eutrophic waters (Samtleben et al., 1995a; Andruleit, 1997; Baumann et al., 2000).

Gephyrocapsa muellerae

The coccolithophore species *Gephyrocapsa muellerae* has not yet been found thriving in the surface waters of the Nordic Seas (Andruleit, 1997; Dylmer et al., 2013, this study).

A previous work on extant populations across an E-W transect located at ~45°N restricted the ecological niche of this species to the mid-latitudes south of the Iceland-Scotland Ridge (10-

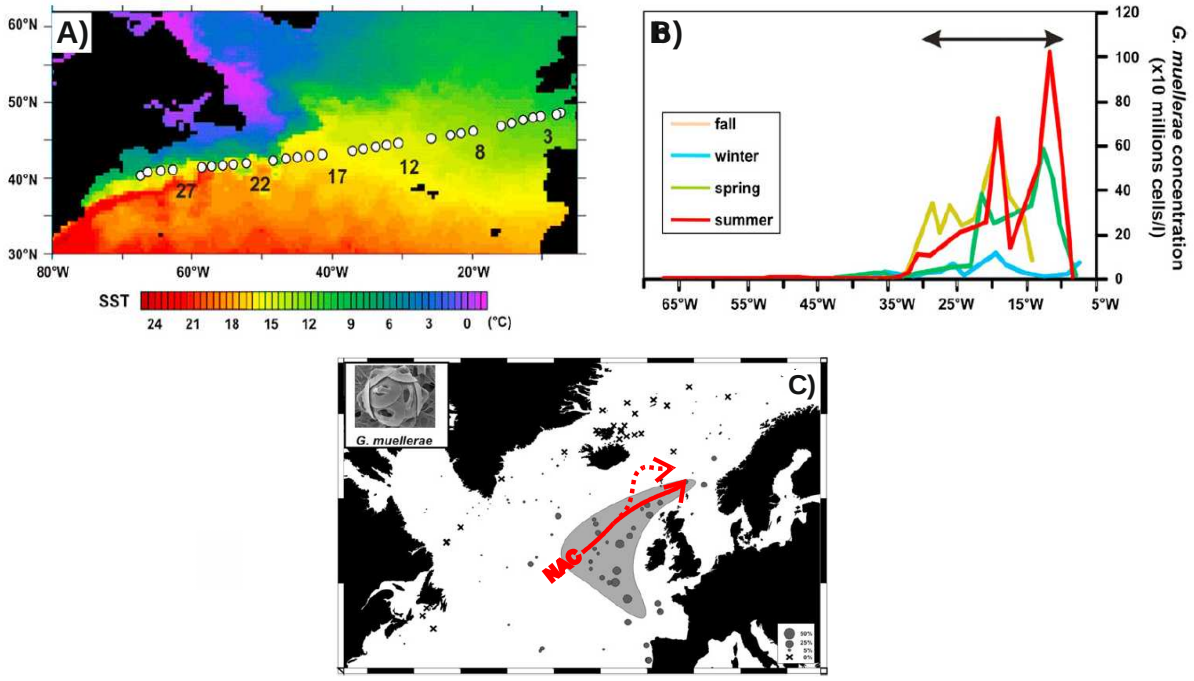

Figure 2.11: Seasonal distribution of *Gephyrocapsa muellerae* standing stocks in North Atlantic surface waters across ~45 °N. A) Satellite-derived SST field in April 2000 with locations of surface water samples. B) Cell concentrations across the studied transect during fall 1999, winter 2000, spring 2000 and summer 2000; the horizontal arrow points to the longitudinal range of peak production (30 °W- 10°W). C) Surface sediment distribution of *G. muellerae* (wt%) in the mid- to high latitudes of the North Atlantic. Modified after Giraudeau et al. (2010), and references therein.

30 °W) (Fig. 2.11) (Giraudeau et al., 2010), with peak production occurring during summer with surface water temperatures ranging from 12 to 18 °C. The optimum temperature of growth was estimated at ca. 14 °C, because *G. muellerae* is seldom found below the thermocline (Samtleben and Schröder, 1992; Giraudeau et al., 2010). Though, in low abundances, skeletal remains of *G. muellerae* are found in surface sediment samples of the Norwegian Sea and as far north as off western Svalbard (Baumann et al., 2000; Giraudeau et

al., 2010; Dylmer et al., 2013), an occurrence explained by meridional transport and drifting of its coccoliths within the NAC (Samtleben and Schröder, 1992; Andruleit, 1997, 2000; Giraudeau et al., 2010; Dylmer et al., 2013). Eventhough the mechanism of poleward transport, as described here for *G. muellerae,* is supposed to affect all species thriving in southern latitudes within the path of the NwAC, it is not expected to hamper the paleorecords of the high in situ production of the dominating species (e.g. *E. huxleyi* and *C. pelagicus*) in the Nordic Seas which is transferred to the sediment surface within weeks by fecal pellets (Samtleben and Schröder, 1992; Andruleit et al., 1997). Given this ecological background, abundance changes of *G. muellerae* in the studied sediment cores will therefore be discussed in terms of relative abundance variations of the depth integrated flow strength of the NwAC to the Nordic Seas up to its northernmost extension off western Svalbard (WSC).

Calcidiscus leptoporus

C. leptoporus is a robust cosmopolitan species, which consists of three sub-taxa described as large, intermediate and small morphotypes or separate sub-species (not distinguished in the present study) (Zivery et al., 2004; Quinn et al., 2004, and references therein). The intermediate form has a wide distribution with an affinity for cool, nutrient poor waters. The large form primarily occurs in higher productivity and mesotrophic environments whereas the distribution of the small form is unclear (Zivery et al., 2004, and reference therein). In the Nordic Seas, *C. leptoporus* is often found associated with *E. huxleyi* and *C. pelagicus* in surface sediments below cold temperate waters in the vicinity of the subarctic front (Giraudeau et al., 2000). The observed abundances restrict the species to surface water masses with a mean annual temperature below ~20 °C and possibly high nutrient content (Zivery et al., 2004).

Syracosphaera spp.

This species group includes all *Syracosphaera* species and has been included into the ”Atlantic coccolithophore assemblage” by Samtleben et al. (1995a). *Syracosphaera* is found in extant populations in the Greenland-Norwegian Seas off the Vøring Plateau at temperatures above 9-10°C and is hence restricted to relatively warm AWs (Samtleben and Schröder, 1992). *Syracosphaera* spp. is mainly distributed in surface sediments along the path of the Atlantic water masses (Samtleben and Schröder, 1992; Samtleben et al., 1995a; Baumann et al., 2000).

Significance of the E. huxleyi/C. pelagicus ratio

The differing regional dominance of the two major species is clearly reflected in the surface sediments of the Nordic Seas (Samtleben et al., 1995a). The abundance ratio between *E. huxleyi* and *C. pelagicus* (E/C ratio) in fossil assemblages of the Nordic Seas was, therefore, proposed by Baumann et al. (2000) to define the location of the AF, which separates the seasonally ice-covered waters of the Polar and Arctic domains (E/C<1) from warmer and saltier Atlantic-derived waters (E/C>1). According to Baumann et al. (2000), the E/C ratio is based on a conversion of coccolith to coccosphere units, where the applied average number of coccoliths per coccosphere for each species was adapted from Samtleben and Schröder (1992).

Allthough the original work by Baumann et al. (2000) were confined to the central areas of the Nordic Seas, we believe the application of this method to be valid in the wider Nordic Seas including its eastern part. The published surface sediment sample dataset by Baumann et al. (2000) only included a few sites far west of the continental margin with coccolith assemblages dominated by *C. pelagicus* (E/C <1). This excess *C. pelagicus* abundance stands as a contrast to our own results from surface sediment assemblages in the northern cores HH11-134-BC and JM09-KA11-GC, as well as to the composition of extant populations northwest of Bjørnøya (Baumann et al., 2000) and across Fram Strait (Dylmer et al., 2013, this study), indicating an expected dominance of *E. huxleyi* below and within AW dominated areas. Based on these evidences we use the definition of the AF (a frontal salinity and temperature gradient separating surface AW masses from mixed ArW) to infer that the E/C ratio (ie. deviations from the treshold of 1) characterizes surface sediments deposited below Atlantic or Arctic surface water masses, when considering pluriannual conditions.

The coccolithophores *Emiliania huxleyi* and *Coccolithus pelagicus*: extant populations from the Norwegian-Iceland Sea and Fram Strait.

C.V. Dylmer[a], J. Giraudeau[a], V. Hanquiez[a], and K. Husum[b].

a Université de Bordeaux, CNRS, UMR 5805 EPOC, Talence, France
b Department of Geology, University of Tromsoe, Tromsoe, Norway

Dylmer, C. V., Giraudeau, J., Hanquiez, V. and Husum, K.: The coccolithophores Emiliania Huxleyi and Coccolithus pelagicus: extant populations from the Norwegian-Greenland Sea and Fram Strait, Biogeosciences Discuss., 10, 15077-15106, 2013.

Abstract
Extant coccolithophores and their relation to the governing oceanographic features in the northern North Atlantic were investigated along two zonal transects of surface water sampling, both conducted during summer 2011 and fall 2007. The northern transects crossed Fram Strait and its two opposing boundary currents (West Spitsbergen Current and East Greenland Current), while the southern transects sampled the Norwegian and Iceland Seas (passing the island Jan Mayen) from the Lofoten Islands to the continental margin off Eastern Greenland. The distribution of the dominant coccolithophore species *Emiliania huxleyi* and *Coccolithus pelagicus* is discussed in view of both the surface hydrology at the time of sampling and the structure of the surface mixed layer. Remote-sensing images as well as CTD and ARGO profiles are used to contrain the physico-chemical state of the surface water at the time of sampling. Both transects were characterized by strong seasonal differences in bulk coccolithophore standing stocks with maximum values of 53×10^3 cells/l for the northern transect and 72×10^3 cells/l for the southern transect in fall and summer, respectively. The highest recorded bulk cell densities are essentially explained by *E. huxleyi*. This species shows a zonal shift in peak abundance in the Norwegian-Iceland Seas from a summer maximum in the Lofoten gyre to peak cell densities around the island Jan Mayen in fall. Vertical mixing of Atlantic waters west of Lofoten Island, a phenomenom related to pervasive summer large scale atmospheric changes in the eastern Nordic Seas, on one hand, and strengthened influence of melt-water and related surface water stratification around the island Jan Mayen during fall, on the other hand, explains the observed seasonal migration of the *E. huxleyi* peak production area, as well as the seasonal change in dominating species within the Iceland Sea. In addition our datasets are indicative of a well-defined maximum boundary temperature of 6°C for the production of *C. pelagicus* in the northern North Atlantic.
The Fram Strait transects provides, to our knowledge, a first view of the zonal distribution of extant coccolithophores in this remote setting during summer and fall. Our datasets are indicative of a seasonal change in the species community from an *E. huxleyi*-dominated assemblage during summer to a *C. pelagicus*-rich population during fall. Here, higher irradiance and increased Atlantic water influence during summer favored the production of the opportunistic species *E. huxleyi* close to the Arctic Front, whereas the peak production area during fall, with high concentrations of *C. pelagicus*, lays in true Arctic/Polar waters.

1. INTRODUCTION

The northern North Atlantic is experiencing unprecedented changes in physical and chemical conditions, which directly influence the ecosystem structure and processes (Hunt and Drinkwater, 2005). The impact of the last decades' increased temperatures linked to the recent "global warming" is particularly felt in those high latitude areas close to the boundary of maximum winter sea-ice extent, defined as the Arctic Front (AF) (IPCC, 2007). There, strong gradients in cryospheric, atmospheric and oceanic processes are prone to enhanced new production (Hunt et al., 2002).

The water mass exchanges between the North Atlantic and Arctic Ocean taking place in the Nordic Seas and Fram Strait have been extensively studied throughout the last decades in order to investigate the manifestations and impacts of the recent global climate change in terms of poleward heat transfer and changes in ecosystem structure. Recent compilations of satellite observations (AVHRR, SeaWiFS and MODIS-Aqua) suggest an increased occurrence of blooms of marine calcifying phytoplankton – coccolithophores – in the Barents Sea and Nordic Seas since the late 80s (Smyth et al., 2004; Burenkov et al., 2011). These blooms are thought to be triggered by modifications in the stratification and temperature of the upper mixed layer linked with extensive sea-ice melting (Parkinson et al., 1999) and increased inflow of Atlantic Water (AW) into the Nordic Seas and adjacent areas (Hatun et al., 2005; Hegseth and Sundfjord, 2008; Dmitrenko et al., 2010). This group of unicellular marine phytoplankton, the most abundant calcifying species on Earth, plays an important role in many biogeochemical cycles, and hence likely contributes to important internal feedbacks to climate changes (e.g. Westbroek et al., 1993).

Recent studies on the biogeography of extant epipelagic coccolithophores in the Northern North Atlantic, and on the distribution of their fossil remains –coccoliths- in surface sediments of the Nordic Seas highlighted the close relationship between the distribution of this species group and major surface water masses of the northern North Atlantic (Samtleben and Schröder, 1990, 1992; Samtleben et al., 1995a, 1995b; Andruleit, 1997; Baumann et al., 2000; Schröder-Ritzrau et al., 2001; Matthiessen et al., 2001; Balestra et al., 2004; Smyth et al., 2004; Dmitrenko et al., 2006; Hegseth and Sundfjord, 2008; Giraudeau et al., 2004, 2010; Burenkov et al., 2011; Charalampopoulou et al., 2011).

The overall surface circulation in the Nordic Seas is governed by two meridional boundary currents. The eastern boundary current is represented by the northward flowing warm and saline Norwegian Atlantic Current (NwAC) (<500-600 m) (Furevik et al., 2007) (Fig. 1), a

topographically steered two branch extension of the North Atlantic Current (NAC) (7-13 °C, ≥35), entering the Nordic Seas through the Iceland-Scotland ridge (ca. 7 Sv, Hansen and Østerhus, 2000; Orvik and Niller, 2002; Andersson et al., 2011). The eastern branch of the NwAC, is accompanied north by the baroclinic shallow Norwegian Coastal Current (NCC) (~34.4) along the continental slope of Norway, and splits into two branches North of Lofoten Island: A meridional branch, the West Spitsbergen Current (WSC), and a zonal component, the North Cape Current (NCaC) (Wassmann et al., 2006; Koszalka et al., 2011).

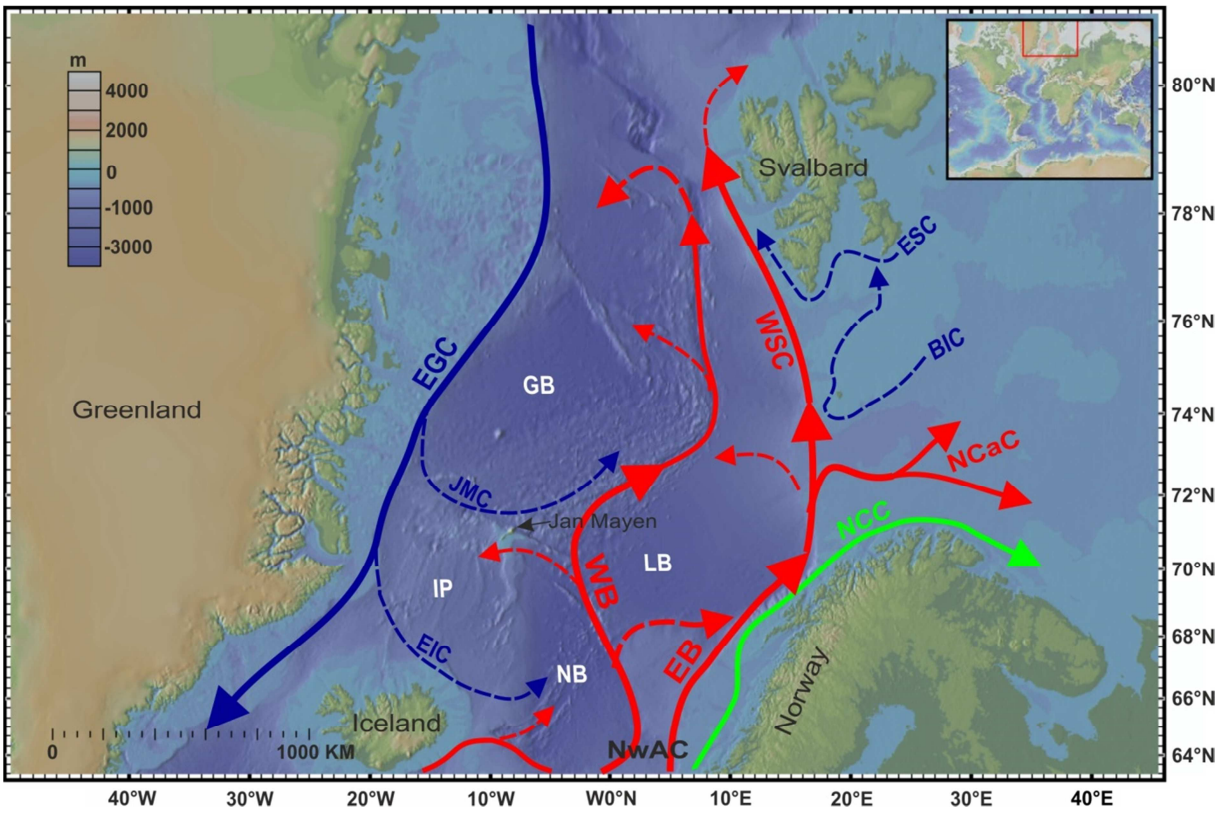

Figure 1: Bathymetric map of the Nordic Seas showing major surface currents after Jakobsen et al. (2003), Olsson et al. (2005) and Andersson et al. (2011). Red arrows show the the flow direction of warm saline Atlantic water. NwAC: Norwegian Atlantic Current, WB: Western Branch (NwAC), EB: Eastern Branch (NwAC), NCaC: North Cape Current, WSC: West Spitsbergen Current). Blue arrows show the flow direction of cold low saline Arctic/Polar waters. EGC: East Greenland Current, JMC: Jan Mayen Current, EIC: East Icelandic Current, BIC: Bear Island Current. Green arrow shows the flow direction of coastal waters. NCC: Norwegian Coastal Current. Other abbrevations; NB: Norwegian Basin, LB: Lofoten Basin, GB: Greenland Basin, IP: Icelandic Plateau.

The WSC flows along the continental margin of the western Barents Sea and western Spitsbergen and is further accompanied on its northern path by shallower Polar Waters (PW) on the shelf (e.g. the Bear Island Current (BIC) and the Sørkapp Current) (Saloranta and Svendsen, 2001; Wassmann et al., 2006) (Fig. 1). It enters the Arctic Ocean as a subsurface current insulated from the atmosphere by fresh PW in the upper mixed layer (3-5 Sv; Blindheim and Østerhus, 2005). The western branch of the NwAC (>34.9) rounds the

southern rim of the Lofoten Basin and flows north as a baroclinic jet along the Mohn Ridge contributing with Atlantic Water (AW) to the development of the Nordic Sea Frontal Zone (Orvik and Niller, 2002; Jakobsen et al., 2003; Koszalka et al., 2011). The western boundary current is represented by the southward flowing East Greenland Current (EGC; <0°C, <34.5), considered as the largest and most concentrated meridional ice flow in the World Oceans (Blindheim and Østerhus, 2005). Its two zonal components, the Jan Mayen Current (JMC) at the Jan Mayen Fracture Zone and the East Icelandic Current (EIC) in the Iceland Sea, supply fresh PW to the gyre systems and hence contribute to the Frontal Zone (Johannessen, 1986; Olsson et al., 2005) (Fig. 1).

The mixing of PW and AW creates Arctic Water (ArW) (0-4°C, 34.6-34.9) (Johannessen, 1986). The northeast-southwest trending boundary between PW and ArW is termed the Polar Front (PF) and characterizes the maximum summer sea-ice extent, whereas the boundary between ArW and AW is referred to as the Arctic Front (AF) and characterizes the maximum winter sea ice extent (Swift, 1986; Van Aken et al., 1995; Saloranta and Svendsen, 2001). Generally, the positions of the fronts in the Nordic Seas are well correlated with bathymetry due to topographic steering of the currents (Johannessen, 1986). This is seen north of the island Jan Mayen along the mid-ocean ridge where the AF only exhibits small fluctuations in contrast to the zone between Iceland and the island Jan Mayen where large shifts within the position of the AF occur due to variations in the inflow of PW/ArW from the EIC (Blindheim et al., 2000). The Frontal Zone term is generally used for the area where horizontal gradients in temperature, salinity and density are high in comparison with the mean parent water types (Van Aken et al., 1995).

A series of cyclonic gyres are present over the Greenland, Lofoten, and Norwegian Basins and the Icelandic Plateau, in-between the two main meridional boundary currents. These four gyres are strongly linked to the local bottom topography and are areas of strong mixing and transformation of water masses (Poulain et al., 1996; Jakobson et al., 2003; Koszalka et al., 2011) (Fig. 1).

Coccolithophores are generally confined to surface waters above or close to the thermocline and only a few species are known to thrive in subsurface waters below this boundary (Schröder-Ritzrau et al., 2001). In addition, coccolithophore production in the Northern Atlantic is strongly related to the seasonal cycle of insolation, nutrient content, grazing pressure and weather conditions, and is usually delayed by diatom production until silica is depleted (Samtleben and Schröder, 1992; Baumann et al., 2000; Charalampopoulou et al.,

2011). The Norwegian Sea is characterized by Atlantic surface waters with a seasonally established thermocline. The uppermost water mass stratification of the Greenland and Iceland Seas are essentially governed by highly variable sea-ice melting, although in years where sea-ice melt waters may be restricted to the margins, thermal warming might initiate the spring stratification. This regional difference obviously lead to important variations in the seasonal development and composition of the fossilizable planktonic community (Wassmann et al., 1991; Samtleben et al., 1995a; Baumann et al., 2000; Schröder-Ritzrau et al., 2001). The coccolithophore production in the southeastern Norwegian Sea may be enhanced as early as May, with a progressive transition towards the Greenland Sea peaking in August (Samtleben and Bickert, 1990; Samtleben et al., 1995a; Baumann et al., 2000; Schröder-Ritzrau et al., 2001). Hence the living coccolithophore community shows a broad seasonal maximum in the Nordic Seas as blooms occur throughout the summer season (Schröder-Ritzrau et al., 2001), with consistently higher cell numbers of living coccolithophores during the high-production periods (summer) than during the low-production periods (fall to early summer) (Samtleben et al., 1995a; Baumann et al., 2000).

As evidenced earlier by Andruleit (1997) and Baumann et al. (2000), the coccolithophore communities in the surface waters across Fram Strait and the Norwegian-Iceland Seas are strongly dominated by the summer blooming species *Emiliania huxleyi* and *Coccolithus pelagicus*, which shows markedly different ecological preferences. An ubiquitous species in the world ocean, *E. huxleyi* exhibits a high growth rate compared to other coccolithophore species which makes it one of the most successful coccolithophores thriving in the world oceans (Baumann et al., 2000; Tyrrell and Merico, 2004). In the Nordic Seas it has been shown to have a strong affinity for the warm and saline Atlantic-derived surface waters and has only occasionally been reported in areas strongly influenced by sea-ice (Baumann et al., 2000; Balestra et al., 2004; Hegseth and Sundfjord, 2008). Additional ecological studies has shown this species to be euryhaline and mainly influenced by variations in stratification, irradiance and to a lesser extent temperature (0-22 °C) of the photic layer (Samtleben and Schröder, 1990, 1992; Samtleben et al., 1995b; Baumann et al., 2000; Beaufort and Heussner, 2001; Schröder-Ritzrau et al., 2001). *C. pelagicus* represents the coldest species of the coccolithophore community, occurring at temperatures between -1 and 14 °C with an optimum at 8 °C (Samtleben et al., 1995a; Baumann et al., 2000). Such a temperature range might explain its very strong dominance, albeit with low standing stocks, in the polar community of the EGC (Samtleben and Schröder, 1992). It might also explain that this

species constitutes the main component of the coccolith assemblages in surface sediments of the Greenland, Iceland, Irminger and Labrador Seas (Solignac et al., 2008). The species has no known salinity preferences, but it has previously been associated with the position of the AF, suggesting an ecology controlled by factors other than temperatures e.g. nutrients and irradiance (Baumann et al., 2000; Schröder-Ritzrau et al., 2001; Balestra et al., 2004; Giraudeau et al., 2004). Furthermore, some studies have suggested turbulence as a possibly important factor preventing the sinking of this heavily calcified species from the photic zone (Cacha and Moita, 2000) hence favoring its production in the highly mixed upper ArW. In these upper water masses the low temperatures probably also further limit the occurrence of other species (Baumann et al., 2000). In addition *C. pelagicus* has been suggested as a reliable proxy of mesostrophic to eutrophic waters in phytoplankton biomass-rich frontal systems of the Nordic Seas (Andruleit, 1997; Samtleben et al., 1995a).

The extant coccolithophore communities compare relatively well with the spatial distribution of their fossil remains in the surface sediments of the Nordic Seas (Samtleben et al., 1995a). Indeed, contrary to siliceous microfossils, dissolution in the water column and in the surface sediments does not alter the general composition of coccolith assemblages and their fluxes remarkably (Andruleit, 1997; Schröder-Ritzrau et al., 2001; Matthiessen et al., 2001). This is consistent with sediment trap studies indicating a dominance of calcareous organisms in the export flux of plankton organisms within the Norwegian Sea. Furthermore, the coccolithophores are the most dominant fossilizable plankton group in terms of mean annual daily flux rates in this region (Schröder-Ritzrau et al., 2001). Previous investigations have demonstrated that coccoliths of *E. huxleyi* and *C. pelagicus* are distributed in surface sediments of the Nordic Seas according to their distribution in extant populations, and accordingly dominate the fossil assemblages below AW and ArW (Baumann et al., 2000).

Remote sensing offers the opportunity to discuss the distribution patterns of phytoplankton communities collected in the upper photic layer, according to geographically and temporally well-constrained large- to meso-scale surface circulation features, and, as in the case of the Nordic Seas, sea-ice occurence. The present investigation, which relies on this analytical strategy to comprehend the seasonal surface hydrology, aims at improving our understanding of the modern distribution of the two dominant coccolithophore species in the Northern North Atlantic: *E. huxleyi* and *C. pelagicus*. It is based on two transects of surface water sampling across Fram Strait and the Norwegian-Iceland Seas (passing Jan Mayen Island), perpendicular

to the flow direction of the primary surface currents, and both carried out during the autumn of 2007 (September-October) and the mid-summer of 2011 (July). Annual and seasonal differences in coccolithophore abundances along both transects will be discussed in view of the surface hydrology at the time of sampling as deduced from Aqua MODIS and AVHRR Pathfinder images.

2. MATERIAL AND METHODS

The present study reports on extant coccolithophore populations collected along two zonal surface water transects across Fram Strait (ca. 73-78°N) and the Norwegian – Iceland Seas (ca. 70°N) during the autumn of 2007 (September 29 - October 14) and summer of 2011 (July 15-27), as part of the cruises SciencePub UiT/WARMPAST and GEO-8144/3144, respectively, of the R/V *Helmer Hanssen* (former 'R/V *Jan Mayen*') (Fig. 2, Tables 1 and 2).

2.1 Coccolithophore Analyses

Sampling was conducted en-route using the ship's deckwash pump (limiting the sampling to the near surface water masses <5 m), and involved onboard membrane filtration of sea water (2-3 litres). Air-dried filter were subsequently mounted between slide and coverslip, and examined under a light microscope at x1000 magnification as described by Giraudeau et al. (1993). A total of 57 samples (31 samples, September/October 2007; 26 samples, July 2011) were investigated for living assemblages (Tables 1 and 2) and the results expressed as coccolithophore standing stocks per litre (number of cells/l). In the present work, *C. pelagicus* includes both the motile holococcolith-bearing phase (*C. pelagicus* f. *hyalinus*) and the non-motile heterococcolith-bearing phase (*C. pelagicus* f. *pelagicus*) (Cachão and Moita, 2000; Balestra et al., 2004)

While the use of a light microscope (compared with Scanning Electron Microscope – SEM - examination) limits a precise taxonomical investigation of the extant coccolithophore population, this approach was found sufficient to identify and to conduct reliable census counts of the dominant fossilizable species in the recovered samples, i.e. *E.huxleyi* and *C. pelagicus.*

Figure 2 : Monthly Sea Surface Temperature (SST) composite maps of the studied area based on satellite grid images (Aqua MODIS 32), extracted from http://oceancolor.gsfc.nasa.gov/ for September 29 - October 14 in 2007 and 15-27 of July 2011. White squares: samples locations; black squares: CTD and ARGO locations; dashed light blue line: sea-ice margin as the 50% sea-ice concentration isoline extracted from AVHRR Pathfinder 5.2 images (http://data.nodc.noaa.gov) from October 5, 2007, and July 20, 2011. Shaded area (October 2007): no data.

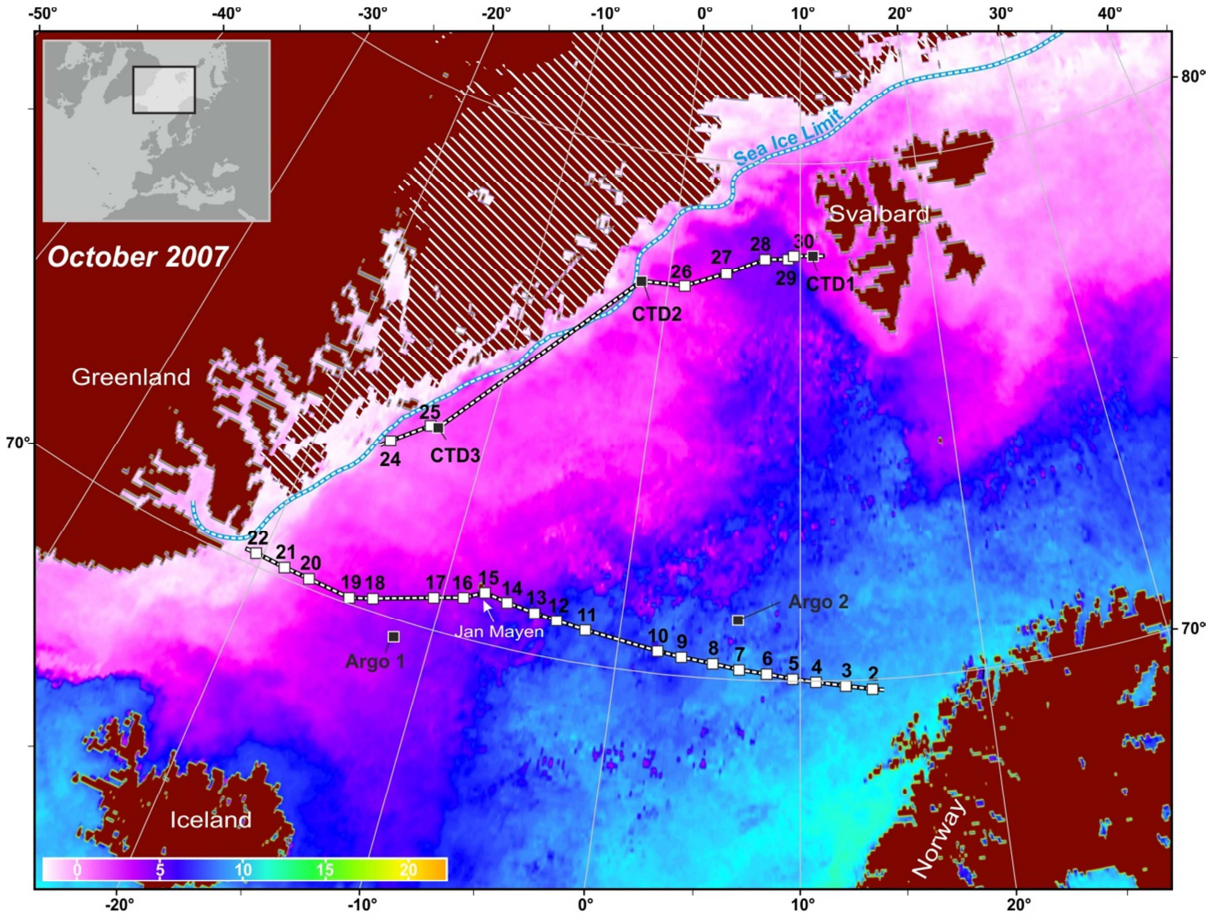
October 2007
Greenland
Iceland
Svalbard
Norway
Sea Ice Limit
CTD1
CTD2
CTD3
Argo 1
Argo 2
Jan Mayen
0
5
10
15
20

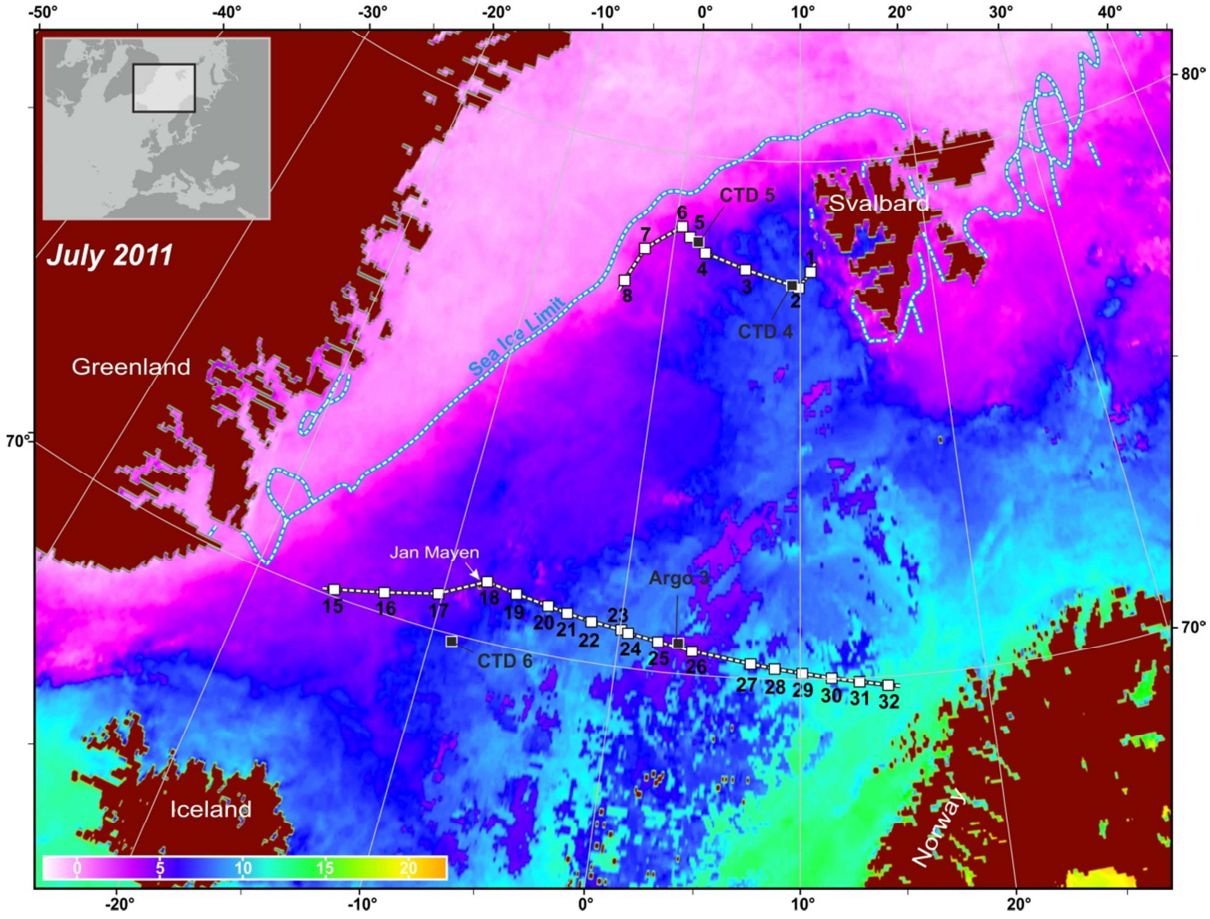
July 2011
Greenland
Iceland
Svalbard
Norway
Sea Ice Limit
CTD 4
CTD 5
CTD 6
Argo 3
Jan Mayen
0
5
10
15
20

Table 1: List of surface water samples for Oct.-Sep. 2007, with collection dates, locations and coccolithophore cell densities.

Sample	Longitude	Latitude	Date	Total Coccolithophores (× 1000/l)	*Coccolithus pelagicus* (× 1000/l)	*Emiliania huxleyI* (×1000/l)	*Algirospheara robusta* (× 1000/l)
1	13.85	69.82	29/09/2007	12.1	0.0	12.1	0.0
2	12.43	69.90	30/09/2007	4.8	0.0	2.4	2.4
3	10.83	69.98	30/09/2007	2.2	0.0	2.2	0.0
4	9.58	70.05	30/09/2007	5.2	0.0	3.9	1.3
5	9.58	70.05	30/09/2007	0.0	0.0	0.0	0.0
6	8.17	70.13	30/09/2007	1.5	0.0	1.5	0.0
7	6.67	70.20	30/09/2007	0.0	0.0	0.0	0.0
8	5.23	70.28	30/09/2007	0.0	0.0	0.0	0.0
9	3.50	70.37	30/09/2007	0.0	0.0	0.0	0.0
10	2.17	70.43	30/09/2007	0.0	0.0	0.0	0.0
11	-1.92	70.65	01/10/2007	0.0	0.0	0.0	0.0
12	-3.57	70.73	01/10/2007	1.3	1.3	0.0	0.0
13	-4.85	70.80	01/10/2007	2.2	0.0	2.2	0.0
14	-6.45	70.88	01/10/2007	11.8	0.0	11.8	0.0
15	-7.78	70.97	01/10/2007	23.5	0.0	23.5	0.0
16	-8.87	70.77	01/10/2007	23.5	2.6	20.9	0.0
17	-10.45	70.62	01/10/2007	66.4	0.0	66.4	0.0
18	-13.60	70.25	02/10/2007	20.7	0.0	20.7	0.0
19	-14.83	70.12	02/10/2007	13.1	0.0	13.1	0.0
20	-17.23	70.18	02/10/2007	2.5	2.5	0.0	0.0
21	-18.68	70.20	02/10/2007	1.9	0.5	1.4	0.0
22	-20.38	70.23	02/10/2007	6.1	3.1	3.1	0.0
24	-15.67	73.23	07/10/2007	6.5	3.3	3.3	0.0
25	-13.65	73.77	08/10/2007	16.3	10.5	5.9	0.0
26	1.25	77.50	11/10/2007	48.3	25.6	22.6	0.0
27	4.32	77.82	12/10/2007	11.5	1.6	9.9	0.0
28	7.23	78.13	12/10/2007	6.1	1.2	3.7	1.2
29	9.03	78.15	12/10/2007	12.7	2.3	9.2	1.2
30	9.48	78.22	12/10/2007	9.1	2.6	3.9	2.6
CTD 1	-13.15	73.78	08/10/2007	9.1	3.9	5.2	0.0
CTD 2	-2.03	77.47	11/10/2007	52.9	29.4	23.5	0.0
CTD 3	10.98	78.22	12/10/2007	7.0	0.0	5.6	1.4

Table 2: List of surface water samples for July 2011, with collection dates, locations, and coccolithophore cell densities.

Sample	Longitude	Latitude	Date	Total Coccolithophores (× 1000/l)	*Coccolithus pelagicus* (× 1000/l)	*Emiliania huxleyi* (× 1000/l)	*Algirospheara robusta* (× 1000/l)
1	10.77	77.88	15/07/2011	1.3	0.0	1.3	0.0
2	9.88	77.58	15/07/2011	1.1	0.0	1.1	0.0
3	5.77	77.90	16/07/2011	27.3	0.0	27.3	0.0

4	2.55	78.15	16/07/2011	46.0	14.7	31.4	0.0
5	1.22	78.42	16/07/2011	29.3	2.0	27.3	0.0
6	0.50	78.60	19/07/2011	10.3	4.8	5.5	0.0
7	-2.17	78.08	19/07/2011	4.0	0.0	4.0	0.0
8	-3.27	77.42	19/07/2011	1.5	0.0	1.5	0.0
15	-15.72	70.13	25/07/2011	5.3	0.0	5.3	0.0
16	-13.10	70.40	25/07/2011	2.6	0.0	2.6	0.0
17	-10.25	70.68	25/07/2011	21.7	12.5	9.3	0.0
18	-7.78	71.15	25/07/2011	3.8	1.0	2.9	0.0
19	-6.03	71.05	25/07/2011	12.2	9.8	2.4	0.0
20	-4.17	70.95	26/07/2011	5.2	3.1	2.1	0.0
21	-3.03	70.88	26/07/2011	9.7	0.0	9.7	0.0
22	-1.65	70.80	26/07/2011	1.0	0.0	1.0	0.0
23	0.05	70.73	26/07/2011	3.6	0.0	3.6	0.0
24	0.47	70.68	26/07/2011	3.5	0.0	3.5	0.0
25	2.15	70.58	26/07/2011	17.9	0.0	17.9	0.0
26	4.05	70.47	26/07/2011	71.3	3.1	68.2	0.0
27	7.28	70.28	26/07/2011	12.6	0.8	11.8	0.0
28	8.60	70.20	27/07/2011	65.4	0.4	65.0	0.0
29	10.10	70.12	27/07/2011	35.8	0.4	35.4	0.0
30	11.67	70.02	27/07/2011	0.0	0.0	0.0	0.0
31	13.17	69.93	27/07/2011	8.9	0.0	8.9	0.0
32	14.70	69.83	27/07/2011	6.1	0.4	5.7	0.0

2.2 Synoptic Views of Sea-Surface Temperatures and Sea-Ice Extents

The presented Sea Surface Temperature (SST) maps (Fig. 2) are based on Aqua MODIS 32 days composite, 0.08° resolution satellite grid images, extracted from http://oceancolor.gsfc.nasa.gov/ for fall 2007 (September 22 – October 23, 2007) and summer 2011 (July 4 – August 4, 2011). In order to convert grid raw values to STTs and to extract SST values along the studied transects, spatial analysis and geoprocessing were performed using ArcGIS (Esri Company). SSTs were calculated from the following equation, derived from information stored in Aqua MODIS grids:

$$SST = (V \times 0.0007178) - 2, \text{ (where V represents grid raw values)}$$

Information on sea-ice fraction in the form of 50% sea-ice concentration were taken from daily AVHRR Pathfinder 5.2 satellite images extracted from http://data.nodc.noaa.gov for

October 5, 2007 (night), and July 20, 2011 (day). They are reported as isolines on the SST maps.

Six Conductivity-Temperature-Depth (CTD) profiles, 5 of them collected as part of the 2007 and 2011 cruises using a Seabird 911 Plus CTD and one extracted together with 3 Argo-floats from the Coriolis database (http://www.coriolis.eu.org/), were all included into the present study (Fig. 2; Appendices A and B), as a mean to validate the satellite extracted monthly average SST profiles as well as to provide additional information on the vertical distribution of watermasses and stratification within the top 500 meters of the water column.

3. RESULTS AND DISCUSSION

The remote sensing-derived maps of surface water conditions during the sampling periods highlight strong differences in temperatures between October 2007 and July 2011 across the northern North Atlantic in terms of both mean average values and horizontal gradients (Fig. 2). The observed differences between the two investigated seasons clearly appear in the temporal and spatial distribution of AW masses between July 2011 and October 2007, showing a generally stronger longitudinal dominance of warmer waters towards the west during summer conditions, which can also be identified by a weaker surface expression of the northern North Atlantic cold currents (EGC, JMC, BIC and EIC), compared to the autumn distribution, where surface ArW masses (0-4°C) contribute to an inverse situation (Fig. 1 and 2). Previous findings of a topographical steering of the AF north of the island Jan Mayen (Blindheim et al., 2000), is hence not obvious based on these observations, in fact the zonal maximum distribution of the AF, with the exception of Fram Strait, show a strong seasonal migration towards the east from summer until autumn, a result which might however be an artifact of the stronger influence of solar irradiance during summer conditions on the upper surface layer, directly influencing the satellite imagery. Sea-ice extent, represented here as the 50% sea-ice concentration limit, do not show any obvious geographical shift between the two periods, with the exception of the area around Svalbard where sea-ice occupied most of the western and southern shelf in July 2011 but is virtually absent in fall 2007.

Sea-ice melting, initiated in summer and completed by fall, might, in addition to seasonal changes in solar irradiance (Cokelet et al., 2008), dominating windpatterns and AW flow (Blindheim et al., 2000), to a high extent explain the observed shift from a dominance in July 2011 of warmer AW carried by the NwAC and WSC in the eastern part of the Nordic Seas to prevailing colder surface waters during the fall of 2007. These changes are particularly indicated by a narrowing of the poleward AW tongue west of Svalbard, as well as by a

strengthened influence of the colder water masses carried by the EGC, JMC, BIC and EIC coupled to an increased temperature gradient across the AF and PF between summer and autumn conditions.

3.1 NORTHERN TRANSECTS

The Fram Strait transects display prominent SST and coccolithophore standing stock gradients over a rather narrow area, as well as noticeable differences in SST ranges and coccolithophore assemblages between summer 2011 (SST~1.5-7 °C, *E. huxleyi* dominated peak coccolithophore standing stocks) and autumn 2007 (SST~ -0.5-5 °C, *C. pelagicus* dominated peak coccolithophore standing stocks) (Fig. 3).

3.1.1 Hydrological Setting During the Sampling Periods

Both SST (sea surface temperature) profiles across Fram Strait show an abrupt temperature increase of ca. 2°C around ~10°E, which relates to the location of the AF off western Svalbard (Fig. 3). Saloranta and Svendsen (2001) investigated the AF position immediately west of Svalbard and identified it as a clear topographically steered temperature-salinity front at the shelf break, separating ArW carried by the Sørkapp Current over the shelf from AW (WSC) over the slope. Our fall 2007 CTD profile recovered east of this frontal boundary (Appendix B, CTD 1), also shows AW-type waters with temperatures and salinities in the range of ~4-5°C and ~35, respectively, submerged under a 50m thick surface mixed layer of ArW (~2-3 °C; <34.8). Both transects reach their highest surface temperatures west of ~10°E, as they cross the main path of the WSC-carried AW. The geographic distribution of WSC varies from ~1.5° E in the summer 2011 to ~5° E in the fall 2007 showing the widest extension during summer. The western boundary of surface AW is marked by a ca. 2°C SST decrease, however the boundary is less pronounced than its eastern counterpart over the Svalbard shelf break, representing the AF and the entrance into the EGC-influenced domain (ArW/PW) (Fig. 3). Temperature differences between the two sampling periods in terms of mean values and width of the surface AW, are most probably related to the seasonal changes in solar irradiance (higher in July) and in distribution of meltwater (higher in October), as well as potential changes in the strength of the meridional currents. ArW located west of the AF is characterized by very homogeneous upper surface temperatures of ca. 1-2°C, as well as a deep mixed layer down to 100 m waterdepth (Fig. 3; Appendix B, CTD 2). PW characterized by a highly stratified upper mixed layer (Appendix B, CTD 3) is found during the fall 2007 close to the sea-ice edge within surface waters with SST around 0°C (Fig. 2).

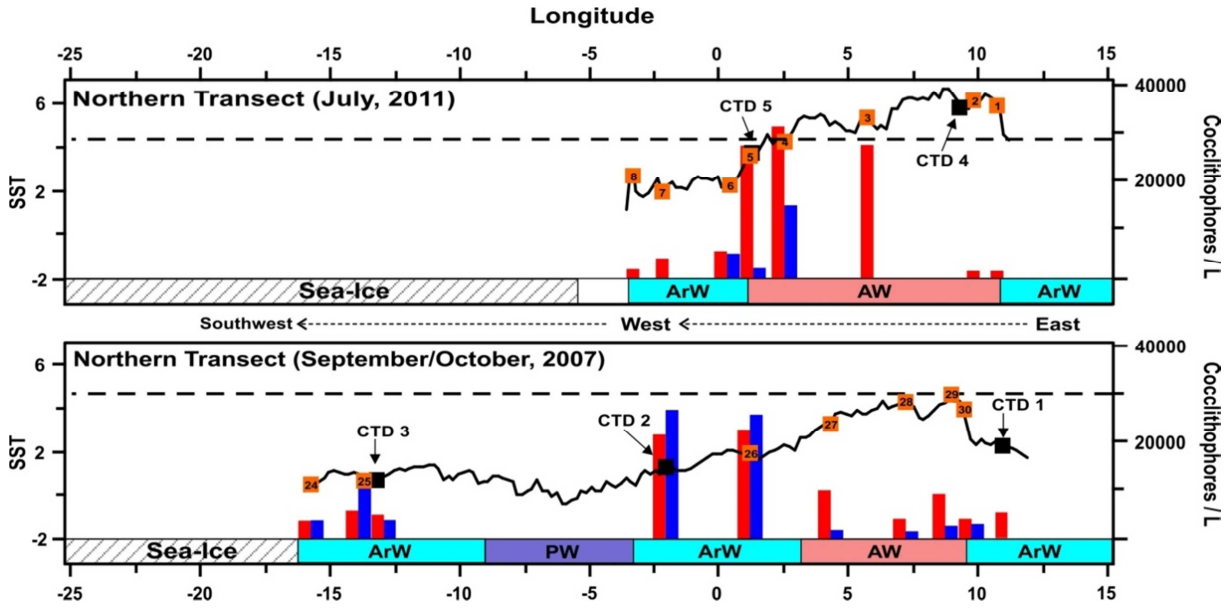

Figure 3: Longitudinal plots of coccolithophore cell densities (coccolithophore standing stock) and SSTs across the Fram Strait transects during July 2011 and October/September 2007. Red bars: *Emiliania huxleyi* coccolithophore standing stocks; blue bars: *Coccolithus pelagicus* coccolithophore standing stocks; black dashed line: maximum temperature of *Coccolithus pelagicus* occurrence observed along the transect; orange boxes: sample locations; black boxes: locations of CTD 1-5; shaded white boxes: sea-ice margin (50% sea-ice concentration); light red bars: surface AW masses; light blue bars: surface ArW masses; purple bars: surface PW masses; dashed arrows: overall transect direction.

3.1.2 Geographic Distribution of Coccolithophores

The coccolithophore standing stocks recorded in the present study across Fram Strait ranges from 1 to 53 $\times 10^3$ cells/l (Fig. 3). The maximum values fall within the range of cell densities from previous observations south of Svalbard, within the influence of the WSC, for the summer and fall-winter seasons (10 to 100 $\times 10^3$ cells/l; Samtleben et al., 1995a).

Peak coccolithophore cell densities occurred on the western edge of the poleward flow of surface AW (Fig. 3), either associated with the AF (July 2011) or within ArW (October 2007). These peak productions are also characterized by a change in dominating species from *E. huxleyi* during the summer period, to *C. pelagicus* during the fall situation. Reduced irradiance from summer until autumn may have had a negative effect on the production of the blooming *E. huxleyi* species (Baumann et al., 2000). Additionally, the differences in the spatial development of the turbulent Frontal Zone between the summer and fall periods, as seen by a reduced distribution of AW in October 2007 compared with July 2011 (Fig. 2 and 3), may also explain this change in coccolithophore assemblage.

C. pelagicus has previously been found to be abundant, if not dominant in ArW (Baumann et al., 2000), hence the onset of the Frontal Zone seems to be surprisingly underrepresented by this species during July 2011. This discrepancy is better explained by the combined

influences, during summer, of enhanced sea-ice melting close to the sea-ice edge, increased importance of AW and higher irradiance, causing strong stratification of the upper photic layer (Appendix B, CTD 4 and 5). This scheme, linked with higher SSTs and a weaker temperature gradient across the Frontal Zone, resulted in *E. huxleyi* dominated coccolithophore assemblages in July 2011 (Fig. 3), in agreement with previous observations (though in more southern latitudes west of the island Jan Mayen) which showed this species as highly successful in ArW close to the PF during summer high production periods (Samtleben and Schröder, 1992; Baumann et al., 2000). The opposite situation, i.e. enhanced mixing of the photic layer and cooler SST within the Frontal Zone area during fall 2007 (Appendix B, CTD 2), a situation associated with a reduced westward influence of surface AW across Fram Strait (Fig. 3), favored the production of the well-mixed and cold water - adapted *C. pelagicus*.

3.2 SOUTHERN TRANSECTS

The Norwegian-Iceland Seas transects display, as expected, markedly higher SSTs (up to 11°C, summer 2011) and coccolithophore standing stocks (up to 72×10^3 cells/l, summer 2011) than the Fram Strait transects. Seasonal differences between July 2011 and October 2007 are limited to an overall SST difference of ca. 1°C, and, more prominently, by a zonal shift in peak *E. huxleyi*-dominated coccolithophore densities (Fig. 4).

3.2.1 Hydrological Setting during the Sampling Periods

Both SST profiles display a pattern of stepwise decrease of SSTs from the NwAC-bathed area off western Norway (~7-11 °C, ~35.1; Fig. 4; Appendix A, Argo 2 and 3) to the EGC-influenced margin off eastern Greenland. The temperature is reduced ca. 2.5 °C twice around 3°W and 17°W, respectively. This show the average locations of the AF and PF. The PF has only been only sampled during fall 2007, when favourable sea-ice conditions allowed the transect to be extended to the eastern Greenland shelf off Scoresby Sund (Fig. 2 and 4). According to van Aken et al. (1995), the AF and PF bounded Frontal Zone (ArW) is here defined as an area of mixed PW and AW fed by the JMC and EIC branches of the EGC and the poleward NwAC (>34.9) (Appendix B, Argo 1 and CTD 6). Surface waters of the Frontal Zone show an AW signature as well as a deep mixed layer during July 2011 (Appendix B, CTD 6), whereas a buoyant, low salinity (<34.8) and highly stratified upper photic layer of PW origin has been found during fall 2007 as a result of mild weather conditions during the

period of sampling (Husum, 2007), as well as eastward spreading of melt waters from the nearby eastern Greenland shelf (Appendix B, Argo 1).

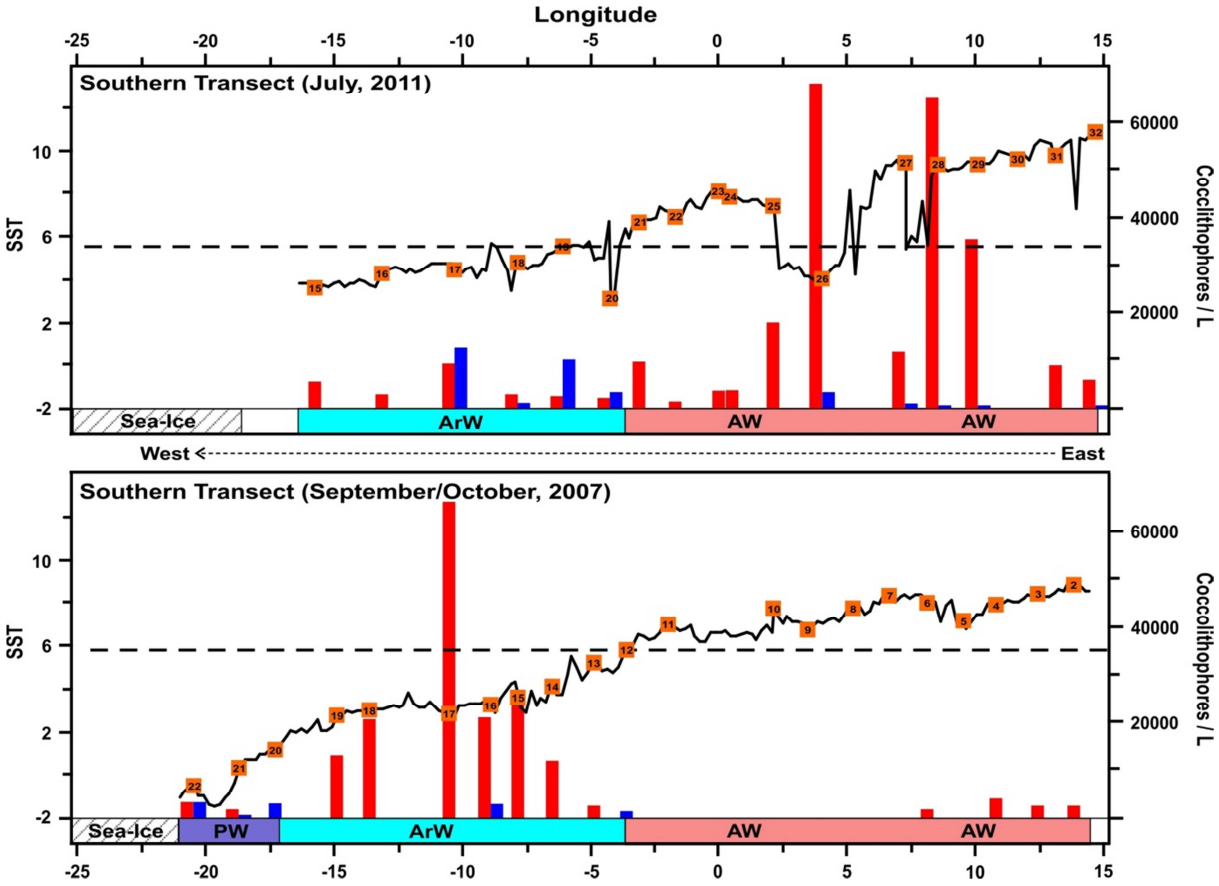

Figure 4: Longitudinal plots of coccolithophore cell densities (coccolithophore standing stocks) and SSTs across the Norwegian-Iceland Seas transects during July 2011 (top) and October/September 2007 (bottom). Red bars: *Emiliania huxleyi* coccolithophore standing stocks; blue bars: *Coccolithus pelagicus* coccolithophore standing stocks; black dashed line: maximum temperature of *Coccolithus pelagicus* occurence observed along the transect; orange boxes: sample locations; shaded white boxes: sea-ice margin (50% sea-ice concentration) ; light red bars: surface AW masses; light blue bars: surface ArW masses; purple bars: surface PW masses; dashed arrows: overall transect direction.

While both transects are characterized by an overall ~2°C SST decrease from east to west across the AW-influenced Norwegian Sea, the July 2011 SST profile displays a low temperature anomaly between ca. 2°E and 8°E with values occasionally as low as 4°C. This is up to ~4°C lower than the surrounding water masses (Fig. 4). The Aqua MODIS image extracted for this period (Fig. 2) suggests that this anomaly is part of the Lofoten Gyre, a semi-permanent feature which is forced by large-scale atmospheric rotational variations effecting the governing wind patterns and the strength of the surface circulations (Jakobsen et al., 2003). The 32 days composite SST Aqua MODIS images representative of spring and fall situations (see database in http://oceancolor.gsfc.nasa.gov/) indicate that the surface water expression of the Lofoton Gyre was observable during 2007 and 2011, but was limited in both

cases to July and August. The Argo record for July 2011 (Appendix B, Argo 3) suggests deep mixing of AW-type waters within this gyre.

3.2.2 Geographic Distribution of Coccolithophores

Our profiles of coccolithophore standing stock values across the Norwegian-Iceland Seas are within the lower range of previously published extant coccolithophore datasets within the Nordic Seas during the summer production period (~3 to 300 $\times 10^3$ cells/l) (Samtleben and Schröder, 1992; Baumann et al., 2000). In addition, the current dataset show and highlight a migration of the peak production (dominated by *E. huxleyi*) toward the west from summer to autumn (Fig. 4).

The coccolithophore peak production area during July 2011 occurs within the Lofoton Gyre system and might be explained by vertical mixing, and hence nutrient enrichment of the upper photic layer. Despite the low abundance the presence of *C. pelagicus* (Fig. 4, sample 26) seems to confirm the particular trophic conditions indicated in the Lofoten Basin during the summer season of 2011 *C. pelagicus* has previously been related to other similar gyre systems south of the Iceland-Scotland Ridge (Tarran et al., 2001).

The Frontal Zone production area is marked by an overall change in species dominance from *C. pelagicus* during summer 2011, when surface waters were affected by deep mixing, to *E. huxleyi* during fall 2007, a period characterized by a highly stratified photic layer.

Both southern transects suggest a maximum boundary temperature of 6°C for the occurence of *C. pelagicus* (Fig. 4), a value which strictly corresponds with earlier suggestions based on the analysis of extant coccolithophore populations across the Norwegian-Greenland Sea (Samtleben and Schröder, 1990). However, our observations in the Fram Strait area also indicate that this upper SST limit becomes somewhat lower (ca. 4°C) in the northermost latitudes (Fig. 3).

4. SUMMARY AND PERSPECTIVES

Although an increased amount of investigations during the recent decades on the distribution of extant coccolithophore populations (e.g. Matthiessen et al., 2001, and references herein) has strongly added to our knowledge of the ecology of this major calcifying species group within the Nordic Seas, our understanding is still hampered by the lack of surface water samples. Phytoplankton samples investigated in the present study were collected en-route using a simple, cost- and time effective method, along two zonal transects perpendicular to the major meridional boundary current systems and hydrological fronts. The combined use of

easily accessible remote sensing images, CTD casts and Argo floats from existing databases, although not sufficient to investigate small-scale physical and biological processes, was found highly relevant for significantly improving our knowledge on the biogeography of the dominant fossilizable coccolithophore species within the northern North Atlantic i.e. *E. huxleyi* and *C. pelagicus*.

Seasonal changes in the distribution and stratification of the main water masses related to sea-ice melts and changes in the drift of Atlantic surface water masses results in an overall westward shift of the peak cocolithophore production areas dominated by the opportunistic *E. huxleyi*. Our datasets across the Norwegian-Iceland Seas confirm previous studies indicating high cell densities in the Vøring Plateau area in July and west of the island Jan Mayen in September-October (Samtleben et al., 1995a). Peak coccolithophore production within the Lofoten gyre in July 2011 was related to increased vertical mixing and nutrient enrichment of the photic layer due to large scale atmospheric changes. In contrast, the change in the dominating species around the island Jan Mayen from *C. pelagicus* in summer to *E. huxleyi* in fall, resulted from a change in stratification from well mixed (summer) to stratified (fall) surface waters. In addition our data are indicative of a strong temperature limitation of *C. pelagicus* production, the maximum boundary value being estimated at 6°C, with a somewhat lower (ca. 4°C) limit in along the northern transects (Fram Strait).
Our dataset obtained in Fram Strait represent to our knowledge a first view of the zonal distribution of extant coccolithophores within this climatically sensitive area during summer and fall. There, seasonal changes in dominance from *E. huxleyi* (summer) to *C. pelagicus* (fall), are related to the combined influence, during summer, of enhanced sea-ice melting close to the sea-ice edge, as well as increased influence of AW and higher irradiance leading to the high production of the opportunitic species *E. huxleyi* within an area usually characterized by *C. pelagicus*-dominated low density populations.

The ongoing intensification of sea-ice melting and sea-ice thinning within the Arctic Ocean, and the associated naturally increased export of ice and melt water to the Nordic Seas (Kwok, 2009), directly results in an overall increased surface water stratification in the western northern North Atlantic (Furevik et al., 2002), a condition which is likely to favor the production of *E. huxleyi*. Remote-sensing investigations already point to the occurence of pervasive blooms of *E. huxleyi* in Arctic to Polar environments such as the Barents Sea

(Smyth et al., 2004) under the influence of increased sea-ice melts and increased inflow of AW, conditions which are equally supposed to characterize the Greenland-Iceland Seas. While the impact of the anthropogenically-forced ocean acidification upon calcifying plankton in polar environments is still debated (Charalampopoulou et al., 2011), ongoing changes in the physico-chemical structure of the surface mixed layer of the northern North Atlantic (stratification, temperature, salinity) might induce regional changes in the structure of the phytoplankton communities with major effects on the carbon cycle as well as the entire food web of the Nordic Seas. Continuing surveys on the distribution of extant coccolithophores, a presumably highly successful group in the presently changing high latitude oceans are therefore of tremendous importance.

Acknowledgements: This work is a contribution to “The Changing Arctic and Subarctic Environment” (CASE) Initial Training Network funded by the European Community's 7th Framework Programme FP7 2007/2013, Marie-Curie Actions, under Grant Agreement No. 238111. Thanks are due to the captain and crew of the R/V "Helmer Hanssen’’ and S. Iversen for CTD collections. Some of the material used in this study was collected as part of the IPY project n°786 “Arctic Ocean Warming in the past” (WARMPAST).

REFERENCES

Andersson, M., Orvik, K. A., La Casce, J. H., Koszalka, I., and Mauritzen, C.: Variability of the Norwegian Atlantic Current and associated eddy fields from surface drifters, J. Geophys. Res., 116, C08032, doi: 10.1029/2011JC007078, 2011.

Andruleit, H.: Coccolithophore fluxes in the Norwegian-Greenland Sea: seasonality and assemblage alterations, Mar. Micropaleontol., 31, 45-64, 1997.

Balestra, B., Ziveri, P., Monechi, S., and Troelstra, S.: Coccolithophorids from the Southeast Greenland Margin (Northern North Atlantic): Production, ecology and the surface sediment record, Mar. Micropaleontol., 50, 23-34, 2004.

Baumann, K.-H., Andruleit, H. A., and Samtleben, C.: Coccolithophores in the Nordic Seas: comparison of living communities with surface sediment assemblages, Deep-Sea Res. II, 47, 1743-1772, 2000.

Beaufort, L., and Heussner, S.: Seasonal dynamics of calcerous nannoplankton on a West European continental margin: the Bay of Biscay, Mar. Micropaleontol., 43, 27-55, 2001.

Blindheim, J., Borovkov, V., Hansen, B., Malmberg, S. Aa., Turrell, W. R., and Østerhus, S.: Upper layer cooling and freshening in the Norwegian Sea in relation to atmospheric forcing, Deep-Sea Res. I, 47, 655-680, 2000.

Blindheim, J., and Østerhus, S.: The Nordic Seas main oceanographic features. In: Drange, H., Dokken, T., Furevik, T., Gerdes, R., and Berger, W. (Eds.), The Nordic Seas: an integrated perspective, Geoph. Monog. Series, 158, 11-37, 2005.

Burenkov, V. I., Kopelevich, O. V., Rat'kova, T. N., and Sheberstov, S. V.: Satellite Observations of the coccolithophorid bloom of the Barents Sea, Oceanology, 51, 766-774, 2011.

Cachão, M., and Moita, M. T.: Coccolithus pelagicus, a productivity proxy related to moderate fronts off Western Iberia, Mar. Micropaleontol., 39, 131-155, 2000.

Cokelet, E. D., Tervalon, N., and Bellingham, J. G.: Hydrography of the West Spitsbergen Current, Svalbard branch: Autumn 2001, J. Geophys. Res., 113, C01006, doi: 10.1029/2007JC004150, 2008.

Dmitrenko, O. B., Lukashin, V. N., and Shevchenko, V. P.: Nannoplankton of the Atlantic Ocean from sediment trap samples, Oceanology, 46, 33-49, 2006.

Dmitrenko, I. A., Kirillov, S. A., Tremblay, L. B., Bauch, D., Hölemann, J. A., Krumpen, T. H., Kassens, Wegner, C., Heinemann, G., and Schröder, D.: Impact of the Arctic Ocean Atlantic water layer on Siberian shelf hydrography, J. Geophys. Res., 115, C08010, doi:10.1029/2009JC006020, 2010.

Furevik, T., Bentsen, M., Drange, H., Johannessen, J. A., and Korablev, A.: Temporal and spatial variability of the sea surface salinity in the Nordic Seas, J. Geophys. Res., 107 (C12), 8009, doi:10.1029/2001JC001118, 2002.

Furevik, T., Mauritzen, C., and Ingvaldsen, R.: The flow of Atlantic Water to the Nordic Seas and Arctic Ocean, In: Arctic - Alpine Ecosystems and People in a Changing Environment, Ørbæk, J. B., Kallenborn, R., Tombre, I., Hegseth, E. N., Petersen, S. F., and Hoel, A. H. (Eds.), Springer Verlag, 123-146, 2007.

Giraudeau, J., Monteiro, P. S., and Nikodemus, K.: Distribution and malformation of living coccolithophores in the northern Benguela upwelling system off Namibia, Mar. Micropaleontol., 22, 93-110, 1993.

Giraudeau, J., Jennings, A. E., and Andrews, J. T.: Timing and mechanisms of surface and intermediate water circulation changes in the Nordic Seas over the last 10000 cal. years: a view from the North Iceland shelf, Quaternary Sci. Rev., 23, 2127-2139, 2004.

Giraudeau, J., Grelaud, M., Solignac, S., Andrews , J. T., Moros, M., and Jansen, E.: Millenial-scale variability in Atlantic water advection to the Nordic Seas derived from Holocene coccolith concentration records, Quaternary Sci. Rev., 29, 1276-1287, 2010.

Hansen, B., and Østerhus, S.: North-Atlantic-Nordic Seas exchanges, Prog. Oceanogr., 45, 109-208, 2000.

Hatun, H., Sando, A. B., Drange, H., Hansen, B., and Valdimarsson, H.: Influence of the Atlantic subpolar gyre on the thermocline circulation, Science, 309, 1841-1844, 2005.

Hegseth. E. N., and Sundfjord, A.: Intrusion and blooming of Atlantic phytoplankton species in the high Arctic, J. Mar. Systems, 74, 108-119, 2008.

Hunt, G. L., Jr., Stabeno, P., Walters, G., Sinclair, E., Brodeur, R. D., Napp, J. M., and Bond, N. A.: Climate change and control of the southeastern Bering Sea pelagic ecosystem, Deep-Sea Res. II, 49, 5821-5853, 2002.

Hunt, G. L. Jr., and Drinkwater, K. F., (Eds.): Ecosystem Studies of Sub-Arctic Seas (ESSAS), Science Plan. GLOBEC Report No.19, VIII, 60pp, 2005.

IPCC 2007: Summary for policymakers. In: Solomon S., Qin, D., Manning, M., Chen, Z., Marquis, M., Averyt, K. B., Tignor, M., and Miller, H. L. (Eds.): Climate change 2007: the physical science basis. Contribution of working group I to the Fourth Assessment Report of the Intergovernmental Panel on Climate Change, Cambridge Univ. Press, Cambridge, UK and New York, NY, USA, 2007.

Jakobsen, P. K., Ribergaard, M. H., Quadfasel, D., Schmith, T., and Hughes, C. W.: Near-surface circulation in the northern North Atlantic as inferred from Lagrangian drifters: Variability from the mesoscale to interannual, J. Geophys. Res., 108, C83251, doi : 10.1029/2002JC001554, 2003.

Johannessen, O. M.: Brief review of the physical oceanography, in The Nordic Seas, edited by Hurdle B. G., Springer-Verlag, New York, 103-128, 1986.

Husum, K.: Cruise report, SciencePub UiT/WARMPAST, Marine geological cruise to East Greenland Margin, 31 pp, 2007.

Koszalka, I., LaCasce, J. H., Orvik, K. A., and Mauritzen, C.: Surface circulation in the Nordic Seas from clustered drifters, Deep-Sea Res. I, 58, 468-485, 2011.

Kwok, R.: Outflow of Arctic Ocean Sea Ice into the Greenland and Barents Seas: 1979–2007, J. Climate, 22, 2438-2457, 2009.

Matthiessen, J., Baumann, K.-H., Schröder-Ritzrau, A., Hass, C., Andruleit, H., Baumann, A., Jensen, S., Kohly, A., Pflaumann, U., Samtleben, C., Schäfer, P., and Thiede, J.: Distribution of calcareous, siliceous and organic-walled planktic microfossils in surface sediments of the Nordic Seas and their relation to surface-water masses, In: The northern North Atlantic: a changing environment, Schäfer, P., Ritzrau, W., Schlüter, M., and Thiede, J. (Eds.), Springer-Verlag, Berlin, 105-127, 2001.

Olsson, K. A., Jeansson, E., Tanhua, T., and Gascard, J.- C.: The East Greenland Current studied with CFCs and released sulphur hexafluoride, J. Marine Syst., 55, 77-95, 2005.

Orvik, K. A., and Niiler, P.: Major pathways of Atlantic water in the northern North Atlantic and Nordic Seas toward Arctic, Geophys. Res. L., 29, doi:10.1029/2002GL015002, 2002.

Parkinson, C. L., Cavalieri, D. J., Gloersen, P., and Zwally, H. J.: Arctic sea ice extents, areas and trends, 1978–1996, J. Geophys. Res.-Oceans, 104, 20837–20856, 1999.

Poulain, P. M., Warn-Varnas, A., and Niiler, P. P.: Near-surface circulation of the Nordic Seas as measured by Lagrangian drifters, J. Geophys. Res., 101, 18237– 18258, 1996.

Saloranta, T. M., and Svendsen, H.: Across the Arctic front west of Spitsbergen: high-resolution CTD sections from 1998-2000, Polar Res., 20, 177-184, 2001.

Samtleben, C., Schaefer, P., Andraluit, H., Baumann, A., Baumann, K.-H., Kohly, A., Matthiessen, J., and Schroeder-Ritzrau, A.: Plankton in the Norwegian-Greenland Sea: from living communities to sediment assemblages an actualistic approach, Geol. Rundsch, 84, 108-136, 1995a.

Samtleben, C., Baumann, K.-H., and Schröder-Ritzrau, A.: Distribution, composition and seasonal variation of coccolithophore communities in the nortern North Atlantic, 5th Conference in Salmanca Proceedings, edited by Flores, J. A., and Sierro, F. J., 219-235, Salamanca, 1995b.

Samtleben, C., and Bickert, T.: Coccoliths in sediment traps from the Norwegian Sea, Mar. Micropaleontol., 16, 39-64, 1990.

Samtleben, C., and Schröder, A.: Coccolithophoriden-Gemeinschaften und Coccolithen-Sedimentation im Europäischen Nordmeer. Zur Abbildung von Planktonzönosen im sediment. Ber Sonderforschungsbereich, Univ. Kiel, 313, 25, 1-52, 1990.

Samtleben, C., and Schröder, A.: Living cocolithophore communities in the Norwegian-Greenland Sea and their record in sediments, Mar. Micropaleontol., 19, 333-354, 1992.

Schröder-Ritzrau, A., Andruleit, H., Jensen, S., Samtleben, C., Schäfer, P., Matthiessen, J., Hass, H. C., Kohly, A., Thiede, J.: Distribution, export and alteration of fossilizable plankton

in the Nordic Seas. In: Schäfer, P., Ritzrau, W., Schlüter, M., and Thiede, J. (Eds.): The Northern North Atlantic: A Changing Environment. Springer, Berlin, 81–104, 2001.

Smyth, T. J., Tyrell, T., and Tarrant, B.: Time series of coccolithophore activity in the Barents Sea, from twenty years of satellite imagery, Geophys. Res. L., 31, L11302, doi:10.1029/2004GL019735, 2004.

Solignac, S., de Vernal, A., and, Giraudeau, J.: Comparison of coccolith and dinocyst assemblages in the northern North Atlantic: How well do they relate with surface hydrography?, Mar. Micropaleontol., 68, 115-135, 2008.

Swift, J. H.: The Arctic Waters. In: Hurdle, B.G. (Eds.): The Nordic Seas, Springer, New York, 129-153, 1986.

Tarran, G. A., Zubkov, M. V., Sleigh, M. A., Burkill, P. H., and Yallop, M.: Microbial community structure and standing stocks in the NE Atlantic in June and July of 1996, Deep-Sea Res. II, 48, 963–985, 2001.

Tyrrell T, and Merico A.: Emiliania huxleyi: bloom observations and the conditions that induce them. In: Thierstein HR, Young JR (eds) Coccolithophores - from Molecular Processes to Global Impact. Springer-Verlag, Berlin, 75-97, 2004.

Van Aken, H. M., Budeus, G., and Hähnel, M.: The anatomy of the Arctic Frontal Zone in the Greenland Sea, J. Geophys. Res., 100, 15999–16014, 1995.

Wassmann, P., Peinert, R., and Smetacek, V.: Patterns of production and sedimentation in the Norwegian coastal zone, the Barents Sea and the Norwegian Sea. In: Wassmann P., Heiskanen A.-S., Lindahl, O. (eds): Sediment trap studies in the Nordic Countries (Symposium Proceedings). Nurmi Print Oy, Nurmijärvi, 137-156, 1991.

Wassmann, P., Reigstad, M., Haug, T., Rudels, B., Carroll, M. L., Hop, H., Gabrielsen, G. W., Falk-Petersen, S., Denisenko, S. G., Arashkevich, E., Slagstad, D., and Pavlova, O.: Food webs and carbon flux in the Barents Sea, Prog. Oceanogr., 71, 232-287, 2006.

Westbroek, P., Brown, C. W., van Bleijswijk, J., Brownlee, C., Brummer, G. J., Conte, M., Egge, J., Fernandez, E., Jordan, R., Knappertsbusch, M., Stefels, J., Veldhuis, M., van der Wal, P., and Young, J.: A model system approach to biological climate forcing. The example of *Emiliania huxleyi*, Global and Planetary Change, 8, 27-46, 1993.

Appendix A

List of CTD casts and Argo Stations used in the present study, with collection dates, locations and water depths

.

Station Nr.	Location	Station	Date	Latitude	Longitude	Water Depth (m)
CTD 1	Fram Strait	# 424	12/10/2007	78 13.84 N	11 00.57 E	340
CTD 2	Fram Strait	# 421	11/10/2007	77 28.61 N	02 02.54 W	3029
CTD 3	Fram Strait	# 417	08/10/2007	73 46.14 N	13 00.60 W	2570
CTD 4	Fram Strait	# 306	16/07/2011	77 36.05 N	09 53.30 E	1381
CTD 5	Fram Strait	# 309	18/07/2011	78 13.98 N	01 36.07 E	1707
CTD 6	Norwegian-Iceland Sea	# 249 (ship 10)	15/07/2011	69 92.98 N	08 70.63 W	717.4
Argo 1	Norwegian-Iceland Sea	# 134	26/09/2007	69 34.90 N	11 51.00 W	1273.9
Argo 2	Norwegian-Iceland Sea	# 6	02/10/2007	71 16.40 N	05 88.00 E	> 1963.4
Argo 3	Norwegian-Iceland Sea	# 39	26/07/2011	70 58.30 N	02 72.60 E	>1976.3

Appendix B

CTD and ARGO profiles (see Fig. 2 and Appendix A for locations) showing temperatures (°C) and salinities within the top 500 meters of the water column. NT, Northern transect; ST, Southern Transect.

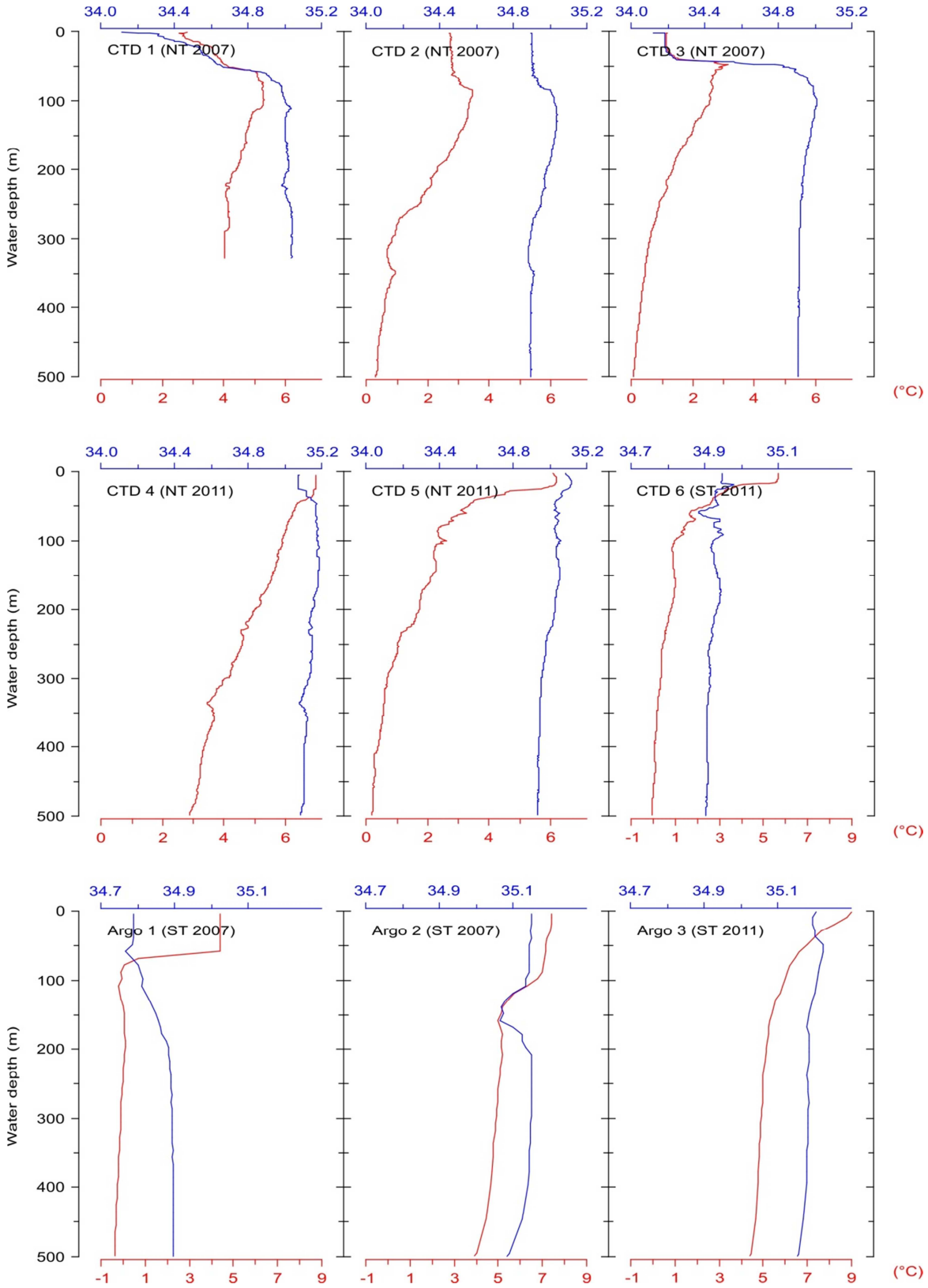

2.5 Generalities on Dinocyst Morphology, Biology, Ecology and Sediment Distribution within the North Atlantic Region.

Dinocysts, the fossil remains of cyst-forming dinoflagellates, are the second major proxy applied in the present study. Dinoflagellates are eukaryotic, unicellular organisms and considered as an important primary producer in the world oceans (Marret and Zonneveld, 2003). In contrast to the strictly marine autotrophic coccolithophores, dinoflagellates include a large variety of feeding strategies (photosyntheses, grazers, predators, parasites and symbionts) and are found within the surface waters of almost all aquatic environments, from strictly marine to fresh water lakes and even within sea ice (Edwards, 1993; Marret and Zonneveld, 2003; Matthiessen et al., 2005).

Dinocysts' large resistance to dissolution and their high diversity within polar regions together with their potential for quantitative estimates of key sea-surface parameters, such as temperature, salinity and sea-ice cover duration through transfer functions, motivated their use for paleoclimate reconstructions in the present research thesis.

2.5.1 The Morphology of Dinoflagellates

Dinoflagellates are found in the size range between 7 and 2000 µm, although most forms are less than 200 µm (20-150 µm). They take their name from the Greek word 'dinos' meaning "whirling", based on their characteristic flagella, which propel them around in a spiral motion. This movement results from the motion of two flagella: a transverse flagellum, which encircles the body in the depression of the cingulum, and a longitudinal flagellum, which extends in the opposite direction of movement, from the mid ventral area (sulcus), towards the apex (Fig. 2.12) (Edwards, 1993). The cell is divided by the cingulum into the anterior epitheca and the posterior hypotheca. The anterior end is called the apex and the posterior is called the antapex. The roughly perpendicular second depression to the cingulum is the sulcus, dividing the cell into left and right halves (Fig. 2.12).

Many dinoflagellates have a theca that is constructed of thin cellulosic pieces called plates that fit together along linear sutures (Fig. 2.12). This arrangement of the plates is commonly known as tabulation and is a valuable tool for identification (Edwards, 1993). Another distinctive and very important identification feature in fossil dinocysts is the archeopyle, the opening in the cyst wall through which the cytoplasm emerges during excystment. The position and nature of the archeopyle is genetically determined and covered by the "operculum" (consisting of either a single plate piece or several plates) (Edwards, 1993). The

processes appear between the theca and the main body of the cyst and can have varying shapes and forms, i.e. spikes or spines (Fig. 2.13). Processes that occur at the intersection of three (or more) paraplates are gonal. The ones that occur along paraplate boundaries away from the triple junctions are named intergonal (Edwards, 1993). The presence of a tabulation pattern is the determining feature separating dinocysts from other palynomorphs, such as acritarchs, and can be expressed in various ways through different types of ornamentation (ridges along plate boundaries, position of spines or processes, etc.) or the shape of the archeopyle (Evitt, 1985).

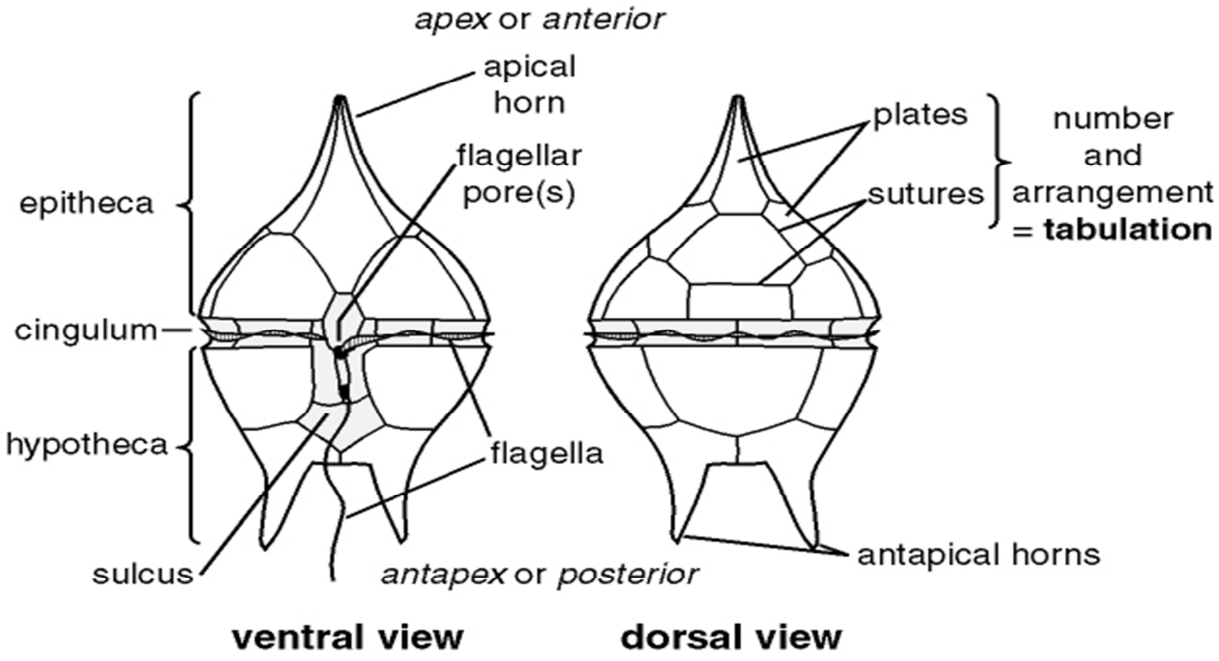

Figure 2.12: Schematic view of the theca of a peridinialean dinoflagellate. Adapted from Edwards et al. (1993), and references therein.

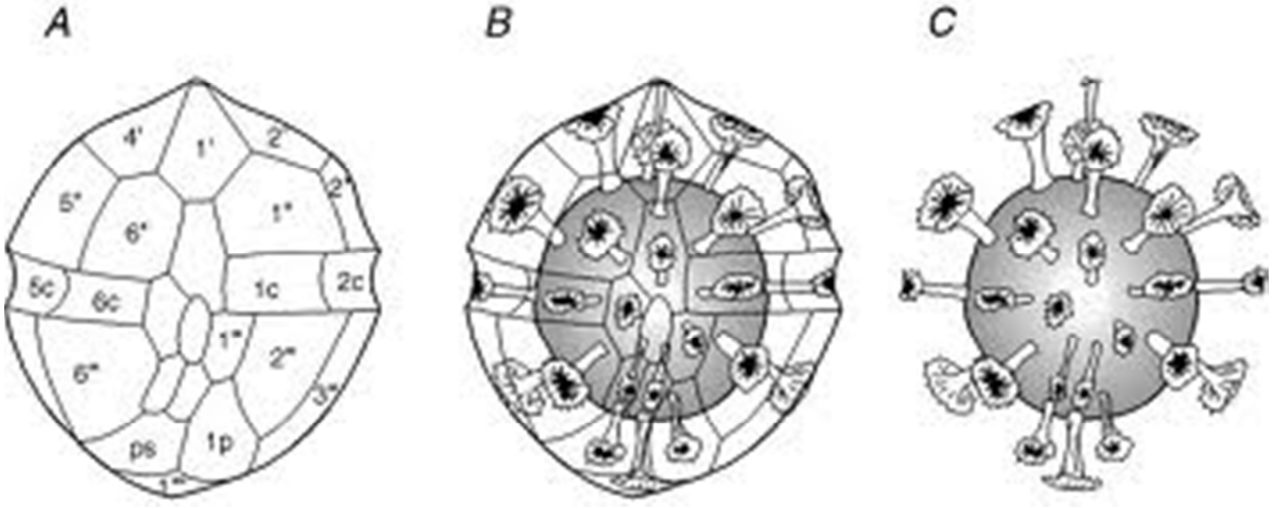

Figure 2.13: (A) A central view of theca showing tabulation; (B) Cyst forming inside theca; (C) Cyst paratabulation reflecting thecal tabulation. Adapted from Edwards et al. (1993), and references therein.

2.5.2 A short Introduction to Dinoflagellate Biology

Dinoflagellates contain typical eukaryotic organelles in the cytoplasm: smooth and rough endoplasmic reticulum, golgi apparatus, mitochondria, lipid and starch grains, and various accumulation bodies such as vacuoles. In addition, they may also contain any of several cytoplasmic inclusions or organelles (Edwards, 1993). The peduncle is a retractable protoplasmic extension, which may play a role in the attachment of the organism to a substrate or a host. The pusule consists of a series of membrane-bound tubules of uncertain function among which nutrition, waste, flotation, and/or osmoregulation have been suggested. The cytoplasm of photosynthetic dinoflagellates contains chloroplasts, and the nucleus is bounded by a nuclear membrane. The dinoflagellate nucleus is rather large in proportion to the cytoplasm (Edwards, 1993).

About half of the known dinoflagellate species are autotrophic and produce organic compounds by photosynthesis. The rest are non-photosynthetic with a heterotrophic, mixotrophic, parasitic, or other more complex nutritional and survival strategy (e.g. Gainesand and Elbrächter, 1987; Schnepf and Elbrächter, 1992; Smayda and Reynolds, 2003).

The vegetative, motile stage of dinoflagellates is often haploid. The life-cycle has many variations between the members of this group, but the following describes a basic pattern: haploid vegetative cells become or produce gametes, gametes fuse and a zygote forms (the zygote often has two long longitudinal flagella). While the zygote enlarges, its walls may thicken and it loses its motility; this stage is called the hypnozygote (Fig. 2.14), which, in palaeontological studies, is usually referred to as a “dinoflagellate cyst” or “dinocyst” embedded in a very resistant, sporopollenine-like organic compounds (Fensome et al., 1993; Head, 1996; Versteegh and Blokker, 2004). As the cyst becomes part of the sediment, the thecal plates break apart or are destroyed. After a period of dormancy (from hours to years), during which the first and sometimes the second meiotic cell divisions occur, the cell or cells emerge(s) through an opening determined by predeveloped structural weakness, the archeopyle. The new cells rapidly form new thecae, and the cycle continues (Fig. 2.14) (Edwards, 1993).

In culture, sexual reproduction can be induced by nutrient depletion, temperature reduction or light reduction. In nature, the triggers are likely to be far more complex. Depending on the species, germination usually occurs between late winter and spring, presumably triggered by extreme environmental conditions. The formation of a hypnozygote (i.e. dinocyst) appears to

be a survival strategy to get through winter and can act as a quick response to environmental stress or as a seed bank for new dinoflagellate populations (Dale, 1983).

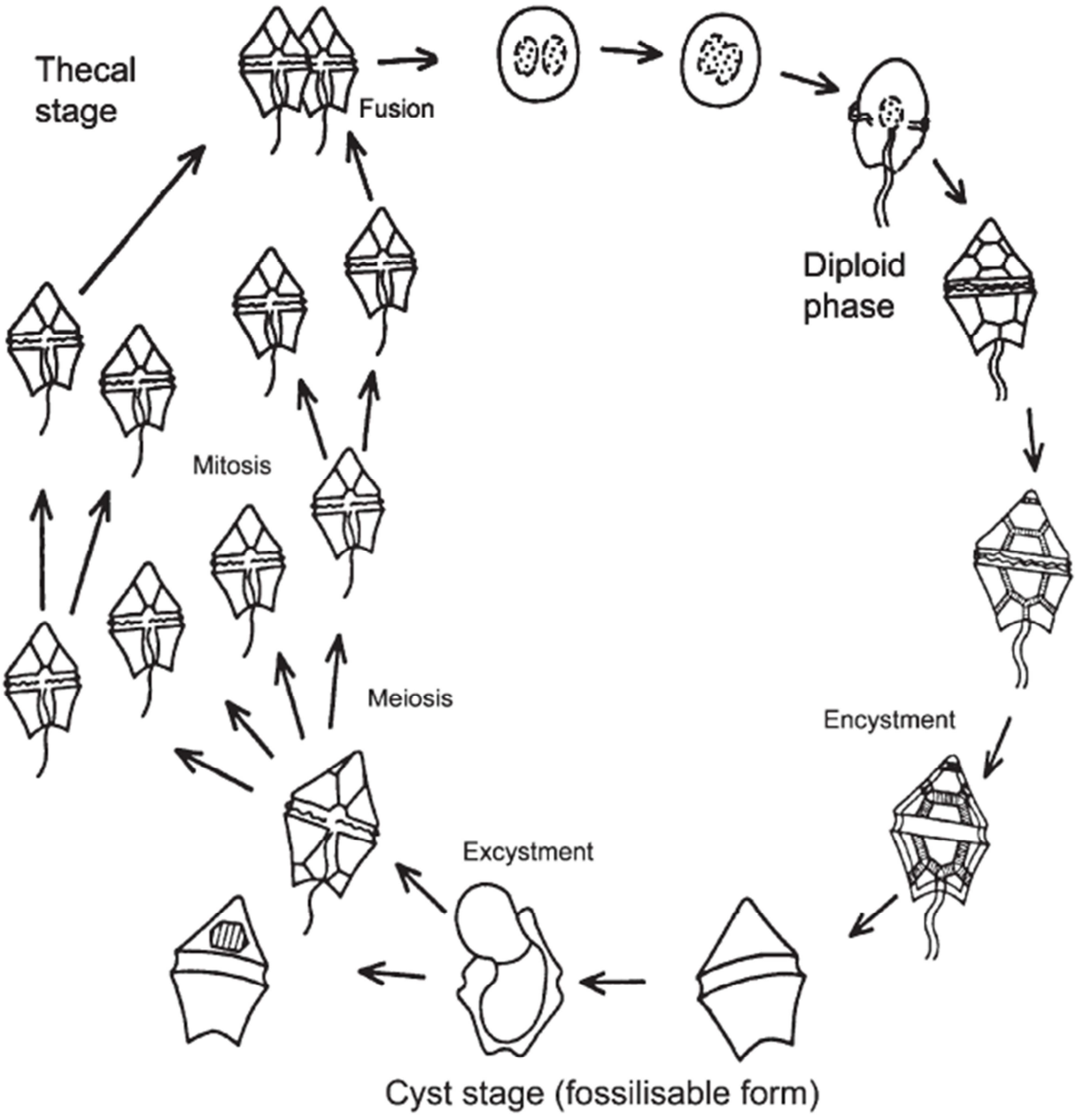

Figure 2.14 : Diagram of the life cycle of a dinoflagellate showing the alternation of the motile stage (cannot be fossilized) and the cyst stage (yielding fossil remains). Schematic life-cycle of a cyst producing dinoflagellate. Asexual reproduction predominates and involves a division of the cell into two halves. Sexual reproduction is known in very few dinoflagellates. Cysts form in the autumn with decreasing temperatures, remaining dormant on the sea floor through the winter. With the amelioration of conditions in spring, the motile stage excysts through the archaeopyle. Before developing any armour, however, the new dinoflagellate must pass through a naked gymnodinioid stage. Adapted from de Vernal and Marret (2007).

The dinocysts, as most of the other known micropaleontological proxies, do not represent the initial living assemblages but only a snapshot (10-15 %) of the initial community, increasing the need to fully understand the ecology of the main dinocyst producing species.

2.5.3 Ecology of the Dominant Dinocysts Species within the Nordic Seas.

The distribution of dinocyst species in modern sediments is strongly related to the biological, physical, and chemical conditions prevailing in the surface water masses and in the sediment. The distributional pattern of fossil dinocysts in sediment samples is, therefore, commonly used to reconstruct past changes in the upper water mass conditions, e.g. eutrophication, salinity, temperature, turbulence, sea-ice extent and nutrients (Dale, 1996; Zonneveld et al., 2013). Such a strategy necessitates detailed information on the relationships between modern oceanic dynamics, environmental conditions and the geographic distribution of cysts in sediments (Zonneveld et al., 2013).

The first worldwide data-set of organic-walled dinoflagellate cyst distribution was published in 2003 in the modern dinocyst atlas by Marret and Zonneveld (2003) and has since been extensively updated with additional data from all over the world (Zonneveld et al., 2013). This new database, together with earlier dinocyst surface sediment studies conducted within the Nordic Seas and adjacent areas, creates a strong basis for the understanding of dinoflagellate ecology and cyst distribution within the present study areas (e.g., Wall et al., 1977; Mudie, 1992; Matthiessen, 1995; Matthiessen et al., 2001, 2005; Dale, 1996; de Vernal et al., 1997, 2001, 2005; Rochon et al., 1999; Harland and Pudsey, 1999; Zonneveld and Brummer, 2000; Devillers and de Vernal, 2000; Head, 1996; Head et al., 2001; Marret and Zonneveld, 2003; Marret et al., 2004; Radi and de Vernal, 2008; Grøsfjeld et al., 2009; Solignac et al., 2009; Zonneveld et al., 2013).
The following is an overview of the ecology and distribution of the most common dinocysts (including one acritarch) species within our studied area (maps of surface sediment distribution follows the species descriptions). Species are listed in alphabetic order, with species names followed by the abbrevations applied within the following chapter figures. All identified species are listed in Appendix 3.

Brigantedinium spp. (BSPP)

Brigantedinium spp. includes the species *B. simplex* and *B. cariacoense* and all spineless, round brown cysts that cannot be determined on species level because of bad preservation or

unfavorable orientation. Since made of a large number of species, this group is distributed within a wide range of sea-surface temperatures (from -2,1 °C during winter to 29,6 °C during summer) and salinities (17 during spring to 36,8 during summer) (Marret and Zonneveld,

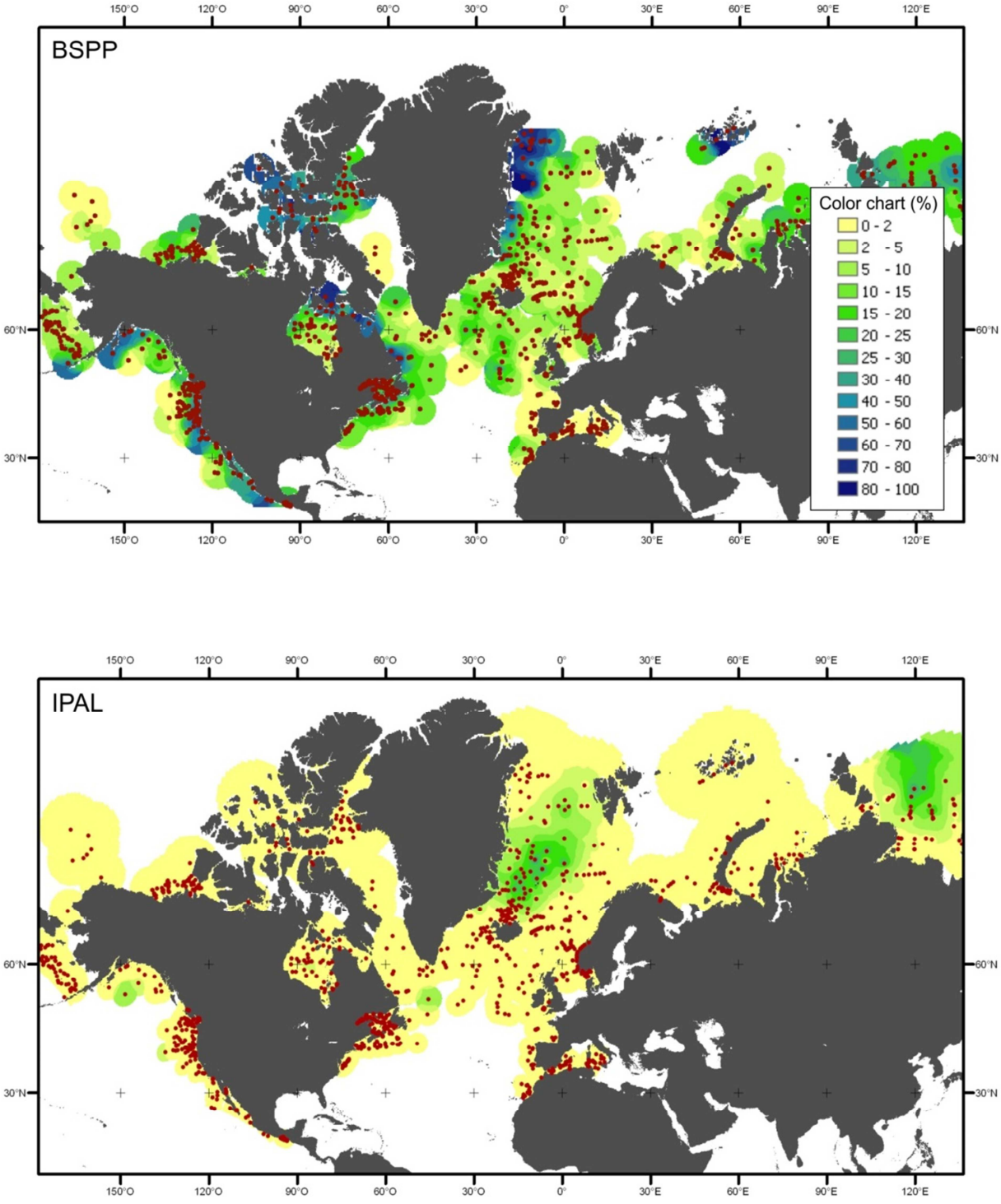

Figure 2.15 : Geographic surface sediment distribution of BSPP and IPAL in the Nordic Seas, based on the 1189 surface sediment database for the North Atlantic and North-Eastern Pacific

2003). Representatives of this cosmopolitan dinocyst group are produced by heterotrophic dinoflagellates. Their occurrence is, therefore, largely dependent on the availability of food, such as diatoms (Marret and Zonneveld, 2003; Zonneveld et al., 2013). They can effectively cope with prolonged periods of sea ice cover (up to 12 months) and are particularly abundant in regions of high productivity, such as upwelling areas and sea-ice margins, and can dominate from coastal to oceanic conditions (e.g. Wall et al., 1977; de Vernal et al., 1997, 2001; Harland and Pudsey, 1999; Zonneveld and Brummer, 2000; Radi and de Vernal, 2008; Zonneveld et al., 2013). *Brigantedinium* spp. is rare to common in surface sediments from the Norwegian Sea, the central Iceland and Greenland Seas and and the Barents Sea (Matthiessen, 1995, and references therein), although its low abundance in surface sediments of the Norwegian Sea has been assumed as due to enhanced degradation in sediments (Matthiessen, 1995).

Impagidinium pallidum (IPAL)

I. pallidum is autotrophic and has a bipolar distribution, which in the NH is restricted to regions north of 45°N. In the North Atlantic, it shows the highest occurrences in surface sediments at the center of the Iceland and Greenland Seas (Matthiessen, 1995; Rochon et al., 1999; Marret and Zonneveld, 2003; Marret et al., 2004; Grøsfjeld et al., 2009). This species rarely contributes more than 1.5% of the total dinocyst assemblages in sediments of the Norwegian Sea, the eastern Fram Strait and the east Greenland shelf (Matthiessen, 1995), corresponding well with a suggested sea-surface temperature optimum for this species of less than ~5 °C (Marret and Zonneveld, 2003). The reported salinity range is rather broad (21.3-36.4) but shows an optimum at 34 (Marret and Zonneveld, 2003; Zonneveld et al., 2013). *I. pallidum* has been reported in regions with sea-ice cover up to 12 months and is generally regarded as a polar oceanic species (de Vernal et al., 2001; Zonneveld et al., 2013).

Islandinium minutum (IMIN)

I. minutum has a bipolar distribution and has been recognized north of 30 °N in the NH, below surface waters with rather broad temperature (-2,1 – 27 °C) and salinity (21,3 - 35,3) ranges. This species, however preferentially thrives in surface water masses with temperatures below 5-7 °C (Head et al., 2001; Marret and Zonneveld, 2003; Zonneveld et al., 2013). Usually, the species is associated with polar to sub-polar environments and it has been suggested that the species is related to ArW masses (Rochon et al., 1999; de Vernal et al.,

2001; Marret and Zonneveld, 2003; Grøsfjeld et al., 2009). *I. minutum* is produced by heterotrophic dinoflagellates, is commonly found in shelf and slope sediments at the eastern margin of Canada, west of Svalbard and close to Greenland (Fig. 2.15), and has its largest

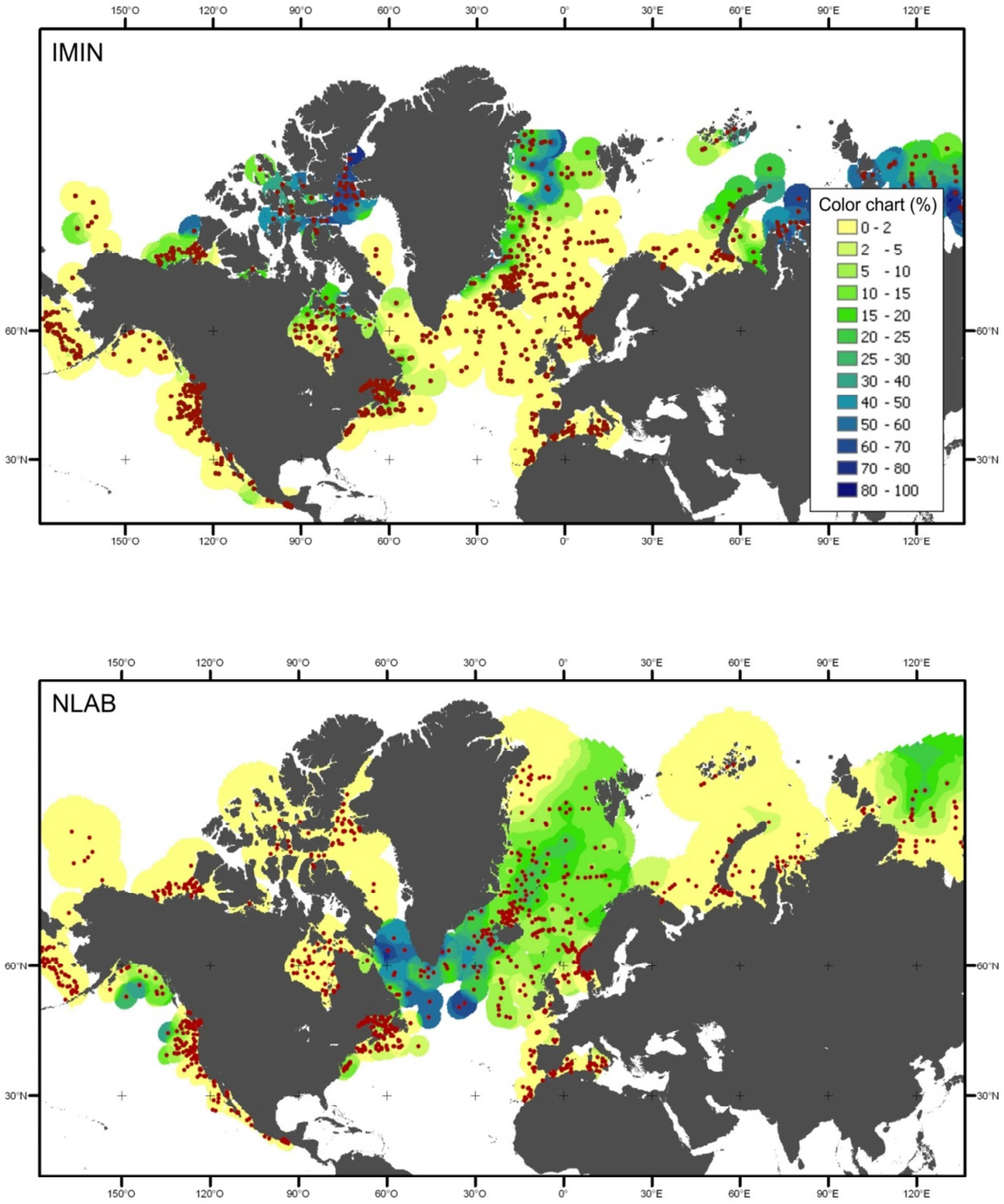

Figure 2.16 : Geographic surface sediment distribution of IMIN and NLAB in the Nordic Seas, based on the 1189 surface sediment database for the North Atlantic and North-Eastern Pacific

abundances (estimated to more than 35%) in areas with sea-ice cover (positive correlation with sea ice duration) during 8-12 months of the year (Matthiessen, 1995; de Vernal et al.,

1997; Rochon et al., 1999; Head et al., 2001; Radi and de Vernal, 2008; Grøsfjeld et al., 2009; Zonneveld et al., 2013).

Nematosphaeropsis labyrinthus (NLAB)

This autotrophic opportunistic cosmopolitan species has been well recorded on the NH within a broad range of surface water conditions (-2.1 to 29.6°C, 16.1 to 26.8) and has been found to occur in high relative abundances in both coastal and oceanic sites (Matthiessen, 1995; Marret and Zonneveld, 2003), with a preference for deep ocean basins (Wall et al., 1977; Matthiessen, 1995, and references therein; Zonneveld et al., 2013). In the North Atlantic, *N. labyrinthus* is found in the highest abundances in the central Greenland and Iceland Seas with decreased abundances in the Norwegian and Barents Sea (Fig. 2.15) (Matthiessen, 1995, and references therein). *N. labyrinthus* has been shown to anti-correlate with the duration of sea-ice cover and show a positive relation with February nutrient content and productivity in the northern North Atlantic (de Vernal et al., 1997; Devillers and de Vernal, 2000; Radi and de Vernal, 2008). The species has been related to oligotrophic environments within the northern North Atlantic (Devillers and de Vernal, 2000).

Operculodinium centrocarpum (OCEN)

O. centrocarpum is autotrophic and is considered as a cosmopolitan opportunistic species. Its ability to adapt quickly to changing or unstable environments explains its overall wide distribution and its tolerance to a wide range of sea-surface temperatures (-2.1 °C-29.6 °C) and salinities (16.1-36.8) (Dale, 1996, 1999; Rochon et al., 1999; de Vernal et al., 2001; Marret and Zonneveld, 2003; Grøsfjeld et al., 2009). The highest relative abundances of this species are found in regions with cold/temperate and nutrient rich surface water masses, e.g. the North Atlantic Drift in the North Atlantic Oceans (up to 91%) (Fig. 2.15) (Matthiessen, 1995; Rochon et al., 1999; Marret and Zonneveld, 2003; Zonneveld et al., 2013). *O. centrocarpum* dominates dinocyst assemblages in surface sediment of the Norwegian Sea (abundances up to 87%) and the Barents Sea, and shows an overall abundance decrease towards the Greenland-Iceland Seas (Matthiessen, 1995). This species is found from coastal to fully oceanic domains but with markedly lower abundances in coastal areas (Wall et al., 1977; Zonneveld et al., 2013). A negative relationship was found between the relative abundances of *O. centrocarpum* and sea-ice cover (Radi and de Vernal, 2008). *O.*

centrocarpum might occur in high abundances in areas affected by reduced surface salinity during the summer season due to either melt water or river discharge (Zonneveld et al., 2013).

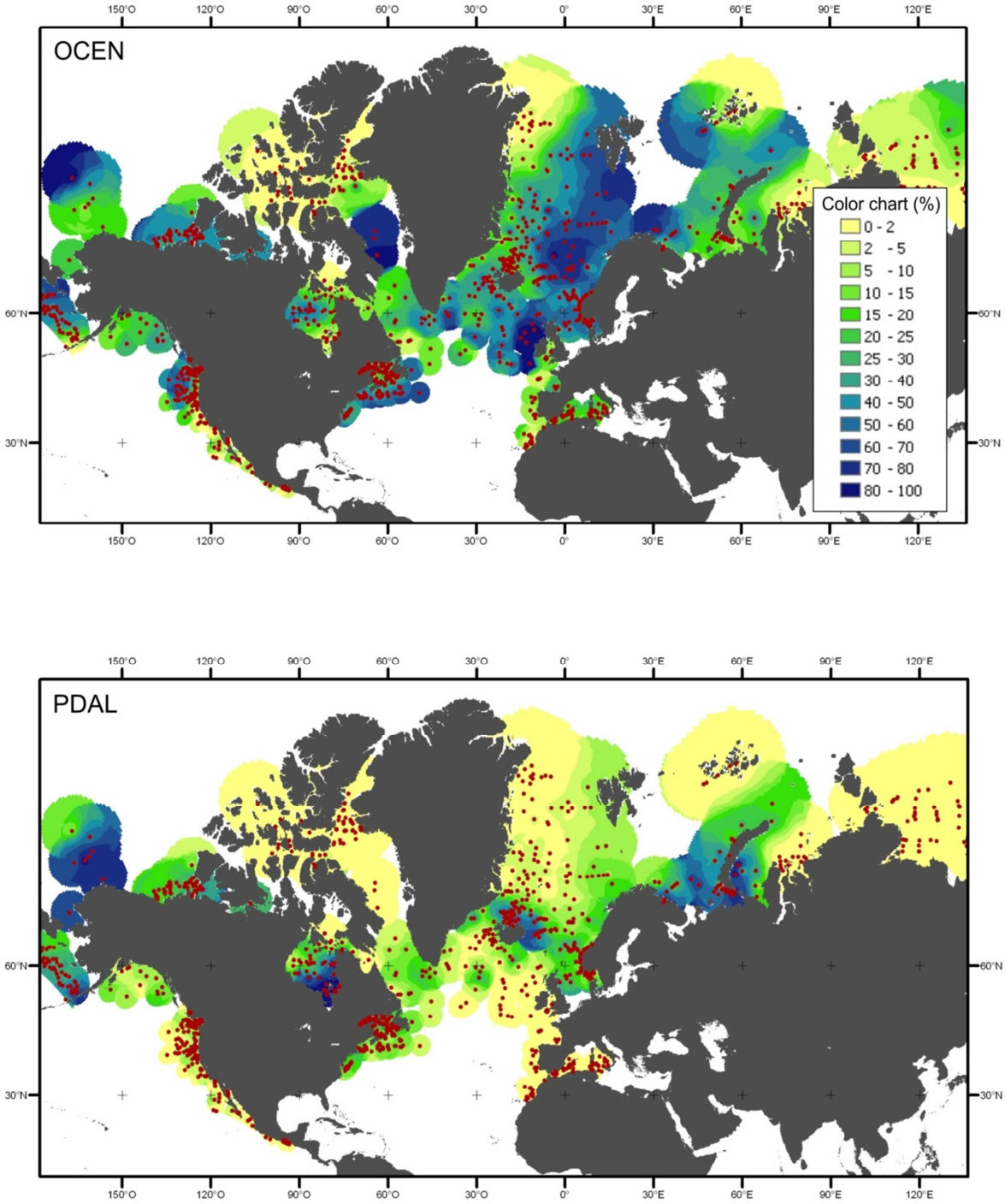

Figure 2.17 : Geographic surface sediment distribution of OCEN and PDAL in the Nordic Seas, based on the 1189 surface sediment database for the North Atlantic and North-Eastern Pacific

Pentapharsodinium dalei (PDAL)

P. dalei is autotrophic and occurs within coastal to oceanic environments north of 62 °S with a wide range of surface temperatures (-2,1°C - 29,6 °C) and salinities (21,3 - 36,7). It may contribute up to 94% of the dinocyst assemblages in coastal surface sediment but less than ~5% in marine environments (Harland and Pudsey, 1999; de Vernal et al., 1997, 2001; Marret and Zonneveld, 2003; Zonneveld et al., 2013). The largest abundances of *P. dalei* cysts have been recorded in sediment samples from the northeast Atlantic (where SSTs > 4°C), especially from along the coast of Norway, within the Barents Sea and around Iceland (Fig. 2.15) (Matthiessen, 1995; Dale, 1996; Rochon et al., 1999; Marret et al., 2004; Grøsfjeld et al., 2009). It is absent from sediments of the east Greenland shelf (Matthiessen, 1995; Zonneveld et al., 2013). Previous studies indicated a strong relation of *P. dalei* to early spring stratification and productivity (Solignac et al., 2009). While showing a preference for coastal environments, this species also occurs in fully marine domains with fall to spring temperatures <1°C and generally reduced upper water salinities due to melt water or river inputs (Zonneveld et al., 2013).

In addition, studies have shown a slight negative relationship between this species and sea-ice cover, although *P. dalei* has been observed below waters with sea-ice cover of up to 9-12 months in the Arctic (de Vernal et al., 1997; Radi and de Vernal, 2008; Zonneveld et al., 2013).

Selenopemphix quanta (SQUA)

S. quanta is a cosmopolitan species found in sediments north of 45°S, below surface waters with a broad temperature (-2,1°C - 29,6 °C) and salinity (16,9 -36,7) range (Marret and Zonneveld, 2003). Maximum abundances of the species were recorded in shallow sediments off Svalbard, the Iceland Sea and over the Barents Sea (Grøsfjeld et al., 2009; Zonneveld et al., 2013, and references therein). Earlier studies suggested that *S. quanta* is heterotrophic, its presence being largely dependent upon the availability of preys, e.g. diatoms (positive correlation to silica/opal and primary productivity) (Devillers and de Vernal, 2000; Marret and Zonneveld, 2003; Radi and de Vernal, 2008; Zonneveld et al., 2013).This species is generally found in high relative abundances in dinocyst assemblages from coastal areas and regions characterized by meso- to eutrophic conditions, e.g. in upwelling areas, close to hydrological fronts and within regions affected by seasonal or permanent river discharge as

well as in areas with sea-ice cover duration of up to 11 months (de Vernal et al., 2001; Marret and Zonneveld, 2003; Zonneveld et al., 2013).

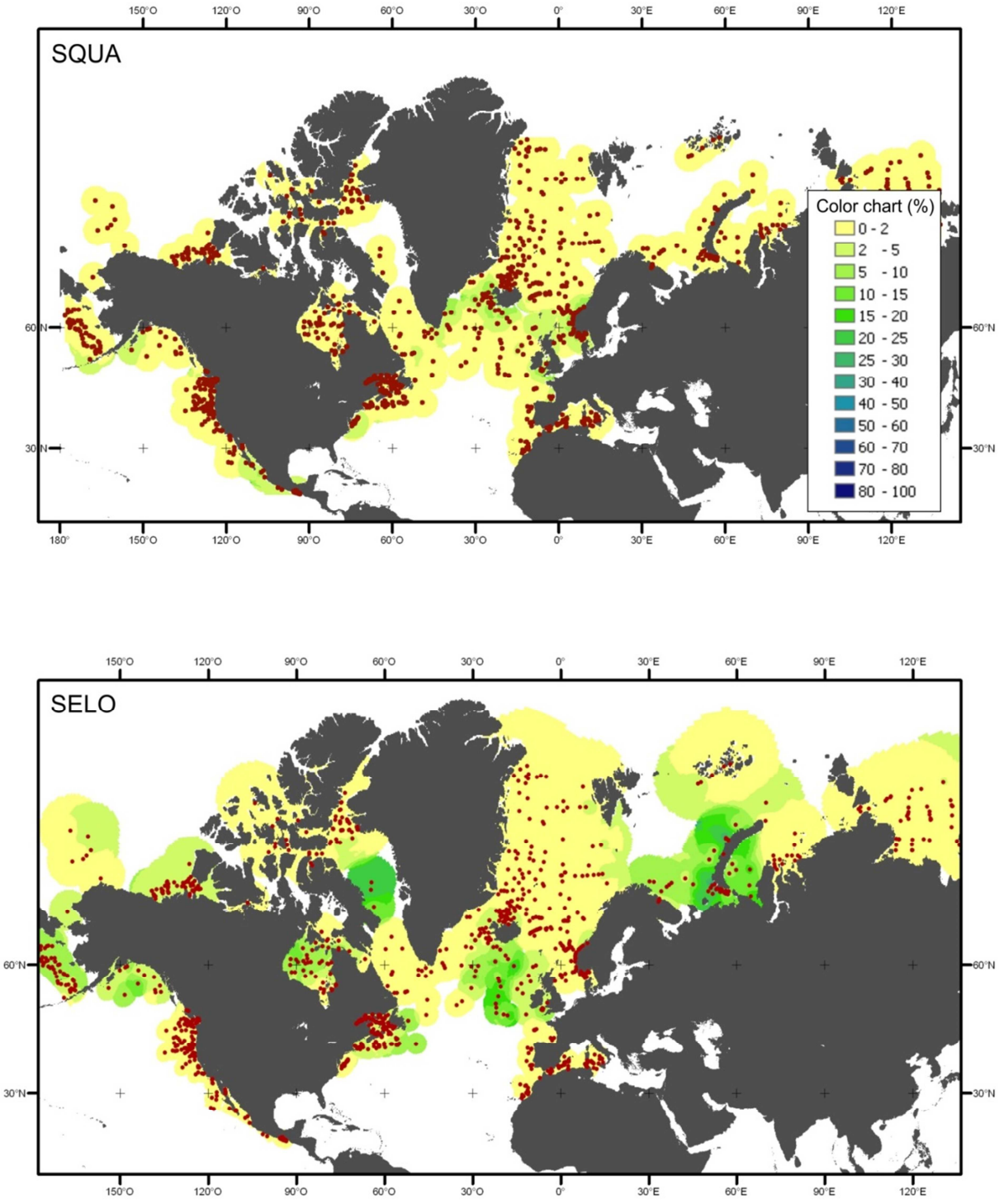

Figure 2.18 : Geographic surface sediment distribution of SQUA and SELO in the Nordic Seas, based on the 1189 surface sediment database for the North Atlantic and North-Eastern Pacific

Spiniferites elongatus (SELO)

S. elongatus is autotrophic and restricted to surface waters of polar to subtropical areas north of 30 °N, within a broad temperature (-2°C – 26,7,6 °C; optimum: -1 to 16°C) and salinity (21,3 -35,9) range (Marret and Zonneveld, 2003). It shows maximum abundances in surface sediments of the central/northern part of the Atlantic Ocean, the Labrador Sea, the Hudson Bay, the Barents Sea and the Nordic Seas (Fig. 2.15) (Marret and Zonneveld, 2003; Grøsfjeld et al., 2009; Zonneveld et al., 2013). This species can be found in areas with ice cover up to 10 months per year, and is particularly successful in meso- to eutrophic environments, which are related to frontal systems (de Vernal et al., 1997; Marret and Zonneveld, 2003; Zonneveld et al., 2013). *S. elongatus* is specifically abundant in coastal surface sediments (Zonneveld et al., 2013).

Spiniferites mirabilis (SMIR)

The autotrophic species *S. mirabilis* includes here both *S. mirabilis* and *Spiniferites hypercanthus*, as determination at species level is difficult and dependent on the orientation of the specimen. *S. mirabilis* has exclusively been observed in fully marine environments with salinities above 28.5 and summer temperatures above 12 °C (Marret and Zonneveld, 2003). The optimum sea-surface temperature preferences were estimated between 10 and 15°C and above 15°C for the winter and summer seasons respectively (de Vernal et al., 1997; Zonneveld et al., 2013). Based on these temperature preferences, *S. mirabilis* is characteristically absent from areas seasonally covered by sea-ice (de Vernal et al., 1994, 1997). In the North Atlantic, abundances of *S. mirabilis* are negatively correlated with the nutrient content of the surface waters (Devillers and de Vernal, 2000).

Spiniferites ramosus (SRAM)

The autotrophic *S. ramosus* cysts are found in a broad range of environments north of 45 °S with surface water temperature and salinity ranges of -1,7 to 29,1°C and 21,3 to 36,7,respectively (Marret and Zonneveld, 2003). The highest relative abundances of *S. ramosus* are recorded in sediments below surface waters with annual salinities above 30. This species can dominate dinocyst assemblages in meso- to eutrophic environments, which are characterized by upwelling or a well-mixed surface layer (Marret and Zonneveld, 2003; Zonneveld et al., 2013), as well as temperate to tropical neritic environments (Wall et al., 1977; Mudie, 1992; Harland et al., 1998; Marret and Zonneveld, 2003, and references

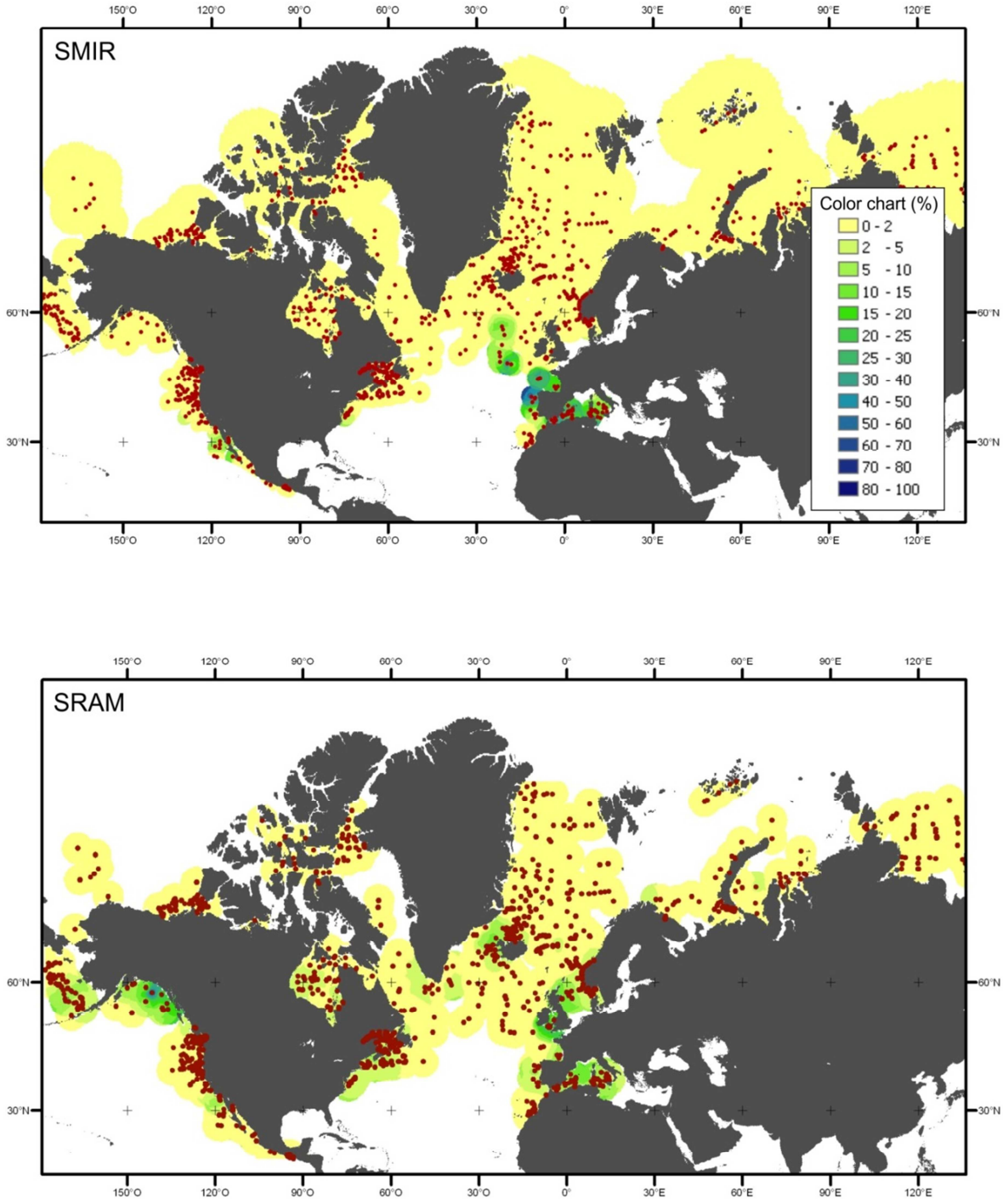

Figure 2.19 : Geographic surface sediment distribution of SMIR and SRAM in the Nordic Seas, based on the 1189 surface sediment database for the North Atlantic and North-Eastern Pacific

therein). *S. ramosus* can be found in areas affected by sea-ice cover up to 8 months a year, although it shows a negative correlation with seasonal ice duration (de Vernal et al., 1997; Radi and de Vernal, 1998). This species occurs in low abundances within the Nordic seas

(Zonneveld et al., 2013) and has been suggested to be related to spring/summer productivity and surface water stratification (Solignac et al., 2009; Grøsfjeld et al., 2009).

Halodinium spp. (Acritarch, HALO)

The acritarch *Halodinium* spp. includes two morphotypes, e.g. *Halodinium minor* (related to colder environments and seasonal sea ice) and *Halodinium major* (restricted to temperate environments) (Matthiessen, 1995). It has been reported from polar to warm-temperate environments within Australian estuaries and Arctic delta environments (Bujak, 1984; McMinn, 1991; Mudie, 1992; Head, 1996), and it has, therefore, been suggested to be related to gradational zones between fresh and marine environments e.g. glacier-meltwater outflow and the MIZ (Mudie, 1992; Head, 1996; Grøsfjeld et al., 2009). *Halodinium* spp. is common in sediments from the east Greenland continental shelf, the western Iceland Sea and the central Greenland Sea and has been reported in high abundances from a surface sediment sample northwest of Bjørnøye (Solignac et al., 2009), whereas only very rare specimens have been found in the southern Norwegian Sea (Matthiessen, 1995).

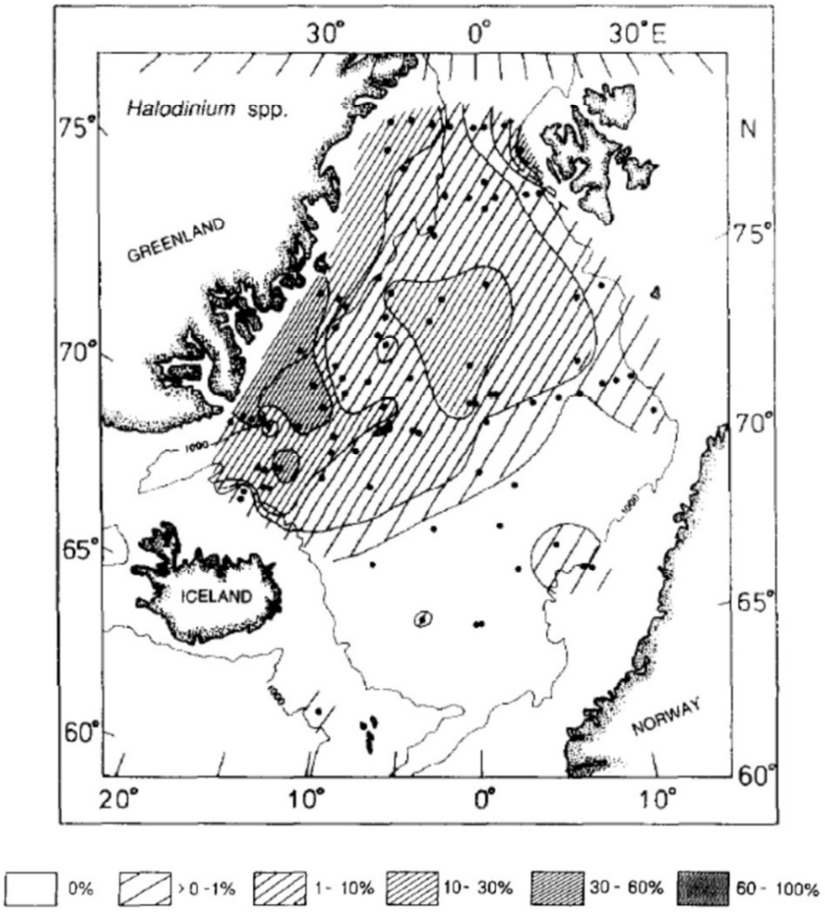

Figure 2.20 : Geographic surface sediment distribution of HALO in the Nordic Seas. Modified after Matthiessen et al. (1995).

Significance of the dinocyst ratios OCEN/NLAB and OCEN/IMIN

The different regional dominance of the two species *O. centrocarpum* and *N. labyrinthus* is clearly reflected in the surface sediments of the Nordic Seas (Matthiessen et al., 2001; Zonneveld et al., 2013) as seen above. Matthiessen et al. (2001) found a somewhat inverse relationship between the relative abundances of the two species with a dominance of *O. centrocarpum* below relatively warm Atlantic-derived water masses of the Norwegian Seas and a dominance of *N. labyrinthus* below Arctic waters. The authors proposed an abundance ratio between the two species (OCEN/NLAB) to define the location of the AF, which separates the Polar and Arctic domains (OCEN/NLAB<4) from warmer and saltier Atlantic-derived waters (OCEN/NLAB>4).

In addition recent investigations of surface sediment samples within the western Barents Sea suggests that the relative abundance of *O. centrocarpum* versus *I. minutum* may be used to indicate whether warm AW flows at the surface or as a subsurface water mass below ArW or sea ice (Grøsfeld et al., 2009), as *I. minutum* has often been associated with Arctic surface water and sea ice (de Vernal et al., 2001; Head et al., 2001; Marret and Zonneveld, 2003).

Based on these evidences we use the definition of the AF (a frontal salinity and temperature gradient separating surface AW masses from mixed ArW) to infer that the OCEN/NLAB ratio (ie. deviations from the treshold of 4) characterizes surface sediments deposited below Atlantic or Arctic surface water masses, when considering pluriannual conditions. In a similar fashion we use the ratio OCEN/IMIN to characterise the surface water masses.

Chapter 3 : Material and Methods

3.1 Chapter Overview

North-western Europe is, today, characterized by a climate 5-10 °C higher than the zonal mean (Hald et al., 2007). This difference is to a large extent attributed to the northward advection of warm AW by the NwAC and its meridional extension the WSC. The contribution of the present study to the understanding of recent climate variability in this region is two-fold. On one hand, we aim at obtaining a more complete knowledge on the Holocene variability of physical parameters (sea-surface temperatures, salinities and sea-ice extent/duration), which affect ecosystem processes within the Nordic Seas (Norwegian-Iceland-Greenland Sea) and Fram Strait in areas presently affected by seasonal sea-ice. On the other hand, we aim at reconstructing the Holocene changes in Atlantic water inflow to the Arctic through the Fram Strait gateway.

Core ID	Latitude	Longitude	Water depth (m)	Core length (m)	SST (winter, °C)	SST (summer, °C)	SSS (winter, PSU)	SSS (summer, PSU)	Location
WOO/SC-3	67° 24.08'N	08°31.25'E	1184	3.85	6.44	11.06	34.96	34.61	Northeast of Vøring Plateau
R248MC010	69° 78.30 N	12,52.98 E	1254	0.49	5.73	10.8	34.6	34.3	West of Lofoten Island
R406MC032	72° 18.97'N	14°82.68'E	1035	0.33	4.85	8.2	35.02	34.09	Southwestern Barents Sea
JM09-KA11-GC	74° 52.48'N	17° 12.21'E	345	3.6	3.03	5.84	34.95	34.7	Midwest Barents Sea (Kveithola Trough)
HH11-134-BC	77° 35.96'N	09° 53.25'E	1383	0.41	2.01	5.4	34.6	34.3	West spitsbergen slope

Table 3.1: Core locations and modern winter (Jan.-Mar.) and summer (Jul.-Sep.) sea surface temperatures and salinities (from World Ocean Database; Boyer et al., 2009). Only the three northern most cores have been affected by sea ice within the last two centuries (Vinje, 2001; Divine and Dick, 2006).

A selection of five records (3 short cores and 2 long cores) were chosen along the continental margin of the eastern North Atlantic, based mainly on their location within the pathway of Atlantic Water to the Arctic Ocean (i.e. NwAC and WSC), between ~67° N and 78° N (Fig. 1.1, 3.1, Table 3.1). The investigation of Holocene climate changes from deep-sea cores has often been hampered by low sedimentation rates or poor preservation. We, therefore, carefully selected sediment materials from depocenter areas on the shelf (troughs or depressions) or along the continental slope, which are characterized by high Holocene accumulation rates

enabling the study of multi-annual to centennial scale climate and hydrological changes. In the present work, qualitative (species assemblages) and quantitative (paleoecological transfer functions) reconstructions of surface water conditions along the meridional flow of AW are essentially derived from two micropaleontological tracers: coccoliths and dinoflagellate cysts. Few additional proxies (XRF-derived elemental concentrations, planktonic foraminiferal assemblages and abundances of large lithic grains) were also investigated in order to get a more comprehensive understanding of the surface and subsurface paleoceanographic changes inferred from coccoliths and dinocysts assemblages. In addition, most cores are investigated by partner institutions (Univ. Plymouth and Univ.Tromsø) within the framework of the ITN project CASE, with a strong focus on the two cores WOO/SC-3 and JM09-KA11-GC.

An additional investigation on extant coccolithophore populations across the Nordic Seas and Fram Strait was conducted with the purpose of improving our understanding of the biogeographical distribution of dominant species in view of the physical and/or chemical conditions of the photic layer at the time of surface water sampling. These results are presented in Chapter 2.

Core ID	**Investigated core length (cm)**	**Sampling resolution in (cm)**						**Bottom age (cal. years BP)**
		Coccoliths	**Dinocysts**	**LLG**	**XRF**	**Forams**	**Bulk $CaCO_3$**	
WOO/SC-3	275	5	5					3172
R248MC010	49	0.5	1	1	0.2	1	1-2	490
R406MC032	34	1	1	1			1	532
JM09-KA11-GC	125	0.5-4	2-4					11769
HH11-134-BC	41	0.5	0.5	0.5	0.1	0.5-1	1-2	6508

Table 3.2: Sampling resolution (in cm) according to the investigated cores and the investigated proxies. Investigated core length and bottom age are provided for information. LLG: Large Lithic Grains, Bulk $CaCO_3$: Bulk carbonate contents. Planktonic foraminifera sensus counts were performed by Linda Rossignol and Jacques Giraudeau.

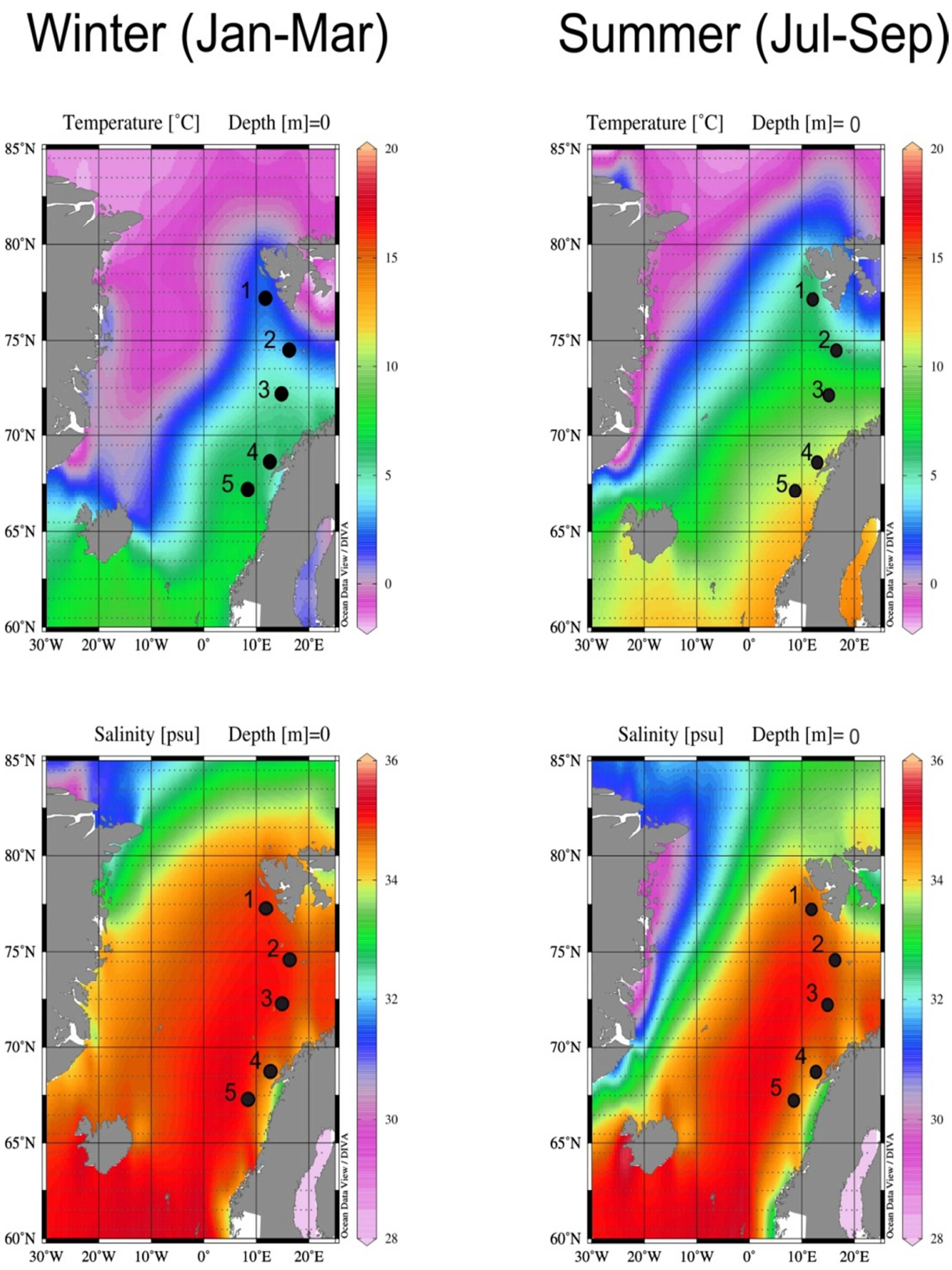

Figure 3.1 :Sea surface temperature and salinity maps for modern summer (Jul.-Sep.) and winter (Jan.-Mar.) conditions within the northern North Atlantic (World Ocean Database; Boyer et al., 2009); plots constructed using Ocean Data View 4. Black filled circles locations of studied cores; 1: HH11-134-BC, 2: JM09-KA11-GC, 3: R406MC032, 4: R248MC010 and 5: WOO/SC-3.

3.2 Core Locations and Descriptions

The present research study was carried out on 5 sediment cores distributed along a latitudinal gradient within the path of the NwAC and its northermost extension the WSC (Fig. 1.1, 3.1). The following paragraph gives an overview of the investigated cores in terms of site location, modern surface water characteristics (currents, temperatures and salinities), lithology and sampling procedure.

3.2.1 WOO/SC-3

This 3.85 m long gravity core was retrieved from the Norwegian continental margin, northeast of the Vøring Plateau (at the entrance to Trænadjupet) within the path of the NwAC (Fig. 1.1, 3.1; Table 3.1; Appendix 1, CTD 1) (Laberg et al., 2002). WOO/SC-3 consists of two lithological units: a deeper diamicton overlayed by a ~270 cm long yellow-brown mud (Fig. 3.2) (Laberg et al., 2002). Sampling for coccolith and dinocyst investigations was conducted every 5 cm at EPOC from 19 cm down to 275 cm (the top 19 cm was missing from our set of sediment samples) (Table 3.2).

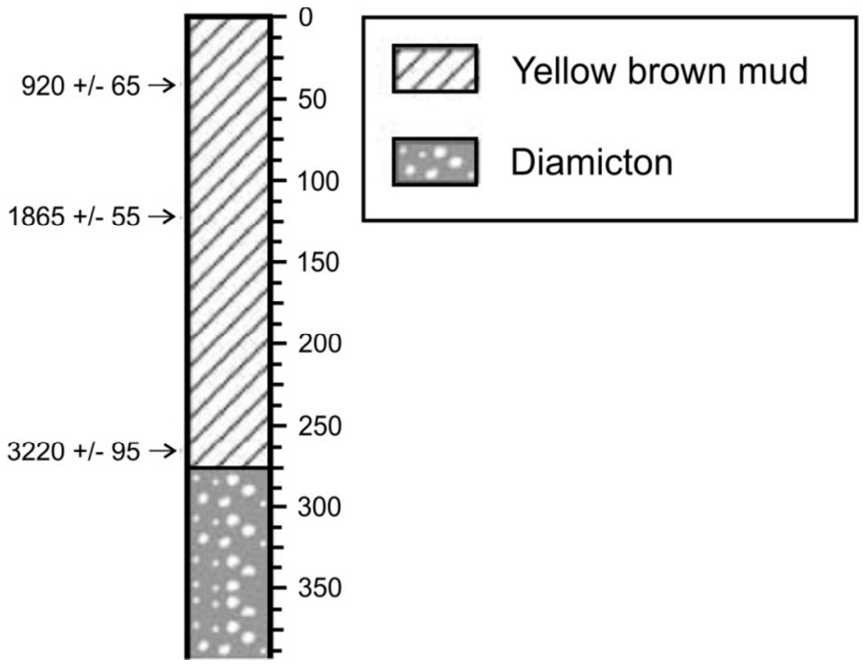

Figure 3.2 : Lithology of core WOO/SC-3 and ^{14}C years BP versus depth (cm). Modified after Laberg et al. (2002).

3.2.2 R248MC010

The site is located in an area influenced both by the NAC and the NCC (Appendix 1, CTD 2), as indicated by CTD 2 showing that the NCC influence the location down to ~35 meters (<34.7, Loeng, 1991) (at least seasonally), followed by a dominance of AW.

The 0.49 m long multi-core R248MC010 consists of gray clayey silt and was retrieved in 2008 west of the Lofoten Islands within the framework of the Norwegian MAREANO program (onboard F/F G.O. Sars) (Fig. 1.1, 3.1, 3.3; Table 3.1) (Jensen et al., 2009). XRF analyses (~0.2 cm) and SCOPIX radiography were conducted at EPOC (Fig. 3.3). The X-ray image provides evidence of bioturbation down the whole section, but does not show any sharp lithological changes and/or erosional surfaces, suggesting that sedimentation was most probably continuous and not affected by gravitational processes. Grain size analyses were conducted every 2 cm at NGU and adapted from Jensen et al. (2009) (Fig. 3.3). They only show minor variability of ~6 % between, mainly, silt and sand. Core sampling for micropaleontological (dinocysts and planktonic foraminifera) and sedimentological (lithic grains and bulk carboinate contents) investigations were carried out at 1 cm resolution with the exception of the coccolith investigation, which was realized at 0.5 cm resolution (Table 3.2).

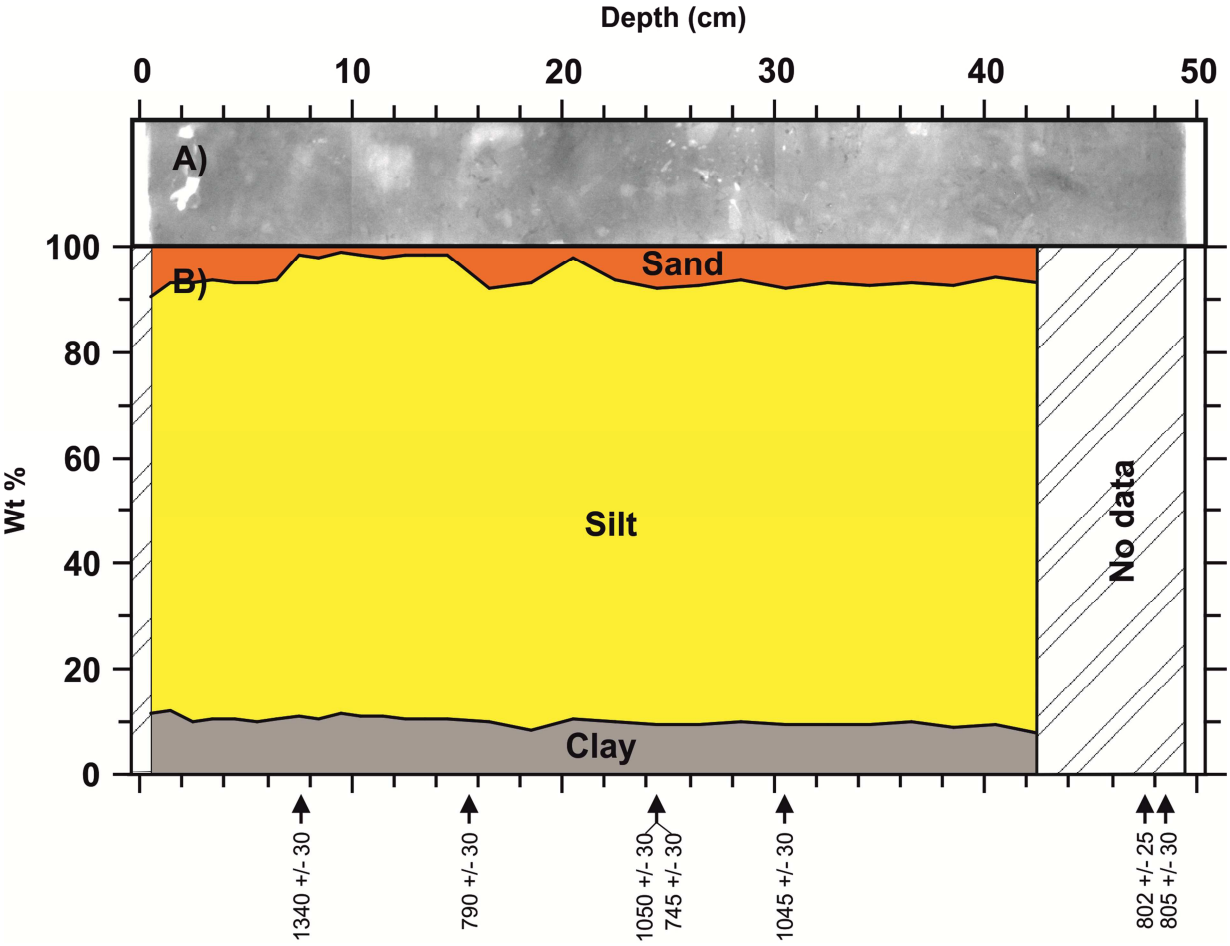

Figure 3.3 : A) SCOPIX image versus depth of core R248MC010 showing bioturbation. B) Grain size analysis (wt %). Clay: <2 µm, Silt: 2-63 µm, Sand: >63µm, based on analyses from Jensen et al. (2009). In addition, ^{14}C ages are marked at their respective depths.

Visual inspection of the core halves after opening indicated that the core top accurately sampled the sediment-water interface, as it contained a very clear ca. 5 cm thick brown reduced layer above a gray oxydated sediment column.

Previous ^{210}Pb dating by Jensen et al. (2009) suggested that core R248MC010, assuming a constant sedimentation rate, represents the last 150 years.

Therefore, this core material was initially intended to be used for high resolution proxy validation.

3.2.3 R406MC032

This 0.34 m long multi-core was retrieved in 2009, within the framework of the Norwegian MAREANO program (onboard F/F G.O. Sars). The site is located along the continental margin of the southwestern Barents Sea, roughly halfway between northern Norway and Bear Island at the entrance to the BIT. The location is overlaid by the WSC meridional branch of the NwAC and is influenced by the NCC during summer (Fig. 1.1, 3.1; Table 3.1; Appendix 1, CTD 3) (Olsen et al., 2003; Jensen et al., 2010).

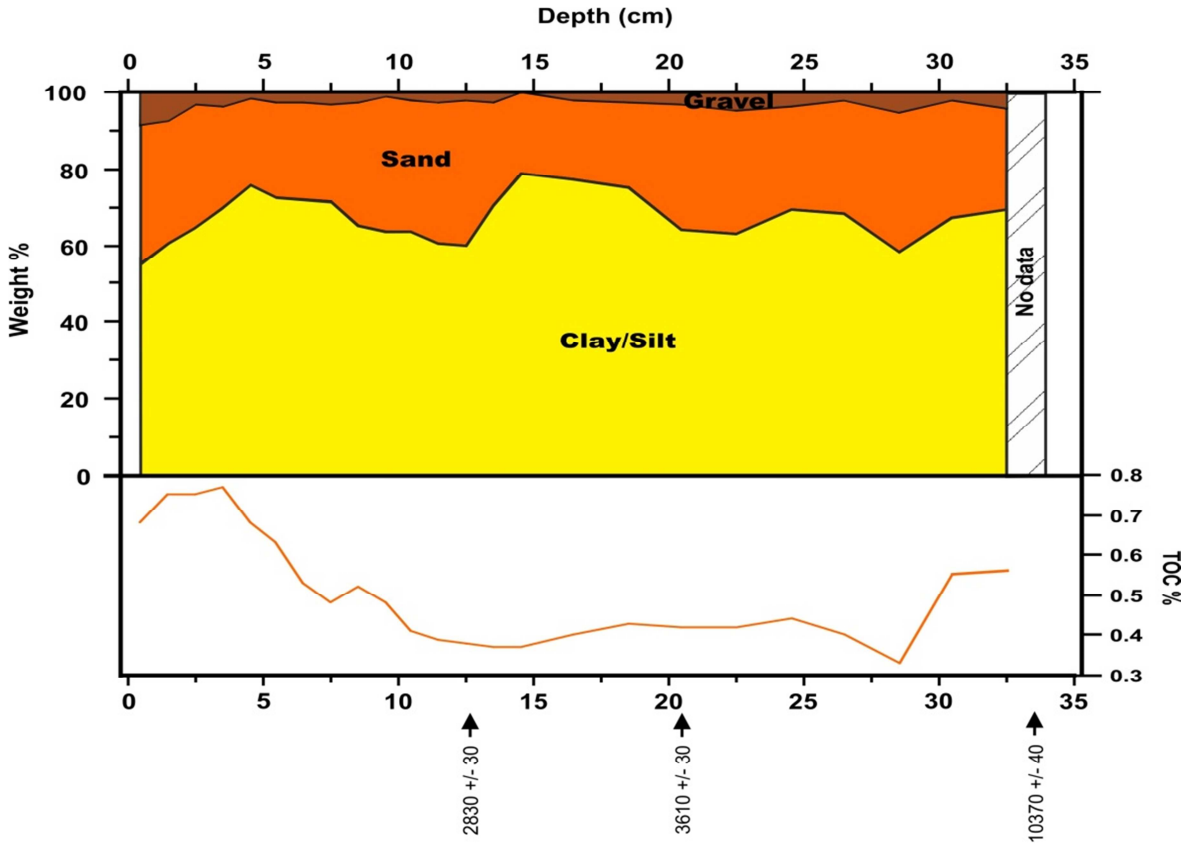

Figure 3.4: Grain size analysis (wt %) and Total Organic Carbon (TOC %) versus core depth (cm) for multicore R406MC032. Clay/Silt: <63 µm, Sand: 63-250 µm, Gravel: >250 µm, based on analyses from Jensen et al. (2010). In addition, ^{14}C ages are marked at their respective depths.

While the core was emptied onboard, subsampling at 1 cm resolution was conducted at EPOC according to the same strategy applied to core R248MC010, i.e. micropaleontological investigations of coccolith and dinocyst assemblages, description and counts of lithic grains, and measurement of bulk carbonate contents (Table 3.2). A previous grain size analysis conducted by the MAREANO research group (Jensen et al., 2010) shows that core R406MC032 is affected by large downcore changes in sand and silt/clay contributions of up to ~20% as well as a strong decrease in the Total Organic Carbon (TOC) content below 5-10 cm (Fig. 3.4). Detailed studies of surface sediments (Steinsund and Hald, 1994) and sediment cores (Jensen et al., 2007) have shown that the formation of metabolic CO_2 together with dense, salty water masses is the main cause of the uneven $CaCO_3$ concentrations in large parts of the Barents Sea. Salty bottom waters with high densities are often found in depressions and troughs along the continental margin where CO_2 enriched water masses accumulate. Carbonate microfossils might, therefore, be stronger effected by dissolution in such environments compared to "higher ground" areas (i.e. along the coast or the continental shelf). The lower carbonate values below ~10 cm in R406MC032 are, thus, not a result of natural variations in the carbonat production but are more likely related to disolution of carbonate foraminifera (Jensen et al., 2010).

Initial ^{210}Pb dating conducted within the framework of the MAREANO program (Jensen et al., 2010) suggested that, assuming a constant sedimentation rate down to the bottom of the core, R406MC032 provides a continuous record of sedimentation throughout the last 300-400 years.

3.2.4 JM09-KA11-GC

The 3.83 meter gravity core was retrieved from the Kveithola Trough northwest of Bear Island onboard R/V *Helmer Hansen* (former R/V 'Jan Mayen') (Fig. 1.1, 3.1; Table 3.1) (Rüther et al., 2012). The site is located within the influence of the poleward flowing WSC in close vicinity to the clockwise flow of ArW on the shelf from the BIC (extension around Bear Island of the PC) and the Sørkapp Current (extension around southern Svalbard of the ESC) (Appendix 1, CTD 4) (Saloranta and Svendsen, 2001; Wassman et al., 2006).

JM09-KA11-GC is situated in a glacial trough, which acts as a natural sediment trap containing relatively thick Holocene sediments (Rüther et al., 2012). Rüther et al. (2012) described the lithofacies in the gravity core JM09-KA11-GC and found an erosive base at the bottom of Lithofacies 1 (LF1), a sharp boundary change from LF2 (crudely laminated, bioturbated mud) to LF4 (layer diamict with muddy matrix) and a sudden increase in the Ice

Rafted Detritus (IRD) content at the boundary between the latter two facies (Fig. 3.5). The core shows a strong downcore variability in sand, silt and clay contents with sandy sediments (~40-60 %) in the top ~0.90-1 m and a dominance of silt and clay (~80-90%) in the deeper parts (Fig. 3.5). The core material was initially sampled in Tromsø and re-sampled at EPOC for the micropaleontological investigations of coccoliths (0.5 cm, <40 cm; 2-4 cm, >40 cm) and dinocysts (~2-4 cm) down to a core depth of ~125 cm (Table 3.2). The chronological framework is based on ^{14}C dates provided by Rüther et al. (2012), Berben et al. (2013) and Groot et al. (2013).

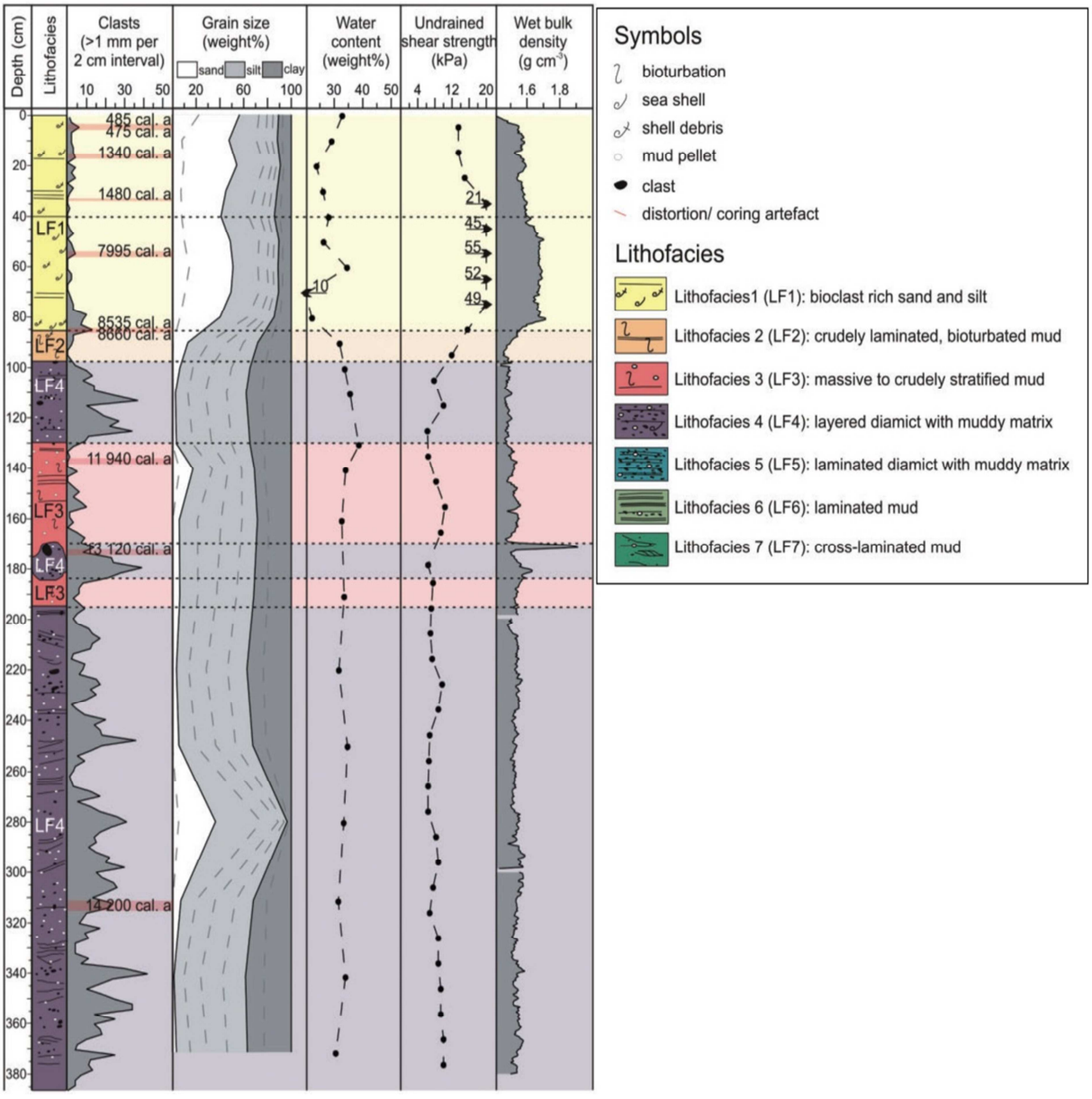

Figure 3.5: Analytical results for gravity core JM09-KA11-GC, incl. the division of lithofacies. Calibrated radiocarbon ages are indicated in the clast-column. Water content and undrained shear strength values are given in numbers when out of the range of the X axis scale. Modified after Rüther et al. (2012).

3.2.5 HH11-134-BC

The 0,41 m long box-core HH11-134-BC was retrieved on the continental slope west of Svalbard at the entrance of Isfjorden and Belsund (Fig 1.1, 3.1; Table 3.1) as part of the GEO-8144/3144 cruise of the RV *Helmer Hansen* (Husum et al., 2011). This core is located within the influence of the WSC (Fig. 3.1; Appendix 1, CTD 5).

The core was cut open at EPOC where XRF core scanning (~0.1 cm resolution) and SCOPIX radiography were conducted (Fig. 3.6). The core consists of homogenous gray clay, although X-Ray images showed a higher abundance of clasts in the upper part of the sediment section. Sampling was achieved at resolutions close to 0.5 cm for micropaleontological (coccoliths, ~0.5 cm; dinocysts, ~0.5 cm; planktonic foraminifera, ~0.5-1 cm in top ~30 cm), sedimentological (lithic grains, ~0.5 cm) and bulk carbonate contents (~2 cm) (Table 3.2). During sampling, a small dropstone of ~2 cm in diameter was identified at a depth of 16-17 cm. In addition, several boulders were found in the left-over sediments of the boxcore when the shipdeck was cleaned.

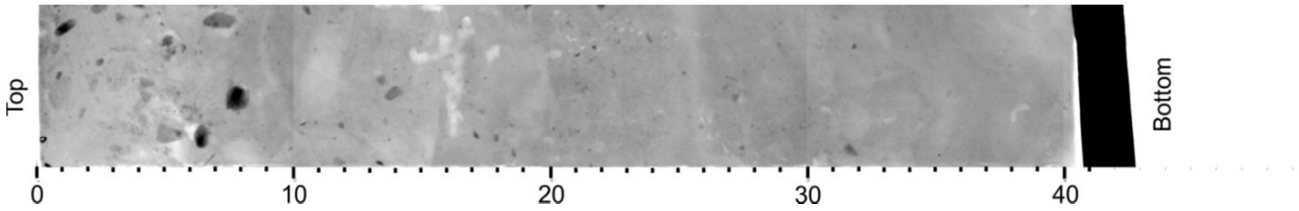

Figure 3.6: SCOPIX radiography of core HH11-134-BC showing a high abundance of clasts in the top 10 cm with an apparent progressive decrease down core.

3.3 Core Chronologies

The chronological framework of the investigated sediment cores is based on ^{210}Pb and ^{14}C datings, their method principles are given in Appendix 2.

The stratigraphic framework of the investigated sediment cores is based on 31 Accelerator mass spectrometry (AMS) ^{14}C- and 16 ^{210}Pb-dates of which 21 have previously been published (Laberg et al., 2002; Rüther et al., 2012; Dylmer et al., 2013; Berben et al., 2013; Groot et al., 2013) (Table 3.3). The dates were calibrated to calendar years before present (Cal. years BP, 1950 AD = 0 BP) by applying the software Calib 6.1.0 (Stuiver and Reimer, 1993) and the marine calibration curve marine09, using a standard reservoir correction of ~400 years ($\Delta R = 0$), if not elsewise stated in Table 3.3.

Table 3.3: Core, sample depth, dated material, 14C age years BP, calibrated years BP, Laboratory ID and reference. ((*) excl. from age model)

Core	Core depth (cm)	Dated material	14C AMS Age years BP	Calibrated Age, cal. years BP	Calibrated ages, 2σ range	ΔR	Lab ID	References
WOO/SC-3	39-41	N. pachyderma	920 ± 65	536.5	435-638	0	TUa-2931	Laberg et al., 2002
WOO/SC-3	119-121	N. pachyderma	1865 ± 55	1410	1291-1529	0	TUa-2930	Laberg et al., 2002
WOO/SC-3	262-264	N. pachyderma	3220 ± 95	3041	2793-3289	0	TUa-2929	Laberg et al., 2002
R248MC010	1			-58				Pb210, from Leinebø (2011)
R248MC010	3.5			-51				Pb210, from Leinebø (2011)
R248MC010	5.2			-42				Pb210, from Leinebø (2011)
R248MC010	7.1			-32				Pb210, from Leinebø (2011)
R248MC010	9.2			-22				Pb210, from Leinebø (2011)
R248MC010	11.2			-11				Pb210, from Leinebø (2011)
R248MC010	13.2			2				Pb210, from Leinebø (2011)
R248MC010	15.2			17				Pb210, from Leinebø (2011)
R248MC010	17.2			36				Pb210, from Leinebø (2011)
R248MC010	19.2			63				Pb210, from Leinebø (2011)
R248MC010*	7-8	Bulk planktic foraminifera	1340 ± 30	871	791-951	0	SacA 29434	
R248MC010*	15-16	Bulk planktic foraminifera	790 ± 30	421.5	350-493	0	SacA 29430	
R248MC010*	24-25	Bulk planktic foraminifera	1050 ± 30	608.5	548-669	0	Beta-307125	
R248MC010*	24-25	Mollusc	745 ± 30	381	303-459	0	SacA 24481	
R248MC010*	30-32	Bulk planktic foraminifera	1045 ± 30	606	546-666	0	SacA 29431	
R248MC010	47-48	Bulk planktic foraminifera	802 ± 25	439	378-500	0	UBA-20059	
R248MC010	48-49	Bulk planktic foraminifera	805 ± 30	434	364-504	0	SacA 24482	
R406MC032	0.5			-56				NGU cruise Report 2010.016

R406MC032	1.5			-49				NGU cruise Report 2010.017
R406MC032	3.5			-29				NGU cruise Report 2010.018
R406MC032	5.5			-7				NGU cruise Report 2010.019
R406MC032	7.5			16				NGU cruise Report 2010.020
R406MC032	9.5			42				NGU cruise Report 2010.021
R406MC032*	12-14	Bulk planktic foraminifera	2830 ± 30	2583.5	2468-2699	0	Beta - 307123	This study
R406MC032*	20-21	Bulk planktic foraminifera	3610 ± 30	3506.5	3411-3602	0	Beta - 307124	This study
R406MC032*	33-34	Bulk planktic foraminifera	10370 ± 40	11432.5	11232-11633	0	SacA 424483	This study
JM09-KA11-GC	3-6	Mollusc dextral part of B. Glacialis	925 ± 30	475.5	396-555	67 ± 34	Tra-1063	Rüther et al., (2012)
JM09-KA11-GC	3-6	Mollusc dextral part of B. Glacialis	900 ± 35*	444	352-536	67 ± 34	Tra-1064	Rüther et al., (2012)
JM09-KA11-GC	15-17	Mollusc sinistralpart of B. Glacialis	1880 ± 35	1375	1268-1482	67 ± 34	Tra-1065	Rüther et al., (2012)
JM09-KA11-GC	27-28	Benthic foraminifera I. Norcrossi/helenae	4430 ± 30	4518	4383-4653	67 ± 34	Beta-324049	Berben et al. (2013) and Groot et al. (2013)
JM09-KA11-GC*	32.5-33.5	Mollusc dextral part of A. Elliptica	1990 ± 35	1469	1345-1593	67 ± 34	Tra-1066	Rüther et al., (2012)
JM09-KA11-GC	39.5-40.5	Benthic foraminifera I. Norcrossi/helenae	5480 ± 30	5779	5665-5893	67 ± 34	Beta-315192	Berben et al. (2013) and Groot et al. (2013)
JM09-KA11-GC	44-45	Benthic foraminifera I. Norcrossi/helenae	6510 ± 40	6943	6783-7103	67 ± 34	Beta-315193	Berben et al. (2013) and Groot et al. (2013)
JM09-KA11-GC	53-57	Mollusc sinistral part of A. Sulcata	7630 ± 45	8037.5	7920-8155	67 ± 34	Tra-1067	Rüther et al., (2012)

JM09-KA11-GC*	80-81	Benthic foraminifera I. Norcrossi/helenae	8770 ± 40*	9367	9249-9485	67 ± 34	Beta-315194	Berben et al. (2013) and Groot et al. (2013)
JM09-KA11-GC	81-83.5	Mollusc paired shell of A. Elliptica	8140 ± 50	8545	8389-8701	67 ± 34	Tra-1068	Rüther et al., (2012)
JM09-KA11-GC	81-83.5	Mollusc sinistral part of N. minuta	8315 ± 50	8782.5	8597-8968	67 ± 34	Tra-1069	Rüther et al., (2012)
JM09-KA11-GC	110.5 - 111.5	Benthic foraminifera E. Excavatum	10540 ± 50	11611.5	11324-11899	67 ± 34	Beta-315195	Berben et al. (2013) and Groot et al. (2013)
JM09-KA11-GC	133-136	Mollusc paired shell of Y. Intermedia	10705 ± 55	11964	11676-12252	67 ± 34	Tra-1070	Rüther et al., (2012)
HH11-134-BC	9.5-10	Bulk planktic foraminifera	826 ± 23	462.5	420-505	0	UBA-20062	This study and Dylmer et al., 2013
HH11-134-BC*	15-16	Bulk planktic foraminifera	2030 ± 30	1601.5	1515-1688	0	SacA 29428	This study and Dylmer et al., 2013
HH11-134-BC	19-20	Bulk planktic foraminifera	1995 ± 28	1571	1473-1669	0	UBA-20061	This study and Dylmer et al., 2013
HH11-134-BC	30-30.5	Bulk planktic foraminifera	3825 ± 30	3774.5	3676-3873	0	SacA 29432	This study and Dylmer et al., 2013
HH11-134-BC	39.5-40	Bulk planktic foraminifera	6045 ± 30	6470.5	6378-6563	0	SacA 29433	This study and Dylmer et al., 2013

Table 3.3 : List of ^{210}Pb and ^{14}C datings in the studied cores. Calibration of ^{14}C dates was done by applying the software Calib 6.1.1 (Stuiver and Reimer, 1993) and the marine calibration curve marine09, using a standard reservoir correction of $\Delta R = 0$, if not otherwise stated. (*) excl. from age model.

A standard reservoir correction $\Delta R = 0$ was chosen for all cores (except JM09-KA11-GC) as a further finetuning of the signals would result in age models differing from published paleoclimate data sets using this standard correction. Nevertheless we are aware of possible errors in our age models due to ΔR-variations along the core transect, especially in areas with 'old' Arctic/Polar waters (Mangerud and Gulliksen, 1975; Mangerud et al., 2006). Indeed, Bondevik and Gulliksen found that the reservoir age is latitude dependent along the Norwegian coast, with ΔR-values increasing from -3 ± 22 years in the south to 105 ± 24 years at Spitsbergen (discussed in Mangerud et al., 2006).

3.3.1 WOO/SC-3

The chronology is based on 3 AMS ^{14}C dates obtained by Laberg et al. (2002) on monospecific samples of planktonic foraminifera (*Neogloboquadrina pachyderma)* (Table 3.3). The final chronology assumes a constant sedimentation rate between each radiocarbon dated level in WOO/SC-3 (linear interpolation) (Fig. 3.7).

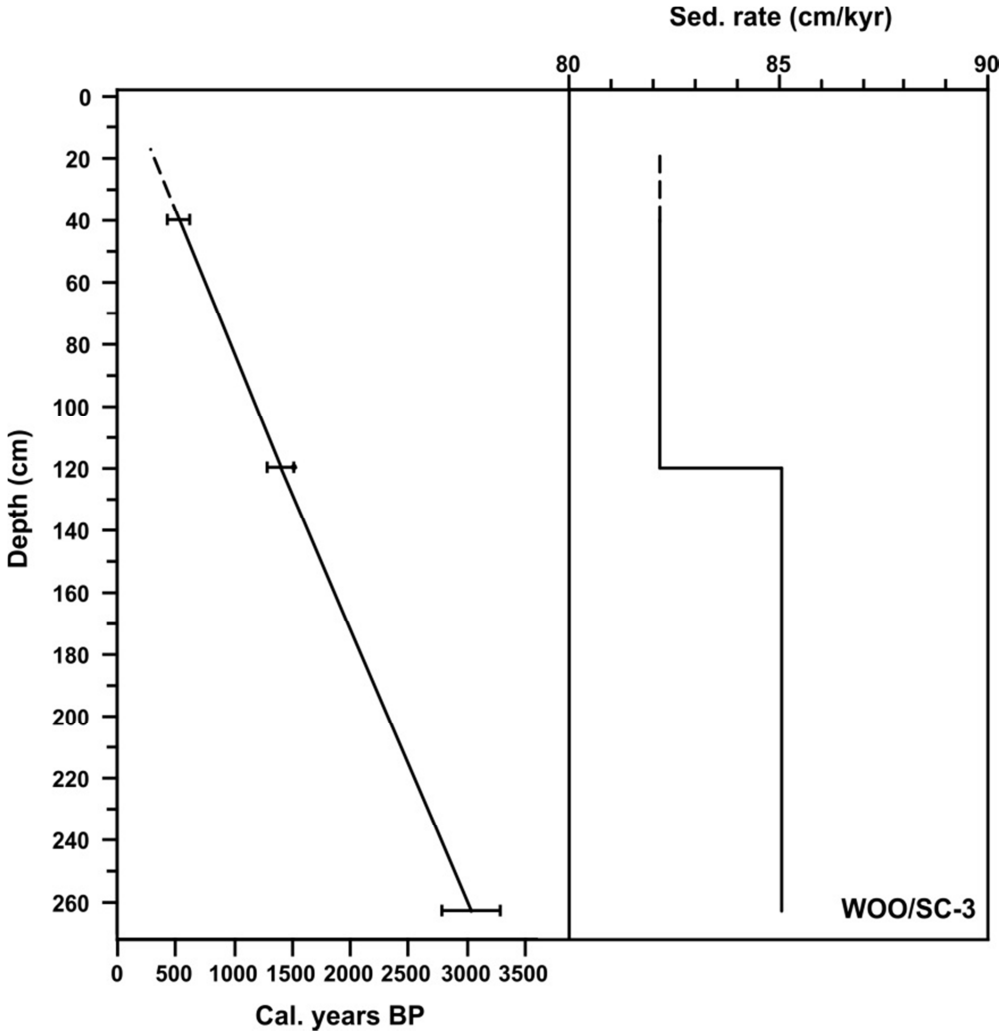

Figure 3.7 : Age-depth model (cal. years BP) and sedimentation rates of WOO/SC-3 based on data from Table 3.3 (linear interpolation between each dated level). Horizontal lines: 2 sigma range of highest probability of calibrated AMS C^{14} dates.

The gravity core (WOO/SC-3) over penetrated the water-sediment interface (explaining the disturbance within the top 19 cm). We, therefore, chose to apply the sedimentation rate estimated from the two AMS dates obtained in the upper levels to the top part of this core. This choice is supported by the homogenous lithology throughout the core as well as rather constant sedimentation rates calculated from the three available AMS dates (Fig. 3.7).

The resulting age model suggests that the core covers the interval ~312 - 3172 Cal. years BP with an apparent sedimentation rate of 82-85 cm/kyr (Fig. 3.7).

3.3.2 R248MC010

As earlier mentioned, this core was initially chosen according to a ^{210}Pb chronology conducted by Jensen et al. (2009) on the top part, suggesting a bottom age of ~150 years. This chronology was later-on revised by Leinebø (2011) based on new ^{210}Pb and ^{137}Cs measurements. This new ^{210}Pb record was found highly coinsistent with the one obtained by Jensen et al. (2009). In addition, the ^{137}Cs dataset obtained in core R248MC010 highlighted the 1986 Chenobyl accident within a core depth corresponding to a ^{210}Pb-based date of 1982, therefore confirming the reliability of the ^{210}Pb-inferred chronology.

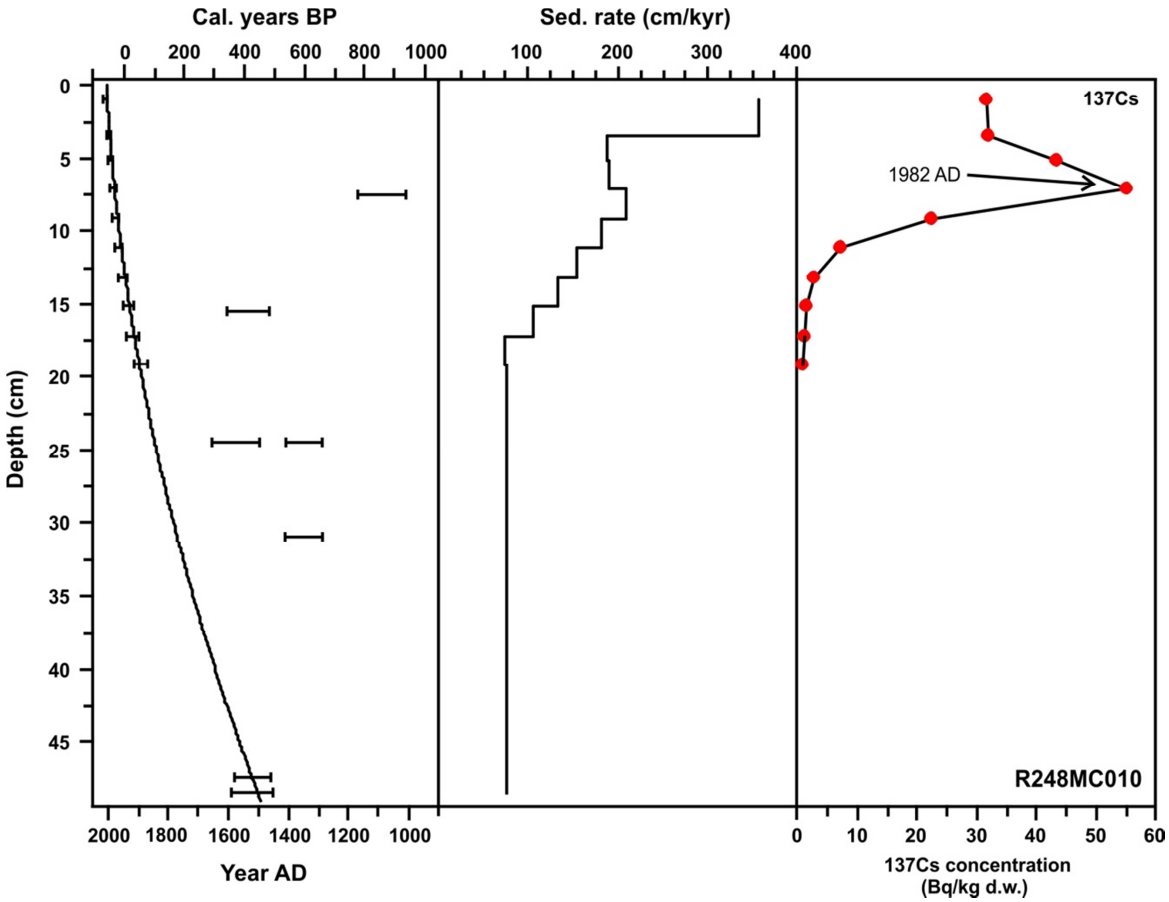

Figure 3.8: Age-depth model, sedimentation rates and ^{137}Cs measurements in core R248MC010, based on data from Table 3.3 and Leinebø (2011) (second order polynomial fit, between each ^{210}Pb dated level and the bottom ^{14}C dates). Horizontal lines: 2 sigma interval of highest probability of the calibrated AMS ^{14}C dates.

A total of six bulk planktonic foraminiferal samples and 1 mollusc sample were submitted to various institutions for AMS ^{14}C dating (Fig. 3.8; Table 3.3). With the exception of two consistent dates obtained at the bottom of core R248MC010, the other five revealed large and variable deviations from the ^{210}Pb -inferred chronology, being older by an average of 500 years (with a maximum of 800 years for the shallower sample in the sediment column) (Fig. 3.8). Reworking and downslope transport of sand-sized material (such as foraminifera shells)

from outer shelf to slope environments are common sedimentary process along the Norwegian continental margin (Fohrman et al., 2001; Schröder-Ritzrau et al., 2001) and is likely to explain the recorded old ages inferred from the mixed planktonic foraminiferal samples. Although bioturbation, as evidenced from the SCOPIX X-Ray image (Fig. 3.3), might act as an additional cause of age excess in core R248MC010, the ^{210}Pb-inferred high sedimentation rate is likely to limit its effect. We must also stress that the foraminiferal samples which were dry-picked for ^{14}C dating contained a significant amount of neanic forms (within the 63 to 90 um size range) as a way to reach the required minimum carbonate weight for measurements. These neanic forms, which are supposed to make up the bulk of planktonic foraminiferal assemblages from shelf environment, are likely to represent an important component of the fossil material which is laterally advected to the core site from shallower environment. This was shown earlier at Gamlembanken southwest of R248MC010 (Rumohr et al., 2001), and hence contribute to the recorded inconsistent measured ages.

According to the final age model (excluding the 5 inconsistent dates), core R248MC010 covers the interval ~2009-1490 AD (-59-460 cal. years BP) with an apparent sedimentation rate of 77 (bottom) -357 (top) cm/kyr (Fig. 3.8). This result is obviously different from the initially expected young age of the sediment core, but still enables us to proceed with a validation of our proxies by comparing with instrumental and historical datasets.

3.3.3 R406MC032

As mentioned earlier, this core was initially chosen according to a ^{210}Pb chronology conducted by Jensen et al. (2010) on the top part, suggesting a bottom age of ~300-400 Cal. years BP. A total of six ^{210}Pb (initial) and three additionel ^{14}C dates were obtained from this core (Table 3.3).

The donwcore grain size analyses show a stronger variability of up to ~20% within the fine fraction of the top 10 cm (Fig. 3.4) compared to the more southern R248MC010 (<6%), a change which might affect the reliability of ^{210}Pb dates, as this element mainly sticks to the finer fraction of the sediments. Nevertheless, as ^{210}Pb dating and the resulting sedimentation rate at R406MC032 (1.4 mm/year; Jensen et al., 2010) fall well within the range of both nearby core sites (Jensen et al., 2010) and the general sedimentation rates recorded within the Barents Sea region (Zaborska et al., 2008; Maiti et al., 2010), we do believe the results to be valid for our age model. The remaining three ^{14}C ages revealed large deviations from the

^{210}Pb -inferred chronology, being older by an average of 5735.5 years, with a maximum of 11290 years for the bottom age (Table 3.3).

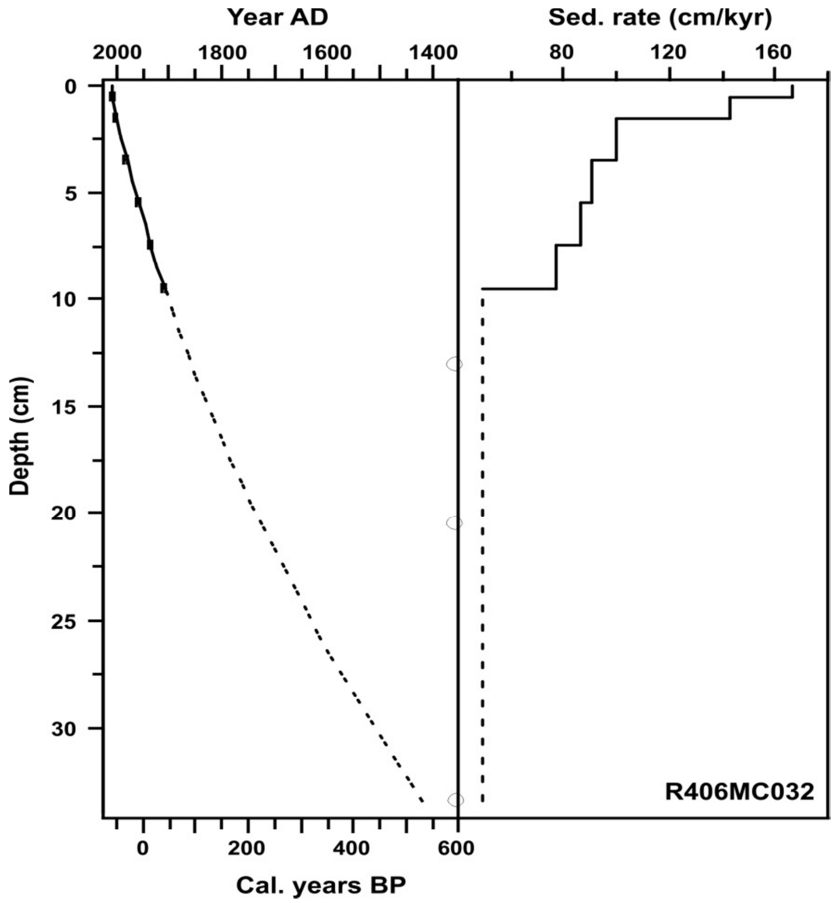

Figure 3.9 : Age-depth model (cal. years BP) and sedimentation rates of R406MC032, based on data from Table 3.3 and Jensen et al. (2010).

A number of studies carried out along the Norwegian (Schröder-Ritzrau et al., 2001) and western Barents Sea (Fohrman et al., 2001; Sarnthein et al., 2003) continental margins (Rumohr et al., 2001), have demonstrated that, in addition to the vertical flux of particles, reworking and downslope transport of sand-sized material (such as foraminiferal shells) from outer shelf to slope environments are a common sedimentary process especially in deep basins and troughs (Fohrman et al., 2001). The location of R406MC032 at the western entrance to the Bear Island Trench, which represents the maximum depth of the Barents Sea (Loeng and Drinkwater, 2007), would therefore most likely be affected by these dense bottom water masses, which flow cross-slope from the shelf edges and down banks such as the Sba and the Gba into the BIT (Navarro-Rodriguez et al., 2012). Hence, lateral advection is likely to explain the recorded old ages inferred from the mixed planktonic foraminiferal samples. Furthermore, the application of a bottom age of 11290 cal. years BP would imply an excessively reduced sedimentation rate within the mid- and early Holocene, a period when,

according to numerous evidences (Bond et al., 2001; Moros et al., 2004; Slubowska et al., 2005; Skirbekk et al., 2010), sediment delivery by the melting of the remnant ice sheets, ice shelves and sea ice was relatively high in the northern North Atlantic region. This sediment input is not shown within the grain size distribution.

These reasonings, therefore, motivated the exclusion of the three ^{14}C ages from the age model, and the construction of the chronology of core R406MC032 was done by applying a second order polynomial fit between the ^{210}Pb dates, extending it to the bottom of the core (Fig. 3.9).

Accordingly, R406MC032 covers the interval ~-57 - 532 cal. years BP with an apparent sedimentation rate of ~49-167 cm/kyr (Fig. 3.9).

3.3.4 JM09-KA11-GC

A total of thirteen ^{14}C dates were measured by Rüther et al. (2012), Berben et al. (2013) and Groot et al. (2013). The ^{14}C dates were calibrated by applying a local reservoir age of $\Delta R = 67 \pm 34$ from south of Bear Island (Mangerud and Gulliksen, 1975), although we did use a standard reservoir correction in an earlier publication (Dylmer et al., 2013). This change has been done according to two recently submitted manuscripts by Berben et al. (2013) and Groot et al. (2013), who applied these reservoir corrections on JM09-K11-GC through the entire Holocene. Two ^{14}C dates were excluded from the age model (Table 3.3), as they showed too young or too old ages when plotted against the chronological framework obtained from the other dates. The age at 32.5-33.5 cm has been excluded because it seems too young and the age at 80-81 cm appears to be to old. Furthermore, based on the lithofacies description by Rüther et al. (2012) (see section 3.2 on JM09-KA11-GC and Fig. 3.5), a boundary was included around 90 cm, to take a possible change in sedimentation rates (Fig. 3.10) into account. Rüther et al. (2012) described an erosive base at the bottom of LF1 (~85 cm), a sharp boundary change from LF2 (crudely laminated, bioturbated mud) to LF4 (layer diamict with muddy matrix) at ~97 cm, a massive shift in the grain size distribution from dominating sand in the top to dominating silt/clay below 85 cm and a sudden increase in the IRD content at the boundary between the latter two facies (Fig. 3.5). In addition, a marked shift can be observed in the interval from ~85-97 cm in most coccolith and dinocyst species, from being fairly stable to a very sudden shift. It is a reasonable assumption that a sedimentation rate shift occurs in relation to strong shifts in the fauna.

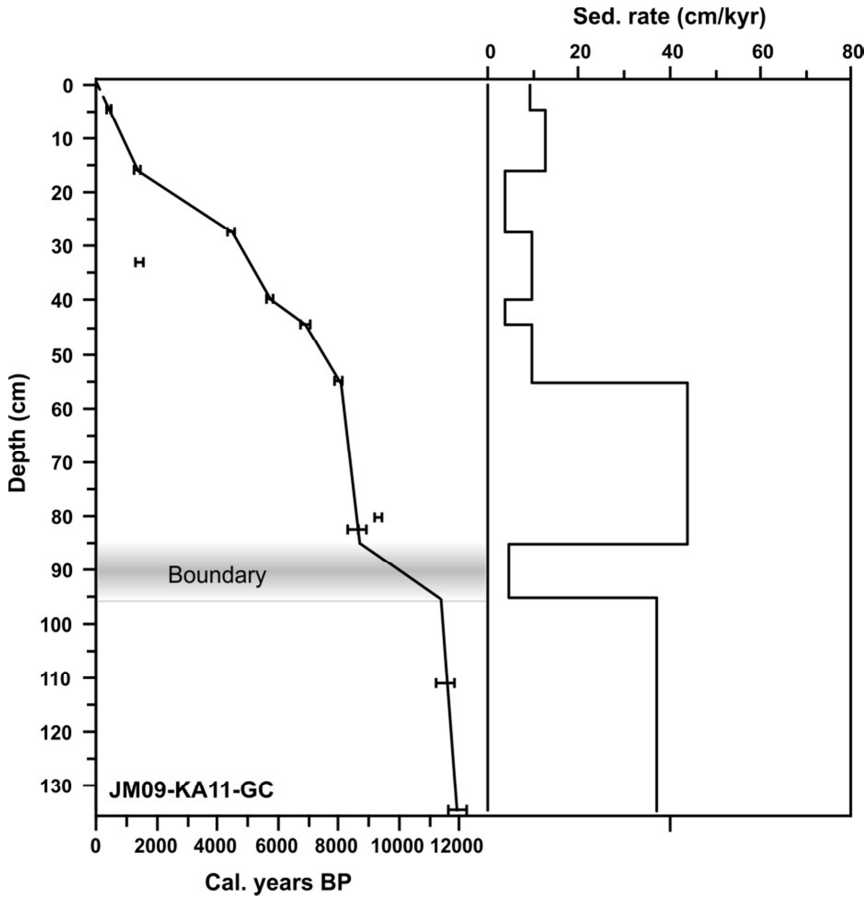

Figure 3.10: Age-depth model (cal. years BP) and sedimentation rates of JM09-KA11-GC, based on data from Table 3.3 (linear interpolation, between each dated level). Horizontal lines: Error range of the AMS C^{14} dating.

The boundary depth has been placed a bit deeper to avoid a sudden change. The chronology was established using the calibrated mean ages for the 2σ interval of highest probability and assuming a constant sedimentation rate between each included radiocarbon dated level of JM09-KA11-GC (linear interpolation) (Fig. 3.10). This was not done at the Boundary. There the equations between the two ^{14}C ages directly above the boundary (53-57 cm and 81-83.5 cm) and directly below (110.5-111.5 cm and 133-136 cm) were applied all the way to the inferred boundary zone at 85 cm and 97 cm, respectively. A liniar interpolation was, then, applied between the following (calculated) boundary top and bottom ages. As with WOO/SC-3, we chose to apply the equation between the first two ^{14}C ages (e.g. 3-6 cm and 15-17 cm) all the way to the top, because of the likelihood of gravity core over penetration.The presented choice of age model differs somewhat from the ones published by Berben et al. (2013) and Groot et al. (2013), as these authors chose to keep the age at 80-81 cm, deleted the two ages at 82.5 cm and did not include an age boundary. Based on these modifications of the age model,

our dataset will most likely differ within the interval ~8000 cal. years BP to 11600 cal. years BP when compared to our Holocene records.

According to the final age model, core JM09-KA11-GC covers the interval ~300-11769 Cal. years BP with sedimentation rates in the range of 4-44 cm/kyr (Fig. 3.10).

3.3.5 HH11-134-BC

Five ^{14}C dates were obtained from this box-core (Table 3.3). The chronology was established by using the calibrated mean ages for the 2σ interval of highest probability and applying a second order polynomial fit between all ages, with the exception of the date obtained at 15.5 cm, which has been excluded because it appeared to be too old (Fig. 3.11; Table 3.3).

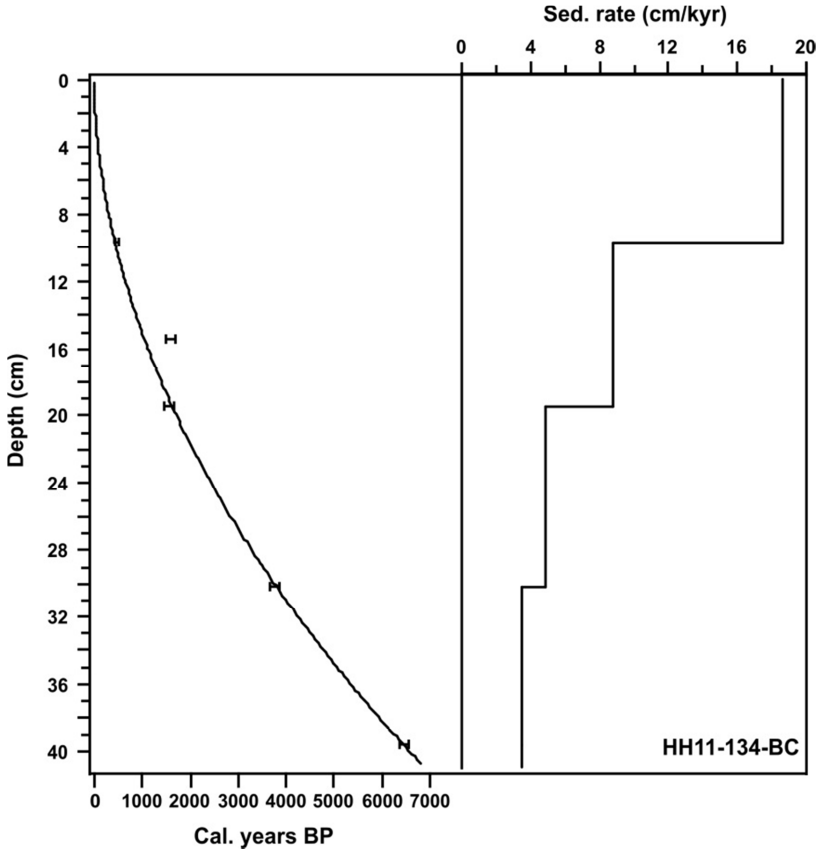

Figure 3.11: Age-depth model (cal. years BP) and sedimentation rates of HH11-134-BC, based on data from Table 3.3 (second order polynomial fit betweeen each dated level). Horizontale lines: Error range of the AMS C^{14} datings.

According to the final age model, core HH11-134-BC covers the interval ~39-6508 Cal. years BP with a sedimentation rate in the range of ~4-19 cm/kyr (Fig. 3.11).

3.4 Geochemical Preparation and Micropaleontological Approach

The following is a short introduction to the different methods applied within this research study, starting with those related to the main proxies used here (e.g. coccolithophores, coccoliths, dinocysts and transfer functions) and then shortly describing those concerning the "minor" proxies (foraminifera, large lithic grains and XRF)

3.4.1 Surface Water Sampling

Surface water sampling was conducted with the purpose of investigating the geographical distribution of the major extant coccolithophore species in the northern North Atlantic (see Chapter 2), hoping that such information might contribute to the understanding of past abundance changes of their fossil remains in the investigated sediment cores. Water sampling was conducted en-route on board the RV *Helmer Hanssen*, using the ship's deck wash pump, which limits the sampling to the near surface water masses (<5 m) and involves on board membrane filtration of 2-3 liter of sea water and air-drying within petri-dishes. Back in the laboratory, a ca 15 mm² of the filter was cut out and mounted in 2-3 drops of immersion oil between slide and cover-slip for examination under a light microscope at ×1000 magnification, as described by Giraudeau et al. (1993). A total of 57 surface water samples (31 samples, September/October 2007, Husum (2007); 26 samples, July 2011, Husum et al. (2011)) were investigated for living assemblages and the results were expressed as coccolithophore standing stocks (number of cells/l). The extant population was dominated by the two major species e.g. *E. huxleyi* and *C. pelagicus* (Appendix 3). *C. pelagicus* includes both the motile holococcolith-bearing phase (*C. pelagicus* f. *hyalinus*) and the non-motile heterococcolith-bearing phase (*C. pelagicus* f. *pelagicus*) (Cachão and Moita, 2000; Balestra et al., 2004).

While the use of a light microscope (compared with Scanning Electron Microscope – SEM - examination) limits a precise taxonomical investigation of the extant coccolithophore population, this approach was found sufficient to identify and to conduct reliable census counts of the dominant fossilizable species in the recovered samples (i.e. *E.huxleyi* and *C. pelagicus*).

3.4.2 Coccolith Preparation from Sediment Samples

The sediment samples for coccolith analysis were prepared according to the « Funnel » method as described by Andruleit (1996). It involves dilution by 10ml of tap water and a few drops of H_2O_2 + $Na_4P_2O_7$, of a preweight amount (0.080 g ± 0.002 g) of dry sediment for

nightcap. These twelve hours is followed by ten seconds ultrasonication of the suspension. The residue is then poured into a larger container and diluted with ~500 ml of tap water, of which 30ml is taken out with a pipette and filtered through a 47 mm diameter and 0.8 µm mesh size membrane filter. A small piece of the air dried filter is then cut out and mounted in 2-3 drops of oil between slide and cover-slip for examination under a light microscope at ×1000 magnification. On average, a total of more than 300 specimens per slide were counted in order to guarantee the statistical reliability of our results (Andruleit, 1996). Census counts were ultimately expressed in terms of relative abundances (species percentage) and absolute concentrations (specimens/gram of dry bulk sediment). The assemblages were found to be dominated by five species (*E. huxleyi, C. pelagicus, G. muellerae, C. leptoporus and Syracosphaera* sp.; Appendix 3). This is in accordance with previous investigations in the area (Samtleben et al., 1995a; Baumann et al., 2000).

Previously repeated analyses of fine fraction sediment samples using the "Funnel" method, have revealed that the method can cause ~15% deviation in the bulk coccolith absolute concentrations (Herlle and Bollmann, 2004). Hence, we will only address species relative abundances as well as "major" (>>15% deviation) absolute concentration changes in the present study.

3.4.3 Dinocyst Preparation from Sediment Samples

The selected samples for dinoflagellate cyst analysis were all processed (<150 µm fraction) using a standard sample preparation procedure (e.g. Stockmarr, 1971; de Vernal et al., 1996), which was slightly modified at EPOC/Université Bordeaux1 (Penaud et al., 2010). A known number of lycopodium clavatum (1-2 tablets) was added prior to the sample treatment in order to calculate absolute concentrations following the method of Stockmarr (1971). The samples were

treated with cold 10, 25 and 50% hydrochloric acid (HCL) in order to get rid of carbonate (depending on the amount of sediment and the carbonate content) and with cold 40 and 70% hydrogen fluoride (HF) for removal of silici-clastic components. Finally the samples was treated again with 25% HCL. The residue was then sieved through 10mm nylon mesh screens. In cases where high amounts of organic material concealed the cysts (spines and processes) organic material was carefully removed by centrifugation and swirling in a large glass, based on the density differences between the cysts and the organic material. The residue containing the dinocysts was hereafter mounted on microscopic slides in a glycerin jelly using a pipette and, finally, covered with a coverslip.

On average, more than 300 specimens per slide were counted using a Zeiss axioscope light microscope at ×40 and ×100 (oil immersion) magnification. A total of 31 species (29 dinocysts and one acritarch; Appendix 3) were identified using the nomenclature of Mudie (1992), Rochon et al. (1999), Head et al. (2001) and Marret and Zonneveld (2003) , which also stands as a base for the following groupings: *Operculodinium centrocarpum* s.l. comprises long-process and short-process forms of *O. centrocarpum* sensu; *Spiniferites membranaceus* includes *Spiniferites belerius*; *Spiniferites mirabilis* contains *Spiniferites hyperacanthus*; *Islandinium minutum* includes *Islandinium cezare*; *Brigantedinium* spp. includes *Brigantedinium simplex, Brigantedinium caracoense* and all spherical brown cysts with smooth walls; *Impagidinium* spp. includes the species *Impagidinium patulum*, *Impagidinium aceulatum* and *Impagidinium sphaericum*; the acritarch *Halodinium* spp. contains the species *Halodinium minor* and *Halodinium major*. The term "spp." refers to cysts which has not been identified beyond the genus level. The relative abundances of the species are calculated based on the total sum of species, excluding reworked cysts, acritarchs and unidentified taxa. The absolute abundances include all unidentified cysts and acritarchs, hence *Halodinium* spp. will only be shown as absolute concentrations.

3.4.4 Modern Analogue Technique (Transfer Function - TF)

Recent studies have shown that dinocyst assemblages in surface sediments of Arctic and sub-Arctic seas have shown a close relationship with sea surface parameters such as temperature, salinity, and seasonal extent of sea ice cover (Mudie, 1992; Voronina et al., 2001; de Vernal et al., 2001, 2005; Zonneveld et al., 2013). On these grounds, and assuming that fossil assemblages developed in environmental conditions similar to the modern analogues, transfer functions using the modern analogue technique (MAT) have been developed. The background of the technique was reported by Overpeck et al. (1985) and Guiot (1990) and originally developed for pollen assemblage. It was later-on adapted for dinocysts by de Vernal et al. (2001, 2005). The MAT technique is the preferred transfer function technique applied to dinocyst assemblages for quantitative reconstruction of sea surface parameters (e.g. temperature, salinity and sea ice cover) as it provides the most reliable and realistic estimates (de Vernal et al., 2001). The technique uses a logarithmic transformation of the relative abundances (per mill) of all taxa in order to increase the importance of the rare species, which are expected to have more specific ecological requirements. Here after follows a search for the best (and closest) 5 analogues amongst the modern spectra on the basis of an even weighting of the taxa by applying the "R" software package ("R" version 2.7.0, R

Development Core Team, 2008). In the present study, we used the modern database containing 1189 surface sediment samples from the Arctic, North Atlantic and North Pacific basins (de Vernal et al., 2008; Radi and de Vernal, 2008; Penaud et al., 2011, and references therein).The hydrological parameters were estimated by calculating an average of the 5 closest analogues (see Appendix 4 - for analogue locations), which are inversely weighted by their respective distance (Radi and de Vernal, 2008; de Vernal et al., 2001, 2005). The technique includes a threshold of a certain distance between the fossil assemblage and a modern analogue, above which the analogue will be rejected. The resulting confidence intervals are calculated from the variances in the closest analogues. Sea ice cover is expressed in terms of months per year with sea ice concentration greater than 50%, a parameter which correlates with the mean annual sea ice concentration but is slightly more sensitive to small ice cover values (de Vernal et al., 2005)

One way to test the approach's degree of accuracy is by comparing modern values (World Ocean Database, 2009, Boyer et al. 2009) with the estimated values reconstructed by MAT within the core-top sample, keeping in mind that the geographical domain of the analogue data set may introduce a bias in the reconstructions (e.g. oceanic site included in fjord areas).

3.4.5 Sample Preparation for the Investigations of Planktic Foraminiferal Assemblages and Large Lithic Grains (or IRD)

All samples of cores R248MC010, R406MC032 and HH11-134-BC were wet sieved through a 63 µm mesh for combined investigations of large lithic grains and foraminiferal assemblages (as well as picking of ^{14}C dates). Foraminiferal and lithic grain identification and counting were done through a light microscope, applying representative splits when necessary.

Investigations on planktonic foraminiferal assemblages were conducted on multi-cores R248MC010 and HH11-134-BC. Species counting was performed on the >100 µm fraction (according to Husum and Hald (2012)) by Linda Rossignol – EPOC - (R248MC010) and Jacques Giraudeau – EPOC - (HH11-134-BC) in order to include small sized species which are frequent in assemblages of the northern North Atlantic. A total of nine planktonic foraminiferal species were recognized and counted (Appendix 3). In addition, counts of bulk benthic foraminiferal shells were done. A taxonomical grouping of sub-polar foraminifera, expressed as the sum of *Globigerinata* species and *Turborotalia quinqueloba,* was applied to the original species counts.

Investigations of large lithic grains have been conducted on cores R248MC010, R406MC032 and HH11-134-BC on the size fraction >150 µm and >500 µm. Descriptive criteria and identification were taken from and follow Wright (1974), Bischof (1994) and Bond et al. (2001). Ice Rafted Detritus (IRD) is sediment that was entrained in floating ice, either icebergs or sea ice, and hat settled to the seafloor when the enclosing ice melted (Hemming, 2004). In the open ocean it is necessary to use a coarse size fraction that has , almost by certainty, not been transported by means other than ice rafting. Here, the size fraction >63 µm are most likely derived by ice rafting and grains >150 µm almost definetely are, if sediment redistribution has not effected the site (Hemming, 2004). Hence when applying IRD in the following chapters we chose to apply the >150 µm size fraction. In addition the size fraction >500 µm will be adapted as a relative iceberg indicator.

3.4.6 XRF Core Scanner Preparation and Measurements

The computer controlled Avaatech X-ray fluorescence (XRF) core scanner is used for scanning and analyzing the chemical composition of sediments directly at the surface of a slab, collected from the sediment core split. XRF core scanners provide a qualitative, non destructive and rapid assessment of major to minor elements from Aluminum (Al, atomic number 13) through to Uranium (U, atomic number 92) (Richter et al., 2006).

The slab surface was covered with a 4 mm thin foil to avoid contamination of the XRF measurement unit and to make sure that the sediment did not dry out. The basic principal is that an X-ray source ionizes the elements in the sediment, which in turn emit an element specific radiation registered by the detector. The XRF radiation passes through three foils between the sediment and the detector: the first covers the sediment surface, the second and the third foil cover the He-flush prism (Tjallingii et al., 2007). To optimize the quality of the XRF measurements, one has to make sure that the sediment surface has first been smoothed and that neither air bubbles nor wrinkles exist under or in the foil. The XRF scanner measurements were carried out with a setting of 10 kV to obtain the element intensities from Al to Fe (on R248MC010 and HH11-134-BC).

Tjallingii et al. (2007) found that the Al and Si counts strongly decrease when the water content of the sediment or between the foil and the sediment surface is elevated. Hence, the XRF core-scanner measured changes in concentration of lighter elements need special attention, i.e. should be compared with Cl profiles, which fluctuate according to seawater content (Tjallingii et al., 2007). In general, elemental records obtained from semi-quantitative

(core scanner) or quantitative XRF measurements should not be interpreted on their own, as elements often originate from different sources: Fe can be lithogenic but can also be produced within the sediment; Sr can be related to in-situ production of biogenic carbonates but may also originate from detrital carbonate sediments of the Barents Sea (Jochen Knies, personal comment).

Chapter 4 : A Late Holocene View on Surface Water changes in the Eastern Nordic Seas

4.1 Chapter Overview

Previous water column and surface sediment investigations of extant and fossil remains (coccoliths) of coccolithophorids and dinocysts suggested that these species groups could be used as qualitative and quantitative proxies of both water mass distribution, sea-surface parameters (temperature, salinity and sea ice) and NAC flow strength in the northern North Atlantic (Samtleben and Schröder, 1992; Samtleben et al., 1995; Matthiessen, 1995; Baumann et al., 2000; Schröder-Ritzrau et al., 2001; de Vernal et al., 2001, 2005; Giraudeau et al., 2010; Zonneveld et al., 2013). The present chapter lies on these exploratory works in applying selected coccolith and dinocyst proxies on a set of marine sedimentary cores distributed along the continental margins off western Norway, western Barents Sea and western Spitsbergen. Our aim is to investigate late Holocene changes in the AW flow and associated surface hydrological frontal variations along the main axis of heat and salt transfer to the Arctic Ocean, which is carried by the Norwegian Atlantic Current (NwAC) and its northernmost extension the West Spitsbergen Current (WSC). Given the major influence of NAO related atmospheric processes on the modern NwAC dynamics and climate of the Nordic Seas region, we will thoroughly discuss our proxy results in view of available NAO paleoreconstructions over the last 3000 years, as well as nearby terrestrial and marine records.

4.2 Introduction

The Late Holocene was governed by a cooling trend known as the Neoglaciation (Porter and Denton, 1967). Compared with the preceding Early to Mid-HTM, the Neoglaciation has been widely recorded in both terrestrial and marine archives in the North Atlantic Region (Jennings et al., 2002; Seidenkrantz et al., 2008; Kaufmann et al., 2009, and references therein; Andresen et al., 2011; Müller et al., 2012) as a time of expansion of Scandinavian glaciers (Nesje et al., 1991; Nesje et al., 2001), increased sea-ice cover and colder surface waters in the Barents Sea and part of Fram Strait (Duplessy et al., 2001; Risebrobakken et al., 2010; Kinnard et al., 2011; Müller et al., 2012), colder surface and subsurface waters off western Norway (Calvo et al., 2002; Moros et al., 2004; Hald et al., 2007; Sejrup et al., 2011) and overall colder conditions over Northern Europe (Bjune et al., 2009). This cooling trend was punctuated by several warm and cold spells such as the Roman Warm Period and Medieval Climate Anomaly (RWP, MCA), and the Little Ice Age (LIA). Over the last century, the LIA was reversed by an overall increase in temperature, as seen in, terrestrial high resolution proxy records of the Arctic region (Overpeck et al., 1997; Kaufman et al., 2009) and proxy records from marine sediment cores of the northern North Atlantic (Spielhagen et al., 2011; Hald et al., 2011; Wilson et al., 2011). Marine proxy-based reconstructions suggest that this recent temperature increase in the subsurface layer west of Spitsbergen (Spielhagen et al., 2011) and in shallow settings off northwest Norway (Hald et al., 2011) were unprecedented over the past two millennia. Both studies implied that this warming was probably caused by enhanced advection of AW to the Arctic Ocean during modern times, although none were able to strictly infer the dynamical history of AW, i.e. the history of the strength of the NwAC.

The hypothesis of an increased AW inflow during the modern period was further supported by Wanamaker et al. (2012) based on living and fossil molluscan remains north of Iceland; these authors additionally related known pre-Anthropocene warm (MCA) and cold (LIA) climatic spells of the last ~1500 years to modulations of the surface Atlantic-derived water dynamics within the North Atlantic. This modulation was further evidenced off Florida, at the inception of the Gulf Stream, by Lund et al. (2006) who estimated a 10 percent decrease in the flow of this current at the transition from the MCA to the LIA. Similarly, in the close Chesapeake Bay, such a modulation was also evidenced by Cronin et al. (2005) who linked this to NAO forcing of sea-surface temperature in the western North Atlantic.

The processes controlling variations in the meridional flow of the NAC to the Nordic Seas and ultimately to the Arctic Ocean are either associated with anomalies in the location and strength of the westerlies, and/or changes in the thermohaline circulation (Müller et al., 2012; Chapter 1). At present the most prominent pattern of atmospheric variability in the North Atlantic Region is known as the NAO, itself depending on the Northern Hemisphere annular mode, the Arctic Oscillation (e.g. Marshall et al., 2001). The NAO is defined as the wintertime difference in atmospheric pressure (sea level) between the Icelandic low and the Azores high, controlling the strength and direction of westerly winds, storm tracks across the North Atlantic, temperature and precipitation over western Europe, and the strength of the poleward NAC and equatorward EGC (Blindheim et al., 2000; Hurrell et al., 2003). A low NAO index (reduced westerly flow across the Atlantic) induces a reduced flow of the NAC, less precipitation in Northern Europe and a more southern direction of the storm tracks (Hurrell et al., 2003). Whereas a high index favors a strengthened NAC flow, stronger precipitation and an eastward shift of the Arctic Front (AF) which separates AW from ArW, toward the slope off Norway (Blindheim et al., 2000). Furthermore modern observations indicate a significant correlation between the NAO indexes and the Barents Sea ice extent, with less sea ice during the positive NAO (warm) phases and conversely more ice during negative NAO (cold) phases (Vinje, 2001; Sorteberg and Kvingedal, 2006), possibly related to variations in southwesterlies, air masses and Atlantic inflow (Blindheim et al., 2000).

Paleorecords from Arctic Canada and Iceland suggest that a series of explosive volcanism centered at the MCA/LIA transition might have triggered an extensive sea ice expansion during the LIA (Miller et al., 2012). A combined switch in NAO patterns from a long-term positive phase during the MCA to negative NAO conditions during the LIA (Trouet et al., 2009; Dylmer et al., 2013) possibly further enhanced the severe increase in sea-ice extent, as decadal and long-term variations in large scale ice concentrations have shown to be significantly correlated with long-term NAO variations (Visbeck et al., 2003).

However, although the importance of the NAO on the modern hydrography and climate of the Nordic Seas is now well established, assessing its significance on paleoceanographical changes of this ocean realm has long been hampered by the lack of instrumental records prior to the 19th century, and by proxy- and model-based reconstructions reaching back only up to one millennia (Lutherbacher et al., 2002; Trouet et al., 2009). A high resolution reconstruction of NAO variability from a lake record in Southwestern Greenland (Olsen et al., 2012), recently extended the NAO record back to 5200 years Before Present (BP), offering a way to

investigate links between atmospheric processes and ocean circulation changes over the mid to late Holocene in the Northern North Atlantic.

The NAC impact on the hydrological and climatic changes in the Nordic Seas and the Arctic Ocean is tremendous, hence motivating investigations aiming at a better understanding of inflow variations, forcing mechanisms and their consequences on the regional and global climate system.

In the following, we discuss late Holocene changes in dinocyst and coccolith assemblages from four sediment cores distributed along the eastern Nordic Seas in terms of qualitative and quantitative (dinocyst-based reconstructions) changes in the surface hydrography of the northern North Atlantic. Details on the core locations, chronologies and species groupings are given in Chapter 3, whereas the species ecology is given in Chapter 2.

4.3 R248MC010 (West of Lofoten Island)

4.3.1 Coccolith Record

The overall preservation of coccolith remains was found to be good within R248MC010, hereby confirming the overall relatively good preservation of calcareous microfossils in recent sediments of the eastern Nordic Seas (Hebbeln et al., 1998; Matthiessen et al., 2001).

Bulk coccolith concentrations throughout the investigated time interval range from ~9 to 32 x 10^8 sp/g. dry sed., a range which falls within typical values of bulk coccolith concentrations in surface sediments of the eastern Nordic Seas below the NwAC and WSC (Baumann et al., 2000). The bulk coccolith concentration record is characterized by overall increasing values towards the core top, punctuated by several lows and highs, with the latter located at 424, 292, 227, 162, 90, 48, 13 and -41 cal. years BP (Fig. 4.1). Relative changes in the amount and temperature of Atlantic-derived surface waters, which sustain most of the calcareous plankton production in the Nordic seas (Schröder-Ritzrau et al., 2001, and references therein), explain to a high extent these observed changes in bulk coccolith accumulation (Andruleit and Baumann, 1998).

Core R248MC010 is only expected to be influenced by terrigeneous inputs from the nearby continental shelf and/or rivers, as sea ice has not been present at the core site during the last centuries including the coldest period of the LIA (Vinje et al., 2001; Divine and Dick, 2006). Dilution of the biogenic component of R248MC010 sediments by terrigenous material carried by the NCC might therefore bias the significance of bulk coccolith concentration records in terms of paleo-productivity patterns.

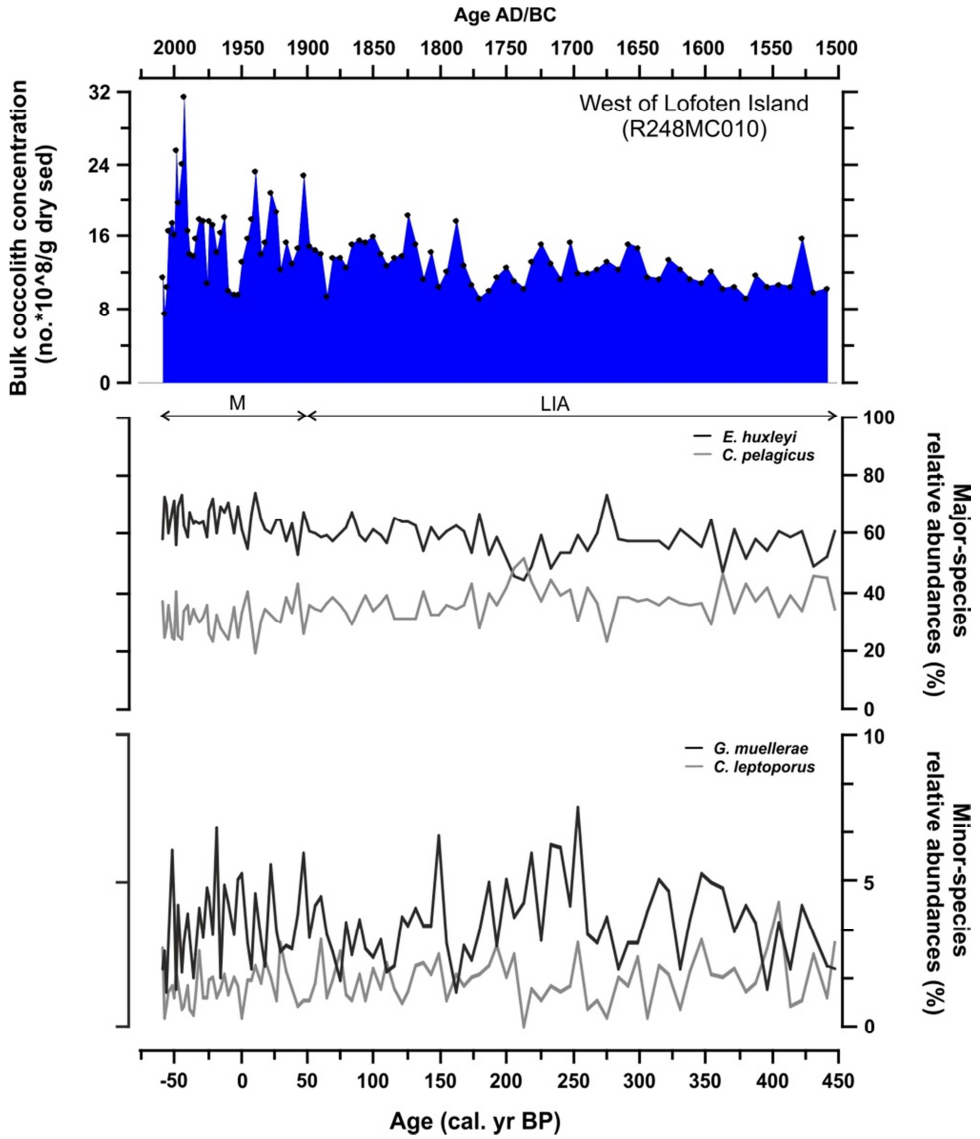

Figure 4.1 : Bulk coccolith concentration record (coccoliths * 10^8/g dry sed.) (top) and relative abundances (%) of major (mid) and minor (bottom) coccolith species within R248MC010.

The coccolith species diversity in core R248MC010 is typically low as expected for this arctic/subarctic setting (e.g. Baumann et al., 2000; Matthiessen et al., 2001) and shows a dominance of *C. pelagicus* (19-51%) and *E. huxleyi* (44-75%), with the latter species contributing on average with more than 50% of the total assemblages (Fig. 4.1).

The core show an overall increased contribution of *E. huxleyi* with relatively high abundances toward the beginning and the end of the record and marked low values between ~220 and 190 cal. years BP. *C. pelagicus* displays opposite patterns of relative abundances in R248MC010 as expected given its overall shared dominance with *E. huxleyi*. The resultant E/C ratio shows values ranging from ~0.5 to 2.7, the ratios decreasing from the base of the record until ~220 - 190 cal. years BP (minimum values), followed by an overall increase toward the Present (Fig. 4.2).

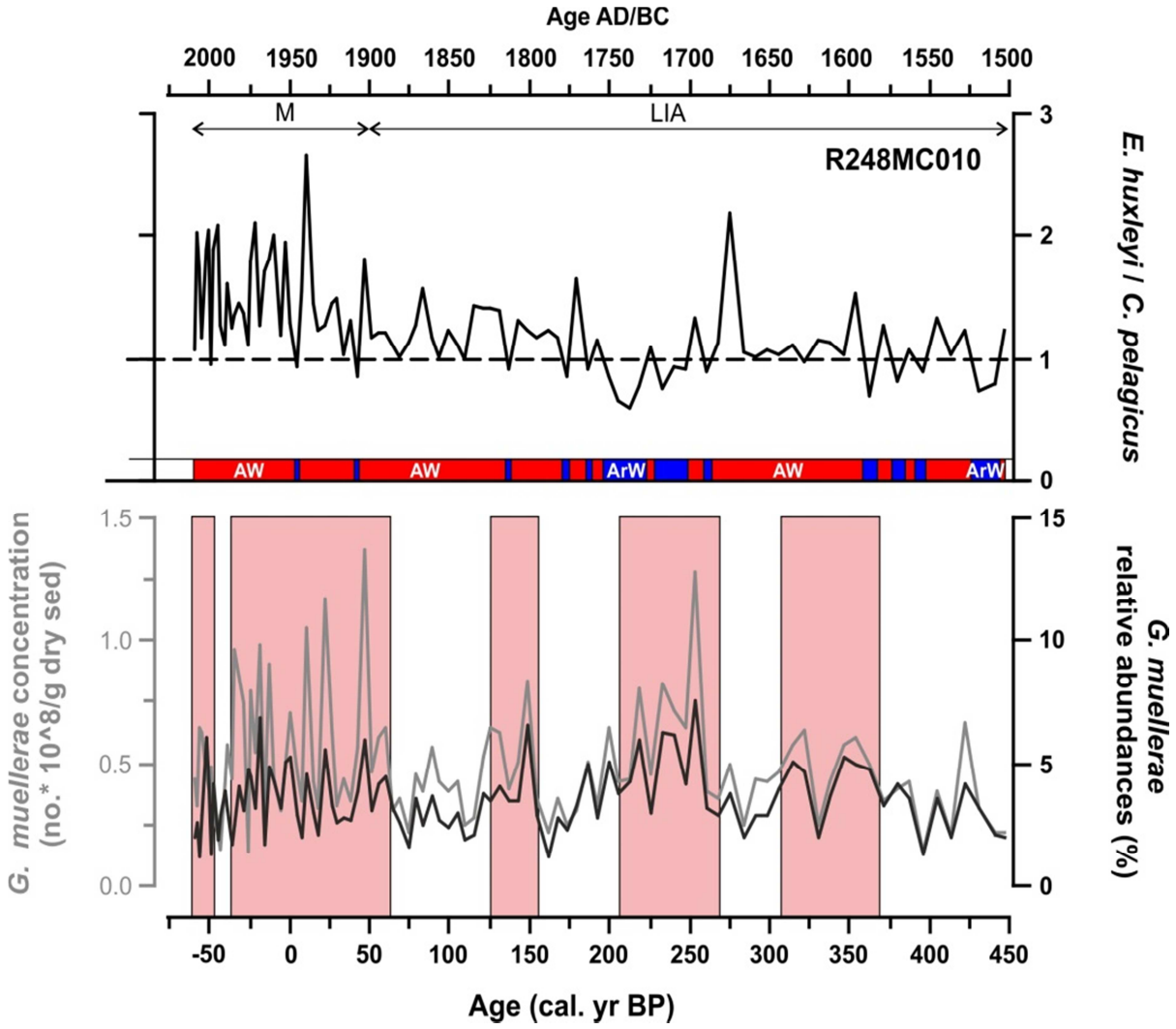

Figure 4.2 : Top : E/C ratios of the dominant coccolithophore species *E. huxleyi* (E) and *C. pelagicus* (C). The bar charts below each E/C plot highlight the dominating surface water masses of R248MC010 according to the "1" threshold: Blue = ArW (E/C<1); Red = AW (E/C >1). Bottom: Relative abundances (black line) and absolute concentrations (grey line) of the AW inflow species *G. muellerae*. The light red shaded areas indicate the marked inflow increases inferred from absolute concentrations of *G. muellerae.*

The species *G. muellerae* (1-8%) and *C. leptoporus* (0-4.5%) account for an average of ~3.5% and 1.5% respectively of the total assemblage, the latter will not be discussed further for this core. The relative abundances of *G. muellerae* increase up to ca. 250 cal. years BP and show a succession of fluctuating abundances with higher values roughly centered at ~370-310, 270-210, 160-130, 60- -35 and -50 cal. years BP to the top (Fig. 4.1). The trends in absolute and relative abundances of this drifted species are nearly identical in this core (Fig. 4.2). Short and/or long term changes in sedimentation of terrigenous material, which most probably affect patterns of microfossil concentration records, including coccoliths, had therefore no obvious influence on *G. muellerae* absolute abundance trends along the studied transect.

Hence *G. muellerae* absolute concentration records can be confidently considered as a proxy for relative changes in the NwAC strength within this record (Fig. 4.2).

4.3.2 Dinocyst Record

The preservation of dinocysts was generally found to be good within R248MC010. This is in accordance with the general high resistance of this species group to degradation processes in the water column and the sediment when compared to other microfossils (Zonneveld et al., 1997). The bulk dinocyst concentrations (sp×10^3/g. dry sed.) fluctuate within the range of 9 to 56 ×10^3 sp/g. dry sed (Fig. 4.3), which is in the range of earlier studies of dinocyst concentrations within surface sediments of the eastern Nordic Seas (Samtleben et al., 1995a; Matthiessen, 1995). The dinocyst concentrations are characterized by an overall decreasing trend toward the top of the record, punctuated by increasing values from the base of the core until ~340 cal. years BP, between 280 and 266 cal. years BP and during the last decades (Fig. 4.3).

The dinocyst diversity is rather high in core R248MC010 and includes a total of up to 25 species (incl. 1 acritarch). The three species *O. centrocarpum* (~43-70%, OCEN), *P. daleii* (~10-35%, PDAL) and *N. labyrinthus* (~5-19%, NLAB) dominate the dinocyst assemblages over the last ~450 years, followed by the two subordinate species *Brigantedinium* spp. (0-12%, BSPP) and *S. ramosus* (0-6%, SRAM) (mean relative abundances of 3.1% and 2.4%, respectively) (Fig. 4.3). All other species contribute with less than 2% of the total assemblages. The reworked dinocysts are expected to origin from river runoff and/or sediment reworking from shallower settings and show a mean absolute concentration of 0.094 sp/g. dry sed.(Fig. 4.3). The average composition of the dinocyst assemblages in core R248MC010 is similar to the ones found in surface sediments along the shelf and slope off northern Norway and of the southwestern Barents Sea (Solignac et al., 2009).

The core show an overall increasing abundance toward the Present of the species OCEN, NLAB, SRAM, *S. elongatus* (SELO) and reworked dinocysts, at the expense of PDAL and BSPP (Fig. 4.3). The OCEN record initiate at the base with an increase until 184 cal. years BP, followed by lower abundances until -42 cal. years BP and a final step of increased abundances during the last decades. PDAL and NLAB show an almost opposite trend with the exception of decreasing abundances initiating at 46 (PDAL) and -28 (NLAB) cal. years BP. BSPP shows two peak relative abundances at 343 and 411 cal. years BP. Finally SRAM shows a trend of increasing abundances from 250 cal.years BP to the Present. Minimum

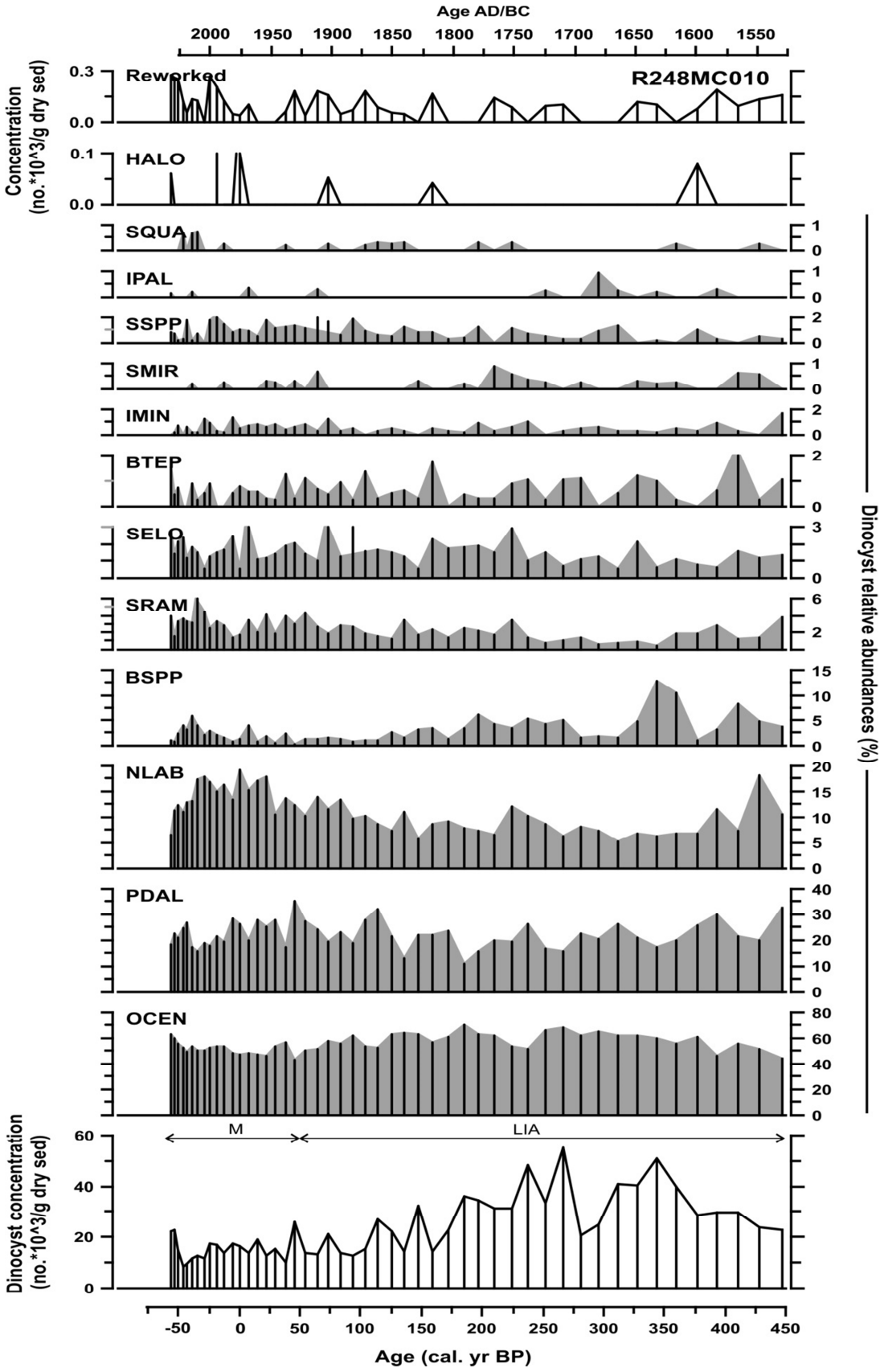

Figure 4.3 : Reworked dinocysts and *Halodinium* spp. (HALO) concentrations (dinocysts * 10^3/g dry sed.) (top), relative abundances (%) of major and minor dinocysts (mid) and dinocyst concentration records (dinocysts * 10^3/g dry sed.) (bottom) of R248MC010. (See chapter II for species names - abrevations).

contributions of SRAM to the dinocyst assemblages encompass the time intervals 350-250, 185-100 and 10-(-)20 cal. years BP (Fig. 4.3).

The resulting ratios OCEN/NLAB (Matthiessen et al., 2001), OCEN/*I. minutum* (IMIN) (Grøsfeld et al., 2009; Solignac et al., 2009) as well as the ratio Autotroph/Heterotroph (A/H) dinocysts, show mean values of 5.8, 116.5 and 31, respectively (Fig. 4.4). OCEN/NLAB and OCEN/IMIN show an overall decrease toward the Present which initiated after a short increase until ~330 cal. years BP. This overall continuous decrease in these dinocyst ratio values is interrupted by a strong low at roughly ~250-225 cal. years BP. The A/H ratio is governed by an overall increasing trend toward Present with maximum values located in the intervals ~330-270 and 100- -20 cal. years BP (Fig. 4.4).

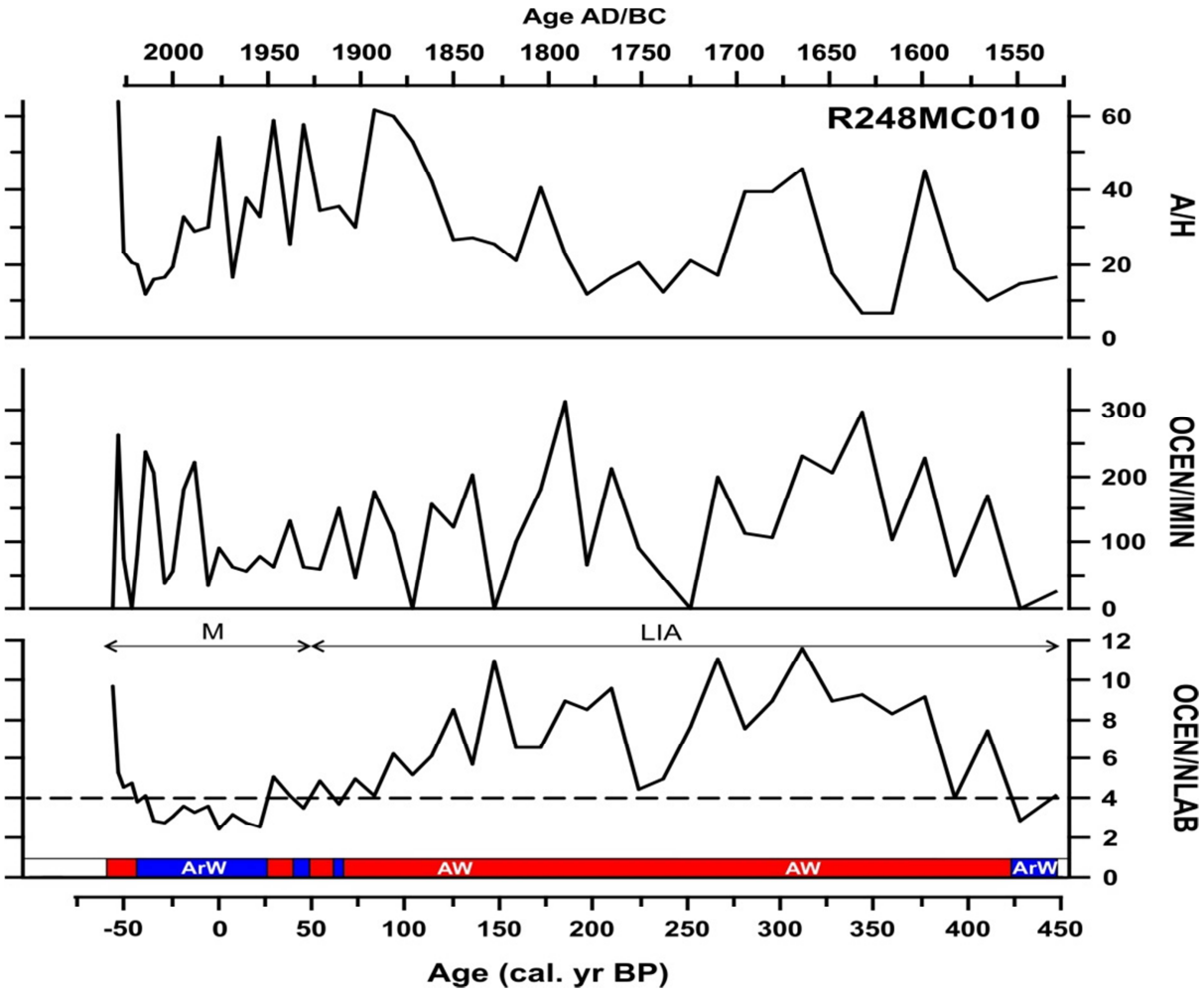

Figure 4.4 : Top: Trophic level ratio between autotrophic (A) and heterotrophic (H) species. Mid: OCEN/NLAB ratio between the AW thriving *O. centrocarpum* (OCEN) and the sea ice related (ArW) *I. minutum* (IMIN). Bottom : OCEN/NLAB ratio of the dominant dinocyst species OCEN and *N. labyrinthus* (NLAB). The bar charts below the OCEN/NLAB plot highlight the dominating surface water masses of R248MC010 according to the "4" threshold: Blue = ArW (OCEN/NLAB<4); Red = AW (OCEN/NLAB >4).

4.3.3 Quantitative Reconstructions of Sea-Surface Conditions

The reconstruction of sea-surface conditions (MAT) resulted in mean winter and summer temperatures of 1.1 °C and 12.3 °C, respectively, for the last ~450 years. The winter and summer temperatures (3.5-12.3 °C) and salinities (33.4-32.3) reconstructed from the uppermost dinocyst assemblages of core R248MC010 lay within the range of modern temperature (5.73-10.8 °C) and salinity (34.3-34.6) values from the World Ocean Database (Chapter 3), salinities being though generally under-estimated by MAT (Fig. 4.5).

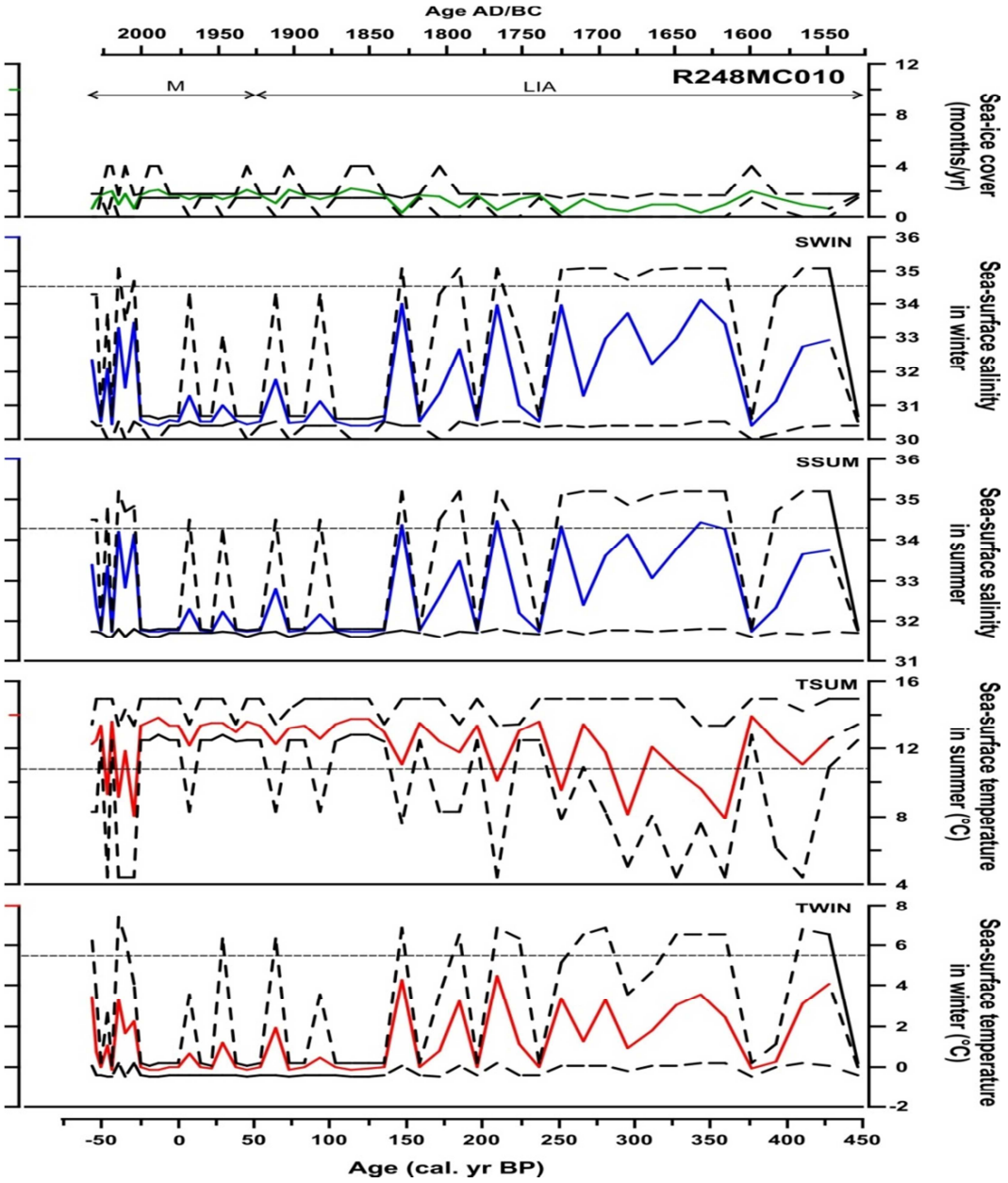

Figure 4.5 : Reconstruction of sea-surface conditions (temperature, salinity, sea ice cover) from dinocyst assemblages of core R248MC010, based on the modern analogue technique (MAT). The surface sediment database (n=1189) of the North Atlantic and North-Eastern Pacific was applied for MAT. Minimum and maximum errors on the estimated parameter are shown by the dashed black lines flollowing the curves. The modern average values are represented by the horisontal dashed lines.

MAT reconstructions display recurring episodes of increased winter temperatures (TWIN, -0.4-4.5 °C) and salinities (summer salinities, SSUM, 30.6-34; winter salinities, SWIN, 31.8-34.4), with an opposing decrease in summer temperatures (TSUM, 8-13.7) (Fig. 4.5). High stable TWIN, SSUM and SWIN, and low TSUM define two intervals centered between 360 and 250 cal. years BP and within the last 30 years. A relatively unstable period is observed in the interval from ~250-150 cal. years BP in all reconstructions. Minimum SSUM and SWIN and TWIN (but higher TSUM) occur continuously from ca. 150 to -25 cal. years BP.

The MAT sea-ice reconstructions are indicative of sea-ice at the core site during 0.4 to 2.2 months/year over the last 450 years (Fig. 4.5). According to the reconstructions, maximum duration of sea-ice characterize the last two centuries including the industrial period and the present global warming period. These results are at odd with historical records of maximum distribution of the Marginal Ice Zone (MIZ) during the last centuries (Vinje et al., 2001; Divine and Dick, 2006) which do not suggest the presence of sea-ice in the vicinity of site R248MC010 during the last ~450 years. The MAT sea-ice reconstructions are also at odd with the location of the studied core below the northward flow of NwAC at a site which is known to be the strongest along the Norwegian coast (Jakobsen et al., 2003) and therefore makes sea ice formation and southward flow of sea ice unlikely.

4.3.4 Inferring the Paleoceanographic changes in Atlantic Water Flow and the Distribution of Surface Waters during the Last ~500 years (R248MC010)

The different proxy data are indicative of paleoceanographic changes in the form of surface temperatures and salinities, distribution of surface water masses, paleoproductivity and strength of the AW flow (Fig. 4.6). The proxies are plotted together with reconstructed bottom water temperatures from the nearby Malangen fjord (Hald et al., 2011) and a combination of instrumental (Dec-Mar; Jones et al., 1997; Osborn, 2006) and reconstructed NAO index (Lutherbacher et al., 2002; 11-year running mean on winter months DJFM) (Fig. 4.6f). Three time zones (and two subzones) have been identified through comparison of all proxy data. ZONE III represents the interval from the core base to 240 cal. years BP (1490-1710 AD) a period which encompasses the main part of the Little Ice Age (LIA). ZONE IV covers the interval 240-60 cal. years BP (1710-1890 AD), i.e. the LIA/Modern transition, and can be subdivided into two subzones IV-a (1710-1800 AD) and IV-b (1800-1890 AD). ZONE V is roughly equal to the last century from 60 to -59 cal. years BP (1890-2009 AD, Modern period) (Fig. 4.6).

In general the proxies shows higher amplitudes during the last two centuries compared to the previous time period. This change in amplitude is attributed to the overall decreasing time resolution down-core and hence increased smoothing of the signals.

ZONE III: 460-240 cal. years BP (1490-1710 AD, Little Ice Age, LIA)

The zone is characterized by a slightly increasing although relatively weak flow of AW (G. muellerae no.*10^8/g, compared to the present level). A minor maximum in flow strength from 370 to 310 cal. years BP occurs synchronously with minimum abundances of subpolar foraminifera (Fig. 4.6b+c). Previous observations identified a clear correspondence between *G. muellerae* absolute abundance datasets and foraminiferal records in Fram Strait sediments (Dylmer et al., 2013). There, subpolar foraminifera are assumed to represent subsurface Atlantic-derived waters (Carsten et al., 1997), hereby confirming the reliability of this coccolith proxy as an indicator of Atlantic water flow strength. Hence assuming that this coccolith proxy is valid west of Norway, the slight inflow of AW during most part of the 15th century seems to be restricted to the upper surface waters, and is supported by high stable surface water salinities (SWIN) and temperatures (TWIN), colder conditions prevailing in the subsurface water masses (Fig. 4.6b+j+k).

The relatively stable relationship throughout this zone, of the two major coccolith proxies (*E.huxleyi* and *C. pelagicus*, E/C) and the strongly decreasing abundance with age of NLAB (together with a slight increase in OCEN), results in a E/C ratio fluctuating around 1 and a strongly increasing OCEN/NLAB ratio toward the top of Zone III (Fig. 4.6g+h). According to earlier studies on the biogeography of the major coccolith and dinocyst species within surface sediments of the Nordic Seas (Samtleben et al., 1995; Matthiessen et al., 2001) (see Chapter 2), the abundance ratios E/C (Baumann et al., 2000) and OCEN/NLAB (Matthiessen, 1995; Matthiessen et al., 2001) have been proposed as proxies for the location of the Arctic Front (AF), which separates the seasonally ice-covered waters of the Polar and Arctic domains (E/C<1; OCEN/NLAB<4) from warmer and saltier Atlantic-derived waters (E/C>1; OCEN//NLAB>4).

Since an overview discussion of the two ratios and of their interpretations as paleoceanographic tracers of the surface expression of ArW and AW is included in a later part of this chapter, the presented ratio interpretations will only be discussed in the light of the relative changes within the zones and subzones currently discussed, and of their relation to the other proxies. Modern observations on the influence of NAO upon the surface hydrology of the eastern Nordic Seas shed light on the understanding of the two ratios. Instrumental records

are indicative of a correlation between changes in the NAO index and surface temperature variations (Blindheim et al., 2000; Miettinen et al., 2011) in the Norwegian Sea. A low NAO index results in a more zonal path of low pressure systems across the Atlantic (a southward storm track), in a generally reduced and wider flow of the NwAC (wider NCC) and in reduced precipitation over Northern Europe (Hurrell et al., 2003). Whereas a high index favors stronger precipitation over Northern Europe, a strengthened NwAC flow and an eastward shift of the Arctic Front toward the slope off Norway (narrower NCC) (Blindheim et al., 2000; Pinto and Raible, 2012). According to these NAO-driven changes in hydrology over the Norwegian continental margin, and comparing our micropaleontological ratios with the NAO index and the temperature reconstruction from the Malangen fjord (Fig. 4.6f-j) we propose that our proxies are related to different controlling factors within sediment core R248MC010. Maximum in OCEN/NLAB ratio occurs during sustained low NAO phases, conditions which induce a westward shift of the AF as expressed by the decreased abundance of the ArW preferring NLAB (Chapter 2). The E/C ratios covary with the bottom water temperatures in the Malangen fjord suggesting a common controlling process e.g. the distribution of the NCC and of the NwAC over the Norwegian margin, and the temperature of the NwAC. *C. pelagicus* has earlier been suggested as a reliable proxy of mesostrophic to eutrophic waters in phytoplankton-rich frontal systems of the Nordic Seas (Samtleben et al., 1995a; Andruleit, 1997), which might indicate that the contribution of *C. pelagicus* in this record is related to the frontal zone between the two site specific currents (NwAC and the NCC; Loeng and Drinkwater, 2007). A narrowing of the NCC during positive NAO conditions would induce a higher contribution of the AW dwelling *E. huxleyi* (Baumann et al., 2000; Dylmer et al., 2013, this study), as well as ventilation of the bottom water in the Malangen fjord by warmer NwAC water. Hence the E/C ratio at site R248MC010 is believed to reflect the varying zonal distribution of NCC waters over the northern Norwegian shelf and slope.

The slight decreasing trend in the Ti/Ca ratio from the base to the top of Zone III suggests decreased terrigenous inputs from from mainland Norway (Ti) and increased carbonate (biogenic) production within the surface and subsurface water masses (Fig. 4.6a), an interpretation which is backed-up by slightly increasing bulk coccolith concentrations. The latter is expected to derive from the increasing influence of Atlantic water as relative changes in the amount and temperature of Atlantic-derived surface waters, as seen from the generally good comparison downcore with the NAO index and the AW flow, are supposed to explain to

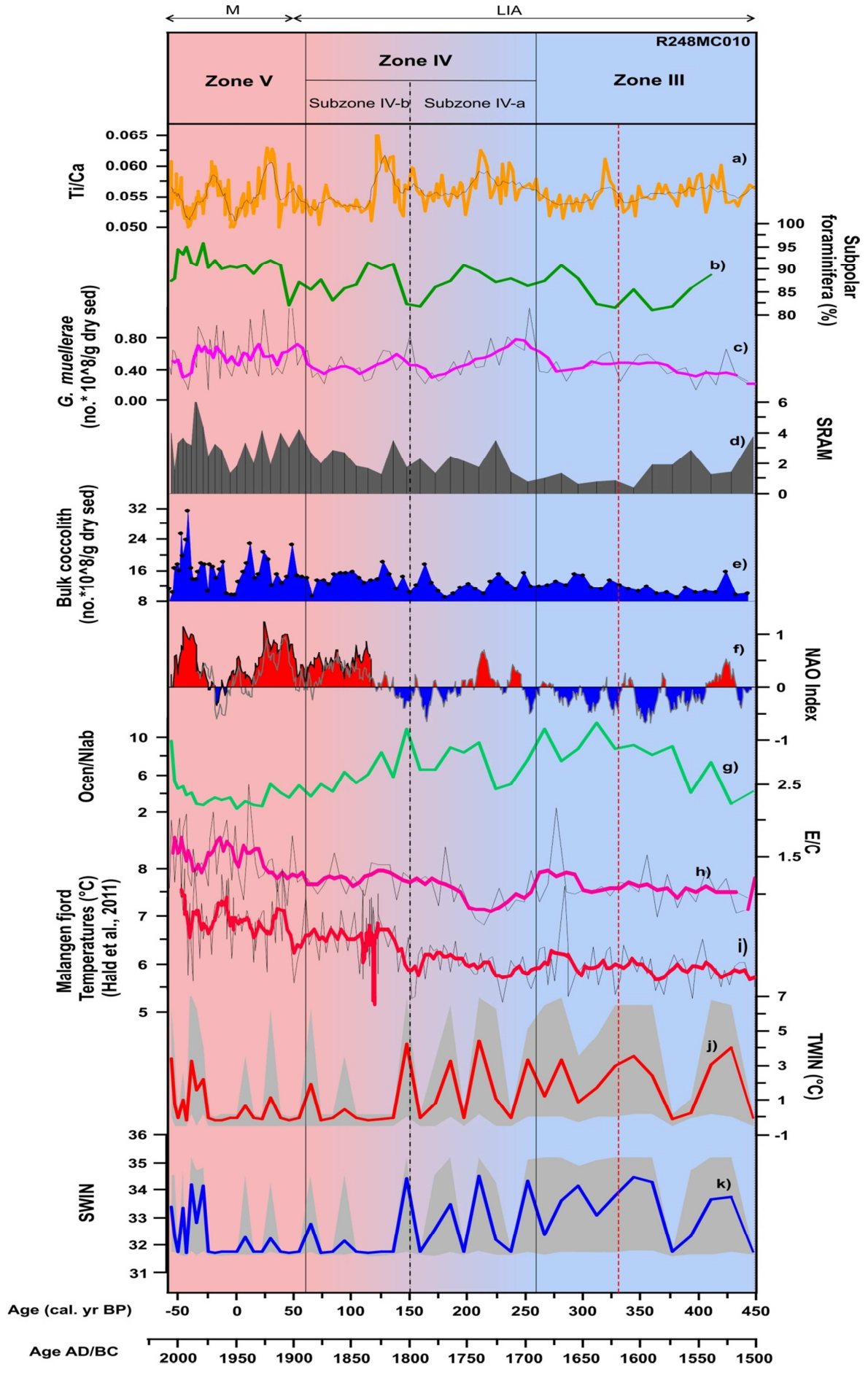
M
LIA
R248MC010
Zone V
Zone IV
Zone III
Subzone IV-b
Subzone IV-a
Ti/Ca
0.065
0.060
0.055
0.050
a)
Subpolar foraminifera (%)
100
95
90
85
80
b)
G. muellerae (no.* 10^8/g dry sed)
0.80
0.40
0.00
c)
SRAM
6
4
2
0
d)
Bulk coccolith (no.*10^8/g dry sed)
32
24
16
8
e)
NAO Index
1
0
-1
f)
Ocen/Nlab
10
6
2
g)
E/C
2.5
1.5
Malangen fjord Temperatures (°C) (Hald et al., 2011)
8
7
6
5
h)
i)
TWIN (°C)
7
5
3
1
-1
j)
SWIN
36
35
34
33
32
31
k)
Age (cal. yr BP)
-50
0
50
100
150
200
250
300
350
400
450
Age AD/BC
2000
1950
1900
1850
1800
1750
1700
1650
1600
1550
1500

Figure 4.6 : Summary plot of surface and subsurface circulation changes west of Lofoten Island (R248MC010) over the past ~500 years. a) : Ti/Ca ratio (XRF) as an index of terrigenous vs. marine (carbonate) biogenic sedimentation, black line represents a 7-running mean. b) : Relative abundances of subpolar foraminifera (fraction > 100 µm) as an index of subsurface AW masses. c) : Absolute concentrations of the *G. muellerae* coccolith species as proxy of the AW flow strength, violet line represents a 5-running mean. d) : relative abundances of SRAM as a proxy for relative variations in primary productivity and width of the NCC. e) : Bulk coccolith concentrations (no.*10^8/g dry sed.) as an index of carbonate productivity. f) : Combined instrumental (Jones et al., 1997; Osborn, 2006) and reconstructed (Lutherbacher et al., 2002) NAO index; Red and blue areas represent long term positive and negative NAO conditions, respectively. g) : OCEN/NLAB ratio as an index of the relative position of the AF (AW/ArW); increased and decreased ratios indicates westward and eastward migrations of the AF, respectively. h) : E/C ratio as a proxy for the zonal expression of the NCC in the Norwegian Sea, violet line represents a 5-running mean. i) : Reconstructed bottom temperatures (November) from the Malangen fjord, Northern Norway (Hald et al., 2011) , red line represents a 5-running mean. j + k) : Dinocyst-based MAT reconstructed winter surface water temperatures and salinities, with the grey shaded area representing the error range of the reconstructions. The summary inferred zones and subzones are highlighted in the top, with boundaries indicated by solid (zones) and dashed (subzones) vertical black lines. The vertical red dashed line represents the younger boundary of a warm pulse identified by Dylmer et al. (2013) in sediments of Fram Strait. Shaded light red and light blue represents inferred relative variations between increased and decreased AW flow periods, respectively.

a high extent the observed changes in bulk coccolith accumulation (Andruleit and Baumann, 1998). Finally the abundance of SRAM, a species which favors Atlantic-like high salinity surface waters with spring/summer productivity and surface water stratification (Solignac et al., 2009; Grøsfjeld et al., 2009; Zonneveld et al., 2013), is governed by an overall decrease across Zone III, as a response to the assumed presence of low saline NCC at the R248MC010 core site (Fig. 4.6d).

ZONE III: *Weak but slightly increasing AW flow toward the top of the zone, AW mainly present at the surface, cold subsurface conditions, westward shift of the AF, strong seasonal presence of NCC at the surface, low primary productivity but slightly improving toward the top of the zone.*

ZONE IV: 240-60 cal. years BP (1710-1890 AD, LIA/M transition)

Zone IV is governed by unstable and changing surface and subsurface conditions compared to the previous zone, with an overall decrease in AW flow, a cooling of the subsurface waters, an increased proximity to the AF and an apparent decreased influence of the NCC (Fig. 4.6).

Subzone IV-a: 240- 150 cal. years BP (1710-1800 AD)

The marked minimum values observed in the E/C (~215 cal. years BP) and OCEN/NLAB ratios (~230 cal. years BP), and in the Malangen fjord bottom temperatures (~230 cal. years BP), indicate generally cold surface conditions (Fig. 4.6h+j) over the core site. The observed minima are remarkable and seem to correspond to a level of strongly increased AW flow and higher subsurface temperatures (subpolar foraminifera). This episode takes place during a

short interval of change in NAO mode toward positive values, which translates into an eastward migration of both the AF and the NCC and a strong AW flow (Fig. 4.6f). This interpretation seems to be supported by the increased abundances of the high salinity index species SRAM, and the reconstructed SWIN and TWIN.

The recorded E/C ratio is at odd with its suggested relation to the NCC: here, *C. pelagicus* reaches its maximum abundances within subzone II-a (~215 cal. years BP), a period when the winter NAO mode implies an eastward shift of NCC waters (Fig. 4.6f+h). As earlier mentioned, the E/C ratio is based on summer blooming coccolithophores species (*E. huxleyi* and *C. pelagicus)*, whereas the NAO index represents the governing wind systems from December until March. Hence it is likely that the E/C ratio expresses summer conditions marked by a westward distribution of the NCC, and the presence at the core site of the turbulent frontal zone separating the NwAC and the NCC. Such a summer situation would explain the marked contribution of SELO in this interval, a species which has earlier been associated to frontal systems (Fig. 4.3) (Chapter 2). This interpretation is further supported by a maximum in the Ti/Ca ratio, suggesting the presence (at least seasonally) of terrigenous rich NCC water (Fig. 4.6a).

Subzone IV-a*: Increased AW flow compared with previous period, eastward migration of the AF, strong seasonal shift in the AW-NCC front,*

Subzone IV-b: 150- 60 cal. years BP (1800-1890 AD)

This interval marks the initiation of the modern period and the termination of the LIA. It is characterized by strong changes in the general circulation of the studied area, represented by a massive decrease in the OCEN/NLAB ratio and a strong increase in bottom water temperatures within the Malangen Fjord (Fig. 4.6g+i). The eastward migration of the AF (decreased OCEN/NLAB) agrees well with the increased NAO index and colder and fresher surface (TWIN and SWIN) and sub-surface temperatures (lower abundance of subpolar foraminifera). The associated narrowing of the NCC is confirmed by the pattern of Ti/Ca, SRAM, E/C and A/H proxies (Fig. 4.6a+d+h, 4.4).

Subzone IV-b: *Decreased AW flow, cooler conditions in the surface and subsurface waters, eastward migration of the AF and NCC.*

Zone V: 60- (-59) cal. years BP (1890-2009 AD, ~Moden period, M)

The Modern period, which is characterized by a sustained positive NAO mode, is unprecedented in terms of AW flow strength (highest), eastward shift of the NwAC and NCC, highest subsurface temperatures, and highest bulk productivity (Fig. 4.6).

The above observations of the Moden period translates in to a closer location of the AF, as indicated by highest productivity and therefore favorable conditions for heterotroph dinocysts as well as lower winter surface temperature and salinity.

ZONE V: *Unprecedented increase in AW flow, high subsurface water temperatures, low winter surface water salinities and temperatures, eastern position of the AF, and narrower NCC, increased productivity.*

4.4 WOO/SC-3 (Northeast of Vøring Plateau)

4.4.1 Coccolith Record

The preservation of coccolith remains was found to be good to very good within gravity core WOO/SC-3. Bulk coccolith concentrations throughout the investigated time interval ranged between ~7 and ~32 x 10^8 sp/g. dry sed and hence within the range of typical bulk coccolith concentrations in the eastern Nordic Seas (Fig. 4.7) (Baumann et al., 2000). The core is characterized by an overall increase in the bulk coccolith concentration towards the top of the record, with relatively stable concentrations until ~2250 cal. years BP followed by a steady increase only punctuated by a marked low at ~960-910 cal. years BP. As the sedimentation is rather constant (Chapter 3) changes in dilution of the biogenic component of WOO/SC-3 sediments by terrigenous material, which might bias the significance of bulk concentration records in terms of paleo-productivity patterns, is not expected to have had a large influence in this record.

The coccolith species diversity in core WOO/SC-3 is low and shows a dominance of *C. pelagicus* (20-38%) and *E. huxleyi* (48-72%) (Fig. 4.7). The latter species shows an overall decreasing abundance from the base to the top of the core, though minimum values are centered at 1500 cal. years BP. On the contrary *C. pelagicus* shows an overall increase with only minor variability. The resultant E/C ratio show values within the range of ~1 to 2.4, characterized by a continuous decrease until ~1500 cal. years BP followed by a relatively steady level towards the top of the record (Fig. 4.8).

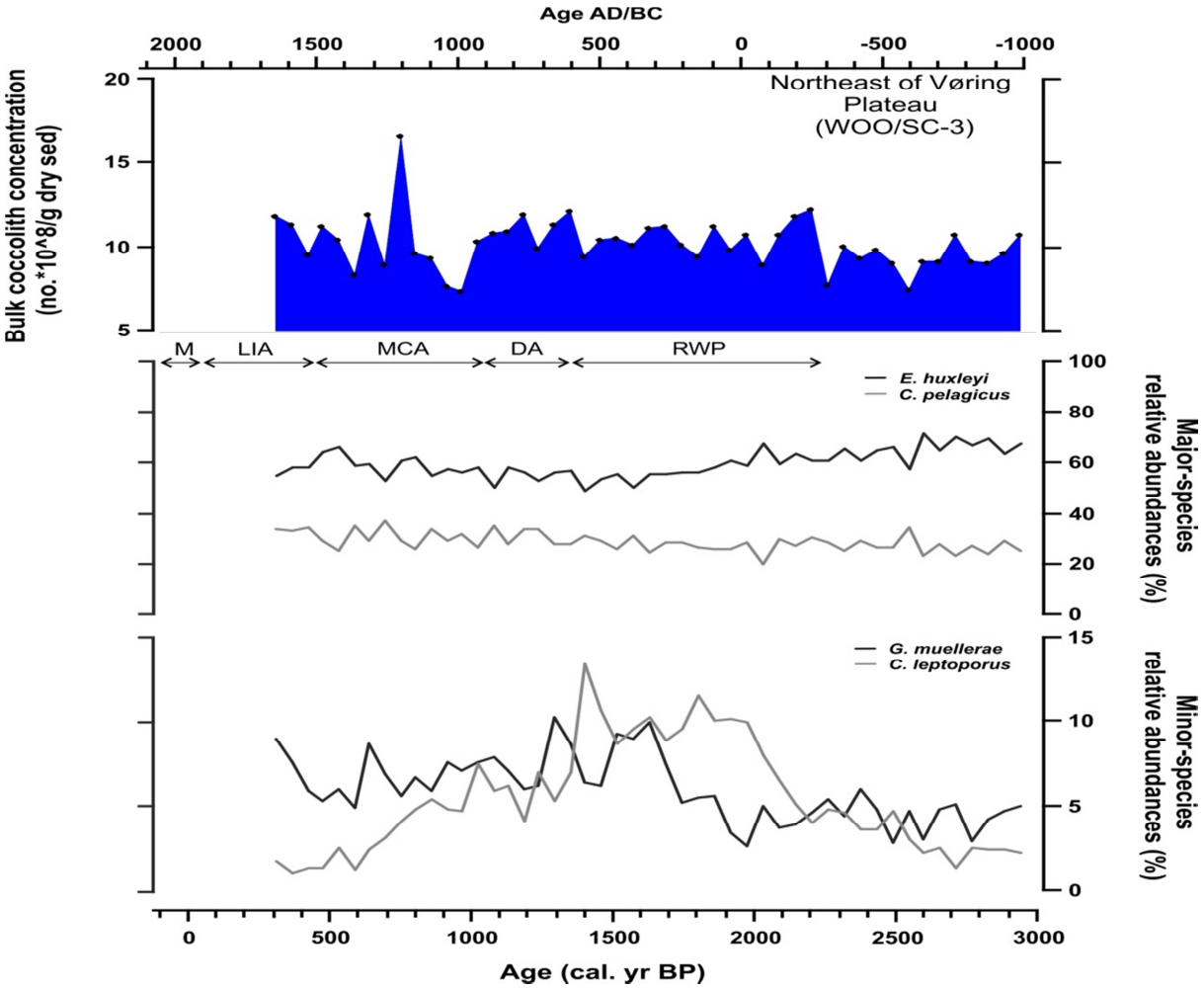

Figure 4.7 : Bulk coccolith concentration record (coccoliths * 10^8/g dry sed.) (top) and relative abundances (%) of major (mid) and minor (bottom) coccolith species within WOO/SC-3.

The subordinate species *G. muellerae* (2-11%) and *C. leptoporus* (1-14%) together account for an average of 10.8% of the total assemblage throughout the studied core. A fifth species, *Syracosphaera sp.*, only contributes with an average of 0.2%, and will not be discussed further. Contrary to *E. huxleyi* and *C. pelagicus*, the relative abundance changes of the drifted species *G. muellerae* and *C. leptoporus* are characterized by similar general trends (Fig. 4.7).

WOO/SC-3 show an overall increase of *G. muellerae* abundances during the last 3000 years, highest values defining an interval from ca. ~1900 to 640 cal. years BP (Fig. 4.7). Trends in absolute concentrations and relative abundances of both drifted species are nearly identical (Fig. 4.8). Hence, according to the suggestions made for core R248MC010, and given the allochtonous origin of *G. muellerae* and *C. leptoporus* as well as the transport mechanisms explaining their presence in Holocene sediments of the eastern Nordic Seas, absolute

concentration records of both species can be considered as significant proxies for relative changes in the NwAC strength within this record.

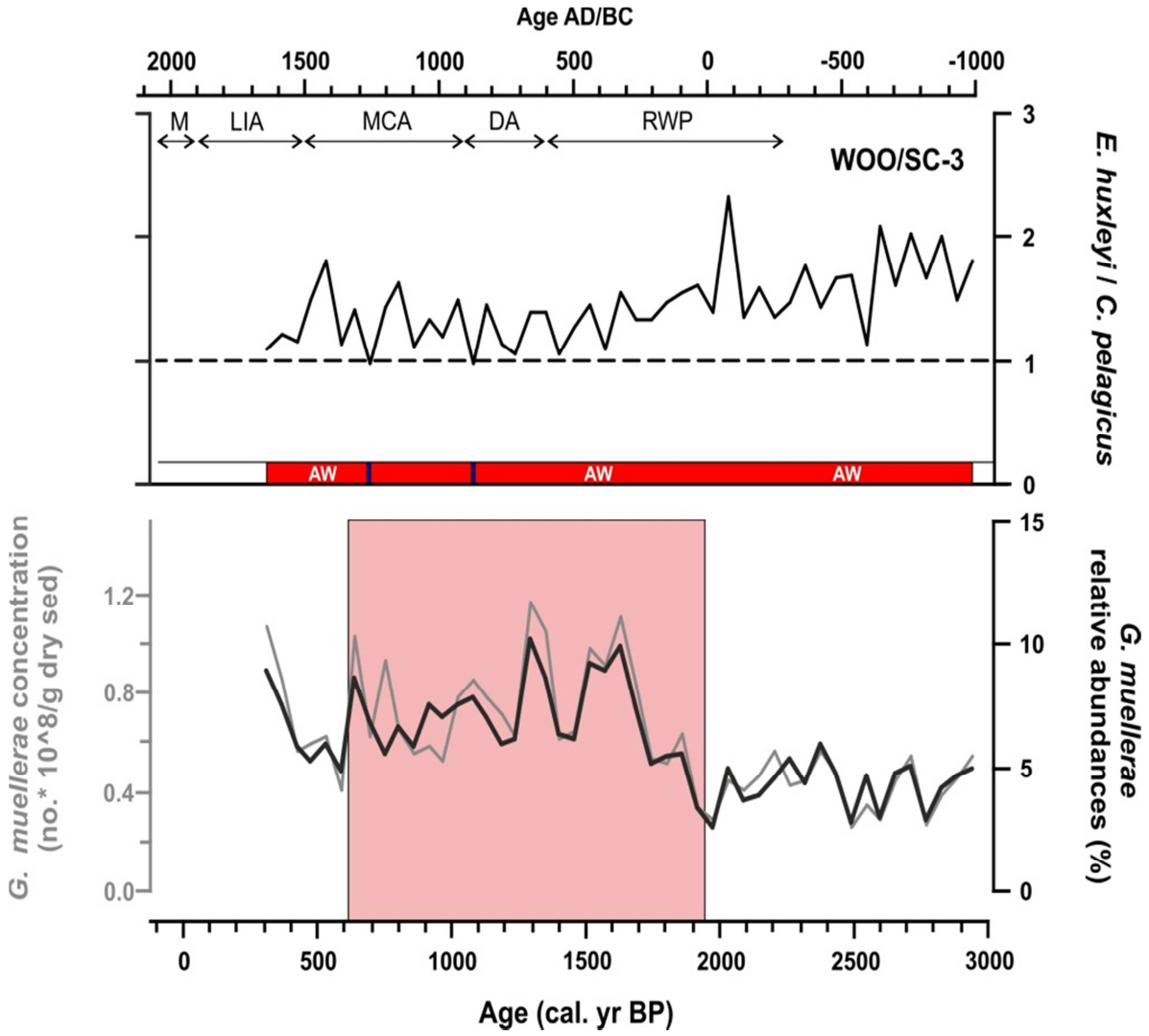

Figure 4.8 : Top : E/C ratios of the dominant coccolithophore species *E. huxleyi* (E) and *C. pelagicus* (C). The bar charts below each E/C plot highlight the dominating surface water masses of WOO/SC-3 according to the "1" threshold: Blue = ArW (E/C<1); Red = AW (E/C >1). Bottom: Relative abundances (black line) and absolute concentrations (grey line) of the AW inflow species *G. muellerae*. The light red shaded areas indicate the marked inflow increases inferred from absolute concentrations of *G. muellerae.*

C. leptoporus shows a peak in relative abundance within the studied core centered at ~2000-1400 cal. years BP (2-10%) (Fig. 4.7). This abundance pattern, different from the other drifted species *G. muellerae*, is enigmatic given the common processes (i.e. poleward transport to the Nordic Seas) affecting both species. One explanation might lay in the less restricted ecological niche of *C. leptoporus* which presently colonizes a wider geographic domain in the North Atlantic from warm to cool temperate areas (i.e. Ziveri et al., 2001) than *G. muellerae*

(Giraudeau et al., 2010), although it has been associated with colder conditions <20 °C and frontal systems (Chapter 2).

4.4.2 Dinocyst Record

The preservation of dinocyst remains within WOO/SC-3 was found to be generally good. The bulk dinocyst concentrations range from 4 to 34 ×10^3 sp/g. dry sed. (Fig. 4.9), within the range of earlier surface sediment studies of dinocyst concentrations in the Nordic Seas (Samtleben et al., 1995a; Matthiessen, 1995). The bulk concentrations are governed by an overall increase toward the core-top punctuated by minimum values in the ~2200-1030 cal. years BP interval (Fig. 4.9).

The dinocyst diversity is high with a maximum of 26 different species identified (incl. one acritarch). The three species OCEN (~55-85%), PDAL (~2-19%) and NLAB (~3-16%) dominate the assemblages with a total mean relative abundance of ~88.4 %, followed by the subordinate species BSPP (~1-12%), SRAM (~0-3%), SELO (~0-5%) and *B. tepikiense* (~0-5%, BTEP) (Fig. 4.9). All other species contribute less than 2% to the total assemblages. The reworked dinocysts show a mean absolute concentration of 0.065 sp/g. dry sed. The overall composition of the WOO/SC-3 dinocyst record is comparable to surface sediment assemblages along the shelf and slope of northern Norway and in the southwestern Barents Sea (Solignac et al., 2009).

The record show an overall increase within the species PDAL, NLAB, SRAM, SELO and the reworked dinocysts, at the expense of OCEN and BSPP. OCEN shows an overall smooth interchanging pattern of relatively high and low abundances with maximum values in the intervals ~3000-2200 and ~1250-925 cal. years BP, followed by an increase from ~425 cal. years BP towards the top of the record (~300 cal. years BP) (Fig. 4.9). NLAB and PDAL show an almost opposite trend to OCEN. BSPP is characterized by relatively high abundances toward the beginning and the end of the record with a marked low between ~1900 and 750 cal. years BP. The temperate to sub-polar species BTEP, which is presently observed in regions covered by sea-ice for less than 4 months/year and has been related to frontal systems (Chapter 2), shows highest relative abundances at 2100-1800 cal. years BP within core WOO/SC-3.

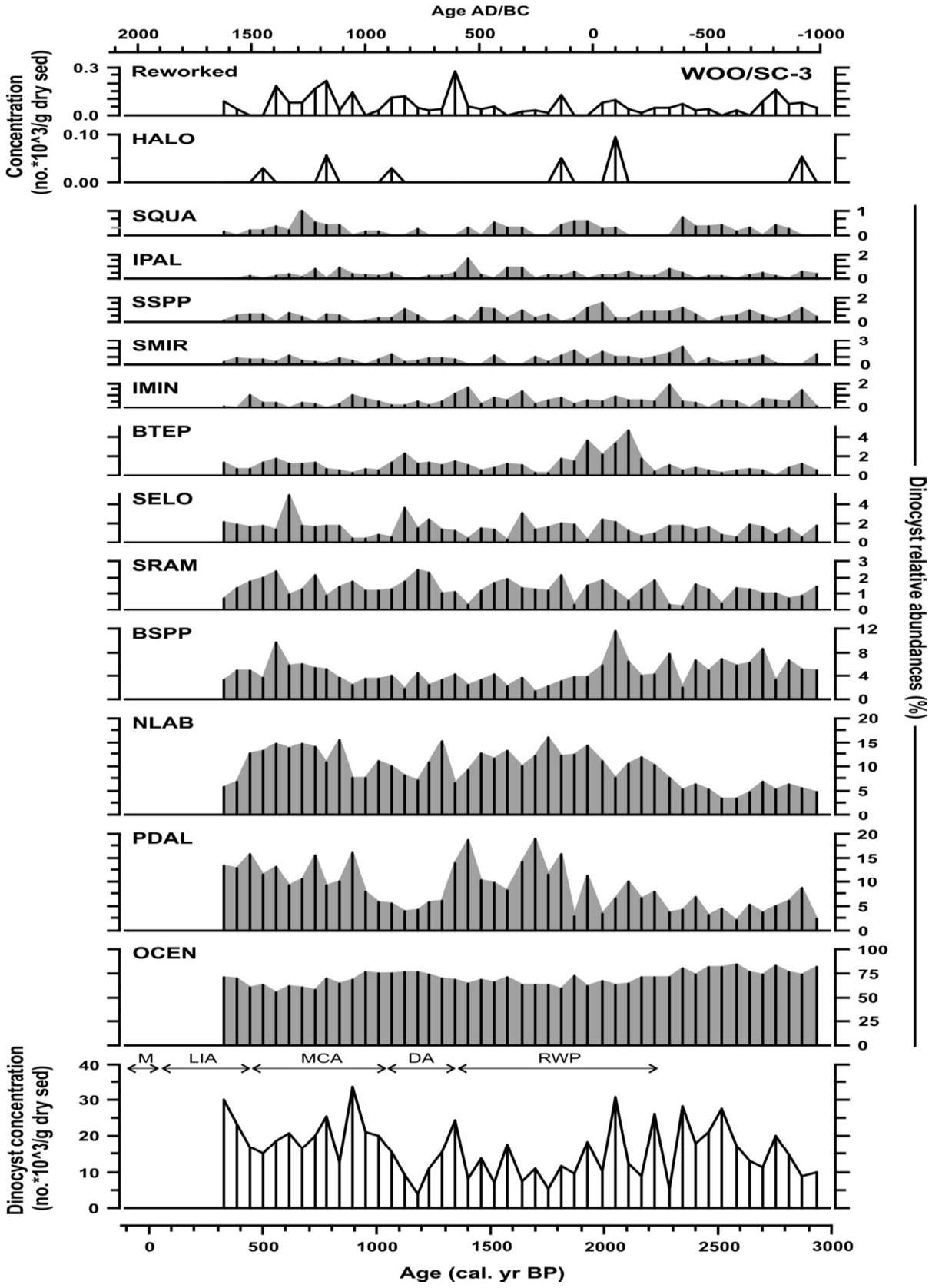

Figure 4.9 : Reworked dinocysts and *Halodinium* spp. (HALO) concentrations (dinocysts * 10^3/g dry sed.) (top), relative abundances (%) of major and minor dinocysts (mid) and dinocyst concentration records (dinocysts * 10^3/g dry sed.) (bottom) of WOO/SC-3. (See chapter 2 for species names - abrevations).

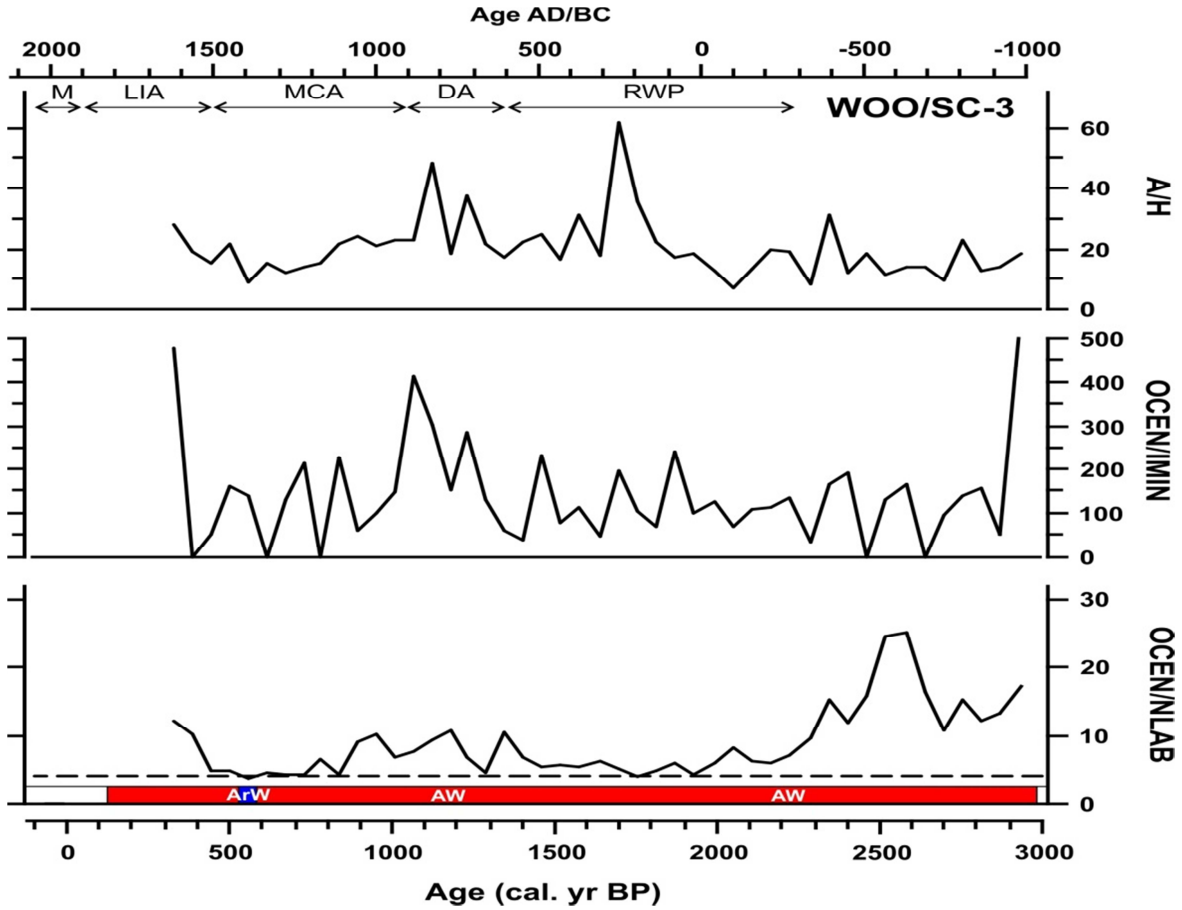

Figure 4.10 : Top: Trophic level ratio between autotrophic (A) and heterotrophic (H) species. Mid: OCEN/NLAB ratio between the AW thriving *O. centrocarpum* (OCEN) and the sea ice related (ArW) *I. minutum* (IMIN). Bottom : OCEN/NLAB ratio of the dominant dinocyst species OCEN and *N. labyrinthus* (NLAB). The bar charts below the OCEN/NLAB plot highlight the dominating surface water masses of WOO/SC-3 according to the "4" threshold: Blue = ArW (OCEN/NLAB<4); Red = AW (OCEN/NLAB >4).

The resulting three ratios OCEN/NLAB, OCEN/IMIN and A/H, show average values of 8.9, 141.6 and 20.3, respectively, with the former governed by an overall decreasing trend and the latter two governed by increasing values toward the top of the record (Fig. 4.10). OCEN/NLAB shows the highest values in the earliest part of the record until 2200 cal. years BP, followed by a generally steady state throughout the rest of the core, except for a short interval of higher values from 1300 to 850 cal. years BP. The final increased ratios of OCEN/NLAB occurs almost synchronously with a maximum value in the ratio of OCEN/IMIN. The A/H ratio is marked by higher values from ~1900 to 750 cal. years BP punctuated by two maximum values at ~1650 and 1090 cal. years BP (Fig. 4.10).

4.4.3 Quantitative Reconstructions of Sea-Surface Conditions

The reconstructed sea-surface conditions fluctuates around mean TWIN and TSUM of 4 °C and 12 °C, and mean SWIN and SSUM of 34 and 33.5. These values fall within the range of

the measured temperatures (6-11 °C) and salinities (34.61-34.96) at the core location (World Ocean Database) (Fig. 4.11).

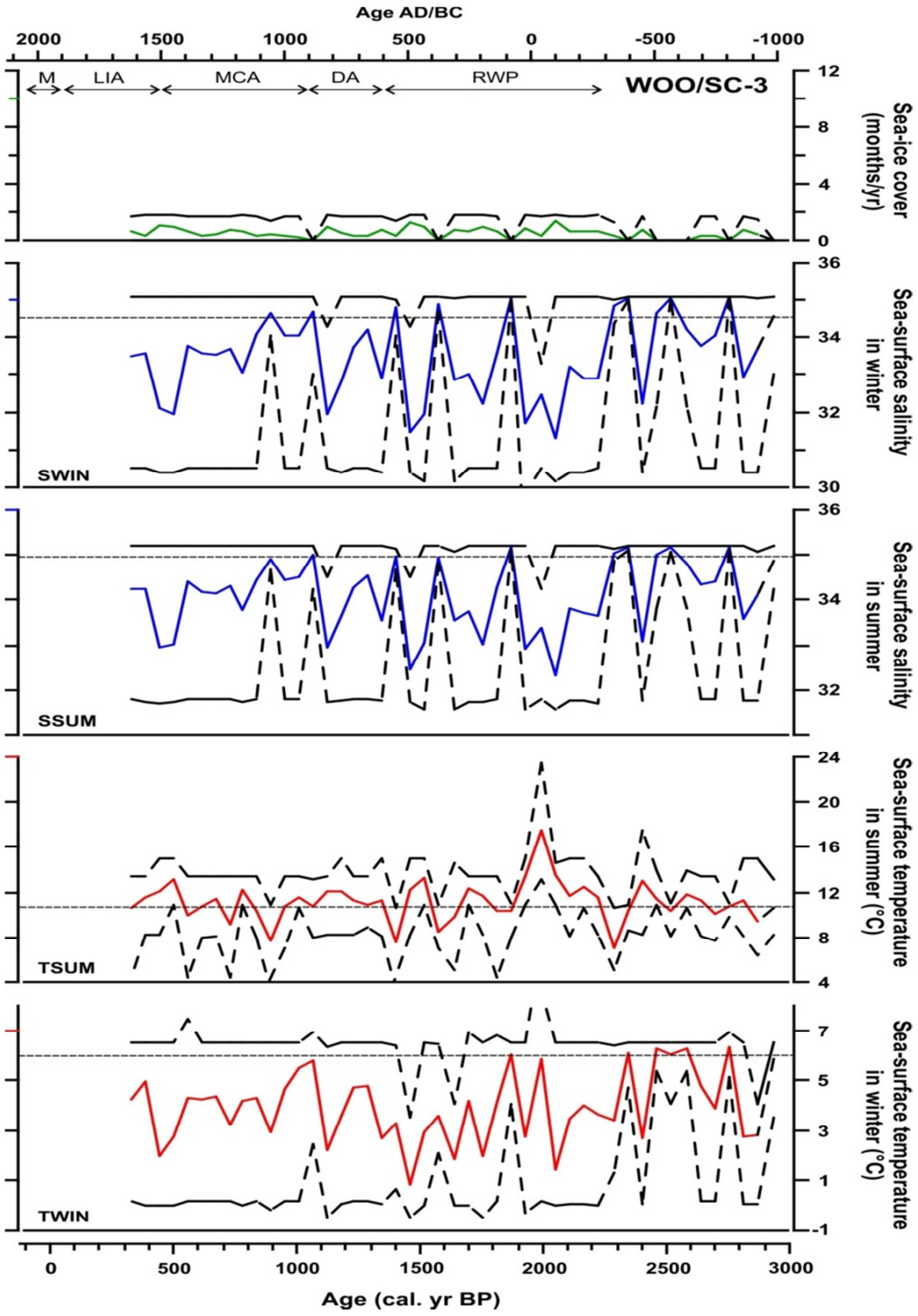

Figure 4.11 : Reconstruction of sea-surface conditions (temperature, salinity, sea ice cover) from dinocyst assemblages of core WOO/SC-3, based on MAT. The surface sediment database (n=1189) of the North Atlantic and North-Eastern Pacific was applied for MAT. Minimum and maximum errors on the estimated parameter are shown by the dashed black lines following the curves. The modern average values are represented by the horisontal dashed lines.

The record display overall decreasing TWIN (0.8-6.3), SSUM (31.3-35) and SWIN (32.4-35), with a general increase in TSUM (7-17.6 °C). The three former records show roughly identical variations throughout the core length. The salinity record initiates with fairly high and stable values until ~2200 cal. years BP, followed by an interval of lower SSUM until 1050 cal. years BP, and finally decreasing towards the core-top (Fig. 4.11). SSUM and SWIN are generally more variable during the interval ~2200 to ~1050 cal. years BP compared to TWIN, which only shows peak values at ~1850 cal. years BP. TSUM is strongly variable and trends are rather difficult to infer with the exception of a single interval of peak values centered at ~1900 cal. years BP.

As in the case of the slightly northern core R248MC010, the MAT sea-ice reconstructions are indicative of sea ice presence at site WOO/SC-3, in line with recent late Holocene dinocyst reconstructions from this area (de Vernal et al., 2013). Nevertheless the reconstructed values are very low and fluctuate around 0.6 months/year, which is toolow a value to be reliable (Fig. 4.11). In addition, according to the same arguments given for R248MC010 (location below northward flowing NwAC, absence of sea-ice at the core location from historical surveys), sea ice formation and/or southward flow of sea ice to the core location was unlikely. Hence sea ice was probably not present at this site during the last ~300-3000 years.

4.4.4 Inferring the Paleoceanographic changes in Atlantic Water Flow and the Distribution of Surface Waters during the Last ~300-3000 Cal. years BP (WOO/SC-3)

The proxy records obtained at core WOO/SC-3 are plotted together with a reconstructed NAO index (Trouet et al., 2009; Olsen et al., 2012). Three zones (and three subzones) have been identified through comparison of all proxy data. ZONE I represents the interval from the base of the core (ca. 3000 cal. years BP) to 2200 cal. years BP (1050 -250 BC). ZONE II, covers the interval 2200-640 cal. years BP (250 BC-1310 AD) and is subdivided into three subzones II-a (2200-1250 cal. years BP, 250 BC-700 AD), II-b (1250-850 cal. years BP, 700-1100 AD) and II-c (850-640 cal. years BP, 1100-1310 AD). ZONE III encompasses the time interval from 640 cal. years BP to the top of WOO/SC-3 record (300 cal. years BP) (Fig. 4.12).

The inferred paleoceanographic changes in WOO/SC-3 are partly based on the results from R248MC010 (located further to the north), as both sites are located west of mainland Norway, under the main flow of AW, and within the main area of influence of NAO-like atmospheric processes. Contrary to core R248MC010, we however do not expect a strong influence of NCC waters at the WOO/SC-3 site given its location.

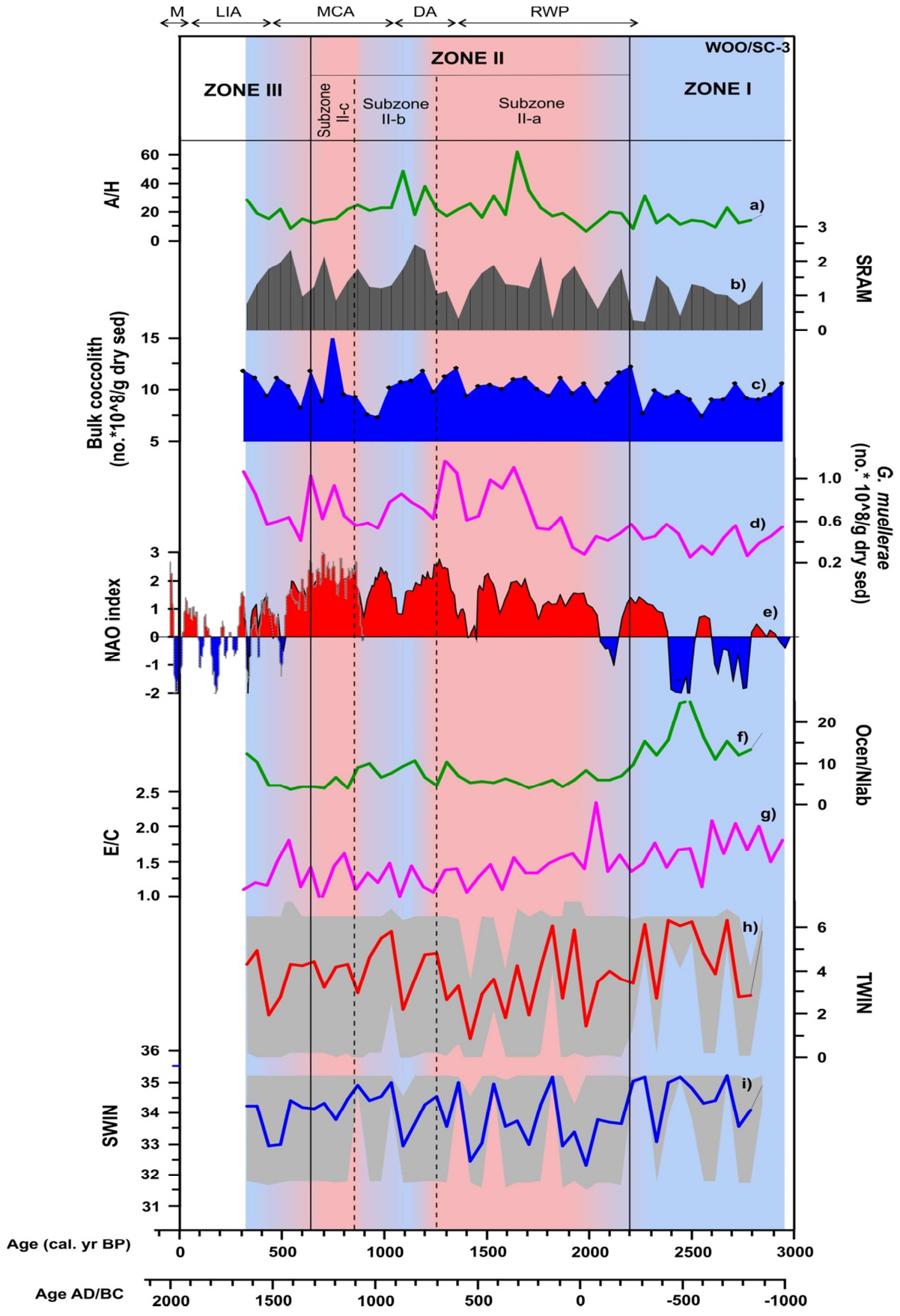
M
LIA
MCA
DA
RWP
WOO/SC-3
ZONE III
ZONE II
ZONE I
Subzone II-c
Subzone II-b
Subzone II-a
A/H
Bulk coccolith (no.*10^8/g dry sed)
SRAM
G. muellerae (no.* 10^8/g dry sed)
NAO index
Ocen/Nlab
E/C
TWIN
SWIN
a)
b)
c)
d)
e)
f)
g)
h)
i)
Age (cal. yr BP)
Age AD/BC

Figure 4.12 : Summary plot of surface and subsurface circulation changes northeast of the Vøring Plateau (WOO/SC-3) over the past 3000 years. a) : A/H ratio as an index of trophic level . b) : Relative abundances of SRAM as a proxy for relative variations in primary productivity and salinity changes. c) : Bulk coccolith concentrations (no.*10^8/g dry sed.) as an index of carbonate productivity. d) : Absolute concentrations of *G. muellerae* as a proxy of the AW flow strength, violet line represents a 5-running mean. e) : Combined NAO index reconstructions based on Trouet et al. (2009) and Olsen et al. (2012); Red and blue areas represent long term positive and negative NAO conditions, respectively. f) : OCEN/NLAB ratio as an index of the relative position of the AF (AW/ArW). g) E/C ratio as a proxy for the relative position of the AF (AW/ArW). h + i): Dinocyst-based MAT reconstructed winter surface water temperatures and salinities, with the grey shaded area representing the error range of the reconstructions. The Summary inferred zones and subzones are highlighted in the top, with the zonations indicated by solid (zones) and dashed (subzones) vertical black lines. Shaded light red and light blue represents inferred relative variations between increased and decreased AW flow periods west of Norway, respectively.

Zone I: ~3000-2200 cal. years BP (1050 -250 BC)

Zone I is characterized by weak AW flow, and a westward extension of the NwAC (western position of the AF), both conditions being triggered by sustained negative NAO conditions (Fig. 4.12d-g). Here as a result of the lack of NCC influence at the location of WOO/SC-3, of the general correspondance between E/C and OCEN/NLAB, and of an overall agreement between NAO modes and changes in E/C ratio, we believe that the earlier suggested application of the E/C ratio as a proxy for the location of the AF is valid at this site. Surface waters are relatively warm and saline (high TWIN and SWIN) thoughout the Zone I interval, with low surface carbonate productivity (bulk coccolith concentrations) (Fig. 4.12h+i).

Zone I: *low AW flow, western location of AF, relatively low carbonate productivity.*

Zone II: 2200-640 cal. years BP (250 BC-1310 AD)

This zone is governed by a strong overall increase in the strength of the AW flow suggesting improved (warmer) conditions west of Norway as a result of the change to a positive NAO mode (Fig. 4.12d+e). The decreasing surface TWIN and SWIN are interpreted as a direct response to an eastward migration of the AF as indicated by the OCEN/NLAB and E/C ratios and more favorable conditions for autotroph phytoplankton (increased bulk coccolith concentration and A/H ratio). As at site R248MC010, the change in the NAO mode agrees well with the general variability in the bulk coccolith concentrations and SRAM, possibly as a result of the increase in AW flow (Fig. 4.12b+c).

Subzone II-a: 2200-1250 cal. years BP (250 BC-700 AD)

A strongly enhanced AW flow can be inferred throughout this subzone, which together with an eastern migration of the AF seems to be related to the major change in the NAO index from a previous negative pattern to a mainly positive one (Fig. 4.12d-g). The decrease in sea surface temperatures and salinities are probably indicative of a subsurface flow of AW below

stratified waters (increased PDAL, Fig. 4.9), as a direct result of an increased influence of ArW in the surface (eastward migration of AF) (Fig. 4.12f-i).
Subzone II-a: *strongly increased AW flow, eastern position of AF, ArW present in the surface waters, increasing carbonate productivity.*

Subzone II-b: 1250-850 cal. years BP (700-1100 AD)
This subzone has been identified based on an apparent decrease in AW flow, and a western migration of the AF as a response to a slight weakening of the NAO index (Fig. 4.12d-g). The warmer and more saline surface waters together with a strong decrease in the carbonate bulk productivity, suggests that colder conditions prevailed during this interval.
Subzone II-b: *weakened AW flow, slight western migration of AF, more AW in the surface and decrease in carbonate productivity.*

Subzone II-c: 850-640 cal. years BP (1100-1310 AD)
This subzone represents the termination of Zone II. It is characterized by a marked increase in AW flow, an eastward migration of the AF and peak carbonate productivity, resulting from the most positive NAO conditions of the entire record (Fig. 4.12). The general correspondance of the reconstructed NAO index with our inflow proxy, the bulk coccolith record and SRAM (as also found in R248MC010) seems to confirm this governing positive NAO like index in most of Zone II.
Subzone II-b: *strong AW flow, eastern position of AF, ArW in the surface, highly increased productivity.*

Zone III: ~640 cal. years BP to the core-top (300 cal. years BP)
The interpretation of the final zone is difficult as it only represents a limited amount of samples which, in addition, might have been mixed during the collection of the core. The transition into Zone III is however marked by detoriating conditions, shown by a strong decrease at 640 cal. years BP in AW and the initiation of a weakened NAO (Fig. 4.12).
The poor age constraint of this core interval (see Chapter 3) limits additional interpretation of the proxy records.
Zone III: *decreased AW flow, western location of AF, AW present in the surface waters, relatively high carbonate productivity.*

4.5 R406MC032 (Southwestern Barents Sea)

4.5.1 Coccolith Record

The preservation of the coccolith remains was found to be moderate to good within R248MC032, with no obvious temporal pattern in dissolution changes. Bulk coccolith concentrations throughout the investigated time interval ranged between ~0.7 and 17 x 10^8 sp/g. dry sed and hence fall well within the range of typical coccolith concentrations in the eastern Nordic Seas (Fig. 4.13) (Baumann et al., 2000). The bulk coccolith concentration record is characterized by overall, low values fluctuating around 1.5 x 10^8 sp/g. dry sed. from the base of the core (ca. 500 cal. years BP) until ca. 125 cal. years BP from when values continously increase up to Present.

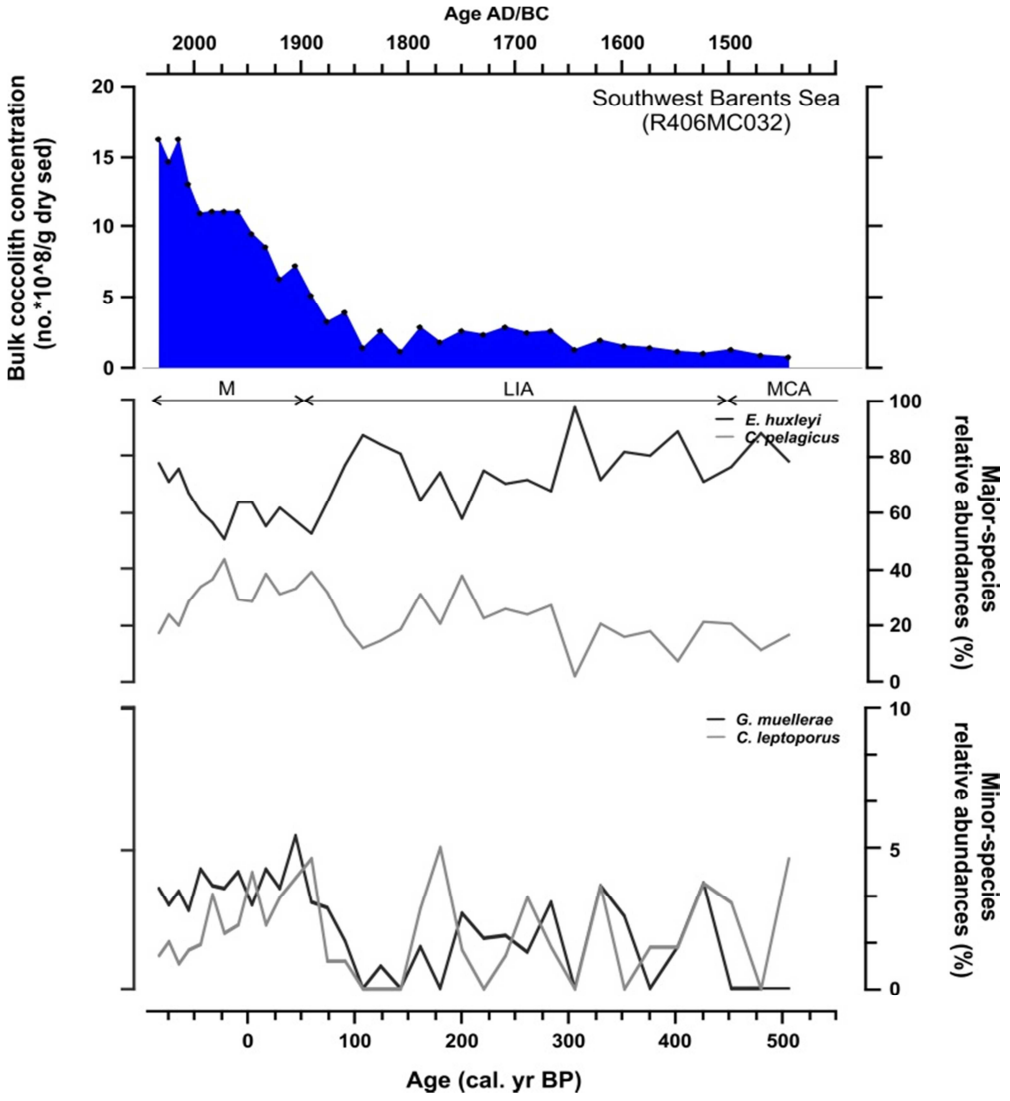

Figure 4.13 : Bulk coccolith concentration record (coccoliths * 10^8/g dry sed.) (top) and relative abundances (%) of major (mid) and minor (bottom) coccolith species within R406MC032.

The peculiar concentration record with sharp increase from ~168 cal. years BP until Present might be a result of changes in carbonate preservation (Chapter 3), variable dilution by lateral transport and/or sea ice inputs of terrigenous material, or a true signature of changes in coccolith production in the surface waters. As discussed in Chapter 3 (Material and Methods) the grain size analysis showed variability within the fine fractions of up to ~20%, which might be in part induced by reworking and/or downslope or lateral transfer of sand sized material from the nearby Barents shelf, as a consequence of brine water formation or storm-events. Downslope sediment transport would be reflected in synchronous variability of species abundances and sediment grain size. This is however not the case. One way to investigate these possible downslope and lateral transfer of shallow Barents Sea shelf material would be to investigate the down core concentrations of benthic foraminifera as their concentrations in slope sediments off the western Barents Sea is assumed to be related to sediment transfer from shelf sediments (e.g. Sarnthein et al., 2003). In the absence of such a dataset, and considering the other evidences listed above, we cannot definitively apply the coccolith bulk concentration record as a productivity indicator.

The coccolith species diversity is low with a dominance of *C. pelagicus* (1-43%) and *E. huxleyi* (51-98%) (Fig. 4.13). The coccolith record shows an overall decreased contribution of *E. huxleyi* toward Present punctuated by several low and high abundance periods. Two intervals with low *E. huxleyi* abundances are apparent at 309-187 and 100-4 cal. years BP. As expected given its overall shared dominance with *E. huxleyi*, *C. pelagicus* displays similar however opposite patterns of relative abundances in R406MC032 (Fig. 4.13). The resultant E/C ratio shows elevated ratios from the base of the core to 309 cal. years BP and in the interval 187-100 cal. years BP (Fig. 4.14).

The subordinate species *G. muellerae* and *C. leptoporus* together account for an average of 4.2% of the total assemblage (Fig. 4.13). R406MC032 displays an overall increase of *G. muellerae* abundances during the last ~550 years punctuated by maximum values in the intervals ~450-200 and 90-(-56) cal. years BP. *G. muellerae* reaches highest abundances during the last 100-150 years. The trends in absolute concentrations and relative abundances of this drifted species are very similar throughout the core, although some short term variabilities in relative abundances prior to 200 cal. years BP are barely reflected in the absolute abundance record (Fig. 4.14). Considering the potential biases on coccolith

concentration records as discussed above, we rather chose to apply the relative abundance of drifted species as a proxy for AW inflow at the location of R406MC032. *C. leptoporus* shows higher abundances at 452, 355, 287, 206 and 85 cal. years BP (Fig. 4.13).

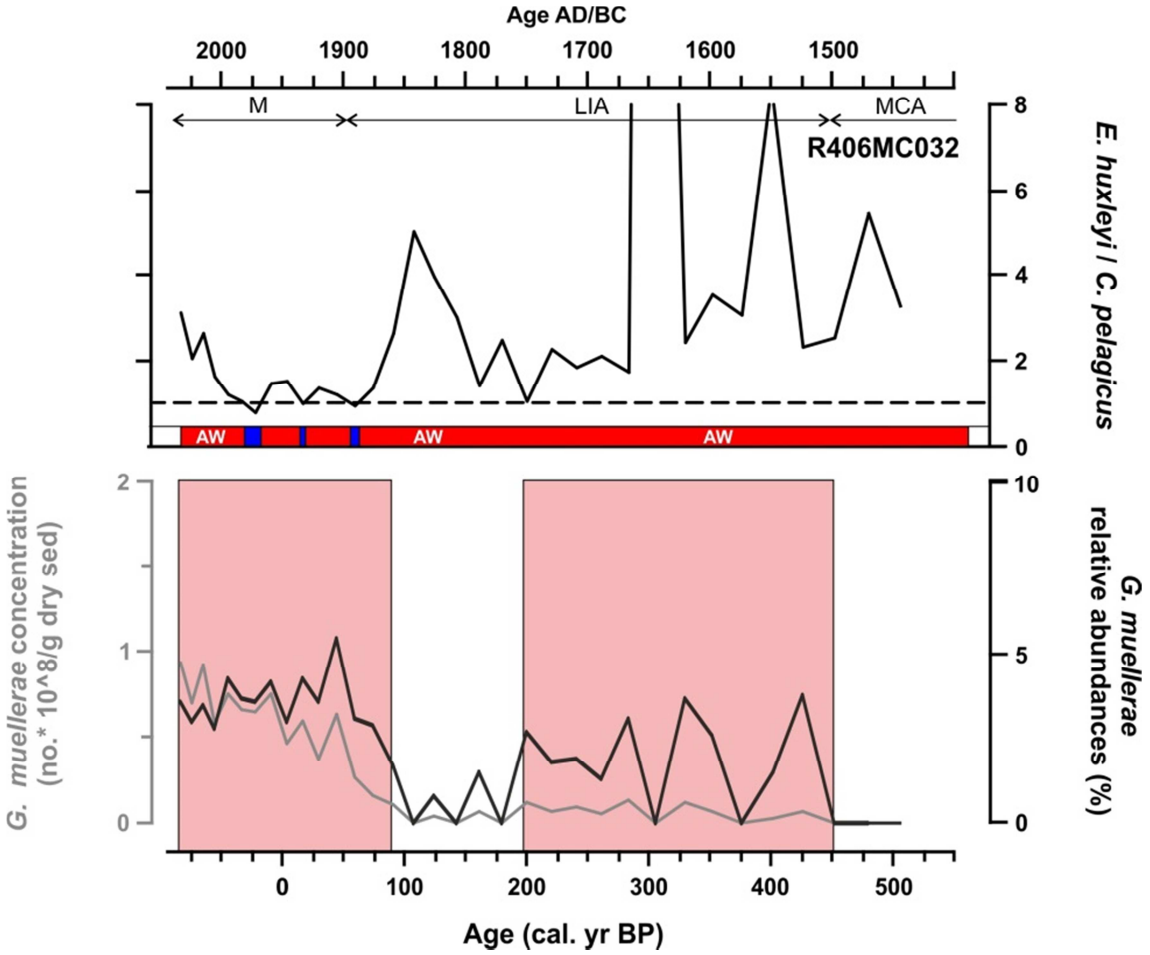

Figure 4.14 : Top : E/C ratios of the dominant coccolithophore species *E. huxleyi* (E) and *C. pelagicus* (C). The bar charts below each E/C plot highlight the dominating surface water masses at R406MC032 according to the "1" threshold: Blue = ArW (E/C<1); Red = AW (E/C >1). Bottom: Relative abundances (black line) and absolute concentrations (grey line) of the AW inflow species *G. muellerae*. The light red shaded areas indicate the marked inflow increases inferred from relative abundances (see text for details) of *G. muellerae.*

4.5.2 Dinocyst Record

The dinocyst preservation within R406MC032 was found to be generally good, with a rather variable bulk dinocyst concentration ranging from 1 to 47 ×10^3 sp/g. dry sed. (Fig. 4.15), although still within the range of values obtained from surface sediment in this area (Matthiessen, 1995). The dinocyst bulk concentration record is peculiar and characterized by an overall increase toward the top of the core. In a similar pattern to the coccolith concentration record, dinocyst concentrations show a massive increase from ca. 100 cal. years BP following relatively steady state low values around 3×10^3 sp/g. dry sed until ca. 170 cal.

years BP (Fig. 4.13, 4.15). The peak bulk dinocyst concentration at ~0 cal. years BP is followed by a decrease towards the top of the record.

A total of up to 23 species (incl. 1 acritarch) has been identified within R406MC032. The three species OCEN (~33-84%), PDAL (~4-22%) and NLAB (~2-13%) dominate the assemblages throughout the last ~500 years, together with the subordinate species SRAM (~1-9%,), SELO (~0-10%) and BSPP (~0-22%) (Fig. 4.15). All other species contribute with less than 2% of the total assemblages. The reworked dinocysts show a mean absolute concentration of 0.065 sp/g. dry sed. The overall composition of the R406MC032 dinocyst record is generally comparable to previous studies of surface sediment assemblages along the shelf and slope of northern Norway and the western Barents Sea shelf (Solignac et al., 2009; Grøsfeld et al., 2009).

R406MC032 shows overall increased abundances toward the Present of the species OCEN, NLAB, SMIR, IPAL and the reworked dinocysts, whereas PDAL, SELO and SRAM shows a general decreasing trend in contribution to the bulk dinocyst assemblages (Fig. 4.15). The relative abundances of OCEN slightly increases from the base of the core until 309 cal. years BP, before a long term plateau, and a slight abundance decrease from ca. 0 cal. years BP. PDAL abundance changes are generally opposite to OCEN, whereas NLAB is characterized by increasing abundances from the core-base to ~187 cal. years BP followed by lower values toward the top of the record. SELO initiates at a high relative abundance at the core base, then shows drastically lower values (minimum at 187 cal. years BP) throughout most of the core with the exception of an all site recovery around 0 cal. years BP (Fig. 4.15). The subordinate species SRAM shows an overall decreased contribution punctuated by several low and high abundance periods. Especially two intervals with low abundances are apparent at 309-245 and 100-4 cal. years BP. The colder dwelling heterotroph species IMIN shows highest relative abundances (~4%) toward the oldest part of the record, peaking at 245 cal. years BP, from which an overall decreasing abundance trend is dominating. The minor species SMIR and IPAL and the reworked dinocysts appear in higher relative abundances from roughly 245-187 cal. years BP to the top of the record (Fig. 4.15).

The resulting ratios OCEN/NLAB, OCEN/IMIN and A/H show average mean values of 12.4, 111.4 and 84.2, respectively (Fig. 4.16). The OCEN/NLAB record is characterized by two intervals of higher values from the oldest part to 225 cal. years BP and from ~100 cal. years BP to the top of the record, only interrupted by a period of lower values at ~225-100 cal. years BP. The OCEN/IMIN record within R406MC032 is governed by higher values at 309-4

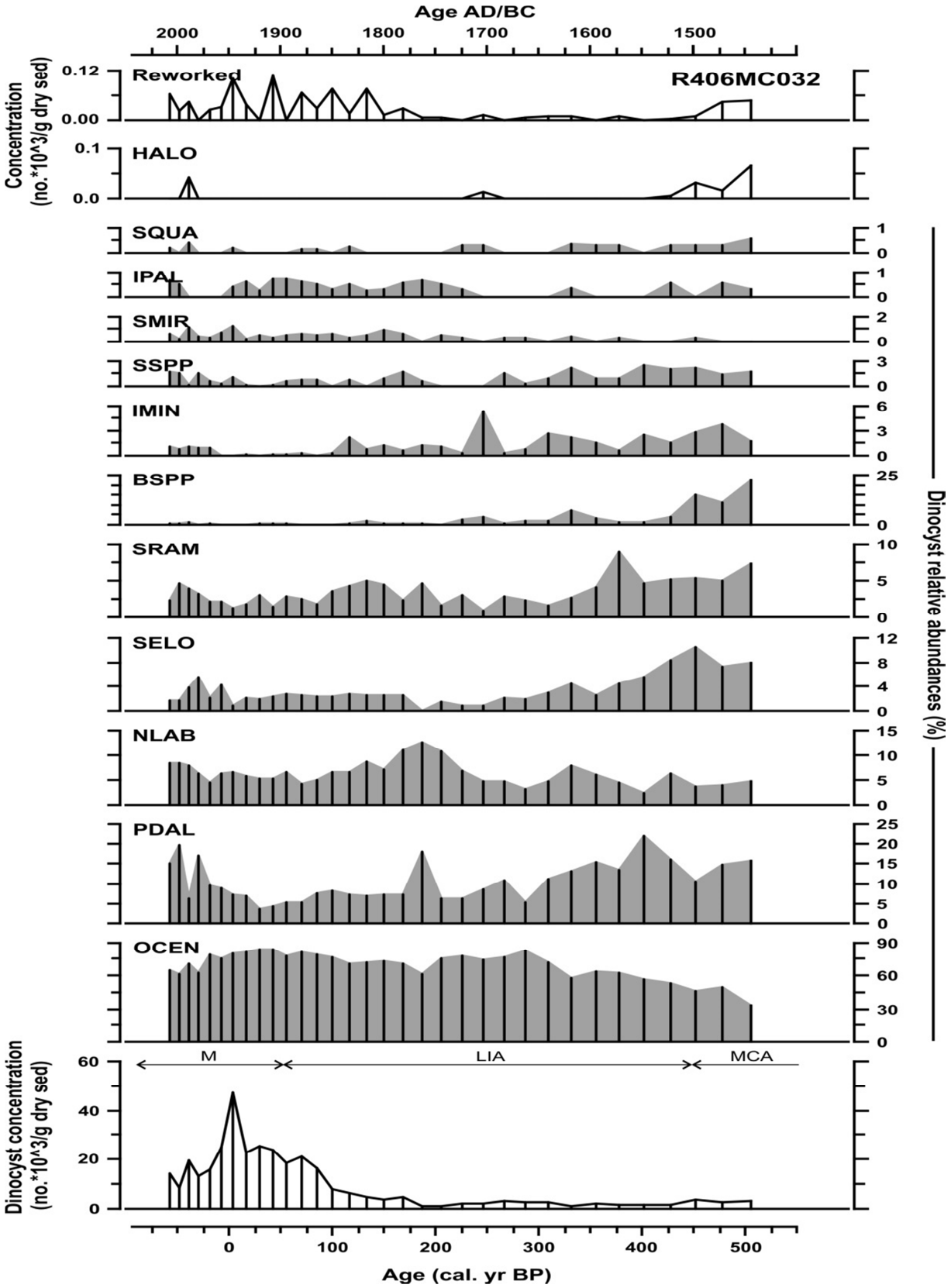

Figure 4.15 : Reworked dinocysts and *Halodinium* spp. (HALO) concentrations (sensus counts * 10^3/g dry sed.) (top), relative abundances (%) of major and minor dinocysts (mid) and dinocyst concentration records (dinocysts * 10^3/g dry sed.) (bottom) of R406MC032. (See Chapter 2 for species names - abrevations).

cal years BP with specifically two periods of very high values at 287-206 and 85-4 cal. years BP. The latter period is not surprising as the bulk coccolith concentration is markedly increased at this level and OCEN accounts for the major relative abundance changes. The A/H ratio roughly follows the trend displayed by OCEN/IMIN, although this record only shows for a single period of maximum values at 85-4 cal. years BP (Fig. 4.16).

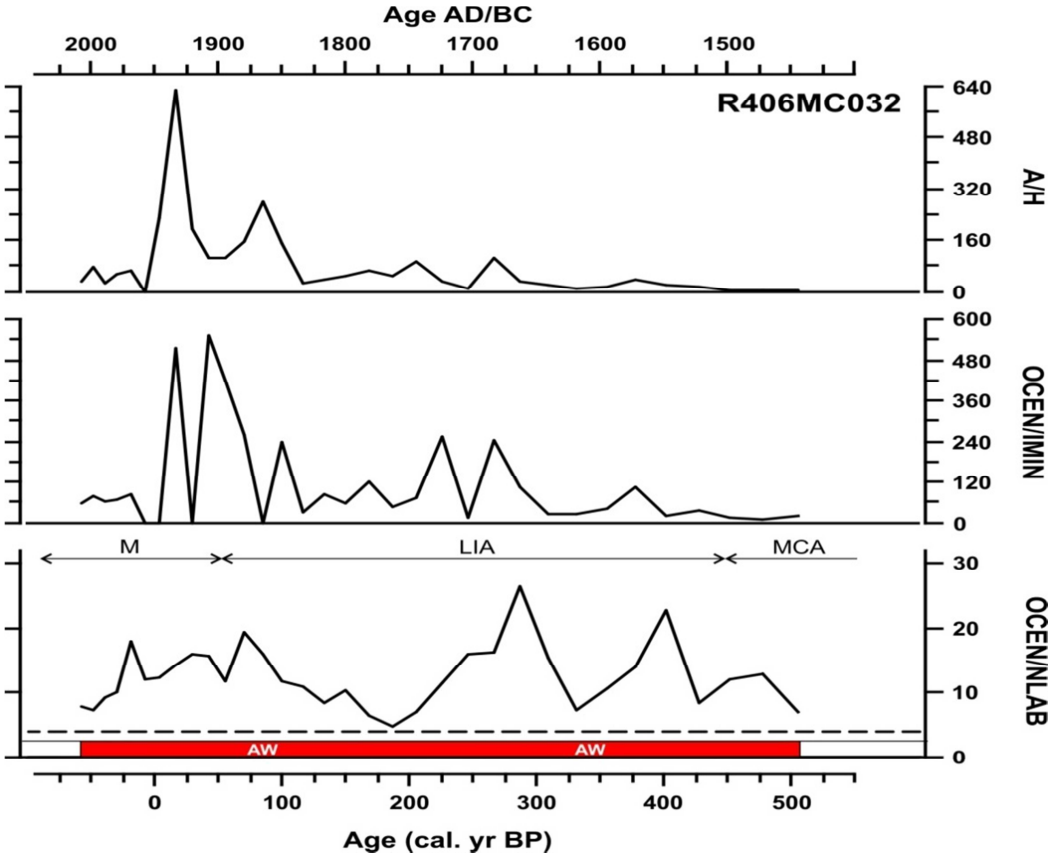

Figure 4.16 : Top: Trophic level ratio between autotrophic (A) and heterotrophic (H) species. Mid: OCEN/NLAB ratio between the AW thriving *O. centrocarpum* (OCEN) and the sea ice related (ArW) *I. minutum* (IMIN). Bottom : OCEN/NLAB ratio of the dominant dinocyst species OCEN and *N. labyrinthus* (NLAB). The bar charts below the OCEN/NLAB plot highlight the dominating surface water masses of R406MC032 according to the "4" threshold: Blue = ArW (OCEN/NLAB<4); Red = AW (OCEN/NLAB >4).

4.5.3 Quantitative Reconstructions of Sea-Surface Conditions

The reconstruction of sea-surface conditions indicate cooler and fresher conditions, compared to the southern core R248MC010 which roughly spans a similar time interval, with mean TWIN and TSUM of 2.5 °C and 11.2 °C, and mean SWIN and SSUM of 33.5 and 32.7 during the last ~500 years (Fig. 4.17). The reconstructed Modern core-top temperatures and salinities of 4.12-11.3 °C and 33.1-34 lay mostly within the range of the measured temperatures (4.9-8.2 °C) and salinities (34.1-35) at the core location (based on the World Ocean Database; Chapter 3). Here again, modern reconstructed salinities appear slightly lower than the measured values.

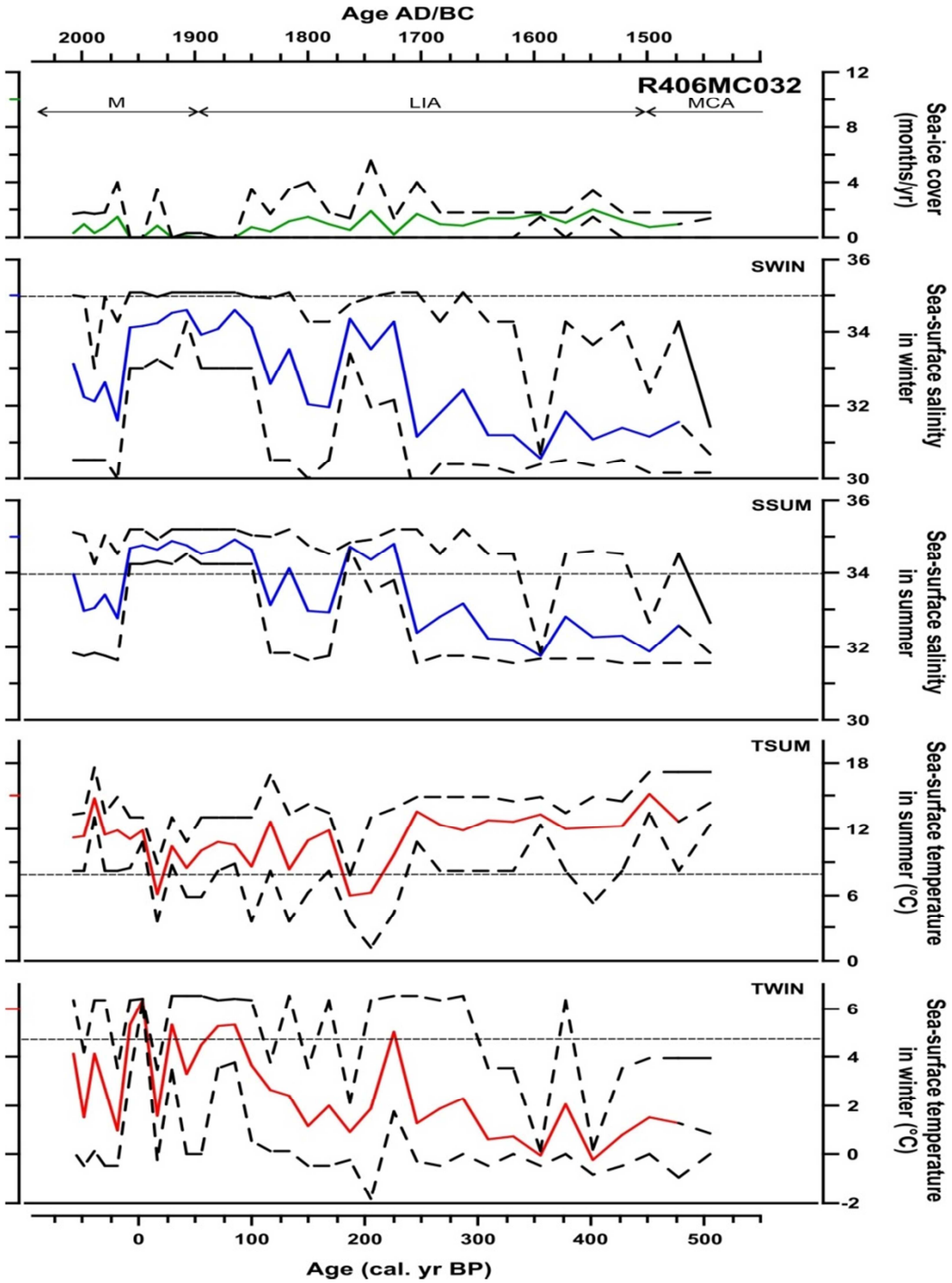

Figure 4.17 : Reconstruction of sea-surface conditions (temperature, salinity, sea ice cover) from dinocyst assemblages of core R406MC032, based on MAT. The surface sediment database (n=1189) of the North Atlantic and North-Eastern Pacific was applied for MAT. Minimum and maximum errors on the estimated parameter are shown by the dashed black lines following the curves. The modern average values are represented by the horisontal dashed lines.

The TWIN, SWIN and SSUM records all display an overall increased tendency, with an opposing decreasing trend from TSUM (Fig. 4.17). The governing increase of the TWIN record toward Recent is punctuated by two intervals of elevated temperatures around 220 cal. years BP and throughout the interval 117 to -18 cal. years BP. On the contrary the TSUM

trend shows a longer interval of decreasing temperatures from the core-base within minimum values describing the interval from ca. 245 to 20 cal. years BP. The reconstructed salinities (SWIN and SSUM) show an overall increasing trend toward Present interrupted at 245 to 168 cal. years BP and 117 to -18 cal. years BP by strongly elevated salinities (Fig. 4.17).

The reconstructed sea ice record (0-2 months/year of sea ice concentrations greater than 50%), is in line with recent late Holocene dinocyst reconstructions from this area (de Vernal et al., 2013), and governed by an overall decreasing trend with minimum values occurring from ca. 120 to -20 cal. years BP (Fig. 4.17). Previous studies on historical records of the maximum distribution of the MIZ (Vinje et al., 2001; Divine and Dick, 2006) shows that it has been located south of the present core site during the last centuries, indicating that the reconstructed sea ice record covering the last ~500 years should not be disregarded.

4.5.4 Inferring the Paleoceanographic changes in AW Flow and the Distribution of Surface Waters during the Last ~550 years (R406MC032)

The proxies obtained at core R406MC032 are plotted against bottom water temperature reconstructions from southeast of Bear Island (Wilson et al., 2011) and the combination of an instrumental (Dec-Mar; Jones et al., 1997; Osborn, 2006) and a reconstructed (Lutherbacher et al., 2002, including a 11 year-running mean) NAO index (Fig. 4.18). Three time zones have been identified through comparison of all proxy data. ZONE III represents the interval from the core-base (530 cal. years BP) to 240 cal. years BP (1420-1710 AD, LIA). ZONE IV, covers the interval ~240 to 100 cal. years BP (1710-1850 AD, LIA/M transition). Finally, ZONE V roughly encompasses the last century from 100 to -58 cal. years BP (1850-2008 AD, Modern period) (Fig. 4.18).

In general the proxy records show higher amplitude of variations during the last two centuries compared to the older part. We attribute this pattern to the overall decreasing time resolution down-core and therefore increased smoothing of the signals.

The core is hampered by the lack of age constrain on the deeper part of the record. Nevertheless, the general trends expressed by the proxies follow the variability of the inferred NAO index in both the upper and the deeper parts of core R406MC032, which to some extent confirm the reliability of the age model.

ZONE III: ~530-240 cal. years BP (LIA)

This zone is characterized by a relatively weak and slightly decreasing flow of AW, and a corresponding decrease of bottom water temperatures (Wilson et al., 2011), as a response to negative NAO conditions (Fig. 4.18c+d+h). The decrease in AW and the low NAO index seems to favor generally colder conditions, which fit well with the MAT reconstruction of sea ice presence and low although slightly increasing TWIN and SWIN conditions (Fig. 4.18h-k). In contrast to the southern R248MC010, earlier publications have shown that the MIZ was at least seasonally present at R406MC032 during the last two centuries (section 4.5.1.3), as also indicated by an elevated level of lithic grains (> 150 µm), and the lack of reworked dinocysts (Fig. 4.18a+b). The latter is supposed to originate either from sediment redistribution or freshwater input from land, hence minimum values indicate that neither process was at work in this interval. We therefore interpret the lithic grains as ice-rafter detritus (IRD). In addition minimum values in both the OCEN/IMIN and A/H ratios during this interval are most likely a result of the high content of heterotrophic dinocysts in Arctic-water assemblages in the vicinity of sea ice, linked with the abundance of diatoms (competing with autotroph dinocysts), a feeding source for heterotrophic organisms (Voronina et al., 2001, and references therein).

High values of the E/C record is observed during this interval (Fig. 4.18g). As indicated from our study of extant coccolithophores across the Norwegian-Iceland Sea (Dylmer et al., 2013, this study), maximum abundances of *E. huxlei* often occur in stratified waters related to sea ice melts during summer, a situation much alike the one identified within the western Barents Sea during this interval. The elevated relative abundances of PDAL confirm this interpretation as this species has earlier been associated with spring/summer productivity and stratification (Fig. 4.15) (Chapter 2).

The application of OCEN/NLAB at this location as a proxy for the AF over the Barents Sea is questionable as NLAB is mainly an oceanic species with maximum distribution in the middle of the Nordic seas along the AF. Hence the ratio is more likely related to the width of the WSC and therefore the distribution of ArW from the west and northwest (AF), which explains the opposite relation at this location to the NAO index (Fig. 4.18e+h). On the contrary the preference of IMIN for ArW and sea ice conditions makes the OCEN/IMIN abundance ratio a more likely proxy for the location of the AF within the southwestern Barents Sea.

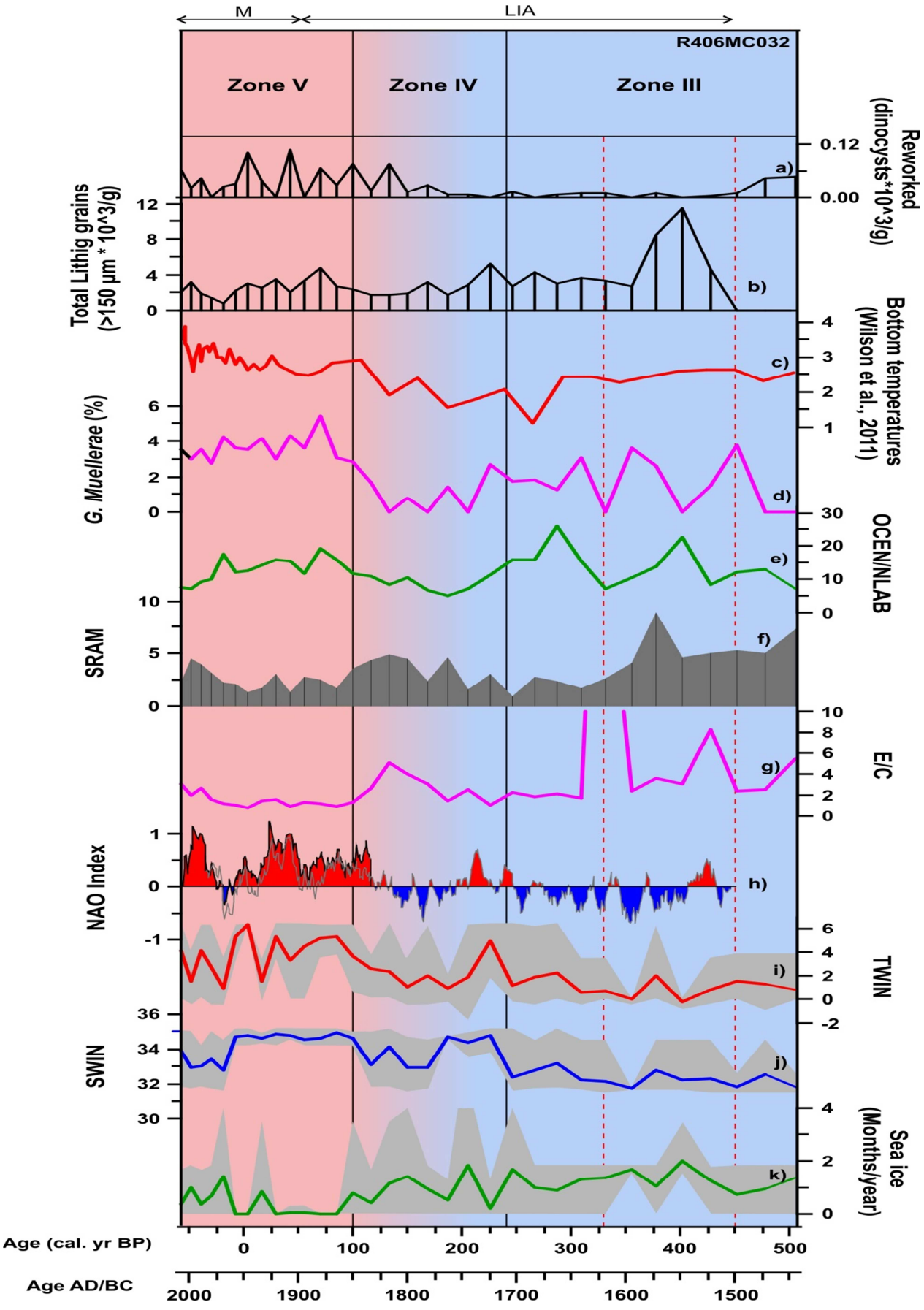
M
LIA
R406MC032
Zone V
Zone IV
Zone III
Reworked (dinocysts*10^3/g)
0.12
0.00
a)
Total Lithig grains (>150 µm * 10^3/g)
12
8
4
0
b)
Bottom temperatures (Wilson et al., 2011)
4
3
2
1
c)
G. Muellerae (%)
6
4
2
0
d)
OCEN/NLAB
30
20
10
0
e)
SRAM
10
5
0
f)
E/C
10
8
6
4
2
0
g)
NAO Index
1
0
-1
h)
TWIN
6
4
2
0
-2
i)
SWIN
36
34
32
30
j)
Sea ice (Months/year)
4
2
0
k)
Age (cal. yr BP)
0
100
200
300
400
500
Age AD/BC
2000
1900
1800
1700
1600
1500

Figure 4.18 : Summary plot of surface and subsurface circulation changes of the southwestern Barents Sea (R406MC032) over the past ~550 years. a) : Reworked dinocysts as an index of input from land (NCC) and/or sediment redistribution b) : Total lithic grains as proxies for IRD (Ice rafted detritus) and/or downslope transport of finer material. c) : Reconstructed bottom water temperatures from southeast of Bear Island (Wilson et al., 2011). d) : Absolute concentrations of *G. muellerae* as a proxy of the AW flow strength. e) : OCEN/NLAB ratio as an index of the width of the WSC. f) : Relative abundances of SRAM as a proxy for relative variations in primary productivity and salinity changes. g) : E/C ratio as an index of the relative position of the AF (AW vs. ArW). h) : Combined modern (Jones et al., 1997; Osborn, 2006) and reconstructed (Lutherbacher et al., 2002) NAO index; Red and blue areas represent long term positive and negative NAO conditions, respectively. i + j + k): Dinocyst-based MAT reconstructed winter surface water temperatures and salinities and sea ice cover (months/year), with the grey shaded area representing the error ranges of the reconstructions. The summary inferred zones and subzones are highlighted in the top, with the zonations indicated by solid (zones) and dashed (subzones) vertical black lines. Shaded light red and light blue represents inferred relative variations between increased and decreased AW flow periods in the southwestern Barents Sea, respectively.

A strong IRD peak is observed in R406MC032 at 430-380 cal. years BP, corresponding to an elevated NAO index (Fig. 4.18b).

ZONE III: *Decrease in AW inflow, relatively warm subsurface conditions, extended sea ice cover, AF south-southwest of the core location, wide WSC.*

Zone IV: 240- 100 cal. years BP (LIA/M transition)

Zone IV is governed by a major decrease in AW flow, the drifted species *G. muellerae* being almost absent from the coccolith assemblages. This marked minimum AW flow correlates with long-term negative NAO conditions and overall low bottom temperatures over the Barents Sea (Wilson et al., 2011). The recorded low OCEN/NLAB ratio translates into a narrowing of the WSC. Relatively low IRD contents confirm the overall cold surface water conditions and probably indicate a strengthened sea ice cover during this period. The increase in SRAM and E/C suggest mild stratified summer/spring conditions (at least during the end of the interval) within the southwestern Barents sea, with an increased seasonal presence of the NCC (increased reworked dinocysts) (Fig. 4.18a+f+g).

ZONE IV: *strongly decreased AW flow, cold subsurface and surface conditions (ArW), strong duration of sea ice, narrow WSC, seasonal presence of NCC at the surface (summer).*

Zone V: 100- (-58) cal. years BP (~Modern period, M)

The zone is characterized by a warming indicated by an unprecedented (over the last ~500 years) increase in AW flow and a widening of the WSC, with implications on reconstructed maximum temperatures of both the bottom waters southeast of Bear Island and the surface temperatures (TWIN) at the core location (Fig. 4.18). The strengthened AW flow naturally coincides with prevailing positive NAO conditions within ZONE V and a decrease in the sea ice extent (increase in IRD). The increase in the reworked dinocysts seems to reflect a

stronger presence of the NCC and seasonally fresher surface waters, confirmed by the marked low within the SRAM and the low E/C ratio.

ZONE V: *unprecedented (for the last 500 years) increase in the AW inflow, warm subsurface and surface conditions, strong decrease in sea ice extent, wide WSC, increased seasonal presence of NCC (summer).*

4.6 HH11-134-BC (Fram Strait, West Spitsbergen Slope)

4.6.1 Coccolith Record

Preservation of coccolith remains was moderate to good within HH11-134-BC. Bulk coccolith concentrations range from 2.4 to 7 $x10^8$ specimens/g and are characterized by increased values towards Present. Peak bulk concentrations is observed at 1400, 500-330, 45 cal. years BP as well as during the last century, with minimum abundances at 990 and 300-160 cal. years BP (Fig. 4.19). As historical and proxy (IRD) based records have shown this core site to have been under the influence of sea ice and icebergs (Chapter 3), and since it is located in the vicinity of Svalbard, it is expected to be influenced by terrigenous inputs from the nearby continental shelfs, sea ice, icebergs coastal areas (Vinje et al., 2001; Divine and Dick, 2006). Changes in dilution of the biogenic component of HH11-134-BC sediments by terrigenous material might therefore bias the significance of bulk concentration records in terms of paleo-productivity patterns.

Coccolith species diversity is low and shows a shared dominance between *C. pelagicus* (~33-63%) and *E. huxleyi* (26-56%) (Fig. 4.19). An overall increased *E. huxleyi* contribution interrupted by several millennial-scale low amplitude changes characterizes the west-Spitsbergen core over the studied time-interval. A short shift in dominance between the major species is apparent in the interval ~1200-800 cal. years BP and more clearly in modern times. As expected given its overall shared dominance with *E. huxleyi*, *C. pelagicus* displays an opposite pattern of relative abundances (Fig. 4.19).

The resultant E/C ratios lay within the range of 1.1 to 0.3. This ratio displays overall increasing values from the base to the top of the core, with higher ratios characterizing the intervals from ca. 3000 to 2100 cal. years BP, from 1200 to 700 cal. years BP, and over the last century (Fig. 4.20).

The subordinate species *G. muellerae* and *C. leptoporus* together account for an average of 8.9% of the total assemblage throughout the studied core. A fifth species, *Syracosphaera sp.*, only contributes on average 0.6%, and will not be discussed further.

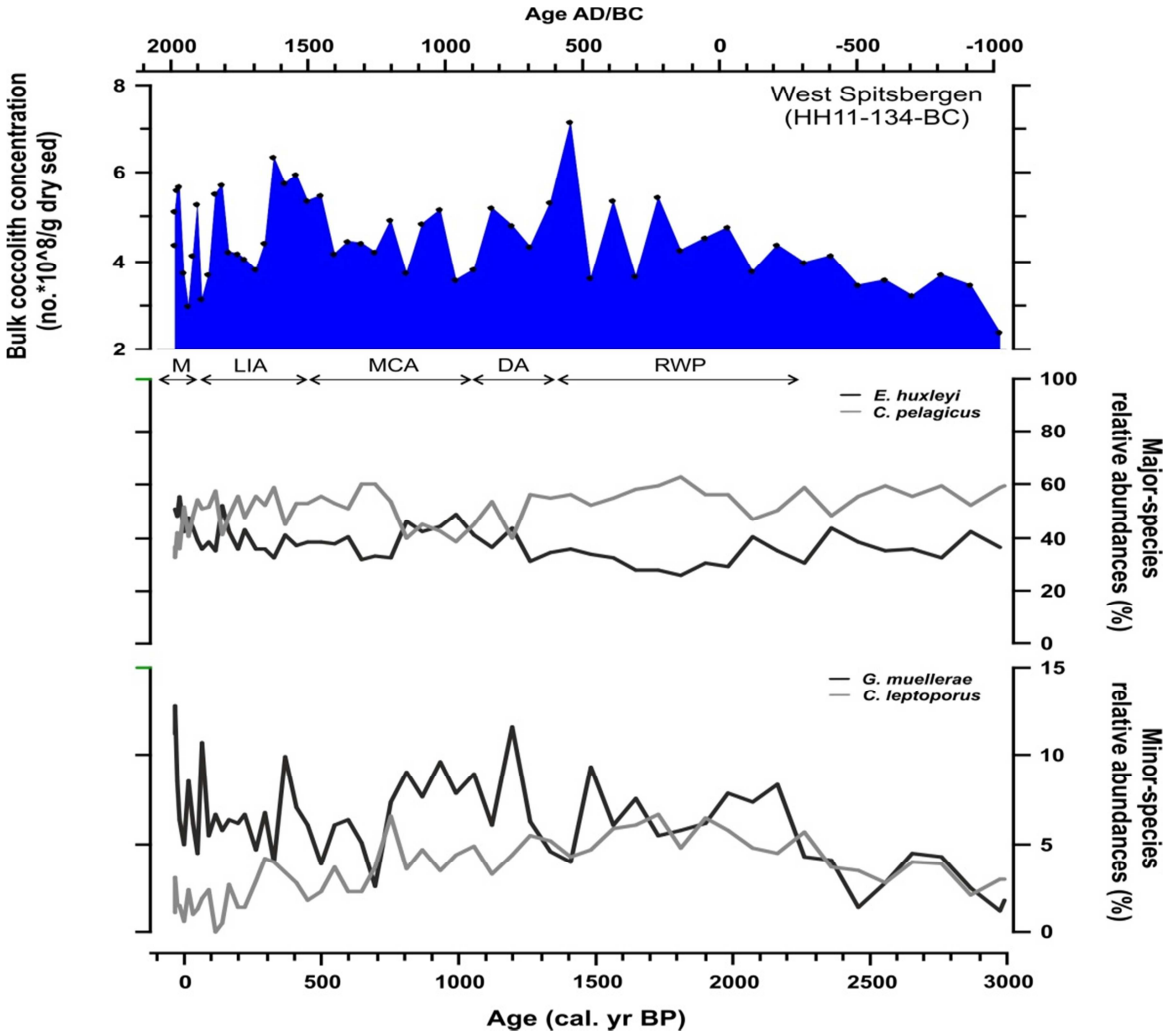

Figure 4.19 : Bulk coccolith concentration record (coccoliths * 10^8/g dry sed.) (top) and relative abundances (%) of major (mid) and minor (bottom) coccolith species within HH11-134-BC.

HH11-134-BC display an overall increase of *G. muellerae* abundances during the last 3000 years punctuated by a low steady level in the 3000-2200 cal. years BP interval, a period of highest abundances from ca. 2200 to ~650 cal. years BP, followed by marked lower values until peak abundances at the beginning of the last century (Fig. 4.19). In addition a peak abundance is observed 450-330 cal. years BP. The trends in absolute concentrations and relative abundances of this drifted species are nearly identical (Fig. 4.20). Short and/or long term changes in sedimentation of sea-ice or continental-margin-derived lithic material, which most probably affect patterns of micro fossil concentration records, including coccoliths, had therefore no obvious influence on *G. muellerae* absolute abundance trends along the studied transect. *C. leptoporus* shows a peak in relative abundance centered at ~1700-2000 cal. years BP (Fig. 4.19).

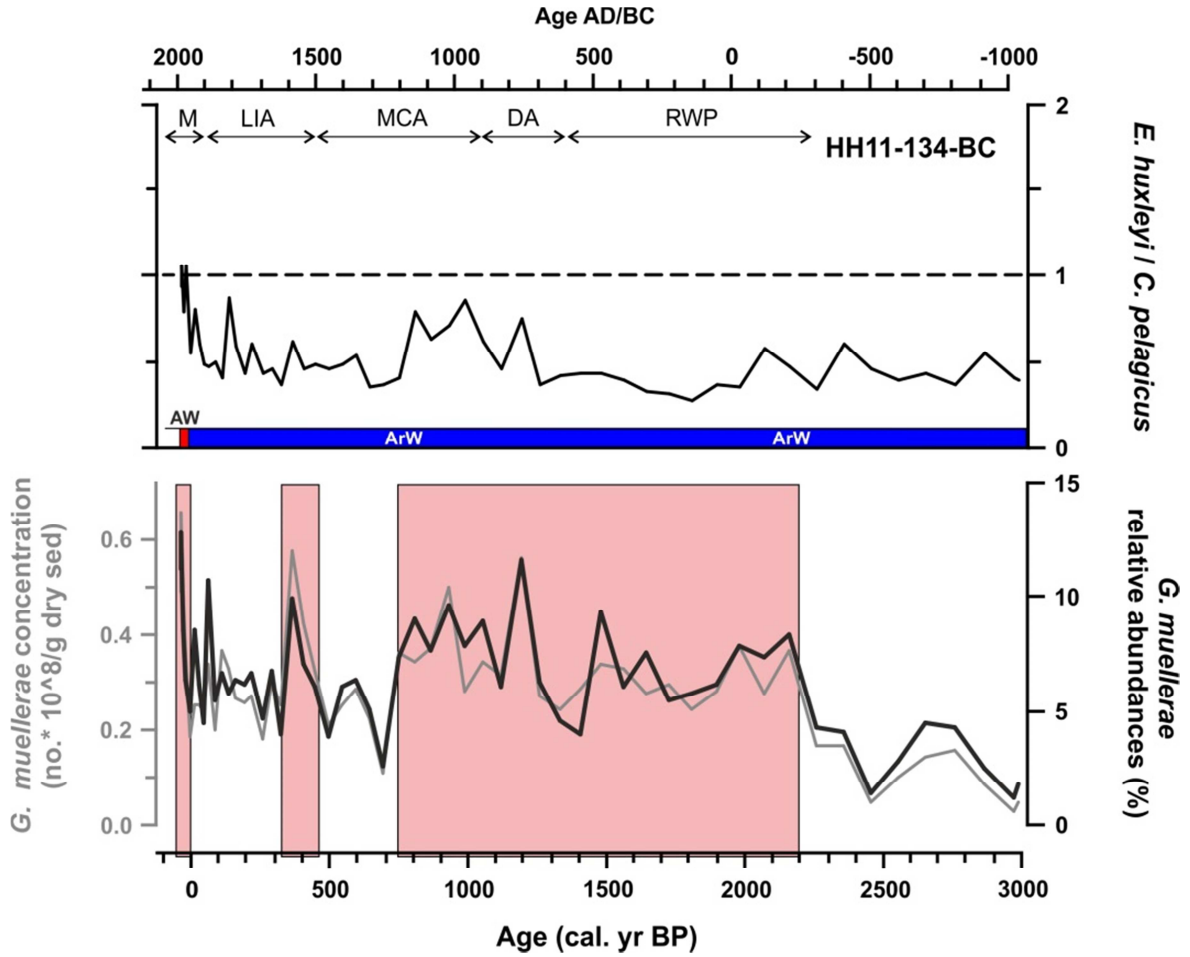

Figure 4.20 : Top : E/C ratios of the dominant coccolithophore species *E. huxleyi* (E) and *C. pelagicus* (C). The bar charts below each E/C plot highlight the dominating surface water masses at HH11-134-BC according to the "1" threshold: Blue = ArW (E/C<1); Red = AW (E/C>1). Bottom: Relative abundances (black line) and absolute concentrations (grey line) of the AW inflow species *G. muellerae*. The light red shaded areas indicate the marked inflow increases inferred from absolute concentrations of *G. muellerae.*

4.6.2 Dinocyst Record

The dinocyst preservation within HH11-134-BC was found to be good. The rather variable bulk dinocyst concentration range from 12 to 43 ×10^3 sp/g. dry sed. (Fig. 4.21) and, hence, fall well within the range of dinocyst concentration within surface sediment assemblages of the studied area (Matthiessen, 1995). The bulk dinocyst concentration record is characterized by increasing values from the core-base until ~2250 cal. years BP followed by a plateau from ~2250 until ~450 cal. years BP and finally decreasing values towards the Present (Fig. 4.21).
A total of up to 24 species (incl. 1 acritarch) was identified within HH11-134-BC. The four species OCEN (~62-87%), PDAL (~1-13%), IMIN (~2-10%) and NLAB (~4-9%) dominated the assemblages throughout the last ~3000 years, together with the subordinate species SELO (~0-6%) (Fig. 4.21). All other species contribute with less than 2% of the total assemblages.

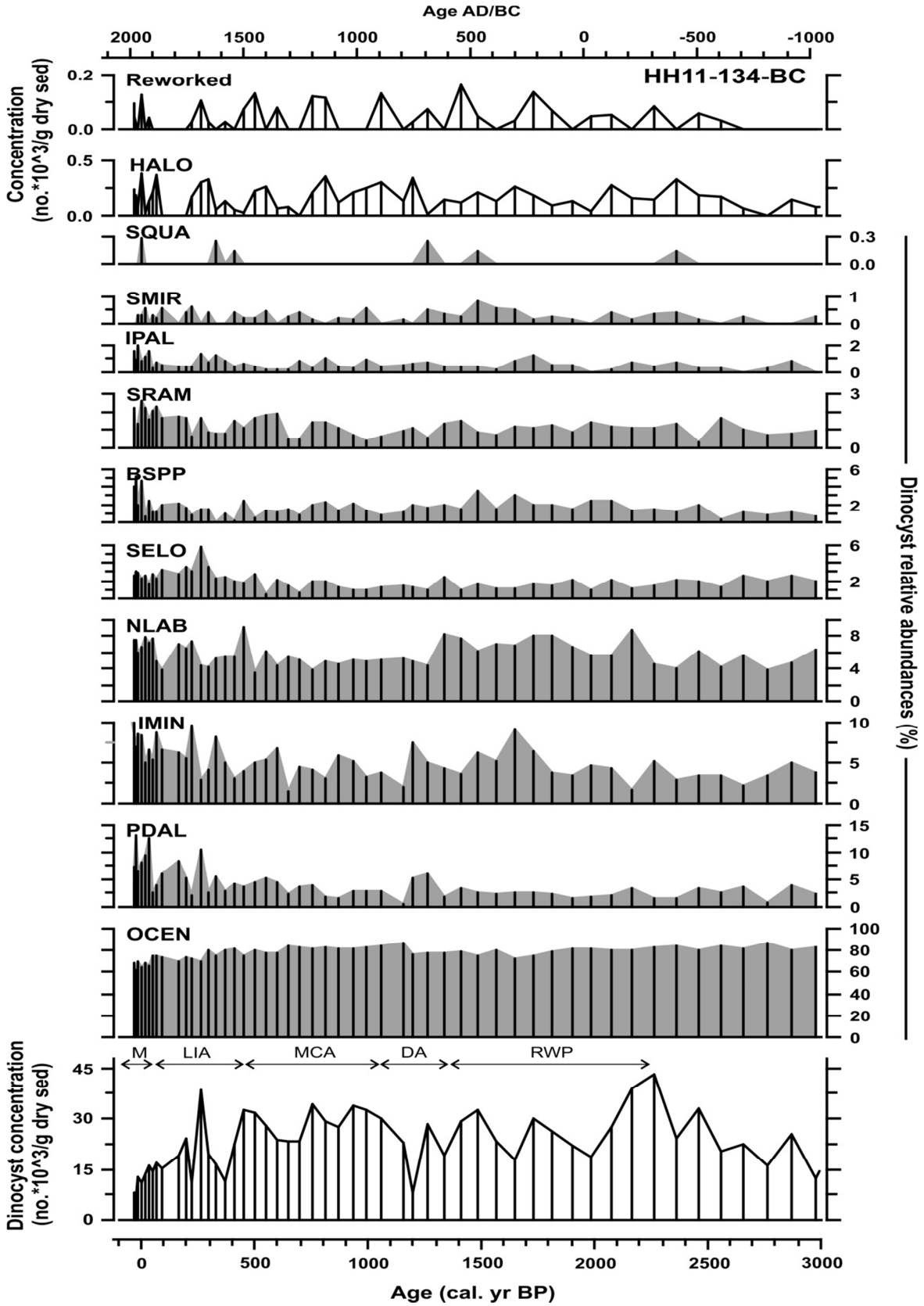

Figure 4.21 : Reworked dinocysts and *Halodinium* spp. (HALO) concentrations (sensus counts * 10^3/g dry sed.) (top), relative abundances (%) of major and minor dinocysts (mid) and dinocyst concentration records (dinocysts * 10^3/g dry sed.) (bottom) of HH11-134-BC. (See chapter 2 for species names - abrevations).

The reworked dinocysts and the palynomorph *Halodinium* spp (HALO) show mean absolute concentrations of 20.79 sp/g. dry sed. and 0.137 sp/g. dry sed., respectively. The overall composition of the HH11-134-BC dinocyst record is generally comparable to previous studies of surface sediment assemblages along the shelf and slope off Svalbard (Grøsfeld et al., 2009).

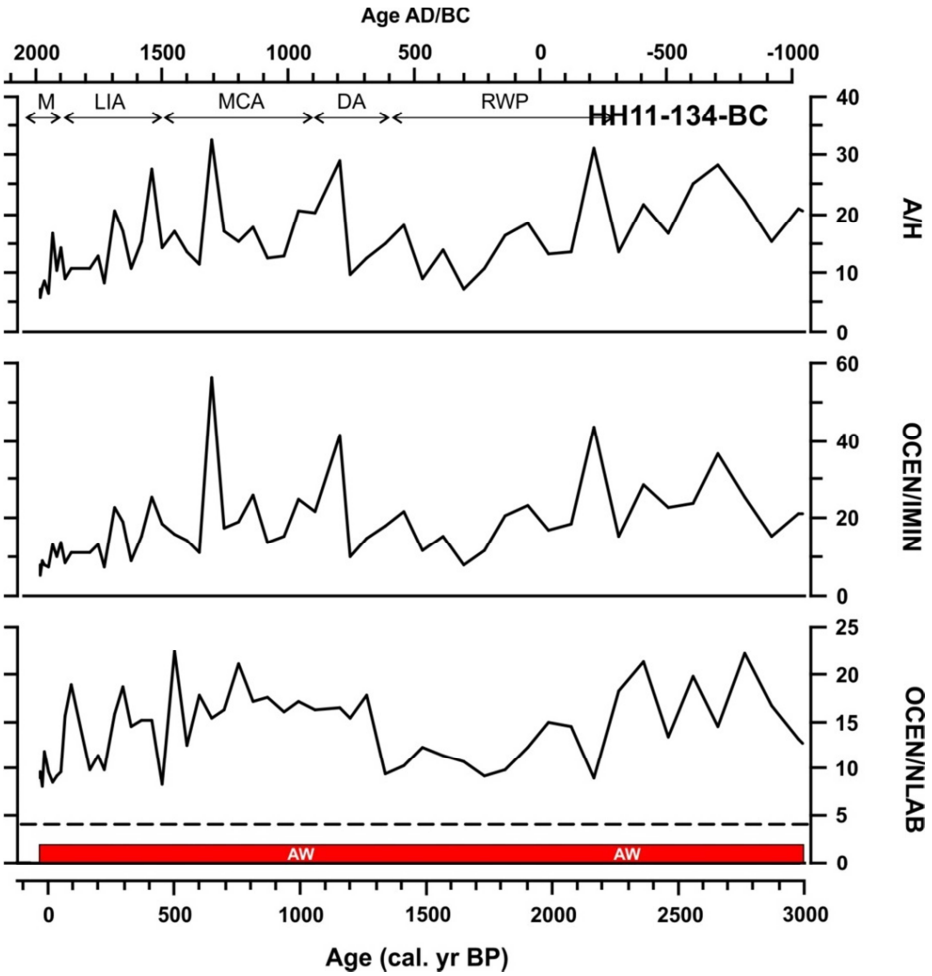

Figure 4.22 : Top: Trophic level ratio between autotrophic (A) and heterotrophic (H) species. Mid: OCEN/NLAB ratio between the AW thriving *O. centrocarpum* (OCEN) and the sea ice related (ArW) *I. minutum* (IMIN). Bottom : OCEN/NLAB ratio of the dominant dinocyst species OCEN and *N. labyrinthus* (NLAB). The bar charts below the OCEN/NLAB plot highlight the dominating surface water masses of HH11-134-BC according to the "4" threshold: Blue = ArW (OCEN/NLAB<4); Red = AW (OCEN/NLAB >4).

Core HH11-134-BC shows overall increased abundances from the core-base of all species including the reworked dinocyst species and HALO, at the expense of OCEN. The OCEN downcore distribution pattern is characterized by high abundance intervals from ~3000-1900 and ~1150-650 cal. years BP slight, followed by a marked decrease during the last 650 years (Fig. 4.21). IMIN shows a roughly inverse relation to OCEN. The most recognizable PDAL abundance features are an interval of high values at ~1260-1200 cal. years BP as well as increasing values from ~650 cal. years BP onward. The species NLAB is characterized by an

interval of higher relative abundances between ~2200 and ~1300 cal. years BP as well as increasing contributions to the dinoccyst assemblages from ~650 cal. years BP onward. The latter period of increased abundances can also be observed in both SELO and SRAM (Fig. 4.21).

The acritarch HALO appears with higher concentrations in the intervals ~2600-2000 and 1300-750 cal. years BP. In the upper part of the record HALO show marked abundance peaks at ~550 and 300 cal. years BP.

The resulting ratios OCEN/NLAB, OCEN/IMIN and A/H show average mean values of 12.3, 17.4 and 15.6, respectively (Fig. 4.22). The OCEN/NLAB record is characterized by two intervals of high values from the bottom of the core to ~2200 cal. years BP and from ~1300 to ~650 cal. years BP. The ratios OCEN/IMIN and A/H are basically identical, which is expected as the major contributors to the autotroph species and the heterotroph species are OCEN and IMIN, respectively. The ratios show elevated values until ~2100 followed by a period of lower values terminating at ~1150-1200 cal. years BP, a period of increased ratios until ~650 cal. years BP and finally a decrease towards the top. Both OCEN/IMIN and A/H show two peak values in the top part of the record at ~400 and 260 cal. years BP (Fig. 4.22).

4.6.3 Quantitative Reconstructions of Sea-Surface Conditions

The reconstruction of sea-surface conditions indicate generally cool conditions, with a reconstructed mean winter and summer temperature of 1.5 °C and 6.2 °C, during the last ~3000 years.

The reconstructed core-top temperatures and salinities of 0.8-3.4 °C and 33.8- 34.3 fall roughly within the range of the temperature (2-5.4 °C) (World Ocean Database), although with generally low reconstructed salinities (34.3-34.6) (Fig. 4.23).

All reconstructed temperatures and salinities are governed by an overall decreasing trend throughout the last 3000 years. The reconstructed TWIN, SWIN and SSUM initiates at the oldest part of the record with high values until ~2200 cal. years BP followed by a stable (to slightly decreasing) pattern until ~700 cal. years BP and finally strongly decreasing values until the top of the record (Fig. 4.23). The former trends are less clear in the SSUM, which seems to show stable to slight decreased values until ~700 cal. years BP followed by enhanced freshening until the top of the record.

The reconstructed sea ice conditions (0-4 months/year) are generally in line with recent (late Holocene) dinocyst reconstructions from this area (de Vernal et al., 2013) and governed by an overall increase during the last 3000 years. The record shows a decrease in sea-ice duration

until ~2200 cal. years BP, followed by a slight increase until ~700 cal. years BP, and terminating in a strong increase during the last 700 years (Fig. 4.23). Previous studies on historical records of the maximum distribution of the MIZ (Vinje et al., 2001; Divine and Dick, 2006) has shown that the MIZ has been located south of the core site during the last two centuries, indicating that our sea ice reconstructions during the last ~3000 years should not be disregarded.

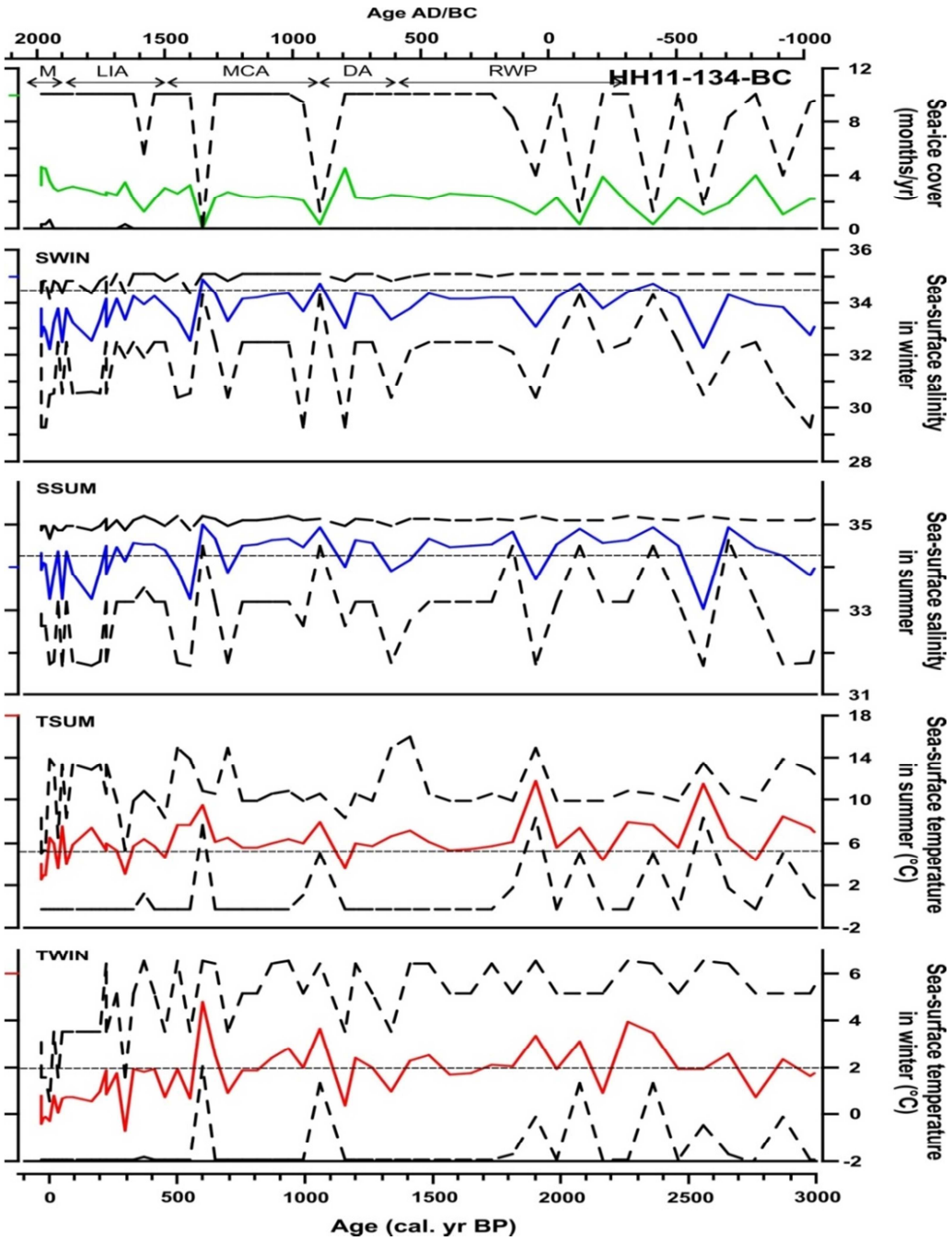

Figure 4.23 : Reconstruction of sea-surface conditions (temperature, salinity, sea ice cover) from dinocyst assemblages of core HH11-134-BC, based on MAT. The surface sediment database (n=1189) of the North Atlantic and North-Eastern Pacific was applied for MAT. Minimum and maximum errors on the estimated parameter are shown by the dashed black lines following the curves. The modern average values are represented by the horisontal dashed lines.

4.6.4 Inferring the Paleoceanographic changes in Atlantic Water Flow and the Distribution of Surface Waters during the Last ~3000 cal. years BP (HH11-134-BC)

The proxies are plotted together with reconstructed Arctic temperatures based on terrestrial records (Kaufmann et al., 2009), a reconstructed NAO index (Trouet et al., 2009; Olsen et al., 2012) and the P_BIP_{25} proxy (A sea ice index provided by Alba Navarro Rodrigez, Univ. Plymouth) (Fig. 4.24, 4.25). Three zones (and three subzones) have been identified through comparison of all proxy data. ZONE I represents the interval from ~the core-base (3000 cal. years BP) to 2200 cal. years BP (1050 – 250 BC). ZONE II, covers the interval 2200-730 cal. years BP (250 BC-1220 AD) and contains the two identified subzones II-a (2200-1250 cal. years BP, 250 BC-700 AD) and II-b+c (1250-730 cal. years BP, 700-1220 AD). ZONE III spans from 730 cal. years BP to ~60 cal. years BP (1220-1890 AD). Finally Zone V encompasses the last ca. 120 years (1890-2011 AD).

Zone I: ~3000-2200 cal. years BP (1050 -250 BC)

The zone appears to be generally governed by cold conditions as shown by the overall low, although slightly improving AW flow and NAO index (Fig. 4.24c+d). The slight increase in TWIN, SWIN and subpolar foraminifera (relative abundances) toward the top of this zone indicate cold however slighly improving conditions, especially in the subsurface waters (Fig. 4.24b+h+i). The slight increase in the AW flow strength possibly results in a low although slightly enhancing summer carbonate productivity possibly induced by sea ice melting (slightly increased IRD > 150 µm, Fig. 4.25g) causing stronger surface water stratification (slightly increased E/C ratio) (Fig. 4.24f). The increase in HALO abundance confirm the presence at the core site of fresh water from sea ice melt related to the MIZ (Fig. 4.25i), this species being related to gradational zones between fresh water and marine environments e.g. glacier-meltwater outflow and the MIZ (Chapter 2). The sea ice reconstructions (MAT) however reveal relatively low duration and slightly decreasing sea-ice cover (month/year) (Fig. 4.25a).

The P_BIP_{25} sea ice index represents a combination of the IP_{25} and brassicasterol concentrations (Fig. 4.25c) (see Navarro-Rodriguez et al., 2012). The former is an organic geochemical biomarker (IP25), which is thought to be biosynthesized by a limited number of sea ice diatoms during the spring blooms and is thus considered to be highly specific as a sea ice proxy (Navarro-Rodriguez et al., 2012, and references therein). The latter (brassicasterol) is considered to be a more general biomarker indicator of phytoplankton since derived from a wide array of algal groups (Navarro-Rodriguez et al., 2012, and references therein). Despite

this lower specificity, the use of brassicasterol alongside IP_{25} has been suggested to provide a potential mean of improving the interpretation of IP_{25} in marine sediments through the calculation of the so-called PIP_{25} index (Müller et al., 2011). Indeed, the absence of IP25 in Arctic sediments has previously been interpreted as representing either ice-free or permanent sea ice conditions (Belt et al., 2007; Müller et al., 2009), hence the relative abundance of brassicasterol provides a way to distinguish between these two extreme scenarios. The P_BIP_{25} index record in core HH11-134BC indicates a relatively strong presence of sea ice.

Of the two XRF ratios e.g. Ca/Ti and Zr/Rb, the former has been interpreted from earlier results, as a ratio between marinebiogenic carbonate production and the lithogenic input from land (Fig. 4.25b+e). Such an interpretation might be biased at the core location by the presence over Svalbard of sedimentary limestones (Vogt and Knies, 2009) (Ti is expected to origine mainly from mainland Norway). We however assume, based on the mear absence of coarse detrital carbonates (>150 µm, strong reaction to 5% HCL) before 1250 cal. years BP (Fig. 4.25h), that a similar pattern is expected to influence the finer fraction, hence the earlier part of the Ca record is expected to represent the biogenic carbonate production fairly well.

The Zr/Rb ratio has been implemented as a proxy of grain size variability within this core. Zr is tracing the coarser fraction (heavier minerals, IRD), whereas Rb is rather associated to the clay fraction (more open water or strong sea ice cover) (Fig. 4.25b).

The overall strong variability of the system is clearly reflected in the grain size record (Zr/Rb) which fluctuates in phase with the IRD abundance. The overall cold conditions are reflected in the low Ca/Ti ratio throughout this zone (low biogenic carbonate production), with the overall conditions slightly improving throughout in relation with increased periods of open water conditions (decreasing Zr/Rb) and decreased sea ice duration (Fig. 4.25). The IRD size fraction >500µm is expected to have a stronger relation to icebergs or locally formed sea ice than the smaller size fration (Fig. 4.25f). The iceberg proxy is similarly low confirming the dominating cold conditions and a decreased supply of icebergs from land.

ZONE I: *low but slightly increasing AW flow strength, presence of AW in subsurface waters, ArW at the surface, low but slightly increasing carbonate productivity, strong seasonal presence of sea ice, low presence of icebergs.*

Zone II: 2200-730 cal. years BP (250 BC-1220 AD)

This zone is governed by a strong overall increase in the AW flow in relation with a shift toward positive NAO conditions, slightly decreasing TWIN, stable SWIN, a warming of subsurface waters, increased productivity, increase in sea ice duration and increased sea ice

melt, increased presence of icebergs, an increase in carbonate productivity and apparently decreasing Arctic air temperatures (Fig. 4.24, 4.25).

Subzone II-a: 2200-1250 cal. years BP (250 BC-700 AD)

This subzone marks the initiation of an interval of an overall strengthened AW flow, possibly related to a change from a governing negative NAO index to a dominating positive NAO pattern (Fig. 4.24c+d). The increased inflow seems to be confirmed by generally warmer subsurface waters (marked by higher subpolar foraminifera abundances), and favors a strengthened carbonate productivity in the near surface water masses (increased bulk coccolith concentration and Ca/Ti ratio) (Fig. 4.24a+b, 4.25e). On the contrary to the ameliorating subsurface conditions, the reconstructed winter surface temperatures (TWIN) seems to follow the generally decreasing trend of Arctic temperatures (Fig. 4.24g+h).

The cold surface temperatures are further confirmed by low values in most of the species ratios, which are likely indicative of an increased presence of ArW in the surface at this location (Fig. 4.24e+f). The reconstructed temperatures and salinities fall well within modern ArW values (0-4°C, 34.6-34.9; Johannessen, 1986), hence confirming the interpretation of ArW in the surface.

The low although slightly increasing IRD (>150 µm) content and the increase in P_BIP_{25} and reconstructed sea ice duration all seems to reflect a strengthening in the sea ice cover during this interval, as also confirmed by the increase in the coarser fraction of the sediments (Zr/Rb) (Fig. 4.25a-c+g).

The increased AW flow might be part of the explanation behind the sudden increase in the coarse IRD size fraction (>500 µm) (Fig. 4.24c, 4.25f). Hence, increased inflow is expected to result in increased evaporation and precipitation which directly affects glacier budgets along

Figure 4.24 : Summary plot of surface and subsurface circulation changes west of Svalbard (HH11-134-BC) over the past ~3000 years. a) : Bulk coccolith concentrations as an index of carbonate productivity. b) : Relative abundances of subpolar foraminifera (fraction > 100 µm) as an index of subsurface AW masses. c) : Absolute concentrations of *G. muellerae* as a proxy of the AW flow strength. d) : Combined NAO index reconstruction based on Trouet et al. (2009) and Olsen et al. (2012); Red area represents positive and blue area negative NAO conditions. e) : OCEN/IMIN ratio as an index of surface water changes (AW/ArW). f) : E/C ratio as an index of the relative position of the AF (AW/ArW). g) : Arctic summer temperatures based on Kaufmann et al. (2009). h + i) : Dinocyst-based MAT reconstructed winter surface water temperatures and salinities, with the grey shaded area representing the error ranges of the reconstructions. The summary inferred zones and subzones are highlighted in the top, with the zonations indicated by solid (zones) and dashed (subzones) vertical black lines. The vertical red dashed line represents the warm pulse at ca. 400 cal. Years BP identified by Dylmer et al., 2013. Shaded light red and light blue represents inferred relative variations between increased and decreased AW flow periods in the eastern Fram Strait, respectively.

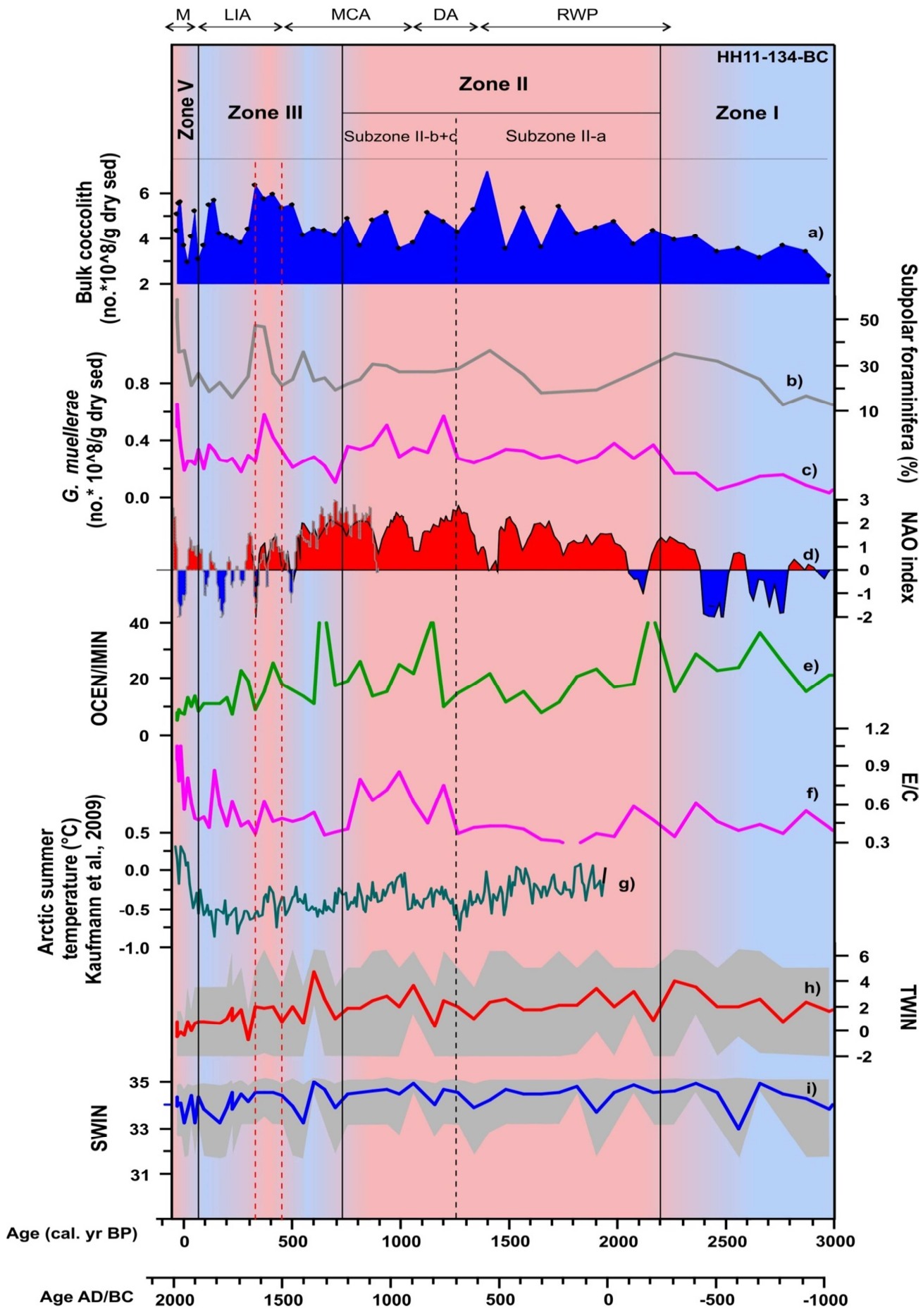
M
LIA
MCA
DA
RWP
HH11-134-BC
Zone V
Zone III
Zone II
Subzone II-b+c
Subzone II-a
Zone I
Bulk coccolith (no.*10^8/g dry sed)
a)
G. muellerae (no.* 10^8/g dry sed)
b)
c)
Subpolar foraminifera (%)
d)
NAO index
OCEN/IMIN
e)
f)
E/C
Arctic summer temperature (°C) Kaufmann et al., 2009)
g)
h)
TWIN
SWIN
i)
Age (cal. yr BP)
Age AD/BC

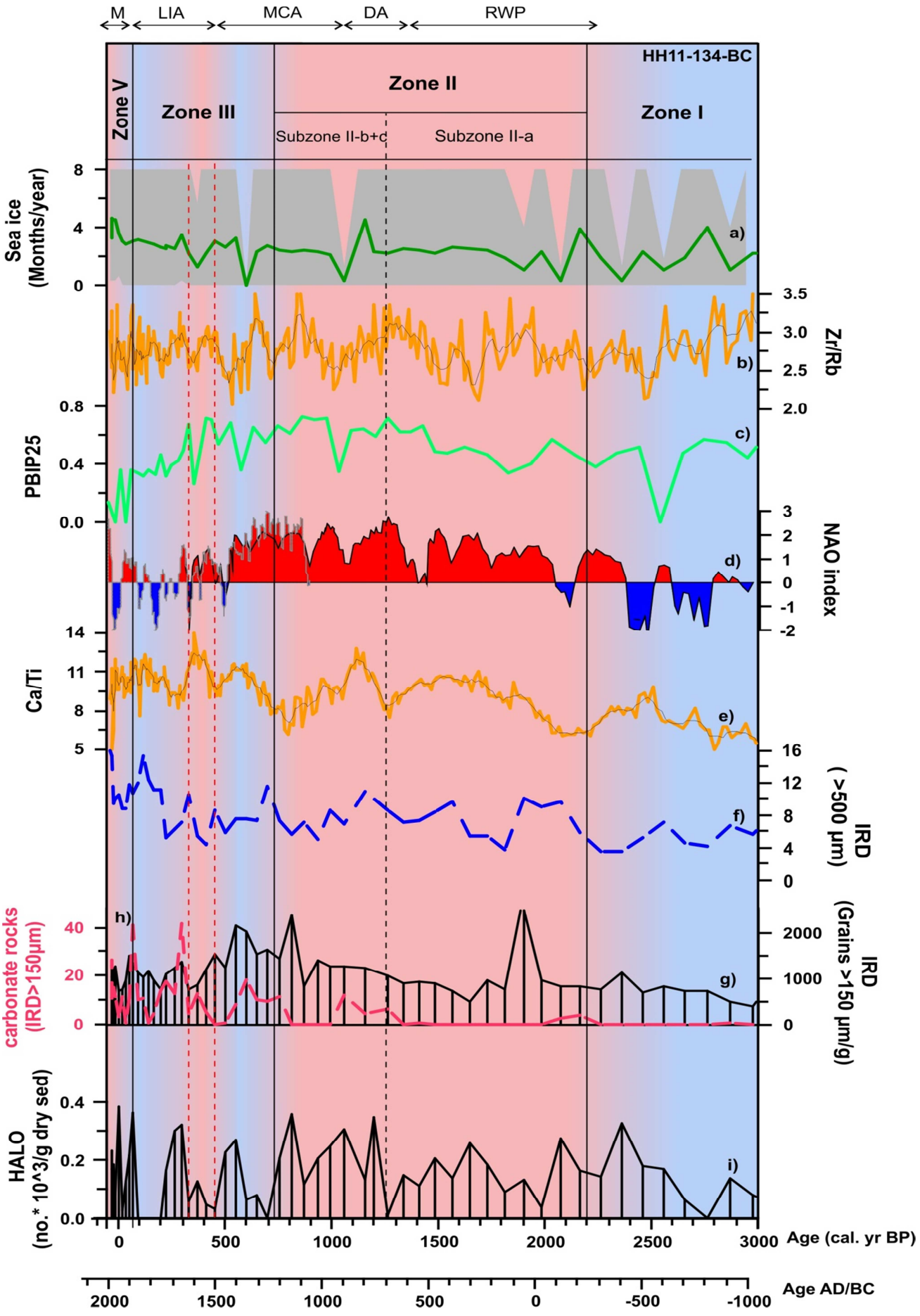
M
LIA
MCA
DA
RWP
HH11-134-BC
Zone V
Zone III
Zone II
Subzone II-b+c
Subzone II-a
Zone I
Sea ice (Months/year)
a)
Zr/Rb
b)
PBIP25
c)
NAO index
d)
Ca/Ti
e)
IRD (>500 µm)
f)
carbonate rocks (IRD>150µm)
h)
g)
IRD (Grains >150 µm/g)
HALO (no.* 10^3/g dry sed)
i)
Age (cal. yr BP)
Age AD/BC

Figure 4.25 : Summary plot of lithology and sea ice variability west of Svalbard (HH11-134-BC) over the past ~3000 years. a) : Dinocyst-based MAT reconstructed sea ice cover (months/year), with the grey shaded area representing the error ranges of the reconstructions. b) : Zr/Rb ratio (XRF) as a grain size indicator and/or sea ice influence indicator; higher values = coarser material (IRD), lower values = fine material (clay), black line indicate a 7-running mean. c) : P_BIP_{25} sea ice index, higher values inferring closer proximity to the MIZ and lower values tracing more open water conditions. d) : Combined NAO index reconstruction based on Trouet et al. (2009) and Olsen et al. (2012); Red area represents positive NAO and blue area negative NAO conditions. e) : Ca/Ti as a tentative index of marine biogenic carbonate vs. terrigenous sedimentation (see text), black line indicate a 7-running mean. f) : IRD (>500 µm) as a relative Iceberg index. g +h) : IRD (>150 µm, incl. carbonate grains) as a proxy for sea ice variability. i) : HALO represents melt water from sea ice and/or land. The summary inferred zones and subzones are highlighted in the top, with the zonations indicated by solid (zones) and dashed (subzones) vertical black lines. The vertical red dashed line represents the warm pulse at ca. 400 cal. years BP identified by Dylmer et al., 2013. Shaded light red and light blue represents inferred relative variations between warmer and cooler periods in the eastern Fram Strait, respectively.

the path of the AW (Nesje et al., 2001) and causes increased iceberg calving following the general governing glacial expansion during the late holocene culminating later during the LIA (Svendsen and Mangerud, 1997).

Subzone II-a*: strengthened AW flow, presence of AW in subsurface, ArW at the surface, increased carbonate productivity, increased presence of sea ice, higher contribution from icebergs.*

Subzone II-b+c: 1250-730 cal. years BP (700-1220 AD)

This subzone is governed by a further strengthening of the AW flow, warmer subsurface waters and a peak in Arctic temperatures at ~1000 cal. years BP (Fig. 4.24b+c+g). The high E/C ratio values express a marked change in dominance between the two major coccolith species in favor of the AW thrieving *E. huxleyi*. This increase most likely suggests a seasonal influence of AW in the surface waters and a retreating MIZ, which is confirmed by the increases in the dinocyst ratios, as well as the increases in ice melt (HALO) (Fig. 4.24e, 4.25i).

The bulk coccolith concentrations indicate a relatively high carbonate production during this interval. (Fig. 4.24a). An observed minimum in the bulk coccolith production at 990-1050 cal. years BP seems to be related to a minimum in Arctic temperatures at 1045 cal. years BP, a cooling event formerly identified during subzone II-b in WOO/SC-3. However except for a minimum in Zr/Rb and P_BIP_{25}, this short cooling is not clearly reflected (Fig. 4.24a, 4.25b+c). The maximum extent of the MIZ reached during this interval (P_BIP_{25} sea ice index), which in combination with an enhanced AW also explain the strong increase in the IRD fraction >150 µm, resulting from the possibly increased sea ice melt, as confirmed by HALO. Which in combination with the elevated E/C ratio are indicative of a strong seasonality of the MIZ during this interval.

The decrease in icebergs (>500 µm) might be a result of increased Arctic temperatures causing a glacier retreat and/or a direct result of the strengthend sea ice cover, as a limited amount of icebergs would be able to reach the site (Fig. 4.24g, 4.25b+c+g+f). The change in the IRD origine (>500 µm, increased carbonate) might be indicative of a general change within the climatic system from ~1000 cal. years BP and onwards.

Subzone II-b+c*: strong AW flow, seasonal presence of AW in subsurface and surface, relatively high carbonate primary productivity, highly fluctuating MIZ, decreased IRD contribution from icebergs.*

Zone III: ~730-60 cal. years BP (1220-1890 AD)

Zone III is characterized by generally cold conditions under long-term negative NAO conditions, as expressed by a strongly decreased AW flow, low TWIN and SWIN, generally low Arctic temperatures, a lower influence of AW in the subsurface and predominantlt ArW at the surface (Fig. 4.24). A strong decrease in HALO further suggests a decrease in ice melting as a result of an increase in sea ice cover (Fig. 4.25).

A decrease in the carbonate productivity seems to occur throughout this interval, although this is inverse to the one observed in the Ca/Ti ratio (Fig. 4.25). The increase in the Ca/Ti ratio is however most likely a response to an increasing delivery of lithogenic carbonate, and is therefore not reliable as a paleoproductivity indicator here.

The first evidences of changes in the sea ice distribution does not occur until before ~550-450 cal. years BP, when a strong decrease is recognized in the IRD >150 µm and the sea ice biomarker P_BIP_{25} (Fig. 4.25), suggesting an increase in sea ice cover, which fit well with earlier findings of glacier advance during the 13th and 14th centuries over Svalbard (Svendsen and Mangerud, 1997).

The sea ice reconstructions by MAT does not correspond to these variations and seems to indicate a continuous increase in duration of the sea ice (Fig. 4.25). This is surprising especially in light of the changes during the later modern period, indicating that the reconstruction of MAT within the top of the record might be biased.

The Zone III is punctuated by a warm pulse between 330 and 450 cal. years BP as expressed by a sudden increase in the AW flow. This warm pulse is supported by warmer temperatures in the subsurface waters, a higher E/C ratio, slightly warmer Arctic temperatures, increased bulk coccolith concentrations, and coincides with the timing of the major decrease in P_BIP_{25} (Fig. 4.24, 4.25). In addition the pulse correlates with a marked increase in IRD in R406MC032 (Fig. 4.18).

ZONE III*: decreased in AW flow, cold conditions in subsurface waters, ArW at the surface, low carbonate productivity, strengthened sea ice cover, high contribution from icebergs, warm puls at 330-450 cal. years BP.*

Zone V: ~60-(-)61 cal. years BP (1890-2011 AD)

Zone V show a strong increase in the AW inflow during the modern period causing an unprecedented presence of AW in both surface and subsurface waters (increased E/C and subpolar foraminifera) (Fig. 4.24). This general trend compares well with the reconstruction of Arctic temperatures, showing a strong increase during the last century. The increases are followed by enhanced bulk coccolith concentrations indicative of stronger carbonate productivity, a stronger meltwater contribution (HALO), a retreat of the MIZ (PBIP25 and low IRD) and finally a high unprecedented production of icebergs (~3000 years) (Fig. 4.24, 4.25).

Zone V: warm conditions, unprecedented increase in AW flow, AW present in surface and subsurface waters, strengthened carbonate productivity, high increase in meltwater, MIZ retreated, high production of icebergs.

4.7 Coccolith and Dinocyst-based NwAC Flow Strength and Water-Mass Proxies

The following section contains a manuscript recently published in *Climate of the Past* (2013) on coccolith evidences for paleoceanographic changes within the eastern North Atlantic during the last 3000 years. This paper especially focus on the use of *G. muellerae* abundances as a proxy for the relative variations in the strength of the NwAC, as well as the application of the E/C ratio to infer changes in the nature of surface water masses (AW vs. ArW) and in the position of the AF.

An additional discussion on the application of coccolith and dinocyst ratios along a north-south transect during the late Holocene will follow this section.

Northward Advection of Atlantic water in the eastern Nordic Seas over the last 3000 years

C.V. Dylmer[a], J. Giraudeau[a], F. Eynaud[a], K. Husum[b], A. De Vernal[c].

a Université de Bordeaux, CNRS, UMR 5805 EPOC, Talence, France
b Department of Geology, University of Tromsoe, Tromsoe, Norway
c GEOTOP, Université du Québec à Montréal, Montréal, Canada

Contact author: Christian V. Dylmer
Address : UMR EPOC, CNRS/INSU – Université Bordeaux 1, Avenue des faculties, 33405 Talence cedex, France.
Email : c.dylmer@epoc.u-bordeaux1.fr

Dylmer, C. V., Giraudeau, J., Eynaud, F., Husum, K., and De Vernal, A.: Northward advection of Atlantic water in the eastern Nordic Seas over the last 3000 yr, Clim. Past, 9, 1505-1518, doi:10.5194/cp-9-1505-2013, 2013.

ABSTRACT

Three marine sediment cores distributed along the Norwegian (MD95-2011), Barents Sea (JM09-KA11-GC), and Svalbard (HH11-134-BC) continental margins have been investigated in order to reconstruct changes in the poleward flow of Atlantic Waters (AW) and in the nature of upper surface water masses within the eastern Nordic Seas over the last 3000 years. These reconstructions are based on a limited set of coccolith proxies: the abundance ratio between *Emiliania huxleyi* and *Coccolithus pelagicus*, an index of Atlantic vs. Polar-Arctic surface water masses; and *Gephyrocapsa muellerae*, a drifted coccolith species from the temperate North Atlantic, whose abundance changes are related to variations in the strength of the North Atlantic Current.

The entire investigated area, from 66 to 77°N, was affected by an overall increase in AW flow from 3000 cal. years BP to the Present. The long-term modulation of westerlies strength and location which are essentially driven by the dominant mode of the North Atlantic Oscillation (NAO), is thought to explain the observed dynamics of poleward AW flow. The same mechanism also reconciles the recorded opposite zonal shifts in the location of the Arctic Front between the area off western Norway and the western Barents Sea-eastern Fram Strait region.

The Little Ice Age was governed by deteriorating conditions, with Arctic/Polar waters dominating in the surface off western Svalbard and western Barents Sea, possibly associated with both severe sea-ice conditions and a strongly reduced AW strength. A sudden short pulse of resumed high WSC flow interrupted this cold spell in eastern Fram Strait from 330 to 410 cal. years BP. Our dataset not only confirms the high amplitude warming of surface waters at the turn of the 19th century off western Svalbard, it also shows that such a warming was primarily induced by an excess flow of AW which stands as unprecedented over the last 3000 years.

1. INTRODUCTION

The Late Holocene was governed by a cooling trend known as the Neoglaciation (Porter and Denton, 1967). Compared with the preceding Early to Mid-Holocene Climate Optimum, the Neoglaciation has been widely recorded in both terrestrial and marine archives in the North Atlantic Region (Jennings et al., 2002; Seidenkrantz et al., 2008; Kaufman et al., 2009, and references therein; Andresen et al., 2011; Müller et al., 2012) as a time of expansion of Scandinavian glaciers (Nesje et al., 1991; Nesje et al., 2001), increased sea-ice cover and colder surface waters in the Barents Sea and part of Fram Strait (Duplessy et al., 2001; Risebrobakken et al., 2010; Kinnard et al., 2011; Müller et al., 2012), colder surface and subsurface waters off western Norway (Calvo et al., 2002; Moros et al., 2004; Hald et al., 2007; Sejrup et al., 2011) and overall colder conditions over Northern Europe (Bjune et al., 2009). This cooling trend was punctuated by several warm and cold spells such as the Roman Warm Period and Medieval Climate Anomaly (RWP, MCA), and the Little Ice Age (LIA). Over the last century, the LIA was reversed by an overall increase in temperature, as seen in, terrestrial high resolution proxy records of the Arctic region (Overpeck et al., 1997; Kaufman et al., 2009) and proxy records from marine sediment cores of the northern North Atlantic (Spielhagen et al., 2011; Hald et al., 2011; Wilson et al., 2011). Marine proxy-based reconstructions suggest that this recent temperature increase in the subsurface layer west of Spitsbergen (Spielhagen et al., 2011) and in shallow settings off Northwest Norway (Hald et al., 2011) were unprecedented over the past two millennia. Both studies implied that this warming was probably caused by enhanced advection of Atlantic Water (AW) to the Arctic Ocean during modern times, although none were able to strictly infer the dynamical history of AW, i.e. the history of the strength of the North Atlantic Current (NAC).

The hypothesis of an increased AW inflow during the modern period was further supported by Wanamaker et al. (2012) based on living and fossil molluscan remains north of Iceland; these authors additionally related known pre-Anthropocene warm (MCA) and cold (LIA) climatic spells of the last ~1500 years to modulations of the surface Atlantic-derived water dynamics within the North Atlantic. This modulation was further evidenced off Florida, at the inception of the Gulf Stream, by Lund et al. (2006) who estimated a 10 percent decrease in the flow of this current at the transition from the MCA to the LIA. Similarly, in the close Chesapeake Bay, such modulations was also evidenced by Cronin et al. (2005) who linked this to North Atlantic Oscillation (NAO) forcing of sea-surface temperature in the western North Atlantic.

The processes controlling variations in the meridional flow of the NAC to the Nordic Seas and ultimately to the Arctic Ocean are either associated with anomalies in the location and strength of the westerlies, and/or changes in the thermohaline circulation (Müller et al., 2012). At present the most prominent pattern of atmospheric variability in the North Atlantic Region is known as the NAO, itself depending on the Northern Hemisphere annular mode, the Arctic Oscillation (e.g. Marshall et al., 2001). The NAO is defined as the wintertime difference in atmospheric pressure (sea level) between the Icelandic low and the Azores high, controlling the strength and direction of westerly winds, storm tracks across the North Atlantic, temperature and precipitation over western Europe, and the strength of the poleward NAC and equatorward EGC (Blindheim et al., 2000; Hurrell et al., 2003). A low NAO index (reduced westerly flow across the Atlantic) induces a reduced flow of the NAC, less precipitation in Northern Europe and a more southern direction of the storm tracks (Hurrell et al., 2003). Whereas a high index favors a strengthened NAC flow, stronger precipitation and an eastward shift of the Arctic Front (AF) which separates Atlantic from Arctic waters (ArW), toward the slope off Norway (Blindheim et al., 2000). Furthermore modern observations indicate a significant correlation between the NAO indexes and the Barents Sea ice extent, with less sea ice during the positive NAO (warm) phases and conversely more ice during negative NAO (cold) phases (Vinje, 2001; Sorteberg and Kvingedal, 2006), possibly related to variations in southwesterlies, air masses and Atlantic inflow (Blindheim et al., 2000).

Paleorecords from Arctic Canada and Iceland suggest that a series of explosive volcanism centered at the MCA/LIA transition might have triggered an extensive sea ice expansion during the LIA (Miller et al., 2012). A combined switch in NAO patterns from a long-term positive phase during the MCA to negative NAO conditions during the LIA (Trouet et al., 2009) possibly further enhanced the severe increase in sea-ice extent, as decadal and long-term variations in large scale ice concentrations have shown to be significantly correlated with long-term NAO variations (Visbeck et al., 2003).

However, although the importance of the NAO on the modern hydrography and climate of the Nordic Seas is now well established, assessing its significance on paleoceanographical changes of this ocean realm has long been hampered by the lack of instrumental records prior to the 19th century, and by proxy- and model-based reconstructions reaching back only one millennia (Trouet et al., 2009). A high resolution reconstruction of NAO variability from a lake record in Southwestern Greenland (Olsen et al., 2012), recently extended the NAO record back to 5200 years Before Present (BP), offering a way to investigate links between

atmospheric processes and ocean circulation changes over the mid to late Holocene in the Northern North Atlantic.

The NAC impact on the hydrological and climatic changes in the Nordic Seas and the Arctic Ocean is enormous, hence the need for an increased understanding of inflow variations, forcing mechanismes and the consequences on the global climate system is crucial in order to fully understand the changes in our present and future climate.

Previous water column and surface sediment investigations of extant and fossil remains (coccoliths) of coccolithophorids suggested that this species group could be used as proxies, though mostly qualitative, of both water mass distribution and flow strength of the NAC in the northern North Atlantic (Samtleben and Schröder, 1992; Baumann et al., 2000; Schröder-Ritzrau et al., 2001). Andrews and Giraudeau (2003) and Giraudeau et al. (2010) thereafter tested these coccolith proxies to infer the Holocene history of AW flow within the Denmark Strait and across the Iceland-Scotland Ridge. The present manuscript lies on these exploratory works in applying selected coccolith proxies on a set of marine sedimentary cores distributed along the continental margins off western Norway, western Barents Sea and western Spitsbergen. Our aim is to investigate late Holocene changes in AW flow and associated surface hydrological fronts along the main axis of heat and salt transfer to the Arctic Ocean, which is carried by the NAC and its northernmost extension (West Spitsbergen Current -WSC-). Given the major influence of NAO related atmospheric processes on the modern NAC dynamics and climate of the Nordic Seas region, we will thoroughly discuss our proxy results in view of available NAO paleoreconstructions over the last 3000 years, as well as to nearby terrestrial and marine records.

2. OCEANOGRAPHY

The study area lies as a South-North transect along the continental slope off western Norway, the western Barents Sea and West of Svalbard (Fig. 1). This area is mainly influenced by three water masses; AW, Polar Water (PW) and Coastal Water. Warm (7-13 °C) and saline (≥35 PSU) AW is advected north by the NAC (Hopkins, 1991), originating from the Iceland-Scotland Ridge, the main passageway of oceanic salt and heat transfer to the Nordic Seas (ca. 7 Sv; Hansen and Østerhus, 2000). This topographically steered poleward flow of AW splits off northern Norway into a meridional branch, the WSC and a zonal component, the North Cape Current (NCaC). The WSC flows along the slope of the western Barents Sea and off western Svalbard, joined on its northern path byArW on the shelf from the Bear Island Current (extension around Bjørnøya of the Persey Current, PC) and the Sørkapp Current

(extension around southern Svalbard of the East Spitsbergen Current, ESC) (Saloranta and Svendsen, 2001; Wassman et al., 2006) (Fig. 1), and transmits a volume of roughly 3-5 Sv of AW to the Arctic Ocean, part of it being recirculated at intermediate depth below the southward flowing East Greenland Current (EGC). North of Svalbard, AW enters the Arctic Ocean as a subsurface current insulated from the atmosphere by fresh PW in the upper mixed layer (Blindheim and Østerhus, 2005). The NCaC transmits 1.8 Sv of AW to the Barents Sea round northern Norway (Skagseth et al., 2008), preventing winter sea-ice to develop in the southern region of the Barents shelf. The Norwegian Coastal Current (NCC), flowing along the Norwegian coast is influenced by freshwater runoff from the Norwegian mainland and from the Baltic Sea, and is therefore characterised by reduced salinities (34.4~PSU) (Wassman et al., 2006).

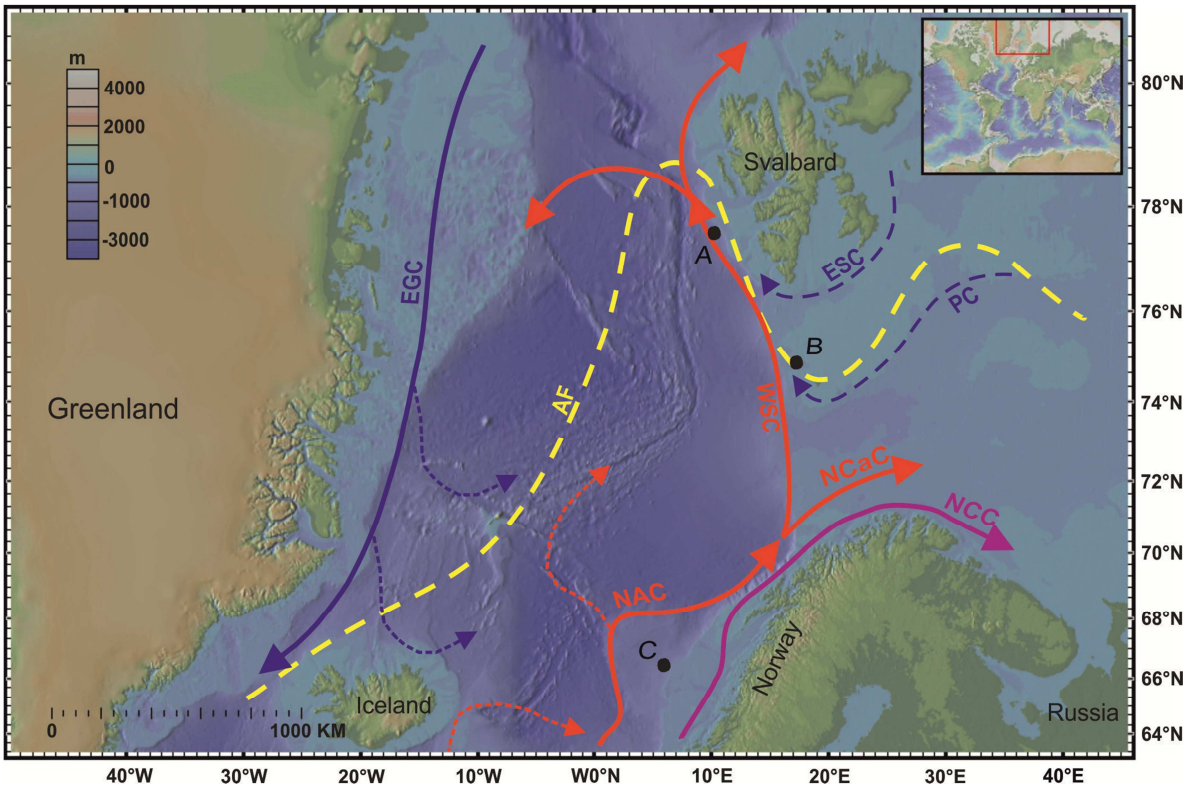

Figure 1: Bathymetric map of the Nordic Seas showing the major oceanic features and site locations. Red arrows: flow direction of warm saline Atlantic water (NAC: North Atlantic Current, NCaC: North Cape Current, WSC: West Spitsbergen Current), blue arrows: flow direction of cold low saline Arctic/Polar waters (EGC: East Greenland Current, ESC: East Spitsbergen Current, PC: Persey Current), purple arrow: flow direction of coastal surface current (NCC: Norwegian Coastal Current). Dashed yellow line: modern distribution of Arctic Front (AF). Core locations A: HH11-134-BC (West of Spitsbergen), B: JM09-KA11-GC (western Barents Sea) and C: MD95-2011(Vøring Plateau).

Sea-ice and fresh water from the Arctic Ocean are essentially transmitted to the Nordic Seas via Fram Strait and the southward flowing cold and fresh EGC (<0°C, <34.5 PSU) (Buch,

2000), the largest and most concentrated meridional ice flow in the World Oceans (Blindheim and Østerhus, 2005) (Fig. 1). The Northeast-Southwest trending boundary between PW and ArW is termed the Polar Front indicating the minimum drift ice extent (summer), whereas the boundary between ArW and AW is known as the AF and represents the maximum drift ice extent (winter) (Baumann et al., 2000; Wassman et al., 2006). Though showing some complex local peculiarities, the interannual changes in sea-ice extent are closely controlled by atmospheric processes acting over the Nordic Seas and surrounding areas. A link with NAO was proposed by Hurrell (1995) and is consistent with anomalies of sea-ice extent in the Barents Sea (Vinje, 2001). Further north in the Greenland Sea, maximum ice export from the Arctic ocean through Fram Strait characterizes positive NAO periods (Kwok et al., 2004).

Table 1: Core location, water depth, length and geographical area

Core ID	Latitude	Longitude	Water depth (m)	Core length (m)	Location
MD95-2011	66°58.19'N	7° 38.36'E	1048	7,45	Mid Norwegian Margin (Vøring Plateau)
JM97_948/2A BC	66°58.19'N	7° 38.36'E	1048	0,30	
JM09-KA11-GC	74°52.489'	17° 12.210'E	345	3,6	Midwest Barents Sea (Kveithola Trough)
HH11-134-BC	77° 35.96	9°53.25'E	1383	0,41	West spitsbergen slope

3. MATERIAL AND METHODS

Three marine sediment cores distributed along the Norwegian, Barents Sea, and Svalbard continental margins were specifically selected for the present work (Fig. 1, Table 1).

The southernmost site (hereafter refered to MD95-2011), representing a splice between a box-core (30 cm) covering the top 560 years (JM97-948/2A) and the MD95-2011 piston core (Giraudeau et al., 2010), was retrieved on the Vøring Plateau off western Norway, located below the main path of the poleward flowing NAC. The present investigation was conducted on the top 220 cm of the composite MD95-2011. The 383 cm long gravity core JM09-KA11-GC, of which the top 25 cm is presented here, was retrieved from the Kveithola trough, representing the western Barents Sea component of the transect, influenced both by the WSC

and Arctic/Polar waters circulating clockwise round Svalbard (Sørkapp Current) and Bjørnøya (Bear Island Current). The 41 cm long box-core HH11-134-BC was retrieved on the West Spitsbergen Margin under the axis of the WSC inflow to the Arctic Ocean. The present study was carried on the top 27 cm of this core.

Table 2: Core, sample depth, dated material, 14C AMS age years BP, calibrated years BP, Laboratory ID and Reference.

Core	Core depth (cm)	Dated material	14C AMS Age years BP	Calibrated Age, cal. Years BP	Calibrated ages, 2σ range	Lab ID	Reference
HH11-134-BC	9.75	Bulk planktic foraminifera	826 +/- 23	462.5	420-505	UBA-20062	
HH11-134-BC	15.5*	Bulk planktic foraminifera	2030 +/- 30	1602	1515-1688	SacA 29428	
HH11-134-BC	19.5	Bulk planktic foraminifera	1995 +/- 28	1571	1473-1669	UBA-20061	
HH11-134-BC	30.25	Bulk planktic foraminifera	3825 +/- 30	3774.5	3676-3873	SacA 29432	
JM09-KA11-GC	4.50	*Bathyarca glacialis*	925 +/- 30	543	482-604	TRa-1063	Rüther et al., (2012)
JM09-KA11-GC	16.00	*Bathyarca glacialis*	1880 +/- 35	1424.5	1332-1517	TRa-1065	Rüther et al., (2012)
JM09-KA11-GC	27.50	*I*. Norcrossi/ helenae	4430 +/- 30	4758	4745-4771	Beta-324049	Berben et al. (2013) and Groot et al. (2013)
JM09-KA11-GC	33*	*A. elliptica*	1990 +/- 35	1556	1441-1671	Tra-1066	Rüther et al., (2012)
JM09-KA11-GC	40.00	*I*. Norcrossi/ helenae	5480 +/- 30	5838.5	5749-5928	Beta - 315192	Berben et al. (2013) and Groot et al. (2013)
JM97_948/2A BC	4.75			-1		210Pb Dated	Risebrobakken et al., (2003)
JM97_948/2A BC	7.75			18		210Pb Dated	Risebrobakken et al., (2003)
JM97_948/2A BC	10.25			29		210Pb Dated	Risebrobakken et al., (2003)
JM97_948/2A BC	21.75	*N. pachyderma (dex)*	735 +/- 40	375.5	290-461	KIA 6285	Risebrobakken et al., (2003)
JM97_948/2A BC	30.75	*N. pachyderma (dex)*	940 +/- 40	553.5	485-622	KIA 4800	Risebrobakken et al., (2003)
MD95-2011	10.5	*N. pachyderma (dex)*	980 +/- 60	573	489-657	Gif 96471	Risebrobakken et al., (2003)
MD95-2011	30.5	*N. pachyderma (dex)*	1040 +/- 40	602.5	534-671	KIA 3925	Risebrobakken et al., (2003)
MD95-2011	47.5	*N. pachyderma (dex)*	1160 +/- 30	709.5	650-769	KIA 5601	Risebrobakken et al., (2003)
MD95-2011	70.5	*N. pachyderma (dex)*	1460 +/- 50	1021	907-1135	KIA 3926	Risebrobakken et al., (2003)
MD95-2011	89.5	*N. pachyderma*	1590 +/- 30	1148.5	1060-1237	KIA	Risebrobakken et

		(dex)				6286	al., (2003)
MD95-2011	154	*N. pachyderma (dex)*	2335 +/- 25	1953	1868-2038	KIA 6287	Risebrobakken et al., (2003)
MD95-2011	170.5	*N. pachyderma (dex)*	2620 +/- 60	2298	2128-2468	Gif 96472	Risebrobakken et al., (2003)
MD95-2011	269.5	*N. pachyderma (dex)*	3820 +/- 35	3768.5	3659-3878	KIA 10011	Risebrobakken et al., (2003)

3.1 Core Chronology

The chronologies of the studied sediment core intervals are based on 22 AMS ^{14}C- and ^{210}Pb-dates of which 13 have previously been published for core JM09-KA11-GC (Rüther et al., 2012), and MD95-2011 (Risebrobakken et al., 2003) (Table 2). The dates were calibrated to calendar years BP (present = 1950 AD) applying the software Calib 6.1.0 (Stuiver and Reimer, 1993) and the marine calibration curve marine09 (Reimer et al., 2009) using a reservoir correction of ~400 years ($\Delta R = 0$). This reservoir correction was chosen as a further finetuning of the signals would result in age models differing from published paleoclimate data sets using the standard variations. Nevertheless we are aware of a possible shift of our age models due to the ΔR effect, especially in areas with 'old' Arctic/Polar waters.

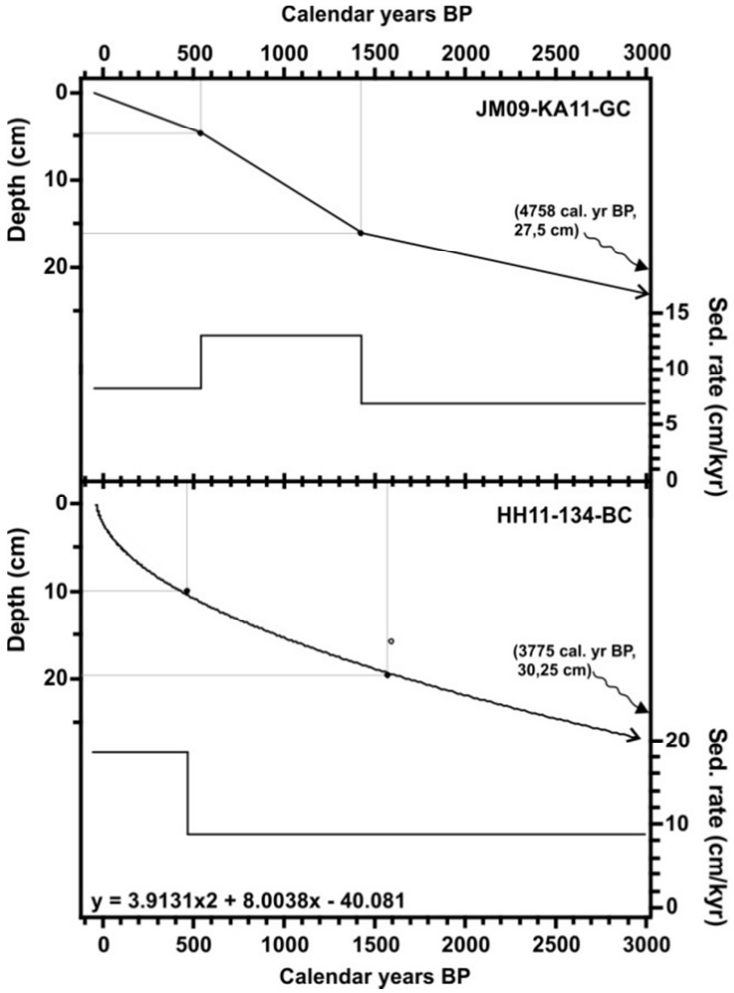

Figure 2: Calendar age-depth model and sedimentation rates of JM09-KA11-GC (linear interpolation between each dated level) and HH11-134-BC (second order polynomia), based on data from table 2. Filled circles: incl. AMS C^{14} datings, hollow circle: excl. AMS C^{14} datings. The stratigraphic framework of core MD95-2011 was developed by Birks and Koç (2002), Risebrobakken et al. (2003) and Andersson et al. (2003).

3.2 Micropaleontological Analyses

The chronologies was established using the calibrated mean ages for the 2σ interval of highest probability and assuming a constant sedimentation rate between each radiocarbon dated level of JM09-KA11-GC (linear interpolation) and a second order polynomial fit for core HH11-134-BC (Fig. 2). The sedimentation rates of the three studied cores range from 5 to 146 cm/kyr, which according to the sampling resolution, lead to a temporal resolution of our micropaleontological dataset of 10 to 105 years. A decadal to multi-decadal resolution has been found sufficient in the present study to identify major centennial scale changes in paleocirculation along our transect.

The sample preparation for the coccolith study was conducted according to the "Funnel" method described by Andruleit (1996). It involves dilution and filtration of a preweight amount of dry bulk sediment on membrane filters, mounting between slide and coverslip, and examination under a light microscope, at x1000 magnification. A total of more than 300 specimens were counted in order to insure the statistical reliability of our results (Andruleit , 1996) and were ultimately expressed in terms of relative abundances (species percentage) and absolute concentrations (specimens/gram of dry bulk sediment). Previous repeated analyses of fine fraction sediment samples using the "Funnel" method revealed that the method can cause ~15% deviation in the bulk coccolith absolute concentrations (Herlle and Bollmann, 2004) and consequently species-specific absolute concentrations. Hence only relative abundances and "major" (>>15% deviation) absolute concentration changes will be adressed in the following.

An additional investigation on planktonic foraminiferal assemblages was conducted on the northernmost sediment core (HH11-134-BC). Samples were wet sieved through a 63 µm mesh. Counting was performed on the >100 µm fraction according to Husum and Hald (2012) in order to include small sized species which are frequent in assemblages of the northern North Atlantic. We will only present here the relative abundance of subpolar planktic foraminifera, expressed as the sum of *Globigerinata* species and *Turborotalia quinqueloba*.

3.3. Rationale for the Selection of Species-Specific Coccolith Proxies.

While an overall presentation of the coccolith assemblages in the sediment cores is provided in the present paper, a focus is made on species-specific coccolith proxies of surface water mass distribution and AW flow dynamics in the studied geographical domain.

Extant populations of coccolithophorids thriving in the Nordic Seas are overwhelmingly dominated by *Emiliania huxleyi* (high to very high cell densities) and *Coccolithus pelagicus* (medium-high cell densities) (Baumann et al., 2000), with rare occurrences of a few representatives of *Syracosphaera* spp. and of the deep-thriving species *Algirosphaera robusta* (Samtleben and Schröder, 1992; Samtleben et al., 1995). Both *E. huxleyi* and *C. pelagicus* dominate settling assemblages and assemblages in the sediment (Schröder-Ritzrau et al., 2001 and reference therein). *E. huxleyi* is a summer blooming ubiquitous species with a strong affinity for Atlantic-derived surface waters in the eastern part of the Nordic Seas. Beside its preferential distribution within areas bathed by the NAC, this species is suggested to be influenced mainly by variations in stratification, irradiance and to a lesser extent temperature of the photic layer (Samtleben and Schröder, 1992; Samtleben et al., 1995; Baumann et al., 2000; Beaufort and Heussner, 2001).

Coccolithus pelagicus, the cold end-member of the extant coccolithophorid populations in the Nordic Seas, thrives preferentially in the vicinity of the Arctic Front and in the Greenland Sea (Samtleben et al., 1995). Turbulence might be an important factor to prevent sinking of this heavily calcified species from the photic zone and therefore favors its dominance in areas with moderate gradients in salinity and temperature (Cachão and Moita, 2000) and/or Arctic to Polar waters.

The different regional dominance of these two species is also reflected in surface sediments (Samtleben et al., 1995). The abundance ratio between *E. huxleyi* and *C. pelagicus* (E/C ratio) in fossil assemblages in the Nordic Seas has therefore been proposed by Baumann et al. (2000) to define the location of the AF, which separates the seasonally ice-covered waters of the Polar and Arctic domains (E/C<1) from warmer and saltier Atlantic-derived waters (E/C>1). According to Baumann et al. (2000), the E/C ratio is based on a conversion of coccolith to coccosphere units; the average number of coccoliths per coccosphere for each species is taken from Samtleben and Schröder (1992).

Allthough the original work by Baumann et al. (2000) were confined to the central areas of the Nordic Seas, we believe the application of this method to be valid in the wider Nordic

Seas including its eastern part. The published surface sediment sample dataset by Baumann et al. (2000) only included a few sites far west of the continental margin with coccolith assemblages dominated by *C. pelagicus* (E/C <1). This excess *C. pelagicus* abundance stands as a contrast to our own results from surface sediment assemblages in the northern cores HH11-134-BC and JM09-KA11-GC, as well as to the composition of extant populations northwest of Bjørnøya (Baumann et al., 2000) and across Fram Strait (Dylmer et al., 2013, this study), which both indicate an expected clear dominance of *E. huxleyi* below and within AW dominated areas. Based on these evidences we use the definition of the AF (a frontal salinity and temperature gradient separating surface AW masses from mixed ArW) to infer that the E/C ratio (ie. deviations from the treshold of 1) characterizes surface sediments deposited below Atlantic or Arctic surface water masses, when considering pluriannual conditions.

Though barely found in modern plankton communities of the Nordic Seas (Andruleit, 1997; Dylmer et al., 2013, this study), coccoliths of *Gephyrocapsa muellerae* and *Calcidiscus leptoporus* commonly contribute together up to ~20% of the fossil assemblages in surface sediments of the eastern Nordic Seas. Drifting with the poleward flow of surface to intermediate NAC waters from the temperate North Atlantic, where these species are preferentially thriving, was proposed as a possible explanation for this discrepancy by Samtleben and Schröder (1992). Based on new datasets on living and fossil communities, Giraudeau et al. (2010) revisited the distributional pattern of *G. muellerae* in the North Atlantic and restricted the ecological niche of this species to the eastern North Atlantic, south of the Iceland-Scotland ridge. Given this ecological background, abundance changes of *G. muellerae* in the studied sediment cores will be discussed in terms of relative variations of the depth integrated flow strength of the NAC to the Nordic Seas up to its northernmost extension off western Svalbard (WSC).

Eventhough the mechanism of poleward transport, as described here for *G. muellerae*, is supposed to affect all species thriving in southern latitudes within the path of the NAC, it is not expected to hamper the paleorecords of the high in situ production of the dominating species (e.g. *E. huxleyi* and *C. pelagicus*) in the Nordic Seas which is transferred to the sediment surface within weeks by fecal pellets (Samtleben and Schröder, 1992; Andruleit et al., 1997).

4. RESULTS AND INTERPRETATION

4.1 Bulk Coccolith Concentrations

Preservation of coccolith remains was good to moderate throughout the three studied cores, hereby confirming the overall relatively good preservation of calcareous microfossils in recent sediments of the eastern Nordic Seas (Hebbeln et al., 1998; Matthiessen et al., 2001). Bulk coccolith concentrations throughout the investigated time interval range from 25±10 $x10^8$ specimens/g. of dry sediment (sp/g. dry sed) in the Vøring Plateau area, to a minimum of 1±0.5 $x10^8$ sp/g. dry sed in the Kveithola through region (Fig. 3). These values fall within the range of typical coccolith concentrations in surface sediments of the eastern Nordic Seas and accurately reproduce the decreasing poleward trend of coccolith absolute concentrations in sediments presently accumulating along the path of the NAC and WSC (Baumann et al., 2000).

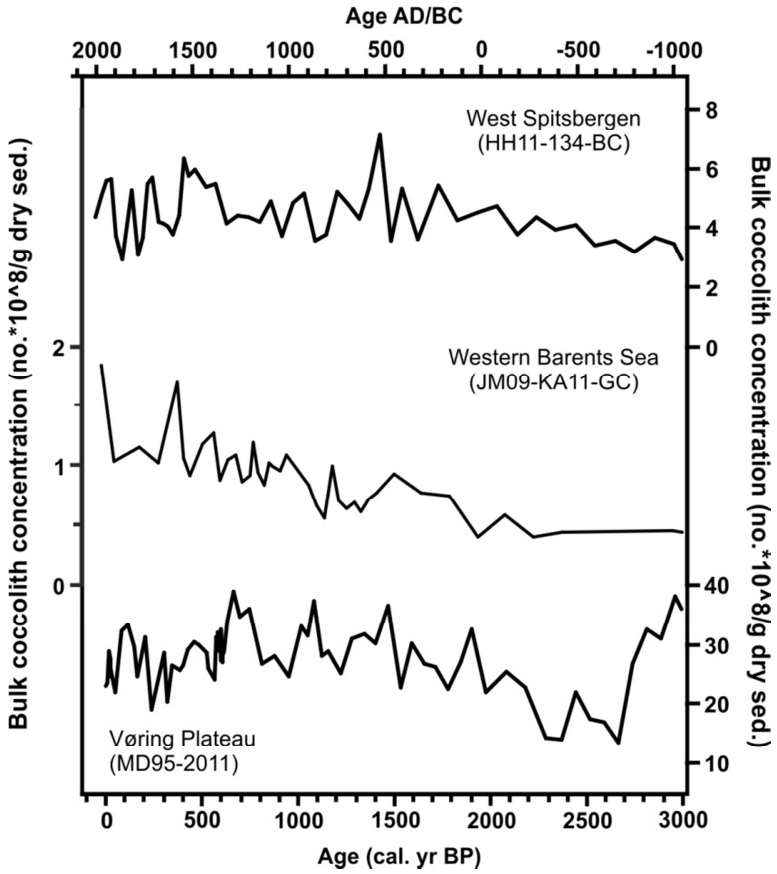

Figure 3: Bulk coccolith concentrations records (coccoliths * 10^8/g dry sed).

While downcore bulk coccolith concentrations are rather stable over the last 3000 years (with the exception of a short low centered at 2500 cal. years BP) at the Vøring Plateau site, the two northernmost locations off western Barents Sea and Svalbard are characterized by increased

values towards the present. Relative changes in the amount and temperature of Atlantic-derived surface waters which sustain most of the calcareous plankton production in the Nordic seas (Schröder-Ritzrau et al., 2001, and references therein) are supposed to explain to a high extent the observed latitudinal and temporal changes in bulk coccolith accumulation (Andruleit and Baumann, 1998). The inferred sedimentation rates in the three studied cores falls within the range of previous investigations carried out in western Barents sea (Sarnthein et al., 2003), off western Spitsbergen (Werner et al., 2011), and at the Vøring Plateau (Sejrup et al., 2011). The late Holocene sedimentation rates show large variations in-between the studied locations which can only be explained by geographical differences in terrigeneous inputs from nearby continental shelfs and/or distribution of sediment-laden sea-ice (Vinje et al, 2001; Divine and Dick, 2006). Spatial and temporal changes in dilution of the biogenic component of Nordic Seas sediments by terrigeneous material are consequently likely to bias the significance of bulk coccolith concentration records in terms of paleoproductivity patterns.

4.2 Species assemblages

Coccolith species diversity is typically low as expected for this arctic/subarctic setting (e.g. Baumann et al., 2000; Matthiessen et al., 2001). The dominance is shared between *C. pelagicus* and *E. huxleyi* in sediments of the two northernmost cores HH11-134-BC and JM09-KA11-GC whereas the latter species always contributes to >50% of the total assemblages over the last 3000 years off Norway (MD95-2011) (Fig. 4). The clear latitudinal shift in dominance from *E. huxleyi* to *C. pelagicus*, which is related to the specific water masses dominating at the core sites (AW/ArW), shows distinct local/regional patterns along the transect with relative abundance changes in the range of 26-56% (*E. huxleyi*) and 33-63% (*C. pelagicus*) West of Spitsbergen, 30-67% and 20-54% in the western Barents Sea, and 46-82% and 8-28% West of Norway. An overall increased *E. huxleyi* contribution interrupted by several millennial-scale low amplitude changes characterizes the west-Spitsbergen core over the studied time-interval, with a short shift in dominance weakly apparent in the interval ~1200-800 cal. years. BP and more clearly in modern times. The western Barents Sea core show an intermediate signal with relatively high *E. huxleyi* abundances toward the beginning and the end of the records and a sustained low between ~1200 and 2300 cal. years BP. West of Norway, although always dominating the coccolith assemblages, *E. huxleyi* displays a steady decreasing abundance from 3000 cal. years BP to the Present.

As expected given its overall shared dominance with *E. huxleyi*, *C. pelagicus* displays opposite patterns of relative abundance in all cores.

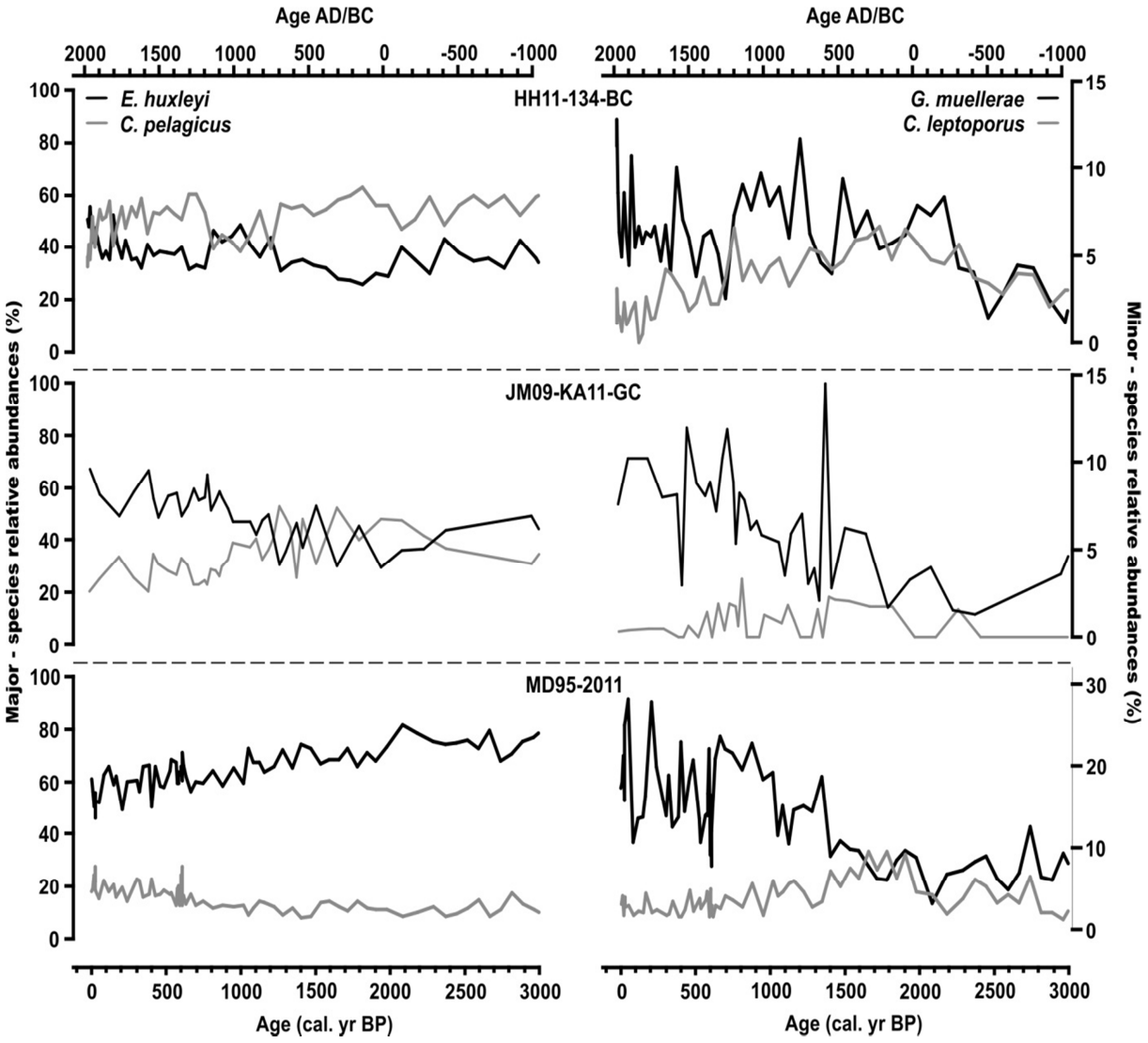

Figure 4: Relative abundances (%) of major (left axes) and minor (right axes) coccolith species throughout the three studied cores.

The resultant E/C ratios show lower values with higher latitudes, ranging from 6.6 to 0.2 (Fig. 5). This ratio displays overall increasing values West of Svalbard and in the western Barents Sea from 3000 years onward, with a contrasting decreasing trend West of Norway. Increased ratios characterize the early part of the three records from ca. 3000 to 2100 cal. years BP, followed by a period of decreased values between 2100 and 1200 cal. years BP. Thereafter, both HH11-134-BC and JM09-KA11-GC share common patterns with higher species ratios until ~700 cal. years BP, followed by a 600 years long interval of lower E/C values, and ending with high ratios over the last century. Contrary to the pattern displayed at the two northermost sites, the species ratios at MD95-2011 shows a marked steady decreasing trend from 1200 cal. years BP to the Present.

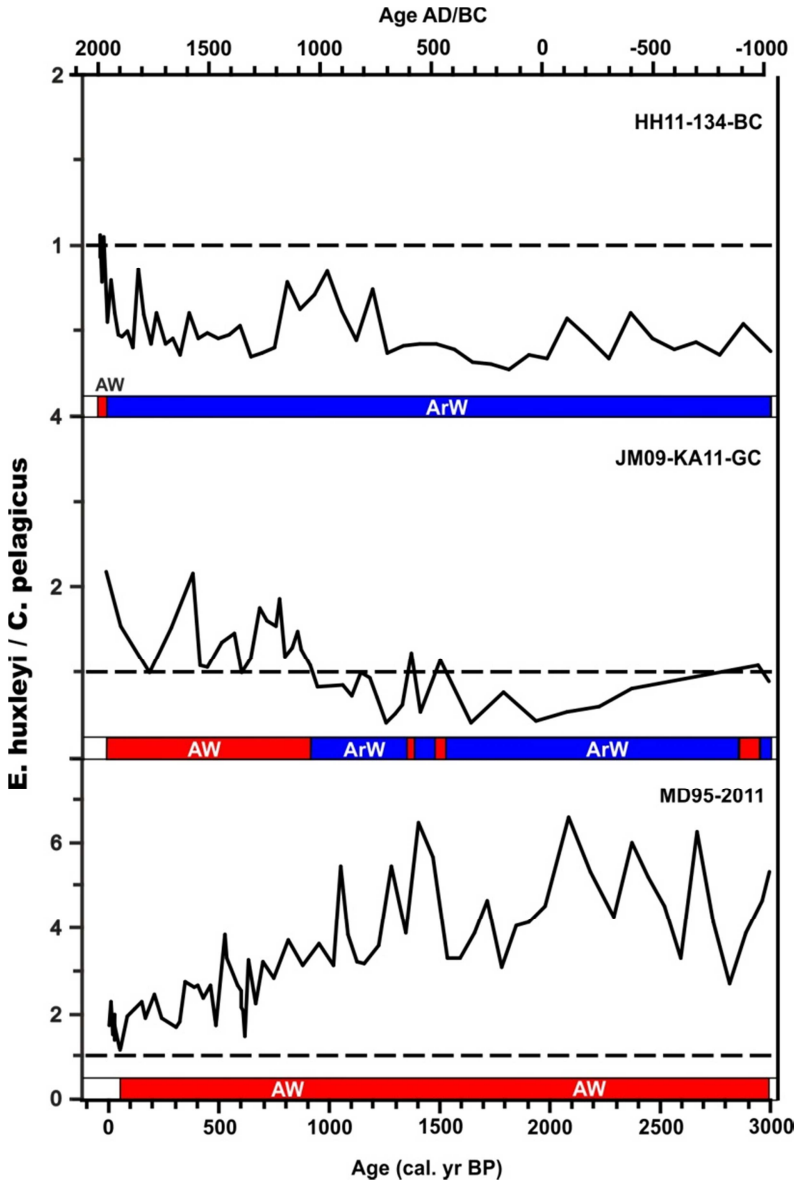

Figure 5: E/C ratios of the dominant coccolithophore species *E. huxleyi* (E) and *C. pelagicus* (C). The bar charts below each E/C plot highlight the dominating surface water masses at the core locations according to the "1" threshold: Blue = ArW (E/C<1); Red = AW (E/C >1).

The subordinate species *G. muellerae* and *C. leptoporus* together account for an average 7.5% of the total assemblage throughout the studied cores (Fig. 4). A fifth species, *Syracosphaera sp*., only contributes on average 1.8%, and will not be discussed further.

Contrary to *E. huxleyi* and *C. pelagicus*, the relative abundance changes of the drifted species *G. muellerae* and *C. leptoporus* are characterized by similar general trends along the whole latitudinal transect (Fig. 4).

All sites display an overall increase of *G. muellerae* abundances during the last 3000 years punctuated by a low steady level in the 3000-2200 cal. years BP interval, a period of highest abundances from ca. 2200 to ~650 cal. years BP, followed by marked lower values until the

beginning of the last century. With the exception of the southernmost core MD95-2011, *G. muellerae* reaches high abundances in the top-most samples (ca. last 100 years) off western Svalbard and western Barents Sea. The trends in absolute concentrations and relative abundances of this drifted species are nearly identical at all studied sites (Fig. 6). Short and/or long term changes in sedimentation of sea-ice or continental-margin-derived lithic material, which most probably affect patterns of microfossil concentration records, including coccoliths, had therefore no obvious influence on *G. muellerae* absolute abundance trends along the studied transect. Hence *G. muellerae* absolute concentration records can be considered as significant proxies for relative changes in the NAC strength.

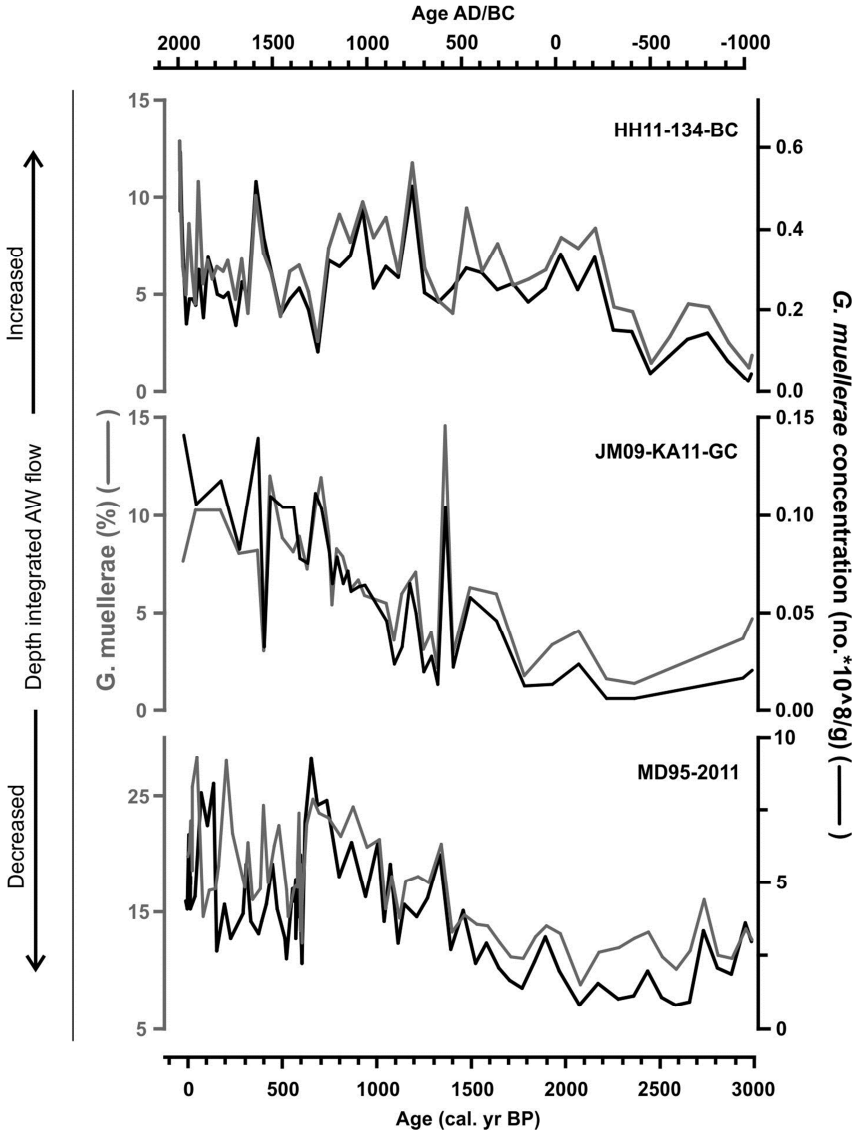

Figure 6: Relative abundances (grey line) and absolute concentrations (black line) of the AW inflow species *G. muellerae*, throughout the three studied cores. The MD95-2011record is a late Holocene zoom of previously published data by Giraudeau et al., (2010).

C. leptoporus shows a peak in relative abundance within all studied cores (though more than twice lower than the maximum values of *G. muellerae*) centered at ~1800-2000 cal. years BP (2-10%) (Fig. 4). This abundance pattern, different from the other drifted species *G. muellerae*, is enigmatic given the common processes (i.e. poleward transport to the Nordic Seas) affecting both species. One explanation might lay in the less restricted ecological niche of *C. leptoporus* which presently colonizes a wider geographic domain in the North Atlantic from warm to cool temperate areas (i.e. Ziveri et al., 2001) than *G. muellerae* (Giraudeau et al., 2010).

4.3 Variability in the Strength of the North Atlantic Current and Fluctuations of the Arctic Front.

Our coccolith records are indicative of important changes in the strength of the NAC and in the dominating surface waters (Arctic vs. Atlantic) within the eastern Nordic Seas over the last 3000 years. Figure 7 summarizes the main paleoceanographic information inferred from our coccolith proxies, together with the abundance record of subpolar planktonic foraminifera in the northernmost studied core. Both the HH11-134-BC foraminiferal abundance record (this study, Fig. 7) and planktonic foraminiferal stable isotopes and species abundances measured in core MD95-2011 (Risebrobakken et al., 2003; Andersson et al., 2003) suggest an increased influence of AW in the Eastern Nordic seas throughout the last 3000 years. The correspondence between our *G. muellerae* abundance datasets and foraminiferal records is particularly obvious in core HH11-134-BC off western Svalbard, where foraminifera are assumed to represent subsurface waters within the main core of Atlantic-derived waters (Carstens et al., 1997), thus confirming the reliability of this coccolith index as a proxy of Atlantic water flow.

The following discussion compares our data with previous marine and terrestrial proxy records of sea-ice distribution, atmospheric circulation (NAO index), and sea-surface and subsurface temperatures in the northern North Atlantic region in order to provide a thorough insight into the paleoceanographical and paleoclimatological development of this climatic sensitive area during the Late Holocene. In the final part we will zoom in on the major climatic changes during the last 700 years covering the interval from the MCA/LIA transition to the Modern Period.

4.3.1 Reconciling the Observed Long-Term Trends in AW Flow and Distribution of Surface Waters with the so-called "Neoglacial Cooling".

The manifestation of the Late Holocene (last ~3000 years) trend toward positive NAO conditions can be inferred from various marine proxy records around Greenland showing colder conditions associated with decreased AW influence in Discobay (western Greenland) related to the so-called "seesaw" pattern (Seidenkrantz et al., 2008; Andresen et al., 2011 and 2012), and an increased flux of sea-ice/icebergs east of Greenland (Jennings et al., 2002). Accordingly, Moros et al. (2004) interpreted the patterns of increased abundance of ice-rafted detritus (IRD) in the western parts of the Nordic Seas (Jennings et al., 2002) and decreased IRD in the Norwegian Sea (their work) to a strengthening of both the NAC and the EGC from the Mid-Holocene to Present. This coupled strengthened circulation affecting the eastern and western parts of the Nordic Seas is consistent with modern observations (Blindheim et al., 2000; Furevik and Nilsen, 2005) and modelling experiments (Nilsen et al., 2003) which relate it to atmospheric processes akin to the present positive phase of the NAO. Finally, a strengthening of the NAC and its WSC extension has earlier been suggested by Sarnthein et al. (2003) based on a general increase in reconstructed subsurface temperatures in the western Barents Sea, which the authors related to a slight increase of the thermohaline circulation (THC). Concurrent glacier expansions on west Spitsbergen (Svendsen and Mangerud, 1997) and increased winter precipitation over mid-western Norway (Nesje et al., 2001) throughout the last 3000 years additionally argue for strengthened southwesterlies and associated increase in NAC and WSC flows, related to the increasingly positive NAO trend, which together constitute the main source of moisture for these high latitude regions.

The surface water expression of the inferred strengthened AW flow toward the northern Nordic Seas is marked by an overall trend of increased influence of surface AW masses in the western Barents Sea and off western Svalbard (Fig. 5). Sustained surface AW conditions occurred earlier at site JM09-KA11-GC from ca. 1000 cal. years BP, than at the northernmost Fram Strait site HH11-134-BC where poleward AW due to the overall dominating sea ice conditions (last 3000 years; Müller et al., 2012) did not affect the surface until the last century. The increased flow of the WSC branch of the NAC throughout the late Holocene has previously been suggested from planktonic foraminiferal-based SST reconstructions off western Barents Sea (Sarnthein et al., 2003) as well as from phytoplankton biomarkers and $CaCO_3$ contents in sediments off western Svalbard (Müller et al., 2012), to which our coccolith proxy (E/C ratio) of surface water masses might further add some constrains and

improve the understanding of changes in the water column distribution of AW in the northern North Atlantic.

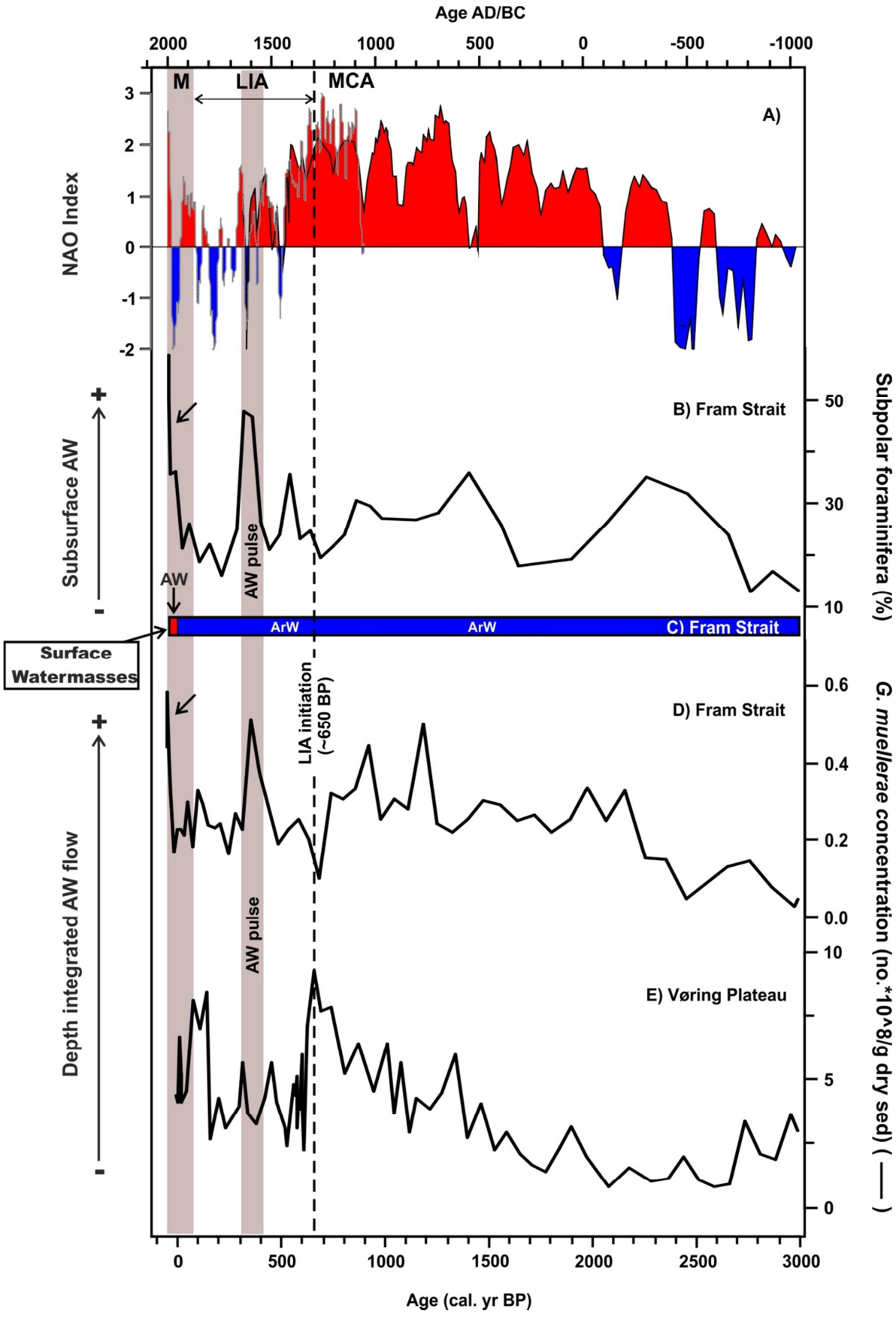

Figure 7: Summary plot of surface and subsurface circulation changes across the eastern Nordic Seas over the past 3000 years. (A) : combined NAO index reconstruction based on Trouet et al. (2009) and Olsen et al. (2012); Red area represents positive NAO and blue area negative NAO conditions. (B) : relative abundance of subpolar foraminifera (fraction > 100 µm) at site HH11-134-BC as an index of subsurface AW masses. (C) : dominating surface water masses at site HH11-134-BC (Fram Strait) inferred from E/C ratios. (D) and (E) : Dynamics of AW flow off western Svalbard (top) and off western Norway (bottom) inferred from absolute concentrations of the AW inflow species *G. muellerae*. The grey shaded areas indicate the marked inflow increases during the Modern period and the intra-LIA event centered at 330-410 cal. years BP. The dashed thick line refers to the initiation of the LIA according to Miller et al. (2012).

The studied site off western Norway shows an opposite surface signature to the northernmost locations (Fig. 5): here, though always overlaid by surface AW mass over the last 3000 years, core MD95-2011 displays a decreasing E/C ratio, most prominent during the last 1200 years (increase in *C. pelagicus*) which translates into an increasing proximity to ArW. Once again, modern observations on the influence of NAO upon the surface hydrology of the eastern Nordic Seas might shed light on this apparent paradox. Instrumental records are indeed indicative of a correlation between changes in the NAO index and surface temperature variations (Blindheim et al., 2000; Miettinen et al., 2011), which is stronger west of Svalbard than off western Norway (Blindheim et al., 2000). Strengthened westerlies (positive NAO index) (Fig. 7), whose track of maximum wind stress in the Eastern Nordic Seas affects the oceanic area off south and mid-Norway, force both an increased flow of AW and a narrowing of the surface expression of the NAC toward the Norwegian slope (Blindheim and Østerhus, 2005, and references therein). An obvious implication at MD95-2011 is an increased proximity of arctic-derived surface water (eastward shift of the AF), throughout the last 3000 years, as suggested by the trend of coccolith E/C ratio (Fig. 5), and confirmed by Norwegian Sea diatom (Andersen et al., 2004; Birks and Koc, 2002) and alkenone-derived SST reconstructions (Calvo et al., 2002).

4.3.2 Zooming in on the Little Ice Age and the Modern Period. Time Interval ~700-0 cal. years BP

The late Holocene trend of increased poleward flow of AW was interrupted by a sudden shift to a period of deteriorating conditions that we assume corresponds to the MCA/LIA transition (Fig. 7). The slight offset in the timing of the observed LIA initiation between the stratigraphically best resolved core MD95-2011 (ie. ca. 660 cal. years BP) and the two northernmost locations can to a large extent be explained by the use in the present study of a standard reservoir correction (R=0) for constraining the stratigraphical framework of all three studied sediment cores, a simplification which does not take into account possible varying contribution of “old” carbon from Arctic/Polar water masses off western Svalbard and

western Barents Sea . The MCA/LIA climatic shift is thought to have been triggered by a combination of a reduction in solar irradiance, explosive volcanism and changes in the internal modes of variability of the ocean-atmosphere system, as one single process cannot usually explain this cold period alone (Wanner et al., 2011). The suggested 660 cal. years BP MCA/LIA age lies within the range of previously proposed ages for the initiation of this climate deterioration in the studied region (Hald et al., 2011; Sejrup et al., 2011), and closely corresponds to recent evidences from Arctic Canada and Iceland (Miller et al., 2012) for a 50 year long explosive volcanism centered at 650 cal. years BP. According to these latter authors, the onset of the LIA was directly linked to such volcanic events which triggered an extensive sea ice expansion causing a self-sustaining sea-ice/ocean feedback until Modern times. As volcanic eruptions seems to modify on short time scales a naturally occurring variability mode similar to the NAO toward its positive phase (Graf et al., 1994), the reconstructed major change to a negative NAO index across the MCA/LIA transition (Fig. 7; Olsen et al., 2012), is most likely related to other forcings i.e. greenhouse gasses, stratospheric ozone and solar irradiance (Gillett et al., 2003). Nevertheless such a concomitant change in NAO pattern from a long-term positive phase to highly fluctuating negative NAO conditions around 640 cal. years BP (Fig. 7A) possibly additionally contributed to an increase in sea-ice extent, as decadal and longterm variations in large scale ice concentrations has shown to be significantly correlated with long-term NAO variations (Visbeck et al., 2003). This major change in turn impacted on the efficiency of the NAC flow to the northern North Atlantic (Fig. 7D), therefore further maintaining, if not strengthening, the sea-ice expansion across the northern Nordic seas (Werner et al., 2011; Müller et al., 2012).

The harsh LIA conditions favored colder surface and subsurface waters in the eastern Fram Strait as also reflected by the E/C ratio and planktonic foraminiferal abundance patterns in core HH11-134BC (Fig. 7B+C). The prevailing Arctic-Polar surface watermasses in eastern Fram Strait stands however as a strong contrast to the dominating surface signature of AW at the western Barents Sea core site (Fig. 5). The specific location of core JM09-KA11-GC within the influence of both AW (WSC) and ArW (Sørkapp Current, Bear Island Current) suggests that although sea ice cover was probably enhanced over the western Barents Sea during this climate deterioration, this local area was affected by a highly fluctuating sea-ice boundary with strong seasonal gradients characterized by an early spring break up of the winter sea ice, and a strong spring/early summer stratification and AW dominance during summer (favoring *E. huxleyi*). The specific surface expression at this site is further confirmed

by the overall similarities between our E/C proxy (JM09-KA11-GC) and reconstructed atmospheric temperatures from a lake record in western Svalbard (D'andrea et al., 2012), an area influenced by similar hydrological features (e.g. sea ice, the Sørkapp Current and the WSC). D'andrea et al., (2012) identified a temperature increase starting at ~1600 AD over western Svalbard as well as mild LIA summer conditions which they explained by a strengthened WSC (NAC), a strengthening only inferred in the present study from our JM09-KA11-GC coccolith record. We therefore suggest the identified warming on Svalbard to be rather due to a decreased flow of polar waters over the shelf via the Sørkapp Current and the Bear Island Current, rather than changes in the strength of the NAC, possibly resulting in a seasonally stronger AW influence on atmospheric temperatures and sea ice extent.

The above described Arctic/Polar LIA conditions in eastern Fram Strait was interrupted by a sudden short pulse of increased WSC flow between ~330 and 410 cal. years BP as depicted in HH11-134-BC by our *G. muellerae* proxy records (Fig. 7B+D) as well as a maximum in subpolar foraminiferal abundance. This strengthened, short-lived AW flow to the northern Nordic Seas was synchronous with a short term increase in the Atlantic Multi-decadal Oscillation (Gray et al., 2004, Winter et al., 2011) and a change towards positive NAO phases. Both processes are likely to explain the minimum sea-ice anomaly in the Nordic Seas during the fifteenth century, compared with the previous and later centuries, as evidenced by Macias Fauria et al. (2009) and Kinnard et al. (2011). The magnitude of this warm pulse, as evidenced by our coccolith proxy record, falls within the range of the AW flow strengthening during the MCA, and is only surpassed by the maximum in AW flow during the Modern period (Fig. 7D).

The reconstructions on Arctic sea-ice by Kinnard et al. (2011) are particularly coherent with the message given by the *G. muellerae* concentrations at core HH11-134-BC with a phasing of the WSC flow pulse and the following deteriorating conditions in both AW flow (our work) and sea-ice extent until the early 20th century (Kinnard et al., 2011), suggesting a generally strong impact of AW flow dynamics on the Arctic sea-ice extent.

The LIA cool climatic period was reversed during the 19th century by an overall increase in atmospheric and sea temperatures, as reconstructed from marine and terrestrial high resolution proxy records from the Arctic region (Overpeck et al., 1997; Kaufman et al., 2009). Recent studies on sea-surface temperature reconstructions over the last 2000 years in Malangen fjord, northwestern Norway (Hald et al., 2011), and West of Spitsbergen (Spielhagen et al., 2011), and evidences herein of high amplitude, rapid temperature increases during the last century,

has intensified the ongoing debate on temperature changes in the Arctic. Spielhagen et al. (2011) used foraminiferal assemblages and geochemical measurements to reconstruct a ~2 °C temperature increase in the subsurface waters of eastern Fram Strait at the transition from the LIA to the Modern period. Our dataset obtained from core HH11-134-BC, not only confirms the high amplitude warming of subsurface waters at the turn of the 19th- century (Fig. 7), it also shows that such a warming was primarily induced by an excess flow of AW along western Svalbard as depicted by our *G. muellerae* proxy record (Fig. 7D). Our coccolith results also indicates that this Modern strengthening of AW flow across Fram Strait was unprecedented over the last 3000 years, and was associated by an exceptional AW shoaling (Fig. 7C), in agreement with reported historical lows in sea ice extent in the Nordic Seas since the second half of the 19th century (Divine and Dick, 2006).

5. CONCLUSIONS

Late Holocene changes in the flow of AW and in the nature of surface waters along the eastern border of the Nordic Seas are reconstructed from coccolith proxy records distributed from the mid-western Norwegian margin to eastern Fram Strait. Our floral records show a general strengthened NAC flow from 3000 cal. years BP to the Present which affected the whole investigated latitudinal range from 66 to 77 °N. This long term modulation in the AW flow appeared linked to atmospheric processes driven by dominant modes of NAO. This mechanism also explains the observed zonal shifts in the location of the AF off western Norway, with increased influence of ArW during strengthened westerlies (positive NAO mode), whereas the western Barents Sea and eastern Fram Strait experienced an overall shoaling of AW which is proportional to its integratedflow to this northernmost settings.

The Little Ice Age, which according to our best-dated records, initiated at ~660 cal. years BP, is seen as an episode of deteriorating conditions, with Arctic/Polar surface waters off western Svalbard and western Barents Sea, possibly associated with severe sea-ice conditions, and a strongly reduced AW flow. This strong cooling was interrupted in eastern Fram Strait by a short resumed high flow of WSC from ca. 330 to 410 cal. years BP, whose magnitude was only surpassed by the one which characterizes the Modern period.

Our dataset not only confirms the high amplitude warming of surface waters at the turn of the 19th century off western Svalbard, it also shows that such a warming was primarily induced by an excess flow of AW which stands as unprecedented over the last 3000 years.

Acknowledgements: This work is a contribution to “The Changing Arctic and Subarctic Environment” (CASE) Initial Training Network funded by the European Community's 7th Framework Programme FP7 2007/2013, Marie-Curie Actions, under Grant Agreement No. 238111. Thanks are due to the captain and crew of the R/V "Helmer Hanssen’’ and S. Iversen for core collection (HH11-134-BC). L. Rossignol and M. Georget (EPOC) assisted with sampling preparation and micropaleontological investigations. We acknowledge supports from the ARTEMIS ^{14}C Accelerator Mass Spectrometry CNRS/MRT/CEA/IRSN/IRD Program. Antoon Kuijpers, Jochen Knies, and an anonymous reviewer are acknowledged for their inspiring comments on an earlier version of this manuscript.

REFERENCES

Andersen, C., Koc, N., Jennings, A., and Andrews, J. T.: Non-uniform response of the major surface currents in the Nordic Seas to insolation forcing: Implications for the Holocene climate variability, Paleoceanography, 19, PA2003, doi: 10.1029/2002PA000873, 2004.

Andersson, C., Risebrobakken, B., Jansen, E., and Dahl, S. O.: Late Holocene surface ocean conditions of the Norwegian Sea (Vøring Plateau), Paleoceanography, 18, PA1044, doi: 10.1029/2001PA000654, 2003.

Andresen, C. S., McCarthy, D. J., Dylmer, C. V., Seidenkrantz, M.-S., Kuijpers, A., and Lloyd, J. M.: Interaction between subsurface ocean waters and calving of the Jakobshavn Isbræ during the late Holocene, The Holocene, 21, 211-224, 2011.

Andresen, C. S., Hansen, M. J., Seidenkrantz, M-S., Jennings, A. E., Knudsen, M. F., Nørgaard-Pedersen, N., Larsen, N. K., Kuijpers, A., and Pearce, C.: Mid- to late-Holocene oceanographic variability on the Southeast Greenland shelf, The Holocene, 23, 167-178, 2012.

Andrews, J. T., and Giraudeau, J.: Multi-proxy records showing significant Holocene variability: the inner N. Iceland shelf (Húnaflói), Quaternary Sci. Rev., 22, 175-193, 2003.

Andruleit, H.: A filtration technique for quantitative studies of coccoliths, Mar. Micropaleontol., 42, 403-406, 1996.

Andruleit, H.: Coccolithophore fluxes in the Norwegian-Greenland Sea: Seasonality and assemblage alterations, Mar. Micropaleontol., 31, 45-64, 1997.

Andruleit, H., and Baumann, K. -H.: History of the last deglaciation and Holocene in the Nordic Seas as revealed by coccolithophore assemblages, Mar. Micropaleontol., 35, 179-201, 1998.

Baumann, K. -H., Andruleit, H., and Samtleben, C.: Coccolithosphores in the Nordic Seas: Comparison of living communities with surface sediment assemblages, Deep-Sea Res. pt. II, 47, 1743-1772, 2000.

Beaufort, L., and Heussner, S.: Seasonal dynamics of calcareous nannoplankton on a West European continental margin: the Bay of Biscay, Mar. Micropaleontol., 43, 27-55, 2001.

Berben, S., Husum, K., Cabedo-Sanz, P., and Belt, S.: Holocene sub-centennial evolution of Atlantic water inflow and sea ice distribution in the western Barents Sea, in preparation, 2013.

Birks, C. J. A., and Koç, N.: A high-resolution diatom record of late-Quaternary sea-surface temperatures and oceanographic conditions from the eastern Norwegian Sea, Boreas, 31, 323-344, 2002.

Bjune, A. E., Seppä, H., and Birks, H. J. B.: Quantitative summer-temperature reconstructions for the last 2000 years based on pollen-stratigraphical data from northern Fennoscandia, J. Paleolimnol., 41, 43-56, 2009.

Blindheim, J., Borovkov, V., Hansen, B., Malmberg, S. Aa., Turrell, W. R., and Østerhus, S.: Upper layer cooling and freshening in the Norwegian Sea in relation to atmospheric forcing, Deep-Sea Res. I, 47, 655-680, 2000.

Blindheim, J., and Østerhus, S.: The Nordic seas, main oceanographic features, in: The Nordic Seas: an integrated perspective Oceanography, Climatology, Biochemistry, and Modelling, Drange, H., Dokken, T., Furevik, T., Gerdes, R., Berger, W., Geophys. Monogr. Ser., 158, 11-37, 2005.

Bonnet, S., de Vernal, A., Hillaire-Marcel, C., Radi, T., and Husum, K.: Variability of sea-surface temperature and sea-ice cover in the Fram Strait over the last two millennia, Mar. Micropaleontol., 74, 59-74, 2010.

Buch, E.: A monograph on the physical oceanography of the Greenland waters, Danish Meteorological Institute Scientific Report 00-12, Greenland Fisheries Research Insitute publication 15 series, 0-244, 1990.

Cachão, M., and Moita, M. T.: Coccolithus pelagicus, a productivity proxy related to moderate fronts off Western Iberia, Mar. Micropaleontol., 39, 131-155, 2000.

Calvo, E., Grimalt, J., and Jansen, E.: High resolution U^{k}_{37} sea surface temperature reconstruction in the Norwegian Sea during the Holocene, Quaternary Sci. Rev., 21, 1385-1394, 2002.

Carstens, J., Hebbeln, D., and Wefer, G.: Distribution of planktic foraminifera at the ice margin in the Arctic (Fram Strait), Mar. Micropaleontol., 29, 257-269, 1997.

Cronin, T. M., Thunell, R., Dwyer, G. S., Saenger, C., Mann, M. E., Vann, C., and Seal, R. R.: Multiproxy evidence of Holocene climate variability from estuarine sediments, eastern North America, Paleoceanography, 20, PA4006, doi: 10.1029/2005PA001145, 2005.

D'Andrea, W. J., Vaillencourt, D. A., Balascio, N. L., Werner, A., Roof, S. R., Reteller, M., and Bradley, R. S.: Mild Little Ice Age and unprecedented recent warmth in an 800 year lake sediment record from Svalbard, Geology, 40, P1007, doi:10.1130/G33365.1, 2012.

Davis, B. A. S., Brewer, S., Stevenson, A. C., Guiot, J., and Data Contibutors: The temperature of Europe during the Holocene reconstructed from pollen data, Quaternary Sci. Rev., 22, 1701-1716, 2003.

Divine, D. V., and Dick, C.: Historical variability of sea ice edge position in the Nordic Seas, J. Geophys. Res., 111, CO1001, doi:10.1029/2004JC002851, 2006.

Duplessy, J. -C., Ivanova, E., Murdmaa, I., Paterne, M., and Labeyrie, L.: Holocene paleoceanography of the northern Barents Sea and variations of the northward heat transport by the Atlantic Ocean, Boreas, 30, 2-16, 2001.

Dylmer, C. V., Giraudeau, J., Hanquiez, V., and Husum, K.: The coccolithophores Emiliania Huxleyi and Coccolithus pelagicus: extant populations from the Norwegian-Greenland Sea and Fram Strait, in preparation, 2013.

Furevik, T., and Nilsen, J. E. Ø.: Large-Scale Atmospheric Circulation Variability and its Impacts on the Nordic Seas Ocean Climate- A Review, Geophys. Monogr. Ser., 158, 105-136, 2005.

Gillett, N. P., Graf, H. F., and Osborn, T. J.: Climate Change and the North Atlantic Oscillation, AGU Geophys. Monogr., 134, in: The North Atlantic Oscillation: Climatic Significance and Environmental Impact, Hurrell, J.W., Kushnir, Y., Ottersen, G., Visbeck, M. (Eds.), American Geophysical Union,Washington, DC, 1-36, 2003.

Giraudeau, J., Grelaud, M., Solignac, S., Andrews , J. T., Moros, M., and Jansen, E.: Millenial-scale variability in Atlantic water advection to the Nordic Seas derived from Holocene coccolith concentration records, Quaternary Sci. Rev., 29, 1276-1287, 2010.

Graf, H. F., Perlwitz, J., and Kirchner, I.: Northern Hemisphere tropospheric mid-latitude circulation after violent volcanic eruptions, report no. 107, Max-Planck-Institut f̈ur Meteorologie, Hamburg, 1–18, 1993.

Gray, S. T., Graumlich, L. J., Betancourt, J. L., and Pederson, G. T.: A tree-ring based reconstruction of the Atlantic Multidecadal Oscillation since 1567 A.D., Geophys. Res. Lett., 31, L12205, doi:10.1029/2004GL019932, 2004.

Groot, D. E., Sørensen, S. Aa., and Husum, K.: Holocene Atlantic Water inflow to the western Barents Sea margin, in preparation, 2013.

Hald, M., Andersson, C., Ebbesen, H., Jansen, E., Klitgaard-Kristensen, D., Risebrobakken, B., Salomonsen, G. R., Sarnthein, M., Sejrup, H. P., and Telford, R. J.: Variations in temperature and extent of Atlantic Water in the northern North Atlantic during the Holocene, Quaternary Sci. Rev., 26, 3423-3440, 2007.

Hald, M., Salomonsen, G. R., Husum, K., and Wilson, L. J.: A 2000 year record of Atlantic Water temperature variability from the Malangen Fjord, northeastern North Atlantic, Holocene, 21, 1049-1059, 2011.

Hansen, B., and Østerhus, S.: North-Atlantic-Nordic Seas exchanges, Prog. Oceanogr., 45, 109-208, 2000.

Hebbeln, D., Henrich, R., and Baumann, K. -H.: Paleoceanography of the Last Interglacial/ Glacial Cycle in the Polar North Atlantic, Quaternary Sci. Rev., 17, 125-153, 1998.

Herrle, J. O., and Bollmann, J.: Accuracy and reproducibility of absolute nannoplankton abundances using filtration techniques in combination with a rotary splitter, Mar. Micropaleontol., 53, 389-404, 2004.

Hopkins, T. S.: The GIN sea—a synthesis of its physical oceanography and literature review 1972–1985, Earth-Science Reviews, 30, 175–318, 1991.

Hurrell, J. W.: Decadal trends in the North Atlantic Oscillation: Regional temperatures and precipitation, Science, 269, 676-679, 1995.

Hurrell, J. W., Kushnir, Y., Ottersen, G., and Visbeck, M.: An overview of the North

Atlantic Oscillation, AGU Geophys. Monogr., 134, in: The North Atlantic Oscillation: Climatic Significance and Environmental Impact, Hurrell, J.W., Kushnir, Y., Ottersen, G., Visbeck, M. (Eds.), American Geophysical Union,Washington, DC, 1-36, 2003.

Husum, K., and Hald, M.: Arctic planktic foraminiferal assemblages: Implications for subsurface temperature reconstructions, Mar. Micropaleontol., 96-97, 38-47, 2012.

Jennings, A. E., Knudsen, K. L., Hald, M., Hansen, C. V., and Andrews, J. T.: A mid-Holocene shift in Arctic sea-ice variability on the East Greenland Shelf, Holocene, 12, 49-58, 2002.

Kaufman, D. S., Schneider, D. P., Mckay, N. P., Ammann, C. M., Bradley, R. S., Briffa, K. R., Miller, G. H., Otto-Bliesner, B. L., Overpeck, J. T., and Vinther, B. M., Arctic Lakes 2k Projekt members: Recent warming reverses long-term Arctic cooling, Science, 325, 1236-1239, 2009.

Kinnard, C., Zdanowicz, C. M., Fisher, D. A., Isaksson, E., de Vernal, A., and Thompson, L. G.: Reconstructed changes in Arctic sea ice over the past 1.450 years, Nature, 479, 509-512, 2011.

Kwok, R., Cunningham, G. F., and Pang, S. S.: Fram Strait sea-ice outflow, J. Geophys. Res., 109, C01009, doi:10.1029/2003JC001785, 2004.

Lund, D. C., Lynch-Stieglitz, J., and Curry, W. B.: Gulf Stream density structure and transport during the past millenium, Nat. Lett., 444, 601-604, 2006.

Macias-Fauria, M., Grinsted, A., Helama, S., Moore, J., Timonen, M., Martma, T., Isaksson, E., and Eronen, M.: Unprecedented low twentieth century winter sea-ice extent in the Western Nordic Seas since A.D. 1200, Clim. Dynam., 34, 781-795, 2009.

Marshall, J., Kushnir, Y., Battisti, D., Chang, P., Czaja, A., Dickson, R., Hurrell, J., McCartney, M., Saravanan, R., and Visbeck, M.: North Atlantic Climate Variability: Phenomena impacts and mechanisms, Int. J. Climatol., 21, 1863-1898, 2001.

Matthiessen, J., Baumann, K. H., Schröder-Ritzrau, A., Hass, C., Andruleit, H., Baumann, A., Jensen, S., Kohly, A., Pflaumann, U., Samtleben, C., Schäfer, P., and Thiede, J.: Distribution of calcareous, siliceous and organic-walled planktic microfossils in surface sediments of the Nordic Seas and their relation to surface-water masses, In: The northern North Atlantic: a changing environment, Schäfer, P., Ritzrau, W., Schlüter, M., and Thiede, J. (Eds.), Springer-Verlag, Berlin, 105-127. 2001

Miettinen, A., Koç, N., Hall, I. R., Godtliebsen, F., and Divine, D.: North Atlantic sea surface temperatures and their relation to the North Atlantic Oscillation during the last 230 years, Clim. Dyn., 36, 533-543, 2011.

Miller, G. H., Geirsdòttir, A., Zhong, Y., Larsen, D. J., Otto-Bliesner, B. L., Holland, M. M., Bailey, D. A., Refsnider, K. A., Lehman, S. J., Southon, J. R., Anderson, C., Björnsson, H., and Thordarson, T.: Abrupt onset of the Little Ice Age triggered by volcanism and sustained by sea-ice/ocean feedbacks, Geophys. Res. Lett., 39, L02708, doi:10.1029/2011GL050168, 2012.

Moros, M., Emeis, K., Risebrobakken, B., Snowball, I., Kuijpers, A., McManus, J., and Jansen, E.: Sea surface temperatures and ice rafting in the Holocene North Atlantic: Climate influences on northern Europe and Greenland, Quaternary Sci. Rev., 23, 2113-2126, 2004.

Müller, J., Werner, K., Stein, R., Fahl, K., Moros, M., and Jansen, E.: Holocene cooling culminates in sea-ice oscillations in Fram Strait, Quaternary Sci. Rev., 47, 1-14, 2012.

Nesje, A., Kvamme, M., Rye, N., and Løvlie, R.: Holocene glacial and climate history of the Jostedalsbreen region, western Norway; evidence from lake sediments and terrestrial deposites, Quaternary Sci. Rev., 10, 87-114, 1991.

Nesje, A., Matthews, J. A., Dahl, S. O., Berrisford, M. S., and Andersson, C.: Holocene glacier fluctuations of Flatebreen and winter-precipitation changes in the Jostedalsbreen region, western Norway, based on glaciolacustrine sediment records, Holocene, 11, 267-280, 2001.

Nilsen, J. E. Ø., Gao, Y., Drange, H., Furevik, T., and Bentsen, M.: Simulated North Atlantic-Nordic Seas water mass exchanges in an isopycnic coordinate OGCM, Geophys. Res. Lett., 30, 1536, *doi:*10.1029/2002GL016597, 2003.

Olsen, J., Anderson, N. J., and Knudsen, M. F.: Variability of the North Atlantic Oscillation over the last 5,200 years, Nat. Geosci., 5, 808-812, 2012.

Overpeck, J., Hughen, K., Hardy, D., Bradley, R., Case, R., Douglas, M., Finney, B., Gajewski, K., Jacoby, G., Jennings, A., Lamoureux, S., Lasca, A., MacDonald, G., Moore, J., Retelle, M., Smith, S., Wolfe, A., and Zielinski, G.: Arctic environmental change of the last four centuries, Science, 278, 1251-1256, 1997.

Porter, S. C., and Denton, G. H.: Chronology of neoglaciation in the North American Cordillera, Am. J. Sci., 265, 177–210, 1967.

Reimer, P. J.: IntCal09 and Marine09 radiocarbon age calibration curves, 0–50,000 years cal BP, Radiocarbon, 51, 1111–1150, 2009.

Risebrobakken, B.,Jansen, E., Andersson, C., Mjelde, E., and Hevrøy, K.: A high-resolution study of Holocene paleoclimatic and paleoceanographic changes in the Nordic Seas, Paleoceanography, 18, PA1017, doi:10.1029/2002PA000764, 2003.

Risebrobakken, B., Moros, M., Ivanova, E. V., Chistyakova, N., and Rosenberg, R.: Climate and oceanographic variability in the SW Barents Sea during the Holocene, Holocene, 20, 609-621, 2010.

Rüther, D. C., Bjarnadòttir, L., R., Junttila, J., Husum, K., Rasmussen, T. L., Lucchi, R. G., and Andreassen, K.: Pattern and timing of the northwestern Barents Sea Ice Sheet deglaciation and indications of episodic Holocene deposition, Boreas, 41, 494-512, 2012

Saloranta, T. M., and Svendsen, H.: Across the Arctic front west of Spitsbergen: high-resolution CTD sections from 1998-2000, Polar Res., 20, 177-184, 2001.

Samtleben, C., Schäfer, P., Andruleit, H., Baumann, A., Baumann, K. H., Kohly, A., Matthiessen, J., and Schröder-Ritzrau, A.: Plankton in the Norwegian-Greenland Sea: from living communities to sediment assemblages – an actualistic approach, Geologische Rundschau, 84, 108-136, 1995.

Samtleben, C., and Schröder, A.: Living cocolithophore communities in the Norwegian-Greenland Sea and their record in sediments, Mar. Micropaleontol., 19, 333-354, 1992.

Sarnthein, M., Van Kreveld, S., Erlenkeuser, H., Grootes, P. M., Kucera, M., Pflaumann, U., and Schulz, M.: Centennial-to-millennial-scale periodicities of Holocene climate and sediment injections off the western Barents shelf, Boreas, 32, 447–461, 2003.

Schröder-Ritzrau, A., Andruleit, H., Jensen, S., Samtleben, C., Schäfer, P., Matthiessen, J., Hass, C., Kohly, A., and Thiede, J.: Distribution, export and alteration of fossilizable plankton in the Nordic Seas, in: The Northern North Atlantic: A Changing Environment, Schäfer, P., Ritzrau, W., Schlüter, M., and Thiede, J., Springer, Berlin, 81–104, 2001.

Seidenkrantz, M. -S., Roncaglia, L., Fischel, A., Heilmann-Clausen, C., Kuijpers, A., and Moros, M.: Variable North Atlantic climate seesaw patterns documented by a late Holocene marine record from Disko Bugt, West Greenland, Mar. Micropaleontol., 68, 66-83, 2008.

Sejrup, H. P., Haflidason, H., and Andrews, J. T.: A Holocene North Atlantic SST record and regional climate variability, Quaternary Sci. Rev., 30, 3181-3195, 2011.

Skagseth, Ø., Furevik, T.**,** Ingvaldsen, R., Loeng, H., Mork, K. A., Orvik, K. A., and Ozhigin, V.: Volume and heat transports to the Arctic Ocean via the Norwegian and Barents Seas, in: Arctic-Subarctic Ocean Fluxes: Defining the role of the Northern Seas in Climate, Dickson, R., Meincke, J., and Rhines, P. (Eds.),. Springer Netherlands, 25-64, 2008.

Sorteberg, A., and Kvingedal B.: Atmospheric forcing on the Barents Sea Winter Ice Extent, J. Climate, 19, 4772-4784, 2006.

Spielhagen, R. F., Werner, K., Aagaard-Sørensen, S., Zamelczyk, K., Kandiano, E., Budeus, G., Husum, K., Marchitto, T. M., and Hald, M.: Enhanced modern heat transfer to the Arctic by Warm Atlantic Water, Science, 331, 450-453, 2011.

Stuiver, M., and Reimer, P. J.: Extended ^{14}C data base and revised CALIB 3.0 ^{14}C age calibration program, Radiocarbon, 35, 215-230, 1993.

Svendsen, J. I., and Mangerud, J.: Holocene glacial and climatic variations on Spitsbergen, Svalbard, Holocene, 7, 45–57, 1997.

Trouet, V., Esper, J., Graham, N. E., Baker, A., Scourse, J. D., and Frank, D. C.: Persistent positive North Atlantic Oscillation mode dominated the Medieval Climate Anomaly, Science, 324, 78-80, 2009.

Vinje, T.: Anomalies and trends of sea-ice extent and atmospheric circulation in the Nordic Seas during the period 1864-1998, J. Climate, 14, 255-267, 2001.

Visbeck, M., Chassignet, E. P., Curry, R. G., Delworth, T. L., Dickson, R. R., and Krahmann, G.: The Ocean's response to North Atlantic Oscillation variability, AGU Geophys. Monogr., 134, in: The North Atlantic Oscillation: Climatic Significance and Environmental Impact, Hurrell, J.W., Kushnir, Y., Ottersen, G., Visbeck, M. (Eds.), American Geophysical Union,Washington, DC, 113-146, 2003.

Wanamaker Jr., A. D., Butler, P. G., Scourse, J. D., Heinemeier, J., Eiŕıksson, J., Knudsen, K. L., and Richardson, C. A.: Surface changes in the North Atlantic meridional overturning circulation during the last millenium, Nat. Commun., 3, 899, doi:10.1038/ncomms1901, 2012.

Wanner, H., Solomina, O., Grosjean, M., Ritz, S. P., and Jetel, M.: Structure and origine of Holocene cold events, Quaternary Sci. Rev., 30, 3109-3123, 2011.

Wassmann, P., Reigstad, M., Haug, T., Rudels, B., Carroll, M. L., Hop, H., Gabrielsen, G. W., Falk-Petersen, S., Denisenko, S. G., Arashkevich, E., Slagstad, D., and Pavlova, O.: Food webs and carbon flux in the Barents Sea, Prog. Oceanogr., 71, 232-287, 2006.

Werner, K., Spielhagen, R. F., Bauch, D., Hass, H. C., Kandiano, E., and Zamelczyk, K.: Atlantic Water advection to the eastern Fram Strait – Multiproxy evidence for late Holocene varibility, Palaeogeogr. Palaeocl. Palaeoecol., 308, 264-276, 2011.

Wilson, L. J., Hald, M., and Godtliebsen, F.: Foraminiferal faunal evidence of twentieth-century Barents Sea warming, Holocene, 21, 527-537, 2011.

Winter, A., Miller, T., Kushnir, Y., Sinha, A., Timmermann, A., Jury, M. R., Gallup, C., Cheng, H., and Edwards, R. L.: Evidence for 800 years of North Atlantic multi-decadal variability from a Puerto Rican speleothem, Earth Planet. Sc. Lett., 308, 23-28, 2011.

Ziveri, P., Kleijne, A., Conte, M., and Weber, J.: Coccolithophorid distribution and alkenone biomarker characterisation from the tropical Equatorial Atlantic, European Geophysical Society (EGS), Nice, XXVI General Assembly, 2001.

4.7.1 Coccolith vs. Dinocyst Ratios as AW/ArW Indicators

Previous studies of surface sediment assemblages within the Nordic Seas have shown that the regional dominance of the coccolithophore species *E. huxleyi* (E) and *C. pelagicus* (C), on one hand, and of the dinocyst species *O. centrocarpum* (OCEN) and *N. labyrinthus* (NLAB), on the other hand, are clearly reflected in surface sediments of the Nordic Seas (Samtleben et al., 1995; Baumann et al., 2000; Matthiessen et al., 2001; Zonneveld et al., 2013) (Fig. 4.26, Chapter 2). Species distribution patterns indicate that *E. huxleyi* and *O. centrocarpum* dominate their fossil group assemblages within areas bathed by Atlantic-derived water masses, wheras *C. pelagicus* and *N. labyrinthus* show highest contributions below Arctic waters (Fig. 4.26). These species distribution patterns in modern sediments led to the definition of two relative abundance ratios (OCEN/NLAB and E/C) (Baumann et al., 2000; Matthiessen et al., 2001), as proxies for the location of the AF which separates the seasonally ice-covered Polar and Arctic waters (E/C<1; OCEN/NLAB<4) from warmer and saltier Atlantic-derived waters (E/C>1; OCEN/NLAB>4).

Allthough Baumann et al. (2000) originally defined the E/C ratio, from surface sediments located in the central areas of the Nordic Seas, we believe that this proxy ratio is valid for the wider Nordic Seas including its eastern part. Baumann et al., (2000)'s dataset only included a few sites far west of the Norwegian continental margin with coccolith assemblages dominated by *C. pelagicus* (E/C <1) (Fig. 4.26). This excess *C. pelagicus* abundance is contradictory to our own observations in recent surface sediment assemblages from the northern cores HH11-134-BC and JM09-KA11-GC, as well as to the composition of extant populations northwest of Bear Island (Baumann et al., 2000) and across Fram Strait (Dylmer et al., 2013, this study; Chapter 2), which both indicate a dominance of *E. huxleyi* below and within AW-dominated surface layers. Based on these evidences we use the definition of the AF (a frontal salinity and temperature gradient separating surface AW masses from mixed ArW) to infer that the E/C ratio (ie. deviations from the threshold of 1) characterizes surface sediments deposited below Atlantic or Arctic surface water masses, when considering pluriannual conditions.

Figure 4.26 : Modern (surface sed.) distribution of key coccolith and dinocyst species in the Nordic Seas e.g. *Emiliania huxleyi* (E), *Coccolithus pelagicus* (C), *Nematosphaeropsis labyrinthus* (NLAB) and *Operculodinium centrocarpum* (OCEN), as well as the ratios E/C and OCEN/NLAB. Modified after Baumann et al. (2000) and Matthiessen et al. (1995, 2001).

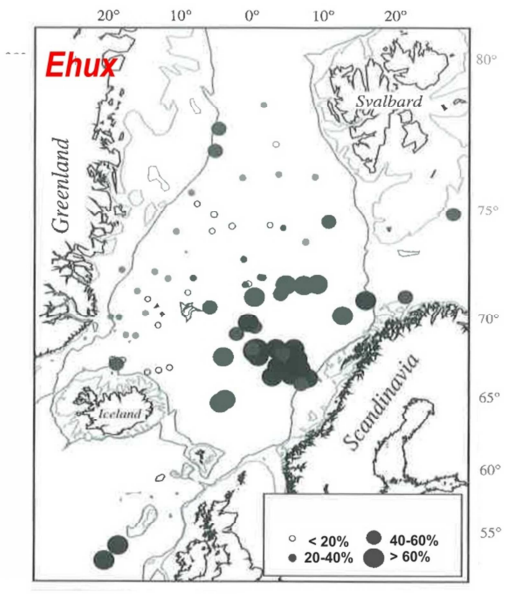
Ehux
Greenland
Svalbard
Iceland
Scandinavia
< 20%
20-40%
40-60%
> 60%

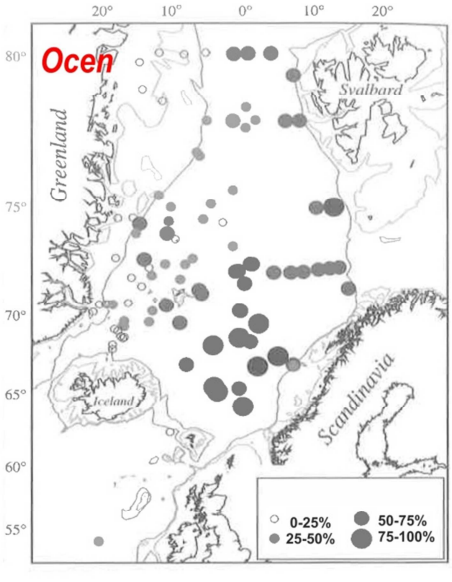
Ocen
Greenland
Svalbard
Iceland
Scandinavia
0-25%
25-50%
50-75%
75-100%

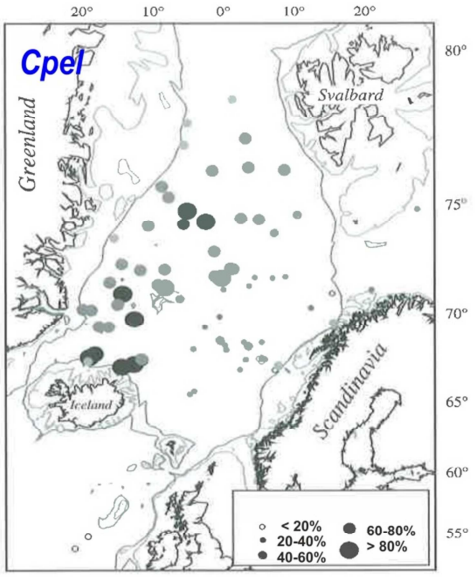
Cpel
Greenland
Svalbard
Iceland
Scandinavia
< 20%
20-40%
40-60%
60-80%
> 80%

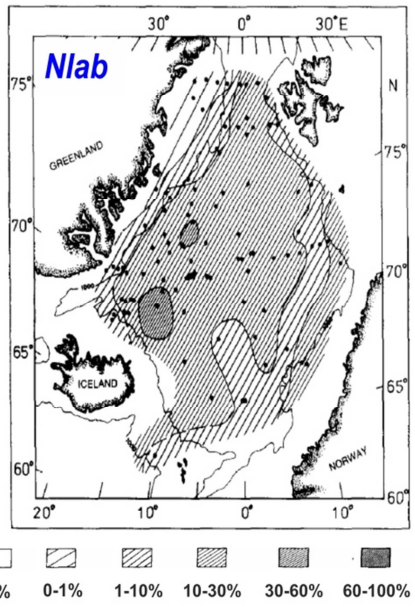
Nlab
GREENLAND
ICELAND
NORWAY
0%
0-1%
1-10%
10-30%
30-60%
60-100%

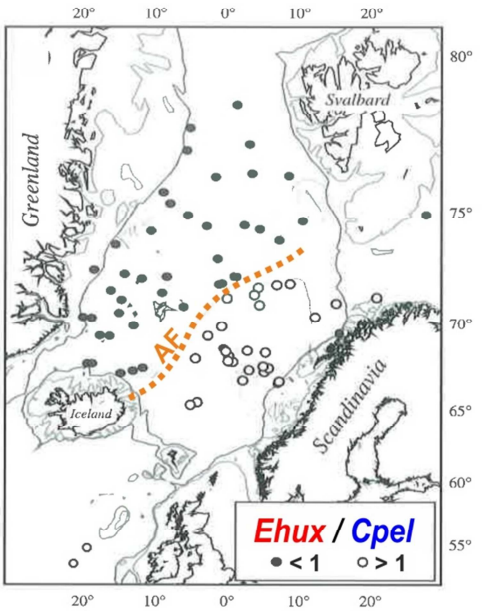
Greenland
Svalbard
Iceland
Scandinavia
AF
Ehux / Cpel
< 1
> 1

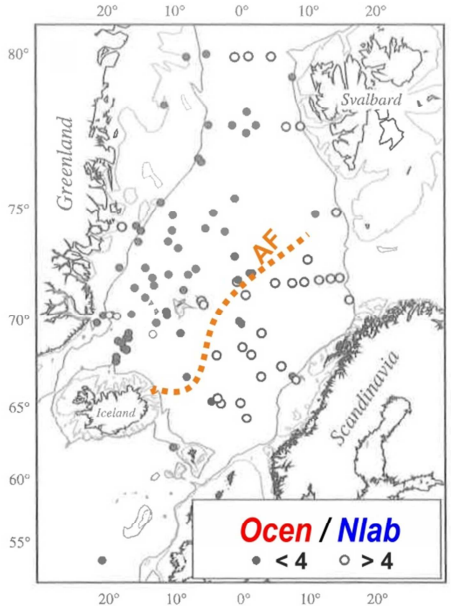
Greenland
Svalbard
Iceland
Scandinavia
AF
Ocen / Nlab
< 4
> 4

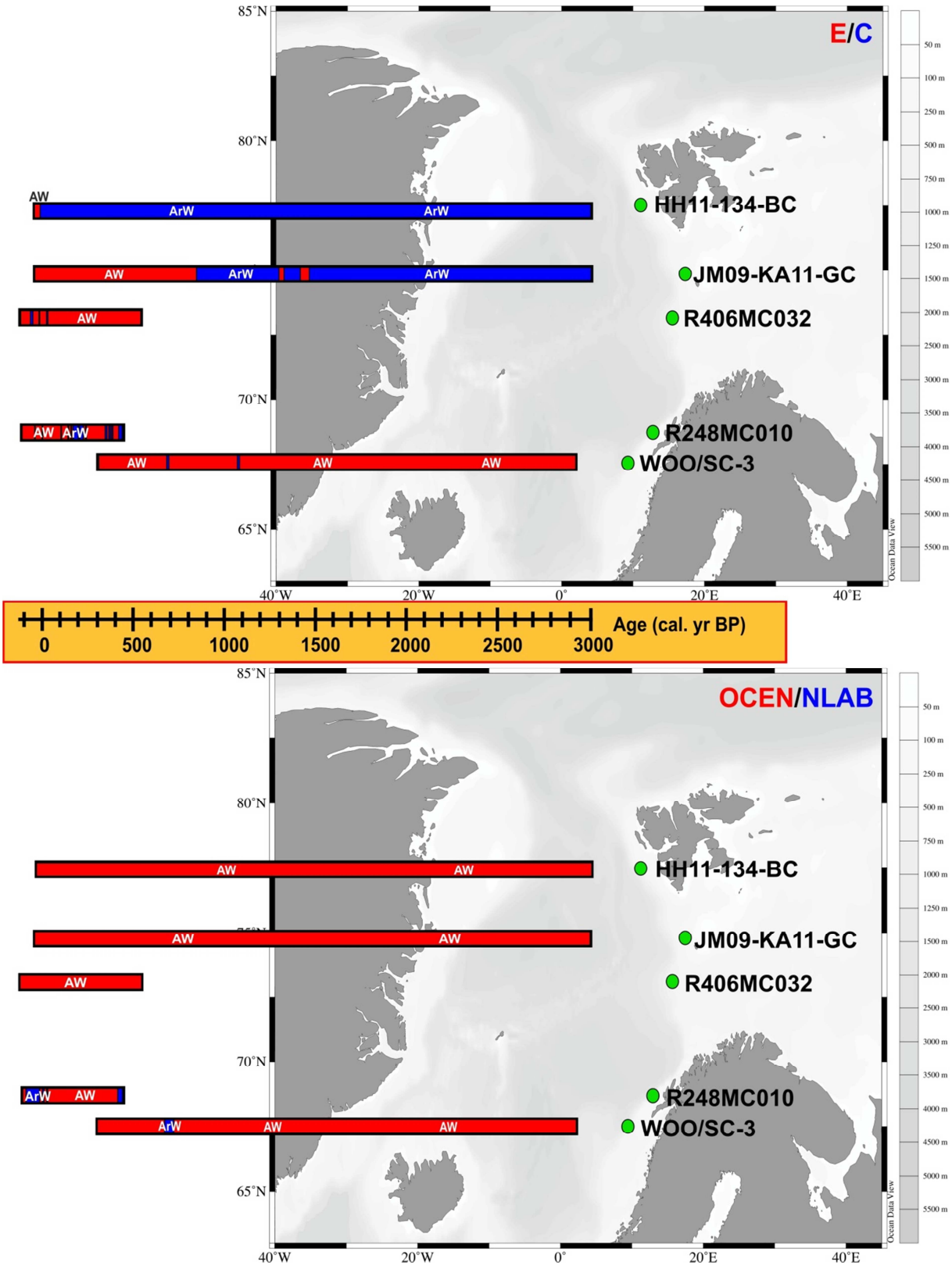

Figure 4.27 : Temporal changes in the nature of surface water masses at the five studied core locations according to the key coccolith and dinocyst ratios (and their threshold values). The dinocyst and coccolith ratios are suggested to reflect the approximate location of the Arctic Front (AF) using various threshold ratios (red bars representing AW, E/C>1 and OCEN/NLAB>4; blue bars representing ArW, E/C<1 and OCEN/NLAB<4).

The original OCEN and NLAB relative abundance datasets used by Matthiessen et al. (2001) to define the OCEN/NLAB ratio was evenly distributed over the Nordic Seas (particularly over its northern part). As suggested in Fig. 4.26, this dinocyst ratio appears as valid for the entire Nordic Seas area.

The resulting temporal changes in the late Holocene surface watermasses along our latitudinal transect of studied cores show strongly contradicting results between the two applied ratios (Fig. 4.27). While the E/C ratio is indicative of an overall time-transgressive increasing influence of AW towards Fram Strait, the downcore distribution of the OCEN/NLAB ratio suggests that AW generally occupied the photic layer over the whole studied latitudinal range throughout the last 3000 years. The latter is peculiar as earlier historical datasets on sea ice extent showed that Fram Strait and the central western Barents Sea are or have been influenced by sea ice (and therefore ArW) during the latter phase of the LIA (~100-51 cal. years BP) (Divine and Dick, 2006) (Fig. 4.28).

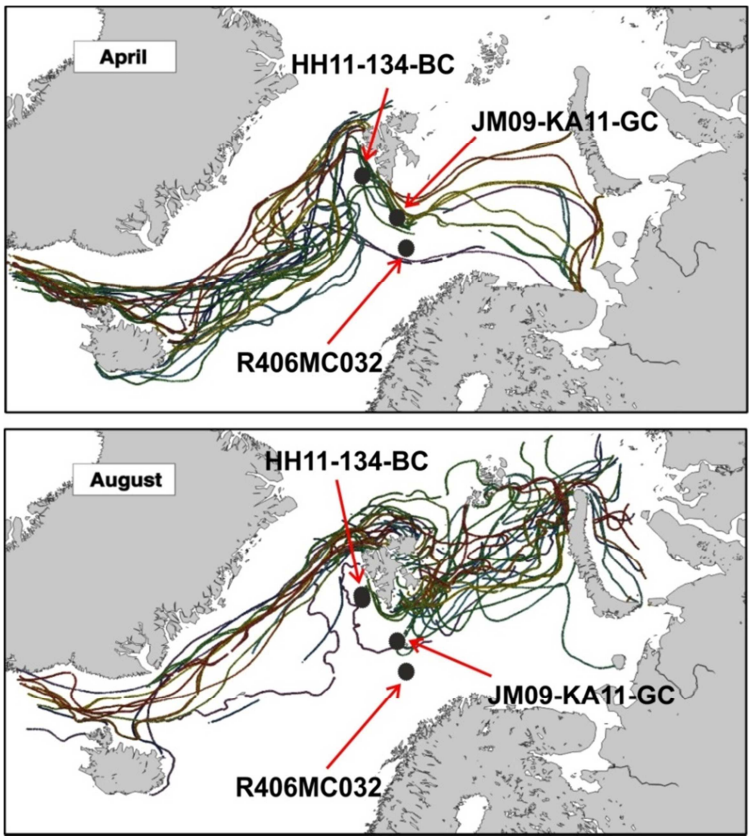

Figure 4.28 : April and August ice edge positions for the period 1850-1899 AD (100-51 cal. years BP), modified from Divine and Dick (2006).

The recent (late LIA) presence of sea-ice is fairly well depicted by the distribution of the E/C ratio in both HH11-134-BC and R406MC032, whereas the record at JM09-KA11-GC

(Kveithola) are indicative of surface AW throughout the last ca. 800 years. The latter, relatively low sedimentation rate, core might however be partly influenced by sediment mixing toward the top of the sediment column as a result of gravity coring. In contrast to the E/C ratio, this LIA interval of extensive sea ice is not reflected by the OCEN/NLAB ratio in the northernmost studied cores. Hence the E/C ratio appears as more reliable than the OCEN/NLAB ratio as a surface water mass proxy along our transect, although several factors might be influencing their interpretation.

One of the key factors affecting the interpretation of these ratios are the threshold values set by Baumann et al. (2000) and Matthiessen et al. (2001) to distinguish between the dominating watermasses. While a threshold of 1 for the E/C ratio looks reasonable in terms of modern and late Holocene approximate location of the AF, the value of 4 for OCEN/NLAB seems too high in the Nordic Seas for describing the rapid, low amplitude changes in surface water masses within the last 3000 years. The latter threshold value howewer might properly describe surface water changes on glacial/interglacial timescale where stronger contrasts are at work in the high latitudes of the North Atlantic.

A second factor which needs to be considered is the spatial distribution of the surface sediment samples used for defining the signatures of the species ratios (Baumann et al., 2000; Matthiessen et al., 2001). Those samples are mainly located in deep ocean settings of the Norwegian-Iceland-Greenland Seas, where hydrological conditions (upper water column mixing, continental impact) are different from those prevailing on slopes and/or continental shelves where our studied cores are located. Hence the OCEN/NLAB threshold might still be valid in the more central part of the Nordic Seas.

Finally a third factor lays in the generally poor knowledge on the ecology of the various species considered in the proxy ratios and the environmental parameters influencing their distribution (Chapter 2).

Taken separately or together these three factors explains most of the contradicting ratio trends measured at each of the studied core location (Fig. 4.27). Accordingly, the significance of the E/C ratio in terms of location of the AF is not conclusive in areas affected by the NCC; here, the strength and zonal extension of this later type of coastal water mass is assumed to drive to a high extent the coccolith ratio. In a similar way, the OCEN/NLAB ratio showed a stronger relation to the AF in cores located in deeper parts of the Nordic Seas.

The preference for strictly oceanic conditions of *N. labyrinthus* (NLAB) is shown by its highest abundances in the central part of the Nordic Seas along the AF. In addition, this

species shows a negative relation to sea ice distribution (Chapter 2) which might hamper any clear interpretations of the OCEN/NLAB ratio as a proxy for the AF in areas strongly affected by sea ice. The application of this ratio should therefore generally be avoided in areas affected by seasonal sea ice and in shelf to upper slope settings, nevertheless the present study west of Norway indicate that the OCEN/NLAB ratio is a strong proxy of relative changes in the zonal extent of the AF within this area.

4.7.2 Comparing G. muellerae Abundances with other Flow Sensitive Proxies

The Neoglaciation (Porter and Denton, 1967) that governed the Late Holocene was punctuated by several warm and cold spells such as the RWP, the MCA, the LIA and the Modern period. Recent terrestrial (Overpeck et al., 1997; Kaufman et al., 2009) and marine proxy records (Spielhagen et al., 2011; Hald et al., 2011; Wilson et al., 2011) from the Arctic and northern North Atlantic, respectively, has shown that the LIA ended with a strong temperature increase during the last century.

The marine proxy-based reconstructions suggested that this recent temperature increase in the subsurface layer west of Spitsbergen (Spielhagen et al., 2011) and in the shallow settings off Northwest Norway (Hald et al., 2011) were unprecedented over the past two millennia. Both studies implied that this warming was probably caused by enhanced advection of Atlantic Water (AW) to the Arctic Ocean during modern times, although none were able to strictly infer the dynamical history of AW, i.e. the history of the strength of the North Atlantic Current (NAC).

The hypothesis of an increased AW flow during the modern period was further supported by Wanamaker et al. (2012) based on living and fossil molluscan remains north of Iceland; these authors additionally related known pre-Anthropocene warm (MCA) and cold (LIA) climatic spells of the last ~1500 years to modulations of the surface Atlantic-derived water dynamics within the North Atlantic. This was further evidenced off Florida, at the inception of the Gulf Stream, by Lund et al. (2006) who estimated a 10 percent decrease in the flow of this current at the transition from the MCA to the LIA and showed a systematically lower current strength during the LIA (~750-100 cal. years BP; AD ~1200-1850) (Fig. 4.29). The North-Icelandic proxy record by Wanamaker et al. (2012) indicates an overall decrease in the flow of AW during the last millenia until 70 cal. years BP (1880 AD), followed by unstable conditions and a marked increase in flow strength from 10 cal. years BP (1940 AD) until present (Fig. 4.29). Both results by Lund et al. (2006) and Wanamaker et al. (2012) are generally consistent with

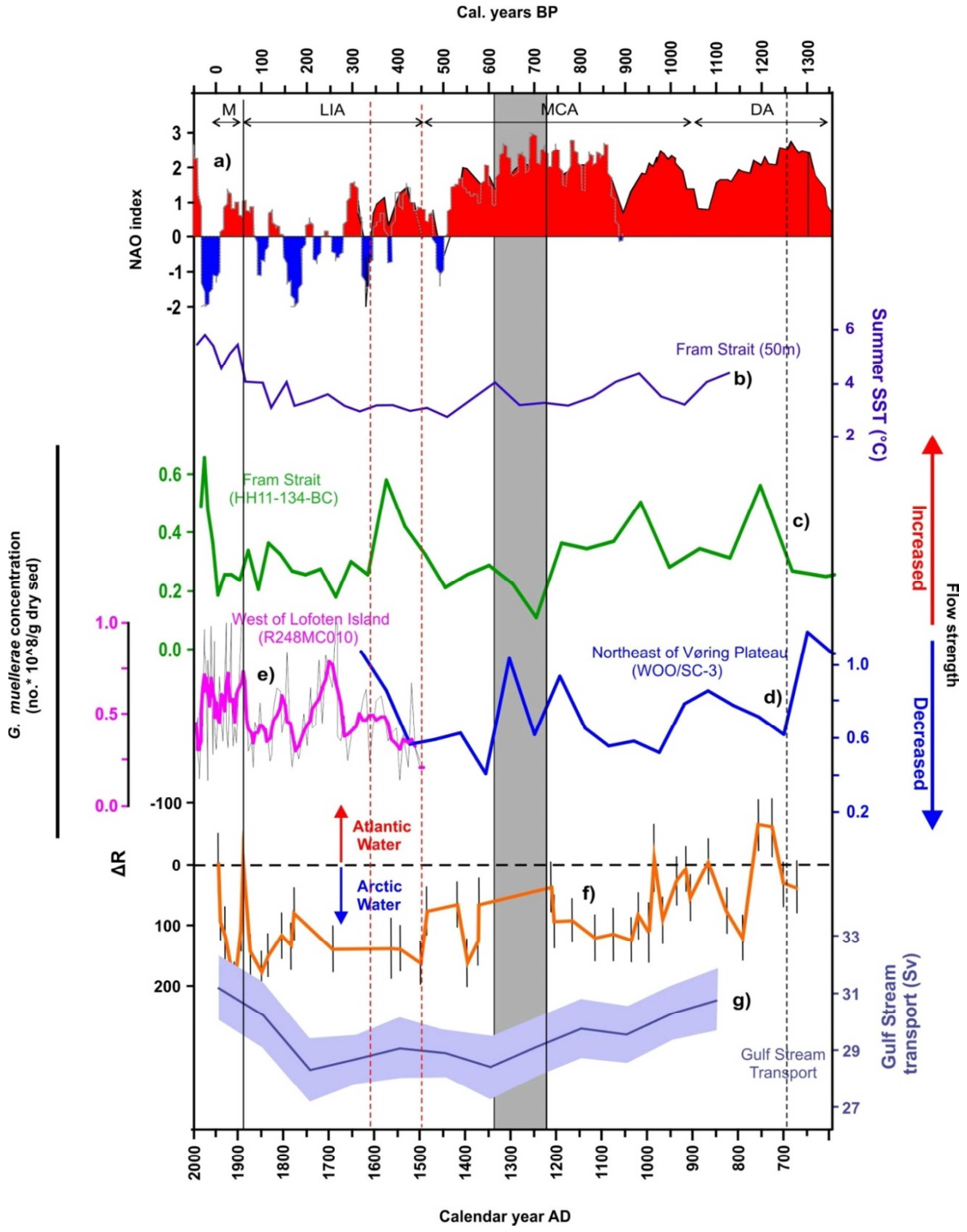

Figure 4.29 : Comparison of *G. muellerae* with other AW flow proxy records during the last millenium. a) : Combined NAO index reconstruction based on Trouet et al. (2009) and Olsen et al. (2012). b) : SST record in Fram Strait off western Svalbard in core MSM5/5-712, due slightly north of HH11-134-BC, after Spielhagen et al. (2011). c+d+e) : AW flow strength inferred from absolute concentrations of the AW inflow species *G. muellerae* (this study). f) : Shell-based ΔR values over northern Iceland after Wannamaker et al. (2012); positive values are representative of Arctic-derived water masses, negative values are indicative of Atlantic-derived surface water masses. g) : Gulf Stream transport estimates in the Florida Strait after Lund et al. (2006). The grey shaded area represents the zone of transition from the MCA to the LIA.

our coccolith (*G. muellerae*) flow proxy records off western Norway and western Svalbard, hence further confirming the reliability of *G. muellerae* abundance as a proxy of poleward AW flow strength within the eastern Nordic Seas (Fig. 4.29).

Wanamaker et al. (2012) connected AW inflow variability over the shelf of Northern Iceland to the Gulf Stream/NwAC flow and the wind-driven (surface) component of AMOC and hypothesized that the variability in surface AMOC and ΔR values north of Iceland were in part driven by the mean state of the NAO system during the last 1,000 years. Such an assumption was also proposed by Cronin et al. (2005) who suggested a modulation of the sea-surface temperature changes in the western North Atlantic (Chesapeake Bay) by a North Atlantic Oscillation (NAO) like atmospheric process. Although short term variability of the reconstructed NAO index (Trouet et al., 2009; Olsen et al., 2012) are not strictly and always connected with rapid changes in the flow proxies shown in Fig. 4.29, the general trends of an overall positive NAO phase during the MCA and the Modern period and a prevaling negative or unstable NAO mode during the LIA fit well with our general understanding of the NAO influence on the northward advection of Atlantic water, according to modern observations (Blindheim et al., 2000).

4.7.3 Reconciling the Observed Trends in AW Flow (HH11-134-BC, Fram Strait) with the Historical Distribution of Arctic Sea Ice

A reconstruction of late summer Arctic sea ice distribution over the last ~1500 years was recently proposed by Kinnard et al. (2011) based mainly on terrestrial records (ice cores, tree rings, lake sediments) and two historical series of sea ice observations from circum Arctic sites. The record indicate a generally increasing sea ice distribution until roughly ~500 cal. years BP, followed by a decrease (Fig. 4.30), a pattern which is fairly similiar to the IRD and P_BIP_{25} records obtained at our northern Fram Strait core site (HH11-134-BC) (Fig. 4.25) as well as to records of ice advances on Svalbard (Svendsen and Mangerud, 1997). Figure 4.30 compares Kinnard et al. (2011) inferred Arctic sea ice distribution with our coccolith flow proxy record obtained in this sediment core over the last 1500 years. The comparison clearly show that recent changes in Arctic sea ice distributions are strongly tied to variations in the advection of warm Atlantic water to Fram Strait, the main gateway to the Arctic. This correlation hold true despite inherent biases linked with differences in time-resolution and age control between the two datasets. In particular, the unprecedented decrease in sea ice extent during the last century is synchronous with a exceptional increase in AW flow strength off western Svalbard, which stands as unprecedented over the last ~1500 year.

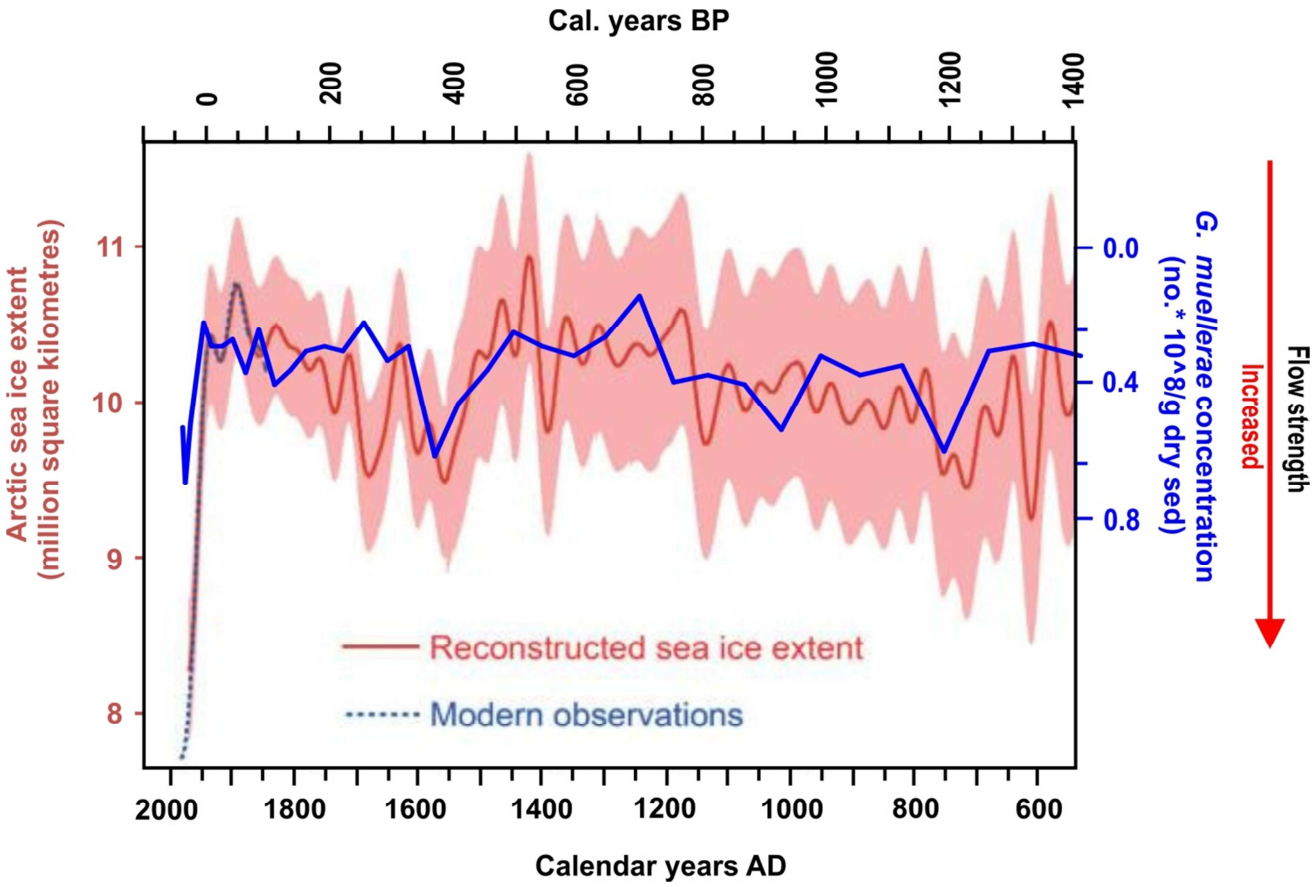

Figure 4.30 : Comparison of *G. muellerae* absolute abundance in the Fram Strait core HH11-134-BC with a 1500 years sea ice reconstruction. Modified after Kinnard et al. (2011).

4.8 Late Holocene Paleoceanographic Variability within Surface and Subsurface Layers of the Eastern Nordic Seas: A General Discussion

The manifestation of the Late Holocene (last ~3000 years) trend toward positive NAO conditions can be inferred from various marine proxy records around Greenland showing colder conditions associated with decreased AW influence in Diskobay (western Greenland) related to the so-called “seesaw” pattern (Seidenkrantz et al., 2008; Andresen et al., 2011, 2012), and an increased flux of sea-ice/icebergs east of Greenland (Jennings et al., 2002). Accordingly, Moros et al. (2004) interpreted the patterns of increased abundance of ice-rafted detritus (IRD) in the western parts of the Nordic Seas (Jennings et al., 2002) and decreased IRD in the Norwegian Sea (their work) to a strengthening of both the NAC and the EGC from the Mid-Holocene to Present. This coupled strengthened circulation affecting the eastern and western parts of the Nordic Seas is consistent with modern observations (Blindheim et al., 2000; Furevik and Nilsen, 2005) and modelling experiments (Nilsen et al., 2003) which relate it to atmospheric processes akin to the present positive phase of the NAO. Finally, a strengthening of the NAC and its WSC extension over the last 3000 years has earlier been

suggested by Sarnthein et al. (2003) based on a general increase in reconstructed subsurface temperatures in the western Barents Sea, which the authors related to a slight increase of the thermohaline circulation. Concurrent glacier expansions over western Spitsbergen (Svendsen and Mangerud, 1997) and increased winter precipitation over mid-western Norway (Nesje et al., 2001) throughout the last 3000 years additionally argue for strengthened southwesterlies and associated increase in NAC and WSC flows, related to the increasingly positive NAO trend (Fig. 4.31a).

Comparing the Observed Late Holocene Circulation and Climate changes with other North Atlantic Terrestrial and Marine Records.

The above core summaries are indicative of the dominating paleoceanographic and paleoclimatic changes which occurred within the surface and subsurface water masses throughout the late Holocene. These changes are discussed in the following section according to the five time Zones identified from the analysis of proxy data within the studied cores. Zone I represents the period ~3000-2200 cal. years BP (1050-250 BC). Zone II covers the interval ~2200-650 cal. years BP and includes the three subzones II-a (2200-1250 cal. years BP), II-b (1250-850 cal. years BP) and II-c (~850-650 cal. years BP). Zone III encompasses the interval from ~650 to ~60 cal. years BP and hence includes ZONE IV (240-60 cal. years BP) with its two subzones IV-a (1710-1800 AD) and IV-b (1800-1890 AD). ZONE V is roughly equal to the last century (1890-present, Modern period) (Fig. 4.31).

ZONE I: ~3000-2200 cal. years BP

The Zone was identified in three (WOO/SC-3, JM09-KA11-GC, HH11-134-BC) out of five cores and was characterized by a generally low AW flow along the entire eastern continental margin of the Nordic Seas (Fig. 4.31b+c+d). The colder and drier conditions prevailing during Zone I which was characterized by persistent negative NAO like atmospheric mode, seemed to be a general phenomenon in the northern North Atlantic region. Evidences from GISP2, indicate an increased transfer of sea-salt aerosols over Greenland from 3150 to 2450 years BP which the authors related to an expansion of the northern polar vortex or a generally intensified meridional air flow (O'Brien et al., 1995). This, together with an observed low in wind strength over Iceland (Jackson et al., 2005) and a possibly increased zonal storm track over central Europe (Sorrel et al., 2012), confirm the generally weak westerlies wind stress

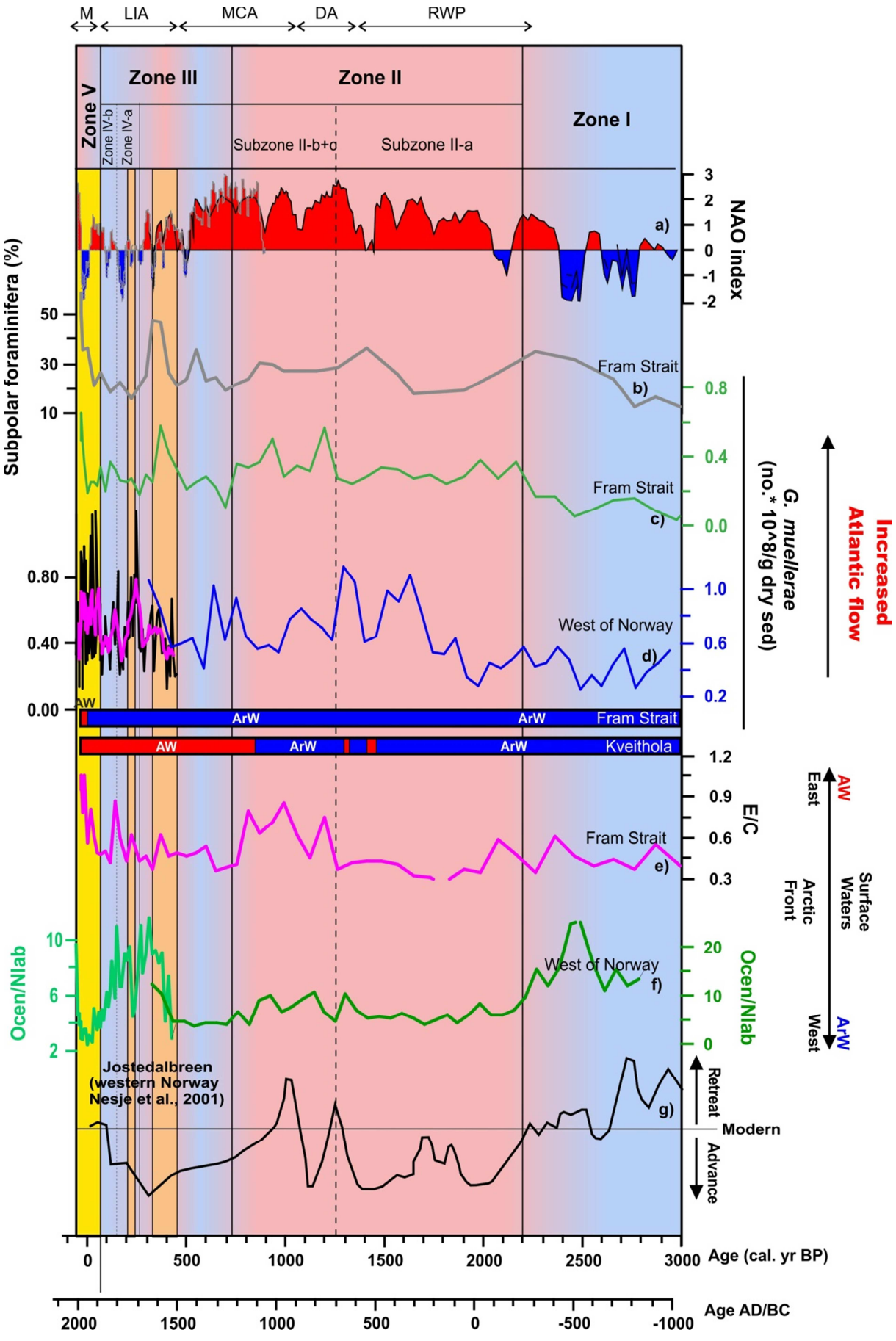
M
LIA
MCA
DA
RWP
Zone V
Zone IV-b
Zone IV-a
Zone III
Zone II
Zone I
Subzone II-b+c
Subzone II-a
NAO index
a)
Subpolar foraminifera (%)
Fram Strait
b)
Fram Strait
c)
West of Norway
d)
G. muellerae (no.* 10^8/g dry sed)
Increased Atlantic flow
AW
ArW
Fram Strait
Kveithola
E/C
Fram Strait
e)
Ocen/Nlab
West of Norway
f)
Jostedalbreen (western Norway Nesje et al., 2001)
g)
Retreat
Modern
Advance
AW East
Arctic Front
Surface Waters
ArW West
Age (cal. yr BP)
Age AD/BC

Figure 4.31 : Summary plot of surface and subsurface circulation changes in the eastern Nordic Seas over the past ~3000 years. a) : Combined NAO index reconstruction based on Trouet et al. (2009) and Olsen et al. (2012); Red area represents positive and blue area negative NAO conditions. b) : Relative abundances of subpolar foraminifera (fraction > 100 µm) as an index of subsurface AW masses. c + d) : Absolute concentrations of *G. muellerae* as a proxy of AW flow strength. e) : E/C ratio as an index of the relative position of the AF (AW/ArW). f) : OCEN/NLAB ratio as an index of the relative position of the AF (AW/ArW). g) : Glaciation curve for Jostedalsbreen area western Norway, modified from Nesje et al. (2001). Also included are watermass distribution bars (red=AW, blue=ArW) from the two most northern records based on the E/C threshold of 1. The summary inferred zones and subzones are highlighted in the top, with the zonations indicated by solid (zones) and dashed (subzones) vertical black lines. Shaded light red and light blue inferred relative variations between increased and decreased AW flow periods in the eastern Nordic Seas, respectively. Shaded base and yellow squares represents the inferred warm pulses and the Modern period flow increases.

over the eastern North Atlantic (negative NAO). This dominating atmospheric pattern resulted in the observed weakened flow of AW and a widening of the surface expression of the NAC and the NCC west of Norway (this study) (Fig. 4.31b+c+f), as indicated by increased sea surface temperatures North of Iceland (and a strengthened Irminger Current) (Solignac et al., 2006). The shallow surface expression of AW is however not expressed in subsurface waters west of Norway at ca. 3000 cal years BP (Anderson et al., 2003; Risebrobakken et al., 2003), but resume in this subsurface layer together with increasing AW flow towards the end of Zone I (Fig. 4.31d). A concurrent increase in the subsurface expression of AW is observed west of Spitsbergen where increasing $CaCO_3$ (wt%), IRD and IP_{25} contents witness a strengthened influence of AW masses and a strong presence of the MIZ (Müller et al., 2012), in agrement with our Fram Strait record (HH11-134-BC) (Fig. 4.31b+c).

Glacier retreats observed in southern Norway (Nesje et al., 2001) (Fig. 4.31g) and on Franz Josef Land in the northeastern Barents Sea (Lubinski et al., 1999), together with an interruption of a prolonged glacier advance on Svalbard (Svendsen and Mangerud, 1997), seem further in line with the prevailing negative NAO conditions which characterized Zone I (Fig. 4.31a). This suggestion agrees with modern observations of winter and snow accumulation on glaciers in maritime southwestern Norway which show that glacier advances and retreats are often related to NAO variability; accordingly, glacier advances are favored by mild and wet winter conditions (positive NAO) whereas retreats are mostly synchronous with cold and dry winters (negative NAO) (Blindheim et al., 2000; Nesje et al., 2001; Pinto and Raible, 2012)

ZONE II: ~2200-650 cal. years BP

The identified Zone II is based on observations from cores WOO/SC-3 (2200-640 cal. years BP), JM09-KA11-GC (2200-650 cal. years BP; Dylmer et al., 2013) and HH11-134-BC (1250-730 cal. years BP). The slight offset in the timing of the upper zone boundary can to a large extent be explained by the use in the present study of a standard reservoir correction

(R=0) for constraining the stratigraphical framework of all studied sediment cores; this simplification does not take into account possible varying contribution of "old" carbon from Arctic/Polar water masses off western Svalbard and western Barents Sea. Hence the upper boundary of Zone II (650 cal. years BP) has been aligned with earlier results by Dylmer et al. (2013) and Miller et al. (2012).

The surface water expression of strengthened AW flow toward the Arctic throughout Zone II is marked by an overall increased influence of surface AW masses in the western Barents Sea and off western Svalbard (Fig. 4.31). Sustained surface AW conditions occurred earlier at site JM09-KA11-GC from ca. 1000 cal. years BP, than at the northernmost Fram Strait site HH11-134-BC due to the sea ice conditions prevailing within this latter area throughout most of the last 3000 years until the last century (Müller et al., 2012). The increased WSC flow throughout the late Holocene was also suggested from planktonic foraminiferal-based SST reconstructions off western Barents Sea (Sarnthein et al., 2003) as well as from phytoplankton biomarkers and $CaCO_3$ contents in sediments off western Svalbard (Müller et al., 2012). In this regard, our coccolith and dinocyst proxy ratio (E/C and OCEN/NLAB) of surface water masses might add further constraints and improve the understanding of changes in the water column distribution of AW in the northern North Atlantic.

The studied sites off western Norway shows an opposite surface signature to the northernmost locations. Here, though always overlaid by surface AW, the studied cores (WOO/SC-3, MD95-2011) display decreasing OCEN/NLAB and E/C ratios, which translates into an increasing proximity of ArW (Fig. 4.31e+f). Modern observations on the influence of the NAO upon the surface hydrology of the eastern Nordic Seas might shed light on this apparent paradox. Instrumental records are indeed indicative of a correlation between changes in the NAO index and surface temperature variations (Blindheim et al., 2000; Miettinen et al., 2011), a correlation which is stronger west of Svalbard than off western Norway (Blindheim et al., 2000). Strengthened westerlies (positive NAO index), whose track of maximum wind stress in the Eastern Nordic Seas affects the oceanic area off south and mid-Norway, force both an increased flow of AW and a narrowing of the surface expression of the NAC and the NCC toward the Norwegian slope (Blindheim and Østerhus, 2005, and references therein). An obvious implication at MD95-2011 and WOO SC/3 is an increased proximity of arctic-derived surface water (eastward shift of the AF), throughout the last 3000 years, as suggested by the trend of our surface water mass proxies (OCEN/NLAB and E/C ratios) (Fig. 4.27), and

as confirmed by Norwegian Sea diatom (Andersen et al., 2004; Birks and Koc, 2002) and alkenone-derived SST reconstructions (Calvo et al., 2002).

In addition, intensified glacier advance in southwestern Norway and Svalbard (Svendsen and Mangerud, 1997; Nesje et al., 2001) (Fig. 4.31g) as well as increased ice rafting from icebergs (and/or sea ice) off western Svalbard (Fig. 4.25) during the period encompassed by Zone II, seem to confirm the governing atmospheric changes and the strengthened meridional flow of the NwAC, a pipeline for precipitation over the northeastern North Atlantic. A short stabilisation or decrease of glacier advances centered around 1000 cal. years BP is observed in Svalbard and southwestern Norway (Svendsen and Mangerud, 1997; Nesje et al., 2001), a short term change which appears to correlate with a weakening of the AW flow as observed during subzone II-b west of Norway (WOO/SC-3) (Fig. 4.31d).

Our observations of increased AW flow throughout Zone II is in line with previous indications of a relation between modulations of the surface Atlantic-derived water dynamics within the North Atlantic and pre-Anthropocene warm and cold climatic spells, as this period covers both the Roman Warm Period (RWP) and the Medieval Climate Anomaly (MCA). The DA is however not clearly reflected in our records although it might correspond to the short circulation and climate change identified during subzone II-b.

ZONE III + IV: ~650-60 cal. years BP (LIA)

The Zone III was observed in all studied cores WOO/SC-3 (~640-300 cal. years BP), R248MC010 (460-240 cal. years BP**)**, R406MC032 (~530-240 cal. years BP), JM09-KA11-GC (650-modern; Dylmer et al., 2013) and HH11-134-BC (~730-60 cal. years BP), although a clear age definition of both the upper or lower boundary was hampered by a limited length of the core or missing/mixed materiel. Hence, as Zone IV was only resolved in two out of 5 investigated cores (R248MC010, 240-60 cal. years BP; R406MC032; 240-100 cal. years BP), and in order to avoid a snapshot discussion of Zone III, we preferred to simplify the discussion of this historically important interval (LIA) by combining both Zones III and IV (Fig. 4.32). The upper boundary of this Zone III + IV was set in accordance to the Pb^{210} dated R248MC010, whose chronology during the last century is expected to be extremely well constrained .

The late Holocene trend of increased poleward flow of AW was interrupted by a sudden shift to a period of deteriorating conditions that we assume corresponds to the MCA/LIA transition

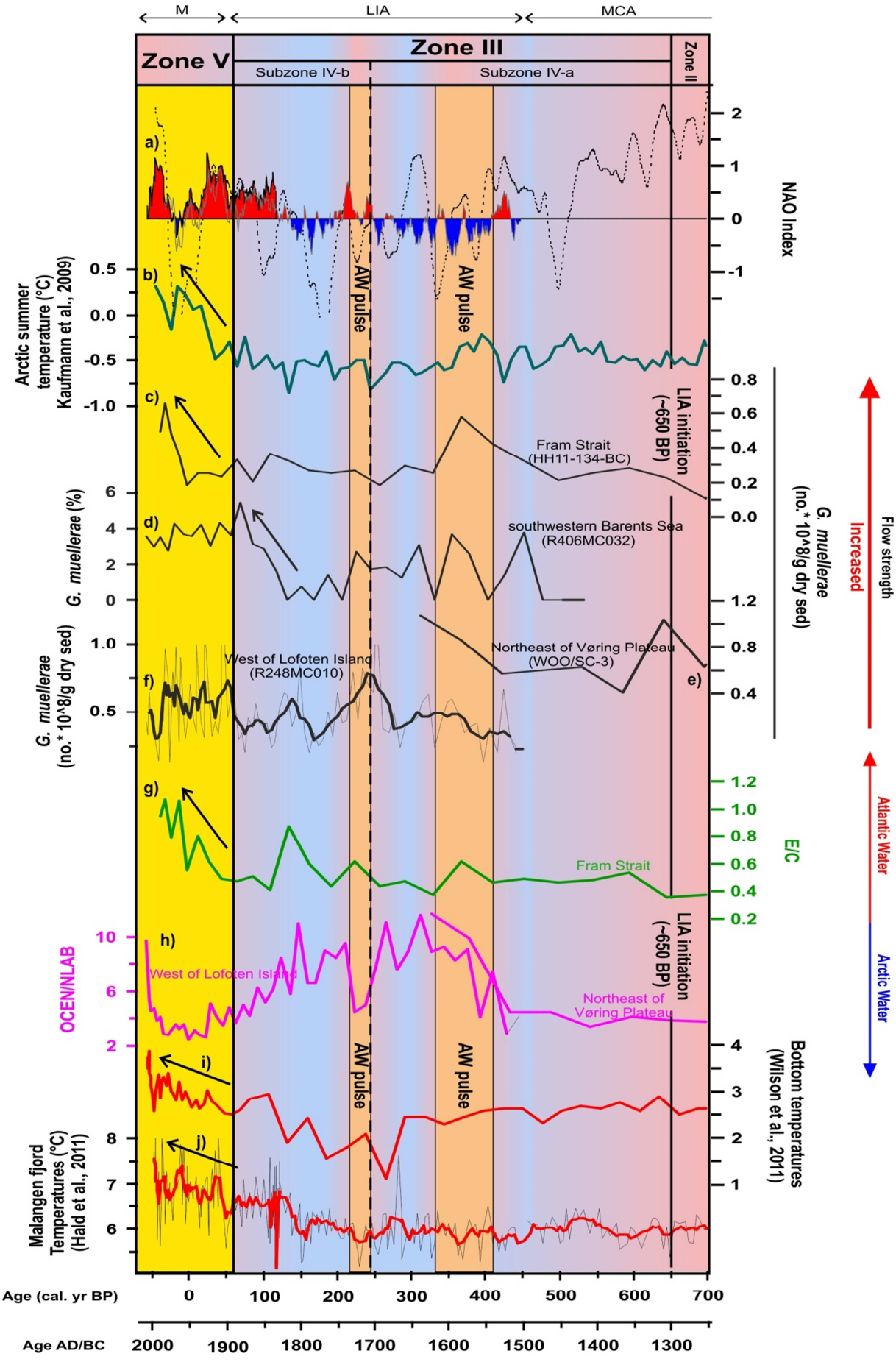
M
LIA
MCA
Zone V
Zone III
Zone II
Subzone IV-b
Subzone IV-a
a)
NAO Index
b)
Arctic summer temperature (°C) Kaufmann et al., 2009)
AW pulse
AW pulse
c)
Fram Strait (HH11-134-BC)
LIA initiation (~650 BP)
d)
G. muellerae (%)
southwestern Barents Sea (R406MC032)
G. muellerae (no.* 10^8/g dry sed)
Northeast of Vøring Plateau (WOO/SC-3)
e)
f)
G. muellerae (no.* 10^8/g dry sed)
West of Lofoten Island (R248MC010)
Flow strength
Increased
g)
Fram Strait
E/C
Atlantic Water
Arctic Water
h)
OCEN/NLAB
West of Lofoten Island
Northeast of Vøring Plateau
LIA initiation (~650 BP)
AW pulse
AW pulse
i)
Bottom temperatures (Wilson et al., 2011)
j)
Malangen fjord Temperatures (°C) (Hald et al., 2011)
Age (cal. yr BP)
Age AD/BC

Figure 4.32 : Summary plot of surface and subsurface circulation changes in the eastern Nordic Seas over the past ~800 years. a) : Combined modern (Jones et al., 1997; Osborn, 2006), reconstructed (Lutherbacher et al., 2002; Trouet et al. (2009), dashed black line) NAO index; Red and blue areas represent long term positive and negative NAO conditions, respectively. b) : Arctic summer temperatures based on Kaufmann et al. (2009). c - f) : Absolute concentrations of *G. muellerae* as a proxy of the AW flow strength. g) : E/C ratio as an index of the relative position of the AF (AW/ArW). h) : OCEN/NLAB ratio as an index of the relative position of the AF (AW/ArW). i) : Reconstructed bottom water temperatures from southeast of Bear Island (Wilson et al., 2011). j) : Reconstructed bottom temperatures (November) from the Malangen fjord, Northern Norway (Hald et al., 2011), red line represents a 5-running mean. The summary inferred zones and subzones are highlighted in the top, with the zonations indicated by solid (zones) and dashed (subzones) vertical black lines. Shaded light red and light blue represents inferred relative variations between increased and decreased AW flow periods in the eastern Nordic Seas, respectively. Shaded base and yellow squares represents the inferred warm pulses and the Modern period flow increases.

(Fig. 4.32). The MCA/LIA climatic shift is thought to have been triggered by a combination of a reduction in solar irradiance, explosive volcanism and changes in the internal modes of variability of the ocean-atmosphere system, as one single process cannot usually explain this cold period alone (Wanner et al., 2011). The suggested ~650 cal. years BP MCA/LIA age lies within the range of previously proposed ages for the initiation of this climate deterioration in the studied region (Hald et al., 2011; Sejrup et al., 2011), and closely corresponds to recent evidences from Arctic Canada and Iceland (Miller et al., 2012) for a 50 year long explosive volcanism centered at 650 cal. years BP. According to these latter authors, the onset of the LIA was directly linked to such volcanic events which triggered an extensive sea ice expansion causing a self-sustaining sea-ice/ocean feedback until Modern times. As volcanic eruptions seem to modify on short time scales a naturally occurring variability mode similar to the NAO toward its positive phase (Graf et al., 1994), the reconstructed major change to a negative NAO index across the MCA/LIA transition (Olsen et al., 2012) is most likely related to other forcings i.e. greenhouse gasses, stratospheric ozone and solar irradiance (Gillett et al., 2003). Nevertheless such a concomitant change in NAO pattern from a long-term positive phase to highly fluctuating negative NAO conditions around 640 cal. years BP possibly additionally contributed to an increase in sea-ice extent (Fig. 4.32a). Indeed, decadal and longterm variations in large scale ice concentrations have shown to be significantly correlated with long-term NAO variations (Visbeck et al., 2003). This major change in turn impacted on the efficiency of the NAC flow to the northern North Atlantic, therefore further maintaining, if not strengthening, the sea-ice expansion across the northern Nordic seas (Werner et al., 2011; Müller et al., 2012). This created cold and favorable conditions for glaciers on Svalbard from the 13^{th} -14^{th} century and onwards (Svendsen and Mangerud, 1997).

The harsh LIA conditions favored colder surface and subsurface waters, sea ice expansion and an increased presence of icebergs in the eastern Fram Strait (Fig. 4.25), which stands as a strong contrast to the dominating surface signature of AW at the western Barents Sea core site

JM09-KA11-GC (Fig. 4.31). The specific location of this site within the influence of both AW (WSC) and ArW (Sørkapp Current, Bear Island Current) implies that although sea ice cover was probably enhanced over the western Barents Sea during this climate deterioration, this local area was affected by a highly fluctuating sea-ice boundary with strong seasonal gradients characterized by an early spring break-up of the winter sea ice, as inferred from a higher level of IP25 (Berben et al., 2013), and a strong spring/early summer stratification and AW dominance during summer (favoring *E. huxleyi*). The specific surface expression at this site is further confirmed by the overall similarities between our E/C proxy (JM09-KA11-GC) and reconstructed atmospheric temperatures from a lake record in western Svalbard (D'andrea et al., 2012), an area influenced by similar hydrological features (e.g. sea ice, the Sørkapp Current and the WSC). D'andrea et al. (2012) identified a temperature increase starting at ~1600 AD (350 cal. years BP) over western Svalbard as well as mild LIA summer conditions which they explained by a strengthened WSC (NAC), a strengthening only inferred in the present study from our JM09-KA11-GC coccolith record. We therefore suggest the identified warming on Svalbard to be due to a decreased flow of polar waters over the shelf via the Sørkapp Current and the Bear Island Current, rather than to changes in the strength of the NAC, possibly resulting in a seasonally stronger AW influence on atmospheric temperatures and sea ice extent. Indeed, paleo-reconstructions from southeast of Bear Island are indicative of an Atlantic-derived bottom water over the continental shelf during the earlier part of the LIA (Wilson et al., 2011) (Fig. 4.32i). Such conditions in a shallow shelf area possibly induced a generally decreased stability of the sea ice cover, earlier spring break-up and increased ice melt in the southwestern Barents Sea.

The surface expression of the LIA west of Norway confirms the overall deteriorating conditions as indicated by a relatively weak AW flow and cool subsurface waters overlaid by AW masses (Fig. 4.6, 4.32). This pattern agrees well with our general understanding of the oceanic circulation in this area, a westward shift of the AF being expected to result in a widening and shallowing of the AW surface layer and hence a cooling in subsurface layers west of Norway. Which is confirmed by a LIA increase in surface temperatures north of Iceland as reconstructed from diatoms (Andersen et al., 2004) and a subsurface cooling west of Norway according to stable isotopes on planktic foraminifera (Sejrup et al., 2011). This comes as a result of the prevailing negative NAO pattern, a pattern that controlled and limited the northern flow of AW and instead caused an increased presence of this water mass off southeastern Greenland (Andresen et al., 2012).

The interval of Arctic/Polar LIA conditions in eastern Fram Strait was interrupted by a sudden short pulse of increased WSC flow between ~330 and 410 cal. years BP as depicted in several proxies within HH11-134-BC (Fig. 4.24, 4.25) and further confirmed in our IRD record from the southwestern Barents Sea (R406MC032) (Fig. 4.18). This short-lived AW flow to the northern Nordic Seas is synchronous with an increase in Arctic temperatures (Kaufmann et al., 2009) (Fig. 4.32b), a short term increase in the Atlantic Multi-decadal Oscillation (Gray et al., 2004; Winter et al., 2011) and a change towards positive NAO mode (Fig. 4.32a). All these rapid, short-term oceanic and atmospheric circulation changes are likely to explain the minimum sea-ice anomaly recorded in the Nordic Seas during the fifteenth century, compared with the previous and later centuries, as evidenced by Macias Fauria et al. (2009) and Kinnard et al. (2011). The magnitude of this warm pulse, as shown by our coccolith proxy record, falls within the range of the AW flow strengthening during the MCA and is only surpassed by a maximum in AW flow during the Modern period.

The sea-ice reconstructions by Kinnard et al. (2011) are particularly coherent with the changes in *G. muellerae* concentrations at core HH11-134-BC, indicating a phasing of increasing (decreasing) WSC flow and decreasing (increasing) sea-ice extent (Kinnard et al., 2011) throughout Zone III (including the ca. 400 cal. years BP warm pulse) up to Present (Fig. 4.30), suggesting as earlier observed a generally strong impact of AW flow dynamics on the Arctic sea-ice extent.

The deterioating conditions that followed the warm pulse was observed along the entire transect and was governed by a decreased AW flow and a dominance of ArW in the surface waters off western Svalbard and in the southwestern Barents Sea (Fig. 4.32c+d). The strengthened dominance of ArW in the surface of the southwestern Barents Sea appeared at a time when both the AW flow and the bottom water temperatures (Wilson et al., 2011) in this region reached a minimum (Fig. 4.32d+i). These processes are indicative of a southwestern migration of the AF over the Barents Sea, which amplified the governing sea ice expansion in the eastern and northern parts of the Barents Sea (Vinje, 2001; Vare et al., 2010).

A significant event identified by our proxy records west of Norway, and dated at ~215-230 cal. years BP, translate into a short-term eastward migration of the frontal systems (e.g. AF and NwAC/NCC) and a short strengthening of the AW flow (Fig. 4.32f+h). The latter represents a second smaller warm pulse within the LIA, and with synchronous with massive advance of glaciers in western Norway, between 1710 and 1735 AD (240-215 cal. years BP) (Nesje and Dahl, 2003; Nesje et al., 2008, and references therein). This glacier advance is

probably a direct result of enhanced precipitations following the slightly strengthened AW flow and positive NAO mode during this short interval (Lutherbacher et al., 2002; Nesje et al., 2008), and is confirmed by higher than normal winter precipitations reconstruction for european land areas showing a higher general winter precipitation during the earlier part of the 18th century (Pauling et al., 2005). In addition this final LIA warm pulse corresponds to a decreased extent of sea ice in the Barents Sea (Vinje, 1998).

ZONE V: 60-present cal. years BP

The LIA cool climatic period was reversed during the 19th century by an overall increase in atmospheric and oceanic temperatures, as reconstructed from marine and terrestrial high resolution proxy records from the Arctic region (Overpeck et al., 1997; Kaufman et al., 2009) (Fig. 4.32a-d, f-j). Recent studies on sea-surface temperature reconstructions over the last 2000 years in Malangen fjord, northwestern Norway (Hald et al., 2011), south of Bear Island (Wilson et al., 2011) and West of Spitsbergen (Spielhagen et al., 2011), and evidences herein of high amplitude, rapid temperature increases during the last century, has intensified the ongoing debate on temperature changes in the Arctic. Spielhagen et al. (2011) used foraminiferal assemblages and geochemical measurements to reconstruct a ~2 °C temperature increase in the subsurface waters of eastern Fram Strait at the transition from the LIA to the Modern period. Our dataset confirms the high amplitude warming of subsurface waters at the turn of the 19th- century; more importantly, it also shows that such a warming was primarily induced by an excess flow of AW along the continental margins of the Eastern Nordic Seas as depicted by our *G. muellerae* proxy records i.e. off western Norway, in the western Barents Sea and off western Svalbard (Fig. 4.32c+d+f). Our results hence indicate that this Modern strengthening of AW flow was unprecedented over the last 3000 years, and was associated with an exceptional AW shoaling (summer, Fram Strait) (Fig. 4.31, 4.32), in agreement with reported historical lows in sea ice extent in the Nordic Seas since the second half of the 19th century (Divine and Dick, 2006) and recent Arctic sea ice reconstructions (Kinnard et al., 2011).

Chapter 5 : General Conclusions and Perspectives

The main objective of this research project was to obtain a more complete knowledge on Late Holocene natural variability of physical parameters affecting ecosystem processes and structure in the eastern Nordic Seas within, or close to areas presently affected by seasonal sea-ice, by applying mainly dinocysts and coccoliths. The goal involved qualitative and quantitative reconstructions of surface water conditions (temperature, salinity, stratification and sea ice distribution) based on dinocyst and coccolith assemblages recovered from high resolution (decadal to centennial scale) Holocene sediment cores, and comparison with other terrestrial and marine datasets. Of particular interest is the reconstruction of late Holocene surface water mass distributions within the eastern Nordic Seas and the dynamics of the Atlantic water flow on its way to the Arctic Ocean via the Fram Strait gateway.
Several take-home messages can be highlighted from this investigation, both concerning the significance of the micropaleontological proxies used in the present study, and the paleo-reconstructions over the last ca. 3000 years.

5.1 The Extant Coccolithophore Populations across the Norwegian-Iceland Seas and Fram Strait.

Phytoplankton samples investigated in the present study (Chapter 2) were collected en-route using a simple, cost- and time effective method, along two zonal transects perpendicular to the major meridional boundary current systems and hydrological fronts. The regional and local oceanography during the sampling periods was derived from the combined use of easily accessible remote sensing images, CTD casts and Argo floats from existing databases. Although not sufficient to investigate small-scale physical and biological processes, this approach was found highly relevant for defining key oceanographic processes and water masses explaining the observed distribution of the dominant fossilizable coccolithophore species within the northern North Atlantic i.e. *E. huxleyi* and *C. pelagicus.*
Observed seasonal changes in the distribution and stratification of the main water masses related to sea-ice melts and changes in the drift of Atlantic surface water masses resulted in an overall westward shift between the observed seasons (July-October) of the peak cocolithophore production areas dominated by the opportunistic *E. huxleyi*. The presented datasets across the Norwegian-Iceland Seas confirm previous studies indicating high cell densities over the Vøring Plateau in July, and west of the Jan Mayen island in September-October (Samtleben et al., 1995a). An observed peak coccolithophore production within the

Lofoten gyre in July 2011 was related to increased vertical mixing and nutrient enrichment of the photic layer due to large scale atmospheric changes. In contrast, the change in dominating species around Jan Mayen from *C. pelagicus* in summer to *E. huxleyi* in fall, resulted from a change in stratification from well mixed (summer) to stratified (fall) surface waters as a result of changing influence of melt water from sea ice. In addition, our data are indicative of a strong temperature limitation of *C. pelagicus* production, which is expressed by a maximum boundary value of 6°C, with a somewhat lower (ca. 4°C) limit across Fram Strait.

To our knowledge, our dataset from Fram Strait represents a first view of the zonal distribution of extant coccolithophores within this climatically sensitive area during summer and fall. The results show a clear seasonal change in dominance from *E. huxleyi* (summer) to *C. pelagicus* (fall) related to the combined influence, during summer, of enhanced sea-ice melting close to the sea-ice edge. This shift in species dominance is also related to the summer increased influence of AW and higher irradiance leading to the high production of the opportunitic species *E. huxleyi* within an area usually characterized by *C. pelagicus*-dominated low density populations.

5.2 Significance of AW/ArW Indicators and of the AW Flow Strength Proxy *G. muellerae*

Surface water mass changes from AW/ArW indicators

The regional dominance of the coccolithophore species *E. huxleyi* (E) and *C. pelagicus* (C), on one hand, and of the dinocyst species *O. centrocarpum* (OCEN) and *N. labyrinthus* (NLAB), on the other hand, has earlier been shown to be strongly reflected in surface sediments of the Nordic Seas (Samtleben et al., 1995; Baumann et al., 2000; Matthiessen et al., 2001; Zonneveld et al., 2013). This led to the definitions of two relative abundance ratios OCEN/NLAB and E/C, for investigating the location of the AF that separates the seasonally ice-covered Polar and Arctic waters (E/C<1; OCEN/NLAB<4) from warmer and saltier Atlantic-derived waters (E/C>1; OCEN/NLAB>4).

The present study lied on these exploratory works in applying these dinocyst and coccolith ratios on a set of five marine sedimentary cores. We identified three key factors, which separately or together, explained contradicting results obtained from this set of cores:

1. The choice of the threshold value.
2. The distribution of the original surface sediment samples used in the species ratio definition.

3. A limited knowledge of the species ecology

Based on these factors and a comparison with other paleo-proxies and historical sea ice observations, the E/C ratio was found to be a reliable proxy for surface water changes (AW vs. ArW, threshold of 1), and is indicative of an overall time-transgressive increasing influence of AW towards Fram Strait throughout the last 3000 years. The significance of the E/C ratio was however not conclusive in areas affected by the NCC. A similar comparison with OCEN/NLAB showed that the initially defined ratio threshold of 4 was to high in our study area for describing rapid, low amplitude changes in surface water masses within the last 3000 years. Furthermore our study indicated that the use of the OCEN/NLAB ratio should be avoided in areas affected by seasonal sea ice as well as in shallow shelf to upper slope settings. Nevertheless, this dinocyst proxy is considered as a valuable proxy for relative changes in the dominating water masses and the position of the AF off western Norway.

The AW drift species G. muellerae

Drifting with the poleward flow of surface to intermediate NAC waters from the temperate North Atlantic, was proposed by Samtleben and Schröder (1992) and later clarified by Giraudeau et al. (2010) for explaining the presence of *G. muellerae* in Holocene sediments of the eastern Nordic Seas. Given the species ecological background and distribution, abundance changes of *G. muellerae* in the studied sediment cores was discussed in terms of relative variations of the depth integrated poleward flow strength of the NAC in relation to the dominating NAO like mode.

Our results showed that short term variability of instrumental and reconstructed NAO index (Jones et al., 1997; Osborn, 2006) and rapid changes in *G. muellerae* did not always strictly correlate during the last ~500 years. This unconformity can be explained by the fact that the meridional flow of the NAC to the Nordic Seas and the Arctic Ocean relates both to anomalies in the location and strength of the westerlies and changes in the thermohaline circulation (Müller et al., 2012). The general trends of an overall positive NAO phase during the MCA and the Modern period and a prevaling negative and/or unstable NAO mode during the LIA (Trouet et al., 2009; Olsen et al., 2012) however translates exceptionnaly well into strengthened and reduced NAC flow strength, respectively, as depicted by our coccolith proxy records, and according the modern processes at play in the Nordci seas (Blindheim et al., 2000). In addition the close correspondence of our *G. muellerae* abundance datasets with foraminiferal records off Norway and western Svalbard, where foraminiferal abundance

changes are assumed to trace subsurface water temperatures, confirms the reliability of this coccolith index as a proxy of Atlantic water flow.

Our coccolith flow proxy variations show a remarkable phasing with changes in Arctic Sea ice distribution over the last ~1500 years, In particular, the reconstructed extensive decrease in sea ice extent during the last century, confirmed by historical reports, is synchronous with an exceptional increase in the AW flow across Frams Strait which stands as unprecedented over the last ~1500 year.

The paleoceanographic potential of *G. muellerae* as a proxy for the strength of AW flow was strongly illustrated within this study and provides a valuable tool to improve our general understanding on past dynamics of the NwAC and its two extensions : the WSC and NCaC.

5.3 A Late Holocene History of Surface Circulation Changes in the Eastern Nordic Seas

A high-resolution study of coccolith and dinocyst assemblages from five sediment cores in the eastern Nordic Seas provided a wealth of information on the surface water dynamics along the path of the AW flow toward Fram Strait throughout the last 3000 years. In particular, a high resolution study of the last ~500 years showed that recent historical climate shifts are expressed by the micropaleontological proxies according to local hydrological and climatological processes which characterize each studied locations. Hence a multi-proxy approach is very much needed to infer paleoceanographic changes in such complex hydrological settings.

The Late Holocene changes in AW flow and in the nature of surface waters in the eastern Nordic Seas along a 66-77°N latitudinal gradient, show a generally strengthened NAC flow from 3000 cal. years BP to the Present. This long term modulation in the AW flow is linked to atmospheric processes driven by dominant modes of NAO. This mechanism also explain the observed zonal shifts in the location of the AF off western Norway, with increased influence of ArW during strengthened westerlies (positive NAO mode), whereas the western Barents Sea and eastern Fram Strait experienced an overall shoaling of AW which is proportional to the integrated flow to this northernmost settings. In general, the late Holocene shifts in AW flow strength relate fairly well with earlier identified pre-Anthropocene warm (RWP, MCA and the Modern period) and cold (LIA, DA) climatic spells. Periods of strong flow (2200-650 cal. years BP; ~60 cal. years BP to Present) were in general characterized by an eastward (west of Norway) and northward (western Fram Strait) migration of the AF, whereas periods of low AW flow (3000-2200 cal. years BP; 650-60 cal. years BP) were related to a reversed

situation of westward (west of Norway) and southward (western Fram Strait) migration of the AF.

The Little Ice Age initiation at ~650 cal. years BP was followed by an episode of deteriorating conditions, with Arctic/Polar surface waters off western Svalbard and in the western Barents Sea, possibly associated with severe sea-ice conditions, and a strongly reduced AW flow. During the earlier stages of this period, the western and southwestern Barents Sea bottom waters were bathed by AW until roughly 300 cal. years BP, causing an unstable fluctuating MIZ. The following period appears exceptional in our record as the AW flow decreased to a minimum over the southwestern Barents Sea shelf and was followed by an extensive sea ice expansion.

The strong LIA cooling was interrupted in the eastern Fram Strait by a short resumed high flow of WSC from ca. 330 to 410 cal. yrs BP, whose magnitude was only surpassed by the excess AW flow who characterized the Modern period and which stands as unprecedented in Fram Strait over the last 3000 years .

5.4 Perspectives

5.4.1 Improving our Paleo-Reconstructions

Improving our knowledge on the ecology of the surface dwelling dinoflagellates and coccolithophores and on the surface distribution of their skeletal remains :

Dinoflagellates and coccolithophores and their fossilizable remains are among some of the most widely used proxies in paleoceanographic and paleoclimatic reconstruction of the northern North Atlantic. An increased amount of investigations during recent decades on the distribution of extant and fossil populations (e.g. Samtleben et al., 1995; Andruleit et al., 1997; Matthiessen et al., 2001) has strongly improved our knowledge of the environmental factors explaining the surface water and surface sediment distribution of these two species groups.

Our study of extant coccolithophores is indicative of the ongoing intensification of sea-ice melts and sea-ice thinning within the Arctic Ocean, the associated naturally increased export of ice and melt water to the Nordic Seas (Kwok, 2009), and the overall increased surface water stratification in the western northern North Atlantic (Furevik et al., 2002). This setting favors the production of *E. huxleyi*. Remote-sensing investigations already point to the occurrence of pervasive blooms of *E. huxleyi* in Arctic to Polar environments such as the Barents Sea (Smyth et al., 2004) under the influence of increased sea-ice melts and increased

inflow of AW, conditions which are equally supposed to characterize the Greenland-Iceland Seas. Ongoing changes in the physico-chemical structure of the surface mixed layer of the northern North Atlantic (stratification, temperature, salinity) might induce regional changes in the structure of the phytoplankton communities with major effects on the carbon cycle as well as the entire food web of the Nordic Seas. Continuing surveys (yearly/monthly) of the distribution of phytoplankton in the presently changing high latitude oceans are therefore of tremendous importance, and could be implemented through an en-route simple, cost- and time effective sampling method such as the one applied in the present study.
Beside living cells, surface water investigations of coccolithophore populations should further include census counts of coccoliths. Understanding the distribution within the water column of the fossil remains of *G. muellerae* would further constrain the use of this species as a proxy for the strength of AW flow. A combination of water sampling and CTD measurements of temperature and salinities along a south to north transect within the main path of the NwAC would indeed be of prime importance in this regard.

The present study of micropaleontological AW/ArW indicators is hampered by the uneven distribution of surface sediment samples used for the definition of these proxy ratios. Zonneveld et al. (2013) recently published an impressive extended version of the 2003 dinocyst surface sediment database by Marret and Zonneveld (2003). This database strongly add to the understanding of dinocysts and their ecology. Unfortunately this improvement only concerns dinocysts. An interdisciplinary work involving several micropaleontolological groups (diatoms, foraminifera, coccoliths, dinocysts and radiolarians) and based on such an extensive surface sediment dataset is of urgent need for the paleoclimatology community.

Improving the records obtained from the five studied cores :
Given its estimated sedimentation rates, WOO/SC-3 is highly relevant for high resolution (up to 10 years resolution) paleoceanographic reconstructions off western Norway. Future work on this core should imply a strong collaboration with our fellow institution in Tromsø in order to combine our phytoplankton-related dataset with plaktic and benthic foraminiferal census counts.
The multicore R248MC010, a very high resolution core encompassing the last 500 years, was the subject within the present study of an extended multi-proxy investigations including a whole range of biotic and abiotic proxies. The modern ages of the core-top offers the

possibilities to constrain the top part of our proxy records with instrumental time-series of environmental datasets. The records of large S, Mg and Fe-coated lithic grains obtained within this core should be thoroughly investigated in combination with XRF-based elemental concentrations, as a proxy record of diagenetic processes. We also intend to implement statistical analyses such as PCA and spectral analyses on this unique set of data, as a way to unravel the recent paleoclimatic history off western Norway.

As mentioned earlier, the problematic location of core R406MC032 at the entrance to the Bear Island Trench might result in downslope transport from upper shelf areas. Hence to clarify the importance of such sedimentary processes, a benthic foraminiferal study is clerly needed (see Chapter 3; Sarnthein et al., 2003).
Future work on core JM09-KA11-GC should include a comparison with published planktic and benthic foraminifera data from Berben et al. (2013) and Groot et al. (2013) and IP25 from the Plymouth group (Cabedo-Sanz, pers. Comm.) and a further investigation of the MAT reconstructions. The latter is motivated by the deviations between reconstructed surface water temperatures and salinities and modern values, as well as sea-ice extent estimates that appears much higher than recent Holocene dinocyst reconstructions from this area (de Vernal et al., 2013).
A higher resolution of the planktic foraminifera record at the base of core HH11-134-BC might strengthen and/or clarify the relation between the *G. muellerae* proxy of AW flow strength and planktic foraminiferal assemblages, tracers of temperature changes in subsurface waters.

5.4.2 Extending the Present Study to Paleoceanographical Reconstructions over the entire Holocene.

An obvious next step for future work will be to extend the investigated timeframe to the entire Holocene, via the implementation of the proxies identified and validated by the present late Holocene study. Some preliminary results obtained from gravity core JM09-KA11-GC are displayed in figure 5.1. The light red boxes represents zones of apparent strengthened AW flow strength (8800-5500 cal. years BP, 2000 cal. years BP- the top) and the dark red box indicate a zone which need to be further stratigraphically constrained. The resulting datasets will be thoroughly discussed and compared with foraminiferal results of Berben et al. (2013), Groot et al. (2013) and sedimentological data by Rüther et al. (2012).

Figure 5.1 : Summary plot of surface and subsurface circulation changes in the western Barents Sea (JM09-KA11-GC) over the past ~12000 years. a) : Bulk coccolith concentrations as an index of carbonate productivity. b) : Absolute concentrations of *G. muellerae* as a proxy of the AW flow strength. c) : relative abundances (%) of the major coccolith species *E. huxleyi* and *C. pelagicus* as proxies for AW and ArW, respectively, within JM09-KA11-GC. d-g) : relative abundances (%) of the dinocyst species OCEN (AW), IMIN (ArW), BSPP (productivity) and SRAM (productivity, salinity) within JM09-KA11-GC. h) : HALO concentrations as a proxy for meltwater. i - k) : Dinocyst-based MAT reconstructed winter surface water temperatures, salinities and sea ice concentrations (months/year), with the grey shaded area representing the error ranges of the reconstructions. Shaded light red represents increased AW flow periods in the western Barents Sea during the Holocene.

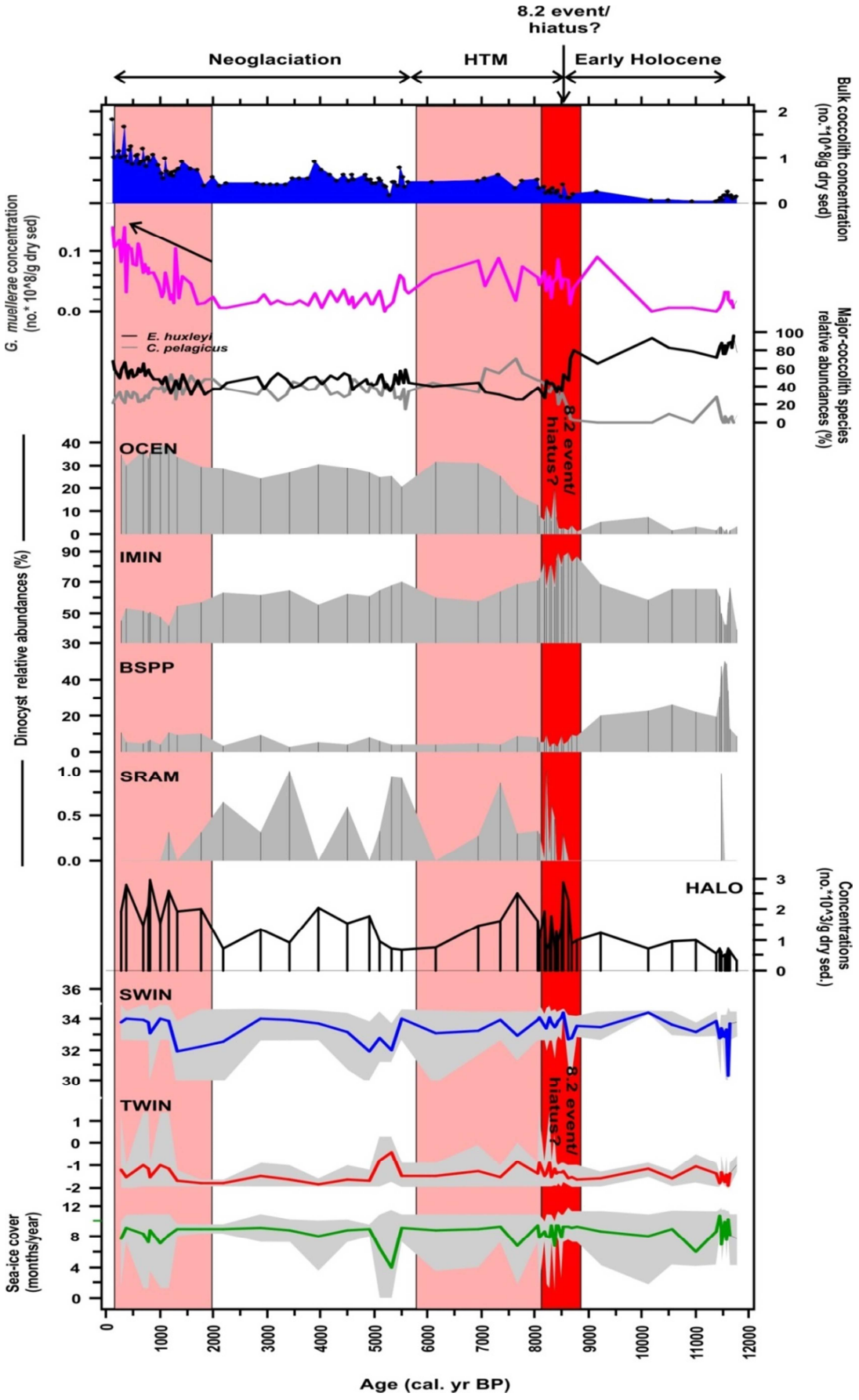
8.2 event/
hiatus?
Neoglaciation
HTM
Early Holocene
Bulk coccolith concentration
(no.*10^8/g dry sed)
G. muellerae concentration
(no.* 10^8/g dry sed)
E. huxleyi
C. pelagicus
Major-coccolith species
relative abundances (%)
8.2 event/
hiatus?
OCEN
IMIN
BSPP
SRAM
HALO
Concentrations
(no.*10^3/g dry sed.)
Dinocyst relative abundances (%)
SWIN
TWIN
8.2 event/
hiatus?
Sea-ice cover
(months/year)
Age (cal. yr BP)

REFERENCES

Aargaard, K. and Carmack, E.: The Arctic Ocean and climate: A perspective, in the Polar Oceans and their role in shaping the global environment: The Nansen Centennial Volume, Geophys. Monogr. Ser., AGU, Washington, D.C., 85, 5-20, 1994.

Andersen, C., Koc, N., Jennings, A. and Andrews, J. T.: Non-uniform response of the major surface currents in the Nordic Seas to insolation forcing: Implications for the Holocene climate variability, Paleoceanography, 19, PA2003, doi: 10.1029/2002PA000873, 2004.

Andersson, C., Risebrobakken, B., Jansen, E. and Dahl, S. O.: Late Holocene surface ocean conditions of the Norwegian Sea (Vøring Plateau), Paleoceanography, 18, PA1044, doi: 10.1029/2001PA000654, 2003.

Andersson, M., Orvik, K. A., La Casce, J. H., Koszalka, I. and Mauritzen, C.: Variability of the Norwegian Atlantic Current and associated eddy fields from surface drifters, J. Geophys. Res., 116, C08032, doi: 10.1029/2011JC007078, 2011.

Andresen, C. S., McCarthy, D. J., Dylmer, C. V., Seidenkrantz, M.-S., Kuijpers, A. and Lloyd, J. M.: Interaction between subsurface ocean waters and calving of the Jakobshavn Isbræ during the late Holocene, The Holocene, 21, 211-224, 2011.

Andresen, C. S., Hansen, M. J., Seidenkrantz, M-S., Jennings, A. E., Knudsen, M. F., Nørgaard-Pedersen, N., Larsen, N. K., Kuijpers, A. and Pearce, C.: Mid- to late-Holocene oceanographic variability on the Southeast Greenland shelf, The Holocene, 23, 167-178, 2012.

Andrews, J. T. and Giraudeau, J.: Multi-proxy records showing significant Holocene variability: the inner N. Iceland shelf (Húnaflói), Quaternary Sci. Rev., 22, 175-193, 2003.

Andruleit, H.: A filtration technique for quantitative studies of coccoliths, Mar. Micropaleontol., 42, 403-406, 1996.

Andruleit, H.: Coccolithophore fluxes in the Norwegian-Greenland Sea: Seasonality and assemblage alterations, Mar. Micropaleontol., 31, 45-64, 1997.

Andruleit, H.: Dissolution-affected coccolithophore fluxes in the Central Greenland Sea (1994/1995), Deep-Sea Res. II, 47, 1719-1742, 2000.

Andruleit, H. and Baumann, K. -H.: History of the last deglaciation and Holocene in the Nordic Seas as revealed by coccolithophore assemblages, Mar. Micropaleontol., 35, 179-201, 1998.

Astthorsson, O. S., Gilason, A. and Jonsson, S.: Climate variability and the Icelandic marine ecosystem, Deep-Sea Res. II, 54, 2456-2477, 2007.

Balestra, B., Ziveri, P., Monechi, S. and Troelstra, S.: Coccolithophorids from the Southeast Greenland Margin (Northern North Atlantic): Production, ecology and the surface sediment record, Mar. Micropaleontol., 50, 23-34, 2004.

Bauerfeind, E., Bodungen, B. V., Arndt, K. and Koeve, W.: Particle flux, and composition of sedimenting matter, in the Greenland Sea, J. Mar. Syst., 5, 411-423, 1994.

Baumann, K. -H., Andruleit, H. and Samtleben, C.: Coccolithosphores in the Nordic Seas: Comparison of living communities with surface sediment assemblages, Deep-Sea Res. II, 47, 1743-1772, 2000.

Beaufort, L. and Heussner, S.: Seasonal dynamics of calcareous nannoplankton on a West European continental margin: the Bay of Biscay, Mar. Micropaleontol., 43, 27-55, 2001.

Belt, S. T., Massé, G., Rowland, S. J., Poulin, M., Michel, C. and LeBlanc, B.: A novel chemical fossil of palaeo sea ice: IP25, Org. Geochem., 38, 16-27, 2007.

Berben, S., Husum, K., Cabedo-Sanz, P. and Belt, S.: Holocene sub-centennial evolution of Atlantic water inflow and sea ice distribution in the western Barents Sea, Clim. Past Discuss., 9, 4893-4938, 2013.

Bianchi, G. G. and McCave, I. N.: Holocene periodicity in North Atlantic climate and deep-ocean flow south of Iceland, Nature, 397, 515–517, 1999.

Billard, C. and Inouye, I*.:* What is new in coccolithophore biology? In Coccolithophores: From Molecular Processes to Global Impact, 1–31, (Eds.) H. R. Thierstein and J. R. Young, Berlin, Springer, 2004*.*

Birgel, D. and Ruediger, S*.:* Northern Fram Strait and Yermak Plateau: distribution, variability and burial of organic carbon and paleoenvironmental implications. In: (Eds.) Stein, R. and Macdonald, R. W., The Organic Carbon Cycle in the Arctic Ocean, Springer Verlag, Berlin, Heidelberg, New York, 279-294, 2004.

Birks, C. J. A. and Koc, N.: A high-resolution diatom record of late-Quaternary sea-surface temperatures and oceanographic conditions from the eastern Norwegian Sea, Boreas, 31, 323–344, 2002.

Bischof, J. F.: The decay of the Barents ice sheet as documented in nordic seas ice-rafted debris, Mar. Geol., 117, 35-55, 1994.

Bjune, A. E., Seppä, H. and Birks, H. J. B.: Quantitative summer-temperature reconstructions for the last 2000 years based on pollen-stratigraphical data from northern Fennoscandia, J. Paleolimnol., 41, 43-56, 2009.

Blindheim, J., Borovkov, V., Hansen, B., Malmberg, S. Aa., Turrell, W. R. and Østerhus, S.: Upper layer cooling and freshening in the Norwegian Sea in relation to atmospheric forcing, Deep-Sea Res. I, 47, 655-680, 2000.

Blindheim, J. and Østerhus, S.: The Nordic seas, main oceanographic features, in: The Nordic Seas: an integrated perspective Oceanography, Climatology, Biochemistry and Modelling, Drange, H., Dokken, T., Furevik, T., Gerdes, R., Berger, W., Geophys. Monogr. Ser., 158, 11-37, 2005.

Bond, G., Showers, W., Cheseby, M., lotti, R., Almasi, P., deMenocal, P., Priore, P., Cullen, H., Hajdas, I. and Bonani, G.: A pervasive millenial-scale cycle in North Atlantic Holocene and glacial climates, Science, 278, 1257-1266, 1997.

Bond, G., Kromer, B., Beer, J., Muscheler, R., Evans, M. N., Showers, W., Hoffmann, S., Lotti-Bond, R., Hajds, I. and Bonani, G.: Persistent solar influence on North Atlantic climate during the Holocene, Science, 294, 2130-2136, 2001.

Bonnet, S., de Vernal, A., Hillaire-Marcel, C., Radi, T. and Husum, K.: Variability of sea-surface temperature and sea-ice cover in the Fram Strait over the last two millennia, Mar. Micropaleontol., 74, 59-74, 2010.

Bown, P.: Calcareous Nannofossil Biostratigraphy, British Micropalaeontological Society Publication Series, Chapman and Hall, Kluwer Academic, London, 1998.

Boyer, T. P., Antonov, J. I., Baranova, O. K., Garcia, H. E., Johnson, D. R., Locarnini, R. A., Mishonov, A. V., O'Brien, T. D., Seidov, D., Smolyar, I. V. and Zweng, M. M.: World Ocean Database 2009, NOAA Atlas NESDIS 66, Ed. S. Levitus, U.S. Gov. Printing Office, Wash., D.C., 216, 2009.

Buch, E.: A monograph on the physical oceanography of the Greenland waters, Danish Meteorological Institute Scientific Report 00-12, Greenland Fisheries Research Insitute publication, 15, 0-244, 1990.

Bujak, J. P.: Cenozoic Dinoflagellate Cysts and Acritarchs from the Bering Sea and Northern North Pacific, DSDP Leg 19, Micropaleontology, 30, 180-212, 1984.

Burenkov, V. I., Kopelevich, O. V., Rat'kova, T. N. and Sheberstov, S. V.: Satellite Observations of the Coccolithophorid Bloom of the Barents Sea, Oceanology, 51, 766-774, 2011.

Cabedo-Sanz, P., Belt, S. T., Knies, J. and Husum, K.: Identification of contrasting seasonal sea ice conditions during the Younger Dryas, Quaternary Sci. Rev., http://dx.doi.org/10.1016 /j.quascirev.2012.10.028, 2012.

Cachão, M. and Moita, M. T.: Coccolithus pelagicus, a productivity proxy related to moderate fronts off Western Iberia, Mar. Micropaleontol., 39, 131-155, 2000.

Calvo, E., Grimalt, J. and Jansen, E.: High resolution U^{k}_{37} sea surface temperature reconstruction in the Norwegian Sea during the Holocene, Quaternary Sci. Rev., 21, 1385-1394, 2002.

Carmack, E., Barber, D., Christensen, J., Macdonald, R., Rudels, B. and Sakshaug, E.: Climate variability and physical forcing of the food webs and the carbon budget on panarctic shelves, Prog. Oceanogr., 71, 2-4, 145-181, 2006.

Carstens, J., Hebbeln, D. and Wefer, G.: Distribution of planktic foraminifera at the ice margin in the Arctic (Fram Strait), Mar. Micropaleontol., 29, 257-269, 1997.

Charalampopoulou, A., Poulton, A. J., Tyrrell, T. and Lucas, M. I. : Irradiance and pH affect coccolithophore community composition on a transect between the North Sea and the Arctic Ocean, Mar. Eco. Progr. Ser., 431, 25-43, 2011.

Cokelet, E. D., Tervalon, N., and Bellingham, J. G.: Hydrography of the West Spitsbergen Current, Svalbard branch: Autumn 2001, J. Geophys. Res., 113, C01006, doi: 10.1029/2007JC004150, 2008.

Comiso, J. C., Parkinson, C. L., Gersten, R. and Stock, L.: Accelerated decline in the Arctic sea ice cover, Geophys. Res. Lett., 35, L01703, 2008.

Cook, E. R.: Multi-proxy reconstructions of the North Atlantic Oscillation (NAO) index: A critical review and a new well-verified winter NAO index reconstruction back to AD 1400, AGU, Geophys. Monogr., 134, in: The North Atlantic Oscillation: Climatic Significance and Environmental Impact, Hurrell, J.W., Kushnir, Y., Ottersen, G., Visbeck, M. (Eds.), American Geophysical Union,Washington, DC, 1-36, 2003.

Cronin, T. M., Thunell, R., Dwyer, G. S., Saenger, C., Mann, M. E., Vann, C. and Seal, R. R.: Multiproxy evidence of Holocene climate variability from estuarine sediments, eastern North America, Paleoceanography, 20, PA4006, doi: 10.1029/2005PA001145, 2005.

Dahl-Jensen, D., Mosegaard, K., Gundestrup, N., Clow, G. D., Johnson, S. J., Hansen, A. W. and Balling, N.: Past temperatures directly from the Greenland Ice sheet, Science, 282, 268-271, 1998.

Dahl, S. O. and Nesje, A.: A new approach to calculating Holocene winter precipitation by combining glacier equilibriumline altitudes and pine-line limits: a case study from Hardangerjokulen, central southern Norway, The Holocene, 6, 381–398, 1996.

Dale, B.: Cyst formation, sedimentation, and preservation/factors affecting dinoflagellate assemblages in recent sediments from Trondheimsfjord, Norway, Rev.
Palaeobot. Palyno., 22, 39-60, 1976.

Dale, B.: Dinoflagellate resting cysts: ‘benthic plankton’, in: Fryxell, G.A. (Ed.), Survival Strategy of the Algae, Cambridge University Press, Cambridge, 69–136, 1983.

Dale, B.: Dinoflagellate cyst ecology: modeling and geological applications, in: Jansonius, J., McGregor, D.C. (Eds.), Palynology: Principles and Applications, 3, American Association of Stratigraphic Palynologists Foundation, Dallas, TX, 1249- 1275, 1996.

Dale, B., Thorsen, T. A. and Fjellsaa, A.: Dinoflagellate cysts as indicators of cultural eutrophication in the Oslofjord, Norway, Estuar. Coast. Shelf S., 48, 371-382, 1999.

Dale, A. L. and Dale, B.: Dinoflagellate contributions to the open ocean sediment flux, in: B. Dale and A.L. Dale (Editors), Ocean Biocoenosis Series, 5: Dinoflagellate Contributions to the Deep Sea. Woods Hole Oceanographic Institution, Woods Hole, 45-73, 1992.

D’Andrea, W. J., Vaillencourt, D. A., Balascio, N. L., Werner, A., Roof, S. R., Reteller, M. and Bradley, R. S.: Mild Little Ice Age and unprecedented recent warmth in an 800 year lake sediment record from Svalbard, Geology, 40, P1007, doi:10.1130/G33365.1, 2012.

Dansgaard, W., Johnsen, S. J., Clausen, H. B., Dahl-Jensen, D., Gundestrup, N. S., Hammer, C. U., Hvidberg, C. S., Steffensen, J. P., Sveinbörnsdottir, A. E., Jouzel, J. and Bond, G.: Evidence for general instability of past climate from a 250-kyr ice-core record, Nature, 364, 218–220, 1993.

Davis, B. A. S., Brewer, S., Stevenson, A. C., Guiot, J. and Data Contibutors: The temperature of Europe during the Holocene reconstructed from pollen data, Quaternary Sci. Rev., 22, 1701-1716, 2003.

De Vernal, A., Turon, L. and Guiot, J.: Dinoflagellate distribution in high-latitude marine environments and quantitative reconstruction of sea-surface salinity, temperature and seasonality, Can. J. Earth Sci., 31, 48-62, 1994.

De Vernal, A., Henry, M. and Bilodeau, G.: Technique de preparation et d'analyse en Micropaleontologie, Les cahiers du GEOTOP 3, unpublished report, Universite du Quebec a Montreal, Montreal, Quebec, Canada, 1996.

De Vernal, A., Rochon, A., Turon, J. L. and Matthiessen, J.: Organic-walled dinoflagellate cysts: Palynological tracers of sea-surface conditions in middle to high latitude marine environments: Geobios, 30, 905-920, 1997.

De Vernal, A., Henry, M., Matthiessen, J., Mudie, P. J., Rochon, A., Boessenkool, K. P., Eynaud, F., Grøsfjeld, K., Guiot, J., Hamel, D., Harland, R., Head, M. J., Kunz-Pirrung, M., Levac, E., Loucheur, V., Peyron, O., Pospelova, V., Radi, T., Turon, J.-L.and Voronina, E.: Dinoflagellate cyst assemblages as tracers of sea-surface conditions in the northern North Atlantic, Arctic and sub-Arctic seas: the new ‘n = 677’ data base and its application for quantitative palaeoceanographic reconstruction, J. Quaternary Sci., 16, 681-698, 2001.

De Vernal, A., Eynaud, F., Henry, M., Hillaire-Marcel, C., Londeix, L., Mangin, S., Matthiessen, J., Marret, F., Radi, T., Rochon, A., Solignac, S. and Turon, J.-L.: Reconstruction of sea-surface conditions at middle to high latitudes of the Northern Hemisphere during the Last Glacial Macimum (LGM) based on dinoflagellate cysts Assemblages, Quaternary Sci. Rev., 24, 897-924, 2005.

De Vernal, A. and Marret, F.: Organic-walled dinoflagellate cysts: tracers of sea-surface conditions. In: proxies in late Cenozoic paleoceanography, developments in marine geology, 1, (Eds.) Hillaire-Marcel C. and de Vernal A., Elsevier, 371-408, 2007.

De Vernal, A.: Dino8 workshop: Quantitative treatments for paleoceanographical reconstructions based on dinocyst assemblages, Dino8 conference, Montŕeal, 2008.

De Vernal, A., Hillaire-Marcel, C., Rochon, A., Fréchette, B., Henry, M., Solignac, S. and Bonnet, S.: Dinocyst-based reconstructions of sea ice cover concentration during the Holocene in the Arctic Ocean, the northern North Atlantic Ocean and its adjacent seas, Quaternary Sci. Rev., 79, 111-121, 2013.

Devillers, R. and de Vernal, A.: Distribution of dinoflagellate cysts in surface sediments of the northern North Atlantic in relation to nutrients content and productivity in surface waters, Mar. Geol., 166, 103-124, 2000.

Dickson, R. R., Meincke, J., Malmberg, S. A. and Lee, A. J.: The “great salinity anomaly” in the northern North Atlantic 1968-1982, Progr. Oceanogr., 20, 103-151, 1988.

Dickson, R., Rudels, B., Dye, S., Karcher, M., Meincke, J. and Yashayaev, I.: Current estimates of freshwater flux through Arctic and subarctic seas, Progr. Oceanogr., 73, 210-230, 2007.

Dmitrenko, O. B., Lukashin, V. N., and Shevchenko, V. P.: Nannoplankton of the Atlantic Ocean from sediment trap samples, Oceanology, 46, 33-49, 2006.

Dmitrenko, I. A., Kirillov, S. A., Tremblay, L. B., Bauch, D., Hölemann, J. A., Krumpen, T. H., Kassens, Wegner, C., Heinemann, G. and Schröder, D.: Impact of the Arctic Ocean Atlantic water layer on Siberian shelf hydrography, J. Geophys. Res., 115, C08010, doi:10.1029/2009JC006020, 2010.

Divine, D. V. and Dick, C.: Historical variability of sea ice edge position in the Nordic Seas, J. Geophys. Res., 111, CO1001, doi:10.1029/2004JC002851, 2006.

Drinkwater, K. F., Belgrano, A., Borja, A., Conversi, A., Edwards, M., Greene, C. H., Ottersen, G., Pershing, A. J. and Walker, H.: The response of marine ecosystems to climate variability associated with the North Atlantic Oscillation. In: Hurrell, J., Kushnir, Y., Ottersen, G., Visbeck, M. (Eds.), The North Atlantic Oscillation, Climatic Significance and Environmental Impact, Geophys. Monogr. Ser., 134, AGU, 211–234, 2003.

Duplessy, J. -C., Ivanova, E., Murdmaa, I., Paterne, M. and Labeyrie, L.: Holocene paleoceanography of the northern Barents Sea and variations of the northward heat transport by the Atlantic Ocean, Boreas, 30, 2-16, 2001.

Dylmer, C. V., Giraudeau, J., Eynaud, F., Husum, K. and de Vernal, A.: Northward advection of Atlantic water in the eastern Nordic Seas over the last 3000 yr, Clim. Past, 9, 1505-1518, doi:10.5194/cp-9-1505-2013, 2013.

Dylmer, C. V., Giraudeau, J., Hanquiez, V. and Husum, K.: The coccolithophores Emiliania Huxleyi and Coccolithus pelagicus: extant populations from the Norwegian-Greenland Sea and Fram Strait, Biogeosciences Discuss., 10, 15077-15106, 2013.

Edwards, L. E.: Dinoflagellates. In: Lipps, J.H. (Ed.), Fossil Prokaryotes and Protists, Blackwell Scientific Publications, Boston, 105-129, 1993.

Eilertsen, H. C.: Spring bloom and stratification, Nature, 363, 24,1993.

Evitt, W. R.: Sporopollenin dinoflagellate cysts: their morphology and and Interpretation, American Association of Stratigraphic Palynologists Foundation, Dallas, TX, 333, 1985.

Fensome, R. A., Taylor, F. J. R., Norris, G., Sarjeant, W. A. S., Wharton, D. I., Williams, G. L.: A classification of fossil and living dinoflagellates, Micropaleontology, Special Paper No. 7, 1-351, 1993.

Fohrmann, H., Backhaus, J. O., Blaume, F., Haupt, B. J., Kämpf, J., Michels, K., Mienert, J., Posewang, J., Ritzrau, W., Rumohr, J., Weber, M. and Woodgate, R.: Modern ocean current-controlled sediment transport in the Greenland-Iceland-Norwegian (GIN) Seas. In: The Northern North Atlantic: A Changing Environment, Schäfer, P., Ritzrau, W., Schlüter, M., and Thiede, J., Springer, Berlin, 81–104, 2001.

Furevik, T., Bentsen, M., Drange, H., Johannessen, J. A., and Korablev, A.: Temporal and spatial variability of the sea surface salinity in the Nordic Seas, J. Geophys. Res., 107 (C12), 8009, doi:10.1029/2001JC001118, 2002.

Furevik, T. and Nilsen, J. E. Ø.: Large-Scale Atmospheric Circulation Variability and its Impacts on the Nordic Seas Ocean Climate - A Review, Geophys. Monogr. Ser., 158, 105-136, 2005.

Furevik, T., Mauritzen, C. and Ingvaldsen, R.: The flow of Atlantic Water to the Nordic Seas and Arctic Ocean. In: Arctic - Alpine Ecosystems and People in a Changing Environment, Ørbæk, J. B., Kallenborn, R., Tombre, I., Hegseth, E. N., Petersen, S. F. and Hoel, A. H. (Eds.), Springer Verlag, 123-146, 2007.

Gaines, G. and Elbrächter, M.: Chapter 6: Heterotrophic nutrition. In: Taylor, F.J.R. (Ed.), The biology of dinoflagellates. Botanical Monographs, 21, Blackwell Scientific Publications, Oxford, 224-268, 1987.

Geisen, M., Young, J., Probert, I., Saez, A., Baumann, K.-H., Bollmann, J., Cros, L., de Vargas, C., Medlin, L. K. and Sprengel, C.: Species level variation in coccolithophores. In: Thierstein, H. R., Young, J. (Eds.), Coccolithophores: From molecular processes to global impact, Springer, Berlin, 327–366, 2004.

Gillett, N. P., Graf, H. F. and Osborn, T. J.: Climate Change and the North Atlantic Oscillation, AGU, Geophys. Monogr., 134. In: The North Atlantic Oscillation: Climatic Significance and Environmental Impact, Hurrell, J. W., Kushnir, Y., Ottersen, G., Visbeck, M. (Eds.), American Geophysical Union,Washington, DC, 1-36, 2003.

Giraudeau, J., Monteiro, P. S. and Nikodemus, K.: Distribution and malformation of living coccolithophores in the northern Benguela upwelling system off Namibia, Mar. Micropaleontol., 22, 93-110, 1993.

Giraudeau, J., Cremer, M., Manthé, S., Labeyrie, L. and Bond, G.: Coccolith evidence for instabilities in surface circulation south of Iceland during Holocene times, Earth Plan. Sci. Lett., 179, 257-268, 2000.

Giraudeau, J., Jennings, A. E. and Andrews, J. T.: Timing and mechanisms of surface and intermediate water circulation changes in the Nordic Seas over the last 10000 cal. years BP: a view from the North Iceland shelf, Quaternary Sci. Rev., 23, 2127-2139, 2004.

Giraudeau, J., Grelaud, M., Solignac, S., Andrews , J. T., Moros, M. and Jansen, E.: Millenial-scale variability in Atlantic water advection to the Nordic Seas derived from Holocene coccolith concentration records, Quaternary Sci. Rev., 29, 1276-1287, 2010.

Graf, H. F., Perlwitz, J. and Kirchner, I.: Northern Hemisphere tropospheric mid-latitude circulation after violent volcanic eruptions, report no. 107, Max-Planck-Institut f̈ur Meteorologie, Hamburg, 1–18, 1993.

Gray, S. T., Graumlich, L. J., Betancourt, J. L. and Pederson, G. T.: A tree-ring based reconstruction of the Atlantic Multidecadal Oscillation since 1567 A.D., Geophys. Res. Lett., 31, L12205, doi:10.1029/2004GL019932, 2004.

Groot, D. E., Sørensen, S. Aa. and Husum, K.: Reconstruction of Atlantic Water variability during the Holocene in the western Barents Sea, Clim. Past Discuss., 9, 4293-4322, 2013.

Grootes, P. M. and Stuiver, M.: Oxygen 18/16 variability in Greenland snow and ice with 10^{-3} to 10^{5}-year time resolution, J. Geophys. Res., 102, 455–26, 1997.

Grøsfjeld, K., Harland, R. and Howe, J.: Dinoflagellate cyst assemblages inshore and ofshore Svalbard reflecting their modern hydrography and climate, Norwegian journal of Geology, 89, 121-134, 2009.

Guan, W. and Gao, K.: Impacts of UV radiation on photosynthesis and growth of the coccolithophore Emiliania huxleyi (Haptophyceae), Environ. Exp. Bot., 67, 502-508, 2010.

Gudmundsson, K.: Long-term variation in phytoplankton productivity during spring in Icelandic waters, ICES, J. Mar. Sci., 55, 635-643, 1998.

Guiot, J.: Methodology of the last climatic cycle reconstruction in France from pollen Data, Palaeogeogr. Palaeocl., 80, 49-69, 1990.

Hald, M., Andersson, C., Ebbesen, H., Jansen, E., Klitgaard-Kristensen, D., Risebrobakken, B., Salomonsen, G. R., Sarnthein, M., Sejrup, H. P. and Telford, R. J.: Variations in temperature and extent of Atlantic Water in the northern North Atlantic during the Holocene, Quaternary Sci. Rev., 26, 3423-3440, 2007.

Hald, M., Salomonsen, G. R., Husum, K. and Wilson, L. J.: A 2000 year record of Atlantic Water temperature variability from the Malangen Fjord, northeastern North Atlantic, The Holocene, 21, 1049-1059, 2011.

Hansen, B. and Østerhus, S.: North-Atlantic-Nordic Seas exchanges, Prog. Oceanogr., 45, 109-208, 2000.

Harland, R., Pudsey, C. J., Howe, J. A. and Fitzpatrick, M. E. J.: Recent dinoflagellate cysts in a transect from the Falklands through to the Weddell Sea, Antarctica, Palaeontology, 41, 1093-1131, 1998.

Harland, R. and Pudsey, C. J.: Dinoflagellate cysts from sediment traps deployed in the Bellingshausen, Weddell and Scotia seas, Antarctica, Mar. Micropaleontol., 37, 77-99, 1999.

Hass, H. C., Andruleit, H., Baumann, A., Baumann, K.-H., Kohly, A., Jensen, S., Matthiessen, J., Samtleben, C., Schäfer, P., Schröder-Ritzrau, A. and Thiede, J.: The potential of synoptic plankton analyses for paleoclimatic investigations: Five plankton groups from the

Holocene Nordic Seas. In: The Northern North Atlantic: a changing environment, Schäfer, P., Ritzrau, W., Schlüter, M., and Thiede, J. (Eds.), Springer-Verlag, Berlin, 291-318, 2001.

Hatun, H., Sando, A. B., Drange, H., Hansen, B. and Valdimarsson, H.: Influence of the Atlantic subpolar gyre on the thermocline circulation, Science, 309, 1841-1844, 2005.

Head, M. J.: Modern dinoflagellate cysts and their biological affinities. In: Jansonius, J., McGregor, D.C. (Eds.), Palynology: Principles and Applications, vol. 3. American Association of Stratigraphic Palynologists Foundation, Dallas, TX, 1197-1248, 1996.

Head, M. J., Harland, R. and Matthiessen, J.: Cold marine indicators of the late Quaternary: the new dinoflagellate cyst genus Islandinium and related morphotypes, J. Quaternary Sci., 16, 621-636, 2001.

Hebbeln, D., Henrich, R. and Baumann, K. -H.: Paleoceanography of the Last Interglacial/ Glacial Cycle in the Polar North Atlantic, Quaternary Sci. Rev., 17, 125-153, 1998.

Hegseth. E. N. and Sundfjord, A.: Intrusion and blooming of Atlantic phytoplankton species in the high Arctic, J. Mar. Syst., 74, 108-119, 2008.

Helland P.: Temperature and salinity variations in the upper layers at Ocean Weather Ship M (66°N 2°E), Aarbok for Universitetet i Bergen 1963, Matematisk-Naturvitenskaplig Serie, 16, 1–26, 1963.

Hemming, S. R.: Heinrich events: Massive late Pleistocene detritus layers of the North Atlantic and their global climate imprint, Rev. Geophys., 42, RG1005, doi:10.1029/2003RG 000128, 2004.

Herrle, J. O. and Bollmann, J.: Accuracy and reproducibility of absolute nannoplankton abundances using filtration techniques in combination with a rotary splitter, Mar. Micropaleontol., 53, 389-404, 2004.

Hirche, H. J. , Baumann, M. E. M. , Kattner, G. and Gradinger, R.: Plankton distribution and the impact of copepod grazing on primary production in Fram Strait, Greenland Sea, J. Mar. Syst., 2 , 477-494, 1991.

Hopkins, T. S.: The GIN sea—a synthesis of its physical oceanography and literature review 1972–1985, Earth-Sci. Rev., 30, 175–318, 1991.

Hughen, K. A., Baillie, M. G. L., Bard, E., Beck, J. W., Bertrand, C. J. H., Blackwell, P. G., Buck, C. E., Burr, G. S., Cutler, K. B., Damon, P. E., Edwards, R. L., Fairbanks, R. G., Friedrich, M., Guilderson, T. P., Kromer, B., McCormac, G., Manning, S., Ramsey, C. B., Reimer, P. J., Reimer, R. W., Remmele, S., Southon, J. R., Stuiver, M., Talamo, S., Taylor, F. W., van der Plicht, J. and Weyhenmeyer, C. E.: Marine04 marine radiocarbon age calibration, 0–26 cal kyr BP, Radiocarbon, 46, 1059–1086, 2004.

Hunt Jr., G. L., Stabeno, P., Walters, G., Sinclair, E., Brodeur, R. D., Napp, J. M. and Bond, N. A.: Climate change and control of the southeastern Bering Sea pelagic Ecosystem, Deep-Sea Res. II, 49, 5821-5853, 2002.

Hunt, G. L. Jr., and Drinkwater, K. F., (Eds.): Ecosystem Studies of Sub-Arctic Seas (ESSAS), Science Plan. GLOBEC Report No.19, VIII, 60p., 2005.

Hurrell, J. W.: Decadal trends in the North Atlantic Oscillation: Regional temperatures and precipitation, Science, 269, 676-679, 1995.

Hurrell, J. W., Kushnir, Y., Ottersen, G. and Visbeck, M.: An overview of the North Atlantic Oscillation, AGU, Geophys. Monogr., 134. In: The North Atlantic Oscillation: Climatic Significance and Environmental Impact, Hurrell, J.W., Kushnir, Y., Ottersen, G., Visbeck, M. (Eds.), American Geophysical Union,Washington, DC, 1-36, 2003.

Husum, K.: Cruise report, SciencePub UiT/WARMPAST, Marine geological cruise to East Greenland Margin, 31, 2007.

Husum, K. and Hald, M.: Arctic planktic foraminiferal assemblages: Implications for subsurface temperature reconstructions, Mar. Micropaleontol., 96-97, 38-47, 2012.

Husum, K., Forwick, M. and Laberg, J. S.: Marine Geological Cruise report, AMGG GEO-8144/3144, West Svalbard – Fram Strait – East Greenland, 44 p., 2011.

Ingvaldsen, R. B.: Width of the North Cape Current and location of the Polar Front in the western Barents Sea, Geophys. Res. Lett., 32, L16603, 2005.

IPCC 2007: Summary for policymakers. In: Solomon S., Qin, D., Manning, M., Chen, Z., Marquis, M., Averyt, K. B., Tignor, M., and Miller, H. L. (Eds.): Climate change 2007: the physical science basis. Contribution of working group I to the Fourth Assessment Report of the Intergovernmental Panel on Climate Change, Cambridge Univ. Press, Cambridge, UK and New York, NY, USA, 2007.

Jackson, M. G., Oskarsson, N., Trønnes, R. G., McManus, J. F., Oppo, D. W., Grönvold, K., Hart, S. R. and Sachs, J. P.: Holocene loess deposition in Iceland: evidence for millennial-scale atmosphere-ocean coupling in the North Atlantic, Geology, 33, 509-512, 2005.

Jakobsen, P. K., Ribergaard, M. H., Quadfasel, D., Schmith, T. and Hughes, C. W.: Near-surface circulation in the northern North Atlantic as inferred from Lagrangian drifters: Variability from the mesoscale to interannual, J. Geophys. Res., 108, C83251, doi : 10.1029/2002JC001554, 2003.

Jennings, A. E., Knudsen, K. L., Hald, M., Hansen, C. V. and Andrews, J. T.: A mid-Holocene shift in Arctic sea-ice variability on the East Greenland Shelf, The Holocene, 12, 49-58, 2002.

Jensen, H. K. B., Knies, J., Finne, T. E. and Thorsnes, T.: MAREANO 2006 – miljøgeokjemiske resultater fra Tromsøflaket, Ingøydjupet og Sørøysundet, NGU-rapport 2007.059, 249 p., 2007.

Jensen, H. K. B., Knies, J., Finne, T. E., and Thorsnes, T.: MAREANO 2008 – miljøgeokjemiske resultater fra havomraaderne utenfor Lofoten - Tromsø, NGU-report 2009.057, 31 p., 2009.

Jensen, H. K. B., Knies, J., Finne, T. E., and Thorsnes, T.: MAREANO 2009 – miljøgeokjemiske resultater fra Eggakanten, NGU-report 2010.016, 31 p., 2010.

Johannessen, O. M.: Brief review of the physical oceanography. In: The Nordic Seas, edited by Hurdle B. G., Springer-Verlag, New York, 103-128, 1986.

Jones, P. D., Jónsson, T. and Wheeler, D.: Extension to the North Atlantic Oscillation using early instrumental pressure observations from Gibraltar and South-West Iceland, Int. J. Climatol., 17, 1433-1450, 1997.

Jones, P. D., Osborn, T. J. and Briffa, K. R.: Pressure-based measures of the North Atlantic Oscillation (NAO): A comparison and an assessement of changes in the strength of the NAO and in its influence on surface climate Parameters, AGU Geophys. Monogr., 134. In: The North Atlantic Oscillation: Climatic Significance and Environmental Impact, Hurrell, J.W., Kushnir, Y., Ottersen, G., Visbeck, M. (Eds.), American Geophysical Union,Washington, DC, 1-36, 2003.

Kaufman, D. S., Ager, T. A., Anderson, N. J., Anderson, P. M., Andrews, J. T., Bartlein, P. J., Brubaker, L. B., Coats, L. L., Cwynar, L. C., Duvall, M. L., Dyke, A. S., Edwards, M. E., Eisner, W. R., Gajewski, K., Geirsdóttir, A., Hu, F. S., Jennings, A. E., Kaplan, M. R., Kerwin, M. W., Lozhkin, A. V., MacDonald, G. M., Miller, G. H., Mock, C. J., Oswald, W. W., Otto-Bliesner, B. L., Porinchu, D. F., Rühland, K., Smol, J. P., Steig, E. J. and Wolfe, B. B.: Holocene thermal maximum in the western Arctic (0-180°W), Quaternary Sci. Rev., 23, 529 – 560, 2004.

Kaufman, D. S., Schneider, D. P., Mckay, N. P., Ammann, C. M., Bradley, R. S., Briffa, K. R., Miller, G. H., Otto-Bliesner, B. L., Overpeck, J. T., Vinther, B. M. and Arctic Lakes 2k Projekt members: Recent warming reverses long-term Arctic cooling, Science, 325, 1236-1239, 2009.

Kinnard, C., Zdanowicz, C. M., Fisher, D. A., Isaksson, E., de Vernal, A. and Thompson, L. G.: Reconstructed changes in Arctic sea ice over the past 1.450 years, Nature, 479, 509-512, 2011.

Koc, N., Jansen, E. and Haflidason, H.: Paleoceanographic reconstruction of surface ocean conditions in the Greenland, Iceland and Norwegian seas through the last 14 kyr based on diatoms, Quaternary Sci. Rev., 12, 115–140, 1993.

Koszalka, I., LaCasce, J. H., Orvik, K. A. and Mauritzen, C.: Surface circulation in the Nordic Seas from clustered drifters, Deep-Sea Res. I, 58, 468-485, 2011.

Kwok, R., Cunningham, G. F. and Pang, S. S.: Fram Strait sea-ice outflow, J. Geophys. Res., 109, C01009, doi:10.1029/2003JC001785, 2004.

Kwok, R.: Outflow of Arctic Ocean Sea Ice into the Greenland and Barents Seas: 1979–2007, J. Climate, 22, 2438-2457, 2009.

Laberg, J. S., Vorren, T. O., Mienert, J., Bryn, P. and Lien, R.: The Trænadjupet Slide: A large slope failure affecting the continental margin of Norway 4,000 years ago, Geo-Mar Lett, 22, 19-24, 2002.

Leinebø, I. B.: Caesium-137 (^{137}Cs) in sediment cores from the Norwegian Sea – including lead-210 (^{210}Pb) dating and comparison with organic contamination levels, Thesis in Environmental Chemistry, Department of Chemistry, University of Bergen, Norway, 2011.

Loeng, H.: A review of the sea ice conditions of the Barents Sea and the area west of Spitsbergen. Fisken og Havet 1979, 2, 29–75, (in Norwegian with English abstract), 1979.

Loeng, H.: Features of the physical oceanographic conditions of the Barents Sea, 5-18. In: Sakshaug, E.. Hopkins, C. C. E., and Britsland, N. A. (eds.): Proceedings of the Pro Mare Symposium on Polar Marine Ecology, Trondheim, 12-16 May 1990, Polar Res., 10, 1, 1991.

Loeng, H. and Drinkwater, K.: An overview of the ecosystems of the Barents and Norwegian Seas and their response to climate variability, Deep-Sea Res. II, 54, 2478-2500, 2007.

Lubinski, D. J., Forman, S. L. and Miller, G. H.: Holocene glacier and climate fluctuations on Franz Josef Land, Arctic Russia, 80°N, Quaternary Sci. Rev., 18, 85-108, 1999.

Lund, D. C., Lynch-Stieglitz, J., and Curry, W. B.: Gulf Stream density structure and transport during the past millenium, Nat. Lett., 444, 601-604, 2006.

Luterbacher, J., Xoplaki, E., Dietrich, D., Jones, P. D., Davies, T. D., Portis, D., Gonzalez-Rouco, J. F., von Storch, H., Gyalistras, D. and Casty, C. : Extending North Atlantic Oscillation Reconstructions Back to 1500, Atmos. Sci. Lett., 2, 114–124, 2002.

Lutz, M. J., Caldeira, K., Dunbar, R. B. and Behrenfeld, M. J.: Seasonal rhythms of net primary production and particulate organic carbon flux to depth describe the efficiency of biological pump in the global ocean, J. Geophys. Res., 112, C10011, 26, 2007.

Macias-Fauria, M., Grinsted, A., Helama, S., Moore, J., Timonen, M., Martma, T., Isaksson, E. and Eronen, M.: Unprecedented low twentieth century winter sea-ice extent in the Western Nordic Seas since A.D. 1200, Clim. Dynam., 34, 781-795, 2009.

Mangerud, J. and Gulliksen, S.: Apparent radiocarbon ages of recent marine shells from Norway, Spitsbergen, and Arctic Canada, Quaternary Res., 5, 263-273, 1975.

Mangerud, J., Bondevik, S., Gulliksen, S., Hufthammer, A. K. and Hoisaeter, T.: Marine C-14 reservoir ages for 19th century whales and molluscs from the North Atlantic, Quaternary Sci. Rev., 25, 3228–3245, 2006.

Maiti, K., Carroll, J. and Benitez-Nelson, C. R.: Sedimentation and particle dynamics in the seasonal ice zone of the Barents Sea, J. Mar. Syst., 79, 185-198, 2010.

Marret, F., Eiríksson, J., Knudsen, K. L., Turon, J.-L. and Scourse, J. D.: Distribution of dinoflagellate cyst assemblages in surface sediments from the northern and western shelf of Iceland, Rev. Palaeobot. Palynol., 128, 35-53, 2004.

Marret, F. and Zonneveld, K. A. F.: Atlas of modern organic-walled dinoflagellate cyst distribution, Rev. Palaeobot. Palynol., 125, 1-200, 2003.

Marshall, J., Kushnir, Y., Battisti, D., Chang, P., Czaja, A., Dickson, R., Hurrell, J., McCartney, M., Saravanan, R. and Visbeck, M.: North Atlantic Climate Variability: Phenomena impacts and mechanisms, Int. J. Climatol., 21, 1863-1898, 2001.

Masarik, J. and Beer, J.: Simulation of particle fluxes and cosmogenic nuclide production in the Earth's atmosphere, J. Geophys. Res., 104, 12099–12111, 1999.

Matthiessen, J.: Distribution patterns of dinoflagellate cysts and other organic-walled microfossils in recent Norwegian-Greenland Sea sediments, Mar. Micropaleontol., 24, 307-334, 1995.

Matthiessen, J., Baumann, K. H., Schröder-Ritzrau, A., Hass, C., Andruleit, H., Baumann, A., Jensen, S., Kohly, A., Pflaumann, U., Samtleben, C., Schäfer, P. and Thiede, J.: Distribution of calcareous, siliceous and organic-walled planktic microfossils in surface sediments of the Nordic Seas and their relation to surface-water masses. In: The northern North Atlantic: a changing environment, Schäfer, P., Ritzrau, W., Schlüter, M. and Thiede, J. (Eds.), Springer-Verlag, Berlin, 105-127, 2001.

Matthiessen, J., de Vernal, A., Head, M., Okolodkov, Y., Zonneveld, K. and Harland, R.: Modern organic-walled dinoflagellate cysts in Arctic marine environments and their (paleo-) environmental significance, Paläontologische Zeitschrift, 79, 3-51, 2005.

McMinn, A.: Recent Dinoflagellate Cysts from Estuaries on the Central Coast of New South Wales, Australia, Micropaleontology, 37, 269-287, 1991.

Miettinen, A., Koç, N., Hall, I. R., Godtliebsen, F. and Divine, D.: North Atlantic sea surface temperatures and their relation to the North Atlantic Oscillation during the last 230 years, Clim. Dyn., 36, 533-543, 2011.

Miller, G. H., Geirsdòttir, A., Zhong, Y., Larsen, D. J., Otto-Bliesner, B. L., Holland, M. M., Bailey, D. A., Refsnider, K. A., Lehman, S. J., Southon, J. R., Anderson, C., Björnsson, H. and Thordarson, T.: Abrupt onset of the Little Ice Age triggered by volcanism and sustained by sea-ice/ocean feedbacks, Geophys. Res. Lett., 39, L02708, doi:10.1029/2011GL050168, 2012.

Moros, M., Emeis, K., Risebrobakken, B., Snowball, I., Kuijpers, A., McManus, J. and Jansen, E.: Sea surface temperatures and ice rafting in the Holocene North Atlantic: Climate influences on northern Europe and Greenland, Quaternary Sci. Rev., 23, 2113-2126, 2004.

Mudie, P.J.: Circum-Arctic Quaternary and Neogene marine palynofloras: paleoecology and statistical analysis. In: Head, M.J., Wrenn, J.H. (Eds.), Neogene and Quaternary Dinoflagellate Cysts and Acritarchs, American Association of Palynologists Foundation, Dallas, TX, 347-390, 1992.

Mudie, P. J.: Fecal Pellets. Pellets of dinoflagellate-eating zooplankton. In: J. Jansonius and D.C. McGregor (Editors), Palynology: principles and applications, 3, AASP Foundation, Salt Lake City, 1087-1089, 1996.

Muscheler, R., Joos, F., Beer, J., Müller, P. S. A., Vonmoos, M. and Snowball, I.: Solar activity during the last 1000yr inferred from radionuclide records, Quaternary Sci. Rev., 26, 82–97, 2007.

Müller, J., Massé, G., Stein, R. and Belt, S. T.: Variability of sea ice conditions in the Fram Strait over the past 30.000 years, Nat. Geosci., 2, 772-776, 2009.

Müller, J., Werner, K., Stein, R., Fahl, K., Moros, M. and Jansen, E.: Holocene cooling culminates in sea-ice oscillations in Fram Strait, Quaternary Sci. Rev., 47, 1-14, 2012.

Mysterud, A., Stenseth, N. C., Yoccoz, N. G., Ottersen, G. and Langvatn, R.: The response of terrestrial ecosystems to climate variability associated with the North Atlantic Oscillation, AGU Geophys. Monogr., 134. In: The North Atlantic Oscillation: Climatic Significance and Environmental Impact, Hurrell, J.W., Kushnir, Y., Ottersen, G., Visbeck, M. (Eds.), American Geophysical Union,Washington, DC, 1-36, 2003.

Navarro-Rodriguez, A., Belt, S. T., Knies, J. and Brown, T. A.: Mapping recent sea ice conditions in the Barents Sea using the proxy biomarker IP_{25}: implications for paleo sea ice reconstructions, Quaternary Sci. Rev., 79, 26-39, 2012.

Nesje, A. and Dahl, S. O.: 'The Little Ice Age'—only temperature?, The Holocene, 13, 139–145, 2003.

Nesje, A., Kvamme, M., Rye, N. and Løvlie, R.: Holocene glacial and climate history of the Jostedalsbreen region, western Norway; evidence from lake sediments and terrestrial deposites, Quaternary Sci. Rev., 10, 87-114, 1991.

Nesje, A., Matthews, J. A., Dahl, S. O., Berrisford, M. S. and Andersson, C.: Holocene glacier fluctuations of Flatebreen and winter-precipitation changes in the Jostedalsbreen region, western Norway, based on glaciolacustrine sediment records, The Holocene, 11, 267-280, 2001.

Nesje, A., Dahl, S. O., Thun , T. and Nordli, Ø.: The 'Little Ice Age' glacial expansion in western Scandinavia: summer temperature or winter precipitation?, Clim. Dyn., 30, 789-801, 2008.

Nilsen, J. E. Ø., Gao, Y., Drange, H., Furevik, T. and Bentsen, M.: Simulated North Atlantic-Nordic Seas water mass exchanges in an isopycnic coordinate OGCM, Geophys. Res. Lett., 30, 1536, *doi:*10.1029/2002GL016597, 2003.

O'Brien, S. R., Mayewski, P. A., Meeker, L. D., Meese, D. A., Twickler, M. S. and Whitlow S. I.: Complexity of Holocene climate as reconstructed from a Greenland ice core, Science, 270, 962– 964, 1995.

Okada, H. and McIntyre, A.: Seasonal distribution of modern coccolithophores in the western North Atlantic Ocean, Mar. Biology, 54, 319-328, 1979.

Olsen, A., Johannessen, T. and Rey, F.: On the nature of the factors that control spring bloom development at the entrance to the Barents Sea and their interannual variability, Sarsia, 88, 379-393, 2003.

Olsen, J., Rasmussen, P. and Heinemeier, J. : Holocene temporal and spatial variation in the radiocarbon reservoir age of three Danish fjords, Boreas, 38, 458-470, 2009.

Olsen, J., Anderson, N. J. and Knudsen, M. F.: Variability of the North Atlantic Oscillation over the last 5,200 years, Nat. Geosci., 5, 808-812, 2012.

Olsson, K. A., Jeansson, E., Tanhua, T. and Gascard, J.- C.: The East Greenland Current studied with CFCs and released sulphur hexafluoride, J. Marine Syst., 55, 77-95, 2005.

Orvik, K. A., Skagseth, Ø. and Mork, M.: Atlantic inflow to the Nordic Seas: Current structure and volume fluxes from moored current meters, VM-ADCP and SeaSoar-CTD observations, 1995– 1999, Deep Sea Res. I, 48, 937–957, 2001.

Orvik, K. A. and Niiler, P.: Major pathways of Atlantic water in the northern North Atlantic and Nordic Seas toward Arctic, Geophys. Res. Lett., 29, doi:10.1029/2002GL015002, 2002.

Osborn T. J.: Recent variations in the winter North Atlantic Oscillation, Weather, 61, 353-355, 2006.

Overpeck, J., Webb, T. and Prentice, I. C.: Quantitative interpretation of fossil pollen spectra: dissimilarity coefficients and the method of modern analogs, Quaternary Res., 23, 87-108, 1985.

Overpeck, J., Hughen, K., Hardy, D., Bradley, R., Case, R., Douglas, M., Finney, B., Gajewski, K., Jacoby, G., Jennings, A., Lamoureux, S., Lasca, A., MacDonald, G., Moore, J., Retelle, M., Smith, S., Wolfe, A. and Zielinski, G.: Arctic environmental change of the last four centuries, Science, 278, 1251-1256, 1997.

Parkinson, C. L., Cavalieri, D. J., Gloersen, P. and Zwally, H. J.: Arctic sea ice extents, areas and trends, 1978–1996, J. Geophys. Res-Oceans, 104, 20837–20856, 1999.

Pauling, A., Luterbacher, J., Casty, C. and Wanner, H.: Five hundred years of gridded high-resolution precipitation reconstructions over Europe and the connection to large-scale circulation, Clim. Dyn., doi:10.107/s00382-005-0090-8, 2005.

Peinert, R., Antia, A., Bauerfeind, E., Bodungen, B. V., Haupt, O., Krumbholz, M., Peeken, I., Ramseier, R. O., Voss, M. and Zeitzschel, B.: Particle flux variability in the Polar and Atlantic biogeochemical provinces of the Nordic Seas. In: The Northern North Atlantic: a changing environment, Schäfer, P., Ritzrau, W., Schlüter, M., and Thiede, J. (Eds.), Springer-Verlag, Berlin, 53-68, 2001.

Penaud, A., Eynaud, F., Turon, J. L., Blamart, D., Rossignol, L., Marret, F., Lopez-Martinez, C., Grimalt, J. O., Malaizé, B. and Charlier, K.: Contrasting paleoceanographic conditions off Morocco during Heinrich events (1 and 2) and the Last Glacial Maximum, Quaternary Sci. Rev., 29, 1923–1939, doi:10.1016/j.quascirev.2010.04.011, 2010.

Penaud, A., Eynaud, F., Voelker, A., Kageyama, M., Marret, F., Turon, J. L., Blamart, D., Mulder, T. and Rossignol, L.: Assessment of sea surface temperature changes in the Gulf of

Cadiz during the last 30 ka: implications for glacial changes in the regional hydrography, Biogeosciences, 8, 2295-2316, 2011.

Porter, S. C. and Denton, G. H.: Chronology of neoglaciation in the North American Cordillera, Am. J. Sci., 265, 177–210, 1967.

Poulain, P. M., Warn-Varnas, A. and Niiler, P. P.: Near-surface circulation of the Nordic Seas as measured by Lagrangian drifters, J. Geophys. Res., 101, 18237– 18258, 1996.

Pinto, J. G. and Raible, C. C.: Past and recent changes in the North Atlantic Oscillation, WIREs Clim. Change, 3, 79-90, 2012.

Quinn, P. S., Sáez, A., Baumann, K.-H., Steel, B. A., Sprengel, C. and Medlin, L. K.: Coccolithophorid biodiversity: evidence from the cosmopolitan species Calcidiscus leptoporus. In: Thierstein, H., Young, J.R. (Eds.), Coccolithophores: From Molecular Processes to Global Impact, 299–326, 2004.

Radi, T. and de Vernal, A. : Dinocysts as proxy of primary productivity in mid-high latitudes of the Northern Hemisphere, Mar. Micropaleontol., 68, doi: 10.1016/ j.marmicro.2008.01.012., 84-114, 2008.

Rahmstorf, S.: Thermohaline Ocean Circulation. In: Encyclopedia of Quaternary Sciences, (Ed.) Elias, S. A., Elsevier, Amsterdam, 2006.

Ramseier, R. O., Garrity, C. and Martin, T.: An overview of sea-ice conditions in the Greenland Sea and the relationship of oceanic sedimentation to the ice regime. In: The northern North Atlantic: a changing environment, Schäfer, P., Ritzrau, W., Schlüter, M., and Thiede, J. (Eds.), Springer-Verlag, Berlin, 105-127, 2001.

Reimer, P. J.: IntCal09 and Marine09 radiocarbon age calibration curves, 0–50,000 years cal BP, Radiocarbon, 51, 1111–1150, 2009.

Reimer, P. J. and Reimer, R. W.: A marine reservoir correction database and on-line interface, Radiocarbon, 43, 461–463, 2001.

Reimer, P. J., Baillie, M. G. L., Bard, E., Bayliss, A., Beck, J. W., Bertrand, C. J. H., Blackwell, P. G., Buck, C. E., Burr, G. S., Cutler, K. B., Damon, P. E., Edwards, R. L., Fairbanks, R. G., Friedrich, M., Guilderson, T. P., Hogg, A. G., Hughen, K. A., Kromer, B., McCormac, G., Manning, S., Ramsey, C. B., Reimer, R. W., Remmele, S., Southon, J. R., Stuiver, M., Talamo, S., Taylor, F. W., van der Plicht, J. and Weyhenmeyer, C. E.: IntCal04 terrestrial radiocarbon age calibration, 0–26 cal kyr BP, Radiocarbon, 46, 1029–1058, 2004.

Ribergaard, M. H.: Koblingen mellem klima, hydrografi og rekruttering af fiskeressourcer ved Vestgrønland, Danmarks Meteorologiske Institut (DMI), Center for Marine Forecasting, Vejret, 104, 1-20, 2005.

Richter, T. O., S. van der Gaast, B. Koster, A. Vaars, R. Gieles, H. C. de Stigter, H. de Haas and T. C. E. van Weering: The Avaatech XRF Core Scanner: Technical description and applications to NE Atlantic sediments, in New Techniques in Sediment Core Analysis, (Ed.) G. Rothwell, Spec. Publ. Geol. Soc., 267, 39–50, 2006.

Risebrobakken, B., Jansen, E., Andersson, C., Mjelde, E. and Hevrøy, K.: A high-resolution study of Holocene paleoclimatic and paleoceanographic changes in the Nordic Seas, Paleoceanography, 18, PA1017, doi:10.1029/2002PA000764, 2003.

Risebrobakken, B., Moros, M., Ivanova, E. V., Chistyakova, N. and Rosenberg, R.: Climate and oceanographic variability in the SW Barents Sea during the Holocene, The Holocene, 20, 609-621, 2010.

Rochon, A., de Vernal, A., Turon, J.-L., Matthiessen, J. and Head, M. J.: Distribution of recent dinoflagellate cysts in surface sediments from the North Atlantic Ocean and adjacent seas in relation to sea-surface parameters, AASP Contribution Series, Dallas, Texas, American Association of Stratigraphic Palynologists Foundation, 1999.

Rost, B. and Riebesell, U.: Coccolithophores and the biological pump: responses to environmental changes. In: Coccolithophores – From Molecular Processes to Global Impact. H.R. Thierstein, J. R. Young (eds.), Springer, New York, 76-99, 2004.

Rumohr, J., Blaume, F., Erlenkeuser, H., Fohrmann, H., Hollender, F.-J., Mienert, J. and Schäfer-Neth, C.: Records of processes of near-bottom sediment transport along the Norwegian-Greenland Sea margins during Holocene and late Weichselian, in: The Northern North Atlantic: A Changing Environment, Schäfer, P., Ritzrau, W., Schlüter, M. and Thiede, J., Springer, Berlin, 81–104, 2001.

Rüther, D. C., Bjarnadòttir, L. R., Junttila, J., Husum, K., Rasmussen, T. L., Lucchi, R. G. and Andreassen, K.: Pattern and timing of the northwestern Barents Sea Ice Sheet deglaciation and indications of episodic Holocene deposition, Boreas, 41, 494-512, 2012.

Saloranta, T. M. and Svendsen, H.: Across the Arctic front west of Spitsbergen: high-resolution CTD sections from 1998-2000, Polar Res., 20, 177-184, 2001.

Samtleben, C. and Bickert, T.: Coccoliths in sediment traps from the Norwegian Sea, Mar. Micropaleontol., 16, 39-64, 1990.

Samtleben, C. and Schröder, A.: Coccolithophoriden-Gemeinschaften und Coccolithen-Sedimentation im Europäischen Nordmeer. Zur Abbildung von Planktonzönosen im sediment. Ber Sonderforschungsbereich, 313, Univ Kiel 25, 1-52, 1990.

Samtleben, C. and Schröder, A.: Living cocolithophore communities in the Norwegian-Greenland Sea and their record in sediments, Mar. Micropaleontol., 19, 333-354, 1992.

Samtleben, C., Schaefer, P., Andraluit, H., Baumann, A., Baumann, K. H., Kohly, A., Matthiessen, J. and Schroeder-Ritzrau, A.: Plankton in the Norwegian-Greenland Sea: from living communities to sediment assemblages an actualistic approach, Geol. Rundsch, 84, 108-136, 1995a.

Samtleben, C., Baumann, K.-H. and Schröder-Ritzrau, A.: Distribution, composition and seasonal variation of coccolithophore communities in he nortern North Atlantic, 5th Conference in Salmanc Proceedings, (Eds.) Flores, J. A., and Sierro, F. J., 219-235, Salamanca, 1995b.

Sarnthein, M., Van Kreveld, S., Erlenkeuser, H., Grootes, P. M., Kucera, M., Pflaumann, U. and Schulz, M.: Centennial-to-millennial-scale periodicities of Holocene climate and sediment injections off the western Barents shelf, Boreas, 32, 447–461, 2003.

Schäfer, P., Thiede, J., Gerlach, S., Graf, G., Suess, E. and Zeitzschel, B.: The environment of the northern North Atlantic Ocean: Modern depositional processes and their historical documentation. In: The northern North Atlantic: a changing environment, Schäfer, P., Ritzrau, W., Schlüter, M. and Thiede, J. (Eds.), Springer-Verlag, Berlin, 105-127, 2001.

Schlüter, M., Sauter, E. J., Schulz-Bull, D., Balzer, W. and Suess, E.: Fluxes of organic carbon and biogenic silica reaching the seafloor: a comparison of high northern and southern latitudes of the Atlantic Ocean. In: The Northern North Atlantic: A Changing Environment, Schäfer, P., Ritzrau, W., Schlüter, M. and Thiede, J. (Eds.), Springer, Berlin, 225-240, 2001.

Schmittner, A., Chiang, J. C. H. and Hemming, S. R.: Introduction: the Oceans Meridional Ocerturning Circulation, AGU, Geophys. Monogr. Ser., 173, 1-4, 2007.

Schnepf, E. and Elbrächter, M.: Nutritional strategies in dinoflagellates – a review with emphasis on cell biological aspects, European J. Protist., 28, 3-24, 1992.

Schröder-Ritzrau, A., Andruleit, H., Jensen, S., Samtleben, C., Schäfer, P., Matthiessen, J., Hass, C., Kohly, A. and Thiede, J.: Distribution, export and alteration of fossilizable plankton in the Nordic Seas, in: The Northern North Atlantic: A Changing Environment, Schäfer, P., Ritzrau, W., Schlüter, M., and Thiede, J. (Eds.), Springer, Berlin, 81–104, 2001.

Schulz, M. and Paul, A.: Holocene climate variability on centennial-to-millennial time scales: 1. Climate records from the North-Atlantic realm. In: Wefer, G., Berger, W. H., Behre, K.-E. and Jansen, E. (eds.): Climate Development and History of the North Atlantic Realm, 41–54. Springer-Verlag, Berlin, 2002.

Seidenkrantz, M. -S., Roncaglia, L., Fischel, A., Heilmann-Clausen, C., Kuijpers, A. and Moros, M.: Variable North Atlantic climate seesaw patterns documented by a late Holocene marine record from Disko Bugt, West Greenland, Mar. Micropaleontol., 68, 66-83, 2008.

Sejrup, H. P., Haflidason, H. and Andrews, J. T.: A Holocene North Atlantic SST record and regional climate variability, Quaternary Sci. Rev., 30, 3181-3195, 2011.

Serreze, M. C., Maslanik, J. A., Scambos, T. A., Fetterer, F., Stroeve, J., Knowles, K., Fowler, C., Drobot, S., Barry, S. G. and Haran, T. M.: A record minimum arctic sea ice extent and area in 2002, Geophys. Res. Lett., 30, 1110, 2003.

Shuman, B., Bartlein, P. J. and Webb, T.: The magnitudes of millennial- and orbital-scale climate change in eastern North America during the late Quaternary, Quaternary Sci. Rev., 24, 20–21, 2005.

Siesser, W.G.: Calcareous nannoplankton. In: Lipps, J.H. (Ed.), Fossil Prokaryotes and Protists, Blackwell Sci. Public., Boston, 169-201, 1993.

Silva, A., Palma, S. and Moita, M. T.: Coccolithophores in the upwelling waters of Portugal: four years of weekly distribution in Lisbon Bay, Continent. Shelf Res., 28, 2601–2613, 2008.

Skagseth, Ø., Orvik, K. A. and Furevik, T.: Coherent variability of the Norwegian Atlantic Slope Current derived from TOPEX/ERS altimeter data, Geophys. Res. Lett., 31, L14304, 2004.

Skagseth, Ø., Furevik, T., Ingvaldsen, R., Loeng, H., Mork, K. A., Orvik, K. A. and Ozhigin, V.: Volume and heat transports to the Arctic Ocean via the Norwegian and Barents Seas. In: Arctic-Subarctic Ocean Fluxes: Defining the role of the Northern Seas in Climate, Dickson, R., Meincke, J. and Rhines, P. (Eds.), Springer Netherlands, 25-64, 2008.

Skirbekk, K., Klitgaard Kristensen, D., Rasmussen, T., Koç, N. and Forwick, M.: Holocene climate variations at the entrance to a warm Arctic fjord: evidence from Kongsfjorden Trough, Svalbard. In: Howe, J.A., Austin, W.E.N., Forwick, M. and Paetzel, M. (Eds.), Fjords: Depositional Systems and Archives, Geological Society, London, Special Publications, 344, 289-304, 2010.

Slubowska, M. A., Koç, N., Rasmussen, T. L. and Klitgaard-Kristensen, D.: Changes in the flow of Atlantic water into the Arctic Ocean since the last deglaciation: evidence from the northern Svalbard continental margin, 80°N, Paleoceanography, 20, PA4014. doi:10.1029/2005PA001141, 2005.

Smayda, T. J. and Reynolds, C. S.: Strategies of marine dinoflagellate survival and some rules of assembly, J. Sea Res., 49, 95-106, 2003.

Smith Jr., W. O., Baumann, M. E. M., Wilson, D. L. and Aletsee, L.: Phytoplankton biomass and productivity in the marginal ice zone of the Fram Strait during summer 1984, J. Geophys. Res.: Oceans (1978-2012), 92, 6777-6786, 1987.

Smith, W. O. and Brightman, R. I.: Phytoplankton biomass and photosynthetic response during the winter-spring transition in the Fram Strait, J. Geophys. Res., 96, C3, 4549-4554, 1991.

Smyth, T. J., Tyrell, T. and Tarrant, B.: Time series of coccolithophore activity in the Barents Sea, from twenty years of satellite imagery, Geophys. Res. L., 31, L11302, doi:10.1029/2004GL019735, 2004.

Solignac, S., Giraudeau, J. and de Vernal, A.: Holocene sea surface conditions in the western North Atlantic: Spatial and temporal heterogeneities, Paleoceanography, 21, PA2004, doi:10.1029/2005PA001175, 2006.

Solignac, S., de Vernal, A. and Giraudeau, J.: Comparison of coccolith and dinocyst assemblages in the northern North Atlantic: How well do they relate with surface hydrography?, Mar. Micropaleontol., 68, 115-135, 2008.

Solignac, S., Grøsfjeld, K., Giraudeau, J. and de Vernal, A.: Distribution of recent dinocyst assemblages in the western Barents Sea: Norsk Geologisk Tidsskrift, 89, 109-119, 2009.

Sorrel, P., Debret, M., Billeaud, I., Jaccard, S. L., McManus, J. F. and Tessier, B.: Persistent non-solar forcing of Holocene storm dynamics in coastal sedimentary archives: Nat. Geosci., 5, 892-896, 2012.

Sorteberg, A. and Kvingedal B.: Atmospheric forcing on the Barents Sea Winter Ice Extent, J. Climate, 19, 4772-4784, 2006.

Spielhagen, R. F., Werner, K., Aagaard-Sørensen, S., Zamelczyk, K., Kandiano, E., Budeus, G., Husum, K., Marchitto, T. M. and Hald, M.: Enhanced modern heat transfer to the Arctic by Warm Atlantic Water, Science, 331, 450-453, 2011.

Steinsund, P. I. and Hald, M.: Recent calcium carbonate dissolution in the Barents Sea: Paleoceanographic applications, Mar. Geo., 117, 303-316, 1994.

Stockmarr, J.: Tablets with spores used in absolute pollen analysis, Pollen et Spores, 8, 615–621, 1971.

Stuiver, M. and Braziunas, T. F.: Modeling atmospheric ^{14}C influences and ^{14}C ages of marine samples to 10,000 BC, Radiocarbon, 35, 137–189, 1993.

Stuiver, M. and Reimer, P. J.: Extended ^{14}C data base and revised CALIB 3.0 ^{14}C age calibration program, Radiocarbon, 35, 215-230, 1993.

Suess, H. E.: Natural Radiocarbon and the Rate of exchange of carbon dioxide between the atmosphere and the Sea. In: Nuclear Processes in Geologic Settings (Ed.), National Research Council Committee on Nuclear Science (Washington, DC: National Academy of Sciences), University of Chicago Press, Chicago, 52–56, 1953.

Svendsen, J. I. and Mangerud, J.: Holocene glacial and climatic variations on Spitsbergen, Svalbard, The Holocene, 7, 45–57, 1997.

Swift, J. H.: The Arctic Waters. In: Hurdle, B.G. (Eds.): The Nordic Seas, Springer, New York, 129-153, 1986.

Sætre R., Aure J. and Ljøen R. : Wind effects on the lateral extension of the Norwegian Coastal Current, Continent. Shelf Res., 8, 239–253, 1988.

Tarran, G. A., Zubkov, M. V., Sleigh, M. A., Burkill, P. H., and Yallop, M.: Microbial community structure and standing stocks in the NE Atlantic in June and July of 1996, Deep-Sea Res. II, 48, 963–985, 2001.

Thordardottir, Th. and Gudmundsson, K.: Plontusvif (Phytoplankton.). Namsgagnastofnun, Hafrannsoknastofnunin, Reykjavik, 12, 1998.

Tjallingii, R., Röhl, U., Kölling, M. and Bickert, T.: Influence of the water content on X-ray fluorescence corescanning measurements in soft marine sediments, Geochem. Geophys. Geosyst., 8, Q02004, doi:10.1029/2006GC001393, 2007.

Trouet, V., Esper, J., Graham, N. E., Baker, A., Scourse, J. D. and Frank, D. C.: Persistent positive North Atlantic Oscillation mode dominated the Medieval Climate Anomaly, Science, 324, 78-80, 2009.

Tyrrell T. and Merico A.: Emiliania huxleyi: Bloom observations and the conditions that induce them. In: Thierstein H. R. and Young J. R. (Eds.), Coccolithophores - from Molecular Processes to Global Impact, Springer-Verlag, Berlin, 75-97, 2004.

Van Aken, H. M., Budeus, G. and Hähnel, M.: The anatomy of the Arctic Frontal Zone in the Greenland Sea, J. Geophys. Res., 100, 15999–16014, 1995.

Vare, L. L., Massé, G. and Belt, S. T.: A biomarker-based reconstruction of sea ice conditions for the Barents Sea in recent sediments, The Holocene, 20, 637-643, 2010.
Versteegh, G. J. M. and Blokker, P.: Resistant macromolecules of extant and fossil Microalgae, Phycological Res., 52, 325-339, , 2004.

Vinje T.: Barents Sea ice edge variations over the past 400 years. Extended abstract. In: Report of the ACSYS Workshop on sea ice charts of the Arctic—scientific achievements from the first 400 years. WMO/TD, 949, 1998.

Vinje, T.: Anomalies and trends of sea-ice extent and atmospheric circulation in the Nordic Seas during the period 1864-1998, J. Climate, 14, 255-267, 2001.

Visbeck, M., Chassignet, E. P., Curry, R. G., Delworth, T. L., Dickson, R. R. and Krahmann, G.: The Ocean's response to North Atlantic Oscillation variability, AGU Geophys. Monogr., 134. In: The North Atlantic Oscillation: Climatic Significance and Environmental Impact, Hurrell, J.W., Kushnir, Y., Ottersen, G. and Visbeck, M. (Eds.), American Geophysical Union, Washington, DC, 113-146, 2003.

Vogt, C. and Knies, J.: Sediment pathways in the western Barents Sea inferred from clay mineral assemblages in surface sediments, Norwegian Journal of Geology, 89, 41-55, 2009.

Voronina, E., Polyak, L., de Vernal, A. and Peyron, O.: Holocene variations of sea-surface conditions in the southeastern Barents Sea, reconstructed from dinoflagellate cyst assemblages, J. Quaternary Sci., 16, 717-726, 2001.

Young, J. R., Bergen, J. A., Bown, P. R., Burnett, J. A., Fiorentino, A., Jordan, R. W., Kleijne, A., van Niel, B. E., Romein, A. J. T. and von Salis, K.: Guidelines for coccolith and calcareous nannofossil terminology, Paleontology, 40, 4, 875-912, 1997.

Wadhams, P.: The ice cover. In: Hurdle, B.G. (Ed.), The Nordic Seas. Springer, New York, 21–84, 1986.

Wanamaker Jr., A. D., Butler, P. G., Scourse, J. D., Heinemeier, J., Eiŕıksson, J., Knudsen, K. L. and Richardson, C. A.: Surface changes in the North Atlantic meridional overturning circulation during the last millenium, Nat. Commun., 3, 899, doi:10.1038/ncomms1901, 2012.

Wall, D., Dale, B., Lohmann, G. P. and Smith, W. K.: The environmental and climatic distribution of dinoflagellate cysts in modern marine sediments from regions in the North and South Atlantic Oceans and adjacent seas, Mar. Micropaleontol., 2, 121- 200, 1977.

Wang, T., Surge, D. and Walker, K. J.: Seasonal climate change across the Roman Warm Period/Vandal Minimum transition using isotope sclerochronology in archaeological shells and otoliths, southwest Florida, USA, Quaternary International, In Press, 2012.

Wanner, H., Beer, J., Bütikofer, J., Crowley, T. J., Cubasch, U., Flückiger, J., Goosse, H., Grosjean, M., Joos, F., Kaplan, J. O., Küttel, M., Müller, S.A., Prentice, I. C., Solomina, O., Stocker, T. F., Tarasov, P., Wagner, M. and Widmann, M.: Mid- to Late Holocen climate change: an overview, Quaternary Sci. Rev., 27, 1791-1828, 2008.

Wanner, H., Solomina, O., Grosjean, M., Ritz, S. P. and Jetel, M.: Structure and origine of Holocene cold events, Quaternary Sci. Rev., 30, 3109-3123, 2011.
Wassmann, P., Peinert, R. and Smetacek, V.: Patterns of production and sedimentation in the boreal and polar Northeast Atlantic, Pol. Res., 10, 1, 209-228, 1990.

Wassmann, P., Peinert, R. and Smetacek, V.: Patterns of production and sedimentation in the Norwegian coastal zone, the Barents Sea and the Norwegian Sea. In: Wassman P, Heiskanen A-S, Lindahl, O (eds): Sediment trap studies in the Nordic Countries (Symposium Proceedings), Nurmi Print Oy, Nurmijärvi, 137-156, 1991.

Wassmann, P., Reigstad, M., Haug, T., Rudels, B., Carroll, M. L., Hop, H., Gabrielsen, G. W., Falk-Petersen, S., Denisenko, S. G., Arashkevich, E., Slagstad, D. and Pavlova, O.: Food webs and carbon flux in the Barents Sea, Prog. Oceanogr., 71, 232-287, 2006.

Werner, K., Spielhagen, R. F., Bauch, D., Hass, H. C., Kandiano, E. and Zamelczyk, K.: Atlantic Water advection to the eastern Fram Strait – Multiproxy evidence for late Holocene varibility, Palaeogeogr. Palaeocl., 308, 264-276, 2011.

Westbroek, P., Brown, C. W., van Bleijswijk, J., Brownlee, C., Brummer, G. J., Conte, M., Egge, J., Fernandez, E., Jordan, R., Knappersbusch, M., Stefels, J., Veldhuis, M., van der Wal, P. and Young, J.: A model system approach to biological climate forcing. The example of Emiliania Huxleyi, Global Planetary Change, 8, 27-46, 1993.

Wilson, L. J., Hald, M. and Godtliebsen, F.: Foraminiferal faunal evidence of twentieth-century Barents Sea warming, The Holocene, 21, 527-537, 2011.

Winter, A., Miller, T., Kushnir, Y., Sinha, A., Timmermann, A., Jury, M. R., Gallup, C., Cheng, H. and Edwards, R. L.: Evidence for 800 years of North Atlantic multi-decadal variability from a Puerto Rican speleothem, Earth Planet. Sc. Lett., 308, 23-28, 2011.

Wright, P. L.: Recent sediments of the southwestern Barents Sea, Mar. Geo., 16, 51-81, 1974.
Wright, H. E., Kutzbach, J. E., Webb III, T., Ruddiman, W. F., Street-Perrot, E. A., Bartlein, P. J. (Eds.): Global Climates Since the Last Glacial Maximum. University of Minnesota Press, Minneapolis, MN, 1993.

Zaborska, A., Carroll, J., Papucci, C., Torricelli, L., Carroll, M. L., Walkusz-Miotk, J. and Pempkowiak, J.: Recent sedimentation accumulation rates for the western margin of the Barents Sea, Deep-Sea Res. II, 55, 2352-2360, 2008.

Ziveri, P., Kleijne, A., Conte, M. and Weber, J.: Coccolithophorid distribution and alkenone biomarker characterisation from the tropical Equatorial Atlantic, European Geophysical Society (EGS), Nice, XXVI General Assembly, 2001.

Zivery, P., Baumann, K.-H., Böckel, B., Bollmann, J. and Young, J. R.: Biogeography of selected Holocene coccoliths in the Atlantic Ocean. In: Thierstein, H. and Young, J.R. (Eds.), Coccolithophores: From Molecular Processes to Global Impact, 299–326, 2004.

Zonneveld, K. A. F., Brummer, G. A.: Ecological significance, transport and preservation of organic walled dinoflagellate cysts in the Somali Basin, NW Arabian Sea, Deep-Sea Research II, Tropical Studies In Oceanography, 47, 2229-2256, 2000.

Zonneveld, K. A. F., Verstegh, G. J. M. and de Lange, G. J.: Preservation of organic-walled dinoflagellate cysts in different oxygen regimes: a 10,000 year natural experiment, Mar. Micropaleontol., 29, 393-405, 1997.

Zonneveld, K. A. F., Versteegh, G. J. M. and de Lange, G. J.: Paleoproductivity and post-depositional aerobic organic matter decay reflected by dinoflagellate cyst assemblages of the Eastern Mediterranean S1 sapropel, Mar. Geol., 172, 181-195, 2001.

Zonneveld, K. A. F., Marret, F., Versteegh, G. J. M., Bogus, K., Bonnet, S., Bouimetarhan, I., Crouch, E., de Vernal, A., Elshanawany, R., Edwards, L., Esper, O., Forke, S., Grøsfjeld, K., Henry, M., Holzwarth, U., Kielt J.-F. , Kim, S.-Y., Ladouceur, S., Ledu, D., Chen, L., Limoges, A., Londeix, L., Lu S.-H., Mahmoud, M. S., Marino, G., Matsouka K., Matthiessen, J. , Mildenhal, D. C., Mudie, P., Neil, H.L., Pospelova, V., Qi, Y., Radi, T., Richerol, T., Rochon, A., Sangiorgi, F., Solignac, S., Turon, J.-L., Verleye, T., Wang, Y., Wang, Z. and Young, M.: Atlas of modern dinoflagellate cyst distribution based on 2405 data points, Rev. Paleobot. Palynol., 191, 1-197, 2013.

Appendices

Appendix 1: Site Specific CTD's

All figures show depth (m) profiles of temperature (°C) and salinities at (or close to) the site location. Only the CTDs associated with JM09-KA11-GC and HH11-134-BC are from the actual sites, the others are from nearby locations (from http://www.imr.no/forskning/forskningsdata/operasjonelledata)

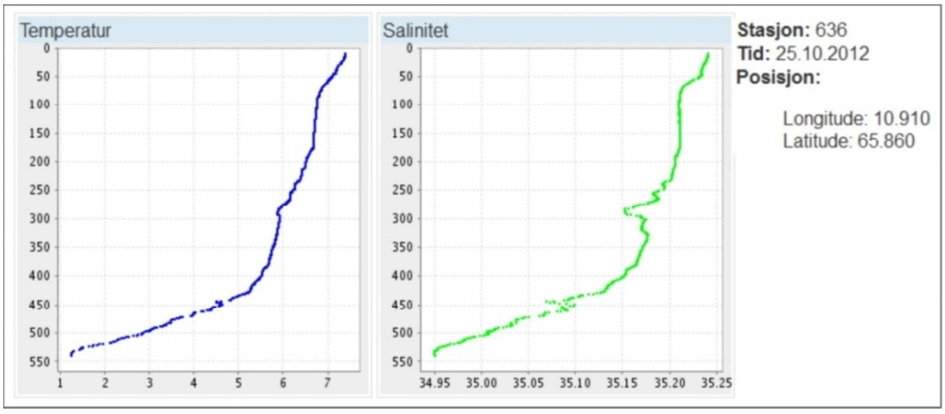

CTD 1: From a location in the viscinity of WOO/SC-3, during fall 2012, showing a clear dominance of AW.

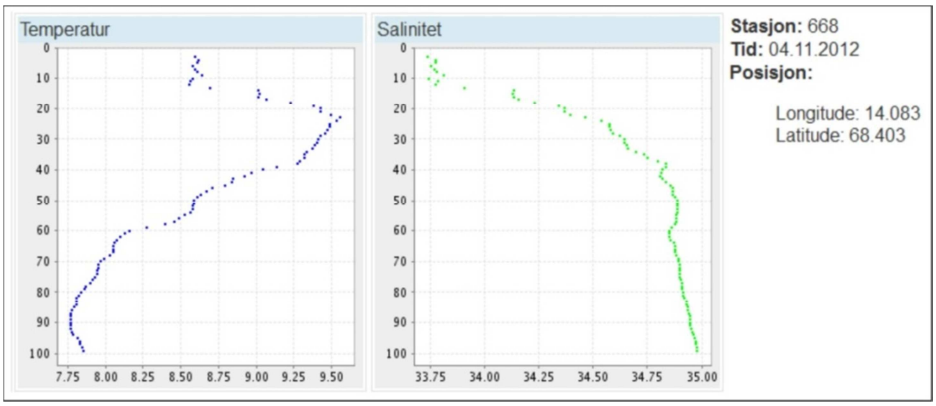

CTD 2: From a location in the vicinity of R248MC010, during fall 2012. The salinity data show a surface layer of low salinity (NCC) at this site, with a dominance in depth of AW.

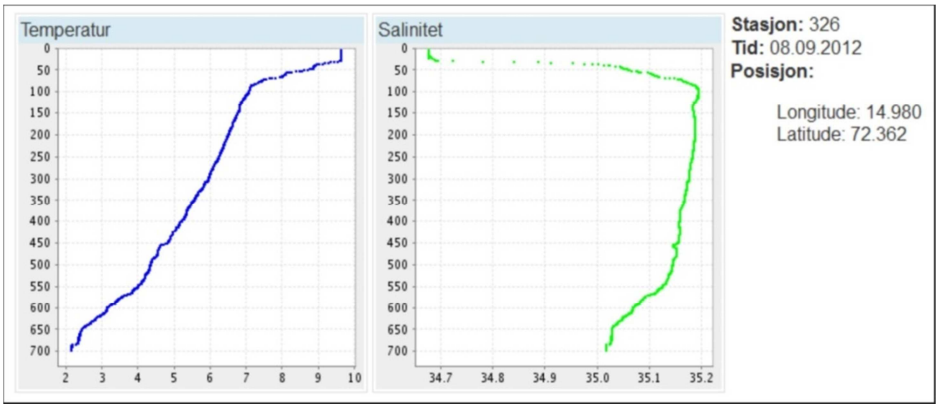

CTD 3: From a site in the viscinity of R406MC032, during summer 2012. The salinity data show the presence of a surface lower salinity layer (NCC) at this site, with a clear dominance in depth of AW.

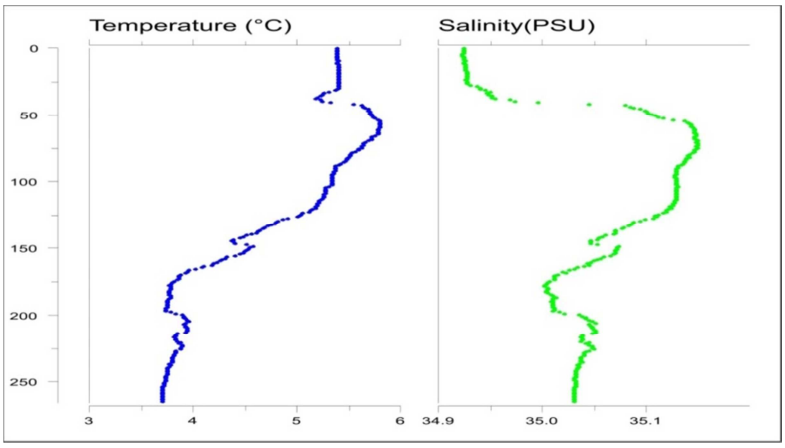

CTD 4: From site JM09-KA11-GC. The salinity data show the dominance of AW with depth (CTD data provided from Denise Rüther).

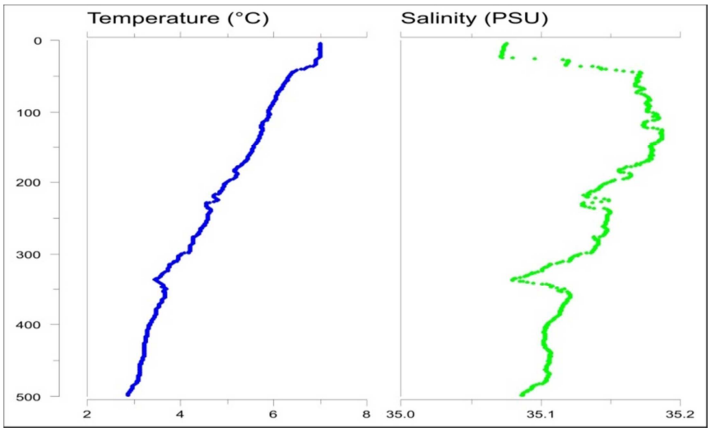

CTD 5: From site HH11-134-BC. The salinity data show the dominance of AW with depth (CTD data collected as part of the 2011 coring cruise, Husum et al. (2011)).

Appendix 2: Introduction to C^{14} and Pb^{210} Dating Methods

The C^{14}-dating method

Carbon (mainly ^{12}C and ^{13}C) is used by plants and animal life forms on Earth to build their hard shells and soft tissues, of which a small part is ^{14}C. The death of the life form closes this addition of ^{14}C and starts the decay clock ticking, with a half life of ~5730 years for ^{14}C (Stuiver and Braziunas, 1993), a "clock" used when applying ^{14}C dating.

The cosmogenic radionuclide ^{14}C isotope is produced in nuclear reactions with nitrogen, as cascades of high-energy galactic cosmic rays (GCR) hits our Earth's atmosphere (Masarik and Beer, 1999; Muscheler et al., 2007). Therefore variability within the production of ^{14}C are indirectly caused by the modulations within the solar wind (and partly the Earths geomagnetic field) produced by the sun, as these winds hampers the access of GCR's to the interior of our solar system (and Earth), causing an inverse relationship between the production of ^{14}C and the strength of the solar wind (Muscheler et al., 2007). The produced ^{14}C oxidizes to CO_2 and stays well mixed within the atmosphere in a gaseous phase for approximately 5 years, as it is finally distributed among the other carbon reservoirs. Changes in atmospheric radiocarbon concentrations can hence naturally be attributed to variations in the ^{14}C production rate and changes in the global carbon cycle (Muscheler et al., 2007).

During the industrial period the human usage of ^{14}C free fossil fuel has lead to an unnatural increase in the atmospheric content of "old" CO_2 causing a reduction in the natural level of ^{14}C, known as the Suess effect (Suess, 1953). The ^{14}C system changed even further as the ^{14}C level increased dramatically with nuclear-bomb testing producing a massive amount of artificial ^{14}C, which, although counteracting the Suess effect, resulted in a uncertain amount of ^{14}C within the atmosphere and hence the term "Before Present - BP" has today been chosen to relate to the year 1950 (Muscheler et al., 2007).

Generally the ocean carbon reservoir is depleted in ^{14}C compared to the atmosphere resulting in an apparent ^{14}C age difference, known as the marine reservoir age R (Stuiver and Braziunas, 1993; Hughen et al., 2004). The marine calibration curve marine09 (Reimer et al., 2004) was constructed to account for this difference, using the terrestrial radiocarbon calibration curve as an input to a global ocean-atmosphere model (Reimer et al., 2004; Hughen et al., 2004; Mangerud et al., 2006; Olsen et al., 2009). Based on this model a globally mean marine reservoir age R was suggested between samples of terrestrial and marine origine of 400 ^{14}C years (Stuiver and Braziunas, 1993), which is obviously a strong simplification as it can vary both spatially and temporally (350-1500 years) (Mangerud and

Gulliksen 1975; Reimer and Reimer, 2001; Mangerud et al., 2006; Olsen et al., 2009), making it necessary to apply an additional offset reservoir age expressed as ΔR. The variations from the global mean reservoir age can possibly be caused by the input of terrestrial organic carbon, dissolved ^{14}C free fossil carbonates (Olsen et al., 2009, and references therein) and old carbon trapped in glaciers and sea-ice.

The ^{210}Pb and ^{137}Cs methods

Lead-210 is one of the daughter isotopes in a naturally existing radioactive decay-series (starting at Uranium-238 with a half life considered near infinite) and because of its short half life of ~22 years, this nuclide is frequently used in dating younger marine sediments (Fig. 3.7).

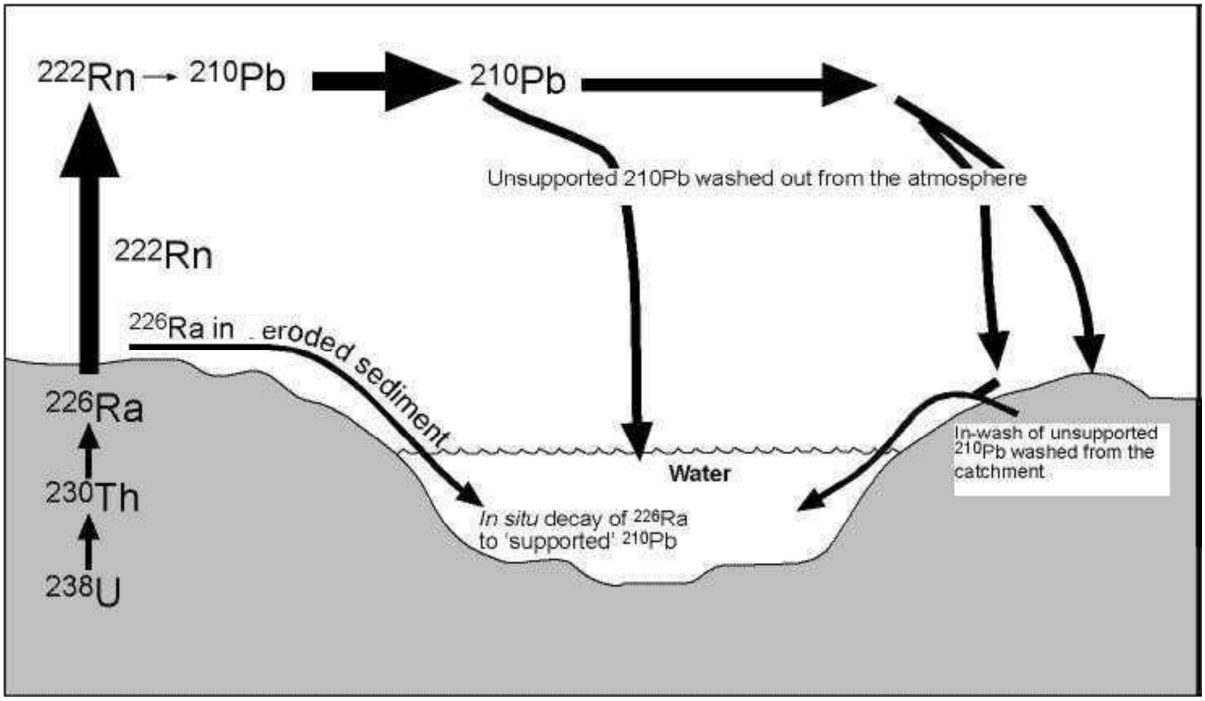

Figure 3.7 : Top; the Uranium-238 decay series showing the major differences in half-lifes of the elements from seconds to near "infinite", http://geoinfo.nmt.edu/resources/uranium/what.html. Bottom; Lead-210 (210Pb) circulation. The noble gas radon-222 (222Rn), escapes from sediments by diffusion. 222Rn decays to the polonium-218 (218Po), which over a period of hours/days fall to the earth with dust and rain. A number of subsequent radioactive decays occur over a period of minutes, and 210Pb is finally produced.

A separate equilibrium is established between the decays in the uranium-series, which means the activity of the different decays will be equal and constant throughout the sediment core. Therefore it does not matter which decay one measures, they will all be the same, provided no disturbances (Leinebø, 2011, and references therein). Measuring the decay of the gamma-emitting ^{226}Ra is therefore done, in order to determine "excess ^{210}Pb".

The measured concentration of ^{210}Pb is the sum of the ^{210}Pb supplied, due to ^{222}Rn-escape (210Pb-unsupported or excess ^{210}Pb) escaping from the earth crust into the atmosphere close to the soil-air interface, and the amount descending from the original ^{238}U (^{210}Pb supported) (Fig. 3.7). The age estimation of the sediment layers is then done by identifying excess ^{210}Pb in each sediment slice, and calculating the age of the layer based on the amount of excess ^{210}Pb, decayed from one layer to the next (Leinebø, 2011 and references therein).

In addition to ^{210}Pb, measurements of ^{137}Cs were conducted on core R248MC010 by Leinebø (2011). The application of ^{137}Cs (half-life of ~30 years) is based on the fact that the element did not exist in nature before the 1940's when the first nuclear weapons were tested (Leinebø, 2011, and references therein). Two peaks are generally important: In 1963 Great Brittani, the Sovjet Union (USSR), and USA signed a partial test-ban treaty, leading to a significant decrease in the global content of ^{137}Cs, a change which today can be observed as a peak on Cs-curves (Leinebø, 2011, and references therein); and the major accident happened at Chernobyl in the USSR in 1986 lead to a release of a huge amount of radioactivity seen as a second peak. ^{137}Cs is a valuable tool to validate recent sediments age models based on ^{210}Pb.

Appendix 3: Taxonomic List

Taxonomic list including all identified taxa of coccoliths, dinocysts, and planktonic foraminifera.

COCCOLITHOPHORES

Calcidiscus leptoporus (Murray and Blackman, 1898) Loeblich and Tappan, 1978
Coccolithus pelagicus (Wallich, 1877) Schiller, 1930
Emiliania huxleyi (Lohmann, 1902) Hay and Mohler, 1967
Gephyrocapsa muellerae Bréhéret, 1978
Syracosphaera spp.

DINOFLAGELLATES (dinocysts) & ACRITARCH

Ataxiodinium choane Reid, 1974
Alexandrium tamarense (Lebour 1925) Balech, 1985
Bitectatodinium tepikiense Wilson, 1973
Brigantedinium spp. Reid, 1977
Echinidinium karaense Head et al., 2001
Echinidinium spp.
Impagidinium aculeatum (Wall 1967) Lentin et Williams, 1981
Impagidinium pallidum Bujak, 1984
Impagidinium patulum (Wall 1967) Stover et Evitt, 1978
Impagidinium sphaericum (Wall 1967) Lentin et Williams, 1981
Impagidinium strialatum (Wall 1967) Stover et Evitt, 1978
Impagdinium spp.
Islandinium? cezare (de Vernal et al. 1989 ex de Vernal in Rochon et al. 1999) Head et al., 2001
Islandinium minutum (Harland et Reid in Harland et al. 1980) Head et al., 2001
Lingulodinium machaerophorum (Deflandre et Cookson 1955) Wall, 1967
Nematosphaeropsis labyrinthus (Ostenfeld 1903) Reid, 1974
Operculodinium centrocarpum sensu Wall et Dale, 1966
Operculodinium centrocarpum sensu Wall et Dale, 1966 - short processes
Pentapharsodinium dalei Indelicato et Loeblich III, 1986
Polykrikos schwartzii Bütschli, 1873
Selenopemphix quanta (Bradford 1975) Matsuoka, 1985
Spiniferites belerius Reid, 1974
Spiniferites bentorii (Rossignol 1964) Wall et Dale, 1970
Spiniferites elongatus Reid, 1974
Spiniferites hyperacanthus (Deflandre et Cookson 1955) Cookson et Eisenack, 1974
Spiniferites membranaceus (Rossignol 1964) Sarjeant, 1970
Spiniferites mirabilis (Rossignol 1967) Sarjeant, 1970
Spiniferites ramosus (Ehrenberg 1838) Mantell, 1854
Spiniferites spp.

Halodinium spp. Bujak, 1984

PLANKTONIC FORAMINIFERA

Globigerina bulloides (d'Orbigny, 1826)
Globigerina falconensis (Blow, 1959)
Globigerinita glutinata (Egger, 1893)
Globigerinita uvula (Ehrenberg, 1861)
Globorotalia inflata (d'Orbigny, 1839)
Globorotalia scitula (Brady, 1882)
Neogloboquadrina pachyderma (Ehrenberg, 1861) sinistral
Neogloboquadrina pachyderma (Ehrenberg, 1861) dextral
Turborotalita quinqueloba (Natland 1838)

Appendix 4: Analogues for MAT (Modern Analogue Technique)

WOO/SC-3

WOO/SC-3															
Depth (cm)	*[ANALOG 1]*	LONG	LATI	[ANALOG 2]	LONG	LATI	[ANALOG 3]	LONG	LATI	[ANALOG 4]	LONG	LATI	[ANALOG 5]	LONG	LATI
20.5	N216	2.66	66.61	G057	-59.78	49.33	A945	-20.83	67.76	N186	3.73	60.63	N214	1.55	66.61
25.5	N186	3.73	60.63	N216	2.66	66.61	G054	-60.17	49.22	N214	1.55	66.61	Z550	30.42	71.42
30.5	G057	-59.78	49.33	N216	2.66	66.61	G052	-60.64	48.51	G061	-58.73	50.12	Z550	30.42	71.42
35.5	N186	3.73	60.63	G057	-59.78	49.33	N216	2.66	66.61	G054	-60.17	49.22	G052	-60.64	48.51
40.5	A945	-20.83	67.76	N216	2.66	66.61	G057	-59.78	49.33	N400	2.07	62.42	N214	1.55	66.61
45.5	N186	3.73	60.63	Z550	30.42	71.42	J311	7.49	71.99	N216	2.66	66.61	G057	-59.78	49.33
50.5	G057	-59.78	49.33	N216	2.66	66.61	N186	3.73	60.63	N214	1.55	66.61	J306	9.27	72.04
55.5	A945	-20.83	67.76	N214	1.55	66.61	G057	-59.78	49.33	N216	2.66	66.61	A983	-17.07	67.58
60.5	N216	2.66	66.61	N214	1.55	66.61	N186	3.73	60.63	G057	-59.78	49.33	G054	-60.17	49.22
70.5	N216	2.66	66.61	A983	-17.07	67.58	N193	-9.31	67	A947	-19.35	67.91	N214	1.55	66.61
65.5	N214	1.55	66.61	N216	2.66	66.61	J311	7.49	71.99	G057	-59.78	49.33	Z550	30.42	71.42
75.5	N216	2.66	66.61	G057	-59.78	49.33	N214	1.55	66.61	L153	-48.38	59.15	N215	2.18	66.61
80.5	N216	2.66	66.61	N214	1.55	66.61	N186	3.73	60.63	G057	-59.78	49.33	J326	5.87	67.69
85.5	N216	2.66	66.61	N214	1.55	66.61	N197	-6.21	67	N186	3.73	60.63	N209	0.02	63.44
90.5	N186	3.73	60.63	Z550	30.42	71.42	G057	-59.78	49.33	G054	-60.17	49.22	G056	-60.8	49.52
95.5	N216	2.66	66.61	N186	3.73	60.63	Z550	30.42	71.42	G057	-59.78	49.33	G052	-60.64	48.51
100.5	N216	2.66	66.61	Z550	30.42	71.42	N185	3.72	60.64	N214	1.55	66.61	G057	-59.78	49.33
105.5	N216	2.66	66.61	J326	5.87	67.69	N214	1.55	66.61	G057	-59.78	49.33	N210	-4.74	65.42
110.5	G052	-60.64	48.51	Z550	30.42	71.42	G057	-59.78	49.33	N216	2.66	66.61	J306	9.27	72.04
115.5	A947	-19.35	67.91	J304	11.14	74.88	N210	-4.74	65.42	N197	-6.21	67	J326	5.87	67.69
120.5	Z550	30.42	71.42	G054	-60.17	49.22	G056	-60.8	49.52	G057	-59.78	49.33	G052	-60.64	48.51
125.5	N186	3.73	60.63	N216	2.66	66.61	G065	-60.03	47.35	G057	-59.78	49.33	G052	-60.64	48.51
130.5	L153	-48.38	59.15	N234	-7.65	65.45	N214	1.55	66.61	N197	-6.21	67	N210	-4.74	65.42
135.5	G057	-59.78	49.33	Z550	30.42	71.42	J285	8.72	78.01	G065	-60.03	47.35	J306	9.27	72.04
140.5	N216	2.66	66.61	N186	3.73	60.63	N209	0.02	63.44	G057	-59.78	49.33	G054	-60.17	49.22
145.5	G057	-59.78	49.33	Z550	30.42	71.42	G054	-60.17	49.22	N216	2.66	66.61	G056	-60.8	49.52
150.5	N216	2.66	66.61	A945	-20.83	67.76	G057	-59.78	49.33	N214	1.55	66.61	N222	3.95	62.75
155.5	N216	2.66	66.61	J326	5.87	67.69	N214	1.55	66.61	N215	2.18	66.61	J311	7.49	71.99
160.5	N186	3.73	60.63	G065	-60.03	47.35	G052	-60.64	48.51	N216	2.66	66.61	G064	-62.54	48.64
165.5	N186	3.73	60.63	G057	-59.78	49.33	A420	-67.92	42.56	C909	-72.69	38.87	C908	-72.72	38.79
170.5	G073	-59.08	46.99	G065	-60.03	47.35	G057	-59.78	49.33	N216	2.66	66.61	G066	-59.88	47.52
175.5	N216	2.66	66.61	G052	-60.64	48.51	G057	-59.78	49.33	J306	9.27	72.04	J326	5.87	67.69
180.5	N216	2.66	66.61	G052	-60.64	48.51	G057	-59.78	49.33	N186	3.73	60.63	J326	5.87	67.69
185.5	N216	2.66	66.61	N186	3.73	60.63	Z550	30.42	71.42	G054	-60.17	49.22	G061	-58.73	50.12
190.5	J286	6.69	78	J326	5.87	67.69	J313	0.66	71.44	J304	11.14	74.88	J285	8.72	78.01
195.5	N216	2.66	66.61	N214	1.55	66.61	J307	11.45	72.14	J326	5.87	67.69	J301	2.91	67.09
200.5	G057	-59.78	49.33	G052	-60.64	48.51	Z550	30.42	71.42	A421	-69.66	42.67	N216	2.66	66.61
205.5	N216	2.66	66.61	N214	1.55	66.61	N215	2.18	66.61	N248	4.23	58.69	N213	1.48	66.67
210.5	N216	2.66	66.61	J326	5.87	67.69	N215	2.18	66.61	N214	1.55	66.61	J306	9.27	72.04
215.5	N216	2.66	66.61	N186	3.73	60.63	N214	1.55	66.61	J326	5.87	67.69	N248	4.23	58.69
220.5	N186	3.73	60.63	N216	2.66	66.61	N215	2.18	66.61	J306	9.27	72.04	G057	-59.78	49.33
225.5	N216	2.66	66.61	N196	-6.59	67.04	Z550	30.42	71.42	J326	5.87	67.69	G057	-59.78	49.33
230.5	N216	2.66	66.61	N214	1.55	66.61	N215	2.18	66.61	J300	3	69.5	N209	0.02	63.44
235.5	G057	-59.78	49.33	N216	2.66	66.61	G052	-60.64	48.51	J306	9.27	72.04	Z550	30.42	71.42
240.5	G052	-60.64	48.51	Z550	30.42	71.42	J306	9.27	72.04	J304	11.14	74.88	J313	0.66	71.44
245.5	N216	2.66	66.61	Z550	30.42	71.42	J326	5.87	67.69	N214	1.55	66.61	N186	3.73	60.63

Table A1 : Analogue list, showing the analogues used by the Modern Analogue Technique for the reconstruction of summer and winter temperatures and salinities as well as sea-ice duration (months/year), within WOO/SC-3.

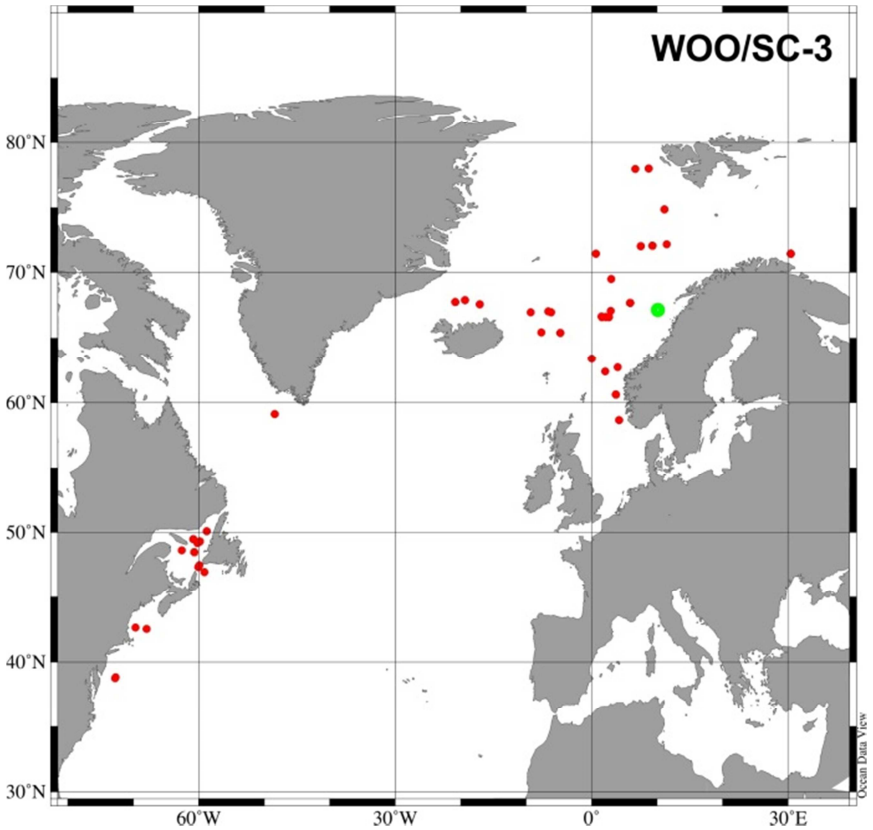

MAP A1: Geographical distribution of all analogues (red dots) applied within the present investigation of core WOO/SC-3 (green dot).

R248MC010

R248MC010															
Depth (cm)	***[ANALOG 1]***	LONG	LATI	**[ANALOG 2]**	LONG	LATI	**[ANALOG 3]**	LONG	LATI	**[ANALOG 4]**	LONG	LATI	**[ANALOG 5]**	LONG	LATI
0.5	N236	-6.79	65.57	J326	5.87	67.69	N195	-7.31	67.08	J298	-3.01	65.5	A699	-10.05	57.03
1.5	G054	-60.17	49.22	G051	-60.64	48.51	G056	-60.8	49.52	Z550	30.42	71.42	G057	-59.78	49.33
2.5	G057	-59.78	49.33	G054	-60.17	49.22	G056	-60.8	49.52	G061	-58.73	50.12	G052	-60.64	48.51
3.5	G1367	-61.5	48.33	G051	-60.64	48.51	A943	-20.31	67.63	A945	-20.83	67.76	A944	-20.5	67.25
4.5	G054	-60.17	49.22	G051	-60.64	48.51	G056	-60.8	49.52	G061	-58.73	50.12	G1367	-61.5	48.33
5.5	G057	-59.78	49.33	A945	-20.83	67.76	N214	1.55	66.61	N216	2.66	66.61	G065	-60.03	47.35
6.5	G1367	-61.5	48.33	G054	-60.17	49.22	G057	-59.78	49.33	A945	-20.83	67.76	A943	-20.31	67.63
7.5	G057	-59.78	49.33	L153	-48.38	59.15	A945	-20.83	67.76	A955	-18.18	67.46	A168	-39.31	59.49
8.5	G056	-60.8	49.52	G061	-58.73	50.12	G054	-60.17	49.22	G052	-60.64	48.51	G065	-60.03	47.35
9.5	G054	-60.17	49.22	G051	-60.64	48.51	G056	-60.8	49.52	G061	-58.73	50.12	G1367	-61.5	48.33
10.5	G1367	-61.5	48.33	G051	-60.64	48.51	G054	-60.17	49.22	G056	-60.8	49.52	G064	-62.54	48.64
11.5	G056	-60.8	49.52	G054	-60.17	49.22	G057	-59.78	49.33	G061	-58.73	50.12	G052	-60.64	48.51
12.5	G054	-60.17	49.22	G056	-60.8	49.52	G052	-60.64	48.51	G061	-58.73	50.12	G051	-60.64	48.51
13.5	G057	-59.78	49.33	Z550	30.42	71.42	G061	-58.73	50.12	G054	-60.17	49.22	G056	-60.8	49.52
14.5	G057	-59.78	49.33	G054	-60.17	49.22	G056	-60.8	49.52	G052	-60.64	48.51	G061	-58.73	50.12
15.5	G054	-60.17	49.22	G056	-60.8	49.52	G061	-58.73	50.12	G051	-60.64	48.51	G052	-60.64	48.51
16.5	G054	-60.17	49.22	G056	-60.8	49.52	N186	3.73	60.63	G051	-60.64	48.51	G057	-59.78	49.33
17.5	G057	-59.78	49.33	G054	-60.17	49.22	G056	-60.8	49.52	G061	-58.73	50.12	G060	-59.46	49.8
18.5	G054	-60.17	49.22	G056	-60.8	49.52	G051	-60.64	48.51	G1367	-61.5	48.33	G061	-58.73	50.12
19.5	G054	-60.17	49.22	G056	-60.8	49.52	G057	-59.78	49.33	G052	-60.64	48.51	G061	-58.73	50.12
20.5	N186	3.73	60.63	G054	-60.17	49.22	G056	-60.8	49.52	Z550	30.42	71.42	N185	3.72	60.64
21.5	G056	-60.8	49.52	G054	-60.17	49.22	G061	-58.73	50.12	G1367	-61.5	48.33	G057	-59.78	49.33
22.5	G054	-60.17	49.22	G056	-60.8	49.52	G057	-59.78	49.33	G052	-60.64	48.51	G061	-58.73	50.12
23.5	G054	-60.17	49.22	G056	-60.8	49.52	G061	-58.73	50.12	Z550	30.42	71.42	G051	-60.64	48.51
24.5	G054	-60.17	49.22	G057	-59.78	49.33	G051	-60.64	48.51	G056	-60.8	49.52	G060	-59.46	49.8
25.5	G1367	-61.5	48.33	G054	-60.17	49.22	G051	-60.64	48.51	G057	-59.78	49.33	G056	-60.8	49.52
26.5	G057	-59.78	49.33	G054	-60.17	49.22	G052	-60.64	48.51	G056	-60.8	49.52	G1367	-61.5	48.33
27.5	G057	-59.78	49.33	G054	-60.17	49.22	G064	-62.54	48.64	G056	-60.8	49.52	G061	-58.73	50.12
28.5	G051	-60.64	48.51	G054	-60.17	49.22	N186	3.73	60.63	N216	2.66	66.61	N209	0.02	63.44
29.5	G052	-60.64	48.51	G054	-60.17	49.22	G056	-60.8	49.52	G057	-59.78	49.33	G061	-58.73	50.12
30.5	G051	-60.64	48.51	G054	-60.17	49.22	G1367	-61.5	48.33	Z539	33.83	69.49	Z550	30.42	71.42
31.5	G054	-60.17	49.22	Z550	30.42	71.42	N186	3.73	60.63	G057	-59.78	49.33	N216	2.66	66.61
32.5	G061	-58.73	50.12	G054	-60.17	49.22	G056	-60.8	49.52	G052	-60.64	48.51	G057	-59.78	49.33
33.5	N216	2.66	66.61	N214	1.55	66.61	A945	-20.83	67.76	G057	-59.78	49.33	N209	0.02	63.44
34.5	G054	-60.17	49.22	G057	-59.78	49.33	G056	-60.8	49.52	G061	-58.73	50.12	N186	3.73	60.63
35.5	G052	-60.64	48.51	G065	-60.03	47.35	G056	-60.8	49.52	G066	-59.88	47.52	G061	-58.73	50.12
36.5	J312	4.99	72.01	J311	7.49	71.99	Z550	30.42	71.42	G051	-60.64	48.51	J308	13.1	72.18
37.5	G052	-60.64	48.51	G066	-59.88	47.52	G057	-59.78	49.33	G065	-60.03	47.35	G054	-60.17	49.22
38.5	G052	-60.64	48.51	G057	-59.78	49.33	N216	2.66	66.61	G054	-60.17	49.22	G056	-60.8	49.52
39.5	N193	-9.31	67	Z550	30.42	71.42	G051	-60.64	48.51	J285	8.72	78.01	N192	-11.66	67.5
40.5	G052	-60.64	48.51	G051	-60.64	48.51	J306	9.27	72.04	G054	-60.17	49.22	J307	11.45	72.14
41.5	N216	2.66	66.61	A945	-20.83	67.76	G057	-59.78	49.33	G052	-60.64	48.51	N214	1.55	66.61
42.5	N216	2.66	66.61	J306	9.27	72.04	G057	-59.78	49.33	N197	-6.21	67	J313	0.66	71.44
43.5	A945	-20.83	67.76	N216	2.66	66.61	A943	-20.31	67.63	G057	-59.78	49.33	L153	-48.38	59.15
44.5	G051	-60.64	48.51	G054	-60.17	49.22	G1367	-61.5	48.33	G056	-60.8	49.52	G057	-59.78	49.33
45.5	G057	-59.78	49.33	G052	-60.64	48.51	G060	-59.46	49.8	A983	-17.07	67.58	G033	-60.72	48.17
46.5	N216	2.66	66.61	A945	-20.83	67.76	G057	-59.78	49.33	G066	-59.88	47.52	C662	-61.69	42.63
47.5	N216	2.66	66.61	N214	1.55	66.61	N186	3.73	60.63	G051	-60.64	48.51	G054	-60.17	49.22
48.5	G052	-60.64	48.51	G061	-58.73	50.12	G057	-59.78	49.33	G056	-60.8	49.52	G054	-60.17	49.22

Table A2: Analogue list, showing the analogues used by the Modern Analogue Technique for the reconstruction of summer and winter temperatures and salinities as well as sea-ice duration (months/year), within R248MC010.

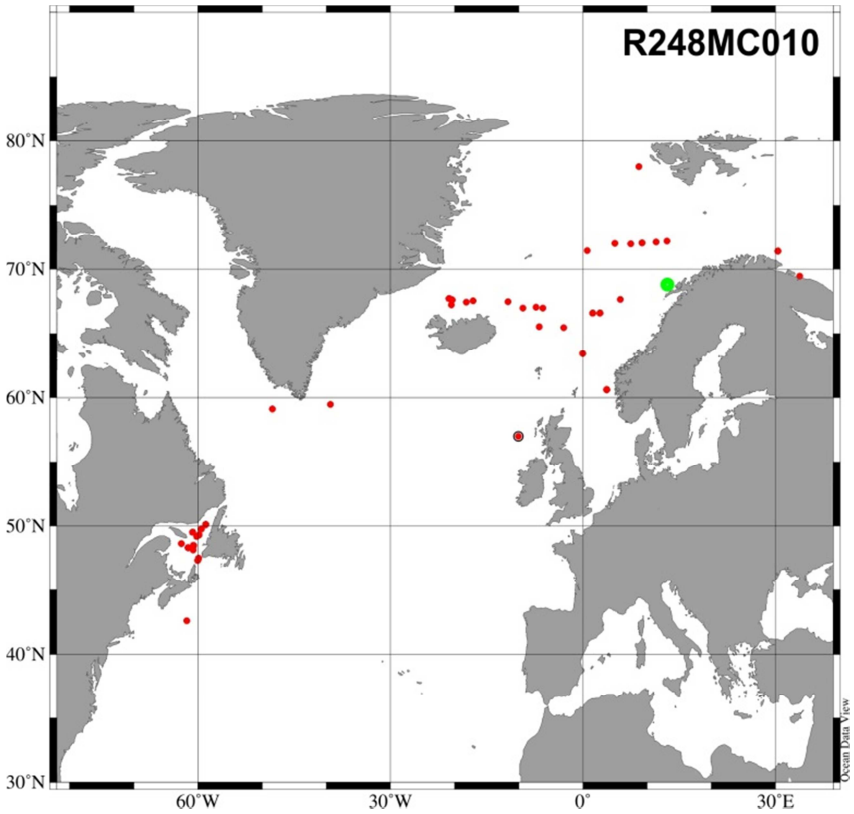

MAP A1: Geographical distribution of all analogues (red dots) applied within the present investigation of core R248MC010 (green dot).

R406MC032

R406MC032															
Depth (cm)	***[ANALOG 1]***	LONG	LATI	**[ANALOG 2]**	LONG	LATI	**[ANALOG 3]**	LONG	LATI	**[ANALOG 4]**	LONG	LATI	**[ANALOG 5]**	LONG	LATI
0.5	G057	-59.78	49.33	Z550	30.42	71.42	J307	11.45	72.14	N185	3.72	60.64	N186	3.73	60.63
1.5	Z550	30.42	71.42	G054	-60.17	49.22	G057	-59.78	49.33	G056	-60.8	49.52	N211	-3.23	65.75
2.5	G057	-59.78	49.33	C666	-61.82	42.92	N185	3.72	60.64	N186	3.73	60.63	C662	-61.69	42.63
3.5	G054	-60.17	49.22	N185	3.72	60.64	G056	-60.8	49.52	Z550	30.42	71.42	N211	-3.23	65.75
4.5	G051	-60.64	48.51	Z550	30.42	71.42	G054	-60.17	49.22	Z539	33.83	69.49	G1367	-61.5	48.33
5.5	N211	-3.23	65.75	N185	3.72	60.64	N212	1.13	66.61	N186	3.73	60.63	Z551	31.97	71.39
6.5	N186	3.73	60.63	N214	1.55	66.61	N185	3.72	60.64	N212	1.13	66.61	N213	1.48	66.67
7.5	N210	-4.74	65.42	Z551	31.97	71.39	A949	-17.75	67.9	A977	-21.78	67.98	A937	-15.38	68.08
8.5	A168	-39.31	59.49	N185	3.72	60.64	N210	-4.74	65.42	N216	2.66	66.61	N214	1.55	66.61
9.5	Z550	30.42	71.42	N210	-4.74	65.42	Z551	31.97	71.39	A936	-15.45	67.91	N216	2.66	66.61
10.5	Z550	30.42	71.42	N185	3.72	60.64	N186	3.73	60.63	N216	2.66	66.61	A936	-15.45	67.91
11.5	Z550	30.42	71.42	N211	-3.23	65.75	N185	3.72	60.64	N186	3.73	60.63	N212	1.13	66.61
12.5	N237	-4.63	65.62	N211	-3.23	65.75	N185	3.72	60.64	N212	1.13	66.61	N214	1.55	66.61
13.5	A977	-21.78	67.98	N211	-3.23	65.75	N185	3.72	60.64	A168	-39.31	59.49	N210	-4.74	65.42
14.5	G057	-59.78	49.33	Z550	30.42	71.42	C666	-61.82	42.92	N237	-4.63	65.62	C660	-59.99	43.12
15.5	Z550	30.42	71.42	A977	-21.78	67.98	N216	2.66	66.61	A983	-17.07	67.58	G057	-59.78	49.33
16.5	Z550	30.42	71.42	G054	-60.17	49.22	G057	-59.78	49.33	G1367	-61.5	48.33	A955	-18.18	67.46
17.5	Z550	30.42	71.42	G054	-60.17	49.22	G057	-59.78	49.33	G056	-60.8	49.52	N186	3.73	60.63
18.5	N193	-9.31	67	A947	-19.35	67.91	N231	-8.81	65.27	A946	-20.68	68.03	N234	-7.65	65.45
19.5	N210	-4.74	65.42	A949	-17.75	67.9	A977	-21.78	67.98	N185	3.72	60.64	A984	-18.47	71.19
20.5	N216	2.66	66.61	N214	1.55	66.61	L153	-48.38	59.15	N248	4.23	58.69	A945	-20.83	67.76
21.5	G1366	-60.01	47.67	G052	-60.64	48.51	N216	2.66	66.61	G063	-62.54	48.64	G033	-60.72	48.17
22.5	G054	-60.17	49.22	Z550	30.42	71.42	N186	3.73	60.63	G051	-60.64	48.51	G056	-60.8	49.52
23.5	Z550	30.42	71.42	N216	2.66	66.61	G052	-60.64	48.51	G057	-59.78	49.33	G054	-60.17	49.22
24.5	G052	-60.64	48.51	G061	-58.73	50.12	G056	-60.8	49.52	Z550	30.42	71.42	G066	-59.88	47.52
25.5	G073	-59.08	46.99	G061	-58.73	50.12	G057	-59.78	49.33	G065	-60.03	47.35	Z550	30.42	71.42
26.5	G057	-59.78	49.33	G061	-58.73	50.12	G052	-60.64	48.51	G056	-60.8	49.52	G054	-60.17	49.22
27.5	G057	-59.78	49.33	Z550	30.42	71.42	N186	3.73	60.63	G054	-60.17	49.22	G061	-58.73	50.12
28.5	G052	-60.64	48.51	G061	-58.73	50.12	G056	-60.8	49.52	G066	-59.88	47.52	Z560	50.72	73.62
29.5	G057	-59.78	49.33	Z550	30.42	71.42	G073	-59.08	46.99	G061	-58.73	50.12	G056	-60.8	49.52
30.5	G065	-60.03	47.35	A813	-57.31	47.69	A423	-69.96	42.82	G073	-59.08	46.99	A419	-65.46	41.92
31.5	A683	-51.8	48.91	G073	-59.08	46.99	G065	-60.03	47.35	Z550	30.42	71.42	A423	-69.96	42.82
32.5	G073	-59.08	46.99	G065	-60.03	47.35	A423	-69.96	42.82	G057	-59.78	49.33	G061	-58.73	50.12

Table A3: Analogue list, showing the analogues used by the Modern Analogue Technique for the reconstruction of summer and winter temperatures and salinities as well as sea-ice duration (months/year), within R406MC032.

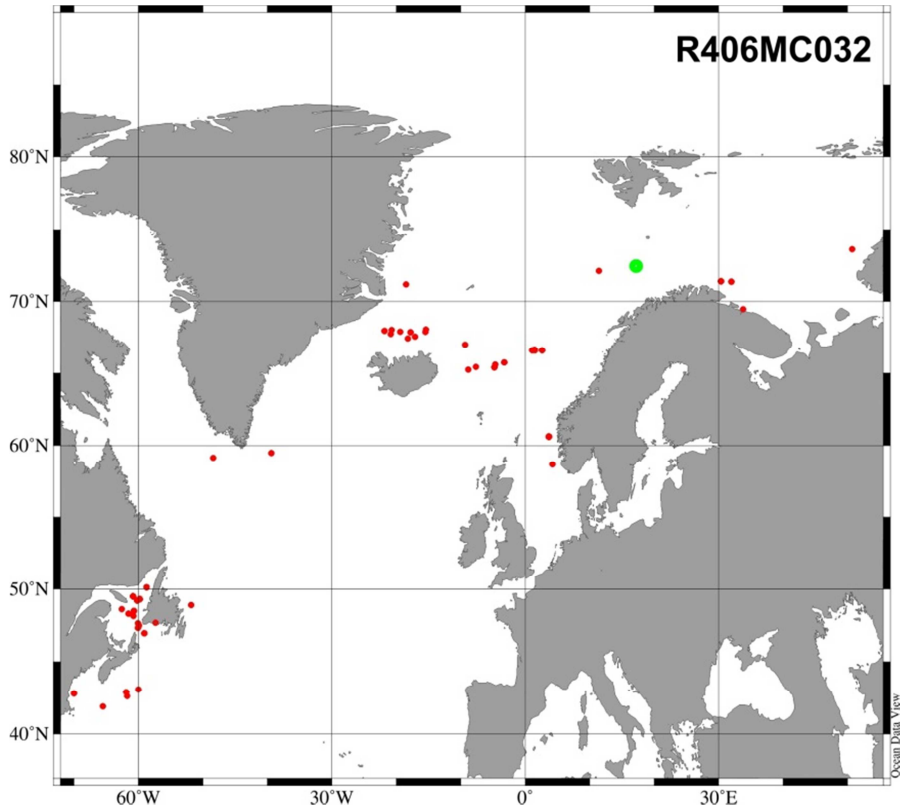

MAP A2: Geographical distribution of all analogues (red dots) applied within the present investigation of core R406MC032 (green dot).

JM09-KA11-GC

JM09-KA11-GC															
Depth (cm)	***[ANALOG 1]***	LONG	LATI	**[ANALOG 2]**	LONG	LATI	**[ANALOG 3]**	LONG	LATI	**[ANALOG 4]**	LONG	LATI	**[ANALOG 5]**	LONG	LATI
2.5	Z558	70.01	77	Z808	57.17	75.48	Z559	70.03	78.32	J286	6.69	78	J366	-6.02	76.92
3.5	J363	-11.57	75.33	Z558	70.01	77	J368	-4.55	77.99	Z555	59.77	76.72	J284	-21.11	70
7.5	Z558	70.01	77	J366	-6.02	76.92	J368	-4.55	77.99	J286	6.69	78	Z559	70.03	78.32
8.5	Z558	70.01	77	J286	6.69	78	Z559	70.03	78.32	J368	-4.55	77.99	Z562	52.43	74.45
9.25	Z558	70.01	77	J368	-4.55	77.99	F1002	-138.38	69.92	J366	-6.02	76.92	Z562	52.43	74.45
11.5	Z558	70.01	77	Z562	52.43	74.45	J368	-4.55	77.99	J286	6.69	78	J366	-6.02	76.92
13.5	Z558	70.01	77	J368	-4.55	77.99	Z559	70.03	78.32	J286	6.69	78	Y697	-70.79	75.58
15.5	Z810	47.87	79.65	F1002	-138.38	69.92	Z558	70.01	77	F997	-133.52	71.15	Y696	-76.08	75.26
17.5	F1002	-138.38	69.92	Z558	70.01	77	Z810	47.87	79.65	Y697	-70.79	75.58	F997	-133.52	71.15
19	Y697	-70.79	75.58	Z558	70.01	77	F1002	-138.38	69.92	Z810	47.87	79.65	F999	-128.52	71.27
21.5	Z558	70.01	77	J368	-4.55	77.99	J366	-6.02	76.92	Y697	-70.79	75.58	J284	-21.11	70
23.5	Z558	70.01	77	Y697	-70.79	75.58	J284	-21.11	70	Z810	47.87	79.65	J363	-11.57	75.33
25.5	Z559	70.03	78.32	Z558	70.01	77	Z809	46.94	79.57	Z562	52.43	74.45	Z557	56.43	75.62
27.5	Z558	70.01	77	Z810	47.87	79.65	J284	-21.11	70	J363	-11.57	75.33	F995	-133.81	71.45
31.5	Z558	70.01	77	Z810	47.87	79.65	F1002	-138.38	69.92	Y696	-76.08	75.26	F997	-133.52	71.15
33.5	Z558	70.01	77	C675	-60.9	45.22	J366	-6.02	76.92	J368	-4.55	77.99	G072	-60.22	46.72
35.5	F1230	-85.6	74.28	Y372	-6.66	80.06	C674	-60.87	45.21	C675	-60.9	45.22	C676	-60.89	45.23
37.5	J368	-4.55	77.99	Z558	70.01	77	J366	-6.02	76.92	Y697	-70.79	75.58	J284	-21.11	70
41.5	Z558	70.01	77	J366	-6.02	76.92	J368	-4.55	77.99	F1002	-138.38	69.92	Z562	52.43	74.45
44.5	Z558	70.01	77	Z559	70.03	78.32	J366	-6.02	76.92	J368	-4.55	77.99	G1366	-60.01	47.67
48.5	Z810	47.87	79.65	J284	-21.11	70	J363	-11.57	75.33	J368	-4.55	77.99	Z558	70.01	77
51.5	Z558	70.01	77	J366	-6.02	76.92	J368	-4.55	77.99	G072	-60.22	46.72	G059	-59.47	49.8
55.5	Z558	70.01	77	J368	-4.55	77.99	J284	-21.11	70	J366	-6.02	76.92	J363	-11.57	75.33
57.5	J368	-4.55	77.99	Z558	70.01	77	J366	-6.02	76.92	J284	-21.11	70	J286	6.69	78
61.5	J284	-21.11	70	Z810	47.87	79.65	Z558	70.01	77	J366	-6.02	76.92	Y696	-76.08	75.26
63.5	Y697	-70.79	75.58	J368	-4.55	77.99	G059	-59.47	49.8	Z559	70.03	78.32	Z558	70.01	77
65.5	Z558	70.01	77	J368	-4.55	77.99	J366	-6.02	76.92	J284	-21.11	70	J286	6.69	78
67.5	J368	-4.55	77.99	Z558	70.01	77	J366	-6.02	76.92	Z559	70.03	78.32	J284	-21.11	70
69.5	H1331	-71.92	62.25	Y697	-70.79	75.58	Z810	47.87	79.65	J366	-6.02	76.92	C671	-60.83	45.16
71.5	J366	-6.02	76.92	Z558	70.01	77	J368	-4.55	77.99	F1230	-85.6	74.28	Z810	47.87	79.65
73.5	J284	-21.11	70	J363	-11.57	75.33	J289	-11.04	78.62	F1230	-85.6	74.28	J368	-4.55	77.99
75.5	J366	-6.02	76.92	J284	-21.11	70	J354	-18.02	69.03	J368	-4.55	77.99	Z558	70.01	77
77.5	J366	-6.02	76.92	J284	-21.11	70	J368	-4.55	77.99	Y697	-70.79	75.58	J363	-11.57	75.33
81.5	Z707	-74.66	76.22	F1230	-85.6	74.28	Y375	-11.32	80.62	Y693	-72.34	77.01	J289	-11.04	78.62
83.5	J289	-11.04	78.62	F1230	-85.6	74.28	J284	-21.11	70	Z707	-74.66	76.22	Y376	-13.66	80.45
85.5	J289	-11.04	78.62	Y376	-13.66	80.45	F1230	-85.6	74.28	J284	-21.11	70	Y693	-72.34	77.01
87.5	J284	-21.11	70	J289	-11.04	78.62	S158	-58.91	56.11	Z558	70.01	77	J368	-4.55	77.99
91.5	J284	-21.11	70	J368	-4.55	77.99	J354	-18.02	69.03	J366	-6.02	76.92	J363	-11.57	75.33
93.5	J284	-21.11	70	J368	-4.55	77.99	Y376	-13.66	80.45	S158	-58.91	56.11	J289	-11.04	78.62
95.5	A534	-31.88	67.14	J289	-11.04	78.62	S160	-55.58	54.72	S159	-56.45	54.71	S158	-58.91	56.11
97.5	J284	-21.11	70	S158	-58.91	56.11	J366	-6.02	76.92	J368	-4.55	77.99	Y376	-13.66	80.45
100.5	J289	-11.04	78.62	Y376	-13.66	80.45	Y378	-15.76	80.08	Y373	-10.71	80.15	Y690	-74.94	76.8
102.5	Y375	-11.32	80.62	J289	-11.04	78.62	H1331	-71.92	62.25	Z707	-74.66	76.22	J284	-21.11	70
103.5	H1331	-71.92	62.25	Y372	-6.66	80.06	J284	-21.11	70	S160	-55.58	54.72	S158	-58.91	56.11
106.5	Y378	-15.76	80.08	J289	-11.04	78.62	Y693	-72.34	77.01	Z707	-74.66	76.22	Y373	-10.71	80.15
108.5	S158	-58.91	56.11	J284	-21.11	70	Y376	-13.66	80.45	J289	-11.04	78.62	S159	-56.45	54.71
110.5	Z803	57.9	80.74	Y376	-13.66	80.45	J289	-11.04	78.62	Z708	-71.04	76.12	Z473	123.84	75.48
114.5	J284	-21.11	70	S158	-58.91	56.11	J366	-6.02	76.92	Z558	70.01	77	J368	-4.55	77.99
121.5	S158	-58.91	56.11	S159	-56.45	54.71	J366	-6.02	76.92	J368	-4.55	77.99	J363	-11.57	75.33

Table A4: Analogue list, showing the analogues used by the Modern Analogue Technique for the reconstruction of summer and winter temperatures and salinities as well as sea-ice duration (months/year), within JM09-KA11-GC.

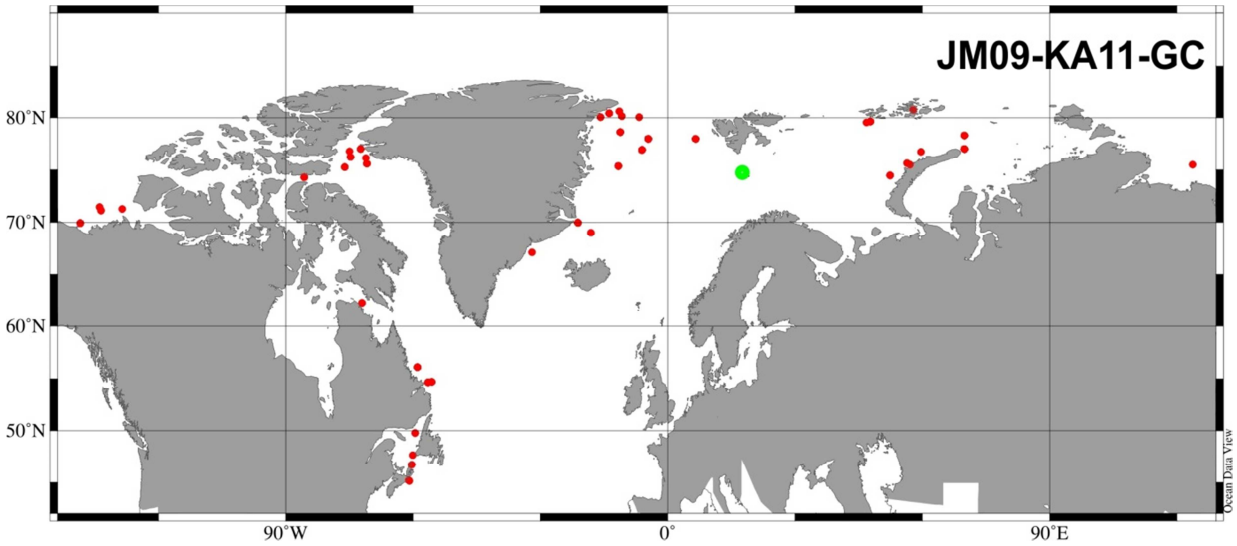

MAP A3 : Geographical distribution of all analogues (red dots) applied within the present investigation of core JM09-KA11-GC (green dot).

HH11-134-BC

HH11-134-BC															
Depth (cm)	***[ANALOG 1]***	LONG	LATI	**[ANALOG 2]**	LONG	LATI	**[ANALOG 3]**	LONG	LATI	**[ANALOG 4]**	LONG	LATI	**[ANALOG 5]**	LONG	LATI
0.25	Z559	70.03	78.32	J285	8.72	78.01	Z550	30.42	71.42	J286	6.69	78	A946	-20.68	68.03
0.75	Z559	70.03	78.32	J285	8.72	78.01	Z558	70.01	77	A946	-20.68	68.03	A950	-17.5	68.08
1.25	J285	8.72	78.01	Z559	70.03	78.32	Z558	70.01	77	J286	6.69	78	J288	-1.05	78
1.75	Z559	70.03	78.32	J285	8.72	78.01	J286	6.69	78	Z558	70.01	77	A946	-20.68	68.03
2.25	Z559	70.03	78.32	A946	-20.68	68.03	A950	-17.5	68.08	G059	-59.47	49.8	G1366	-60.01	47.67
2.75	Z559	70.03	78.32	Z550	30.42	71.42	J285	8.72	78.01	G057	-59.78	49.33	J286	6.69	78
3.25	Z559	70.03	78.32	A946	-20.68	68.03	A947	-19.35	67.91	J285	8.72	78.01	N193	-9.31	67
3.75	Z559	70.03	78.32	Z550	30.42	71.42	J285	8.72	78.01	G057	-59.78	49.33	G061	-58.73	50.12
4.25	Z559	70.03	78.32	A946	-20.68	68.03	A947	-19.35	67.91	J286	6.69	78	Z550	30.42	71.42
4.75	Z559	70.03	78.32	Z550	30.42	71.42	J285	8.72	78.01	J286	6.69	78	G057	-59.78	49.33
6.25	Z550	30.42	71.42	Z559	70.03	78.32	J285	8.72	78.01	G061	-58.73	50.12	G056	-60.8	49.52
6.75	Z550	30.42	71.42	Z559	70.03	78.32	J285	8.72	78.01	J286	6.69	78	G057	-59.78	49.33
7.25	J285	8.72	78.01	J286	6.69	78	Z559	70.03	78.32	Z550	30.42	71.42	J326	5.87	67.69
7.75	Z550	30.42	71.42	Z559	70.03	78.32	J285	8.72	78.01	G057	-59.78	49.33	A946	-20.68	68.03
8.25	Z559	70.03	78.32	J285	8.72	78.01	Z550	30.42	71.42	J286	6.69	78	J300	3	69.5
8.75	A984	-18.47	71.19	A937	-15.38	68.08	Z559	70.03	78.32	J285	8.72	78.01	A953	-15.75	68.33
9.25	J285	8.72	78.01	J286	6.69	78	J300	3	69.5	Z559	70.03	78.32	Z550	30.42	71.42
9.75	A984	-18.47	71.19	A937	-15.38	68.08	A955	-18.18	67.46	N216	2.66	66.61	Z551	31.97	71.39
10.25	J286	6.69	78	J285	8.72	78.01	Z550	30.42	71.42	Z559	70.03	78.32	J300	3	69.5
10.75	Z559	70.03	78.32	Z550	30.42	71.42	J285	8.72	78.01	J286	6.69	78	Z560	50.72	73.62
11.25	Z559	70.03	78.32	N216	2.66	66.61	Z550	30.42	71.42	G052	-60.64	48.51	J286	6.69	78
11.75	Z550	30.42	71.42	Z559	70.03	78.32	J285	8.72	78.01	G1366	-60.01	47.67	G061	-58.73	50.12
12.25	J326	5.87	67.69	N216	2.66	66.61	Z550	30.42	71.42	J300	3	69.5	N196	-6.59	67.04
12.75	J300	3	69.5	J286	6.69	78	J285	8.72	78.01	Z559	70.03	78.32	J326	5.87	67.69
13.25	Z550	30.42	71.42	Z559	70.03	78.32	J285	8.72	78.01	G052	-60.64	48.51	J286	6.69	78
13.75	Z550	30.42	71.42	Z559	70.03	78.32	J285	8.72	78.01	J300	3	69.5	J286	6.69	78
14.25	J286	6.69	78	J285	8.72	78.01	Z559	70.03	78.32	Z550	30.42	71.42	J300	3	69.5
14.75	Z559	70.03	78.32	J300	3	69.5	J286	6.69	78	J285	8.72	78.01	J326	5.87	67.69
15.25	J326	5.87	67.69	Z559	70.03	78.32	J286	6.69	78	J285	8.72	78.01	N216	2.66	66.61
15.75	J300	3	69.5	J285	8.72	78.01	J286	6.69	78	Z550	30.42	71.42	Z558	70.01	77
16.5	J300	3	69.5	J326	5.87	67.69	Z550	30.42	71.42	J286	6.69	78	J285	8.72	78.01
16.75	Z559	70.03	78.32	J285	8.72	78.01	J286	6.69	78	Z558	70.01	77	Z550	30.42	71.42
17.25	J285	8.72	78.01	J286	6.69	78	Z559	70.03	78.32	J300	3	69.5	J326	5.87	67.69
17.75	Z550	30.42	71.42	J286	6.69	78	J285	8.72	78.01	J300	3	69.5	Z559	70.03	78.32
18.25	Z550	30.42	71.42	J285	8.72	78.01	J286	6.69	78	Z559	70.03	78.32	G052	-60.64	48.51
18.75	J286	6.69	78	Z559	70.03	78.32	J285	8.72	78.01	A420	-67.92	42.56	J326	5.87	67.69
19.25	J286	6.69	78	J300	3	69.5	J285	8.72	78.01	J326	5.87	67.69	Z559	70.03	78.32
19.75	Z559	70.03	78.32	J286	6.69	78	J285	8.72	78.01	Z550	30.42	71.42	J300	3	69.5
20.25	Z559	70.03	78.32	J286	6.69	78	J285	8.72	78.01	J300	3	69.5	Z550	30.42	71.42
20.75	Z550	30.42	71.42	Z559	70.03	78.32	J285	8.72	78.01	J286	6.69	78	J326	5.87	67.69
21.25	J286	6.69	78	J300	3	69.5	J285	8.72	78.01	Z550	30.42	71.42	Y697	-70.79	75.58
21.75	N216	2.66	66.61	J326	5.87	67.69	Z550	30.42	71.42	G052	-60.64	48.51	G1366	-60.01	47.67
22.25	Z550	30.42	71.42	J286	6.69	78	Z559	70.03	78.32	J285	8.72	78.01	J300	3	69.5
22.75	J300	3	69.5	Z550	30.42	71.42	J285	8.72	78.01	J286	6.69	78	J281	-3.64	68.3
23.25	J300	3	69.5	J286	6.69	78	Y697	-70.79	75.58	Z559	70.03	78.32	J285	8.72	78.01
23.75	J300	3	69.5	N216	2.66	66.61	Z550	30.42	71.42	Z559	70.03	78.32	J326	5.87	67.69
24.25	J285	8.72	78.01	J286	6.69	78	J300	3	69.5	J326	5.87	67.69	Z550	30.42	71.42
24.75	Z550	30.42	71.42	Z559	70.03	78.32	J285	8.72	78.01	J286	6.69	78	J300	3	69.5
25.25	Z550	30.42	71.42	G054	-60.17	49.22	G056	-60.8	49.52	G061	-58.73	50.12	N216	2.66	66.61
25.75	J300	3	69.5	J286	6.69	78	J285	8.72	78.01	Y697	-70.79	75.58	J326	5.87	67.69
26.25	Z559	70.03	78.32	J285	8.72	78.01	J286	6.69	78	J300	3	69.5	Z555	59.77	76.72
26.75	Z550	30.42	71.42	J300	3	69.5	J286	6.69	78	J285	8.72	78.01	G1366	-60.01	47.67
27.25	Z550	30.42	71.42	J285	8.72	78.01	J300	3	69.5	Z558	70.01	77	G056	-60.8	49.52
27.75	Z550	30.42	71.42	Z559	70.03	78.32	J285	8.72	78.01	J286	6.69	78	N216	2.66	66.61
28.25	Y697	-70.79	75.58	J286	6.69	78	J300	3	69.5	Z559	70.03	78.32	Z550	30.42	71.42
28.75	Z550	30.42	71.42	Z559	70.03	78.32	J285	8.72	78.01	J286	6.69	78	A946	-20.68	68.03
29.25	Z559	70.03	78.32	Z550	30.42	71.42	G052	-60.64	48.51	G061	-58.73	50.12	N216	2.66	66.61
29.75	Z559	70.03	78.32	Z550	30.42	71.42	J286	6.69	78	J285	8.72	78.01	J300	3	69.5
30.25	Z550	30.42	71.42	Z559	70.03	78.32	J285	8.72	78.01	J286	6.69	78	G061	-58.73	50.12
30.75	J285	8.72	78.01	A947	-19.35	67.91	A953	-15.75	68.33	N193	-9.31	67	A946	-20.68	68.03
32.25	Z550	30.42	71.42	N216	2.66	66.61	J286	6.69	78	J300	3	69.5	J285	8.72	78.01
32.75	Z550	30.42	71.42	Z559	70.03	78.32	A984	-18.47	71.19	J285	8.72	78.01	J286	6.69	78
33.75	Z550	30.42	71.42	N216	2.66	66.61	G057	-59.78	49.33	Z559	70.03	78.32	G061	-58.73	50.12
34.25	Z550	30.42	71.42	J285	8.72	78.01	G061	-58.73	50.12	Z559	70.03	78.32	J286	6.69	78
34.75	Z550	30.42	71.42	G061	-58.73	50.12	G056	-60.8	49.52	G054	-60.17	49.22	G057	-59.78	49.33
35.25	Z550	30.42	71.42	A946	-20.68	68.03	G061	-58.73	50.12	G057	-59.78	49.33	N193	-9.31	67
35.75	Z550	30.42	71.42	J300	3	69.5	G061	-58.73	50.12	J286	6.69	78	A946	-20.68	68.03
36.25	G061	-58.73	50.12	Z550	30.42	71.42	G056	-60.8	49.52	G054	-60.17	49.22	N216	2.66	66.61
36.75	Z550	30.42	71.42	Z559	70.03	78.32	G057	-59.78	49.33	J285	8.72	78.01	G061	-58.73	50.12
37.25	Z550	30.42	71.42	J286	6.69	78	J285	8.72	78.01	Z559	70.03	78.32	J300	3	69.5
37.75	J285	8.72	78.01	J286	6.69	78	G061	-58.73	50.12	Z550	30.42	71.42	Z559	70.03	78.32
38.25	Z559	70.03	78.32	J285	8.72	78.01	J286	6.69	78	Z550	30.42	71.42	A951	-16.93	68.58
38.75	Z559	70.03	78.32	J285	8.72	78.01	J286	6.69	78	Z550	30.42	71.42	G061	-58.73	50.12
39.25	A947	-19.35	67.91	A946	-20.68	68.03	J285	8.72	78.01	A953	-15.75	68.33	J368	-4.55	77.99

Table A5: Analogue list, showing the analogues used by the Modern Analogue Technique for the reconstruction of summer and winter temperatures and salinities as well as sea-ice duration (months/year), within HH11-134-BC.

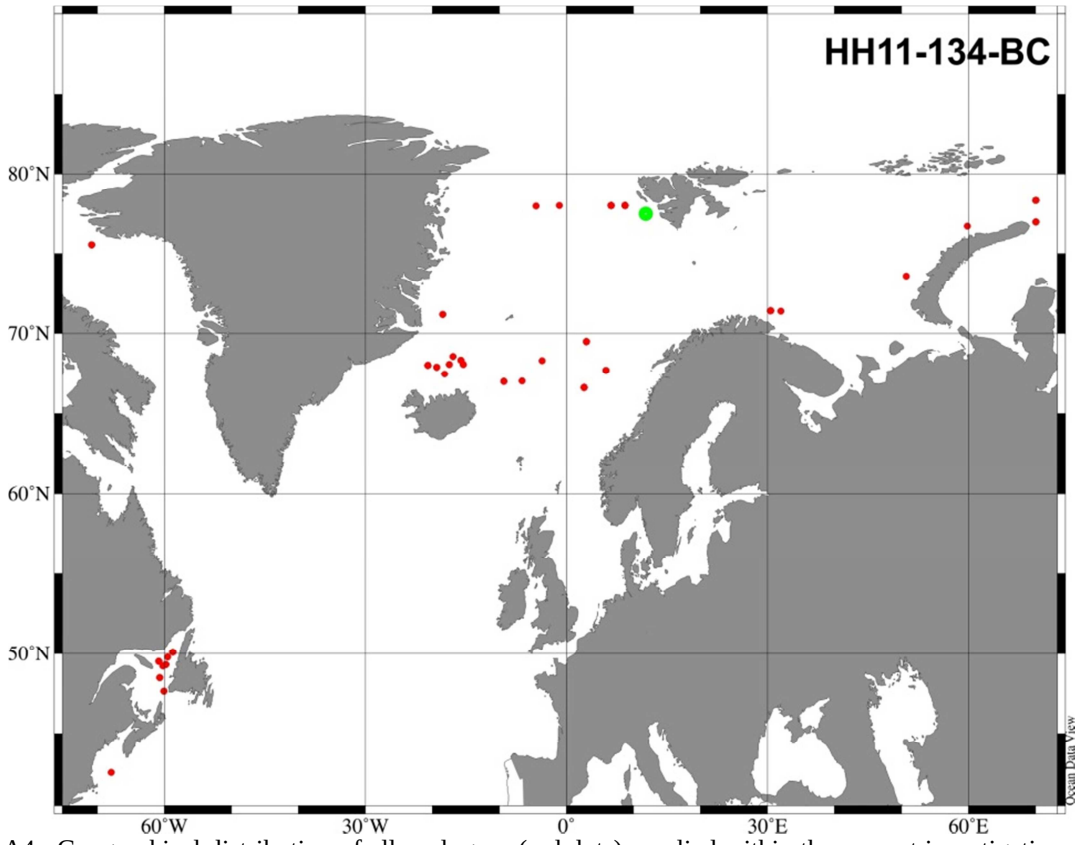

MAP A4 : Geographical distribution of all analogues (red dots) applied within the present investigation of core HH11-134-BC (green dot).

Appendix 5: R248MC010 relative abundances and absolute concentrations of microfossils, MAT reconstructions and XRF count datasets

A5.1 Coccoliths

Depth (cm)	Age (cal. years BP)	*E. huxleyi* (wt. %)	*C. pelagicus* (wt. %)	*G. muellerae* (wt. %)	*C. leptoporus* (wt. %)	Bulk coccoliths (no.*10^8/g)
0.25	-57.3	58.5	36.9	2.0	2.7	11.6
0.75	-55.9	72.7	24.4	2.6	0.3	7.5
1.25	-54.4	70.3	27.8	1.2	0.7	10.6
1.75	-52.8	60.6	35.4	2.9	1.2	16.8
2.25	-51.2	68.2	24.4	6.1	1.3	17.7
2.75	-49.4	71.2	23.6	4.2	1.0	16.4
3.25	-47.6	56.5	40.3	1.3	1.9	25.6
3.75	-45.7	69.4	25.0	4.2	1.5	20.0
4.25	-43.7	73.6	23.9	1.9	0.6	24.2
4.75	-41.7	62.7	33.7	2.9	0.7	31.7
5.25	-39.5	58.9	35.8	3.9	1.4	16.8
5.75	-37.3	67.7	28.6	3.1	0.6	14.1
6.25	-35.0	63.5	34.3	1.7	0.4	13.9
6.75	-32.6	64.0	32.4	2.5	1.0	15.9
7.25	-30.2	63.4	29.9	4.1	2.6	18.0
7.75	-27.6	64.0	31.9	3.1	1.0	17.8
8.25	-25.0	58.6	35.6	4.8	1.0	11.0
8.75	-22.3	68.0	25.9	4.5	1.6	17.8
9.25	-19.6	72.0	23.2	3.1	1.7	17.3
9.75	-16.7	60.0	32.1	6.9	1.0	14.4
10.25	-13.8	69.4	27.7	1.7	1.3	16.5
10.75	-10.8	67.8	25.5	4.9	1.8	18.3
11.25	-7.7	70.7	23.9	4.3	1.1	10.3
11.75	-4.5	60.5	34.6	3.1	1.7	9.8
12.25	-1.2	69.3	24.2	5.0	1.4	9.8
12.75	2.1	61.7	32.7	5.3	0.3	13.3
13.25	5.5	55.2	40.4	2.9	1.6	15.9
13.75	9.0	67.1	29.4	1.9	1.6	18.1
14.25	12.6	74.3	19.0	4.5	2.1	23.3
14.75	16.2	64.9	30.6	3.0	1.5	14.2
15.25	20.0	61.6	34.0	2.1	2.3	15.4
15.75	23.8	60.4	32.3	5.6	1.7	21.0
16.25	27.7	65.2	30.6	3.3	0.9	18.9
16.75	31.6	64.8	29.7	2.6	2.9	12.5
17.25	35.7	57.4	37.9	2.8	1.9	15.4
17.75	39.8	63.3	32.7	2.6	1.3	13.2
18.25	44.0	52.9	42.5	3.9	0.7	14.8

Depth (cm)	Age (cal. years BP)	*E. huxleyi* (wt. %)	*C. pelagicus* (wt. %)	*G. muellerae* (wt. %)	*C. leptoporus* (wt. %)	Bulk coccoliths (no.*10^8/g)
18.75	48.3	67.6	25.5	6.0	0.9	23.0
19.25	52.7	60.6	35.4	3.1	0.9	15.0
19.75	57.1	60.4	34.0	4.1	1.5	14.7
20.25	61.6	59.3	33.3	4.5	3.0	14.3
20.75	66.2	59.5	36.3	3.2	1.0	9.6
21.25	70.9	57.5	38.4	2.6	1.5	13.8
21.75	75.7	60.1	35.8	1.6	2.6	13.8
22.25	80.5	62.1	33.1	3.6	1.1	12.6
22.75	85.5	67.4	29.2	2.5	0.9	15.3
23.25	90.5	59.7	34.9	3.6	1.8	15.7
23.75	95.5	57.5	38.9	2.7	0.9	15.6
24.25	100.7	61.8	33.8	2.4	2.0	16.0
24.75	105.9	59.4	36.4	3.0	1.2	14.3
25.25	111.3	56.9	39.0	1.9	2.2	13.0
25.75	116.7	65.6	31.1	2.0	1.3	13.8
26.25	122.1	64.5	31.0	3.8	0.8	14.1
26.75	127.7	64.3	31.0	3.5	1.2	18.5
27.25	133.3	63.2	30.7	4.1	2.0	15.3
27.75	139.1	54.2	40.1	3.4	2.2	11.5
28.25	144.9	62.3	32.4	3.5	1.7	14.5
28.75	150.7	58.5	32.5	6.5	2.5	10.7
29.25	156.7	60.8	35.4	2.9	0.9	12.4
29.75	162.7	62.6	34.3	1.2	1.8	17.9
30.25	168.9	60.6	35.3	2.8	1.4	12.9
30.75	175.1	53.5	42.5	2.3	1.7	10.9
31.25	181.3	67.1	27.8	3.3	1.8	9.3
31.75	187.7	53.2	39.7	5.0	2.1	10.2
32.25	194.1	59.2	35.2	2.8	2.8	11.7
32.75	200.6	51.7	41.5	5.1	1.7	12.8
33.25	207.2	45.9	47.8	3.8	2.5	11.3
33.75	213.9	44.3	51.4	4.3	0.0	10.3
34.25	220.7	49.2	43.5	6.0	1.3	13.4
34.75	227.5	59.4	36.8	3.0	0.9	15.2
35.25	234.4	48.6	43.8	6.2	1.4	13.2
35.75	241.4	53.6	39.0	6.2	1.2	11.5
36.25	248.5	54.0	40.5	4.2	1.4	15.5
36.75	255.6	59.3	30.2	7.6	2.9	12.1
37.25	262.9	54.6	41.7	3.2	0.6	12.1
37.75	270.2	60.2	36.1	2.9	0.9	12.4
38.25	277.6	73.2	22.8	3.8	0.3	13.3
38.75	285.0	58.4	38.0	2.0	1.7	12.4
39.25	292.6	57.3	38.4	2.8	1.4	15.2

Depth (cm)	Age (cal. years BP)	*E. huxleyi* (wt. %)	*C. pelagicus* (wt. %)	*G. muellerae* (wt. %)	*C. leptoporus* (wt. %)	Bulk coccoliths (no.*10^8/g)
39.75	300.2	57.9	36.8	2.9	2.4	14.8
40.25	307.9	57.9	37.8	4.0	0.3	11.7
40.75	315.7	57.5	35.3	5.1	2.1	11.4
41.25	323.6	55.2	38.4	4.6	1.8	13.7
41.75	331.5	61.3	36.1	2.0	0.6	12.6
42.25	339.6	59.1	35.4	3.7	1.8	11.4
42.75	347.7	55.4	36.3	5.3	3.0	10.9
43.25	355.9	64.6	28.7	5.0	1.8	12.2
43.75	364.1	47.3	46.2	4.8	1.7	10.3
44.25	372.5	61.8	32.9	3.3	2.0	10.6
44.75	380.9	51.5	43.1	4.2	1.2	9.4
45.25	389.4	58.3	36.6	3.6	1.5	11.9
45.75	398.0	54.5	41.5	1.3	2.7	10.5
46.25	406.7	60.9	31.3	3.6	4.3	10.7
46.75	415.4	58.6	38.8	2.0	0.7	10.7
47.25	424.2	61.1	33.8	4.2	0.9	15.9
47.75	433.1	49.1	45.2	3.2	2.5	10.0
48.25	442.1	52.4	44.5	2.1	1.0	10.3
48.75	451.2	62.4	32.3	2.0	3.3	10.9

A5.2 Dinocysts

Depth (cm)	Age (cal. years BP)	OCEN (wt. %)	PDAL (wt. %)	NLAB (wt. %)	BSPP (wt. %)	SRAM (wt. %)	SELO (wt. %)	BTEP (wt. %)	IMIN (wt. %)	SMIR (wt. %)
0.5	-56.6	63.4	18.3	6.6	1.0	4.0	2.7	1.5	0.0	0.0
1.5	-53.6	60.1	22.8	11.3	0.7	1.6	1.4	0.5	0.2	0.0
2.5	-50.3	55.8	20.9	12.3	2.4	3.4	2.2	0.7	0.7	0.0
3.5	-46.7	52.5	24.6	11.1	4.0	3.7	2.4	0.0	0.0	0.0
4.5	-42.7	49.2	26.7	12.8	3.3	3.3	1.2	0.0	0.6	0.0
5.5	-38.4	54.1	17.2	13.1	6.0	3.2	1.8	0.9	0.2	0.2
6.5	-33.8	50.7	15.9	17.4	4.0	6.2	1.5	0.2	0.2	0.0
7.5	-28.9	50.4	19.0	18.0	2.1	4.4	0.5	0.5	1.3	0.0
8.5	-23.7	52.8	17.8	16.9	3.1	2.5	1.2	0.9	0.9	0.0
9.5	-18.1	53.3	21.4	14.9	2.1	3.3	1.5	0.0	0.3	0.0
10.5	-12.3	53.4	19.5	16.3	1.7	2.9	1.7	0.0	0.2	0.2
11.5	-6.1	48.9	28.6	13.5	0.8	1.4	2.4	0.5	1.4	0.0
12.5	0.4	47.4	26.3	19.3	1.3	1.8	0.5	0.8	0.5	0.0
13.5	7.2	48.7	20.0	15.3	4.0	3.4	3.6	0.6	0.8	0.0
14.5	14.4	47.7	27.7	17.1	0.9	2.0	1.1	0.6	0.9	0.0
15.5	21.8	46.3	25.2	17.8	1.8	4.2	1.2	0.3	0.6	0.3
16.5	29.6	53.5	28.0	10.5	0.6	1.9	1.4	0.3	0.8	0.3
17.5	37.7	56.4	17.2	13.6	2.5	4.0	1.9	1.3	0.4	0.0
18.5	46.1	43.3	35.2	12.3	0.3	3.1	2.0	0.3	0.7	0.3
19.5	54.9	50.6	27.5	10.4	1.4	4.2	1.4	1.1	0.8	0.0
20.5	63.9	51.4	24.1	13.9	1.4	2.7	1.0	0.7	0.3	0.7
21.5	73.3	57.9	19.7	11.6	1.5	2.0	3.2	0.5	1.2	0.0
22.5	83.0	55.9	23.2	13.3	1.3	2.9	1.3	1.0	0.3	0.0
23.5	93.0	61.7	18.9	9.8	0.8	2.7	3.0	0.3	0.5	0.0
24.5	103.3	53.8	27.9	10.4	1.2	1.8	1.6	1.4	0.0	0.0
25.5	114.0	52.5	32.3	8.6	1.0	1.7	1.7	0.3	0.3	0.0
26.5	124.9	63.1	21.5	7.4	2.6	1.3	1.5	0.5	0.5	0.0
27.5	136.2	64.5	13.1	11.2	1.6	3.5	1.3	0.6	0.3	0.0
28.5	147.8	63.6	22.2	5.8	3.2	1.7	0.6	0.3	0.0	0.3
29.5	159.7	57.3	22.2	8.6	3.5	2.3	2.3	1.7	0.6	0.0
30.5	172.0	61.3	23.6	9.2	1.4	1.4	1.7	0.0	0.3	0.0
31.5	184.5	70.4	11.0	7.8	3.6	2.5	1.8	0.4	0.2	0.2
32.5	197.4	63.0	15.8	7.5	6.2	2.2	1.9	0.3	0.9	0.0
33.5	210.6	62.5	19.9	6.5	4.2	1.8	1.5	0.3	0.3	0.9
34.5	224.1	54.1	19.7	12.1	3.5	3.5	2.9	0.9	0.6	0.6
35.5	237.9	51.1	26.1	10.2	5.3	1.4	1.1	1.1	1.1	0.4
36.5	252.1	65.9	16.8	8.7	4.3	0.8	1.5	0.3	0.0	0.3
37.5	266.5	68.3	15.9	6.2	5.2	1.0	0.7	1.0	0.3	0.0
38.5	281.3	61.7	22.8	8.2	1.6	1.4	1.1	1.1	0.5	0.3
39.5	296.4	65.7	20.4	7.4	1.9	0.6	1.2	0.0	0.6	0.0

Depth (cm)	Age (cal. years BP)	SSPP (wt. %)	IPAL (wt. %)	SQUA (wt. %)	HALO (no.*10^3/g)	Reworked (no.*10^3/g)	Dinocyst concentrations (no.*10^3/g)
0.5	-56.6	0.8	0.1	0.0	0.1	0.3	22.4
1.5	-53.6	0.7	0.0	0.0	0.0	0.3	23.0
2.5	-50.3	0.2	0.0	0.0	0.0	0.3	14.9
3.5	-46.7	0.3	0.0	0.7	0.0	0.1	8.5
4.5	-42.7	1.8	0.0	0.0	0.0	0.1	9.4
5.5	-38.4	0.2	0.2	0.7	0.0	0.1	11.7
6.5	-33.8	0.7	0.0	0.7	0.0	0.1	12.6
7.5	-28.9	0.0	0.0	0.0	0.0	0.0	11.5
8.5	-23.7	1.8	0.0	0.0	0.0	0.3	17.5
9.5	-18.1	2.1	0.0	0.0	0.1	0.2	17.0
10.5	-12.3	1.4	0.0	0.2	0.0	0.1	13.5
11.5	-6.1	0.8	0.0	0.0	0.0	0.0	17.3
12.5	0.4	1.0	0.0	0.0	0.1	0.0	16.5
13.5	7.2	0.9	0.4	0.0	0.0	0.1	13.9
14.5	14.4	0.6	0.0	0.0	0.0	0.0	19.0
15.5	21.8	1.8	0.0	0.0	0.0	0.0	12.8
16.5	29.6	1.1	0.0	0.0	0.0	0.0	15.5
17.5	37.7	1.3	0.0	0.2	0.0	0.1	9.9
18.5	46.1	1.4	0.0	0.0	0.0	0.2	26.1
19.5	54.9	1.1	0.0	0.0	0.0	0.0	13.8
20.5	63.9	2.0	0.3	0.0	0.0	0.2	13.1
21.5	73.3	1.7	0.0	0.2	0.1	0.2	21.0
22.5	83.0	0.6	0.0	0.0	0.0	0.0	14.0
23.5	93.0	1.9	0.0	0.0	0.0	0.1	12.9
24.5	103.3	0.9	0.0	0.2	0.0	0.2	15.5
25.5	114.0	0.7	0.0	0.3	0.0	0.1	27.2
26.5	124.9	0.5	0.0	0.3	0.0	0.1	22.2
27.5	136.2	1.3	0.0	0.3	0.0	0.0	14.2
28.5	147.8	0.9	0.0	0.0	0.0	0.0	32.5
29.5	159.7	0.9	0.0	0.0	0.0	0.2	14.6
30.5	172.0	0.3	0.0	0.0	0.0	0.0	22.9
31.5	184.5	0.4	0.0	0.0	0.0	0.0	36.1
32.5	197.4	1.2	0.0	0.3	0.0	0.0	34.4
33.5	210.6	0.0	0.0	0.0	0.0	0.1	31.4
34.5	224.1	1.2	0.0	0.3	0.0	0.1	31.1
35.5	237.9	0.7	0.0	0.0	0.0	0.0	48.5
36.5	252.1	0.5	0.3	0.0	0.0	0.1	33.6
37.5	266.5	0.3	0.0	0.0	0.0	0.1	55.4
38.5	281.3	0.3	0.0	0.0	0.0	0.0	20.7
39.5	296.4	0.9	0.9	0.0	0.0	0.0	24.7

Depth (cm)	Age (cal. years BP)	OCEN (wt. %)	PDAL (wt. %)	NLAB (wt. %)	BSPP (wt. %)	SRAM (wt. %)	SELO (wt. %)	BTEP (wt. %)	IMIN (wt. %)	SMIR (wt. %)
40.5	311.8	61.9	26.3	5.4	1.6	0.8	0.5	0.5	0.3	0.0
41.5	327.6	61.6	21.1	6.9	4.8	0.9	2.1	1.2	0.3	0.3
42.5	343.6	59.6	17.3	6.4	12.9	0.4	0.6	1.0	0.2	0.2
43.5	360.0	55.8	19.8	6.8	10.6	1.9	1.1	0.3	0.5	0.3
44.5	376.7	61.2	25.6	6.7	1.1	1.9	0.8	0.0	0.3	0.0
45.5	393.7	46.8	29.9	11.5	3.2	2.9	0.6	0.6	1.0	0.0
46.5	411.0	55.3	21.4	7.4	8.4	1.3	1.6	2.3	0.3	0.6
47.5	428.7	51.6	20.1	18.1	4.9	1.4	1.1	0.3	0.0	0.6
48.5	446.6	44.5	32.5	10.6	3.8	3.8	1.4	1.0	1.7	0.0

Depth (cm)	Age (cal. years BP)	SSPP (wt. %)	IPAL (wt. %)	SQUA (wt. %)	HALO (no.*10^3/g)	Reworked (no.*10^3/g)	Dinocyst concentrations (no.*10^3/g)
40.5	311.8	1.3	0.3	0.0	0.0	0.0	40.9
41.5	327.6	0.0	0.0	0.0	0.0	0.1	40.3
42.5	343.6	0.2	0.2	0.0	0.0	0.1	50.9
43.5	360.0	0.0	0.0	0.3	0.0	0.0	40.0
44.5	376.7	1.1	0.0	0.0	0.1	0.1	28.8
45.5	393.7	0.3	0.3	0.0	0.0	0.2	29.8
46.5	411.0	0.0	0.0	0.0	0.0	0.1	29.8
47.5	428.7	0.6	0.0	0.3	0.0	0.1	23.9
48.5	446.6	0.3	0.0	0.0	0.0	0.2	22.8

A5.3 Modern Analogue Technique Results (MAT)

Reconstructed sea-surface temperatures and salinities during winter and summer, and sea ice durations (i and s → estimated lower and upper error ranges, respectively).

Depth (cm)	Age (cal. years BP)	TWIN	TWIN_i	TWIN_s	SWIN	SWIN_i	SWIN_s	TSUM	TSUM_i	TSUM_s
0.5	-56.6	3.5	0.0	6.4	33.4	31.7	34.5	12.3	8.3	13.5
1.5	-53.6	0.7	-0.4	3.5	32.3	31.7	34.5	12.5	8.3	14.9
2.5	-50.3	0.0	-0.4	0.2	31.7	31.7	31.8	13.4	12.5	14.9
3.5	-46.7	1.0	-0.5	2.6	33.3	31.6	34.8	9.3	4.4	14.9
4.5	-42.7	-0.1	-0.5	0.1	31.7	31.6	31.8	13.6	12.5	14.9
5.5	-38.4	3.3	0.2	7.4	34.2	31.8	35.2	9.1	4.4	13.3
6.5	-33.8	1.6	-0.5	6.3	32.8	31.6	34.7	11.9	4.4	14.3
7.5	-28.9	2.2	0.2	4.1	34.1	31.8	34.8	8.1	4.4	13.3
8.5	-23.7	0.0	-0.4	0.2	31.7	31.7	31.8	13.4	12.5	14.9
9.5	-18.1	-0.1	-0.5	0.1	31.7	31.6	31.8	13.7	12.5	14.9
10.5	-12.3	-0.1	-0.5	0.2	31.7	31.6	31.8	13.8	12.8	14.9
11.5	-6.1	0.0	-0.4	0.2	31.8	31.7	31.8	13.4	12.5	14.9
12.5	0.4	0.0	-0.4	0.2	31.7	31.7	31.8	13.4	12.5	14.9
13.5	7.2	0.7	-0.4	3.5	32.3	31.7	34.5	12.1	8.3	13.5
14.5	14.4	0.0	-0.4	0.2	31.8	31.7	31.8	13.4	12.5	14.9
15.5	21.8	-0.1	-0.4	0.1	31.7	31.7	31.8	13.5	12.5	14.9
16.5	29.6	1.1	-0.4	6.3	32.2	31.7	34.3	13.5	12.8	14.9
17.5	37.7	0.0	-0.4	0.2	31.8	31.7	31.8	13.0	12.5	13.5
18.5	46.1	-0.2	-0.5	0.1	31.7	31.6	31.8	13.6	12.5	14.9
19.5	54.9	0.0	-0.4	0.2	31.8	31.7	31.8	13.4	12.5	14.9
20.5	63.9	1.9	-0.4	6.3	32.8	31.7	34.5	12.3	8.3	13.5
21.5	73.3	-0.1	-0.5	0.2	31.7	31.6	31.8	13.3	12.5	14.3
22.5	83.0	0.0	-0.4	0.2	31.7	31.7	31.8	13.4	12.5	14.9
23.5	93.0	0.5	-0.4	3.5	32.2	31.7	34.5	12.6	8.3	14.9
24.5	103.3	0.0	-0.4	0.2	31.8	31.7	31.8	13.4	12.5	14.9
25.5	114.0	-0.1	-0.5	0.2	31.7	31.6	31.8	13.8	12.8	14.9
26.5	124.9	-0.1	-0.5	0.2	31.7	31.6	31.8	13.8	12.8	14.9
27.5	136.2	0.0	-0.4	0.2	31.8	31.7	31.8	13.0	12.5	13.5
28.5	147.8	4.3	0.0	6.9	34.4	31.8	35.2	11.1	7.6	14.9
29.5	159.7	0.0	-0.4	0.2	31.7	31.7	31.8	13.5	12.5	14.9
30.5	172.0	0.8	-0.5	3.5	32.6	31.6	34.5	12.4	8.3	14.9
31.5	184.5	3.3	0.0	6.5	33.5	31.7	35.2	11.8	8.3	13.5
32.5	197.4	0.0	-0.4	0.2	31.7	31.7	31.8	13.4	12.5	14.9
33.5	210.6	4.5	0.2	6.9	34.5	31.8	35.2	10.1	4.4	13.3
34.5	224.1	1.1	-0.4	6.3	32.2	31.7	34.3	13.1	12.5	13.5
35.5	237.9	0.0	-0.4	0.2	31.7	31.7	31.8	13.6	12.5	14.9

Depth (cm)	Age (cal. years BP)	SSUM	SSUM_i	SSUM_s	Sea ice duration (months/yr)	Sea ice_i	Sea ice_s
0.5	-56.6	32.3	30.5	34.3	0.7	0.0	1.8
1.5	-53.6	31.3	30.4	34.3	1.3	0.0	1.8
2.5	-50.3	30.5	30.4	30.7	1.7	1.5	1.8
3.5	-46.7	32.1	30.0	33.7	1.9	0.2	4.0
4.5	-42.7	30.4	30.0	30.7	2.0	1.5	4.0
5.5	-38.4	33.3	30.5	35.1	0.9	0.0	1.7
6.5	-33.8	31.5	30.0	33.5	1.8	0.0	4.0
7.5	-28.9	33.5	30.5	34.7	0.7	0.0	1.7
8.5	-23.7	30.5	30.4	30.7	1.7	1.5	1.8
9.5	-18.1	30.4	30.0	30.7	2.0	1.5	4.0
10.5	-12.3	30.4	30.0	30.6	2.1	1.5	4.0
11.5	-6.1	30.5	30.4	30.7	1.7	1.5	1.8
12.5	0.4	30.5	30.4	30.7	1.7	1.5	1.8
13.5	7.2	31.3	30.5	34.3	1.4	0.0	1.8
14.5	14.4	30.5	30.4	30.7	1.7	1.5	1.8
15.5	21.8	30.5	30.4	30.7	1.6	1.5	1.8
16.5	29.6	31.0	30.4	33.0	1.3	0.0	1.8
17.5	37.7	30.6	30.5	30.7	1.7	1.5	1.8
18.5	46.1	30.4	30.0	30.7	2.1	1.5	4.0
19.5	54.9	30.5	30.4	30.7	1.7	1.5	1.8
20.5	63.9	31.7	30.5	34.3	1.0	0.0	1.8
21.5	73.3	30.5	30.0	30.7	2.1	1.5	4.0
22.5	83.0	30.5	30.4	30.7	1.7	1.5	1.8
23.5	93.0	31.1	30.4	34.3	1.4	0.0	1.8
24.5	103.3	30.5	30.4	30.6	1.6	1.5	1.8
25.5	114.0	30.4	30.0	30.6	2.2	1.5	4.0
26.5	124.9	30.4	30.0	30.6	2.0	1.5	4.0
27.5	136.2	30.6	30.5	30.7	1.7	1.5	1.8
28.5	147.8	34.0	30.4	35.1	0.3	0.0	1.5
29.5	159.7	30.5	30.4	30.7	1.7	1.5	1.8
30.5	172.0	31.3	30.0	34.3	1.5	0.0	4.0
31.5	184.5	32.7	30.5	35.1	0.7	0.0	1.8
32.5	197.4	30.5	30.4	30.7	1.7	1.5	1.8
33.5	210.6	34.0	30.5	35.1	0.6	0.0	1.7
34.5	224.1	31.0	30.5	33.0	1.4	0.0	1.8
35.5	237.9	30.5	30.4	30.7	1.7	1.5	1.8

Depth (cm)	Age (cal. years BP)	TWIN	TWIN_i	TWIN_s	SWIN	SWIN_i	SWIN_s	TSUM	TSUM_i	TSUM_s
36.5	252.1	3.3	0.0	5.2	34.3	31.8	35.1	9.5	7.8	14.9
37.5	266.5	1.3	0.0	6.5	32.4	31.7	35.2	13.5	10.9	14.9
38.5	281.3	3.3	0.0	6.9	33.6	31.8	35.2	11.8	8.3	14.9
39.5	296.4	0.9	-0.2	3.5	34.2	31.8	34.9	8.1	5.0	14.9
40.5	311.8	1.7	0.0	4.7	33.1	31.7	35.1	12.1	8.1	14.9
41.5	327.6	3.0	0.0	6.5	33.8	31.8	35.2	10.8	4.4	14.9
42.5	343.6	3.5	0.2	6.5	34.4	31.8	35.2	9.7	7.6	13.3
43.5	360.0	2.5	0.2	6.5	34.3	31.8	35.2	7.9	4.4	13.3
44.5	376.7	-0.1	-0.5	0.2	31.7	31.6	31.8	13.9	12.8	14.9
45.5	393.7	0.3	0.0	1.1	32.3	31.7	34.7	12.4	6.1	14.9
46.5	411.0	3.1	0.2	6.8	33.7	31.7	35.2	11.0	4.4	14.3
47.5	428.7	4.1	0.0	6.5	33.7	31.7	35.2	12.6	10.9	14.9
48.5	446.6	0.0	-0.4	0.2	31.7	31.7	31.8	13.5	12.5	14.9

Depth (cm)	Age (cal. years BP)	SSUM	SSUM_i	SSUM_s	Sea ice duration (months/yr)	Sea ice_i	Sea ice_s
36.5	252.1	34.0	30.4	35.1	0.3	0.0	1.5
37.5	266.5	31.3	30.4	35.1	1.4	0.0	1.8
38.5	281.3	33.0	30.4	35.1	0.7	0.0	1.7
39.5	296.4	33.8	30.4	34.7	0.4	0.0	1.5
40.5	311.8	32.2	30.4	35.0	1.0	0.0	1.8
41.5	327.6	33.0	30.4	35.1	0.9	0.0	1.7
42.5	343.6	34.1	30.5	35.1	0.3	0.0	1.7
43.5	360.0	33.4	30.5	35.1	0.9	0.0	1.7
44.5	376.7	30.4	30.0	30.6	2.0	1.5	4.0
45.5	393.7	31.1	30.2	34.3	1.5	0.6	1.8
46.5	411.0	32.8	30.4	35.1	1.0	0.0	1.8
47.5	428.7	33.0	30.4	35.1	0.6	0.0	1.8
48.5	446.6	30.5	30.4	30.7	1.7	1.5	1.8

A5.4 Planktic foraminifera

Depth (cm)	Age (cal. years BP)	G. bulloides (wt %)	G. uvula (wt %)	G. glutinata (wt %)	G. quinqueloba (wt %)	Planktonic Foram./g
0.5	-56.6	6.0	4.6	1.1	30.5	184.2
1.5	-53.6	5.0	3.9	2.1	33.9	269.1
2.5	-50.3	6.8	4.5	1.6	38.3	538.7
3.5	-46.7	6.5	7.0	1.3	47.4	759.1
4.5	-42.7	4.5	8.1	2.4	47.4	770.4
5.5	-38.4	4.1	9.1	1.8	45.1	658.4
6.5	-33.8	4.1	8.9	0.5	47.8	557.8
7.5	-28.9	5.4	9.4	2.4	51.6	752.1
8.5	-23.7	4.7	8.1	1.1	45.0	456.1
9.5	-18.1	5.8	11.4	1.1	41.3	387.3
10.5	-12.3	8.8	10.1	0.8	37.1	313.6
11.5	-6.1	6.1	14.5	2.8	41.8	257.6
12.5	0.4	5.1	8.3	1.3	46.5	317.3
13.5	7.2	4.5	14.9	1.8	42.7	466.1
14.5	14.4	4.1	14.6	1.4	42.8	427.7
15.5	21.8	6.6	16.7	1.1	37.3	629.1
16.5	29.6	4.4	14.0	0.8	42.3	371.9
17.5	37.7	3.6	15.6	1.0	44.9	423.1
18.5	46.1	2.7	13.2	0.8	39.6	308.4
19.5	54.9	2.0	17.1	1.7	42.4	411.6
20.5	63.9	2.3	14.2	1.8	45.9	332.2
21.5	73.3	4.3	14.0	2.2	42.0	327.6
22.5	83.0	5.0	13.2	1.2	38.8	199.7
23.5	93.0	4.2	16.2	1.7	32.0	153.4
24.5	103.3	5.3	18.2	0.8	33.7	0.0
25.5	114.0	3.3	17.8	1.3	40.5	282.9
26.5	124.9	4.2	8.9	0.6	43.0	197.4
27.5	136.2	5.7	13.4	1.6	42.3	237.0
28.5	147.8	3.6	9.9	1.0	39.5	196.6
29.5	159.7	4.8	10.5	0.9	42.7	283.8
30.5	172.0	3.2	11.1	1.2	42.3	442.2
31.5	184.5	4.6	13.1	1.0	41.3	568.6
32.5	197.4	3.9	11.6	1.2	42.9	465.1
33.5	210.6	5.9	12.4	1.1	39.3	392.3
34.5	224.1	3.9	9.4	0.8	47.4	347.8
35.5	237.9	5.0	9.1	2.1	38.9	313.6
36.5	252.1	2.9	10.8	0.8	45.0	402.0
37.5	266.5	2.4	11.9	1.1	37.7	373.1
38.5	281.3	1.7	14.2	1.4	46.3	355.2
39.5	296.4	2.9	7.9	1.0	47.5	358.0
Depth (cm)	**Age (cal.**	***G. bulloides***	***G. uvula***	***G. glutinata***	***G. quinqueloba***	**Planktonic**

	years BP)	(wt %)	(wt %)	(wt %)	(wt %)	Foram./g
40.5	311.8	4.4	8.9	1.4	45.7	286.3
41.5	327.6	3.7	11.9	1.1	41.0	306.0
42.5	343.6	3.3	10.7	2.3	46.2	326.9
43.5	360.0	5.1	7.6	2.0	39.4	496.7
44.5	376.7	3.1	8.5	3.4	45.6	276.6
45.5	393.7	3.4	17.0	1.1	35.5	383.8
46.5	411.0	4.6	15.8	1.4	39.4	542.5

A5.5 XRF core scanning (counts)

Depth (cm)	Age (cal. years BP)	Ca	Ti	Depth (cm)	Age (cal. years BP)	Ca	Ti
0.2	-57.5	74369	4316	8.4	-24.222928	97696	5544
0.4	-56.9	84701	4799	8.6	-23.144888	95968	5495
0.6	-56.3	84811	5162	8.8	-22.054112	94572	5575
0.8	-55.8	97120	5150	9	-20.9506	90515	5506
1	-55.2	100947	5561	9.2	-19.834352	101181	5751
1.2	-54.6	103175	5748	9.4	-18.705368	100239	6019
1.4	-53.9	105274	5908	9.6	-17.563648	99282	5827
1.6	-53.298368	107627	5950	9.8	-16.409192	103168	5977
1.8	-52.653352	106998	5852	10	-15.242	102175	5649
2	-51.9956	102337	6022	10.2	-14.062072	104251	6009
2.2	-51.325112	109438	6035	10.4	-12.869408	106778	5894
2.4	-50.641888	110025	5902	10.6	-11.664008	103405	5746
2.6	-49.945928	114879	6184	10.8	-10.445872	105679	5950
2.8	-49.237232	115578	6294	11	-9.215	106831	5563
3	-48.5158	115855	6434	11.2	-7.971392	105072	5694
3.2	-47.781632	116013	6744	11.4	-6.715048	106363	6142
3.4	-47.034728	115626	6438	11.6	-5.445968	106678	5470
3.6	-46.275088	115586	6072	11.8	-4.164152	108406	5534
3.8	-45.502712	117610	6188	12	-2.8696	111455	5243
4	-44.7176	113170	5820	12.2	-1.562312	106997	5418
4.2	-43.919752	116986	6243	12.4	-0.242288	105382	5605
4.4	-43.109168	118228	6082	12.6	1.090472	106485	5484
4.6	-42.285848	119296	6016	12.8	2.435968	108439	5647
4.8	-41.449792	116749	5846	13	3.7942	109855	5808
5	-40.601	118091	6277	13.2	5.165168	111245	6086
5.2	-39.739472	117536	5911	13.4	6.548872	109256	6079
5.4	-38.865208	114281	5846	13.6	7.945312	111622	5788
5.6	-37.978208	115929	6029	13.8	9.354488	108894	5730
5.8	-37.078472	113708	6127	14	10.7764	102063	5859
6	-36.166	110181	5670	14.2	12.211048	97985	5305
6.2	-35.240792	112689	6193	14.4	13.658432	92203	4971
6.4	-34.302848	110237	5915	14.6	15.118552	98725	5160
6.6	-33.352168	105686	5738	14.8	16.591408	97464	5342
6.8	-32.388752	108083	6051	15	18.077	96940	5172
7	-31.4126	104606	5620	15.2	19.575328	94102	5620
7.2	-30.423712	105349	5769	15.4	21.086392	91657	5091
7.4	-29.422088	105682	5559	15.6	22.610192	96316	5540
7.6	-28.407728	108010	5647	15.8	24.146728	96866	5289
7.8	-27.380632	102304	5668	16	25.696	83002	5064
8	-26.3408	102774	5626	16.2	27.258008	87493	5517
8.2	-25.288232	93548	5342	16.4	28.832752	87796	5327

Depth (cm)	Age (cal. years BP)	Ca	Ti	Depth (cm)	Age (cal. years BP)	Ca	Ti
16.6	30.420232	85068	5349	25	108.595	114357	6001
16.8	32.020448	90263	5600	25.2	110.730128	111280	5877
17	33.6334	93323	5531	25.4	112.877992	113576	6020
17.2	35.259088	98900	5467	25.6	115.038592	113514	6151
17.4	36.897512	102513	5568	25.8	117.211928	113721	5805
17.6	38.548672	105066	5187	26	119.398	110885	6154
17.8	40.212568	102506	5525	26.2	121.596808	100248	5909
18	41.8892	101464	5440	26.4	123.808352	81782	5657
18.2	43.578568	100580	5569	26.6	126.032632	87373	5287
18.4	45.280672	91856	5541	26.8	128.269648	102484	6286
18.6	46.995512	97609	5611	27	130.5194	99628	5903
18.8	48.723088	99718	5724	27.2	132.781888	90979	5593
19	50.4634	100442	5258	27.4	135.057112	95036	5851
19.2	52.216448	101761	5444	27.6	137.345072	102042	5511
19.4	53.982232	100913	5731	27.8	139.645768	103341	5965
19.6	55.760752	103005	5803	28	141.9592	107767	5704
19.8	57.552008	106214	5561	28.2	144.285368	110618	5734
20	59.356	107855	5885	28.4	146.624272	102631	5860
20.2	61.172728	110226	5911	28.6	148.975912	101780	5711
20.4	63.002192	105654	5561	28.8	151.340288	101379	6061
20.6	64.844392	105815	5510	29	153.7174	105838	6313
20.8	66.699328	109856	5969	29.2	156.107248	108169	6082
21	68.567	108724	5734	29.4	158.509832	109165	6050
21.2	70.447408	110906	5910	29.6	160.925152	112461	6308
21.4	72.340552	112347	5671	29.8	163.353208	113003	5948
21.6	74.246432	105775	5695	30	165.794	109492	6072
21.8	76.165048	106819	5939	30.2	168.247528	108913	6073
22	78.0964	111608	6366	30.4	170.713792	112244	6077
22.2	80.040488	109859	6031	30.6	173.192792	101884	5826
22.4	81.997312	107866	5898	30.8	175.684528	105610	5790
22.6	83.966872	110037	6013	31	178.189	104769	6140
22.8	85.949168	111487	5947	31.2	180.706208	102774	5588
23	87.9442	109521	5933	31.4	183.236152	107646	5747
23.2	89.951968	111411	5947	31.6	185.778832	105128	5738
23.4	91.972472	114440	6120	31.8	188.334248	110398	6254
23.6	94.005712	114663	6154	32	190.9024	106315	5826
23.8	96.051688	114583	6035	32.2	193.483288	100783	5780
24	98.1104	111381	5974	32.4	196.076912	104004	5918
24.2	100.181848	107819	5785	32.6	198.683272	106690	5542
24.4	102.266032	109506	5809	32.8	201.302368	104928	5759
24.6	104.362952	112860	6159	33	203.9342	87591	5077
24.8	106.472608	111721	5941	33.2	206.578768	92035	5184

Depth (cm)	Age (cal. years BP)	Ca	Ti	Depth (cm)	Age (cal. years BP)	Ca	Ti
33.4	209.236072	88282	5351	41.8	332.343448	106433	5909
33.6	211.906112	84912	5320	42	335.5484	110520	5802
33.8	214.588888	93969	5788	42.2	338.766088	108306	5771
34	217.2844	100029	5972	42.4	341.996512	109735	6064
34.2	219.992648	100356	5501	42.6	345.239672	110202	5703
34.4	222.713632	101750	5715	42.8	348.495568	112228	6364
34.6	225.447352	104481	6091	43	351.7642	113969	6258
34.8	228.193808	98491	5296	43.2	355.045568	116759	6431
35	230.953	92146	5560	43.4	358.339672	116821	6375
35.2	233.724928	95941	5291	43.6	361.646512	113802	6220
35.4	236.509592	94701	5737	43.8	364.966088	112539	6426
35.6	239.306992	94480	5620	44	368.2984	112627	6273
35.8	242.117128	102116	5559	44.2	371.643448	116127	6611
36	244.94	98073	5514	44.4	375.001232	114962	6402
36.2	247.775608	99010	5609	44.6	378.371752	117521	6423
36.4	250.623952	99351	5641	44.8	381.755008	116583	6230
36.6	253.485032	98225	5614	45	385.151	119310	6802
36.8	256.358848	98823	5544	45.2	388.559728	118702	6563
37	259.2454	97161	5632	45.4	391.981192	122345	7090
37.2	262.144688	97371	5292	45.6	395.415392	123066	6805
37.4	265.056712	101043	5551	45.8	398.862328	123708	7235
37.6	267.981472	103909	5870	46	402.322	119006	7009
37.8	270.918968	104044	5387	46.2	405.794408	121524	6367
38	273.8692	104898	5689	46.4	409.279552	118959	6498
38.2	276.832168	101157	5388	46.6	412.777432	122551	7172
38.4	279.807872	104557	5796	46.8	416.288048	122775	6926
38.6	282.796312	103924	5333	47	419.8114	116061	6992
38.8	285.797488	103671	5603	47.2	423.347488	125652	6789
39	288.8114	104639	5768	47.4	426.896312	126272	6817
39.2	291.838048	106498	5603	47.6	430.457872	128813	7016
39.4	294.877432	105075	5761	47.8	434.032168	127748	6811
39.6	297.929552	105268	5537	48	437.6192	124806	6859
39.8	300.994408	106167	5885	48.2	441.218968	126343	7068
40	304.072	104184	5704	48.4	444.831472	124401	7090
40.2	307.162328	84398	4469	48.6	448.456712	120657	6810
40.4	310.265392	99534	5406	48.8	452.094688	115590	6541
40.6	313.381192	100299	5550	49	455.7454	111536	6674
40.8	316.509728	104762	5871	49.2	459.408848	109021	6143
41	319.651	103320	6318				
41.2	322.805008	98898	5703				
41.4	325.971752	102655	5838				
41.6	329.151232	99833	5334				

Appendix 6: WOO/SC-3 relative abundances and absolute concentrations of microfossils and MAT reconstructions.

A6.1 Coccoliths

Depth (cm)	Age (cal. years BP)	*E. huxleyi* (wt. %)	*C. pelagicus* (wt. %)	*G. muellerae* (wt. %)	*C. leptoporus* (wt. %)	Bulk coccoliths (no.*10^8/g)
19.5	312.7	55.2	34.1	9.0	1.7	11.9
24.5	367.3	58.1	32.8	7.6	1.0	11.3
29.5	421.9	58.3	34.4	6.0	1.3	9.6
34.5	476.5	64.1	29.3	5.3	1.3	11.2
39.5	531.1	66.2	25.0	6.0	2.4	10.5
44.5	585.6	58.6	35.1	4.9	1.2	8.4
49.5	640.2	59.7	28.8	8.7	2.4	11.9
54.5	694.8	52.9	37.1	6.9	3.1	9.0
59.5	749.4	61.2	29.0	5.6	4.1	16.6
64.5	804.0	62.3	26.1	6.7	4.7	9.7
69.5	858.6	54.6	33.6	5.9	5.3	9.4
74.5	913.2	57.8	29.4	7.6	4.8	7.7
79.5	967.8	56.1	31.8	7.1	4.7	7.4
84.5	1022.4	58.1	26.6	7.6	7.4	10.4
89.5	1077.0	50.6	35.0	7.9	5.9	10.9
94.5	1131.6	58.3	27.5	7.1	6.2	11.0
99.5	1186.2	56.2	33.5	6.0	4.1	11.9
104.5	1240.8	52.7	34.1	6.2	6.9	10.0
109.5	1295.4	56.4	27.7	10.3	5.2	11.4
114.5	1350.0	56.6	27.7	8.7	7.0	12.2
119.5	1404.6	48.8	31.2	6.5	13.4	9.5
124.5	1461.4	53.9	28.8	6.2	10.6	10.5
129.5	1518.4	55.6	26.0	9.3	8.7	10.6
134.5	1575.4	50.3	31.2	9.0	9.5	10.2
139.5	1632.5	55.4	24.4	10.0	10.2	11.2
144.5	1689.5	55.4	28.3	7.5	8.9	11.2
149.5	1746.5	56.1	28.6	5.2	9.5	10.2
154.5	1803.6	56.6	26.2	5.5	11.6	9.5
159.5	1860.6	58.5	25.7	5.6	10.0	11.2
164.5	1917.6	60.8	25.6	3.5	10.1	9.9
169.5	1974.6	58.6	28.6	2.7	10.0	10.7
174.5	2031.7	67.2	19.6	5.0	8.0	9.0
179.5	2088.7	59.7	29.9	3.8	6.4	10.8
184.5	2145.7	63.6	27.1	4.0	5.1	11.8
189.5	2202.8	61.0	30.5	4.6	3.9	12.3
194.5	2259.8	61.0	28.2	5.5	4.7	7.8
199.5	2316.8	65.7	25.2	4.4	4.6	10.1

Depth (cm)	Age (cal. years BP)	*E. huxleyi* (wt. %)	*C. pelagicus* (wt. %)	*G. muellerae* (wt. %)	*C. leptoporus* (wt. %)	Bulk coccoliths (no.*10^8/g)
204.5	2373.9	61.2	29.2	6.0	3.6	9.4
209.5	2430.9	65.1	26.4	4.8	3.6	9.9
214.5	2487.9	66.0	26.4	2.8	4.7	9.1
219.5	2544.9	57.7	34.6	4.7	3.0	7.5
224.5	2602.0	71.5	23.3	3.1	2.2	9.2
229.5	2659.0	65.2	27.5	4.8	2.5	9.1
234.5	2716.0	70.2	23.4	5.1	1.3	10.8
239.5	2773.1	67.2	27.4	2.9	2.5	9.2
244.5	2830.1	69.7	23.5	4.2	2.4	9.1
249.5	2887.1	63.7	29.2	4.7	2.4	9.7
254.5	2944.2	67.4	25.4	5.0	2.2	10.8
259.5	3001.2	70.4	25.0	3.3	1.3	11.4
264.5	3058.2	74.5	20.6	3.9	1.1	11.7
269.5	3115.2	82.4	14.3	2.7	0.5	1.3
274.5	3172.3	70.5	21.2	3.8	3.8	0.9

A6.2 Dinocysts

Depth (cm)	Age (cal. years BP)	OCEN (wt. %)	PDAL (wt. %)	NLAB (wt. %)	BSPP (wt. %)	SRAM (wt. %)	SELO (wt. %)	BTEP (wt. %)	IMIN (wt. %)	SMIR (wt. %)
20.5	323.6	71.7	13.5	5.8	3.1	0.7	2.1	1.3	0.1	0.3
25.5	378.2	70.0	12.8	6.9	4.9	1.3	1.8	0.7	0.0	0.8
30.5	432.8	60.0	15.8	12.5	4.8	1.8	1.5	0.7	1.1	0.7
35.5	487.4	63.6	11.7	13.2	3.7	1.9	1.8	1.4	0.4	0.6
40.5	542.0	55.6	13.3	14.8	9.6	2.3	1.4	1.8	0.4	0.4
45.5	596.6	61.3	9.3	13.8	5.8	1.0	4.9	1.2	0.0	1.2
50.5	651.2	61.1	10.5	14.6	6.0	1.2	1.7	1.2	0.5	0.5
55.5	705.8	57.6	15.5	13.9	5.3	2.1	1.6	1.3	0.3	0.3
60.5	760.3	69.5	9.2	10.7	5.1	0.9	1.7	0.6	0.0	0.2
65.5	814.9	63.9	9.9	15.6	3.5	1.4	1.7	0.6	0.3	0.8
70.5	869.5	68.9	16.1	7.7	2.4	1.8	0.4	0.2	1.1	0.4
75.5	924.1	76.9	8.0	7.6	3.5	1.2	0.5	0.6	0.8	0.0
80.5	978.7	74.8	5.7	11.1	3.4	1.2	0.8	0.5	0.5	0.7
85.5	1033.3	74.7	5.6	9.9	4.0	1.3	0.5	1.3	0.2	1.3
90.5	1087.9	76.5	4.0	8.1	1.8	1.8	3.5	2.3	0.3	0.3
95.5	1142.5	76.7	4.2	7.2	4.5	2.5	1.5	1.2	0.5	0.5
100.5	1197.1	73.1	5.7	10.9	2.3	2.3	2.3	1.3	0.3	0.8
105.5	1251.7	69.1	6.0	15.2	3.1	1.0	1.3	1.0	0.5	0.8
110.5	1306.3	68.7	14.0	6.6	4.3	1.1	1.1	1.4	1.1	0.6
115.5	1360.9	64.1	18.6	9.3	2.3	0.3	0.3	1.0	1.7	0.0
120.5	1415.8	68.2	10.3	12.6	3.2	1.2	1.5	0.6	0.3	0.0
125.5	1472.8	66.4	9.8	11.5	4.4	1.6	1.4	0.8	0.8	1.1
130.5	1529.8	71.1	8.1	13.0	2.2	1.9	0.3	1.2	0.6	0.0
135.5	1586.8	62.9	14.2	9.9	3.6	1.3	3.0	1.0	1.3	0.0
140.5	1643.9	62.5	19.0	12.1	1.3	1.3	1.3	0.3	0.3	1.0
145.5	1700.9	63.7	11.6	16.2	2.1	1.2	1.5	0.3	0.6	0.3
150.5	1757.9	59.6	15.8	12.2	3.0	2.1	1.9	1.7	0.9	1.1
155.5	1815.0	72.7	3.0	12.3	3.9	0.3	1.8	1.5	0.3	1.8
160.5	1872.0	61.2	11.3	14.3	3.9	1.5	0.3	3.6	0.6	0.6
165.5	1929.0	67.3	3.4	11.1	5.8	1.8	2.4	2.1	0.5	1.6
170.5	1986.1	62.8	6.7	7.6	11.6	1.2	2.1	3.4	0.9	0.9
175.5	2043.1	64.1	9.9	10.5	6.4	0.6	1.2	4.7	0.6	0.9
180.5	2100.1	71.1	6.6	11.8	4.1	1.2	0.6	1.7	0.6	0.6
185.5	2157.1	71.7	7.8	10.3	4.3	1.8	0.9	0.4	0.5	0.9
190.5	2214.2	71.4	3.6	7.5	7.8	0.3	1.7	1.1	1.9	1.4
195.5	2271.2	80.6	4.3	5.3	1.9	0.2	1.7	0.5	0.5	2.2
200.5	2328.2	74.3	7.0	6.2	6.6	1.5	1.4	0.8	0.4	0.0
205.5	2385.3	81.6	3.0	5.2	4.8	1.3	1.6	0.5	0.0	0.7
210.5	2442.3	81.2	4.5	3.3	6.8	0.4	0.8	0.2	0.6	0.2
215.5	2499.3	84.3	2.0	3.3	5.9	1.3	0.5	0.5	0.5	0.5

Depth (cm)	Age (cal. years BP)	SSPP (wt. %)	IPAL (wt. %)	SQUA (wt. %)	HALO (no.*10^3/g)	Reworked (no.*10^3/g)	Dinocyst concentrations (no.*10^3/g)
20.5	323.6	0.1	0.0	0.1	0.0	0.1	30.2
25.5	378.2	0.5	0.0	0.0	0.0	0.0	23.2
30.5	432.8	0.7	0.2	0.2	0.0	0.0	16.9
35.5	487.4	0.6	0.0	0.2	0.0	0.0	15.3
40.5	542.0	0.0	0.2	0.4	0.0	0.2	18.9
45.5	596.6	0.8	0.4	0.2	0.0	0.1	20.8
50.5	651.2	0.5	0.2	1.1	0.0	0.1	16.6
55.5	705.8	0.0	0.8	0.5	0.0	0.2	20.2
60.5	760.3	0.6	0.0	0.4	0.1	0.2	25.3
65.5	814.9	0.6	1.0	0.4	0.0	0.0	12.8
70.5	869.5	0.0	0.4	0.0	0.0	0.1	33.8
75.5	924.1	0.2	0.3	0.2	0.0	0.0	21.3
80.5	978.7	0.3	0.2	0.2	0.0	0.0	20.2
85.5	1033.3	0.4	0.5	0.0	0.0	0.1	15.7
90.5	1087.9	1.0	0.0	0.0	0.0	0.1	9.3
95.5	1142.5	0.5	0.0	0.2	0.0	0.0	3.9
100.5	1197.1	0.0	0.3	0.0	0.0	0.0	10.9
105.5	1251.7	0.0	0.3	0.0	0.0	0.0	15.4
110.5	1306.3	0.6	0.6	0.0	0.0	0.3	24.5
115.5	1360.9	0.0	1.7	0.3	0.0	0.1	8.2
120.5	1415.8	1.2	0.3	0.0	0.0	0.0	13.7
125.5	1472.8	1.1	0.0	0.5	0.0	0.1	6.9
130.5	1529.8	0.3	0.9	0.3	0.0	0.0	17.7
135.5	1586.8	1.0	1.0	0.3	0.0	0.0	7.5
140.5	1643.9	0.3	0.0	0.0	0.0	0.0	10.9
145.5	1700.9	0.6	0.3	0.0	0.0	0.0	5.3
150.5	1757.9	0.0	0.2	0.4	0.0	0.1	11.7
155.5	1815.0	0.3	0.6	0.6	0.0	0.0	9.6
160.5	1872.0	1.2	0.0	0.6	0.0	0.0	18.5
165.5	1929.0	1.6	0.3	0.3	0.0	0.1	10.3
170.5	1986.1	0.3	0.3	0.3	0.1	0.1	30.8
175.5	2043.1	0.3	0.6	0.0	0.0	0.0	12.5
180.5	2100.1	0.8	0.2	0.0	0.0	0.0	8.9
185.5	2157.1	0.9	0.2	0.0	0.0	0.0	26.3
190.5	2214.2	0.8	0.8	0.0	0.0	0.0	5.2
195.5	2271.2	1.2	0.5	0.7	0.0	0.1	28.3
200.5	2328.2	0.6	0.0	0.4	0.0	0.0	18.0
205.5	2385.3	0.0	0.2	0.4	0.0	0.0	21.4
210.5	2442.3	0.4	0.2	0.4	0.0	0.0	27.5
215.5	2499.3	0.5	0.0	0.2	0.0	0.0	17.5

Depth (cm)	Age (cal. years BP)	OCEN (wt. %)	PDAL (wt. %)	NLAB (wt. %)	BSPP (wt. %)	SRAM (wt. %)	SELO (wt. %)	BTEP (wt. %)	IMIN (wt. %)	SMIR (wt. %)
220.5	2556.4	75.9	5.2	4.6	6.2	1.2	1.9	0.6	0.0	0.6
225.5	2613.4	73.9	3.7	6.8	8.6	1.0	1.6	0.5	0.8	1.0
230.5	2670.4	82.5	5.0	5.4	3.2	1.0	0.8	0.0	0.6	0.2
235.5	2727.4	76.2	6.1	6.3	6.6	0.7	1.5	0.7	0.5	0.0
240.5	2784.5	73.9	8.7	5.5	5.2	0.9	0.6	1.2	1.4	0.0
245.5	2841.5	81.4	2.3	4.7	5.0	1.4	1.7	0.5	0.2	1.2

Depth (cm)	Age (cal. years BP)	SSPP (wt. %)	IPAL (wt. %)	SQUA (wt. %)	HALO (no.*10^3/g)	Reworked (no.*10^3/g)	Dinocyst concentrations (no.*10^3/g)
220.5	2556.4	0.9	0.3	0.3	0.0	0.0	13.2
225.5	2613.4	0.5	0.5	0.0	0.0	0.1	11.4
230.5	2670.4	0.2	0.2	0.4	0.0	0.2	20.2
235.5	2727.4	0.5	0.0	0.2	0.0	0.1	14.8
240.5	2784.5	1.2	0.6	0.0	0.1	0.1	8.9
245.5	2841.5	0.5	0.5	0.0	0.0	0.0	9.8

A6.3 Modern Analogue Technique Results (MAT)

Reconstructed sea-surface temperatures and salinities during winter and summer, and sea ice durations (i and s → estimated lower and upper error ranges, respectively).

Depth (cm)	Age (cal. years BP)	TWIN	TWIN_i	TWIN_s	SWIN	SWIN_i	SWIN_s	TSUM	TSUM_i	TSUM_s
20.5	323.6	4.3	0.2	6.5	34.2	31.8	35.2	10.6	4.4	13.3
25.5	378.2	4.9	0.0	6.5	34.2	31.7	35.2	11.6	8.3	13.5
30.5	432.8	2.0	0.0	6.5	32.9	31.7	35.2	12.1	8.3	14.9
35.5	487.4	2.8	0.0	6.5	33.0	31.7	35.2	13.1	10.9	14.9
40.5	542.0	4.3	0.2	7.5	34.4	31.8	35.2	9.9	4.4	13.3
45.5	596.6	4.3	0.2	6.5	34.2	31.8	35.2	10.8	7.9	13.3
50.5	651.2	4.4	0.2	6.5	34.1	31.8	35.2	11.4	8.1	13.3
55.5	705.8	3.2	0.2	6.5	34.3	31.8	35.2	9.2	4.4	13.3
60.5	760.3	4.2	0.0	6.5	33.8	31.7	35.2	12.2	10.9	13.5
65.5	814.9	4.3	0.2	6.5	34.4	31.8	35.2	10.3	7.9	13.3
70.5	869.5	2.9	-0.2	6.5	34.9	34.7	35.2	7.7	3.9	10.9
75.5	924.1	4.6	0.2	6.5	34.4	31.8	35.2	10.7	7.1	13.3
80.5	978.7	5.5	0.2	6.5	34.5	31.8	35.2	11.6	10.6	13.3
85.5	1033.3	5.8	2.5	6.9	35.0	34.3	35.2	10.8	8.0	13.1
90.5	1087.9	2.2	-0.4	6.3	33.0	31.7	34.5	12.1	8.3	13.5
95.5	1142.5	3.6	0.0	6.5	33.6	31.8	35.2	12.0	8.3	14.9
100.5	1197.1	4.8	0.2	6.5	34.3	31.8	35.2	11.3	8.3	13.3
105.5	1251.7	4.8	0.2	6.5	34.5	31.8	35.2	11.0	8.9	13.3
110.5	1306.3	2.7	0.0	6.5	33.5	31.8	35.2	11.3	8.1	14.9
115.5	1360.9	3.3	0.7	6.4	35.0	34.7	35.1	7.5	3.9	10.6
120.5	1415.8	0.9	-0.4	3.5	32.5	31.7	34.5	12.3	8.3	14.9
125.5	1472.8	2.9	0.0	6.5	33.0	31.6	35.2	13.3	10.9	14.9
130.5	1529.8	3.6	2.1	6.4	35.0	34.8	35.2	8.5	7.1	10.9
135.5	1586.8	1.8	0.0	4.1	33.5	31.6	35.1	9.9	5.0	14.5
140.5	1643.9	4.2	0.0	6.9	33.8	31.7	35.2	12.3	10.9	13.5
145.5	1700.9	2.0	-0.4	6.5	33.0	31.7	35.2	11.7	8.3	13.5
150.5	1757.9	4.2	0.2	6.8	34.3	31.8	35.2	10.4	4.4	13.4
155.5	1815.0	6.0	4.1	6.5	35.2	35.1	35.2	10.3	7.9	11.0
160.5	1872.0	2.7	-0.3	6.5	32.9	31.6	35.2	13.4	10.9	14.9
165.5	1929.0	5.8	0.2	9.2	33.4	31.8	34.3	17.6	13.1	23.5
170.5	1986.1	1.4	0.0	6.5	32.3	31.6	35.2	13.6	10.9	14.6
175.5	2043.1	3.5	0.0	6.5	33.8	31.8	35.2	11.6	8.1	14.9
180.5	2100.1	4.0	0.0	6.5	33.7	31.8	35.2	12.5	10.6	14.9
185.5	2157.1	3.6	0.0	6.5	33.6	31.7	35.2	11.6	8.3	13.5
190.5	2214.2	3.4	1.4	6.4	35.0	34.9	35.1	7.0	5.0	10.6
195.5	2271.2	6.1	4.7	6.5	35.2	35.1	35.2	10.4	8.7	10.9
200.5	2328.2	2.7	0.0	6.5	33.1	31.8	35.2	13.1	8.3	17.6

Depth (cm)	Age (cal. years BP)	SSUM	SSUM_i	SSUM_s	Sea ice duration (months/yr)	Sea ice_i	Sea ice_s
20.5	323.6	33.5	30.5	35.1	0.6	0.0	1.7
25.5	378.2	33.6	30.5	35.1	0.3	0.0	1.8
30.5	432.8	32.1	30.4	35.1	1.0	0.0	1.8
35.5	487.4	32.0	30.4	35.1	1.0	0.0	1.8
40.5	542.0	33.8	30.5	35.1	0.6	0.0	1.7
45.5	596.6	33.6	30.5	35.1	0.3	0.0	1.7
50.5	651.2	33.5	30.5	35.1	0.4	0.0	1.7
55.5	705.8	33.7	30.5	35.1	0.7	0.0	1.7
60.5	760.3	33.0	30.5	35.1	0.6	0.0	1.8
65.5	814.9	34.1	30.5	35.1	0.3	0.0	1.7
70.5	869.5	34.7	34.1	35.1	0.4	0.0	1.3
75.5	924.1	34.1	30.5	35.1	0.4	0.0	1.7
80.5	978.7	34.0	30.5	35.1	0.3	0.0	1.7
85.5	1033.3	34.7	33.0	35.1	0.0	0.0	0.0
90.5	1087.9	31.9	30.5	34.3	0.9	0.0	1.8
95.5	1142.5	32.8	30.4	35.1	0.6	0.0	1.7
100.5	1197.1	33.7	30.5	35.1	0.3	0.0	1.7
105.5	1251.7	34.2	30.5	35.1	0.3	0.0	1.7
110.5	1306.3	32.9	30.4	35.1	0.7	0.0	1.7
115.5	1360.9	34.8	34.1	35.0	0.3	0.0	1.3
120.5	1415.8	31.5	30.4	34.3	1.2	0.0	1.8
125.5	1472.8	32.0	30.1	35.1	0.9	0.0	1.8
130.5	1529.8	34.9	34.7	35.1	0.0	0.0	0.0
135.5	1586.8	32.8	30.1	35.0	0.8	0.0	1.8
140.5	1643.9	33.0	30.5	35.1	0.6	0.0	1.8
145.5	1700.9	32.2	30.5	35.1	1.0	0.0	1.8
150.5	1757.9	33.6	30.5	35.1	0.7	0.0	1.7
155.5	1815.0	35.1	35.0	35.1	0.0	0.0	0.0
160.5	1872.0	31.7	29.6	35.1	0.8	0.0	1.8
165.5	1929.0	32.5	30.5	33.3	0.3	0.0	1.7
170.5	1986.1	31.3	30.1	35.1	1.4	0.0	1.8
175.5	2043.1	33.2	30.4	35.1	0.6	0.0	1.7
180.5	2100.1	32.9	30.4	35.1	0.6	0.0	1.7
185.5	2157.1	32.9	30.5	35.1	0.6	0.0	1.8
190.5	2214.2	34.9	34.4	35.0	0.3	0.0	1.2
195.5	2271.2	35.1	35.0	35.1	0.0	0.0	0.0
200.5	2328.2	32.2	30.4	35.1	0.7	0.0	1.7

Depth (cm)	Age (cal. years BP)	TWIN	TWIN_i	TWIN_s	SWIN	SWIN_i	SWIN_s	TSUM	TSUM_i	TSUM_s
205.5	2385.3	6.3	5.4	6.5	35.0	33.8	35.2	11.4	10.8	13.9
210.5	2442.3	6.0	4.1	6.5	35.2	35.1	35.2	10.4	8.1	11.0
215.5	2499.3	6.3	5.4	6.5	34.8	33.8	35.2	11.8	10.6	13.9
220.5	2556.4	4.8	0.2	6.5	34.3	31.8	35.2	11.3	8.1	13.3
225.5	2613.4	3.9	0.2	6.5	34.4	31.8	35.2	10.1	7.7	13.3
230.5	2670.4	6.3	5.1	6.9	35.2	35.1	35.2	10.8	9.9	11.1
235.5	2727.4	2.8	0.0	6.5	33.6	31.8	35.2	11.3	8.1	14.9
240.5	2784.5	2.8	0.0	4.1	34.1	31.8	35.1	9.5	6.4	14.9
245.5	2841.5	5.8	3.5	6.5	34.9	34.3	35.2	10.7	8.3	13.1

Depth (cm)	Age (cal. years BP)	SSUM	SSUM_i	SSUM_s	Sea ice duration (months/yr)	Sea ice_i	Sea ice_s
205.5	2385.3	34.6	32.1	35.1	0.0	0.0	0.0
210.5	2442.3	35.1	35.0	35.1	0.0	0.0	0.0
215.5	2499.3	34.2	32.1	35.1	0.0	0.0	0.0
220.5	2556.4	33.8	30.5	35.1	0.3	0.0	1.7
225.5	2613.4	34.1	30.5	35.1	0.3	0.0	1.7
230.5	2670.4	35.1	35.1	35.1	0.0	0.0	0.0
235.5	2727.4	32.9	30.4	35.1	0.7	0.0	1.7
240.5	2784.5	33.7	30.4	35.0	0.4	0.0	1.5
245.5	2841.5	34.6	33.0	35.1	0.0	0.0	0.0

Appendix 7: R406MC032 relative abundances and absolute concentrations of microfossils and MAT reconstructions.

A7.1 Coccoliths

Depth (cm)	Age (cal. years BP)	*E. huxleyi* (wt. %)	*C. pelagicus* (wt. %)	*G. muellerae* (wt. %)	*C. leptoporus* (wt. %)	Bulk coccoliths (no.*10^8/g)
0.5	-56.7	78.2	17.0	3.6	1.2	16.2
1.5	-48.0	71.5	23.8	3.0	1.7	14.6
2.5	-38.8	76.0	19.6	3.5	0.9	16.3
3.5	-28.9	67.8	28.1	2.8	1.4	13.1
4.5	-18.5	60.8	33.3	4.2	1.6	11.0
5.5	-7.5	57.1	35.9	3.7	3.4	11.1
6.5	4.0	51.1	43.3	3.6	2.0	11.2
7.5	16.1	64.4	29.1	4.2	2.3	11.1
8.5	28.8	64.6	28.2	3.0	4.2	9.6
9.5	42.1	55.5	37.9	4.3	2.3	8.5
10.5	55.9	62.1	31.0	3.6	3.3	6.4
11.5	70.3	57.9	32.7	5.4	4.0	7.3
12.5	85.3	53.3	38.9	3.1	4.7	5.2
13.5	100.8	64.4	31.7	2.9	1.0	3.3
14.5	117.0	77.4	20.0	1.6	1.0	4.0
15.5	133.6	88.1	11.9	0.0	0.0	1.4
16.5	150.9	84.7	14.5	0.8	0.0	2.7
17.5	168.7	81.7	18.3	0.0	0.0	1.2
18.5	187.2	65.0	30.7	1.5	2.9	2.9
19.5	206.1	74.7	20.2	0.0	5.1	1.8
20.5	225.7	58.5	37.4	2.7	1.4	2.7
21.5	245.8	75.7	22.6	1.7	0.0	2.4
22.5	266.5	71.2	25.8	1.8	1.2	3.0
23.5	287.8	72.1	23.4	1.3	3.2	2.5
24.5	309.6	68.5	26.9	3.1	1.5	2.7
25.5	332.0	98.2	1.8	0.0	0.0	1.4
26.5	355.0	72.5	20.2	3.7	3.7	2.0
27.5	378.5	81.8	15.6	2.6	0.0	1.6
28.5	402.7	80.6	17.9	0.0	1.5	1.4
29.5	427.3	89.7	7.4	1.5	1.5	1.3
30.5	452.6	71.7	20.8	3.8	3.8	1.1
31.5	478.4	76.6	20.3	0.0	3.1	1.3
32.5	504.9	88.9	11.1	0.0	0.0	0.9
33.5	531.8	79.1	16.3	0.0	4.7	0.8

A7.2 Dinocysts

Depth (cm)	Age (cal. years BP)	OCEN (wt. %)	PDAL (wt. %)	NLAB (wt. %)	SELO (wt. %)	SRAM (wt. %)	BSPP (wt. %)	IMIN (wt. %)	SSPP (wt. %)	SMIR (wt. %)
0.5	-56.7	65.2	15.2	8.4	1.8	2.3	0.5	1.1	1.8	0.7
1.5	-48.0	61.2	19.6	8.4	1.8	4.6	0.5	0.8	1.5	0.3
2.5	-38.8	71.3	6.2	7.8	3.8	4.0	1.6	1.1	0.2	1.1
3.5	-28.9	63.1	17.2	6.2	5.5	3.2	0.2	0.9	1.6	0.5
4.5	-18.5	79.3	9.5	4.4	2.1	2.2	0.5	0.9	0.6	0.3
5.5	-7.5	76.2	9.0	6.3	4.3	2.1	0.0	0.0	0.4	0.7
6.5	4.0	80.2	7.1	6.5	0.9	1.3	0.2	0.0	1.1	1.3
7.5	16.1	82.2	6.8	5.7	2.2	1.7	0.0	0.2	0.2	0.2
8.5	28.8	83.5	3.5	5.3	2.0	3.0	0.5	0.0	0.0	0.5
9.5	42.1	84.0	4.3	5.3	2.4	1.4	0.8	0.2	0.2	0.3
10.5	55.9	78.7	5.3	6.6	2.8	2.8	0.8	0.2	0.6	0.6
11.5	70.3	81.6	5.3	4.2	2.7	2.5	0.2	0.3	0.8	0.6
12.5	85.3	79.6	7.5	5.0	2.3	1.8	0.2	0.0	0.7	0.5
13.5	100.8	77.3	8.1	6.5	2.3	3.6	0.0	0.3	0.0	0.6
14.5	117.0	71.6	7.1	6.6	2.7	4.4	0.5	2.2	0.8	0.3
15.5	133.6	72.6	6.9	8.6	2.5	5.0	1.7	0.8	0.0	0.6
16.5	150.9	73.8	7.3	7.0	2.6	4.5	0.6	1.3	1.0	1.0
17.5	168.7	71.6	7.4	10.9	2.7	2.4	0.6	0.6	1.8	0.6
18.5	187.2	61.3	18.0	12.7	0.0	4.7	0.7	1.3	0.7	0.0
19.5	206.1	75.8	6.2	10.8	1.5	1.5	0.0	1.0	0.0	0.5
20.5	225.7	77.7	6.1	6.7	0.9	3.1	2.4	0.3	0.0	0.3
21.5	245.8	75.0	8.5	4.7	0.9	0.9	3.8	5.3	0.0	0.0
22.5	266.5	76.4	10.7	4.7	2.2	2.8	0.6	0.3	1.6	0.3
23.5	287.8	83.1	5.3	3.2	1.8	2.4	2.1	0.8	0.3	0.3
24.5	309.6	72.5	11.1	4.7	3.0	1.7	1.7	2.7	1.0	0.0
25.5	332.0	57.7	13.1	7.9	4.5	2.6	7.1	2.2	2.2	0.4
26.5	355.0	64.1	15.4	6.1	2.6	4.2	3.5	1.6	1.0	0.0
27.5	378.5	62.3	13.4	4.5	4.5	8.9	1.5	0.6	0.9	0.3
28.5	402.7	56.3	22.0	2.5	5.6	4.6	1.2	2.5	2.5	0.0
29.5	427.3	52.7	16.3	6.3	8.4	5.1	3.9	1.5	2.1	0.0
30.5	452.6	45.7	10.4	3.8	10.4	5.4	15.1	2.8	2.2	0.3
31.5	478.4	49.7	14.7	3.8	7.4	5.0	10.9	3.8	1.5	0.0
32.5	504.9	33.1	15.7	4.7	8.0	7.4	22.2	1.8	1.8	0.0

Depth (cm)	Age (cal. years BP)	IPAL (wt. %)	SQUA (wt. %)	HALO ((no.*10^3/1000)/g)	Reworked (no.*10^3/g)	Dinocyst concentrations (no.*10^3/g)
0.5	-56.7	0.7	0.2	0.0	0.1	14.2
1.5	-48.0	0.5	0.0	0.0	0.0	8.6
2.5	-38.8	0.0	0.4	0.0	0.0	19.5
3.5	-28.9	0.0	0.0	0.0	0.0	13.5
4.5	-18.5	0.0	0.0	0.0	0.0	16.1
5.5	-7.5	0.0	0.0	0.0	0.0	25.2
6.5	4.0	0.4	0.2	0.0	0.1	47.3
7.5	16.1	0.6	0.0	0.0	0.0	22.9
8.5	28.8	0.3	0.0	0.0	0.0	25.4
9.5	42.1	0.8	0.0	0.0	0.1	23.7
10.5	55.9	0.8	0.0	0.0	0.0	18.6
11.5	70.3	0.6	0.2	0.0	0.1	21.5
12.5	85.3	0.5	0.2	0.0	0.0	16.4
13.5	100.8	0.3	0.0	0.0	0.1	7.8
14.5	117.0	0.5	0.3	0.0	0.0	6.3
15.5	133.6	0.3	0.0	0.0	0.1	4.5
16.5	150.9	0.3	0.0	0.0	0.0	3.7
17.5	168.7	0.6	0.0	0.0	0.0	4.9
18.5	187.2	0.7	0.0	0.0	0.0	1.0
19.5	206.1	0.5	0.0	0.0	0.0	1.3
20.5	225.7	0.3	0.3	0.0	0.0	2.3
21.5	245.8	0.0	0.3	0.0	0.0	2.4
22.5	266.5	0.0	0.0	0.0	0.0	3.3
23.5	287.8	0.0	0.0	0.0	0.0	2.4
24.5	309.6	0.0	0.0	0.0	0.0	2.6
25.5	332.0	0.4	0.4	0.0	0.0	1.1
26.5	355.0	0.0	0.3	0.0	0.0	1.9
27.5	378.5	0.0	0.3	0.0	0.0	1.7
28.5	402.7	0.0	0.0	0.0	0.0	1.5
29.5	427.3	0.6	0.3	0.0	0.0	1.5
30.5	452.6	0.0	0.3	0.0	0.0	3.5
31.5	478.4	0.6	0.3	0.0	0.0	2.5
32.5	504.9	0.3	0.6	0.1	0.0	3.1

A7.3 Modern Analogue Technique Results (MAT) + IRD

Reconstructed sea-surface temperatures and salinities during winter and summer, and sea ice durations (i and s → estimated lower and upper error ranges, respectively) + IRD >150µm.

Depth (cm)	Age (cal. years BP)	TWIN	TWIN_i	TWIN_s	SWIN	SWIN_i	SWIN_s	TSUM	TSUM_i	TSUM_s
0.5	-56.7	4.1	0.2	6.4	34.0	31.8	35.1	11.3	8.3	13.3
1.5	-48.0	1.5	-0.4	4.2	33.0	31.7	35.0	11.4	8.3	13.5
2.5	-38.8	4.1	0.2	6.4	33.1	31.8	34.3	14.8	13.1	17.6
3.5	-28.9	2.7	-0.4	6.4	33.4	31.7	35.0	11.5	8.3	13.5
4.5	-18.5	1.0	-0.5	3.5	32.8	31.6	34.5	12.0	8.3	14.9
5.5	-7.5	5.3	3.2	6.4	34.7	34.3	35.2	11.1	8.5	13.1
6.5	4.0	6.4	6.3	6.4	34.8	34.3	35.2	11.9	10.8	13.1
7.5	16.1	1.6	-0.2	3.5	34.7	34.3	34.9	6.2	3.6	8.9
8.5	28.8	5.3	3.5	6.5	34.9	34.3	35.2	10.5	8.7	13.1
9.5	42.1	3.3	0.0	6.5	34.8	34.5	35.2	8.4	5.8	10.9
10.5	55.9	4.5	0.0	6.5	34.5	34.3	35.2	10.1	5.8	13.1
11.5	70.3	5.3	3.5	6.4	34.6	34.3	35.2	10.9	8.3	13.1
12.5	85.3	5.3	3.8	6.4	34.9	34.3	35.2	10.6	8.9	13.1
13.5	100.8	3.7	0.6	6.4	34.7	34.3	35.0	8.7	3.6	13.1
14.5	117.0	2.7	0.2	3.8	33.2	31.8	35.0	12.7	8.3	16.9
15.5	133.6	2.4	0.2	6.5	34.1	31.8	35.2	8.4	3.6	13.3
16.5	150.9	1.1	-0.5	3.5	33.0	31.6	34.8	11.0	6.3	14.3
17.5	168.7	2.0	-0.4	6.3	32.9	31.7	34.5	11.9	8.3	13.5
18.5	187.2	0.9	-0.2	2.1	34.7	34.7	34.8	5.9	3.6	7.8
19.5	206.1	1.8	-1.8	6.4	34.4	33.5	34.9	6.2	1.1	13.1
20.5	225.7	5.0	1.8	6.5	34.8	33.8	35.2	9.7	4.4	13.9
21.5	245.8	1.2	-0.3	6.5	32.4	31.6	35.2	13.6	10.9	14.9
22.5	266.5	1.9	-0.4	6.3	32.8	31.7	34.5	12.4	8.3	14.9
23.5	287.8	2.3	0.0	6.5	33.2	31.7	35.2	11.9	8.3	14.9
24.5	309.6	0.6	-0.4	3.5	32.2	31.7	34.5	12.8	8.3	14.9
25.5	332.0	0.8	0.0	3.5	32.2	31.6	34.5	12.8	8.3	14.6
26.5	355.0	0.0	-0.4	0.2	31.8	31.7	31.8	13.4	12.5	14.9
27.5	378.5	2.0	0.0	6.3	32.8	31.7	34.5	12.1	8.3	13.5
28.5	402.7	-0.2	-0.8	0.2	32.3	31.7	34.6	12.1	5.3	14.9
29.5	427.3	0.8	-0.4	3.5	32.3	31.6	34.5	12.3	8.3	14.6
30.5	452.6	1.5	0.0	4.0	31.9	31.6	32.7	15.2	13.5	17.2
31.5	478.4	1.3	-1.0	4.0	32.6	31.6	34.5	12.8	8.3	17.2
32.5	504.9	0.9	0.0	4.0	31.8	31.6	32.7	14.5	12.5	17.2

Depth (cm)	Age (cal. years BP)	SSUM	SSUM_i	SSUM_s	Sea ice duration (months/yr)	Sea ice_i	Sea ice_s	Total Lithic Grains (>150 µm * 10^3/g)
0.5	-56.7	33.1	30.5	35.0	0.4	0.0	1.7	2.1
1.5	-48.0	32.2	30.5	35.0	1.0	0.0	1.8	3.2
2.5	-38.8	32.1	30.5	33.0	0.4	0.0	1.7	1.8
3.5	-28.9	32.6	30.5	35.0	0.7	0.0	1.8	1.4
4.5	-18.5	31.6	30.0	34.3	1.4	0.0	4.0	0.7
5.5	-7.5	34.1	33.0	35.1	0.0	0.0	0.0	2.2
6.5	4.0	34.2	33.0	35.1	0.0	0.0	0.0	2.9
7.5	16.1	34.2	33.2	35.0	0.8	0.0	3.5	2.5
8.5	28.8	34.5	33.0	35.1	0.0	0.0	0.0	3.4
9.5	42.1	34.6	34.3	35.1	0.1	0.0	0.3	2.1
10.5	55.9	33.9	33.0	35.1	0.1	0.0	0.3	3.4
11.5	70.3	34.1	33.0	35.1	0.0	0.0	0.0	4.7
12.5	85.3	34.6	33.0	35.1	0.0	0.0	0.0	2.7
13.5	100.8	34.1	33.0	35.0	0.8	0.0	3.5	2.4
14.5	117.0	32.6	30.5	34.9	0.4	0.0	1.7	1.8
15.5	133.6	33.5	30.5	35.1	1.1	0.0	3.5	1.8
16.5	150.9	32.0	30.0	34.3	1.4	0.0	4.0	1.8
17.5	168.7	32.0	30.5	34.3	0.9	0.0	1.8	3.1
18.5	187.2	34.4	33.4	34.8	0.5	0.0	1.3	1.8
19.5	206.1	33.5	31.9	35.0	1.8	0.0	5.6	2.8
20.5	225.7	34.3	32.1	35.1	0.2	0.0	1.3	5.1
21.5	245.8	31.2	29.6	35.1	1.7	0.0	4.0	2.6
22.5	266.5	31.8	30.4	34.3	1.0	0.0	1.8	4.3
23.5	287.8	32.4	30.4	35.1	0.9	0.0	1.8	2.9
24.5	309.6	31.2	30.4	34.3	1.3	0.0	1.8	3.6
25.5	332.0	31.2	30.1	34.3	1.4	0.0	1.8	3.3
26.5	355.0	30.5	30.4	30.7	1.7	1.5	1.8	2.7
27.5	378.5	31.8	30.5	34.3	1.1	0.0	1.8	8.5
28.5	402.7	31.1	30.4	33.6	2.0	1.5	3.4	11.5
29.5	427.3	31.4	30.5	34.3	1.3	0.0	1.8	4.5
30.5	452.6	31.2	30.1	32.3	0.7	0.0	1.8	0.0
31.5	478.4	31.6	30.1	34.3	0.9	0.0	1.8	0.0
32.5	504.9	30.7	30.1	31.5	1.4	0.0	1.8	0.0

Appendix 8: HH11-134-BC relative abundances and absolute concentrations of microfossils and MAT reconstructions.

A8.1 Coccoliths

Depth (cm)	Age (cal. years BP)	*E. huxleyi* (wt. %)	*C. pelagicus* (wt. %)	*G. muellerae* (wt. %)	*C. leptoporus* (wt. %)	Bulk coccoliths (no.*10^8/g)
0.25	-37.8	50.8	36.5	11.3	1.1	4.4
0.75	-31.9	51.0	32.6	12.8	3.1	5.1
1.25	-24.0	48.2	41.5	8.5	1.5	5.6
1.75	-14.1	55.3	35.5	6.3	1.5	5.7
2.25	-2.3	42.4	51.7	5.0	0.6	3.7
2.75	11.5	47.9	40.5	8.6	2.3	3.0
3.25	27.3	43.9	48.6	6.1	1.0	4.1
3.75	45.0	39.2	54.5	4.5	1.3	5.3
4.25	64.6	35.8	50.9	10.7	1.8	3.1
4.75	86.2	38.5	51.8	5.4	2.3	3.7
5.25	109.8	35.2	57.7	6.6	0.0	5.5
5.75	135.3	52.2	40.8	5.7	0.5	5.7
6.25	162.8	42.5	48.2	6.3	2.7	4.2
6.75	192.2	35.7	55.8	6.1	1.4	4.2
7.25	223.6	43.0	47.6	6.6	1.4	4.1
7.75	257.0	35.5	55.4	4.7	2.9	3.8
8.25	292.3	36.0	52.1	6.8	4.2	4.4
8.75	329.5	32.5	58.9	4.0	4.0	6.4
9.25	368.8	41.1	45.3	10.0	3.4	5.8
9.75	409.9	36.8	53.3	7.1	2.8	6.0
10.25	453.1	38.5	53.1	6.0	1.8	5.4
10.75	498.2	38.1	55.5	3.8	2.3	5.5
11.25	545.2	37.5	52.7	6.1	3.7	4.2
11.75	594.2	40.3	50.8	6.4	2.2	4.5
12.25	645.2	31.9	60.4	5.1	2.2	4.4
12.75	698.1	33.3	60.1	2.6	3.7	4.2
13.25	753.0	32.2	53.5	7.3	6.6	4.9
13.75	809.8	46.6	39.8	9.1	3.6	3.8
14.25	868.6	42.2	45.2	7.6	4.7	4.9
14.75	929.3	44.4	42.2	9.7	3.5	5.2
15.25	992.0	48.8	38.6	7.9	4.3	3.6
15.75	1056.7	41.3	45.0	8.9	4.8	3.8
16.25	1123.3	36.3	53.8	6.0	3.3	5.2
16.75	1191.9	44.0	39.9	11.7	4.4	4.8
17.25	1262.4	31.2	56.4	6.2	5.4	4.3
17.75	1334.9	34.2	55.3	4.6	5.1	5.4
18.25	1409.3	35.6	56.0	4.0	4.2	7.2

Depth (cm)	Age (cal. years BP)	*E. huxleyi* (wt. %)	*C. pelagicus* (wt. %)	*G. muellerae* (wt. %)	*C. leptoporus* (wt. %)	Bulk coccoliths (no.*10^8/g)
18.75	1485.7	33.5	52.5	9.3	4.7	3.6
19.25	1564.0	32.4	54.6	6.1	5.8	5.4
19.75	1644.3	28.0	58.0	7.6	6.1	3.7
20.25	1726.6	27.7	59.9	5.4	6.7	5.5
20.75	1810.8	26.0	62.8	5.7	4.7	4.3
21.25	1897.0	30.3	56.3	6.2	6.5	4.5
21.75	1985.1	29.2	56.3	7.8	5.7	4.8
22.25	2075.2	40.3	46.9	7.3	4.8	3.8
22.75	2167.3	35.3	50.6	8.3	4.5	4.4
23.25	2261.3	30.1	59.2	4.3	5.7	4.0
23.75	2357.2	43.6	48.7	4.0	3.7	4.1
24.25	2455.2	38.1	55.9	1.4	3.4	3.5
24.75	2555.0	34.9	59.6	2.7	2.7	3.6
25.25	2656.9	35.8	55.3	4.4	4.0	3.2
25.75	2760.6	32.3	59.5	4.3	3.9	3.7
26.25	2866.4	42.6	52.5	2.5	2.0	3.5
26.75	2974.1	36.1	59.0	1.2	3.0	2.4
27.25	3083.7	29.8	62.4	3.9	3.1	3.0
27.75	3195.4	33.2	59.8	2.7	2.3	2.6
28.25	3308.9	37.5	49.3	6.6	6.6	1.9
28.75	3424.4	35.0	58.4	3.3	1.9	3.6
29.25	3541.9	23.3	67.9	5.2	3.1	2.3
29.75	3661.4	24.4	68.9	2.9	2.9	2.5
30.25	3782.8	27.9	66.2	1.5	4.4	2.0
30.75	3906.1	34.4	61.0	3.9	0.6	2.2
31.25	4031.4	33.5	57.8	3.7	4.1	3.0
31.75	4158.7	40.2	47.1	4.9	7.8	1.5
32.25	4287.9	33.9	61.4	0.5	3.7	2.2
32.75	4419.1	37.1	53.8	3.7	4.0	3.6
33.25	4552.2	33.2	61.3	1.5	4.0	2.9
33.75	4687.3	40.1	50.5	1.6	7.1	2.6
34.25	4824.4	29.0	63.9	1.9	3.2	1.9
34.75	4963.4	34.6	57.2	3.7	4.1	3.1
35.25	5104.3	33.6	55.5	5.3	5.0	4.2
35.75	5247.2	25.6	68.4	1.8	4.2	3.3
36.25	5392.1	30.6	59.9	5.4	3.7	4.2
36.75	5538.9	20.7	75.7	1.4	1.7	7.2
37.25	5687.7	31.3	61.3	4.1	1.8	3.1
37.75	5838.5	34.1	56.6	7.2	2.0	3.6
38.25	5991.2	23.8	69.8	2.7	3.7	3.5
38.75	6145.8	24.7	69.3	3.9	1.2	8.1

Depth (cm)	Age (cal. years BP)	E. huxleyi (wt. %)	C. pelagicus (wt. %)	G. muellerae (wt. %)	C. leptoporus (wt. %)	Bulk coccoliths (no.*10^8/g)
39.25	6302.4	34.2	59.1	3.0	2.3	4.2
39.75	6461.0	33.3	57.9	6.9	1.2	5.6
40.25	6621.5	40.1	50.5	6.4	3.1	4.7
40.75	6784.0	35.9	55.8	4.8	2.9	4.4

A8.2 Dinocysts

Depth (cm)	Age (cal. years BP)	OCEN (wt. %)	PDAL (wt. %)	IMIN (wt. %)	NLAB (wt. %)	SELO (wt. %)	BSPP (wt. %)	SRAM (wt. %)	IPAL (wt. %)	SMIR (wt. %)	SQUA (wt. %)
0.25	-37.8	67.9	4.8	8.6	7.6	1.9	4.1	2.2	1.6	0.0	0.0
0.75	-31.9	64.9	7.2	12.8	6.7	2.6	2.0	2.0	1.2	0.0	0.0
1.25	-24.0	62.0	13.1	7.0	7.6	3.0	5.2	0.0	0.9	0.0	0.0
1.75	-14.1	69.5	6.6	8.5	5.9	3.0	2.0	1.3	2.0	0.3	0.0
2.25	-2.3	64.6	8.1	8.4	6.7	2.3	4.6	2.6	0.9	0.3	0.3
2.75	11.5	67.8	9.5	5.0	7.8	2.6	0.6	2.2	1.2	0.6	0.0
3.25	27.3	66.1	12.6	6.6	7.1	1.6	2.4	1.6	1.6	0.0	0.0
3.75	45.0	75.2	2.7	5.4	7.8	2.7	1.2	2.1	0.3	0.3	0.0
4.25	64.6	75.0	4.1	8.7	4.8	2.3	1.2	2.3	0.8	0.2	0.0
4.75	86.2	73.4	6.1	6.6	3.9	3.3	1.9	1.7	0.6	0.6	0.0
6.25	162.8	69.3	8.5	6.3	7.0	2.8	2.2	1.7	0.4	0.0	0.0
6.75	192.2	73.9	5.4	5.6	6.4	3.5	1.7	1.7	0.4	0.4	0.0
7.25	223.6	72.7	2.2	9.7	7.3	3.0	0.9	0.6	0.4	0.6	0.0
7.75	257.0	70.1	10.5	3.0	4.4	5.8	1.4	1.7	1.4	0.0	0.0
8.25	292.3	80.3	2.7	4.1	4.3	3.6	1.4	0.9	0.7	0.4	0.0
8.75	329.5	75.5	5.5	8.3	5.3	2.3	0.0	0.8	1.3	0.0	0.3
9.25	368.8	80.8	2.9	5.2	5.4	2.5	1.0	0.8	0.8	0.0	0.0
9.75	409.9	82.1	4.2	3.2	5.4	1.9	0.1	1.5	0.4	0.4	0.1
10.25	453.1	75.2	3.6	4.1	9.1	1.8	2.5	1.1	0.7	0.2	0.0
10.75	498.2	80.4	4.4	5.1	3.6	2.7	0.4	1.7	0.4	0.2	0.0
11.25	545.2	77.5	5.3	5.5	6.2	0.5	1.4	1.8	0.2	0.5	0.0
11.75	594.2	78.2	4.4	6.9	4.4	2.0	1.2	1.9	0.2	0.0	0.0
12.25	645.2	84.5	2.3	1.5	5.5	1.5	1.5	0.5	0.3	0.3	0.0
12.75	698.1	82.5	3.8	4.6	5.1	0.7	0.9	0.4	0.9	0.4	0.0
13.25	753.0	81.1	3.9	4.2	3.9	1.9	1.9	1.4	0.4	0.2	0.0
13.75	809.8	82.5	2.0	3.1	4.8	2.0	2.2	1.4	1.0	0.0	0.0
14.25	868.6	81.8	1.7	5.9	4.6	1.3	1.3	1.1	0.4	0.2	0.0
14.75	929.3	81.9	2.9	5.2	5.1	1.0	2.0	0.7	0.3	0.1	0.0
15.25	992.0	83.4	2.8	3.4	4.9	0.9	1.3	0.4	0.9	0.6	0.0
15.75	1056.7	84.1	3.0	3.9	5.2	1.3	0.9	0.6	0.4	0.0	0.0
16.5	1157.3	86.3	0.6	2.1	5.3	1.4	1.1	1.0	0.5	0.2	0.0
16.75	1191.9	76.1	5.4	7.5	5.0	1.3	1.9	1.1	0.6	0.0	0.0
17.25	1262.4	77.8	5.9	5.2	4.4	1.0	1.5	0.5	0.8	0.5	0.3
17.75	1334.9	77.5	2.0	4.3	8.2	2.4	2.0	1.4	0.4	0.4	0.0
18.25	1409.3	78.9	3.5	3.6	7.7	1.0	1.5	1.5	0.4	0.3	0.0
18.75	1485.7	75.1	2.5	6.3	6.2	1.7	3.6	0.8	0.4	0.8	0.1
19.25	1564.0	80.0	2.4	5.2	7.0	1.1	1.5	0.7	0.2	0.6	0.0
19.75	1644.3	72.9	2.6	9.2	6.8	1.2	3.1	1.2	0.9	0.5	0.0
20.25	1726.6	75.1	2.8	6.4	8.1	1.7	2.0	1.1	1.2	0.2	0.0
20.75	1810.8	78.8	2.3	3.8	8.1	1.5	2.0	1.3	0.5	0.3	0.0

Depth (cm)	Age (cal. years BP)	HALO ((no.*10^3)/g)	Reworked (no.*10^3/g)	Dinocyst concentrations (no.*10^3/g)
0.25	-37.8	0.2	0.1	7.4
0.75	-31.9	0.2	0.0	8.2
1.25	-24.0	0.2	0.0	6.7
1.75	-14.1	0.1	0.0	12.8
2.25	-2.3	0.4	0.1	11.0
2.75	11.5	0.0	0.0	13.6
3.25	27.3	0.1	0.0	16.2
3.75	45.0	0.2	0.0	14.3
4.25	64.6	0.4	0.0	17.0
4.75	86.2	0.0	0.0	15.3
6.25	162.8	0.0	0.0	19.0
6.75	192.2	0.0	0.0	24.4
7.25	223.6	0.2	0.0	11.0
7.75	257.0	0.3	0.1	38.8
8.25	292.3	0.3	0.0	19.5
8.75	329.5	0.1	0.0	16.7
9.25	368.8	0.1	0.0	11.6
9.75	409.9	0.0	0.0	22.7
10.25	453.1	0.0	0.1	32.9
10.75	498.2	0.2	0.1	31.7
11.25	545.2	0.3	0.0	28.2
11.75	594.2	0.1	0.1	23.8
12.25	645.2	0.1	0.0	23.3
12.75	698.1	0.0	0.0	23.3
13.25	753.0	0.2	0.1	34.2
13.75	809.8	0.4	0.1	29.5
14.25	868.6	0.1	0.0	27.8
14.75	929.3	0.2	0.0	33.9
15.25	992.0	0.2	0.0	32.7
15.75	1056.7	0.3	0.1	30.0
16.5	1157.3	0.1	0.0	22.9
16.75	1191.9	0.3	0.0	8.0
17.25	1262.4	0.0	0.1	28.6
17.75	1334.9	0.1	0.0	19.1
18.25	1409.3	0.1	0.2	29.4
18.75	1485.7	0.2	0.0	32.5
19.25	1564.0	0.1	0.0	23.2
19.75	1644.3	0.3	0.0	18.0
20.25	1726.6	0.2	0.1	30.1
20.75	1810.8	0.1	0.1	26.3

Depth (cm)	Age (cal. years BP)	OCEN (wt. %)	PDAL (wt. %)	IMIN (wt. %)	NLAB (wt. %)	SELO (wt. %)	BSPP (wt. %)	SRAM (wt. %)	IPAL (wt. %)	SMIR (wt. %)	SQUA (wt. %)
21.25	1897.0	81.9	1.5	3.5	6.6	2.2	1.5	0.8	0.5	0.2	0.0
21.75	1985.1	82.2	1.9	4.8	5.5	1.0	2.4	1.4	0.0	0.0	0.0
22.25	2075.2	80.0	2.0	4.4	5.5	2.2	2.4	1.2	0.2	0.4	0.0
22.75	2167.3	80.1	3.5	1.8	8.8	1.1	1.3	1.1	0.7	0.2	0.0
23.25	2261.3	82.6	1.7	5.3	4.5	1.5	1.5	1.1	0.4	0.4	0.0
23.75	2357.2	84.6	1.6	3.0	4.0	2.1	1.2	1.3	0.7	0.4	0.1
24.25	2455.2	80.8	3.5	3.5	6.1	2.0	2.0	0.3	0.3	0.2	0.0
24.75	2555.0	84.6	2.7	3.5	4.3	1.4	0.3	1.7	0.3	0.0	0.0
25.25	2656.9	82.1	3.7	2.3	5.7	2.5	1.2	1.1	0.0	0.3	0.0
25.75	2760.6	87.3	0.9	3.4	3.9	1.9	0.9	0.7	0.3	0.0	0.0
26.25	2866.4	79.8	3.8	5.1	4.8	2.5	1.1	0.8	0.8	0.0	0.0
26.75	2974.1	82.7	2.4	3.8	6.3	1.9	0.7	1.0	0.0	0.2	0.0
27.25	3083.7	77.0	6.1	3.8	6.6	1.3	1.0	1.5	0.3	0.0	0.0
27.75	3195.4	83.0	2.3	4.2	4.6	2.1	0.4	1.5	0.2	0.4	0.0
28.25	3308.9	82.1	0.4	4.6	4.6	2.7	1.3	1.1	0.5	0.4	0.0
28.75	3424.4	75.7	4.7	6.0	6.0	1.4	1.9	2.5	0.6	0.0	0.0
29.25	3541.9	74.8	5.1	5.5	8.0	0.7	1.7	2.3	0.3	0.1	0.0
29.75	3661.4	77.4	2.3	4.3	7.0	1.8	1.3	2.2	0.8	0.5	0.0
30.25	3782.8	77.6	2.8	4.8	4.8	1.8	3.0	3.2	0.6	0.2	0.0
30.75	3906.1	72.4	7.6	5.4	8.9	0.8	0.5	1.9	1.4	0.0	0.0
32.25	4287.9	80.7	2.5	3.7	7.5	1.4	1.1	1.6	0.2	0.5	0.0
32.75	4419.1	77.7	1.6	4.4	7.7	2.1	0.9	2.8	0.9	0.2	0.0
33.75	4687.3	72.4	4.8	3.6	9.7	2.2	2.4	2.6	0.4	0.6	0.0
34.25	4824.4	74.6	3.0	4.3	8.0	3.3	1.1	3.4	0.5	0.0	0.0
34.75	4963.4	71.8	4.4	4.2	11.5	1.5	1.1	2.4	0.2	0.4	0.0
35.25	5104.3	72.0	3.4	2.6	12.0	2.4	1.4	4.2	0.6	0.0	0.0
35.75	5247.2	70.0	2.9	4.1	13.5	0.9	1.8	4.4	0.6	0.3	0.0
36.25	5392.1	72.1	1.8	3.1	15.1	1.1	1.1	3.6	0.0	0.2	0.0
36.75	5538.9	69.0	4.2	3.7	13.7	2.1	1.3	2.5	1.0	0.2	0.0
37.25	5687.7	70.4	2.4	4.1	14.4	2.8	1.3	1.7	0.6	0.8	0.0
37.75	5838.5	48.8	2.1	9.3	27.7	3.9	1.5	2.7	0.6	0.3	0.0
38.25	5991.2	46.1	3.6	8.7	31.3	3.1	1.4	2.2	1.4	0.3	0.0
38.75	6145.8	47.1	4.4	9.7	25.8	4.4	1.4	2.8	1.1	0.6	0.0
39.25	6302.4	45.1	6.5	14.0	26.6	1.0	2.3	2.6	1.3	0.0	0.0

Depth (cm)	Age (cal. years BP)	HALO ((no.*10^3)/g)	Reworked (no.*10^3/g)	Dinocyst concentrations (no.*10^3/g)
21.25	1897.0	0.1	0.0	21.9
21.75	1985.1	0.0	0.0	18.8
22.25	2075.2	0.3	0.1	27.6
22.75	2167.3	0.2	0.0	39.2
23.25	2261.3	0.1	0.1	43.1
23.75	2357.2	0.3	0.0	24.4
24.25	2455.2	0.2	0.1	33.1
24.75	2555.0	0.2	0.0	20.5
25.25	2656.9	0.1	0.0	22.4
25.75	2760.6	0.0	0.0	16.1
26.25	2866.4	0.1	0.0	25.3
26.75	2974.1	0.1	0.0	12.2
27.25	3083.7	0.1	0.0	21.4
27.75	3195.4	0.1	0.1	15.5
28.25	3308.9	0.1	0.0	18.9
28.75	3424.4	0.0	0.0	23.8
29.25	3541.9	0.1	0.0	19.7
29.75	3661.4	0.1	0.0	17.6
30.25	3782.8	0.0	0.2	30.6
30.75	3906.1	0.2	0.0	10.5
32.25	4287.9	0.1	0.1	19.2
32.75	4419.1	0.0	0.0	11.0
33.75	4687.3	0.0	0.1	16.8
34.25	4824.4	0.1	0.0	13.3
34.75	4963.4	0.0	0.1	23.2
35.25	5104.3	0.0	0.0	15.7
35.75	5247.2	0.0	0.0	10.9
36.25	5392.1	0.0	0.0	17.3
36.75	5538.9	0.3	0.0	16.1
37.25	5687.7	0.1	0.0	18.4
37.75	5838.5	0.2	0.1	8.6
38.25	5991.2	0.1	0.0	10.2
38.75	6145.8	0.1	0.0	10.8
39.25	6302.4	0.1	0.1	8.4

A8.3 Modern Analogue Technique Results (MAT)

Reconstructed sea-surface temperatures and salinities during winter and summer, and sea ice durations (i and s → estimated lower and upper error ranges, respectively).

Depth (cm)	Age (cal. years BP)	TWIN	TWIN_i	TWIN_s	SWIN	SWIN_i	SWIN_s	TSUM	TSUM_i	TSUM_s
0.25	-37.8	0.8	-2.0	3.5	34.3	33.2	35.0	4.0	-0.3	8.3
0.75	-31.9	-0.4	-2.0	1.6	34.0	32.6	34.9	2.5	-0.3	5.0
1.25	-24.0	-0.2	-2.0	1.6	34.1	32.6	35.0	2.9	-0.3	5.2
1.75	-14.1	-0.1	-2.0	1.6	34.1	32.6	35.0	2.9	-0.3	5.2
2.25	-2.3	-0.3	-2.0	0.6	33.3	31.7	34.7	6.5	-0.3	13.9
2.75	11.5	0.8	-2.0	3.5	33.9	31.8	35.0	5.9	-0.3	13.3
3.25	27.3	0.1	-2.0	1.6	34.4	33.2	34.9	3.6	-0.3	6.5
3.75	45.0	0.7	-2.0	3.5	33.3	31.7	34.9	7.5	-0.3	13.3
4.25	64.6	0.7	-2.0	3.5	34.4	33.2	35.0	4.0	-0.3	8.3
4.75	86.2	0.8	-2.0	3.5	33.8	31.8	35.0	5.8	-0.3	13.3
6.25	162.8	0.6	-2.0	3.5	33.3	31.7	34.9	7.5	-0.3	12.8
6.75	192.2	1.0	-2.0	3.5	33.9	31.8	35.0	6.2	-0.3	13.3
7.25	223.6	1.9	-2.0	6.4	34.5	33.2	35.1	5.3	-0.3	10.6
7.75	223.6	0.9	-2.0	3.5	33.9	31.8	34.9	5.9	-0.3	13.3
8.25	257.0	1.7	-2.0	5.1	34.5	33.2	35.1	5.3	-0.3	9.9
8.75	292.3	-0.7	-2.0	1.6	34.1	33.2	34.9	3.0	-0.3	5.2
9.25	329.5	2.0	-2.0	5.1	34.6	33.2	35.1	5.6	-0.3	9.9
9.75	368.8	1.8	-1.8	6.5	34.5	33.5	35.2	6.3	1.1	10.9
10.25	409.9	1.9	-2.0	5.1	34.6	33.2	35.1	5.6	-0.3	9.9
10.75	453.1	0.8	-2.0	3.5	34.4	33.2	35.0	4.6	-0.3	8.3
11.25	498.2	1.9	-2.0	6.5	33.9	31.8	35.2	7.7	-0.3	14.9
11.75	545.2	0.7	-2.0	3.5	33.3	31.7	34.9	7.7	-0.3	13.9
12.25	594.2	4.8	2.1	6.5	35.0	34.5	35.2	9.5	7.7	10.9
12.75	645.2	2.5	-2.0	6.4	34.7	33.2	35.1	6.1	-0.3	10.6
13.25	698.1	0.9	-2.0	3.5	33.9	31.8	35.0	6.5	-0.3	14.9
13.75	753.0	1.9	-2.0	5.1	34.5	33.2	35.1	5.5	-0.3	9.9
14.25	809.8	1.9	-2.0	5.1	34.5	33.2	35.1	5.6	-0.3	9.9
14.75	868.6	2.4	-2.0	6.4	34.6	33.2	35.1	6.0	-0.3	10.6
15.25	929.3	2.8	-2.0	6.5	34.7	33.2	35.2	6.3	-0.3	10.9
15.75	992.0	2.0	-2.0	5.1	34.5	32.6	35.1	6.0	1.0	9.9
16.50	1056.7	3.7	1.4	6.4	34.9	34.5	35.1	7.9	5.0	10.6
16.75	1157.3	0.4	-2.0	3.5	34.0	32.6	35.0	3.6	-0.3	8.3
17.25	1191.9	2.4	-2.0	6.4	34.7	33.2	35.1	5.9	-0.3	10.6
17.75	1262.4	2.0	-2.0	5.1	34.6	33.2	35.1	5.7	-0.3	9.9
18.25	1334.9	1.0	-2.0	3.5	33.9	31.8	35.0	6.6	-0.3	14.9
18.75	1409.3	2.3	-2.0	6.4	34.2	32.8	35.1	7.1	-0.3	16.1

Depth (cm)	Age (cal. years BP)	SSUM	SSUM_i	SSUM_s	Sea ice duration (months/yr)	Sea ice_i	Sea ice_s
0.25	-37.8	33.8	32.5	34.8	3.2	0.0	10.1
0.75	-31.9	32.7	29.3	34.4	4.7	0.4	10.1
1.25	-24.0	33.1	29.3	34.8	4.5	0.4	10.1
1.75	-14.1	32.9	29.3	34.8	4.5	0.4	10.1
2.25	-2.3	32.3	30.5	34.1	3.6	0.6	10.1
2.75	11.5	33.3	30.5	34.8	3.1	0.0	10.1
3.25	27.3	33.8	32.5	34.7	2.9	0.0	10.1
3.75	45.0	32.5	30.5	34.4	2.9	0.0	10.1
4.25	64.6	33.8	32.5	34.8	3.1	0.0	10.1
4.75	86.2	33.3	30.5	34.8	3.2	0.0	10.1
6.25	162.8	32.6	30.6	34.4	2.8	0.0	10.1
6.75	192.2	33.4	30.5	34.8	2.7	0.0	10.1
7.25	223.6	34.2	32.5	35.0	2.5	0.0	10.1
7.75	223.6	33.1	30.5	34.4	2.7	0.0	10.1
8.25	257.0	34.1	32.5	35.1	2.6	0.0	10.1
8.75	292.3	33.4	31.9	34.4	3.5	0.3	10.1
9.25	329.5	34.2	32.5	35.1	2.2	0.0	10.1
9.75	368.8	34.0	31.9	35.1	1.3	0.0	5.6
10.25	409.9	34.2	32.5	35.1	2.2	0.0	10.1
10.75	453.1	33.9	32.5	34.8	3.1	0.0	10.1
11.25	498.2	33.4	30.4	35.1	2.7	0.0	10.1
11.75	545.2	32.5	30.6	34.4	3.3	0.0	10.1
12.25	594.2	34.9	34.3	35.1	0.0	0.0	0.0
12.75	645.2	34.4	32.5	35.1	2.3	0.0	10.1
13.25	698.1	33.3	30.4	34.8	2.7	0.0	10.1
13.75	753.0	34.2	32.5	35.1	2.4	0.0	10.1
14.25	809.8	34.2	32.5	35.1	2.3	0.0	10.1
14.75	868.6	34.3	32.5	35.1	2.4	0.0	10.1
15.25	929.3	34.3	32.5	35.1	2.3	0.0	10.1
15.75	992.0	33.7	29.3	35.1	2.1	0.0	9.5
16.50	1056.7	34.7	34.3	35.1	0.3	0.0	1.2
16.75	1157.3	33.0	29.3	34.8	4.6	0.0	10.1
17.25	1191.9	34.3	32.5	35.1	2.4	0.0	10.1
17.75	1262.4	34.2	32.5	35.1	2.2	0.0	10.1
18.25	1334.9	33.3	30.4	34.8	2.5	0.0	10.1
18.75	1409.3	33.8	32.2	35.0	2.4	0.0	10.1

Depth (cm)	Age (cal. years BP)	TWIN	TWIN_i	TWIN_s	SWIN	SWIN_i	SWIN_s	TSUM	TSUM_i	TSUM_s
19.25	1485.7	2.5	-2.0	6.4	34.7	33.2	35.1	6.1	-0.3	10.6
19.75	1564.0	1.7	-2.0	5.1	34.5	33.2	35.1	5.2	-0.3	9.9
20.25	1644.3	1.8	-2.0	5.1	34.5	33.2	35.1	5.4	-0.3	9.9
20.75	1726.6	2.1	-2.0	6.4	34.5	33.2	35.1	5.7	-0.3	10.6
21.25	1810.8	2.1	-1.7	5.1	34.8	34.5	35.1	6.1	1.7	9.9
21.75	1897.0	3.3	-0.1	6.5	33.7	31.7	35.2	11.7	8.3	14.9
22.25	1985.1	1.9	-2.0	5.1	34.5	33.2	35.1	5.6	-0.3	9.9
22.75	2075.2	3.1	1.4	5.1	34.9	34.5	35.1	7.5	5.0	9.9
23.25	2167.3	0.9	-2.0	5.1	34.6	33.2	35.1	4.4	-0.3	9.9
23.75	2261.3	4.0	-2.0	6.5	34.6	33.2	35.2	7.9	-0.3	10.9
24.25	2357.2	3.5	1.4	6.4	34.9	34.5	35.1	7.7	5.0	10.6
24.75	2455.2	1.9	-2.0	5.1	34.5	33.2	35.1	5.6	-0.3	9.9
25.25	2555.0	1.9	-0.4	6.5	33.0	31.7	35.2	11.5	8.3	13.5
25.75	2656.9	2.6	-1.7	6.4	35.0	34.6	35.1	6.5	1.7	10.6
26.25	2760.6	0.7	-2.0	5.1	34.5	33.2	35.1	4.3	-0.3	9.9
26.75	2866.4	2.3	-0.1	5.1	34.3	31.7	35.1	8.4	5.0	13.9
27.25	2974.1	1.6	-2.0	5.1	33.8	31.8	35.1	7.4	1.0	12.8
27.75	3083.7	2.2	-2.0	6.5	34.5	33.2	35.2	5.8	-0.3	10.9
28.25	3195.4	1.2	-2.0	5.1	34.5	33.2	35.1	4.9	-0.3	9.9
28.75	3308.9	1.0	-2.0	3.5	34.4	33.2	35.0	4.4	-0.3	8.3
29.25	3424.4	1.6	-2.0	6.5	33.3	31.7	35.2	9.1	-0.3	14.9
29.75	3541.9	1.8	-2.0	5.1	34.5	33.2	35.1	5.5	-0.3	9.9
30.25	3661.4	1.0	-2.0	3.5	33.9	31.7	35.0	6.1	-0.3	12.5
30.75	3782.8	0.4	-0.6	1.6	34.7	34.7	34.9	4.7	3.6	6.5
32.25	3906.1	3.7	1.4	6.5	34.9	34.5	35.2	7.9	5.0	10.9
32.75	4287.9	0.6	-2.0	3.5	34.2	33.2	35.0	3.9	-0.3	8.3
33.75	4419.1	1.7	-2.0	6.5	33.3	31.7	35.2	8.9	-0.3	13.3
34.25	4687.3	1.0	-2.0	3.5	33.9	31.7	35.0	6.2	-0.3	12.5
34.75	4824.4	0.7	-0.4	3.5	32.3	31.7	34.5	12.0	8.3	13.5
35.25	4963.4	0.9	-0.2	3.5	33.5	31.7	34.8	8.8	3.6	13.3
35.75	5104.3	2.2	0.0	5.1	34.2	31.7	35.1	8.0	3.6	12.5
36.25	5247.2	1.9	-0.4	6.5	33.0	31.7	35.2	11.6	8.3	13.5
36.75	5392.1	0.7	-2.0	3.5	33.3	31.7	34.9	7.6	-0.3	13.3
37.25	5538.9	1.9	-2.0	5.1	34.5	33.2	35.1	5.6	-0.3	9.9
37.75	5687.7	0.9	-2.0	3.5	33.9	31.7	35.0	6.1	-0.3	12.5
38.25	5838.5	0.7	-2.0	3.5	34.4	33.2	35.0	4.3	-0.3	8.3
38.75	5991.2	0.9	-2.0	3.5	33.9	31.7	35.0	6.0	-0.3	12.5
39.25	6145.8	0.2	-1.2	1.6	34.7	34.5	34.9	3.4	-0.1	5.0

Depth (cm)	Age (cal. years BP)	SSUM	SSUM_i	SSUM_s	Sea ice duration (months/yr)	Sea ice_i	Sea ice_s
19.25	1485.7	34.4	32.5	35.1	2.3	0.0	10.1
19.75	1564.0	34.1	32.5	35.1	2.7	0.0	10.1
20.25	1644.3	34.2	32.5	35.1	2.5	0.0	10.1
20.75	1726.6	34.2	32.5	35.0	2.4	0.0	10.1
21.25	1810.8	34.2	32.2	35.1	1.8	0.0	8.3
21.75	1897.0	33.1	30.4	35.1	1.1	0.0	4.0
22.25	1985.1	34.2	32.5	35.1	2.3	0.0	10.1
22.75	2075.2	34.7	34.3	35.1	0.3	0.0	1.2
23.25	2167.3	33.8	32.2	35.1	3.9	0.0	10.1
23.75	2261.3	34.4	32.5	35.1	1.9	0.0	10.1
24.25	2357.2	34.7	34.3	35.1	0.3	0.0	1.2
24.75	2455.2	34.2	32.5	35.1	2.3	0.0	10.1
25.25	2555.0	32.3	30.5	35.1	1.0	0.0	1.8
25.75	2656.9	34.3	32.2	35.1	1.9	0.0	8.3
26.25	2760.6	34.0	32.5	35.1	4.0	0.0	10.1
26.75	2866.4	33.9	30.6	35.1	1.1	0.0	4.0
27.25	2974.1	32.8	29.3	35.1	2.2	0.0	9.5
27.75	3083.7	34.2	32.5	35.1	2.4	0.0	10.1
28.25	3195.4	33.8	32.2	35.1	4.0	0.0	10.1
28.75	3308.9	33.9	32.5	34.8	2.7	0.0	10.1
29.25	3424.4	32.6	30.4	35.1	2.8	0.0	10.1
29.75	3541.9	34.2	32.5	35.1	2.4	0.0	10.1
30.25	3661.4	33.4	30.7	34.8	2.7	0.0	10.1
30.75	3782.8	34.2	33.4	34.7	0.7	0.0	1.3
32.25	3906.1	34.7	34.3	35.1	0.3	0.0	1.2
32.75	4287.9	33.6	31.9	34.8	3.5	0.0	10.1
33.75	4419.1	32.7	30.5	35.1	2.6	0.0	10.1
34.25	4687.3	33.4	30.7	34.8	2.5	0.0	10.1
34.75	4824.4	31.4	30.5	34.3	1.3	0.0	1.8
35.25	4963.4	32.8	30.5	34.7	0.9	0.0	1.8
35.75	5104.3	33.7	30.7	35.1	0.9	0.0	1.8
36.25	5247.2	32.2	30.5	35.1	1.0	0.0	1.8
36.75	5392.1	32.5	30.5	34.4	2.8	0.0	10.1
37.25	5538.9	34.2	32.5	35.1	2.3	0.0	10.1
37.75	5687.7	33.3	30.7	34.8	2.7	0.0	10.1
38.25	5838.5	34.0	32.5	34.8	2.7	0.0	10.1
38.75	5991.2	33.3	30.7	34.8	2.8	0.0	10.1
39.25	6145.8	33.7	32.4	34.4	2.8	0.3	10.8

A8.4 Planktic foraminifera

Depth (cm)	Age (cal. years BP)	G. bulloides (wt %)	G. uvula (wt %)	G. glutinata (wt %)	G. quinqueloba (wt %)	Planktonic Foram./g
0.25	-37.8	1.0	10.1	6.1	35.4	1041.7
0.75	-31.9	1.1	6.7	2.2	36.0	572.4
1.25	-24.0	4.5	5.4	2.7	18.8	428.9
2.25	-2.3	1.0	4.8	1.9	21.9	157.8
3.25	27.3	0.8	2.4	0.0	15.9	101.1
4.25	64.6	1.5	3.1	1.5	20.0	135.9
5.25	109.8	0.0	0.0	0.0	14.5	82.8
6.25	162.8	1.6	2.4	0.8	15.9	282.9
7.25	223.6	1.7	0.0	0.0	12.7	129.8
8.25	292.3	2.6	0.9	0.9	16.4	314.5
8.75	329.5	0.0	4.5	1.8	36.9	717.2
9.25	368.8	2.1	4.3	1.4	35.5	760.2
9.75	409.9	3.6	0.0	0.0	19.3	199.3
10.25	453.1	2.0	0.0	0.0	13.0	290.7
10.75	498.2	0.0	6.0	0.0	11.2	1053.1
11.25	545.2	0.7	3.0	0.7	28.9	874.1
11.75	594.2	0.0	6.3	0.9	12.5	1033.4
12.25	645.2	0.9	2.8	0.9	16.5	445.0
12.75	698.1	0.9	4.4	1.8	10.6	649.8
13.25	753.0	0.0	2.2	1.1	15.2	390.6
13.75	809.8	2.8	6.5	0.0	10.2	619.3
14.25	868.6	0.9	4.5	0.9	20.7	566.0
14.75	929.3	0.0	2.7	0.0	20.5	884.8
15.25	992.0	0.0	5.0	0.8	15.7	535.3
16.5	1157.3	0.0	3.1	2.1	18.6	482.9
17.25	1262.4	0.8	1.7	0.8	23.3	472.6
18.25	1409.3	1.6	0.8	0.8	29.6	528.4
19.25	1564.0	2.4	0.0	0.0	19.4	425.5
19.75	1644.3	1.6	0.8	0.0	11.6	743.7
21.25	1897.0	2.9	0.0	1.0	12.5	849.6
22.25	2075.2	0.0	1.8	0.0	19.3	483.4
23.25	2261.3	0.9	9.3	1.9	21.3	705.4
24.25	2455.2	1.1	2.1	0.0	26.6	382.5
25.25	2656.9	0.0	0.9	0.9	16.7	603.6
25.75	2760.6	1.0	0.0	1.0	9.9	544.0
26.25	2866.4	0.9	0.0	0.0	12.1	604.9
27.25	3083.7	0.8	0.0	0.8	7.6	1175.5
28.25	3308.9	0.0	0.9	0.0	6.0	1201.1

Depth (cm)	Age (cal. years BP)	G. bulloides (wt %)	G. uvula (wt %)	G. glutinata (wt %)	G. quinqueloba (wt %)	Planktonic Foram./g
29.25	3541.9	0.0	0.8	0.0	6.1	1096.9
31.25	4031.4	1.0	0.0	0.0	9.0	669.4
32.25	4287.9	1.9	0.9	0.0	4.6	1003.8
39.75	6461.0	0.0	0.0	0.9	11.3	701.6

A8.4 XRF core scanning (counts)

Depth (cm)	Age (cal. years BP)	Ca	Ti	Zr	Rb	Depth (cm)	Age (cal. years BP)	Ca	Ti	Zr	Rb
0.1	-39.2	11621	1299	1628	539	4.1	58.5	13022	1112	1631	507
0.2	-38.3	11250	1143	1456	575	4.2	62.6	13826	1376	1802	536
0.3	-37.3	10994	974	1354	466	4.3	66.7	14824	1337	1528	604
0.4	-36.3	9573	1053	1374	419	4.4	70.9	14815	1275	1704	644
0.5	-35.1	10746	1119	1610	635	4.5	75.2	14681	1226	1762	641
0.6	-33.9	11372	1099	1895	729	4.6	79.5	14790	1263	1488	570
0.7	-32.6	10198	1194	2082	808	4.7	84.0	14783	1305	1430	615
0.8	-31.2	10320	1152	2234	832	4.8	88.5	14707	1324	1736	577
0.9	-29.7	9871	986	2299	848	4.9	93.1	14816	1772	1928	603
1	-28.2	10126	1093	2519	980	5	97.8	14923	1976	1515	596
1.1	-26.5	7830	1193	2439	1076	5.1	102.5	15330	1295	1432	584
1.2	-24.8	7164	1452	2240	995	5.2	107.3	14536	1289	1451	569
1.3	-23.1	10758	1205	1806	817	5.3	112.3	14669	1304	1707	572
1.4	-21.2	12565	1197	1572	610	5.4	117.2	15482	1349	1584	583
1.5	-19.3	13928	1184	1573	583	5.5	122.3	14998	1211	1641	597
1.6	-17.3	13993	1168	1586	594	5.6	127.5	14557	1266	1513	648
1.7	-15.2	13416	1223	1465	586	5.7	132.7	14511	1371	1553	588
1.8	-13.0	13401	1397	1712	569	5.8	138.0	15078	1506	1952	635
1.9	-10.7	13531	1199	1609	606	5.9	143.4	14818	1234	1648	612
2	-8.4	13443	1222	1539	457	6	148.8	15789	1386	1606	591
2.1	-6.0	13326	1353	1596	571	6.1	154.3	14038	1324	1682	575
2.2	-3.5	13249	1345	1669	591	6.2	160.0	12885	1218	1687	573
2.3	-1.0	12596	1310	1588	598	6.3	165.7	11925	1259	1539	508
2.4	1.7	12839	1262	1614	560	6.4	171.4	13665	1251	1493	529
2.5	4.4	13661	1298	1678	590	6.5	177.3	14287	1509	1576	596
2.6	7.2	13639	1311	1538	560	6.6	183.2	14171	1359	1664	580
2.7	10.1	13826	1340	1550	610	6.7	189.2	14341	1385	1585	582
2.8	13.0	13488	1184	1449	579	6.8	195.3	14610	1380	1569	631
2.9	16.0	12929	1255	1469	577	6.9	201.4	14784	1414	1520	629
3	19.1	11969	1109	1390	483	7	207.7	14950	1418	1645	593
3.1	22.3	11373	1062	1539	566	7.1	214.0	14601	1282	1607	579
3.2	25.6	11754	1310	1468	533	7.2	220.4	14000	1427	1513	577
3.3	28.9	12057	1264	1391	566	7.3	226.9	13534	1317	1538	594
3.4	32.4	12707	1302	1457	580	7.4	233.4	13641	1616	1725	616
3.5	35.9	13190	1393	1494	659	7.5	240.1	13086	1480	1672	642
3.6	39.4	13421	1320	1552	610	7.6	246.8	12982	1381	1692	562
3.7	43.1	13078	1232	1289	567	7.7	253.6	13137	1400	1698	579
3.8	46.8	11410	1090	1377	466	7.8	260.4	12690	1357	1846	625
3.9	50.7	10691	1039	1469	534	7.9	267.4	12641	1368	1628	576
4	54.5	12472	1324	1428	505	8	274.4	12848	1558	1664	622

Depth (cm)	Age (cal. years BP)	Ca	Ti	Zr	Rb	Depth (cm)	Age (cal. years BP)	Ca	Ti	Zr	Rb
8.1	281.5	13109	1319	2052	630	12.2	639.9912	14018	1388	2098	663
8.2	288.7	12571	1328	1917	649	12.3	650.4	13378	1354	2107	584
8.3	295.9	12297	1325	1699	603	12.4	660.8	12188	1435	1949	650
8.4	303.3	12738	1451	1854	603	12.5	671.4	12801	1307	1782	567
8.5	310.7	13580	1377	1813	625	12.6	682.0	13521	1321	1589	562
8.6	318.2	13652	1254	1818	629	12.7	692.7	12852	1520	1749	584
8.7	325.7	15411	1365	1618	638	12.8	703.5	12123	1310	1524	621
8.8	333.4	15831	1333	1416	555	12.9	714.3	11793	1524	1466	611
8.9	341.1	16290	1302	1463	552	13	725.3	10876	1343	1737	675
9	348.9	15600	1343	1674	609	13.1	736.3	12175	1559	1764	636
9.1	356.8	16537	1176	1633	634	13.2	747.4	12224	1471	1707	627
9.2	364.8	15989	1292	1429	572	13.3	758.6	12405	1517	1779	620
9.3	372.8	15463	1366	1593	547	13.4	769.8	11424	1304	1831	662
9.4	380.9	15816	1351	1633	563	13.5	781.1	9864	1498	1791	611
9.5	389.1	16315	1332	1645	559	13.6	792.5	8698	1396	2018	660
9.6	397.4	15571	1234	1767	625	13.7	804.0	9543	1364	1635	646
9.7	405.7	14690	1259	1767	586	13.8	815.6	10637	1545	1669	635
9.8	414.2	14327	1242	1841	598	13.9	827.2	11888	1321	1921	628
9.9	422.7	12943	1437	1669	576	14	838.9	11889	1310	1976	591
10	431.3	13232	1194	1689	632	14.1	850.7	11936	1340	2240	588
10.1	439.9	12935	1263	1652	559	14.2	862.6	10469	1533	2182	661
10.2	448.7	12801	1338	1694	561	14.3	874.6	11609	1404	1733	649
10.3	457.5	12956	1411	1686	561	14.4	886.6	12580	1281	1827	674
10.4	466.4	13947	1404	1552	596	14.5	898.7	11692	1300	1749	577
10.5	475.4	13547	1486	1687	634	14.6	910.9	10202	1319	1867	588
10.6	484.4	13949	1288	1621	604	14.7	923.2	12228	1527	1440	523
10.7	493.6	14483	1400	1432	588	14.8	935.5	12699	1428	1578	576
10.8	502.8	14384	1398	1631	678	14.9	947.9	13853	1330	1689	583
10.9	512.1	13859	1286	1580	638	15	960.4	14325	1364	1570	654
11	521.4	14168	1355	1497	645	15.1	973.0	13589	1357	1756	668
11.1	530.9	14633	1275	1425	689	15.2	985.7	13365	1344	1674	646
11.2	540.4	15522	1328	1696	571	15.3	998.4	13234	1557	1685	588
11.3	550.0	14916	1335	1651	624	15.4	1011.2	13403	1378	1473	649
11.4	559.7	15276	1367	1514	571	15.5	1024.1	14025	1428	1475	631
11.5	569.5	14382	1287	1408	637	15.6	1037.1	13874	1459	1557	616
11.6	579.3	15305	1324	1625	568	15.7	1050.1	13491	1512	1807	639
11.7	589.2	14649	1372	1703	606	15.8	1063.2	13735	1329	1590	620
11.8	599.2	14477	1246	1660	575	15.9	1076.5	14520	1345	1841	657
11.9	609.3	14239	1470	1546	682	16	1089.7	15093	1316	1627	570
12	619.5	14989	1375	1871	602	16.1	1103.1	15805	1399	1533	647
12.1	629.7	15452	1434	1664	549	16.2	1116.5	16386	1274	1550	584

Depth (cm)	Age (cal. years BP)	Ca	Ti	Zr	Rb	Depth (cm)	Age (cal. years BP)	Ca	Ti	Zr	Rb
16.3	1130.1	14732	1264	1742	567	20.4	1751.672	13054	1419	1929	635
16.4	1143.6	14831	1186	1680	579	20.5	1768.5	13500	1489	1908	698
16.5	1157.3	14134	1258	1390	529	20.6	1785.4	13639	1462	1681	665
16.6	1171.1	13903	1350	1793	601	20.7	1802.3	12033	1397	1760	673
16.7	1184.9	14039	1287	1493	557	20.8	1819.4	12456	1405	1790	651
16.8	1198.8	13617	1281	1885	562	20.9	1836.5	12489	1525	1987	576
16.9	1212.8	12550	1252	1784	645	21	1853.7	13734	1344	1791	662
17	1226.9	11685	1307	1713	697	21.1	1871.0	13859	1489	1744	628
17.1	1241.0	11690	1454	1945	585	21.2	1888.3	13056	1454	1729	590
17.2	1255.2	11533	1359	1809	652	21.3	1905.7	13332	1488	1815	586
17.3	1269.5	11474	1541	1966	584	21.4	1923.2	13453	1501	1748	571
17.4	1283.9	12356	1367	1833	624	21.5	1940.8	12637	1513	1883	567
17.5	1298.4	12916	1383	1988	626	21.6	1958.5	11684	1561	1470	601
17.6	1312.9	12272	1427	1906	596	21.7	1976.2	10930	1365	1558	616
17.7	1327.5	13303	1438	1797	615	21.8	1994.1	10376	1431	1769	623
17.8	1342.2	13572	1448	1803	616	21.9	2012.0	10589	1389	1757	710
17.9	1357.0	13983	1438	2062	625	22	2029.9	9854	1571	1901	706
18	1371.8	13078	1356	1821	649	22.1	2048.0	9097	1451	1736	621
18.1	1386.8	14295	1425	1928	646	22.2	2066.1	9739	1438	1798	693
18.2	1401.8	14691	1446	1769	664	22.3	2084.3	9488	1568	1739	691
18.3	1416.8	14827	1414	1941	617	22.4	2102.6	8499	1383	1893	655
18.4	1432.0	14922	1497	1912	621	22.5	2121.0	8474	1361	1895	707
18.5	1447.2	15333	1514	1592	621	22.6	2139.5	8903	1449	1948	646
18.6	1462.6	14836	1541	1644	666	22.7	2158.0	9353	1411	1930	686
18.7	1478.0	14688	1446	1755	600	22.8	2176.6	8706	1377	1716	759
18.8	1493.4	14529	1376	1745	647	22.9	2195.3	9265	1435	1654	690
18.9	1509.0	15228	1419	1520	647	23	2214.0	9255	1530	1901	677
19	1524.6	15550	1479	1556	664	23.1	2232.9	9726	1410	1705	706
19.1	1540.3	15148	1414	1612	694	23.2	2251.8	10634	1490	1724	685
19.2	1556.1	15141	1421	1737	606	23.3	2270.8	10807	1445	1841	683
19.3	1572.0	14927	1440	1574	557	23.4	2289.9	11134	1468	1760	632
19.4	1587.9	15073	1452	1602	598	23.5	2309.0	11609	1392	1926	663
19.5	1603.9	14559	1457	1900	602	23.6	2328.2	12025	1509	1666	643
19.6	1620.0	14667	1372	1576	664	23.7	2347.6	11869	1429	1795	662
19.7	1636.2	14766	1423	1557	595	23.8	2366.9	11329	1470	1856	616
19.8	1652.5	14818	1558	1477	637	23.9	2386.4	11537	1400	1697	678
19.9	1668.8	15781	1501	1496	682	24	2406.0	12412	1539	1903	683
20	1685.2	15007	1363	1415	669	24.1	2425.6	11930	1593	1627	658
20.1	1701.7	14584	1475	1617	680	24.2	2445.3	12957	1417	1761	630
20.2	1718.3	14087	1333	1899	581	24.3	2465.1	13662	1448	1380	647
20.3	1734.9	13369	1457	1919	642	24.4	2484.9	13016	1499	1496	690

Depth (cm)	Age (cal. years BP)	Ca	Ti	Zr	Rb	Depth (cm)	Age (cal. years BP)	Ca	Ti	Zr	Rb
24.5	2504.9	12887	1309	1733	697	28.6	3389.587	10421	1397	1852	653
24.6	2524.9	11218	1381	1683	695	28.7	3412.8	10779	1365	2082	605
24.7	2545.0	11180	1531	1868	636	28.8	3436.1	10950	1334	1973	625
24.8	2565.1	11389	1590	2181	653	28.9	3459.5	10792	1485	1721	632
24.9	2585.4	10360	1419	1972	707	29	3482.9	10791	1435	1916	672
25	2605.7	10427	1482	1749	661	29.1	3506.5	11540	1427	1831	627
25.1	2626.1	9525	1385	1851	656	29.2	3530.1	11442	1414	1931	631
25.2	2646.6	9254	1398	1966	650	29.3	3553.8	11178	1441	1709	601
25.3	2667.2	9889	1403	1918	634	29.4	3577.6	10709	1405	1865	658
25.4	2687.8	10296	1337	1799	672	29.5	3601.4	10339	1309	1711	617
25.5	2708.5	11338	1390	1843	711	29.6	3625.3	10327	1369	1857	713
25.6	2729.3	10785	1558	1949	673	29.7	3649.3	10392	1597	1915	670
25.7	2750.2	10165	1547	1709	698	29.8	3673.4	8903	1442	1669	670
25.8	2771.1	9456	1445	1891	639	29.9	3697.6	8209	1465	1931	692
25.9	2792.2	8011	1591	2116	611	30	3721.8	9091	1549	1973	711
26	2813.3	8075	1475	2031	656	30.1	3746.1	8587	1540	1800	695
26.1	2834.5	10043	1476	2140	637	30.2	3770.5	8497	1477	1811	677
26.2	2855.7	9865	1459	1793	692	30.3	3795.0	8716	1557	1784	685
26.3	2877.1	8622	1454	1834	644	30.4	3819.6	8562	1530	1786	629
26.4	2898.5	8909	1403	1993	689	30.5	3844.2	9429	1419	1788	731
26.5	2920.0	8851	1402	2081	642	30.6	3868.9	8684	1462	1681	700
26.6	2941.6	9102	1299	2136	650	30.7	3893.7	7956	1536	1791	634
26.7	2963.2	8083	1353	1870	644	30.8	3918.6	7997	1379	1879	719
26.8	2985.0	7870	1350	2184	591	30.9	3943.5	8251	1608	1727	648
26.9	3006.8	7383	1378	1919	589	31	3968.5	8640	1546	1818	754
27	3028.7	7359	1353	1888	678	31.1	3993.6	8382	1707	1716	653
27.1	3050.6	7218	1382	2083	732	31.2	4018.8	8276	1557	1671	730
27.2	3072.7	7008	1406	2162	677	31.3	4044.1	8519	1641	1648	689
27.3	3094.8	8121	1453	1967	620	31.4	4069.4	8575	1524	1747	743
27.4	3117.0	6863	1467	2085	617	31.5	4094.8	9125	1592	1790	688
27.5	3139.3	6737	1416	1848	611	31.6	4120.3	8555	1462	1945	750
27.6	3161.7	6996	1324	1681	700	31.7	4145.9	8318	1365	1746	731
27.7	3184.1	8771	1647	1757	632	31.8	4171.5	7727	1559	2089	631
27.8	3206.6	8914	1416	1712	636	31.9	4197.2	7948	1517	1877	695
27.9	3229.2	9300	1423	1938	627	32	4223.1	7805	1270	1686	656
28	3251.9	9466	1438	1828	616	32.1	4248.9	7869	1397	2000	710
28.1	3274.6	9596	1424	1894	692	32.2	4274.9	8607	1548	1783	721
28.2	3297.5	9365	1408	1847	672	32.3	4300.9	8741	1451	1733	634
28.3	3320.4	9766	1405	1862	712	32.4	4327.1	8462	1664	1779	710
28.4	3343.4	10294	1562	1914	640	32.5	4353.3	8564	1562	2220	713
28.5	3366.4	9912	1428	1834	662	32.6	4379.5	8699	1558	2089	686

Depth (cm)	Age (cal. years BP)	Ca	Ti	Zr	Rb	Depth (cm)	Age (cal. years BP)	Ca	Ti	Zr	Rb
32.7	4405.9	8216	1269	1932	683	36.8	5553.735	7324	1312	2069	632
32.8	4432.3	7771	1264	2190	647	36.9	5583.4	7370	1057	2032	726
32.9	4458.8	7215	1341	1668	613	37	5613.1	7066	1189	1847	617
33	4485.4	7222	1185	1881	657	37.1	5642.9	7324	1228	1794	656
33.1	4512.1	8155	1559	2084	704	37.2	5672.8	7102	1151	1784	686
33.2	4538.8	7394	1412	1552	702	37.3	5702.7	7881	1211	2106	733
33.3	4565.6	6932	1365	2023	681	37.4	5732.7	7923	1428	1793	711
33.4	4592.5	6750	1358	2064	634	37.5	5762.9	8003	1283	1659	688
33.5	4619.5	6712	1288	2096	719	37.6	5793.0	8132	1201	1714	735
33.6	4646.6	7132	1354	2011	762	37.7	5823.3	7986	1356	1747	664
33.7	4673.7	8335	1464	1770	718	37.8	5853.7	7514	1218	1870	709
33.8	4700.9	8583	1496	1827	653	37.9	5884.1	8071	1261	1686	744
33.9	4728.2	7649	1404	1999	703	38	5914.6	8565	1222	1645	601
34	4755.6	7433	1475	2047	631	38.1	5945.2	8906	1306	1487	667
34.1	4783.0	7530	1310	1780	701	38.2	5975.8	8511	1381	1647	755
34.2	4810.6	7665	1412	1768	702	38.3	6006.6	9625	1533	1560	682
34.3	4838.2	7692	1344	1887	607	38.4	6037.4	9015	1449	1973	737
34.4	4865.9	8325	1469	1830	706	38.5	6068.3	8652	1265	1723	639
34.5	4893.6	8867	1429	1853	705	38.6	6099.2	9591	1390	1544	728
34.6	4921.5	8402	1457	2062	701	38.7	6130.3	10500	1348	1719	782
34.7	4949.4	9555	1354	1922	693	38.8	6161.4	11211	1449	1714	710
34.8	4977.4	9339	1411	1842	653	38.9	6192.6	10520	1381	1495	705
34.9	5005.4	8779	1474	1892	730	39	6223.9	10268	1237	1531	709
35	5033.6	8087	1476	1874	626	39.1	6255.3	9999	1272	1806	654
35.1	5061.8	7598	1489	1705	645	39.2	6286.7	10098	1296	1595	662
35.2	5090.1	7748	1423	1663	684	39.3	6318.2	9788	1263	1783	734
35.3	5118.5	7278	1192	1746	652	39.4	6349.8	10417	1389	1941	680
35.4	5147.0	7184	1177	1903	715	39.5	6381.5	10149	1262	1874	679
35.5	5175.5	7777	1460	2136	603	39.6	6413.2	8850	1100	1703	686
35.6	5204.2	7941	1253	1925	677	39.7	6445.1	8064	1193	1676	748
35.7	5232.9	7561	1232	2067	666	39.8	6477.0	8707	1349	1819	690
35.8	5261.6	7895	1322	2232	688	39.9	6509.0	10053	1388	1716	733
35.9	5290.5	7886	1462	2433	661						
36	5319.4	7634	1331	2151	708						
36.1	5348.4	8711	1505	1780	699						
36.2	5377.5	8417	1538	1895	704						
36.3	5406.7	7751	1322	1650	716						
36.4	5436.0	7525	1141	1864	681						
36.5	5465.3	7719	1382	2116	667						
36.6	5494.7	8137	1301	1990	623						
36.7	5524.2	8212	1367	2202	682						

A8.5 Ice Rafted Debris (number/gram dry sed.)

Depth (cm)	Age (cal. years BP)	Carbonate rocks (>150µm)	Total (>150µm)	Total (>500µm)
0.25	-37.8	26.8	1369.7	19.8
0.75	-31.9	11.0	1020.7	15.5
1.25	-24.0	15.1	1190.7	9.5
1.75	-14.1	11.4	1281.1	10.0
2.25	-2.3	3.1	729.1	10.4
2.75	11.5	11.2	770.7	8.8
3.25	27.3	0.6	982.8	8.8
3.75	45.0	10.6	1501.7	11.7
4.25	64.6	40.8	1342.1	10.6
4.75	86.2	10.2	1147.6	11.9
5.25	109.8	10.4	1025.4	15.3
5.75	135.3	0.5	1174.5	12.4
6.25	162.8	4.1	965.0	11.1
6.75	192.2	13.9	777.2	11.1
7.25	223.6	17.8	1086.8	5.3
7.75	257.0	12.8	1226.9	6.4
8.25	292.3	41.6	1368.2	7.2
8.75	329.5	4.4	776.9	10.4
9.25	368.8	12.8	864.4	5.5
9.75	409.9	5.0	1214.4	4.4
10.25	453.1	0.1	1543.0	8.6
10.75	498.2	0.4	1219.8	5.9
11.25	545.2	8.0	2159.3	7.6
11.75	594.2	18.5	2042.7	7.7
12.25	645.2	10.0	1517.5	7.3
12.75	698.1	9.2	1632.5	11.7
13.25	753.0	11.2	1441.3	7.3
13.75	809.8	0.0	2396.3	5.6
14.25	868.6	0.0	824.5	7.2
14.75	929.3	0.2	1415.0	5.0
15.25	992.0	0.1	1262.5	8.6
15.75	1056.7	12.2	1267.2	6.9
16.5	1157.3	4.5	1245.0	11.0
17.25	1262.4	6.3	1082.7	8.6
17.75	1334.9	0.3	886.0	7.2
18.25	1409.3	0.6	931.0	7.3
18.75	1485.7	0.2	915.3	8.4
19.25	1564.0	0.2	728.4	9.7
19.75	1644.3	0.2	515.4	5.5

Depth (cm)	Age (cal. years BP)	Carbonate rocks (>150µm)	Total (>150µm)	Total (>500µm)
20.25	1726.6	0.0	969.5	5.6
20.75	1810.8	0.0	778.8	3.8
21.25	1897.009	0.0	2678.3	10.2
21.75	1985.143	0.0	963.6	9.1
22.25	2075.233	2.4	828.5	9.7
22.75	2167.279	3.6	822.9	5.8
23.25	2261.282	0.0	760.8	3.6
23.75	2357.242	0.0	1145.5	3.6
24.25	2455.159	0.0	710.2	5.2
24.75	2555.031	0.0	826.4	7.2
25.25	2656.861	0.0	724.8	4.6
25.75	2760.647	0.0	746.5	4.3
26.25	2866.389	0.4	511.3	6.7
26.75	2974.088	0.0	405.8	5.6
27.25	3083.744	2.1	877.2	7.1
27.75	3195.356	0.0	883.8	5.2
28.25	3308.925	0.0	706.9	6.4
28.75	3424.45	0.0	810.6	6.6
29.25	3541.932	0.0	777.5	3.9
29.75	3661.37	0.0	757.0	4.9
30.25	3782.765	0.1	339.1	5.1
30.75	3906.116	0.0	565.5	5.0
31.25	4031.424	0.0	414.4	2.7
31.75	4158.689	0.0	586.8	5.7
32.25	4287.91	0.0	457.4	3.4
32.75	4419.088	0.0	502.5	3.3
33.25	4552.222	0.0	733.4	4.4
33.75	4687.313	0.0	551.6	4.4
34.25	4824.36	0.0	552.2	5.3
34.75	4963.364	0.0	269.9	2.8
35.25	5104.324	0.7	336.6	1.8
35.75	5247.241	0.2	177.2	2.1
36.25	5392.115	0.0	106.4	0.3
36.75	5538.945	2.1	40.9	1.5
37.25	5687.731	0.0	27.3	0.3
37.75	5838.475	0.0	99.3	1.8
38.25	5991.174	0.0	73.2	0.9
38.75	6145.83	0.0	74.9	0.9
39.25	6302.443	0.2	125.9	1.0

Depth (cm)	Age (cal. years BP)	Carbonate rocks (>150µm)	Total (>150µm)	Total (>500µm)
39.75	6461.013	0.7	118.5	2.0
40.25	6621.539	0.0	147.9	3.0
40.75	6784.021	3.1	231.5	4.4